REPORT DOCUMENTATION PAGE

Form Approved
OMB No. 0704-0188

Public reporting burden for this collection of information is estimated to average 1 hour per response, including the time for reviewing instructions, searching existing data sources, gathering and maintaining the data needed, and completing and reviewing the collection of information. Send comments regarding this burden estimate or any other aspect of this collection of information, including suggestions for reducing this burden, to Washington Headquarters Services, Directorate for Information Operations and Reports, 1215 Jefferson Davis Highway, Suite 1204, Arlington, VA 22202-4302, and to the Office of Management and Budget, Paperwork Reduction Project (0704-0188), Washington, DC 20503.

1. AGENCY USE ONLY (Leave blank)	2. REPORT DATE	3. REPORT TYPE AND DATES COVERED
	1982	Final

4. TITLE AND SUBTITLE
Proceedings of the Tri-Service Gun Tube Wear and Erosion Symposium, ARRADCOM, Dover, NJ, 25-27 October 1982

5. FUNDING NUMBERS
Unknown

6. AUTHOR(S)
Picard, Jean-Paul
Ahmad, Iqbal
Bracuti, Arthur

7. PERFORMING ORGANIZATION NAME(S) AND ADDRESS(ES)
American Defense Preparedness Association at U.S. Army Armament Research and Development Command, Dover, New Jersey

8. PERFORMING ORGANIZATION REPORT NUMBER
Unknown

9. SPONSORING/MONITORING AGENCY NAME(S) AND ADDRESS(ES)
same as above

10. SPONSORING/MONITORING AGENCY REPORT NUMBER
Unknown

11. SUPPLEMENTARY NOTES
Proceedings of the 1977 Symposium are available in the DTIC collection ADA046606

12a. DISTRIBUTION/AVAILABILITY STATEMENT
Approved for Public Release

12b. DISTRIBUTION CODE
A/01

13. ABSTRACT *(Maximum 200 words)*

This volume consists of reprints of the technical papers presented at the Tri-Service Gun Tube Wear and Erosion Symposium, held at Picatinny Arsenal, Dover, New Jersey, on October 25-27, 1982, but was updated to reflect the current findings. It was the second Tri-Service Symposium hosted at the Army Armament Research and Development Command (ARRADCOM).

forty papers authored by scientists and engineers from the Tri-Services, Industries, and the Academia, were presented in six sessions, namely: (1) Overview of the Current Properties; (II) Phenomenology and Characterization; (III) Mechanisms and Modeling; (IV) Coatings; (V) Liners, Rotating Bands and Design; (VI) Propellants and Additives. This was followed by remarks made by the Chairman of each session stressing the major points made in each session, with identification of the central areas where future R&D efforts should be concentrated.

It was intended for this symposium to enhance coordination of activities between the services and industries.

14. SUBJECT TERMS	15. NUMBER OF PAGES
GUN BARRELS, GUN PROPELLANTS, EROSION RESISTANCE, WEAR REISTANCE, HEAT RESISTANT ALLOYS, INTERIOR BALLISTICS, MUZZLE VELOCITY, GUN BARREL ATTACHMENTS, SYMPOSIA, JOINT MILITARY ACTIVITIES	554
	16. PRICE CODE

17. SECURITY CLASSIFICATION OF REPORT	18. SECURITY CLASSIFICATION OF THIS PAGE	19. SECURITY CLASSIFICATION OF ABSTRACT	20. LIMITATION OF ABSTRACT
U	U	U	U

GENERAL INSTRUCTIONS FOR COMPLETING SF 298

The Report Documentation Page (RDP) is used in announcing and cataloging reports. It is important that this information be consistent with the rest of the report, particularly the cover and title page. Instructions for filling in each block of the form follow. It is important to ***stay within the lines*** to meet ***optical scanning requirements***.

Block 1. Agency Use Only *(Leave blank)*.

Block 2. Report Date. Full publication date including day, month, and year, if available (e.g. 1 Jan 88). Must cite at least the year.

Block 3. Type of Report and Dates Covered. State whether report is interim, final, etc. If applicable, enter inclusive report dates (e.g. 10 Jun 87 - 30 Jun 88).

Block 4. Title and Subtitle. A title is taken from the part of the report that provides the most meaningful and complete information. When a report is prepared in more than one volume, repeat the primary title, add volume number, and include subtitle for the specific volume. On classified documents enter the title classification in parentheses.

Block 5. Funding Numbers. To include contract and grant numbers; may include program element number(s), project number(s), task number(s), and work unit number(s). Use the following labels:

C	- Contract	**PR**	- Project
G	- Grant	**TA**	- Task
PE	- Program Element	**WU**	- Work Unit Accession No.

Block 6. Author(s). Name(s) of person(s) responsible for writing the report, performing the research, or credited with the content of the report. If editor or compiler, this should follow the name(s).

Block 7. Performing Organization Name(s) and Address(es). Self-explanatory.

Block 8. Performing Organization Report Number. Enter the unique alphanumeric report number(s) assigned by the organization performing the report.

Block 9. Sponsoring/Monitoring Agency Name(s) and Address(es). Self-explanatory.

Block 10. Sponsoring/Monitoring Agency Report Number. *(If known)*

Block 11. Supplementary Notes. Enter information not included elsewhere such as: Prepared in cooperation with...; Trans. of...; To be published in.... When a report is revised, include a statement whether the new report supersedes or supplements the older report.

Block 12a. Distribution/Availability Statement. Denotes public availability or limitations. Cite any availability to the public. Enter additional limitations or special markings in all capitals (e.g. NOFORN, REL, ITAR).

- **DOD** - See DoDD 5230.24, "Distribution Statements on Technical Documents."
- **DOE** - See authorities.
- **NASA** - See Handbook NHB 2200.2.
- **NTIS** - Leave blank.

Block 12b. Distribution Code.

- **DOD** - Leave blank.
- **DOE** - Enter DOE distribution categories from the Standard Distribution for Unclassified Scientific and Technical Reports.
- **NASA** - Leave blank.
- **NTIS** - Leave blank.

Block 13. Abstract. Include a brief *(Maximum 200 words)* factual summary of the most significant information contained in the report.

Block 14. Subject Terms. Keywords or phrases identifying major subjects in the report.

Block 15. Number of Pages. Enter the total number of pages.

Block 16. Price Code. Enter appropriate price code *(NTIS only)*.

Blocks 17. - 19. Security Classifications. Self-explanatory. Enter U.S. Security Classification in accordance with U.S. Security Regulations (i.e., UNCLASSIFIED). If form contains classified information, stamp classification on the top and bottom of the page.

Block 20. Limitation of Abstract. This block must be completed to assign a limitation to the abstract. Enter either UL (unlimited) or SAR (same as report). An entry in this block is necessary if the abstract is to be limited. If blank, the abstract is assumed to be unlimited.

PROCEEDINGS OF THE TRI-SERVICE GUN TUBE WEAR AND EROSION SYMPOSIUM

25-27 OCTOBER 1982

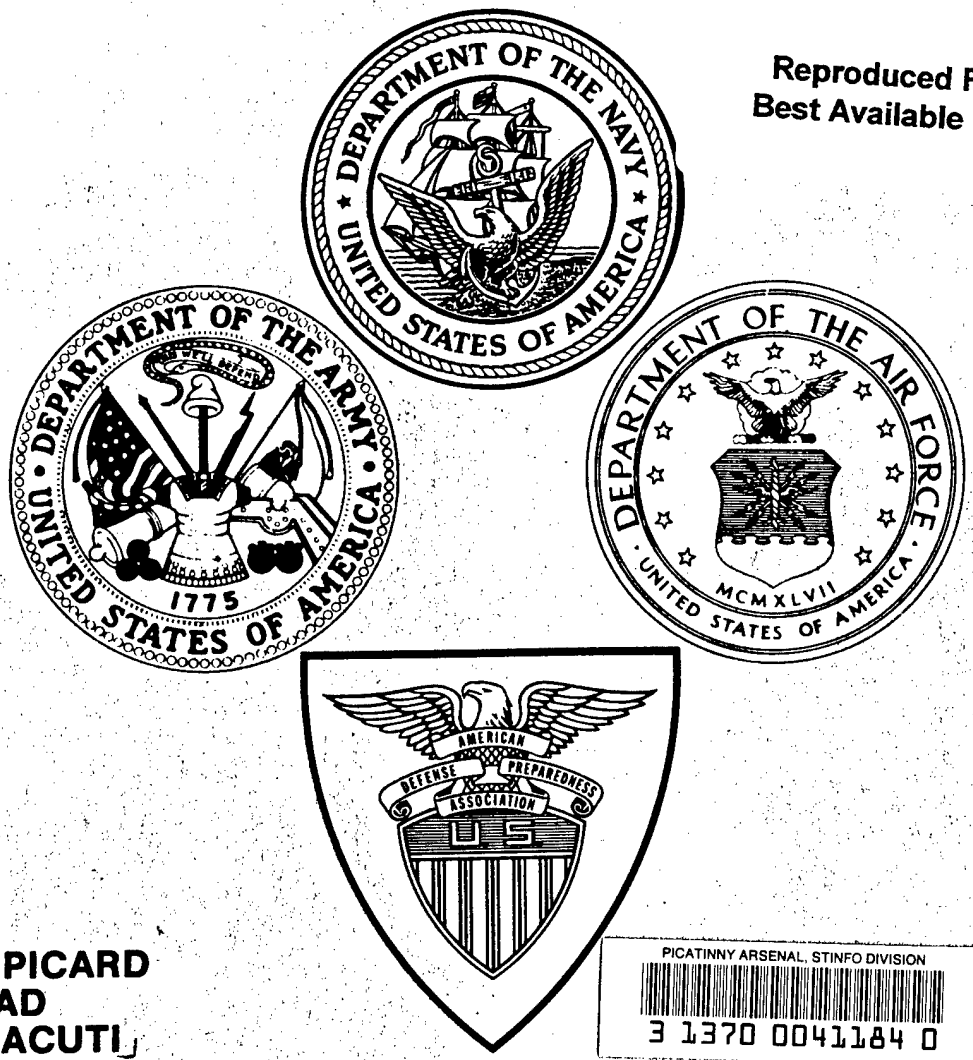

Reproduced From
Best Available Copy

EDITORS:
JEAN-PAUL PICARD
IQBAL AHMAD
ARTHUR BRACUTI

PICATINNY ARSENAL, STINFO DIVISION
3 1370 0041184 0

ARMAMENT RESEARCH & DEVELOPMENT CENTER
SCIENTIFIC AND TECHNICAL INFORMATION DIVISION

SPONSORED BY

AMERICAN DEFENSE PREPAREDNESS ASSOCIATION

AT

U.S. ARMY ARMAMENT RESEARCH
AND DEVELOPMENT COMMAND
DOVER, NEW JERSEY

ARMAMENT RESEARCH & DEVELOPMENT CENTER
SCIENTIFIC AND TECHNICAL INFORMATION DIVISION

20020108 111

UI60,1982
MTG./25-27 Oct 1982
(2)

ARMAMENT RESEARCH & DEVELOPMENT CENTER
SCIENTIFIC AND TECHNICAL INFORMATION DIVISION

TECHNICAL PROGRAM COMMITTEE

Dr. Jean-Paul Picard, LCWSL, ARRADCOM, Dover, NJ - Chairman
Dr. Arthur Bracuti, LCWSL, ARRADCOM, Dover, NJ
Dr. Iqbal Ahmad, Benet Weapons Lab, LCWSL, Watervliet, NY
Dr. Austin Barrows, BRL, ARRADCOM, Aberdeen Proving Ground, MD
Dr. S. Johnston, Army Material and Mechanics Research Center, Watertown, MA
Dr. Robert R. Reeber, US Army Research Office, Research Triangle Park, NC
Mr. Otto Heiney, Armament Division, Eglin Air Force Base, FL
Mr. James S. O'Brasky, Naval Surface Weapons Center, Dahlgren, VA

The Assistant Secretary of Defense for Public Affairs has determined that this event complies with Department of Defense guidance in the conduct of Association activities.

ARMAMENT RESEARCH & DEVELOPMENT CENTER
SCIENTIFIC AND TECHNICAL INFORMATION DIVISION

GENERAL COMMENTS

This volume consists of reprints of the technical papers presented at the Tri-Service Gun Tube Wear and Erosion Symposium, held at Picatinny Arsenal, Dover, New Jersey, on October 25-27, 1982, but was updated to reflect the current findings. It was the second Tri-Service Symposium hosted at the Army Armament Research and Development Command (ARRADCOM).

The last symposium on this subject was held at Dover, NJ, in March 1977. Therefore, it was the objective of this symposium to present an up-to-date review of the work carried out in the field of gun tube wear and erosion in the United States and foreign countries. Attention was directed to the development and application of coatings and liner materials, rotating band designs, propellant formulations, additives, modeling, and mechanisms responsible for wear and erosion. The development of a technical base for design of extended life for gun barrels was also discussed.

It was intended for this symposium to enhance coordination of activities between the services and industries.

Following the welcoming remarks by Mr. Victor Lindner, Associate Technical Director, and the keynote address by Colonel Ronald Philip, Deputy Commander, forty papers authored by scientists and engineers from the Tri-Services, Industries, and the Academia, were presented in six sessions, namely: (1) Overview of the Current Properties; (II) Phenomenology and Characterization; (III) Mechanisms and Modeling; (IV) Coatings; (V) Liners, Rotating Bands and Design; (VI) Propellants and Additives. This was followed by remarks made by the Chairman of each session stressing the major points made in each session, with identification of the central areas where future R&D efforts should be concentrated.

Sincere thanks are due to Colonel G. Gustafson, USA (Ret), ADPA representative for his assistance, participation, and devotion to the advancement of Munitions Technology.

TABLE OF CONTENTS

	Page No.
Summary	vi
Session I: Symposium Overview -- Chairman: Dr. John T. Frasier	
U.S. Army Gun Barrel Wear and Erosion Program a Review J. Lannon LCWSL, ARRADCOM, Dover, NJ	I-1
The Operational Impact of Naval Gun Erosion J.S. O'Brasky Naval Surface Weapons Center, Dahlgren, VA	I-27
Basic Research Related to Gun Tube Wear and Erosion Robert R. Reeber U.S. Army Research Office Research Triangle Park, NC	I-52
Status of Gun Barrel Wear and Erosion in the USA Jean-Paul Picard LCWSL, ARRADCOM, Dover, NJ	I-63
Session II: Phenomenology and Characterizations -- Chairman: Dr. Joseph A. Lannon	
GAU-8/A Barrel Life Improvement Program Microflash Photography, Post Test Metallographic Results S.R. Duke, D.P. Perrin, M.A. Blair General Electric Company, Burlington, VT	II-72
White Layer Development on Gun Steel in Ballistic Compressor Tests R.J. Arnott, W.J. Croft, L.A. Shepard AMMRC, Watertown, MA	II-89
Metallurgical Characterization of the Eroded Bore Surface of a High Performance Barrel K. Iyer SCWSL, ARRADCOM, Dover, NJ A. Schmacher, H. Weiss IFAM, Bremen, West Germany	II-100
Auger Electron Spectroscopic Analysis on Gun Tube Erosion Sin-Shong Lin AMMRC, Watertown, MA	II-111

Electrochemical Studies of Chromium in Molten LIF- NAF-RF II-126
R.A. Bailey, T. Yoko
Dept. of Chem., Rensseler Polytechnic Institute
Troy, NY

Monitoring Interior Surface Conditions of Large Caliber Gun Barrels at Aberdeen Proving Grounds II-133
R. A. Gillery
Material Testing Directorate, Aberdeen Proving Grounds, MD

Metallographic Studies of Erosion and Cracking of Cannon Tubes II-151
R.M. Fisher, A. Szirmae
U.S. Steel Corp., Research Laboratory, Monroeville, PA
M.H. Kamdar
ARRADCOM, LCWSL, Benet Weapons Laboratory,
Watervliet NY

Session III: Mechanism and Modeling: -- Chairman: Dr. Austin Barrows

A Ballistic Compressor for Studies of Corrosion and Erosion of Metals Exposed to a Hot, Dense Gas III-162
M. Takeo, J. Dash, C.E. Sanford
Dept of Physics, PSU, Portland OR

Calibration of the Nordheim-Soodak Heat Transfer Model to the Large Caliber Artillery Tube Heating Problem III-172
John E. Kovacs
ARRADCOM, Requirements and Analysis Office
Dover, NJ

Role of Surface Oxide on Gun Barrel Wear III-182
I.C. Stobie, J.R. Ward
ARRADCOM, BRL
Aberdeen Proving Grounds, MD

Two-Dimensional, Turbulent, Two-Phase Interior Ballistic Flows Using Implicit Numerical Algorithm III-192
N.E. Banks
ARRADCOM, BRL
Aberdeen Proving Grounds, MD
H.J. Giberling, H. Mc Donald
Scientific Research Associates, Inc, Glastonbury, CT

Modeled Heating and Surface Erosion Comparing Mobile (Gas Borne) and Stationary (Surface Coating) Inert Particle Additive III-203
A.C. Buckingham, W.J. Sickhaus
University of California, Lawrence Livermore National Laboratory
Livermore, CA

Gun Wear: An Account of Recent UK Research and New Wear Mechanisms III-221
D.C.A. Izod, R.G. Baker
RARDE, Fort Halstead, Sevenoaks, Kent, UK

Session IV: Coatings: -- Chairman: Dr. Iqbal Ahmad,

GAU-8/A Barrel Live Improvement Program IV-253
David Perrin, Steven Duke
General Electric Co., Burlington, VT

Evaluation of Diffusion Coatings on Gun Barrel IV-269
G.R. Lakshminarayanan, W.T. Ebihara
ARRADCOM, SCWSL, Dover, NJ

High Rate Sputtering of Tantalum on to Gun Steel IV-277
J.F. Fox
ARRADCOM, LCWSL
Dover, NJ
E.D. Mc Clanahan
Battle Pacific Northwest Laboratories, Richmond, VA

A New Concept for Deposition of Chrome Coatins in Tubes IV-289
A. Niiler, W.F. Henshawt, J.R. White
ARRADCOM, LCWSL, Dover, NJ

Electro-deposition of Refractory Metal Coatings IV-299
(Tantalum and Columbium) From Fused Salt Electrolytes
Ahmad, G.J. Janz, J. Spiak, E.S. Chen
ARRADCOM, LCWSL, Benet Laboratory
Watervliet, NY

Advances in Electro-deposition of Chromium IV-334
E.S. Cheh, W. Baldauf, R.S. Carter
ARRADCOM, LCWSL, Benet Laboratory
Watervliet, NY

Erosion Resistant Coatings for Gun Tube Bore Protection IV-344
J.A. Sheward
RARDE, Fort Halstead, Sevenoaks, Kent, UK

Refractory Metal For Control of Gun Tube Erosion IV-354
M. Levy, S.K. Pan
AMMRC, Watertown, MA

Session V: Liners, Rotating Bands, and Design: -- Chairman:
James S. O'Brasky

Material For De-Coppering Erosion-Resistant Gun Tube V-368
G.C. Vezzoli, M. Otooni
ARRADCOM, LCWSL, Dover, NJ

Ceramic Material for Lightweight Guns V-382
P. Wong
AMMRC, Watertown, MA

Feasibility of Glass Matrix Composite Cylinders for Gun Barrel Liner Applications V-392
R.A. Giles, E. Bunning
Saco Defense Systems Division
Maremont Corporation, Saco, ME

Advanced High Performance Guns with Refractory Liners for Erosion Resistance V-404
P.D. Aalto, G.P. O'Hara, G.D. Andres
ARRADCOM, LCWSL
Benet Laboratory, Watervliet, NY

Engraving of Rotating Bonds: A Modification of Metal Flow Pattern V-416
Boaz Aritzur,
ARRADCOM, LCWSL, Benet Laboratory
Watervliet, NY

Interface Considerations in Medium and Major Caliber Guns V-444
J.S. O'Brasky
Naval Surface Weapons Center
Dahlgreen, VA

Session VI: Propellants and Aditives -- Chairman:
Dr. Arthur J. Bracuti
Dr. Jean-Paul Picard

Mitigation of Heating and Erosion in High Energy Anti-Armor Automatic Cannons VI-461
Franklin A. Vassallo
Calspan Corporation, Buffalo, NY

A Comparison of Barrel-Heating Processes for Granular and Stick Propellant Charges VI-479
A.W. Horst
ARRADCOM, BRL, Aberdeen Proving Grounds, MD

Erosivity of Stick Propellant VI-489
J.R. Ward, I.C. Stobie
ARRADCOM, BRL,
Aberdeen Proving Grounds, MD

A Critical Examination of the Concept of Worn Gun Charge Assessment VI-506
B.Z. Jablorski, J.S. O'Brasky
Naval Surface Weapon Center
Dahlgren, VA

Wear Testing of M30A1 and M31E1 Propellant in Stick Configuration Packaged in Bags and Combustible Cases

J.A. Lannon, A.J. Bracuti, C.J. Gardner
ARRADCOM, LCWSL, Dover, NJ
D. Adams, G. Sturbutzel
Calsban Corporation, Buffalo, NY

SUMMARY

This is the third symposium on the subject of erosion of gun tubes. The previous ones were held at Watervliet, NY and Dover, NJ in 1970 and 1977 respectively.

In the 1977 symposium a number of areas for research and development necessary to control erosion were indicated. In the summary of its proceedings an active, well coordinated effort under the supervision of a Working Group/Committee was also emphasized. The Army, being the major developer and user of guns, established such a committee.* This committee stimulated R&D both in the Government and industrial laboratories. Also in UK, the Royal Armament Research and Development Establishment (RARDE) initiated a number of complementary research projects, and under TCCP-P1 agreement has been working very closely with the committee. Consequently, since the end of World War II, 1977-1982 became a peak period for active studies of the phenomenon of erosion and its control.

Because of limitations of time, papers presented in this symposium represent only a part of the results obtained in this five year period. A complete listing of the Government reports and open literature publications is covered in the bibliography included in this volume.

The symposium consisted of six sessions, namely (I) Overview, (II) Phenomenology and Characterization, (III) Mechanisms and Modelling, (IV) Coatings, (V) Liners, Rotating Bands, and Design, (VI) Propellants and Additives.

*Members of the Erosion Committee: Dr. J. Lannon, ASD, ARRADCOM (Chairman); Dr. I. Ahmad, BWL, ARRADCOM; Dr. R. Ward, BRL, ARRADCOM; Dr. S. Johnson, AMMRC; Dr. O. Hiney, Eglin AFB; Mr. J. O'Brasky, Navy; and Dr. P. Parrish, ARO. Consultants: Dr. J. Picard, ARRADCOM; Dr. W. Rostocker, University of Illinois, Chicago; Dr. J. Sharma, ARRADCOM.

Deputy Commanding Officer, ARRADCOM, COL Philipp, in his keynote address, reemphasized that the statement made by Sir Fredrick Abel in 1866, "The great increase....in the power of artillery has brought the subject of erosion of gun barrels into prominence, and it is not too much to say that it now forms one of the chief difficulties to be encountered by the makers of a heavy gun. As far as can be seen at present its sufficient investigation is the one great difficulty which seems likely to impose a limit on the size and power of ordnance in future" and quoted in the keynote address of the 1977 symposium, was still valid. Inspite of the great progress made in the control of erosion in the conventional guns, new challenges were appearing, for example, in the form of ICAS and EM guns development, and must be met.

Dr. J. Lannon, Chairman of the Army Erosion Committee, summarized the salient advances in the understanding and control of erosion made during the last five years. Dr. Reeber of ARO enumerated the program sponsored by ARO, which included: electrodeposition of chromium in magnetic fields, electrode kinetics of the electrodeposition of chromium from fused salt electrolytes including fluoride eutectics, pulsed electrodeposition of amorphous metals and alloys, and modelling of heating and bore surface erosion in the presence of mobile and stationary inert particle additives. In a review of the Navy's involvement in the erosion control, J. O'Brasky indicated that in the conventional naval guns, because of the use of low temperature propellants supported by additives, erosion is not a worrisome problem. However, in future systems designed for superior performance, serious erosion problems were expected. The Air Force's major effort has been in the development of plastic rotating bands for GAU-8.

As reported in the papers included in these proceedings, a number of significant advances both in the understanding of the mechanisms of erosion and control can be identified.

While the application of new surface characterization techniques continued to be used to obtain additional insight into the nature of the products formed at the bore surface as a result of firing propellants with and without additives and ablatives, laboratory studies involving a 37 mm blow out gun showed that propellants containing additives leave a thin layer of residue which insulates the bore surface and thus contributes to the reduction of erosion. Even charges containing no additives leave an oxide film which reduces erosion by the subsequent round. The thickness of the film depends on the propellant flame temperature. Supportive evidence was obtained from the heat input data in the instrumented 105 mm M68 gun. Heat transfer to the bore surface when M392A2 charge was fired after a 'clean out' round of a charge with high flame temperature (such as M30, in M490 rd.), was higher than that with low flame temperature propellant (such as M1, in M467 rd.).

Theoretical work sponsored jointly by ARO and ARRADCOM further confirmed the above observation. Besides, it was shown theoretically that the most effective reduction in erosion was caused by the mobile gas born additive particles (as in the conventional charges in which an additive jacket consisting of rayon gauze impregnated with TiO_2 + wax or talc + wax is incorporated). Extensive work at BRL on the heat transfer both in 105 mm M68 and 155 mm instrumented guns has provided data for both modelling studies at LLNL, as well as for developing semi-empirical relationships to predict erosion life of guns. Significant contributions have been made at Calspan Corporation where unique thermal/erosion research facilities involving both 60

mm and 90 mm fixtures have been developed, not only to measure the heat transferred to the bore, but also the rate of erosion of the bore surface using a Knoop indentation technique. These facilities have been used effectively to evaluate candidate materials for bore surface protection and the efficiency of erosion inhibitors, particularly dimethyl silicone ablative compositions, as well as the design of the rounds containing these ablatives and their influence on the interior ballistics of the guns.

Progress in low erosivity propellants such as those reported in the 1977 symposium has not been significant. Major emphasis has been on the study of the erosivity of the stick propellants. It has been shown that, as has been suggested by Nordheim, the M30 stick propellant was more erosive than the granular form, probably because the unburnt propellant remained in the chamber longer and therefore the heat transferred to the commencement of rifling area was higher.

In the 1977 symposium the need for the improvement of the conventional HC chromium was emphasized and development of technology of using refractory metals (other than the brittle chromium) and ceramics was highlighted. As is evident from the number of papers presented in Sessions IV and V, there has been considerable activity in this area and many outstanding contributions have been made.

The process of electroplating of chromium was introduced in the 1920-1930 time frame, with the main objective of achieving resistance to mechanical wear and bright appearance for application on shafts, cylinders, car bumpers, and other household items. The same process was being applied until now in the gun barrels. In ARRADCOM it is now well recognized that for successful and reliable performance of the electrodeposited chromium, it is necessary to

modify the process to achieve superior mechanical properties (such as tensile and shear strength). Some of the salient results of the R&D projects initiated with that objective include: (a) HC chromium applied in 105 mm M68 tubes both by the conventional immersion process and the pump thru process was evaluated by test firing. The pump thru chrome behaved better than that applied by the immersion process. Also, partially plated barrels gave a better accuracy than that given by the fully plated tubes. (b) Mechanical strength was identified as one of the necessary properties for the coating to be successful in gun barrels. Therefore, a systematic study of the effect of aging, current density, plating temperature, additives, flow rate of the electrolyte, etc., on the mechanical properties, microstructure, internal residual stresses, and texture of the HC chromium has been made at BWL. (c) Low contractile chromium coating applied at 85°C, 100-120 amp/dm^2 and using a pump thru system gave the best mechanical properties. Its erosion behavior as determined by test firing in 20 mm M24A1 gun barrel using a severe AF firing schedule was superior to HC chromium. (d) Both improved HC and LC chromium coating processes developed under 6.1/6.2 programs were used to plate 105 mm and 120 mm M256 barrels. On preliminary test firing, LC coating in 120 mm M256 showed much better performance as compared with HC coating (very little chipping). Currently under MMT and OMA projects these coatings are being evaluated by test firing. (e) Another important advancement made is the introduction of computer controlled microprocessor technology in the pump thru process used for plating 105 mm and 120 mm tubes at BWL. (f) Of special interest is the work reported by the GE Burlington on the successful use of HC chromium coating-plastic band system for GAU-8, with a coating thickness of 8 mil. This combination improved the life of the tube by a factor of three.

Of the refractory metals other than chromium, tantalum was the one the most extensively studied. The coating applied from a fused eutectic mixture of KF-LiF-NaF at 800°C, in 20 mm liners was found to give excellent performance as compared with HC chromium. The process was successfully scaled up to coat 20 inch long 105 mm diameter liners. One of these liners was shrink fitted in 105 mm M68 tube, using a specially designed and in-house fabricated facility. Test firing of this gun indicated not only that the design of the liner was satisfactory, but also that inspite of the fact that the coating was not optimized (3-4 mil in thickness and non-uniform), but also it was superior to 5 mil HC chromium, test fired under the similar conditions. This work is expected to be transitioned to MMT in FY85. Columbium coating has also been applied successfully in 20 mm liners. Fundamental studies of electrodeposition of Ta-Cr alloys, electrode kinetics of electrodeposition of chromium from both fused fluorides and low melting chloride eutectic mixtures have been made. In this connection it is of interest to note that under a UK sponsored project in Imperial College, dense chromium coating of high purity was successfully applied from a fused salt bath at a temperature of 450°C. Coating of tantalum and molybdenum has also been successfully applied in 20 mm rifled liners by high rate sputtering and is currently being evaluated. In this case the substrate temperature is kept below 300°C by water cooling.

Although not reported in these proceedings, considerable progress has been made in developing the technology of fabrication of 105 mm liners from high temperature steels such as Pyrotool V and molybdenum alloys. Molybdenum is the only refractory metal available in the country. It has shown good erosion resistance in gun barrel environments. It is cheaper than other refractory metals, and is therefore quite attractive for application as liner

material in future advanced guns.

Preliminary studies on the use of silicon carbide liners in 0.5 cal rifles also showed encouraging results. Work is in progress on the evaluation of other ceramics (e.g., silicon carbide fiber reinforced glasses) for application in small caliber high performance guns.

From the above it is evident that positive progress has been made and in a number of cases 6.1/6.2 work has been translated into MMT. However, much more has to be done to bring these advances to fruition. Unfortunately for the last two years, because of the overall shrinking of R&D funds, a number of projects have to be closed out. The remaining are also under squeeze because while in 1978-81 gun tube erosion was DOD's high thrust areas of research, since FY82 it is being categorized as priority II. Consequently there is a possibility that some of the excellent technical progress made thus far, if not brought to successful implementation, may be lost.

In conclusion, the following recommendations can be made.

1. As the keynote speaker emphasized, in view of the continued challenge from the high performance guns including hypervelocity and EM guns, a steady R&D effort at a reasonable level be maintained in the Army laboratories to develop base technology for application in the 1990's.

2. In view of the significant results obtained in the materials such as those in the improvement of chromium technology and refractory metal coatings and liners, emphasis be placed to further develop these technologies for implementation in the near future.

3. Efforts to develop low erosivity propellants and erosion reducing additives must be encouraged.

4. Because of the very high cost of the ammunition and test firing, an economical and reliable simulator for evaluating both the materials and propellants should be developed.

5. Basic work on understanding the mechanisms and developing predictive models should be continued.

6. Also, new approaches to the development and design of light weight barrels with high erosion life should be explored.

7. Development of suitable organic polymers and design of rotating bands for large caliber guns is another area which requires emphasis. Very little progress has been made so far.

8. Finally, active collaboration between the three services and industry in developing concepts and design of high weight light performance guns with good erosion life must continue. Also, coordination of these efforts with our allies should be strengthened.

Iqbal Ahmad
Jean-Paul Picard

SESSION I

SYMPOSIUM OVERVIEW

CHAIRMAN: Dr. John T. Frasier

US ARMY GUN BARREL WEAR AND EROSION PROGRAM - A REVIEW

J. Lannon
US Army Armament Research and Development Command
Large Caliber Weapon Systems Laboratory
Dover, New Jersey 07801

ABSTRACT

The progress made under the Army Gun Barrel Wear and Erosion Program since 1977 is reviewed. The areas covered include diagnostics, propellants and additives and coatings/liners. Significant achievements in these areas have potential for application in the conventional and future armament systems. In view of the evolving concepts such as L.P. and E.M. guns, continued funding for R&D in the erosion control is strongly recommended.

INTRODUCTION

In this paper I would like to review the progress made under the Army Gun Barrel Wear and Erosion Program since 1977. Following are some definitions that should be kept in mind during this discussion:

> Wear Life of Gun Barrel - Is determined by unacceptable ammunition performance - Muzzle velocity drop, precision, fuze malfunction stripped rotating band.
>
> Fatigue Life - The number of rounds that may be fired before the gun barrel fails catastrophically.
>
> Gun Barrel Wear and Erosion - Physical and Chemical processes leading to enlargement or deformation of a gun barrel.

A key point is that the wear life of a gun barrel is not determined by its enlargement at the origin of rifling. It is determined by unacceptable ammunition performance such as muzzle velocity drop, a loss in precision, a malfunction of a round fired short of its target. This unacceptable ammunition performance is related to the barrel enlargement at the origin of rifling which is then established as the condemnation criteria. The critical elements influencing gun barrel wear and erosion are given in Table I. It has been clearly demonstrated that lower flame temperature propellants consisting of mainly nitrate esters produce lower wear and erosion and that wear reducing additives such as TiO_2/wax can greatly reduce the erosion in the gun barrel. Mixed results have been obtained with rotating bands. It is not clear whether non-metallic rotating bands reduce erosion more than metallic rotating bands. Some Air Force results with plastic vs. copper rotating bands in a chrome plated tube indicate the plastic to be better. In steel tubes, plastic bands do not seem to out perform the metallic bands. There has been significant progress in gun barrel lining and/or coating with erosion resistant materials

Distribution limited to US Government Agencies only because of test and evaluation; September 1982. Other requests for this document must be referred to Commander, AMCCOM, Attn: DRSMC-DCG(ASD), Dover, New Jersey 07801

such as refractory materials in the past few years, which will be described later and which offers promise for erosion reduction.

SCOPE OF THE PROGRAM

The Army's gun barrel wear and erosion program covered three main areas: Mechanisms, modelling and control. Table II shows the agencies working on erosion mechanisms, including Lawrence Livermore National Laboratory (LLNL), CALSPAN, Army Materiel and Mechanics Research Center (AMMRC), Large Caliber Weapon Systems Laboratory (LCWSL), and the Army Research Office, Durham (ARO). Also listed are those working on modelling, erosion control especially platings and liners, on wear reducing additives and finally those working on coating evaluations. By coating evaluation is meant erosion testing in controlled apparatuses, not testing in the gun tube.

STATUS OF EROSION CONTROL IN 1977

The status of wear and erosion control in 1977 is summarized in Table III. In propellants, the M30 propellant was used with the high zone 8" and the 155mm M203 propelling charges. Diagnostic techniques for predicative capability were not well established. TiO_2/wax was used as additive in high zone artillery charges. There was a serious secondary wear problem in the 105mm M68 tank gun even though the TiO_2/wax wear reducing liner was used. Gun tube coatings were not used, but uncharacterized high contractile chrome was applied to the chambers of artillery cannons. There was little work in refractory coatings and/or liners and little progress was made in understanding the wear and erosion mechanism since the Second World War. Table IV shows the barrel life of guns as established in 1977. In the M68 tank gun, the wear life was 750 rounds because of secondary wear, and the fatigue life was 1000 rounds. The barrel wear life in the 155mm M198 Howitzer System was 1750 rounds effective full charge (EFC) with a fatigue life of 11,000 rounds and the barrel wear life in the 8" M201 cannon was 1500 EFC with about a 10,000 rounds fatigue life.

PROGRESS SINCE 1977

Diagnostic Techniques:

Some of the diagnostic techniques developed and tested over the past few years will now be discussed. Figure 1 demonstrates the technique used to install thermocouples into the gun barrel wall. The thermocouples are placed into the wall about 1mm from the surface at various distances from the rear face of the tube with at least one sensor near the origin of rifling. From these measurements, the total heat input into the gun barrel at each sensor location can be calculated. This technique is especially valuable for comparing types, quantities and geometric arrangements of wear reducing additives within the propelling charge. It has been successfully used in both artillery and tank ammunition. Figure 2 demonstrates how the erosion sensor is placed into the gun barrel. This erosion sensor can be placed in the lands and/or the grooves of tank artillery barrels. Figure 3 shows the geometric configuration of a typical knoop impression on the sensor face. Only the change in length of knoop impression on the sensing face need to be measured since there is a constant ratio between the length and depth and the depth can easily be calculated. A Scanning Electron Microscope (SEM) is used to measure this length before firing and after a predetermined number of rounds (usually 5-10 rounds) and the results averaged to yield a measurement value per shot. Figure 4 gives more insight into what the erosion sensor surface looks like. Here we observe the surface of two erosion sensors.

The one on the left shows an erosion sensor before firing and after firing in which the propelling charge contained no wear reducing additive. This was an M188 8" propelling charge, Zone 9. The one on the right shows the surface before firing and after firing in which the propelling charge contained TiO_2/wax wear reducing additive. It is clear that the propelling charge without the wear reducing additive removed all the knoop impressions on the erosion sensor, meaning that this propelling charge is highly erosive. In comparison after firing, the propelling charge with the TiO_2/wax wear reducing additive, some of the knoop impression on the erosion sensors can still be observed, especially the more deeply imprinted ones. From the deeper knoop impressions the erosion was measured as about .02 mils per shot.

A radiation technique was developed by Dr. Andy Niiler of the Ballistic Research Laboratory (BRL). With this technique the gun barrel surface is irradiated with a proton source, converting the iron in the steel from a non-radioactive isotope to one radioactive emitting gamma rays. The gamma rays emitted from the gun barrel surface are measured both before and after each shot. From the difference in gamma rays, the amount of erosion in the gun barrel can be determined. The disadvantage of this technique is that it is extremely slow. It can take 15-30 minutes to get sufficient gamma ray counts to obtain an accurate reading, but an accurate measurement of the erosion per shot can be obtained. The disadvantage of the knoop technique is that it must be used over a series of shots. The number of shots varies anywhere from 5 to 10 rounds and the amount eroded per shot is then calculated by taking the total amount of erosion observed in all shots and dividing by total number of shots. This does not tell us how much erosion occurs in each shot. Figure 5 shows a plot comparing the wear measured by the knoop and radiation techniques measured during the firing of one ten round series of a wear test with the M203 propelling charge. This shows that the difference between the two techniques is not great. Please note that in measurement #1 of Figure 5, part of the erosion sensor was chipped away and this probably caused the large difference between the two techniques. Table V summarizes the amount of erosion measured by the radiation technique for each shot over a series of ten shots. It clearly shows that the amount of erosion for each shot is not the same. In fact, there is a wide variation in the amount of erosion among shots. However, if one averages the erosion over ten shots for the radiation technique and computes the same average using the knoop sensor technique, the two techniques compare well. This gives some insight to the mechanism of wear and erosion in gun barrels. There seems to be no erosion for several shots and then a large amount of erosion occurs and then this cycle seems to repeat itself. This does not always occur in a regular pattern but it appears that a layer buildup must happen before erosion occurs.

The above described diagnostic techniques offer a substantial cost savings. For example, in 1979, for artillery applications, projected cost to evaluate a given wear reducing additive configuration was about $170,000. This includes the firing of about 200 rounds. Two hundred rounds were picked because this is the number of rounds needed to be fired to get an accurate measurement of the wear and erosion at the origin of rifling with a standard star gauge. The cost of using thermal and erosion sensors is only about $10K per test. During this fiscal year in the artillery systems about 35 different configurations were evaluated leading to a total cost avoidance of over 5.6 million dollars for artillery systems and a similar cost avoidance of 3.8 million dollars was realized for the tank systems in FY79. Thus wear reducing additives can now be optimized in all new propelling charges at very low cost.

Propelling Charges:

The properties of the charge contributing to the gun barrel wear and erosion, are the flame temperature, the charge weight and the rate of heat input to the barrel. It is a much more erosive condition to put a large amount of heat quickly into the gun barrel than to put the same amount of heat slowly into the gun barrel. Higher pressures, of course, mean more molecular collisions with the gun barrel walls and consequently more heat transfer. Higher rates of fire tend to raise the ambient temperature of the gun barrel, thus allowing the barrel wall temperature to reach its melting point (or a very erosive condition) easier. Table VI shows some of the improvements in gun barrel wear life due to changes in propellant charge. One of the biggest achievements was in 8" artillery. A switch from M30A2 to M31A1 propellant in the M188 propelling charge more than doubled the wear life. In the 155mm artillery system, it was shown that the M119 base ignited propelling charge was equal to or better in wear than the center core ignited M119 propelling charge. In the 105mm M724 tank round it was demonstrated that the TiO_2/wax wear reducing liner was not necessary.

Figure 6 shows the 8" propelling charge containing the M30A2 propellant. The TiO_2/wax wear reducing liner is used in both the Zone 8 and Zone 9 parts of the M188 propelling charge. This propelling charge left residue in the chamber after firing. The new 8" propelling charge is shown in Figure 7. Here the wear reducing additive is used in only the Zone 9 part of the propelling charge because of the use of the cooler M31A1 propellant. This decision was based solely on the heat input data obtained using our new diagnostic techniques. The decision was later confirmed in a limited wear test. Table VII gives a comparison of the heat input data of the 8" propelling charge containing the M30A2 and the M31A1 propellant. Comparing the two propelling charges at Zone 8, it can be seen that a reduction occurs in heat input with a corresponding increase in wear life for the M31A1 propellant, and the same can be observed for the Zone 9 part of the charge. Some idea of the cost savings realized in terms of FY80 dollars in the 8" system as a result of switching to cooler propellants can be had from the estimate that only ½ the current production quantity of tubes would be required. This would mean a saving of about 8.7 million dollars for this year alone.

Figure 8 shows a picture of a current, fielded M203 propelling charge containing M30A1 granular propellant. M31A1 granular propellant cannot be substituted for M30A1 granular propellant in this charge because there is not enough room in the gun chamber if the loading density is to be kept at 0.65 lbs./cu inch or less. This loading density is required to prevent ignition problems with granular charges. Table VIII shows the heat inputs and total rounds fired for the M203 propelling charge containing the TiO_2/wax wear reducing liner with the usual lower melting point wax (71°C) and that containing the new TiO_2/wax wear reducing liner containing a higher melting point wax (96°C). Table IX gives possible reasons for the superior function of synthetic wax. The melting point of a wax is not a true melting point. Wax is a mixture of polymers of different chain lengths. It does not have a sharply defined melting point. It has a range of melting point depending upon the distribution of polymers contained within the wax. The heat input data indicates that if the wax is softened by temperature conditioning or by contact with the hot gun barrel walls, it does not reduce the heat input to the barrel as much as it would if it remained hard and brittle. If the wear reducing additive does not function properly, residue may occur as it did in the M203 charge. So the wax

Table XI gives some results for some small caliber systems. Here the different additives, molybdenum trioxide, talc and calcium carbonate, contained in the propellant for 7.62mm ammunition are compared. The calcium carbonate is more effective than either molybdenum trioxide or the talc. Also seen in this table is that the calcium carbonate coated on the surface of the propellant grains offer an improvement over incorporating it directly into the propellant formulation.

Refractory Metal Coatings and Liners

The following have been examined as coatings and liners; chromium, tantalum, columbium and molybdenum, ceramic liners such as silicon carbide, diffusion coatings and replacements for the cobalt alloy liners, specifically the stellite liner for the 0.50 caliber machine gun barrel. The stellite liner has to be replaced because of the unavailability of cobalt in the United States and the difficulty in procuring it from foreign sources. Some of the accomplishments in the past few years are summarized in Table XII. Chrome coatings have been fielded in the 8" howitzer systems but not recommended for field use. The reason will be discussed later in the talk. Chrome has also been tested in the M68 tank gun where it was shown that partial plating was superior in wear performance to the steel barrel but that full barrel length chrome plating was not as good. Low contractile chrome was demonstrated to be superior to conventional high contractile chrome. It is now being tested in the 120mm system and will also be tested in the future in the 155mm artillery system. Tantalum liners have been tested in 20mm guns and shown to be superior to high contractile chrome. They have also been shrink fitted into M68 tank guns but only limited firings have taken place. Silicon carbide liner has been successfully shrink fitted into a .50 caliber machine gun and has survived 1000 firings in a single shot mode.

The main requirements of materials for coating and lining gun barrels include melting points, yield strength at high temperature, elastic modulus fracture toughness and impact strength, hot hardness, chemical inertness to powder gases,coefficient of thermal expansion, thermal conductivity, specific heat, inertness with the rotating band material, phase transition, ease of fabricability and cost. Figure 12 shows a comparison of wear vs. round numbers in a 20mm test of low contractile chrome with high contractile chrome. In this test the low contractile chrome outperformed the high contractile chrome by at least a factor of 2. In Figure 13 we see a comparison in a wear test of steel liners coated with high contractile chrome and tantalum. Again, the tantalum liners outperformed the high contractile chrome by about a factor of 2. This indicates that the tantalum and the low contractile chrome are coatings that should be given serious consideration in future systems where erosion might be a problem.

In the next series of Figures beginning with Figure 14, the 155mm tube wear test in which a chrome coated barrel is compared with a steel barrel will be presented. The chrome plated barrels in two separate tests outperformed the steel barrel if barrel wear at the origin of rifling from a star gauge report is the only consideration. The reader is reminded of the definition of the condemnation criteria of a gun barrel. Condemnation criteria is determined from ammunition malfunctions after firing a given number of rounds. Figure 15 shows 155mm projectiles recovered after being fired from a steel tube. Figure 16 shows 155mm projectiles recovered after being fired from a chrome tube. These tubes had previously fired about 1500 M203 charges. The projectiles fired and recovered from the steel tube were engraved normally. Those fired and recovered from the chrome tube have less

must be brittle enough to break up in order to function properly in the wear reducing additive. The higher melting wax contains a distribution of polymers that have higher melting points and thus it will not soften as easily at the higher operating gun temperatures as does the previously used lower melting point wax.

The present M198 gun tube has a wear life of 1750 rounds EFC. This is based on firing the M203 propelling charge (EFC=1) using M30A1 granular propellant. The wear life goal for the M203 propelling charge is 2600 EFC. A product improvement program (PIP) is currently being worked on to achieve this. In this charge, a cooler propellant, M31A1, similar to that used in the 8" propelling charge will be used in stick form, not granular. A combustible case containing 8-10% talc will also aid in reducing the gun barrel erosion, and evaluation early in the development cycle is planned. The new proposed product improved M203 propelling charge is shown in Figure 9. This propelling charge uses M31A1 stick propellant, a combustible case containing talc but no TiO_2/wax wear reducing liner and contains only a base igniter.

Some wear reducing liners used in tank ammunition will now be discussed. Two tank rounds, namely M724A1 and M490 show in Figure 10 and 11, will first be described. The M724A1 originally contained a TiO_2/wax wear reducing liner and used M30 propellant but later M1, a much cooler propellant, was substituted for M30 and the round was never tested to determine if the wear additive was still required (probably because no diagnostic techniques were available). The M724 is a training round that simulates the M392 kinetic energy round in the 105mm tank systems. The M490, the training round for the M456 HEAT round, contains M30 granular propellant and also uses TiO_2/wax wear reducing liner to help control the erosion in the gun barrel. Table X shows heat input data from these rounds obtained from previously described diagnostic techniques. Comparing heat input data among the M724 with the wear reducing liner and M1 propellant, called the standard round, this same round without the wear reducing liner and also with the M724 containing M30 propellant and the TiO_2/wax wear reducing liner shows that both rounds with the M1 propellant have less heat input to the gun barrel than the round containing the M30 propellant and the wear reducing liner. The data also show that TiO_2/wax wear reducing liner does not significantly reduce the heat input to the gun barrel in the round with the M1 propellant. The table also shows the heat input data for an M490 heat round fired after other M490 rounds, fired after a standard M724 round and a M724 round without the wear reducing liner. Previous firings demonstrated that heat inputs were highest for an M490 round which had one M724 round without wear reducing additive fired before it. We test fired an M490 round preceeded by two M724 rounds and also an M490 round preceeded by three M724 rounds. These two cases were no worse than one M490 preceeded by one M724. This series of tests demonstrated the following: the M724 round without the wear reducing liner but with M1 propellant is far superior in wear and erosion characteristics to the M724 round containing the M30 propellant and the TiO_2/wax wear reducing liner. Second, the M724 without the wear reducing liner has slightly greater heat input than the M724 round with the wear reducing liner and thus the wear reducing liner does not add much to the erosion control for this round. The utilization of the M1 propellant seems sufficient to control the erosion in the M724 round. The data shows that the firing of the M724 before the M490 does not adversely affect its heat input even if the round does not contain a wear reducing liner. This table contains both the heat input at the origin of rifling and at the secondary wear position because a serious secondary wear problem existed in the tank guns. The table also shows that removing the wear reducing liner from the M724 round will not have an adverse affect on the secondary wear in the tank gun.

material on the rotating band and are close to being stripped. Figure 17 is a picture of steel tube heat checking after 200 rounds. The rounding of the lands, the lands being the narrower of the two in the picture, can also be observed. Figure 18 shows the chrome tube after about 200 rounds. This tube looks new. No heat checking nor rounding of the lands has occurred. Figure 19 shows the steel tube after about 1500 rounds where loss of definition of the lands and considerable wear in the gun barrel has occurred. Figure 20 is a chrome tube after the same number of rounds. At the origin of rifling, evidence of heat checking is beginning to appear. The barrel looks good at the origin of rifling but at the commencement of rifling where the lands reach full height, a necking down of the lands is evident. This necking down of the lands is believed to be the cause of the excess wear on the rotating bands. If enough rounds were fired from this tube, there would eventually be a hole occurring at the commencement of rifling. The necking down starts when the projectile engraves the rifling enough times to chip away the chrome plating from the edge of the lands, leaving the steel exposed on these edges but the chrome still on the top of the lands. Then the hot gases erode away the steel faster than the chrome, thus resulting in the observed necking down of the lands. This condition has also been shown to lead to a high torsional impulse, indicating a projectile free run in the tube, and this high torsional impulse can cause serious ammunition malfunctions in the fuze, projectile or the explosive filler, and thus will result in the condemnation of the gun tube. So, for a chrome gun tube the condemnation criteria will be quite different than for a steel gun tube. It was for this reason and because the chrome did not add a significant number of rounds to the wear life in the 155mm system, that chrome was not recommended for field use.

FUTURE TRENDS

All high performance systems will require increased muzzle velocity, range and increased rates of fire which will definitely lead to higher wear and erosion in conventional systems. If liquid propulsion or electromagnetic propulsion are utilized to achieve higher performance, different wear patterns than are presently observed may occur. Table XIII shows the barrel life of guns in 1982. Improvements in wear life in the tank gun and in the 8" artillery system have been achieved while a program to improve the wear life of the 155mm system has been initiated.

CONCLUSIONS

Significant progress and cost savings have been made in wear and erosion measurement techniques and reduction since 1977. Some of these have been applied to existing systems while other technological advances have been made which may be applicable to future systems. Continued funding is required for this technology to be applied to future systems. Novel systems such as liquid and electromagnetic propulsion may surface new wear and erosion problems which may require increased funding to solve.

ACKNOWLEDGMENTS

The Army Gun Barrel Wear and Erosion Program was managed by a Committee consisting of the following: Dr. J. Lannon (Chairman) LCWSL(ASD), Dr. R. Ward, BRL, Dr. I. Ahmad, LCWSL (BWL), Mr. E. Wurzel, LCWSL, Dr. L. Rosendorf, LCWSL, Mr. H. Kahn, FC and SCWSL, Dr. S. Cytron, FC and SCWSL, Dr. S. Johnson, AMMRC, Dr. P. Parrish. ARO consultants: Professor N. Suh, MIT, Professor W. Rostocker, University of Illnois and Dr. J. P. Picard, ARRADCOM. Currently Dr. R. Ward, Dr. Lannon and Dr. Johnson have been respectively replaced by Dr. I. Stobie, Dr. A. Bracuti, and Mr. M. Levy.

TABLE I. CRITICAL ELEMENTS INFLUENCING WEAR AND EROSION

Propellants	Low flame temperature Liquid propellants Consolidated Nitramines
Wear Reducing Additives	Talc, TiO_2, Other Ablatives Improved configuration
Rotating Bands	Non-metallic Improved design Other metals
Platings/Liners	Fixed Replaceable Coating optimization New techniques

TABLE II. ARMY GUN BARREL WEAR AND EROSION PROGRAM

Mechanisms	Modeling	Control
LLNL	LLNL	Wear reducing additive
CALSPAN	BRL	CALSPAN
AMMRC	ARO	LCAL
LCAL	LCAL	BRL
ARO		SCAL
		ARO
		Coating Evaluation
		LCAL
		BRL

TABLE III. STATUS OF WEAR AND EROSION CONTROL IN 1977

Propellants -	M30 propellant used with high zone 8" propelling charge and XM201 and XM203 propelling charges.
Diagnostic techniques -	Predicative capability not well established.
Additives -	TiO_2 wax used in high zone artillery charges, secondary wear in the 105mm M68 with TiO_2/wax.
Gun tube coatings -	Uncharacterized H.C. chrome applied in chamber.
Gun Tube liners -	No work
Mechanisms -	Little progress

TABLE IV. BARREL LIFE OF GUNS

Gun Barrel	Wear Life (Rds)	Fatigue Life
M68 (105mm)	750 Rds	1000 Rds
M185 (155mm)	7500 Rds	5000 Rds
M199 (155mm)	1700 Rds	11000 Rds
M201 (8")	1500 Rds	10000 Rds

TABLE V. AVERAGE EROSION MEASURED FROM CHANGES IN RADIATION COUNTS FROM THE SENSOR FACES (MICRONS)

SHOT #	SENSOR[a] 1	SENSOR[b] 2	SENSOR[c] 3
1	0.60	0.0	0.0
2	1.91	0.31	0.31
3	0.11	1.72	0.05
4	1.03	0.23	0.31
5	0.05	0.90	-0.29
6	3.21	0.41	0.25
7	0.25	1.32	0.10
8	0.07	1.12	0.08
9	2.06	0.32	0.11
10	0.28	0.03	0.50
1 - 10	0.957	0.636	0.126

a - Located at 1.06 meters rft

b - Located at 1.09 meters rft

c - Located at 1.65 meters rft

TABLE VI. IMPROVEMENTS IN WEAR LIFE DUE TO CHANGES IN PROPELLING CHARGES

8" ARTILLERY

Switch from M30A2 to M31A1 doubled the wear life.

155MM ARTILLERY

M119 base ignited charge equal to or better than center core ignited charge.

Wax in TiO_2/wax wear reducing additive in M203 functions better with high melting wax at 145°F.

105MM TANK

TiO_2/wax reducing additive is not necessary in the M724 training round.

Optimization of wear reducing additive in KE rounds.

Cooler propellant/improved geometry reduces wear in the spin stabilized M490 round.

TABLE VII. HEAT INPUT AT ORIGIN OF RIFLING FOR 8" GUN

DESCRIPTION	AVE HEAT INPUT ($J/M^2 \times 10^{-4}$)	WEAR LIFE (RDS)
M188 E1, Standard Liner, Zone 8, M30A2 Propellant	202	3000
M188 E2, Standard Liner, Zone 9, M30A2 Propellant	215	1500
M188 A1, No liner, Zone 8 M31A1 Propellant	187	6000*
M188 A1, Liner only in Zone 9, M31A1 Propellant	168	3000*

*Estimated values based on firing 250 rounds.

TABLE VIII. HEAT INPUT AND ROUNDS FIRED BEFORE CONDEMNATION WITH THE M203 PROPELLING CHARGE

CHARGE	HEAT INPUT (BTU/FT^2)	TOTAL RDS BEFORE CONDEMNATION
M203 IND-78J-69806	99.6±7 (7)	1750
M203 CHARGE WITH HIGH MELTING POINT WAX	97.8±7 (7)	1750

TABLE IX. TiO_2/WAX IN M203 PROPELLING CHARGE

PETROLEUM BY PRODUCT WAX SOFTENS OVER A BROAD RANGE OF TEMPERATURE DUE TO DISTRIBUTION OF MOLECULAR WEIGHTS.

IF WAX SOFTENS DUE TO HIGH TEMPERATURE CONDITIONS, WEAR ADDITIVE DOES NOT FUNCTION PROPERLY AND RESIDUE MAY OCCUR.

HIGHER MELTING POINT SYNTHETIC WAX DOES NOT LEAVE RESIDUE IN CHARGE CONDITIONED TO 145°F AND ADDITIVE FUNCTIONS PROPERLY.

WAX MUST BE BRITTLE ENOUGH TO BREAK UP IN ORDER TO FUNCTION PROPERLY IN TiO_2/WAX WEAR REDUCING ADDITIVE.

TABLE X. TEST RESULTS (ECP ALT 8701)

TYPE RD	NUMBER FIRED	ORIGIN GROOVE (25" RFT)	MINIMUM GROOVE (26.5"RFT)	SECONDARY GROOVE (35" RFT)	SECONDARY LAND (35" RFT)
M724A1 (STD)	8	60.5±5.5	58.1±3.5	57.6±5.7	55.0±4.3
M724A1 W/O LINER	8	64.7±3.7	62.5±2.5	65.1±2.3	58.9±2.2
M724 W M30	10	74.1±6.8	70.5±6.0	65.6±4.3	61.6±4.3
M490	8	86.0±3.7	83.0±2.7	94.4±2.4	87.9±2.6
M490/M724A1 STD (ALTERNATE FIRING)	10/10	87.7±5.5	83.0±4.3	93.3±4.9	87.2±5.1
M490/M724A1 W/O LINER (ALTERNATE FIRING)	12/12	83.1±6.1	82.1±4.6	91.9±4.4	86.6±3.0

TABLE XI. AVERAGE BARREL LIFE RESULTS - 7.62MM

Propellant Type	Wear Reducing Agent	%	Nature of Distribution	Bullet Jacket	Average Barrel Life (rounds)
Single Base Extruded	-	-	-	GMCS	7,750
	MoO_3	0.45	Incorporated	GMCS	10,417
	Talc	0.68	Incorporated	GMCS	8,458
	$CaCO_3$	0.52	Incorporated	GMCS	15,750
Double Base Extruded	-	-	-	GMCS	6,333
	MoO_3	1.05	Incorporated	GMCS	8,625
	$CaCO_3$	0.37	Incorporated	GMCS	19,125
Double Base Ball	$CaCO_3$	0.15	Incorporated	GMCS	10,417
	$CaCO_3$	0.57	Incorporated	GM	18,042
	$CaCO_3$	0.46	Incorporated	GMCS	13,342
	$CaCO_3$	0.80	Coated	GMCS	29,488
	$CaCO_3$	0.50	Coated	GMCS	21,508

TABLE XII. COATINGS/LINER

CHROME

FIELDED IN 8" HOWITZER SYSTEM

TESTED IN 155MM HOWITZER SYSTEM BUT NOT RECOMMENDED FOR FIELD USE

TESTED IN 105MM TANK SYSTEM. IT SHOWED PARTIAL PLATING (40") WAS SUPERIOR TO STEEL BARREL.

L.C. CHROME WAS SUPERIOR TO CONVENTIONAL H.C. CHROME IN 20MM BARREL - NOW BEING TESTED IN 120MM SYSTEM AND PROPOSED FOR THE 155MM SYSTEM.

TANTALUM

COATED LINERS SUPERIOR TO H.C. CHROME AND STEEL IN 20MM TESTING SHRUNK FIT INTO 105MM M68 TANK CANNON WITH LIMITED FIRINGS.

CERAMICS

SiC SUCCESSFULLY TESTED IN 0.50 CALIBER MACHINE GUN IN THE SINGLE SHOT MODE.

TABLE XIII. BARREL LIFE OF GUNS

GUN BARREL	WEAR LIFE (RDS)	FATIGUE LIFE
M68 (105MM)	1000 RDS	1000 RDS
M185 (155MM)	7500 RDS	5000 RDS
M199 (155MM)	2600 RDS	11000 RDS
M201 (8")	3000 RDS	10000 RDS
M256 (120MM)	400 RDS	1800 RDS

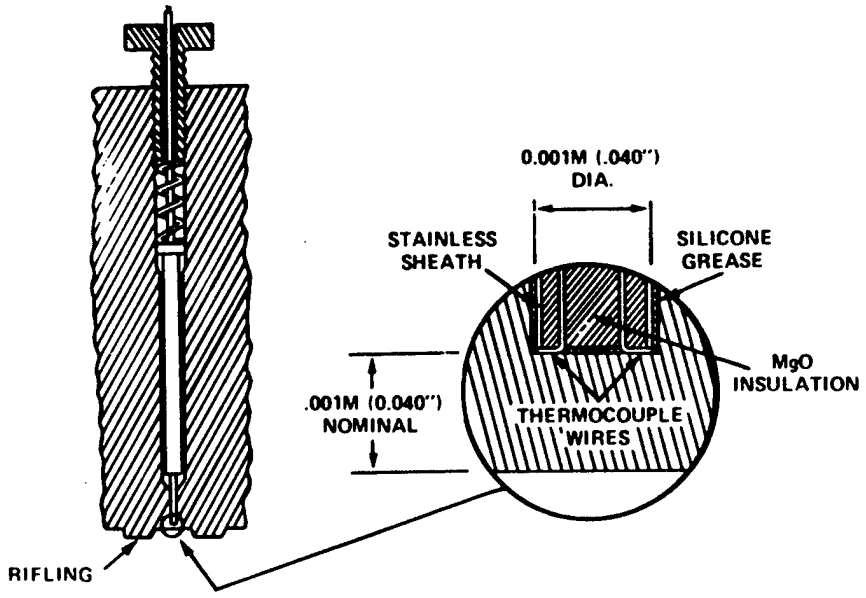

Figure 1 - Thermocouple (heat sensor) Installation in the Tube Wall

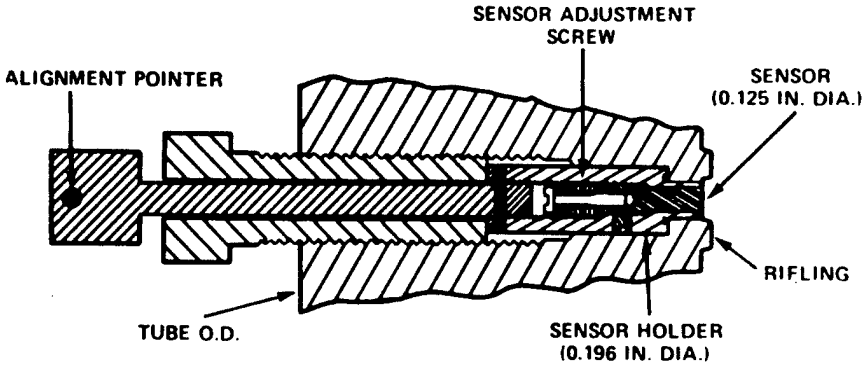

Figure 2 - Erosion Sensor Installation in the Tube Wall

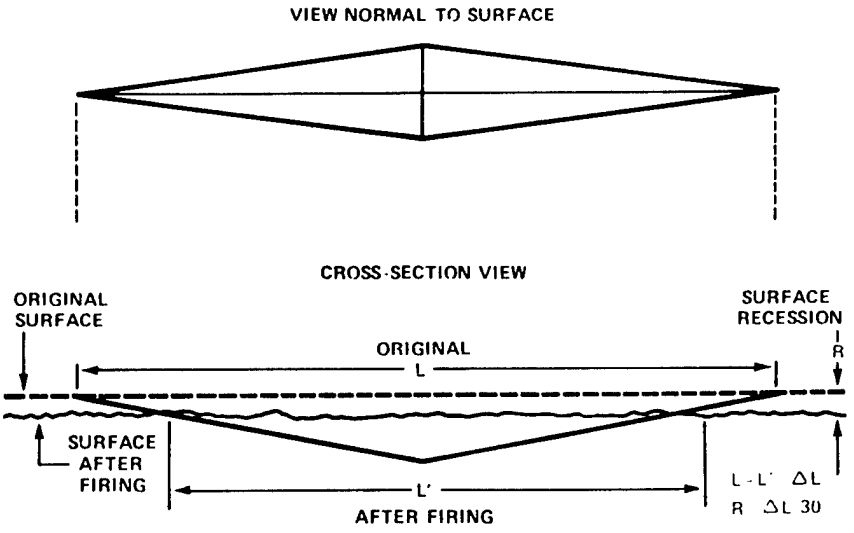

Figure 3 - Knoop microhardness indenter configuration. In practice actual length of indentation is 10-400 microns.

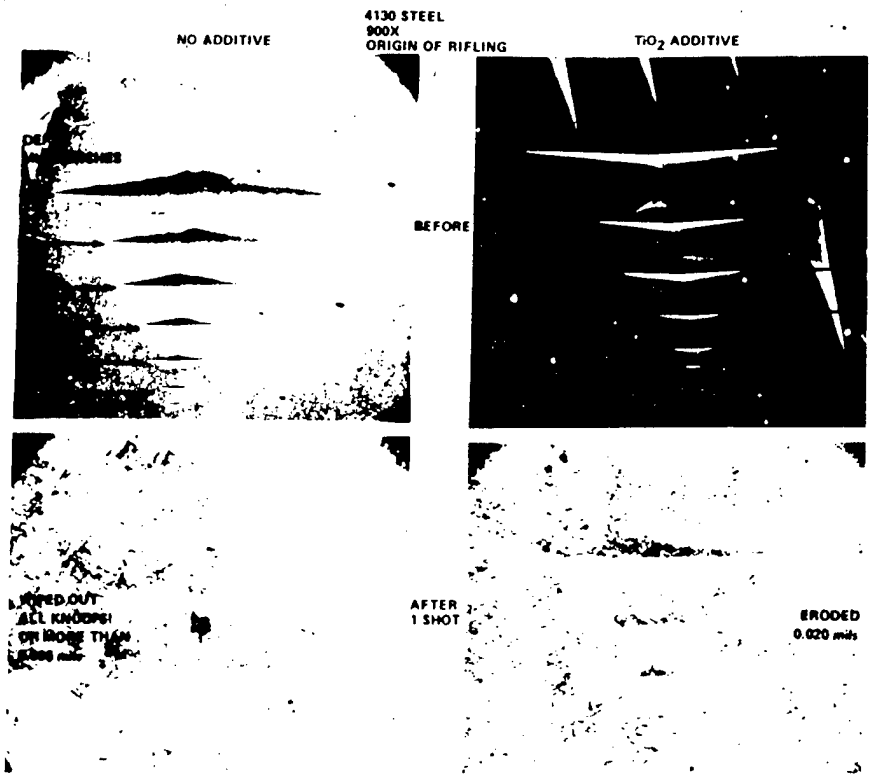

Figure 4 - Typical indentations in 8" Howitzer before and after one round; left without additive, right with additive.

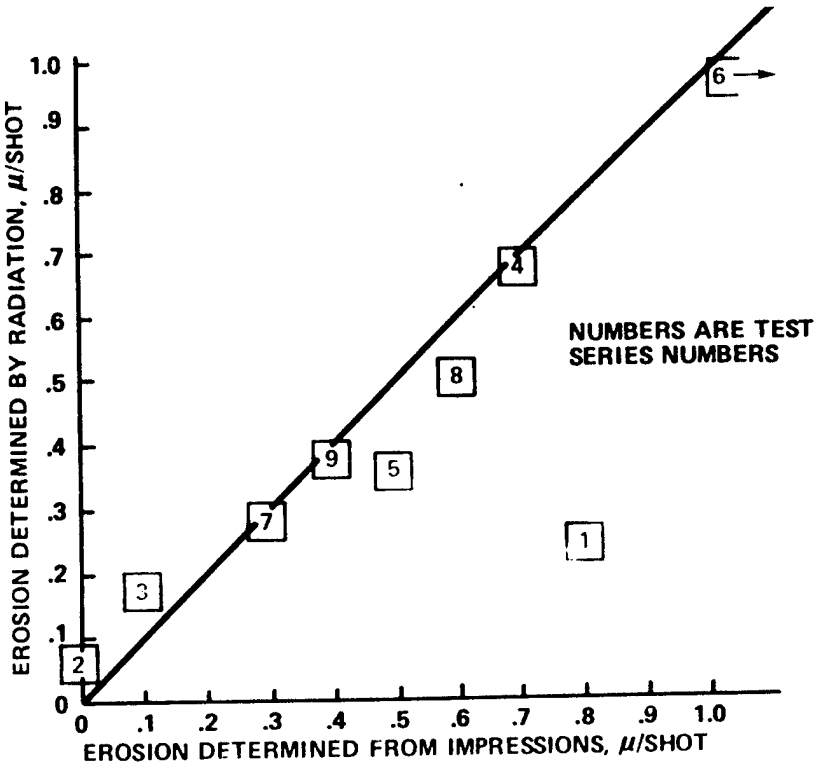

Figure 5 - Comparison of Knoop and radiation measurement on erosion sensors location 1.06M RFT.

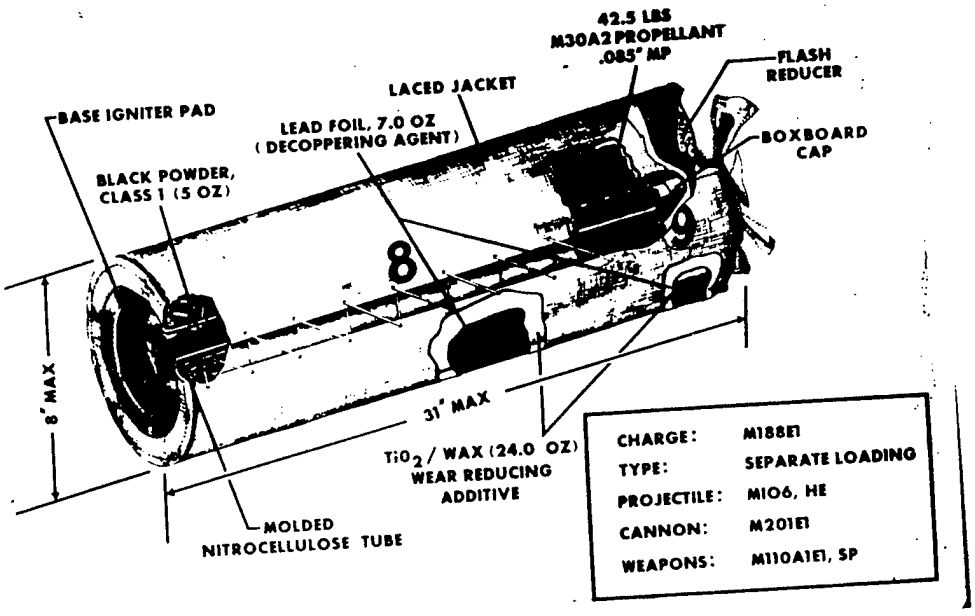

Figure 6 - 8" Propelling charge (M188E1) containing M30A2 Propellant.

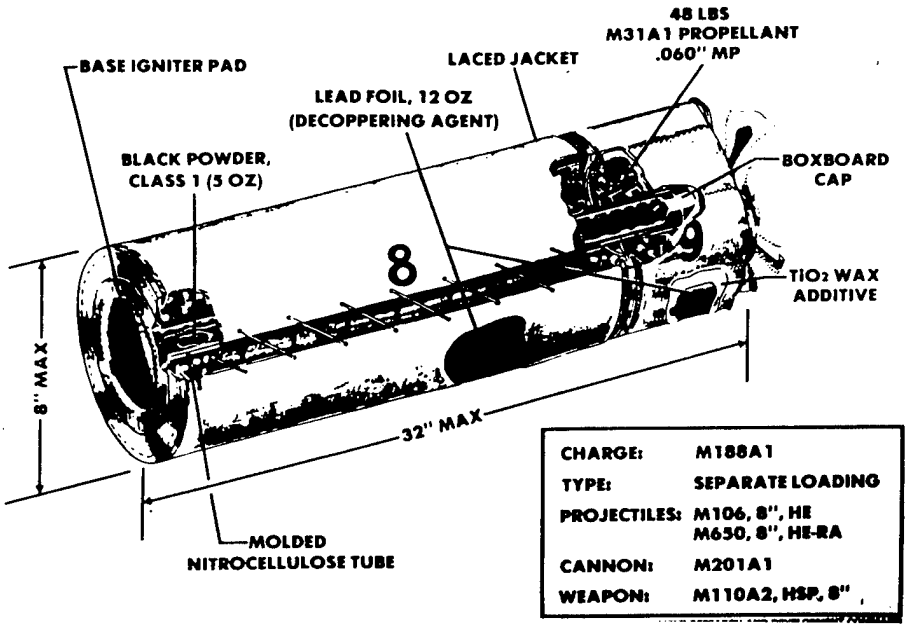

Figure 7 - New 8" propelling charge (M188A1) with M31A1 propellant. Additive is needed only in zone 9 part of charge.

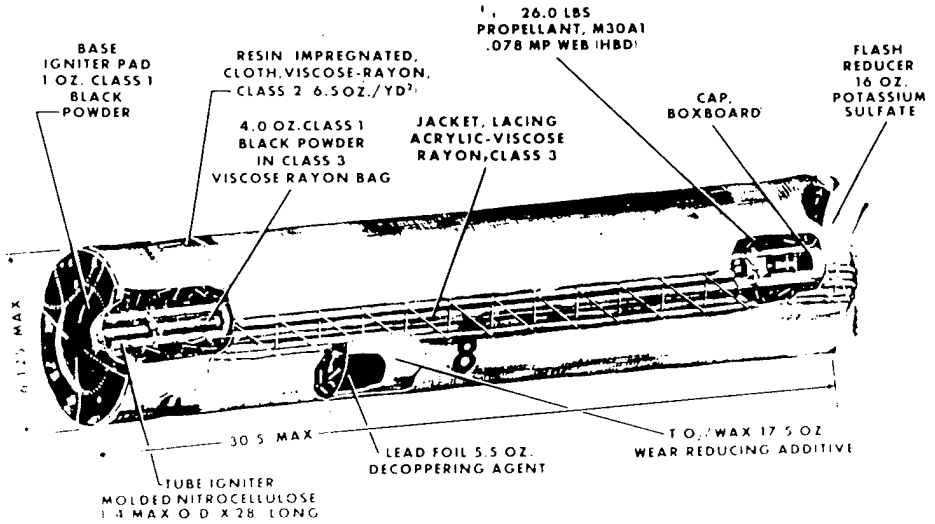

Figure 8 - Currently fielded 155mm M203 propelling charge.

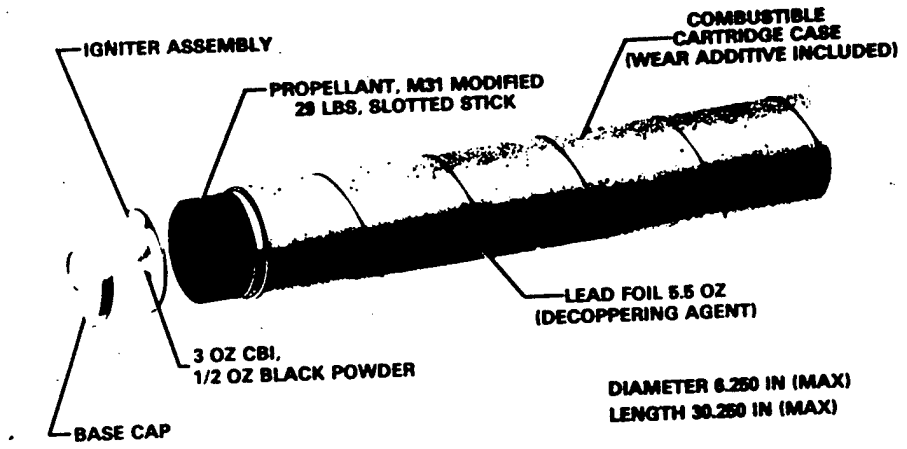

Figure 9 - New proposed M203 (zone 8) propelling charge, which will use stick propellant and combustible cartridge containing talc.

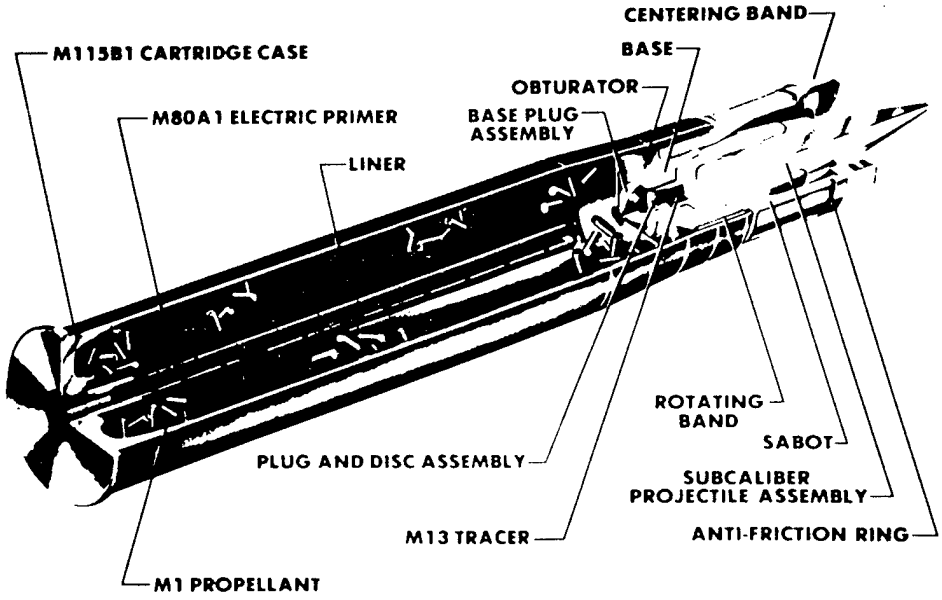

Figure 10 - Cartridge, 105mm TPDS-T, M724A1

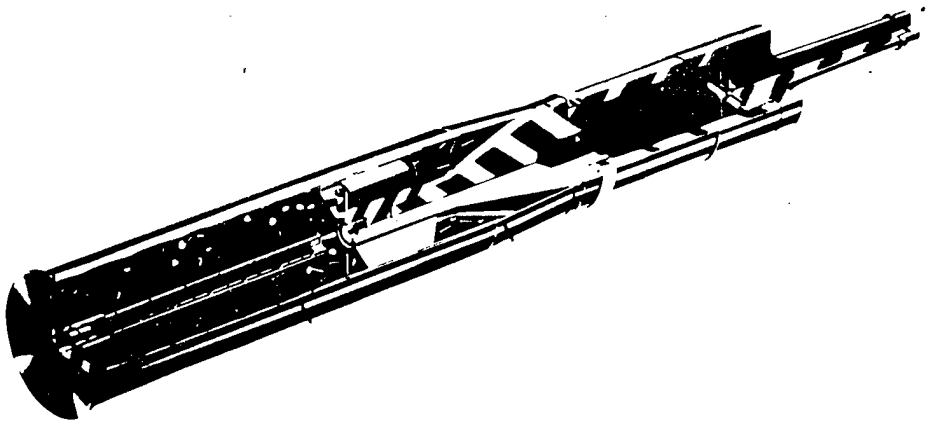

Figure 11 - Cartridge, 105mm TP-T, M490

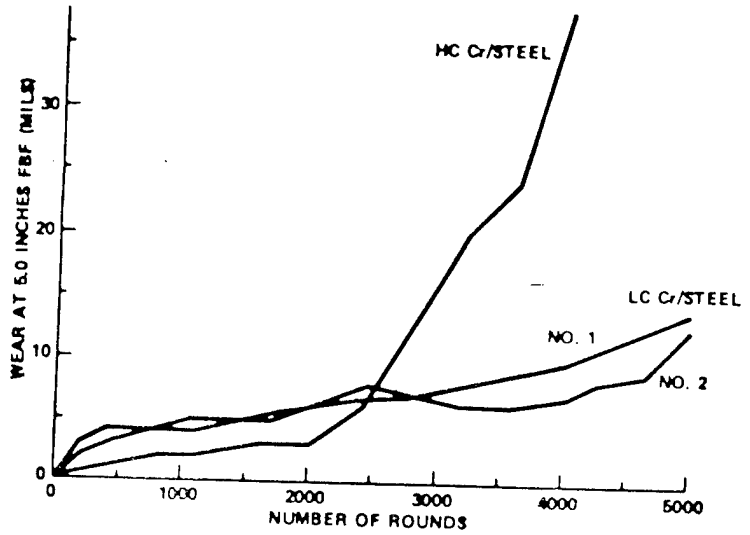

Figure 12 - Comparison of HC and LC erosion behavior (wear vs. rounds) in 20mm M24A1 firing test.

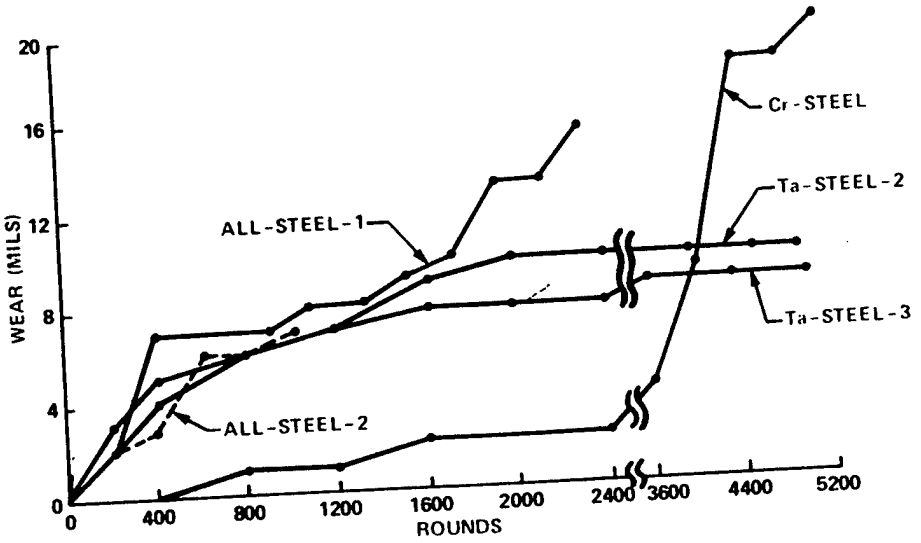

Figure 13 - Erosion behavior of HC chromium and tantalum coatings in 20mm M24A1 firing tests (wear vs. rounds)

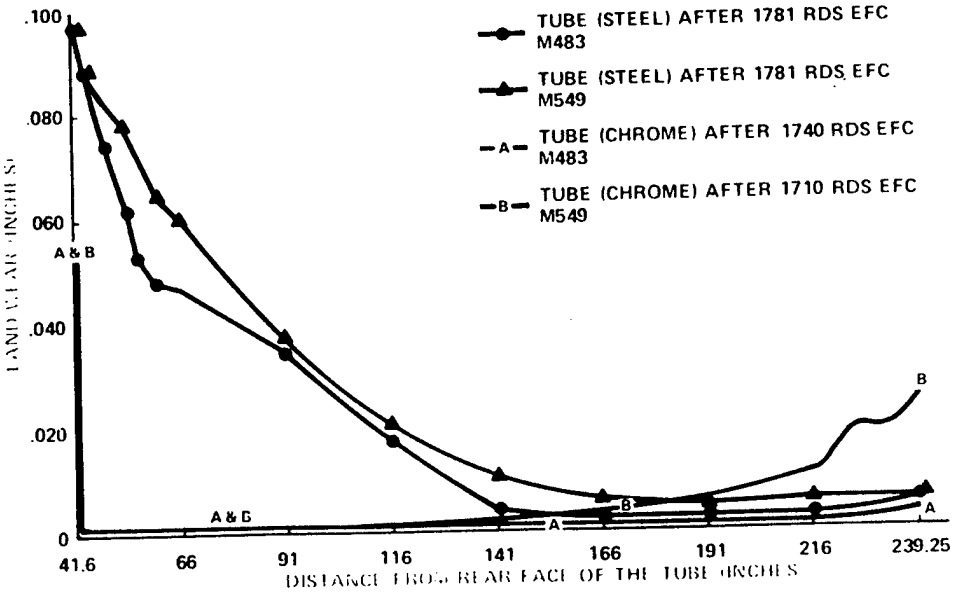

Figure 14 - Wear profiles of 155mm M199 tube. Unplated vs. chromium plated.

Figure 15 - 155mm projectiles recovered after being fired from unplated tube (after 1,500 rounds)

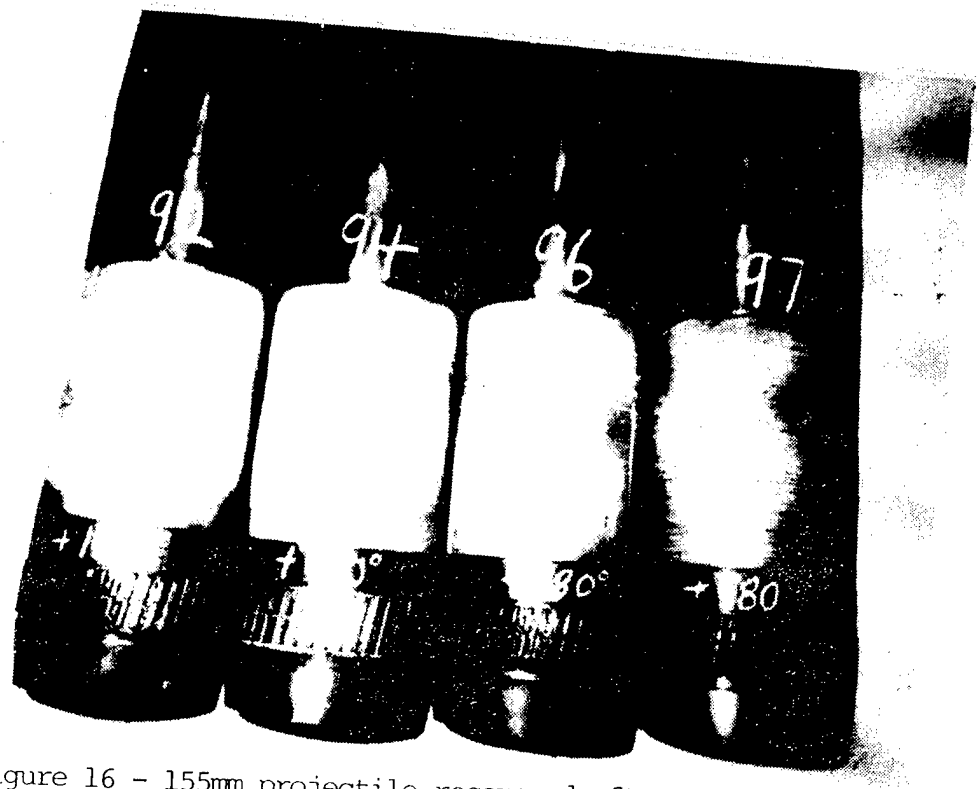

Figure 16 - 155mm projectile recovered after being fired from chrome plated tube. (after 1,500 rds) Notice wear of the rotating band.

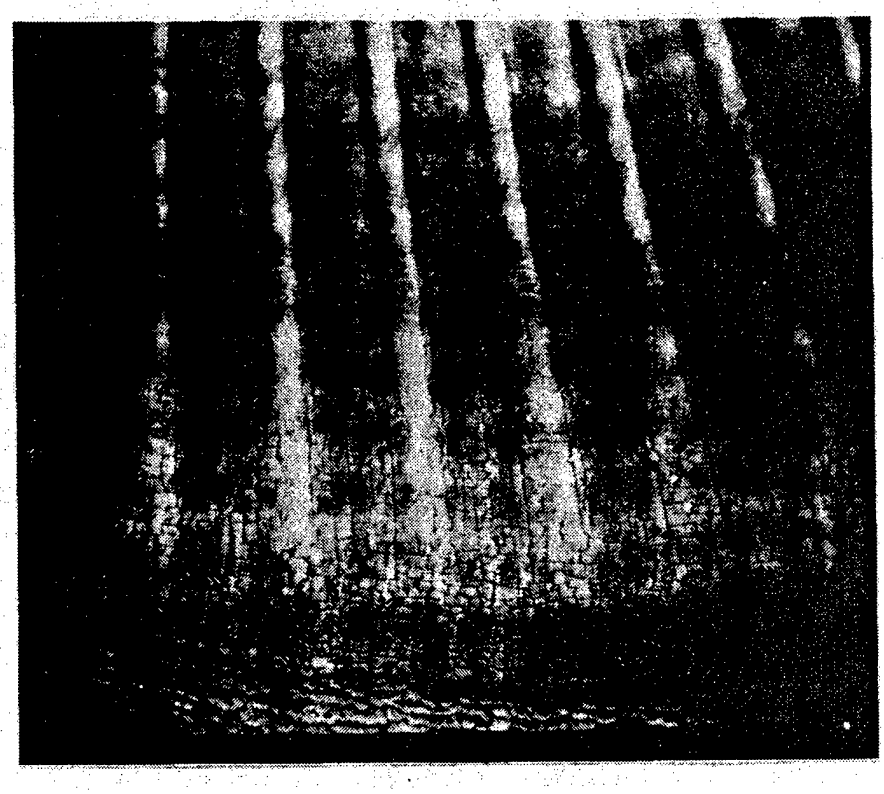

Figure 17 - Showing heat checking in an unplated 155mm M199 tube after 200 rounds.

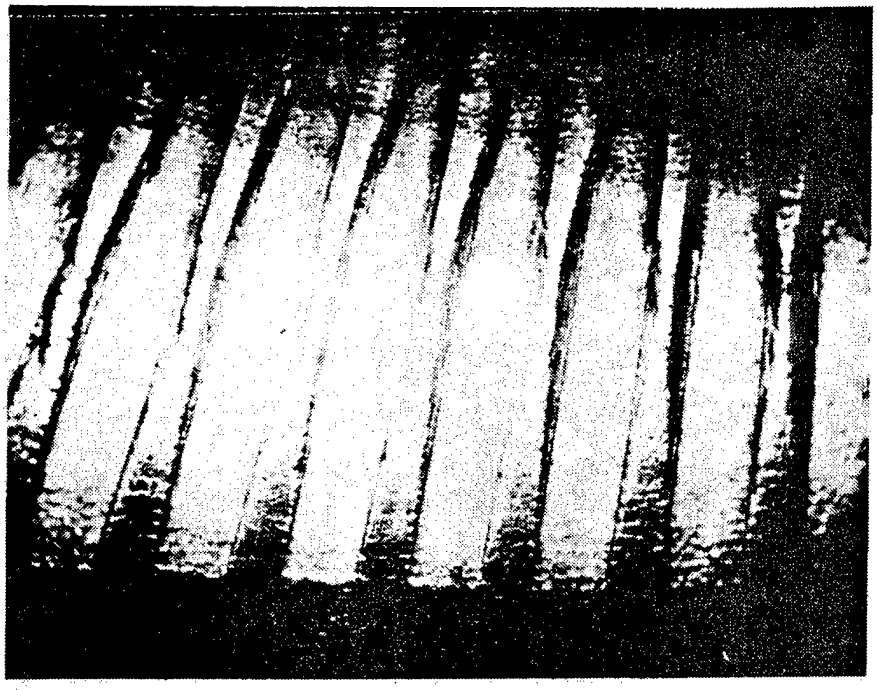

Figure 18 - Showing O.R. area of a chromium plated 155mm M199 tube after 200 rounds.

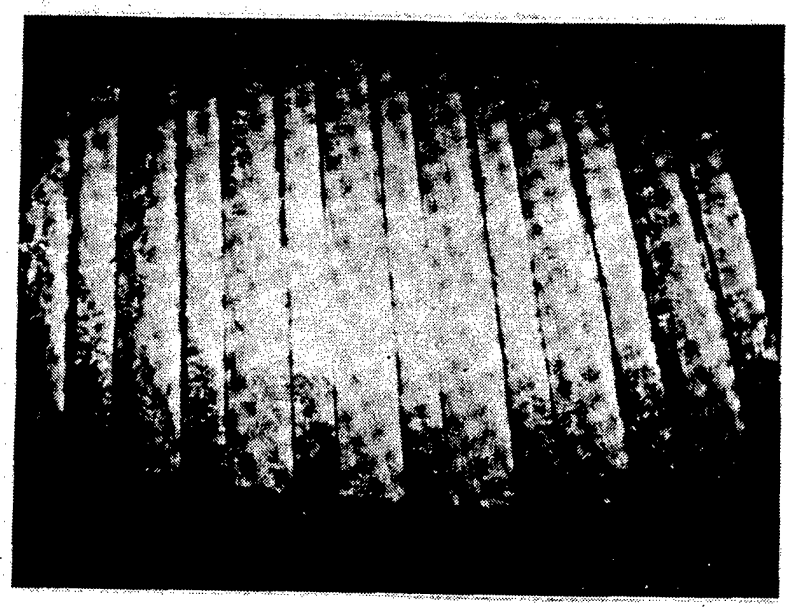

Figure 19 - Showing the O.R. area of unplated 155mm M199 tube after 1,500 rounds.

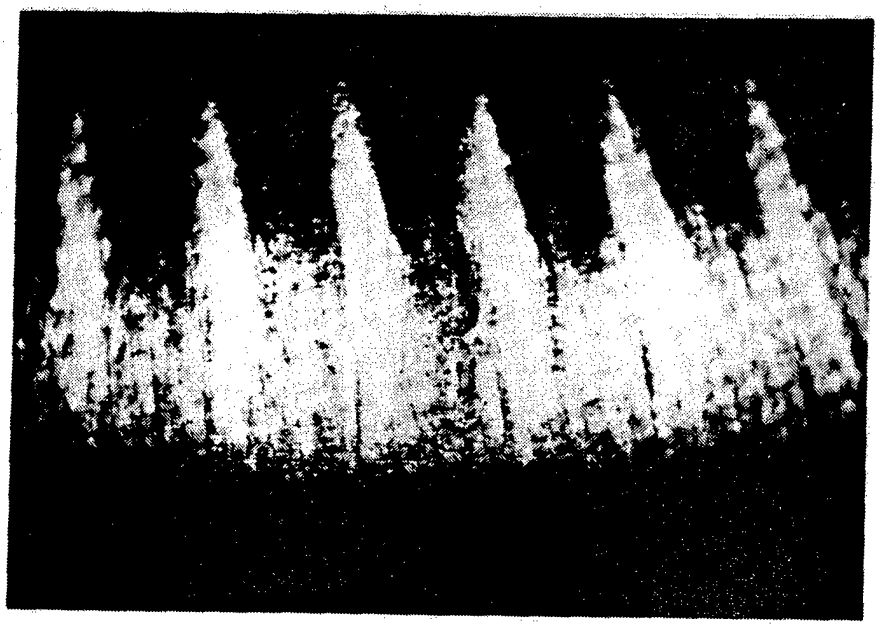

Figure 20 - Showing O.R. area of a chrome plated 155mm M199 tube after 1,500 rounds.

THE OPERATIONAL IMPACT OF NAVAL GUN EROSION

J. S. O'Brasky

Naval Surface Weapons Center
Dahlgren, Virginia

ABSTRACT

An overview is presented of the role of the gun within the Navy and of the operational impact of Naval gun erosion. A short review of the present status of naval gun tube erosion investigative activity is also provided.

CAVEAT

This paper constitutes the author's opinion concerning the subject matter discussed and cannot be construed to represent the official position of the Department of the Navy or any other government activity.

INTRODUCTION

Any attempt to assess the impact of gun erosion on naval operations must consider the following:

1. The Navy mission and warfare areas.
2. The Naval force structure.
3. The Naval gunnery roles.
4. Generic operational scenarioes.
5. Logistics.

Each of these elements generates a technical emphasis which is peculiar to the naval application.

THE NAVY MISSION AND WARFARE AREAS

The U. S. Navy's mission as established by Title X, U. S. Code. "The Navy shall be organized, trained and equipped primarily for prompt and sustained combat incident to operations at sea. The Marine Corps shall be organized, trained, and equipped to provide fleet marine forces of combined arms, together with supporting air components, for service with the fleet in the seizure or defense of advanced naval bases and for the conduct of such land operations as may be essential to the prosecution of a naval campaign." (Reference 1).

For the purposes of developing platforms and weapons, the U. S. Navy has defined warfare areas. The warfare areas which apply to the surface fleet are the following:

1. Anti-air warfare (AAW)
2. Anti-Submarine Warfare (ASW)
3. Anti-Surface Warfare (ASUW)
4. Amphibious Warfare (AMW)

As might be imagined a variety of different platforms might support each warfare area. For example, aircraft, surface ships, and submarines are all employed as sensor and weapon platforms in anti-submarine warfare. The technology and technical problems thus would be shared by all platforms. The net effect is to create within the Navy an anti-submarine warfare community with its own set of viewpoints, skills, and operating procedures. These warfare area communities have a decisive impact on selection of technical approaches and resource allocation. The newest and weakest denomination is the ASUW community. Each naval surface combatant ship has some competence in each warfare area.

THE NAVAL FORCE STRUCTURE

In Fiscal Year 1982, the U. S. Navy operated 199 surface combatant ships. (Reference 2.) These ships supported 274 immediate caliber gun mounts. The Navy is in the midst of a force structure build-up leading to a 600 ship Navy. In 1990, the planned surface combatant inventory objective is 248 ships. These 248 ships will mount 406 intermediate and major caliber guns. The details of these structures are contained in Table I with data taken from References 3 and 4. In addition, almost every naval ship will be equipped with one or more close-in weapons system (CIWS). The CIWS is a close range, last ditch air defense system optimized against cruise missiles.

The specific point of this discussion is that the Navy must execute its mission with a relatively small number of gun weapons systems. The 406 Navy medium and major caliber gun barrels stand in sharp contrast to the 3500 medium and major caliber gun barrels in active U. S. Army field artillery alone and the 10,000(+) tank guns field in the armored force.

NAVAL GUNNERY ROLES

In 1974, the Navy Department promulgated a "Gun Policy", Reference 5. This policy contained the following elements:

1. Small caliber (C) gun systems (C < 76mm) will be employed principally in an anti-air mode taking advantage of any anti-surface target capability which might be inherent in the weapon system.

2. Intermediate caliber gun systems (76mm < C < 200mm) will be employed in an anti-surface target role taking advantage of any anti-air target capability which might be inherent in the weapon system.

3. Major caliber gun systems (C > 200mm) will be employed only against surface targets.

This gun policy recognized the technical limitations of the existing naval gun systems and provided a reasonable basis for resource allocation at the time of its promulgation. As a result of this policy the naval gun was recognized as having two surface-to-surface and one air defense role:

1. Short range (R) (C < 200mm), surface strike, short ranged (R < 40 km)

2. Shore bombardment in amphibious warfare

3. Short range (R < 10 km) air defense.

Of more particular importance the naval guns were effectively disqualified from other uses both by policy and by the lack of an effective warfare area advocate. Guns as short range weapons have little utility in the long ranged plans of the Navy.

The naval gun policy did not anticipate the possibility that the major caliber naval gun could become a medium ranged (range approximately 75 km with excursions to 200 km) multi-purpose launcher for an immediate ranged combat system. The potential of solid propellant ramjet gun launch flight vehicles, autonomous seekers, and solid state gun hardened electronics is not well appreciated in the naval service. The idea that a flight vehicle could be launched from a 203mm or larger naval gun and have flight performance which exceeds that of the best area defense AAW missile presently under development seems to the naval AAW community to be a flight of shear fantasy. Even if such a capability were realizable, the development and deployment of such a system would require major changes in resource allocation. Such changes tend to disrupt the community.

Table II is a listing of the warfare areas with weapons and platforms associated with them and their approximate maximum ranges and target type. As one can see, the gun policy limits the naval gun to only a small fraction of the surface weapons functions.

Figures 1 and 2 show typical naval combatant ships. Note that there are typically four or five weapon positions on a given ship and that any surface combatant must be competent in all warfare areas. The net result of this philosophy is that only one or two weapon positions on a given ship are available for any single warfare area. This is the major limiting factor in naval gun system employment under the Naval Gun Policy as they are not considered multipurpose players.

GENERIC OPERATIONAL SCENARIOES

The following scenarioes were created by this writer for the purpose of illustrating typical naval gun uses. These scenarioes have no standing within the Navy.

Anti-Air Warfare - Point Defense. The principal threat in this scenario is a M = 0.9 to M = 2.5 cruise missile which may have leaked through the outer air defense and area air defense system or which was not detected for a variety of reasons. Thus, one or more threat missiles appear at a range of about 12 nm and must be engaged. The gun systems having capability against such a threat are the 20mm MK 16 CIWS, the 76mm MK 75, and the 5"/54 MK 45. For purposes of estimating the significance of the gun tube erosion issue in this scenario, a Mach 0.8 target was selected to maximize the ammunition expenditure. The 5"/54 system is assumed to fire guided projectiles. Table 3 gives the probable first shot engagement range, the maximum number of shots per engagement, and the amount of ammunition expended per 1000 engagements. This last number provides a reasonable estimate of the life-time naval ammunition expenditure in this scenario. As one can see, the average number of rounds expended per weapon in wartime is quite small. One must conclude that the AAW point defense application is not a gun tube erosion driver. The only exception to this rule is that a badly worn gun (generated on other duty) might reduce the reliability of a guided projectile.

Anti-Surface Warfare. In this scenario a threat surface ship or boat appears at a relatively close (less than 15nm) range probably against a friendly background. The objective of this action is to get a firepower or mobility kill against such a target quickly. If the target is a boat, sinking may be a reasonable objective. If the target is a destroyer sized or larger ship, sinking by gunfire is not economical. The weapon of choice is a guided projectile if such is available or conventional HE projectiles if guided munitions are not available. The applicable naval gun mounts are the 5"/54 MK 45 and the 76mm MK 75. Table III contains an estimate of the number of rounds required in each engagement, the number of rounds per 1000 engagements and 5000 engagements. Note that in the entire history of the U. S. Navy there probably have been less than 5000 surface-ship-to-surface-ship engagements. Again we see that this scenario is not a gun tube erosion driver.

Amphibious Warfare. Amphibious operations are recognized as the single most complicated and challenging type of military endeavor. Such operations involve crossing air-land and sea-land interfaces simultaneously and the rapid establishment and build-up of combat power ashore from a zero baseline. If an amphibious assault must be conducted in the face of a strong, skilled, and alert enemy, only overwhelming and responsive fire support makes such an assault feasible. As will be seen, the support of an amphibious assault is the single most intensive application of naval gun systems.

The classic World War II amphibious assaults were either conducted against enemy forces which occupied the target area in strength or were so lacking in mobility as to preclude rapid concentration agains the lodgement. Examples of such situations are Iwo Jima; an eight square mile island with 26,000 defenders, and the Normandy Invasion in which a German Army with a horse drawn and rail based logistic system was subjected to overwhelming air interdiction and a carefully coordinated sabotage campaign. In the classic situation, the prerequisites for successfull assault were the existence of enough fire support to destroy or neutralize the enemy force in the target area and to interdict enemy reinforcemtnts slowly approaching the lodgement. Under these circumstances, the assaults were always successful and sea based logistics could always win the battle of the build-up.

The present situation is somewhat different. In much of the world today, land forces consist of armored and mechanized combat units supported by motorized logistics systems with extensive engineer support. These forces are covered by air defense systems down to the platoon level. In the last decade, eight nations have employed multi-divisional forces of this description, sometimes with great skill. None of these nations are superpowers. For the purposes of this discussion, a Soviet model combined arms army can be taken as the threat (a western model would be equally appropriate, but not so well known). This force consists of a tank division and three motorized rifle divisions. Figure 3 shows a deployment. Figure 4 shows the time required for this force to close the lodgement. Note that if a mechanized opponent is not interdicted, large forces can be concentrated in 24 to 48 hours. This situation is a massive departure from World War II amphibious assault models. Today, the "standard scheme" of defense against amphibious assault is to keep the coast-line under observation, defend only ports and airfields, and concentrate mechanized, air assault, and armored units against the lodgement before it can be consolidated. In addition, the amphibious assault force must be denied air superiority. The purpose of the Naval Fire Support System is to

defeat this response.

The Naval Fire Support System performs five functions in amphibious assault operations:

1. Beach Preparation
2. Direct Support of Maneuver Elements
3. General Support of the Landing Force
4. Air Defense Suppression
5. Interdiction

Table V identifies the capabilities of the components of the Naval Fire Support System. The naval gun supports the first three functions due to its all-weather-day-night capability and its responsiveness. Unfortunately, naval gun systems do not have sufficient range to support the air defense suppression and interdiction functions in more than the most marginal sense. Figure 5 is a typical Soviet air defense system envelope taken from Reference f. Note that no capability exists or is presently programmed which would allow the Naval Surface Fire Support System to deal with moving targets and mobile air defenses located more than 20 km inland. On the other hand, a superb capability will exist to deal with fixed targets which have been in place at least 24 hours at very long ranges.

A Marine Amphibious Force (MAF) consists of a Marine Division and a Marine Air Wing. This organization is a Corps command and is the largest force for which assault amphibious lift exists in peace time. Figure 6 gives a profile of the fire support available to an MAF level amphibious assault for X-1 to X+10 days. Note that the unit of measure is the Artillery Battery Equivalent (ABE). This device is an invention of this writer for use in discussions such as this. The ABE is defined as a unit of fire power equivalent to an eight gun 155mm Howitzer Battery operating at the assault rate of 220 rounds per gun per day. Fifteen (15%) of the munitions are assumed to be guided. Table VI is an estimate of the naval fire support assets available to an MAF amphibious assault. As can be seen, an amphibious operation of this size would tie up about 25% of the naval surface and air forces. The amount of ammunition required to support an MAF amphibious assault through X+10 days is given in Table VII. In a war in which the amphibious option is unconstrained a maximum of two Marine Amphibious Forces and two Marine Amphibious Brigade assaults could be expected in a year. Note that in supporting an MAF landing 8 5"/54 and 7 16"/50 gun barrels would be worn out. As can be seen the Amphibious Warfare Area is a gun erosion driver. Figure 7 illustrates the situation in a MAF amphibious operation at X-Day. Figure 8 represents X+3. Note that once the Marine Artillery becomes firmly established ashore, the naval gunnery component serves principally to extend the flanks. The defense of the lodgement from this point becomes a case of massed firepower and mobile defense. Note that even in the case of lodgement shown in Figure 9, most of the area is subject to three or more battalion massing. Incidently, a lodgement this size is required if the beach support area is to be free of enemy divisional level artillery fire, an absolute necessity to win the battle of the build-up.

LOGISTICS

Naval forces are largely self contained. Ammunition transfer at sea is a routine procedure. Regunning of 5" to 8" gun mounts must be performed along side a pier or tender in sheltered waters. Regunning a 16"/50 turret requires the services of a Navy yard with the ability to lift 125 tons at a radius of 100 to 150 feet. Figure 10 shows the major U. S. Naval bases. Ships can economically sail 500 miles per day. Table VIII shows the effects of gun tube life on ship availability time for a calendar year for 3, 5, and 7 day transit times. As can be seen, long life naval gun barrels are a must.

SUMMARY

The naval gun exists in a relatively small niche in the overall naval picture largely due to the Naval Gun Policy and the lack of investment resulting therefrom. Naval gun systems are highly automated but used intermittently. The Naval force structure is small by Army standards and operates far from bases. For all these reasons a long gun barrel life is vital for naval gun systems.

SUMMARY OF NAVAL GUN EROSION EFFORTS

No naval gun erosion research program has existed since 1956. All of the results reported in the 1977 Tri-Service Symposium (Reference 7) were the products of development and malfunction investigations undertaken between 1968 and 1974. There has been no active Navy gun development program since 1977 although several have been proposed. Present naval gun barrel lives are operationally satisfactory with the exception of that of the 76mm MK 75 gun mount. The technology exists to solve this problem. Indeed, technology exists to make the next step in performance level should that ever be required.

TABLE I

U. S. NAVY SURFACE COMBATANT GUN POPULATION

GUN BARREL	1982	1990	2000
16"/50 MK 7	0	36	36
5"/54 MK 19	82	138	211
5"/54 MK 18	150	112	46
5"/38 MK 12	6	54	54
76mm MK 34	36	66	66
Total	274	406	413

TABLE II
NAVAL WARFARE AREAS AND PLATFORMS

WARFARE AREA	MISSION	TARGET	PLATFORMS	MAX RANGE (KM)	WEAPONS
Anti-Air Warfare	Point Defense (PD)	Cruise Missile	Ships	10	GUNS, Surface-to-Air Missile (SAMs)
	Area Defense	Cruise Missiles Aircraft	Ships	200	SAMs
	Outer Air Defense	Cruise Missiles Aircraft	Aircraft	600	Air-Intercept Missile System (AIMS), Aircraft, Guns
Anti-Submarine Warfare	Kill	Submarines	Submarines Ships Aircraft	20 16 4000	Homing Torpedoes
Anti-Surface Ship Warfare	Strike	Surface Ships	Submarines Ships	90-600 90-600	Cruise Missiles
			Aircraft	600-4000	Cruise Missiles, Tactical Missiles, Bombs
	Short Range Strike	Surface Ships	Submarines Ships	20 30	Homing Torpedoes
Amphibious Warfare	Beach Preparation Direct Support General Support	Vehicles Field Fortifi-cations	Ships Aircraft	40 km 100 km	Major & Med. Caliber Guns Tactical missiles, Bombs
	Air Defense Suppression Intradiction	Vehicles, SAMs	Aircraft Ships	300 km	Cruise Missiles Tactical Missiles Anti-Radiation Missiles (ARMs), Bombs

TABLE III

AAW POINT DEFENSE SCENARIO

CALIBER	MAXIMUM ENGAGEMENT RANGE	NO. SHOTS/ ENGAGEMENT	NO. SHOTS/ 1000 ENGAGEMENTS	10 ENGAGEMENTS NO. SHOTS/ WEAPON
20mm	4 km	300	300,000	Approx 3000
76mm	7 km	40	40,000	Approx. 400
5"/54 GP	10 km	5	5,000	Approx. 50
5"/54 Conv.	10 km	15	15,000	Approx. 150

TABLE IV

ANTI-SURFACE SHIP SCENARIO

CALIBER	MAXIMUM ENGAGEMENT RANGE	NO. SHOTS/ ENGAGEMENT	NO. SHOTS/ 1000 ENGAGEMENTS	10 ENGAGEMENTS NO. SHOTS/ WEAPON
76mm	16 km	160	160,000	1600
5"/54 GP	28 km	10	10,000	100
5"/54 Conv.	28 km	100	100,000	1000

TABLE V

NAVAL FIRE SUPPORT SYSTEM COMPONENTS

PLATFORM	WEAPON	MISSION	MAX RANGE (KM)	TARGET
Ship	5"/54 Gun	Beach Preparation	19*	Troops, light material
		Direct Support	18*	Vehicles, field fortifications
		General Support	19*	
	16"/50 Gun	Beach Preparation	25**	Large structures, Bridges
		Interdiction	25**	
	Tomahawk (TLAM)	Interdiction	1000	Fixed targets, bridges, airfields, etc.
Aircraft A6, A7, F18	Std. ARM	Air Defense Suppression	60	Radar emitters and SAMs
	Tomahawk (TLAM)	Interdiction	1000	Fixed Targets
	Bombs	Interdiction	2	Moving Targets
	Tactical Missiles	Interdiction	5	
	Guns	Interdiction	1	

*10 km - Hydrographic Standoff.

**15 km - Hydrographic Standoff.

TABLE VI

TYPICAL MAF AMPHIBIOUS ASSAULT FIRE SUPPORT ASSETS (1990)

NAVAL SOURCES ONLY

SHIP PLATFORMS	NO.	TLAM	16"/50	5"/54	5"/38	ABE
BB-61	2	64	18	-	24	7.86
DD-963/993	15	-	-	30	-	3.47
FF-1052	15	-	-	15	-	2.52
					Subtotal	13.85

AIRCRAFT	NO.	SORTIE/DAY	ABE		
A-6	36	3	4.91		
F-18	72	4	9.82		
AV/10B	48	6	9.82		
				Subtotal	24.55
				Total	38.4

TLAM = Tomahawk Land Attack Missile
ABE = Artillery Battery Equivalent

TABLE VII

NAVAL GUN AMMUNITION EXPENDATURES

NOTIONAL 1990 MAF AMPHIBIOUS ASSAULT (X-1 TO X+10 DAYS)

	CONVENTIONAL	GUIDED
16"/50	4,900	2,000
5"/54	34,500	4,250
5"/38	3,000	-

TABLE VIII

EFFECTS OF 5"/54 GUN TUBE LIFE ON SHIP AVAILABILITY

BARREL LIFE	TIME ON LINE (DAYS)	TIME REARMING (DAYS)	TIME IN TRANSIT	FRACTION AVAILABLE IN AOA	DAYS IN TRANSIT
1500	130.3	52.1	182.6	0.50	3
3000	173.8	69.5	121.7	0.67	
6000	202.7	91.3	71.0	0.81	
1500	101.4	40.6	223.0	0.39	5
3000	146.0	58.4	160.6	0.56	
6000	182.5	82.1	100.4	0.73	
1500	83.0	33.2	248.8	0.32	7
3000	125.8	50.3	188.9	0.48	
6000	165.9	74.7	124.4	0.66	

Note: Assumes - 300 rounds/gun-day
1 day rearm
365 day year

REFERENCES

1. Title 10 "Armed Forces" United States Code, Annotated
   Section 5012 (West Publishing Company, St. Paul, MN, 1959 with 1982 packet)
   Section 5013

2. Brent Baker, "Counting the 600-Ship Navy", Proceedings, (U. S. Naval Institute - Annapolic, Md.) May 1982, Vol. 108/5/951, pg 208

3. Normal Polmar, "The U. S. Navy: A New Destroyer Class", Proceedings, (U. S. Naval Institute - Annapolic, Md.), Aug 1982, Vol. 108/8/954, pg 122

4. Armament of Naval Vessels of the United States, (Naval Sea Systems Command, Washington, D. C.), 1 Jan 1982

5. Naval Gun Concept, CNO Message R202039Z, Feb 1975

6. Deitchman, Seymour J., "The Future of Tactical Air Power in Land Warfare", Astronautics and Aeronautics, July/August 1980, Vol 18, No. 7, 8, pg 37, F-2. Note: Originally derived from Mar/Apr 1976, Electronic Warfare, pg 66.

7. Proceedings of the Tri-Service Gun Tube Wear and Erosion Symposium - 29-31 March 1977

Figure 1

TICONDEROGA CG 47 (ex-DDG 47) 566 FT. o.a.
FROM: FRIEDMAN "US DESTROYERS" pg 323

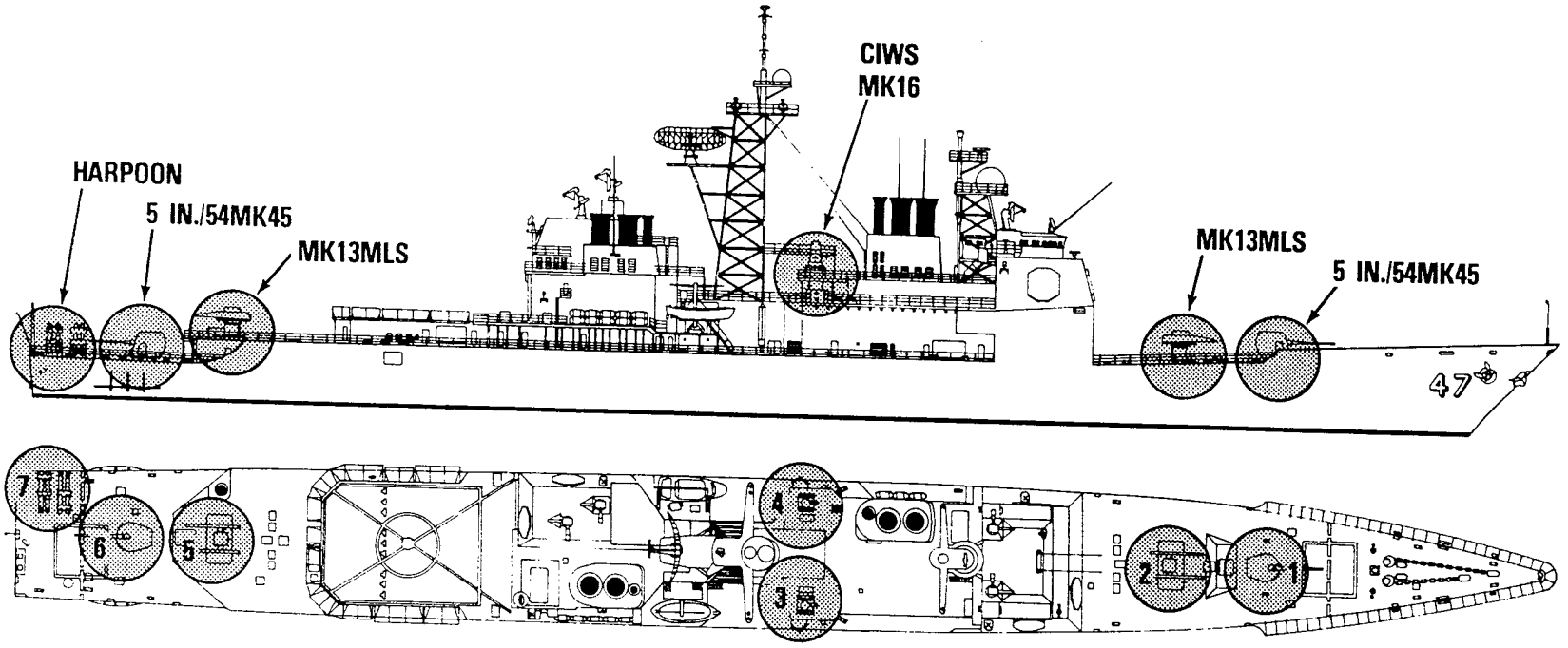

I-42

FIGURE 2

FF 1052 FRIGATE
FROM: FRIEDMAN "US DESTROYERS" pg 359

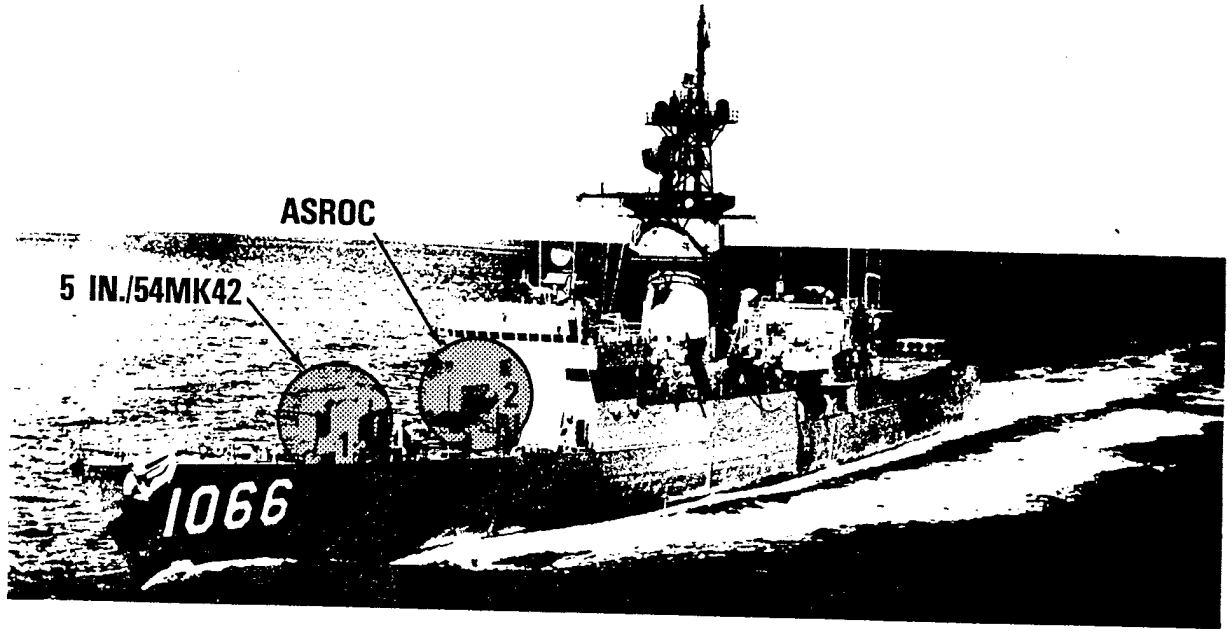

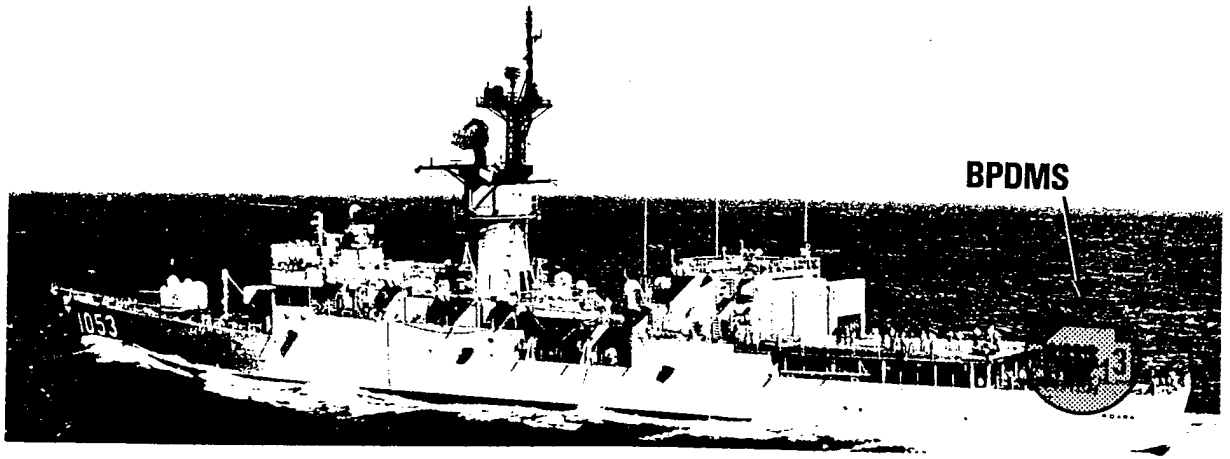

FIGURE 3

NOTIONAL ANTI-AMPHIB DEPLOYMENT

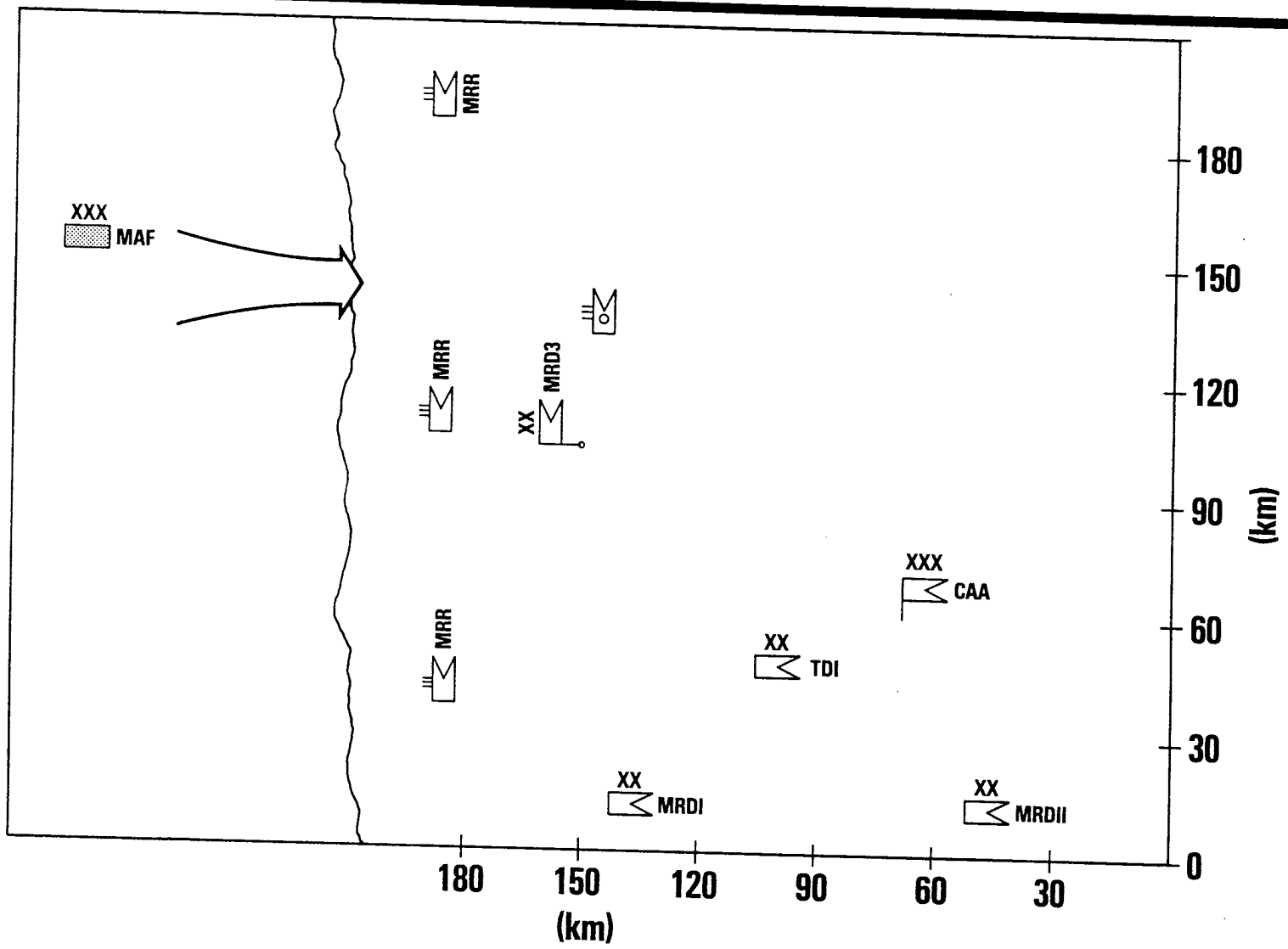

FIGURE 4

TARGET BUILDUP RATE

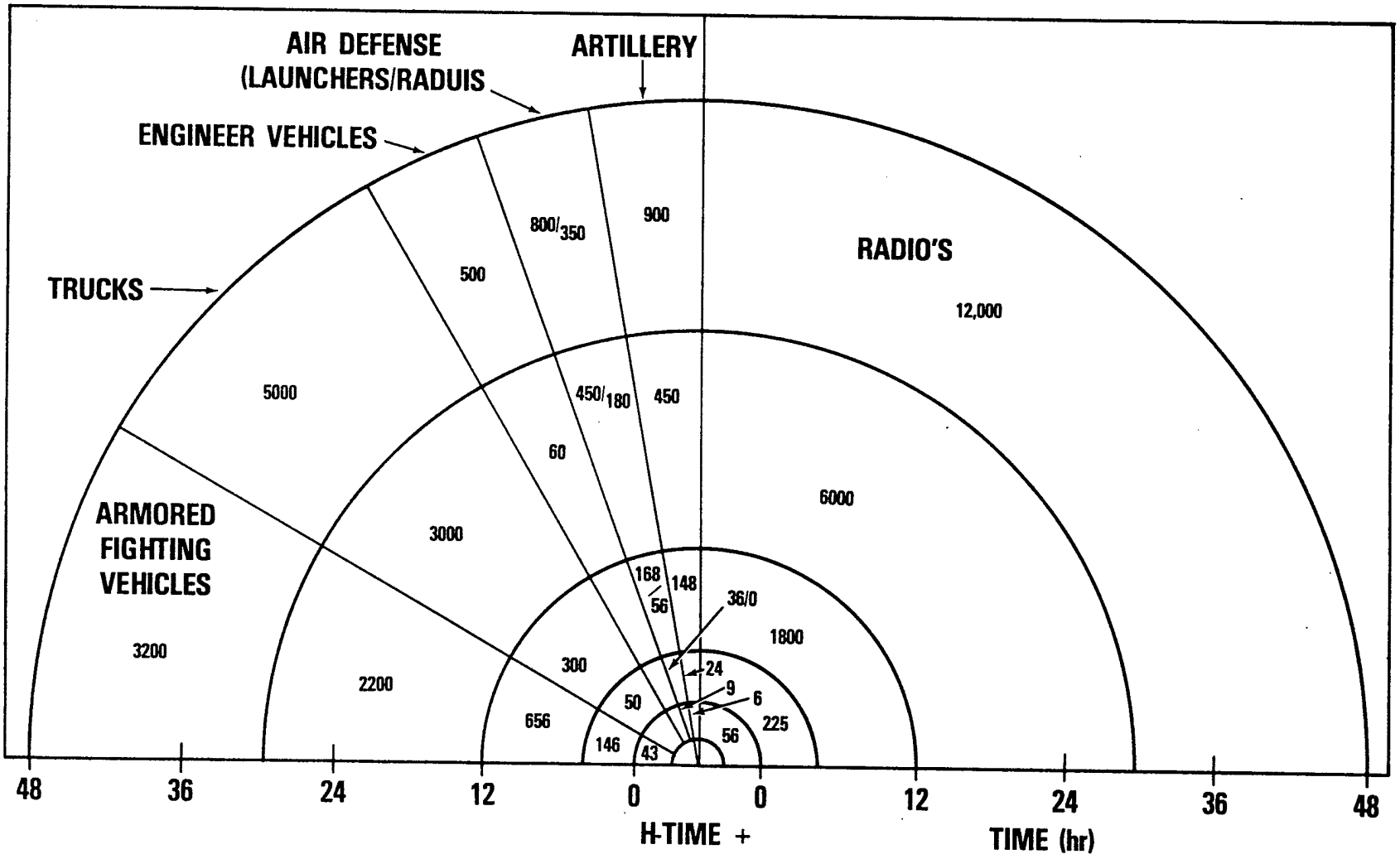

FIGURE 5

COMPARATIVE SAM ENVELOPES

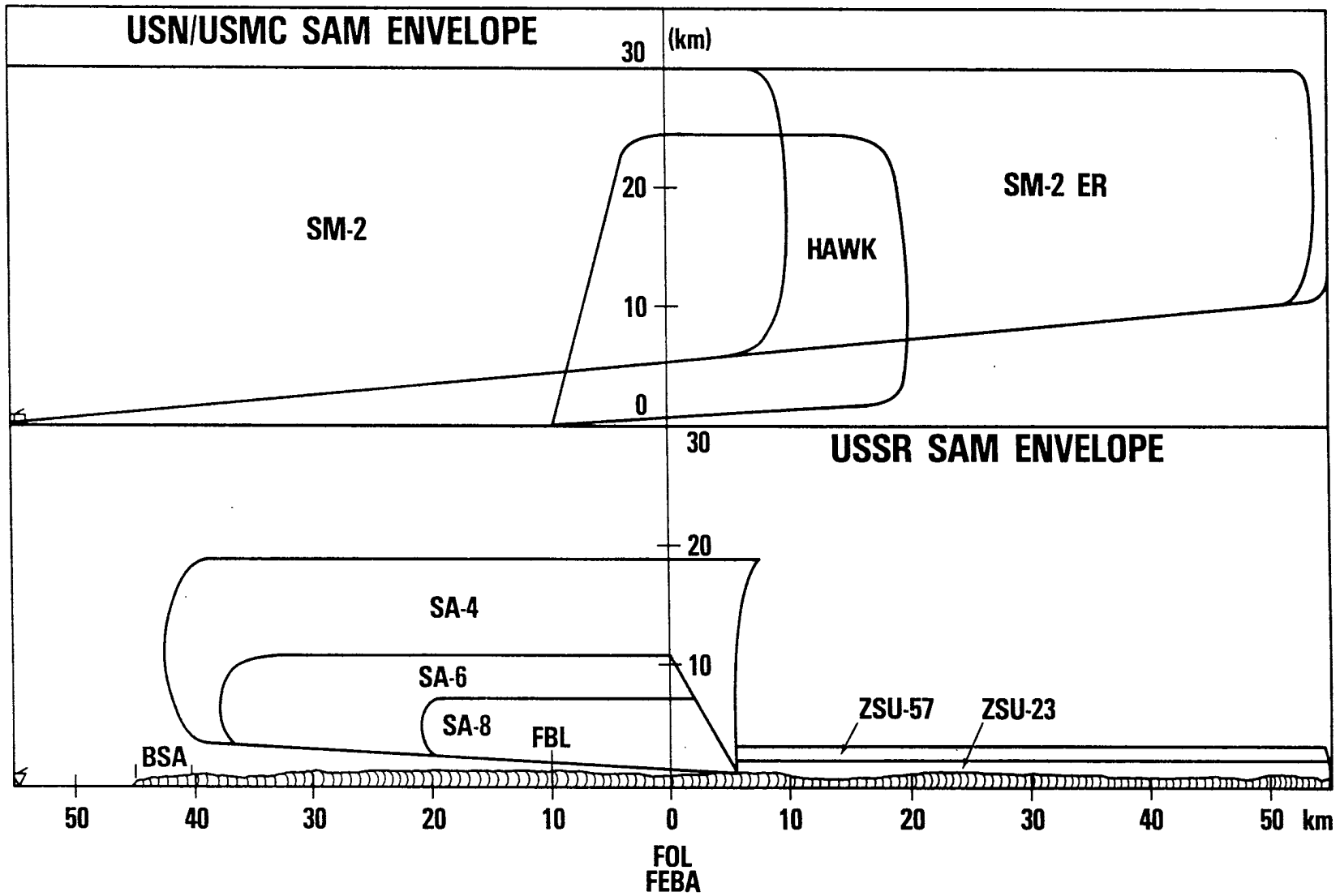

FIGURE 4

TARGET BUILDUP RATE

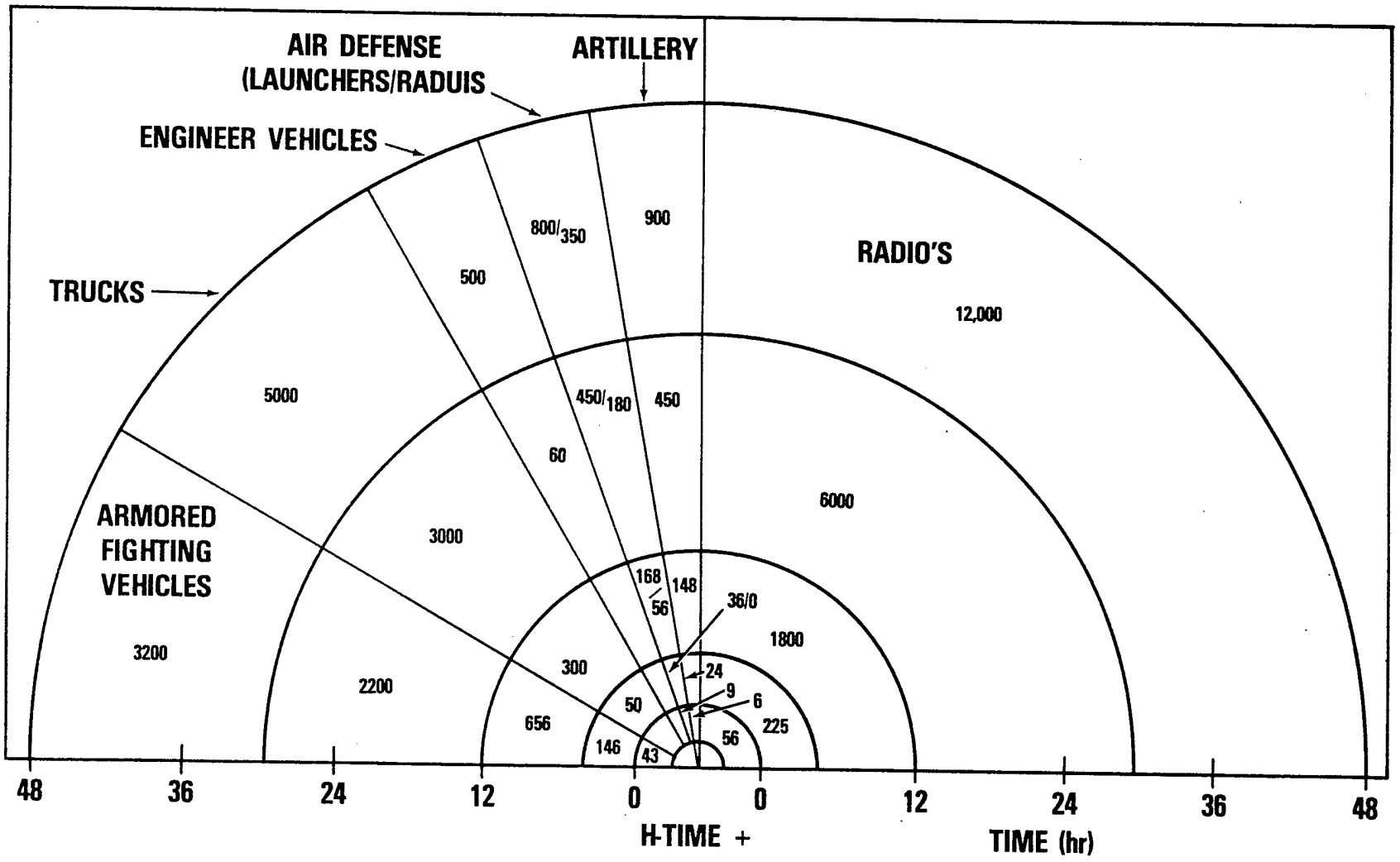

FIGURE 5

COMPARATIVE SAM ENVELOPES

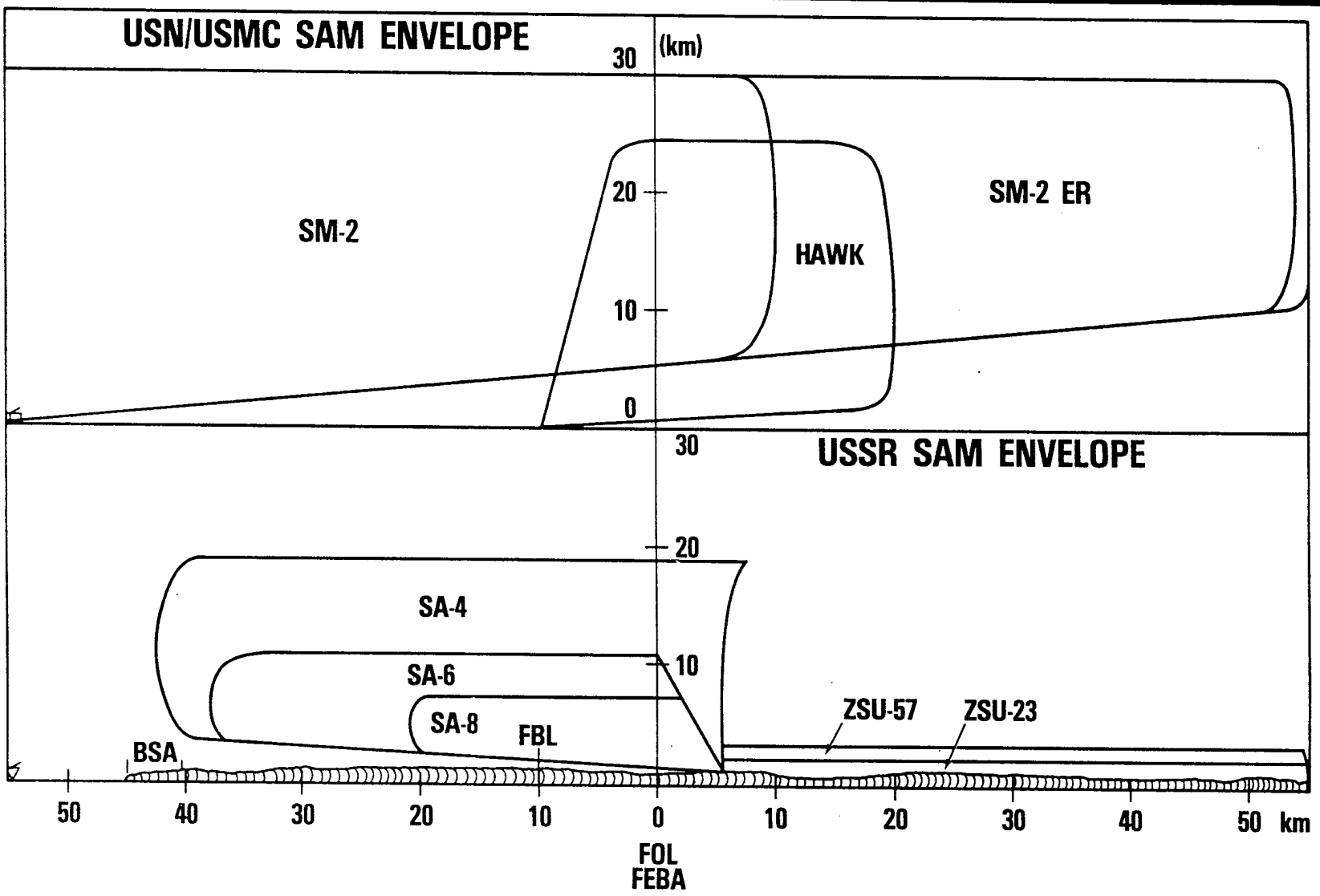

FIGURE 6

FIRE SUPPORT ASSETS—MARINE AMPHIBIOUS FORCE ASSAULT LANDING

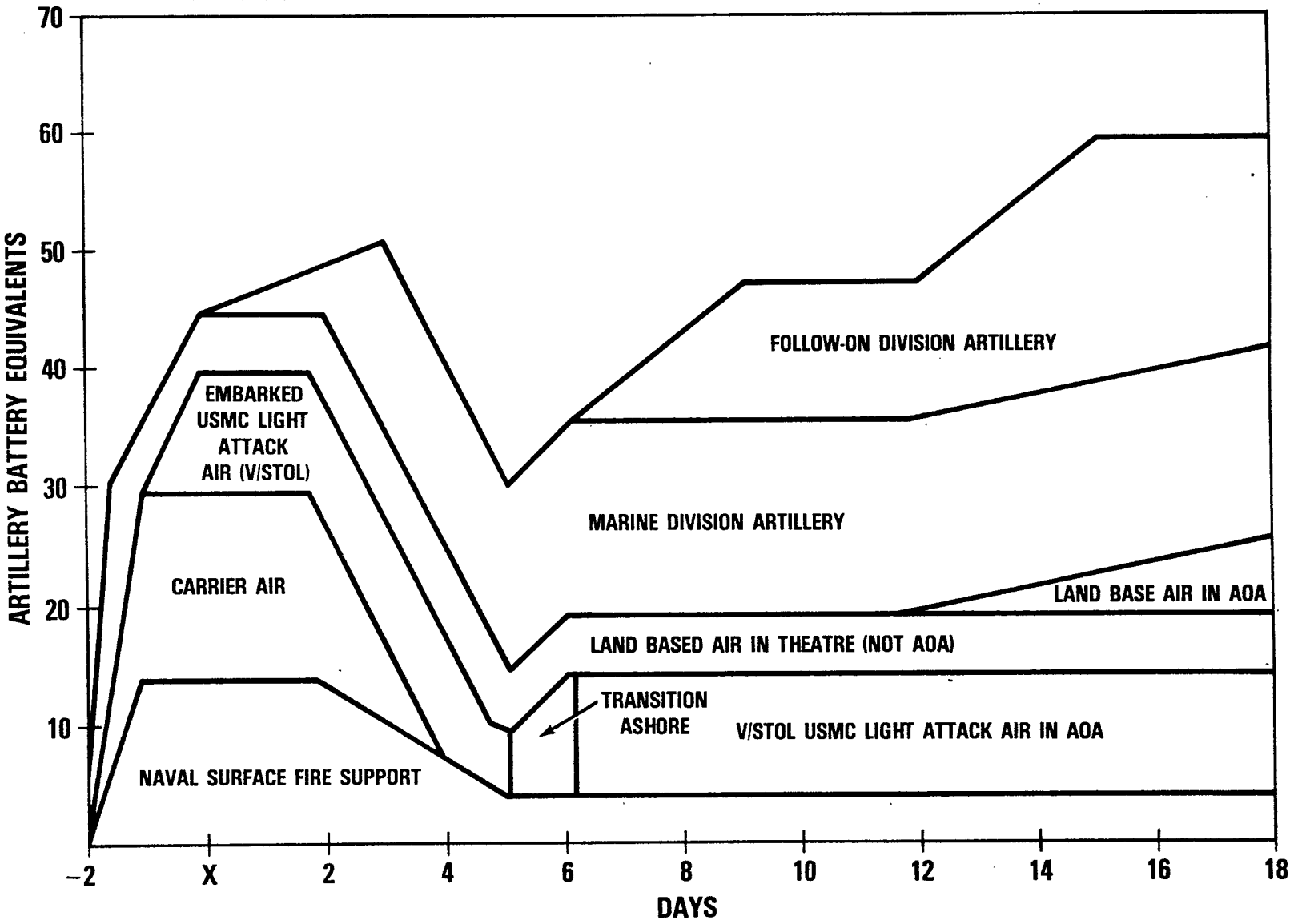

FIGURE 7

MAF LANDING SITUATION
END OF X DAY

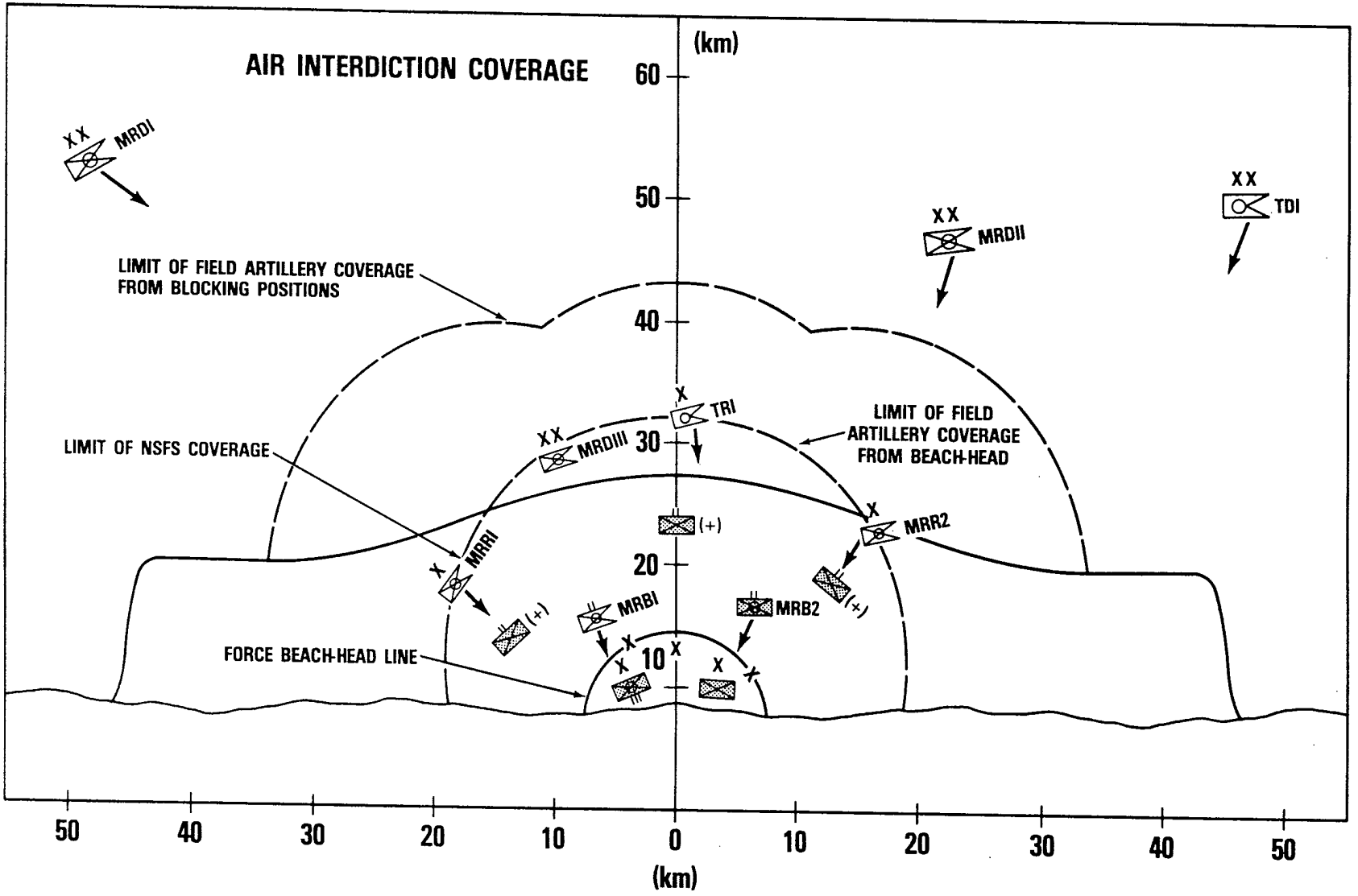

FIGURE 8

MARINE AMPHIBIOUS FORCE LODGEMENT SITUATION ON X+3 DAY

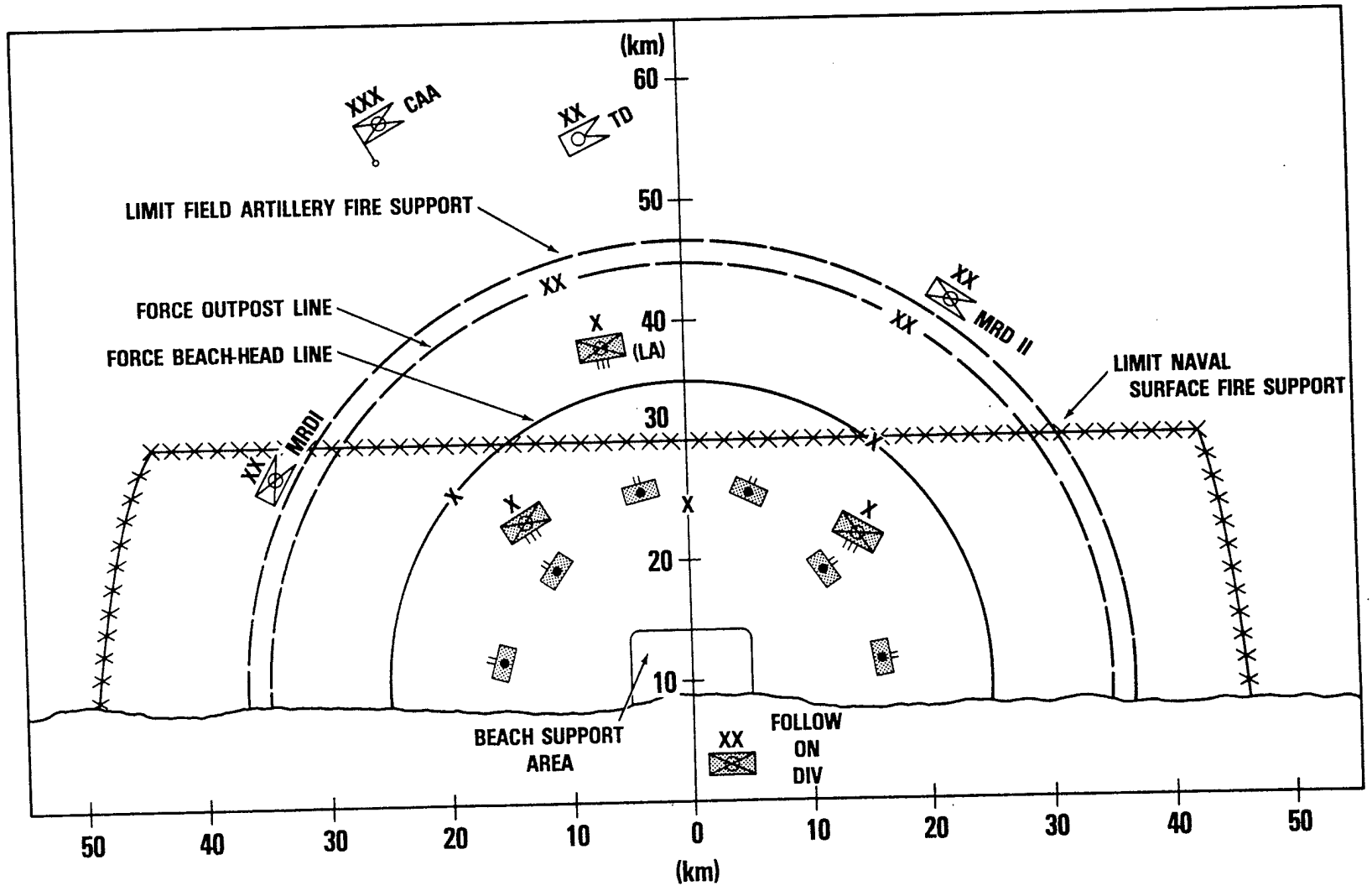

FIGURE 9

MAF BEACH-HEAD X+3 DAY FIELD ARTILLERY MASSING ZONES

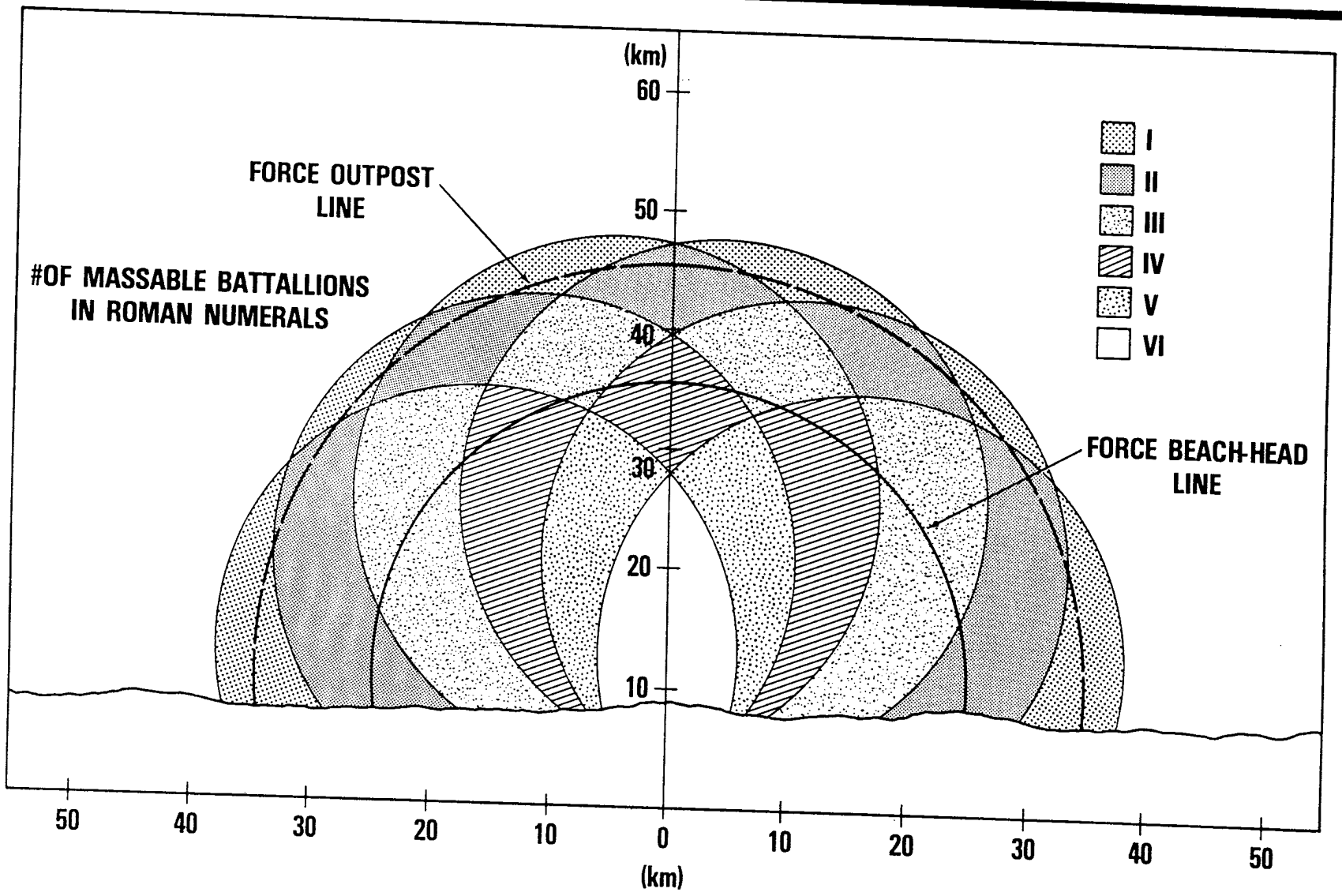

FIGURE 10

SAILING TIME IN DAYS FROM MAJOR US BASES

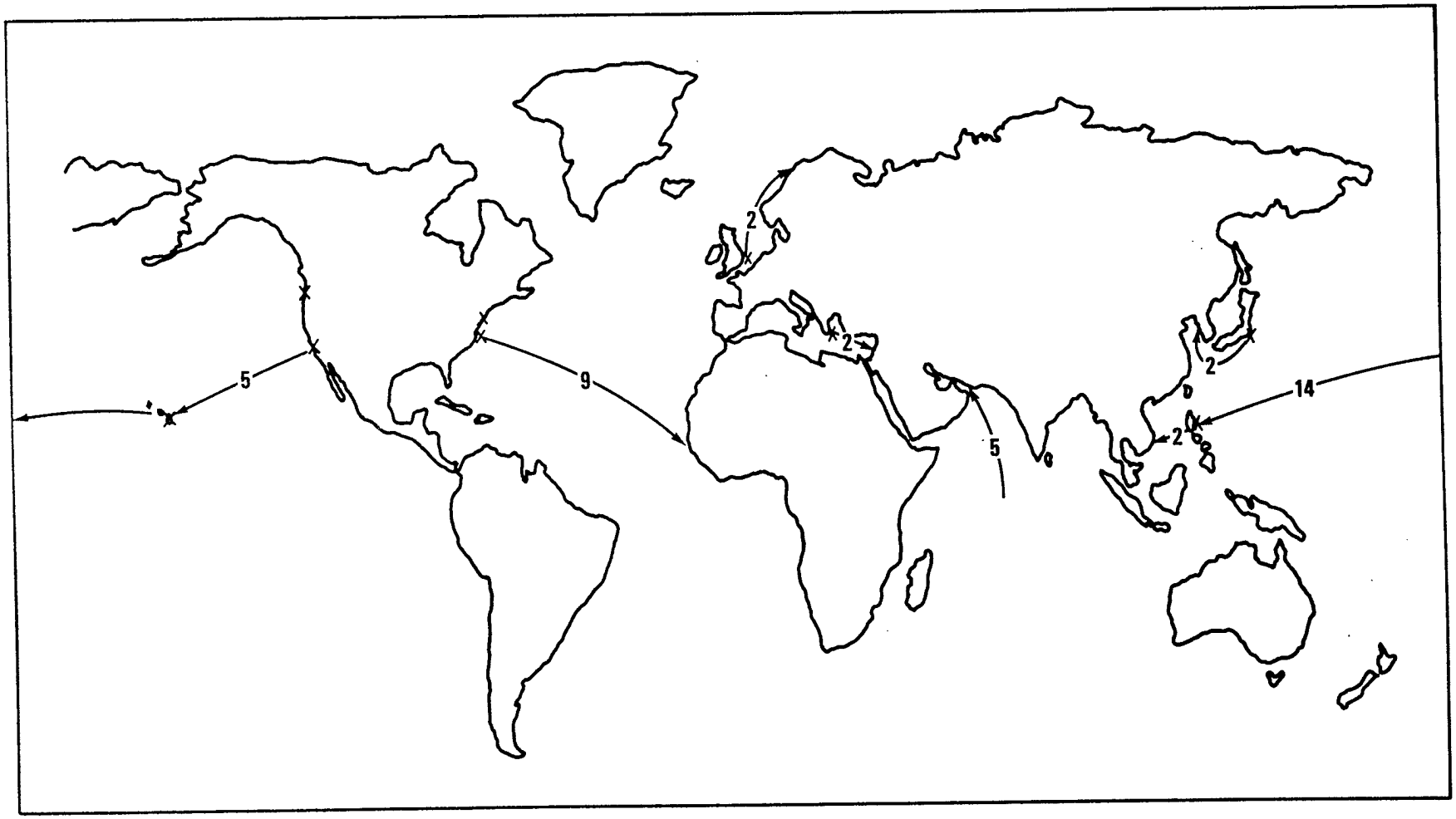

BASIC RESEARCH RELATED TO GUN TUBE WEAR AND EROSION

Robert R. Reeber*
U. S. Army Research Office
P. O. Box 12211
Research Triangle Park, NC 27709

ABSTRACT

Several of our investigations relate, at least in part, to problems arising in large caliber gun tubes. The objectives of two of these projects, at Lawrence Livermore Laboratory (LLL) and the University of Pittsburgh, involve characterization of the mechanisms of interaction of hot multiphase erosion/corrosion phenomena occurring in gun tubes and high temperature combustion engines. The LLL project, at least in its initial stages, was cofunded by Large Caliber and Ballistic Research Laboratories.

The second group of projects relates to the more general topic of plating refractory metal coatings that have application for the development of improved performance gun tubes, the manufacture of metallic glasses for electronic applications and the development of wear resistant surfaces for other military hardware. These projects, although basic research, have a two-fold thrust that includes:

1. Development of an understanding of the plating process that could eventually lead to improved wear and erosion resistance performance and;

2. Evaluation of specific high risk/high payoff aspects of plating technology that can lead to significantly lower costs for the plating process.

Technology aspects of each project as well as technology transfer arrangements with Army laboratories will be briefly reviewed. Related projects in Chemistry and Engineering Divisions are also briefly reviewed.

* Materials Engineer, U. S. Army Research Office program on Degradation, Reactivity and Protection of Materials, Metallurgy and Materials Science Division (919) 549-0641.

BASIC RESEARCH RELATED TO GUN TUBE WEAR AND EROSION

Robert R. Reeber
U. S. Army Research Office
P. O. Box 12211
Research Triangle Park, NC 27709

The U. S. Army Research Office sponsors a number of projects that relate at least in part to erosion problems in large caliber gun tubes. Choice of these unsolicited projects results from external peer review for technical merit, Army laboratory review for program relevance and the availability of funds as prioritized by Army management. The projects can generally be grouped into the following three categories:

(1) Theoretical and experimental characterization of complex thermodynamic and kinetic phenomena.

(2) Performance improvements of chemicals, materials, structures or control equipment stemming from an improved understanding of design principles, physical and mechanical properties of materials, and reaction chemistry.

(3) Developments/breakthroughs in characterization and sensing methodology that can later impact categories (1) and (2).

Work considered most relevant to the erosion area includes: Metallurgy and Materials Sciences (6 projects), Chemistry (7 projects), Engineering (4 projects). The principal thrust of the Engineering effort is directed at high temperature engine research related to combustion and surface/gas reactions.

Because of the interdisciplinary nature of several of these projects, their funding, as indicated, is shared between several divisions. Funding for all areas is summarized in Table 1.

Approved for public release; distribution unlimited.

Metallurgy and Materials Sciences Division
Project Monitor: Dr. Robert R. Reeber, Telephone: (919) 549-0641, Ext 318

1. An Investigation of the Electrode Kinetics and Electrochemistry of Refractory Metal Deposition. Project Number 19554-MS 25 April 1983

EIC Corporation, Newton, Massachusetts.
Principal Investigator: Dr. S. H. White

Preliminary studies are evaluating zinc chloride for application as a low temperature electrolyte for molybdenum and tungsten deposition. Electrochemical spectroscopic techniques will be used to identify conditions for coherent metal deposition. In parallel with these studies, literature information is being collected to evaluate alternate low temperature fused salt electrolytes. Proposed novel electrolyte formulations designed from such information will be examined experimentally with techniques applied for zinc chloride.

Annual Funding: M&MS, 44K
Chemistry, 44K

SC: ARRADCOM (Lakshminarayan)
SC: BWL (AHMAD)
SL: AMMRC (Pan)
SC: NASA LEWIS (May)

2. Electrodeposition of Chromium in Magnetic Fields. Project Number 15104-MS 31 December 1982

Portland State University, Portland, Oregon.
Principal Investigator: Professor John Dash

This work involves assessing the effect of magnetic fields on electrodeposition processes. Work to date indicates that magnetic fields increase the current efficiency of chromium deposition, improve the uniformity of the deposits and reduce the volume of hydrogen gas present. Magnetic field strengths of zero to 13.4 kiloguass were employed. Deposits were characterized with transmission and scanning electron microscopy. Current efficiency increases were small. Additional activities on this project relate to bath additives for improvement of chromium plating efficiency. A United States Patent Application was filed in June, "Methods to obtain current efficiencies in chromium plating of up to 70% are presented in this disclosure."

Presently, industrial practice operates in the 15 to 25% range. Several publications have been presented on this work, the latest at the 69th Annual Technical Conference of the American Electroplater's Society.

Annual Funding: M&MS, 41K

SL: BWL (Chen)
SC: AMMRC (Morrossi)
SC: MERADCOM (Levine)
SC: FCSCWSL (Ebihara)

TABLE 1

EROSION RELATED* RESEARCH

FUNDING SUMMARY

	1982 ANNUAL $K
ELECTROPLATING	208
EROSION	323
REACTION KINETICS	202
BORON CHEMISTRY	297
HEAT FLUX TO SURFACES	108
CATALYTIC SURFACE REACTIONS	114

* SOME PROJECTS MAY BE OF INTEREST ONLY BECAUSE OF DIAGNOSTIC AND MATHEMATICAL TECHNIQUES USED.

3. Electroplating of Refractory Metals and Alloys from Fluoride Melts. Project Number 15916-MS 31 August 1982

Rensselaer Polytechnic Institute, New York.
Principal Investigator: Professor R. A. Bailey

The project is evaluating electroplating of chromium from molten LiF-NaFKF (FLINAK). The primary object of this research is to determine the mechanisms of the electrode reduction of Cr^{3+} ion in the molten FLINAK based on results obtained from cyclic voltammetry and chronopotentiometry. Chromium deposits obtained to date have had marginal potential for applications requiring quality chromium electroplated material. Chromium deposits that are adherent, soft and free of dendrites can be obtained but only at high temperatures where grain size is excessively large. Present work is concentrating on the use of codeposited species to control grain size and changing melt properties in a way that might favor the stability of the chromium species.

Annual Funding: M&MS, 13.5K
Chemistry, 18.5K

SL: BWL (Ahmad)
SC: FCSCWSL (Ebihara)

4. Pulsed Electrodeposition of Amorphous and Composite Alloys. Project Number 16782-MS 1 June 1983

Stevens Institute of Technology, Hoboken, New Jersey.
Principal Investigator: Professor Rolf Weil

The object of this research is to investigate the effect of pulse plating on compositional variation and hydrogen codeposition effects in electrodeposited alloys. The plating of amorphous nickel-phosphorus and nickelmolybdenum alloys in a range of plating solutions is being studied. Films obtained are being characterized by transmission electron microscopy and mechanical property tests. Several papers have been presented to the Electrochemical Society, TMS AIME and the Penn State Conference on Electrodeposition.

Annual Funding: M&MS, 42K

SL: BWL (Ahmad)
SL: ETDL (Tauber)
SC: AMMRC (Aabielski)
SC: MERADCOM (Horner)

5. Interactions Between Erosion and Corrosion of Metals and Alloys at Elevated Temperatures. Project Number 17421-MS 4 January 1984

University of Pittsburgh.
Principal Investigators: Professors N. Birks and F. S. Pettit

The work will investigate the effects of a hot gas stream with and without particulates on erosion of refractory metals and metal alloys. Typical temperatures and speeds are 910 C at 140 ms^{-1} and 865 C at 240 ms^{-1}. Particle control and monitoring is accomplished with a Sylco particle dispenser and a computer monitored laser doppler anemometer. As work proceeds, higher temperatures and

particle flow rates are expected. Eroded samples are examined by a variety of metallurgical, analytical and microscopical techniques.

Annual Funding: M&MS, 73K

SL: AMMRC (Levy)
SC: RTL/EUSTIS (Cale)
SC: RTL/EUSTIS (Santoro)
SC: TACOM (Rose)

6. An Investigation of the Mechanisms of Hot, Multiphase Erosion/ Corrosion Phenomena. Project Number 15812 1 October 1982

Lawrence Livermore Laboratory. Principal Investigator: Dr. A. Buckingham

Theoretical modeling and experimental work involving laser simulation of erosive phenomena. This project will be reviewed separately.

Annual Funding: Engineering, 100K
M&MS, 100K
Large Caliber, 50K

SL: BWL (Ahmad)
SL: LCWSL (Lannon)
SL: BRL (Ward)
SC: MICOM (Walker)

The Chemistry Division has two program areas that relate in part to the erosion problem. These include three projects addressing heterogeneous reaction kinetics; other potential applications of this work relate to catalysts and chemical reactivity, and four boron chemistry projects (with relevance for explosives with low flame temperatures).

Brief descriptions are as follows:

Heterogeneous Reaction Kinetics:

Project Manager: Dr. David R. Squire, Telephone: (919) 549-0641, Ext 208

1. Interactions of Vibrationally Excited Molecules with Solid Surfaces. Project Number 17349-C 14 June 1983

Cornell University.
Principal Investigators: Professors P. L. Houston and R. P. Merrill

Molecules contained in an ultrahigh vacuum chamber were excited with a pulsed CO_2 laser. Relaxation phenomena for CO_2 vibrational modes at stainless steel, silver and nickel surfaces were obtained. Thermal accommodation on surfaces subjected to the same treatment as experimental surfaces is being used to determine the extent and effect of adsorbed species on the vibrational relaxation efficiencies.

Annual Funding: Chemistry, 61.5K

SC: BRL (Keller)
SC: LCWSL (Harris)
SC: AMMRC (Johnson)

2. Study of Gas-Surface Interactions by Laser-Induced Fluorescence Detection. Project Number 17355.3-CH 8 December 1983

Stanford University.
Principal Investigator: Professor R. N. Zare

A theoretical/experimental study of the form of the gas-surface interaction potential. Measurements will include chemiluminescence that accompanies exposure of clean surfaces to bombarding gas molecules and internal state distributions of H_2 that is formed by atom recombination on a metal surface.

Annual Funding, Chemistry, 80K

SC: CSL (Harden)
SC: BRL (Anderson)
SC: BRL (Beyer)
SC: AMMRC (Johnson)
SL: LCWSL (Sharma)

3. Determination of the Microscopic Structure of Surfaces and Overlayers, Adsorbate-Adsorbate Interaction Energies and Rates of Surface Processes. Project Number 16273.5-C 24 September 1982

California Institute of Technology.
Principal Investigator: Professor W. Henry Weinberg

A versatile multiprobe molecular beam ultrahigh vacuum apparatus is in final testing. Scattering of a variety of rare gases (He, Ar, Ne, Xe) from Fe single crystals will provide information concerning the gas-surface interaction potential. Later experiments will focus on the scattering of reactive gases (H_2S, H_2O, O_2, PH_3) from the iron crystal surfaces. Reactant and product molecules scattered from the iron surface will be measured as a function of crystal temperature and geometric and dynamical variables of the experiments.

Annual Funding: Chemistry 60K

SL: MERADCOM (Joebstl)
SL: LCWSL (Habermand)
SC: BRL (Beyer)
SC: AMMRC (Harrison)
SC: BWL (Kamdar)

Boron Chemistry

Project Manager: Dr. Bernard Spielvogel, Telephone: (919) 549-0641, Ext 230.

ARO research on boron compounds has involved a long-term effort that includes Dr. Spielvogel's staff research at ARO. In the middle 70's, the potential for NHC, N-Hexylcarborane was recognized as essential for the new Viper antitank weapon. Since this material currently costs $1200/lb, there was a critical need for less expensive synthesis routes. Figure 1 from a management briefing by Dr. Spielvogel indicates the success to date of the basic research efforts in this area.

FIGURE 1

EFFICIENT ROUTES TO NHC

CASE HISTORY (CONTINUING)

NHC, N-HEXYLCARBORANE - BURNING RATE MODIFIER ESSENTIAL FOR NEW VIPER ANTITANK WEAPON

CONVENTIONAL ROUTE: DIBORANE ---------- DECABORANE ---------- NHC
VERY EXPENSIVE PROCESS CURRENT COST $1,200/LB CRITICAL NEED FOR LESS EXPENSIVE PROCESS

JAN 77 ARO SPONSORS WORKSHOP ON TOPIC AT MICOM - STIMULATES 9 PROPOSALS, 4 FUNDED

AUG 78 ARO CONTRACTOR S. G. SHORE, OHIO STATE, REPORTS INDIRECT EVIDENCE FOR PREPARATION OF DECABORANE FROM PENTABORANE. AIR FORCE HAS 100 TONS OF SURPLUS PENTABORANE FROM 1950S CANCELLED BORON FUELS PROGRAM.

OCT 79 SHORE ISOLATES DECABORANE IN RESPECTABLE YIELD (40%)

JAN/
FEB 80 SHORE AND SPIELVOGEL OF ARO VISIT MICOM AND DISCUSS RESULTS WITH VIPER PROJECT OFFICERS

APR 80 SHORE PRESENTS DETAILED REPORT TO MICOM

AUG 81 U. S. PATENT FILED FOR PREPARATION OF DECABORANE FROM PENTABORANE
ESTIMATED GOVERNMENT COST SAVINGS $2,000,000/YEAR

MAY 82 PATENT TO ISSUE; SCALE-UP OF SHORE PROCESS PLANNED

An aim of the boron compound research program has been to achieve lower molecular weight combustion products and higher impetus solid propellants. Nitrogen-boron-hydrogen compounds (N-B-H) have been identified that have 60 to 80% higher theoretical impetuses than conventional propellants at the same flame temperatures.

1. Synthesis of Polyhedranes and Polyhedral Carboranes. Project No. 17398-C
14 June 1983

University of Georgia
Principal Investigator: Professor R. B. King

Annual Funding: Chemistry, 46K

SL: LCWSL (Gilbert
SC: BRL (Schroeder)
SC: MICOM (Carver)

2. The Conversion of Smaller Borane Fragments to Larger Structures - The Systematics of Boron Hydrides Reactions. Project No. 18151-C 18 June 1984

University of Utah
Principal Investigators: Professors R. W. Parry and G. Kodama

Annual Funding: Chemistry, 102K

SC: MICOM (Carver)
SC: BRL (Fifer)

3. Studies on the Synthesis of Boron Hydride Systems. Project No. 19129-C
31 March 1985

Ohio State University
Principal Investigator: Professor S. G. Shore

Annual Funding: Chemistry, 100K

SC: MICOM (Carver)
SC: BRL (Fifer)

4. New Synthetic Routes to Boron Cage Compounds. Project No. 18563-C

University of Pennsylvania
Principal Investigator: Professor L. G. Sneddon

Annual Funding: Chemistry, 48.6K

SC: MICOM (Carver)

5. Studies in Boron Chemistry. Project No. 17650-C

Duke University
Principal Investigators: Dr. B. F. Spielvogel and Dr. A. T. McPhail

Annual Funding: Chemistry, 48.6K

Projects in the Engineering Division, although not directly relevant to the erosion problem, are of interest because of similarities in experimental, diagnostic and mathematical approaches.

Engineering Division

Project Manager: Dr. Dave Mann, Telephone: (919) 549-0641 Ext 249

Heat Flux to Surfaces

1. Wall Effects on Combustion in an Engine. Project No. 15048-E

TRW, Inc. 14 December 1982
Principal Investigator: F. E. Fendell

This project undertakes experimental and theoretical investigations of the interaction of planar, premixed, fuel-lean, hydrocarbon-air flames with planar, isothermal, noncatalytic walls. This work entails numerical solution of a transcendentally nonlinear, elliptical eigenvalue problem, expressing a Shvab-Zeldovich formulation of the aerothermochemical flow.

The adequacy of such a formulation is to be indicated by comparing predictions for a single-sidewall quench layer with experimental measurements of isotherms and isoconcentration surfaces for hydrocarbons. The laboratory data is obtained by laser Raman spectroscopy for a flame stabilized on a heat sinktype burner, with a water-cooled sidewall of various materials. The preliminary comparison is fairly adequate--theory gives a somewhat too slow burn-up of hydrocarbons relative to observations.

Annual Funding: Engineering 56K SL: MERADCOM (Quillian)
SC: TACOM (McClelland)

2. Diesel Engine Cylinder Gas-Side Heat Flux to a Ceramic Surface. Project No. 18188-E 17 February 1983

University of Wisconsin
Principal Investigator: G. L. Borman

The research is to provide experimental data on the heat flux to the cylinder gas side surface of a transducer constructed from materials which may be used for the cylinder surfaces in a low heat rejection diesel engine. Such data are to be used to obtain an improved understanding of the heat transfer phenomena in such engines and to provide improved correlations for use in cycle simulation and combustion modeling.

Annual Funding: Engineering, 52K SL: TACOM (Klein)
SC: MERADCOM (Kinser)

Catalytic Surface Reactions

Surface Ignition and Heterogeneous Catalysis of Hydrocarbon Fuels. Project No. 16914-E
13 April 1983

University of Illinois-Urbana
Principal Investigators: Richard I. Masel, R. O. Buckius

This research project consists of a parallel experimental and analytical study investigating catalytic combustion for piston engine applications. The objective of this study is to obtain a better fundamental picture of the chemical and physical processes that lead to substantially improved engine performance. The experimental program has successfully measured ignition temperatures for hydrogen, propane, propylene, methanol, and toluene. Detailed kinetics for catalytic combustion of a model hydrocarbon fuel, formaldehyde, are being obtained. The analytical efforts are directed towards a two-dimensional transient investigation for catalytic combustion.

Annual Funding: Engineering, 52K SL: TACOM (Bryzik)

An Investigation of the Kinetics of Catalyzed Combustion of Fuel. Project No. 17267-E
30 September 1983

United Technologies Research Center
Principal Investigator: Pierre J. Marteney

The fundamental aspects of catalytic combustion are under investigation in this program. Argon-diluted mixtures of hydrocarbon fuels and oxygen are preheated and reacted on catalytic surfaces. A two-step reaction mechanism is presumed, with fuel coverting sequentially to CO and CO_2. Tests to date have been conducted with single-component fuels, principally propane.

Annual Funding: Engineering, 62K SL: NASA LEWIS (Mularz)

The Mathematics Division also has some work that may aid in complex calculations and computations related to theoretical models of erosion and heterogeneous reaction kinetics. Those interested in further information on this area should contact Dr. J. Chandra, Director of the Mathematics Division, (919) 549-0641 Ext 254.

The Physics Division has no programs directly relevant to erosion. Projects relating to theoretical aspects of structure and strength of materials are under the direction of Dr. Robert Lontz, Director of the Physics Division, (919) 549-0641 Ext 237.

STATUS OF GUN BARREL WEAR AND EROSION IN THE USA

THE THIRD TRI-SERVICE SYMPOSIUM ON

"GUN TUBE WEAR AND EROSION" (1), (2)

By

Jean-Paul Picard

ARRADCOM, Dover, N. J.

*The previous two were held in 1970 at Watervliet (1), and in 1977 here at Dover, New Jersey, respectively (2).

OUTLINE

I. Historical

II. The Magnitude of the Problem of Erosion

III. Mechanism of Erosion

IV. Approaches to Solve the Problem

V. Low Flame Temperature Propellant

VI. Modern Propellant

VII. Conclusion

I. Historical

The useful life of gun tubes under the wear and erosive environments of gun propulsion has been and continues to be one of the major problems in artillery technology.

Since the advent of guns in the beginning of the 14th century, there has been a continuous effort to increase their capability, in terms of, propelling heavier projectiles faster for longer distance with greater accuracy.

In the 19th century, becuase of advances in chemistry, mechanics, metallurgy and associated disciplines, elongated projectiles replaced sperical iron projectiles and rifled guns were introduced. In that period, for the first time, through the effort of Captain Rodman (USA), a progressive burning gun propellant was used. In Germany, through the effort of Alfred Krupp, the process of fabricating gun barrel by casting was introduced. All of these made possible the development of guns with increased chamber pressure, muzzle velocity, rate of fire and range; but these led to increased erosion to a point that it was recognized as a serious problem.

In 1886, the French Scientist, Frederic Abel, wrote "The great increase in the power of artillery has brought the subject of erosion of gun barrels into prominance, and it now forms one of the chief difficulties to be encountered by the makers of a heavy gun, its sufficient mitigation is the one great difficulty likely to impose a limit on the size and power of ordnance in future."

This prophesy has become an axiom of ballistics technology and a proof of that is this symposium.

In some conventional systems such as howitzers and mortars, due to the advancements in the technology of materials, propellants and design, the erosion problem has been kept under control. In advanced systems, however, which are designed for rapid fire, increased range and high muzzle velocity, the seriousness of erosion often requires that they be condemned prematurely. Consequently, there has been considerable R&D effort to understand it and to develop the technology to overcome it. Some of this work was reported in the 1970 and 1977 symposia, (1)(2); this symposium gives an account of the work done since then.

The thesis of these remarks is that erosion is a ballistic factor that must be continually addressed if improved gun systems are to be fielded. This is predicted on the fact that although significant progress has been made in some areas of erosion control, the constant demands for increased range, higher muzzle velocity and rates of fire place greater strain on the gun and result in drastic increases in erosion.

II. The Magnitude of the Problem of Erosion

The seriousness of the erosion problem in currently used artillery is quite severe, and some of the advanced systems such as the 75mm high velocity gun or the

Whenever there is a problem with one particular weapon, funding is provided to solve that problem, but with little attention to identification of its root cause. There is little doubt that a more systematic and persistent approach is necessary.

Erosion-reduction additives may be considered as an interim solution to the problem. This is not to say that additives such as talc, TiO_2 and polyurethane have little value but it becomes apparent that additives do not perform with equal degree of effectiveness in all systems. In other words, there is still no satisfactory way to predict whether a given additive will be effective in a given weapon.

Work done in recent years on refractory metal coating technology has advanced in many different areas. At Benet Weapons Laboratory, work on chrome plating technology has resulted in considerable improvement of the properties of conventional chromium coatings. For example, improved low contractile chromium evaluated in 20mm M24A1 (4) guns showed a performance much superior to the high contractile chromium tested under the same conditions. The flow-through method appears to give coating with superior properties.

Other refractory coatings such as Tantalum and Columbium have been laboratory tested on short liners shrink-fitted into 20mm M24A1 barrels and, on 105mm liners for the M68 gun. Preliminary results indicate a potential pay off.

V. Low Flame Temperature Propellant

As already stated, the flame temperature of the propellant is probably the single most important factor contributing to erosion; accordingly, there is a continuing effort by all the Services to formulate low flame temperature propellants. The M-30 developed at Picatinny in the mid-fifties, was a product of such an effort. In this case, the incorporation of nitroguanidine with nitrocellulose and nitroglycerine did provide somewhat cooler propellant than its counterpart made up of nitroglycerin and nitrocellulose. In the same development, a cooler burning propellant than M-30, known as M-31, when substituted for M-30 in the 8-inch gun resulted in less gun barrel erosion.

VI. Modern Propellant

An important development of the sixties was the introduction by Picatinny of the nitramine based propellants. It was realized that RDX, or HMX, in combination with nitrocellulose or a hydrocarbon binder, could provide the most unique propellant system with a relatively high force and low flame temperature.

Attempts to introduce propellants with low flame temperature and high impetus show promising results; the combustion products of some of these, however, are quite erosive. In the development of any artillery system, it is important that

95mm gun, cannot be brought to fruition unless satisfactory methods of controlling it are found. Additives such as dimethyl silicone have exhibited anti-erosion effects in these systems.

The needs for more frequent exchange of tubes on the battlefield, and the slowing down of advanced systems development especially those requiring long range, rapid fire rate and high muzzle velocity are neither cost nor performance effective, resulting in premature condemning of tubes at DOD's expense.

The consequences of erosion, in terms of logistics, ballistic performance and accuracy, have to be recognized and addressed. For too long, erosion has been passively tolerated and its importance slighted. As we advance further and further towards the development of high pressure, high velocity weapons, constraints of erosion become more apparent and increasingly more significant.

III. Mechanisms of Erosion

Numerous approaches have been pursued to characterize erosion mechanisms and predict the useful life of a gun barrel. By measuring the temperature at various points along the barrel, Thornhill (3) was able to correlate the average rate of wear, one-inch from origin of rifling, with temperature, and to estimate the maximum bore temperature at this point. He showed that at temperatures below 660°C erosion was negligible, while above 660°C, there was a marked increase, and even more so above 1000°C (probably due to ablation).

It is obvious that the high velocity gases and their chemical composition play an important role in the extent of erosion, as do high pressure and high temperature.

Heat measurement in combination with various additives used for the purpose of mitigating the heat transfer, has been examined with some success.

The design of rotating bands to improve the band-rifling interaction, engraving stresses and gas obturation, has also been very much in the forefront.

The research effort expended to understand the erosion process and to identify the essential parameters show that one of the most important factors is the flame temperature of the propellant.

Ideally, propellant capable of high force and low flame temperature is highly desirable.

IV. Approaches to Solve the Problem

Never in the history of ammunition has there been a subject so important and yet so neglected in terms of research and development. Due to lack of adequate funding, most of the approaches could not be conducted to full conclusion.

the evaluation of erosion be carried out simultaneously to avoid unexpected results.

"The propellant testing should be performed as early as possible in the weapon development cycle for which it is intended."

Finally, we become aware of the fact that no one single factor will reduce erosion in all cases. The potential for success is increased through the use of appropriate gun barrel design, low flame temperature propellant and, if necessary, additives. Although the relevance of the type of ignition used, has been omitted in this address, it should not be neglected. The practical use of combustible cartridge cases should also be noted; this provides an opportunity to locate additives such as talc and TiO_2 at the proper positions along the gun barrel wall.

It is hoped that this meeting will lead to a better appreciation of the problem and that it will promote more intense cooperation among the Services, Industries and the University.

It was soon realized, however, that the composition of the gas resulting from the combustion of such propellants also caused gun barrel erosion; at that time the appearance of anti-erosion additives was a reassuring factor.

Tracing back to the origin of additive, we find that in the mid-fifties, Canadian Scientists (5) explored the use of polyurethane foam, which through its thermal degradation generated a cool boundary layer. Tests made in the U.S. (6) in 90mm, 105mm, and 120mm tank guns showed similar findings to those obtained in Canada. However, although in the 105mm M68 the wear life did improve, an unacceptable dispersion value was recorded.

In the sixties, the Swedish inventors (7) suggested the use of propelling charge liners made of rayon coated with TiO_2 (titanium dioxide) dispersed in molten wax. The results obtained were encouraging.

Furthermore, work in this direction was done at Picatinny (8,9). A number of oxides and silicates were found usable for this purpose, and in particular, Hydrated Magnesium Silicate or Talc has gained prominence. The superiority of talc-wax over TiO_2-wax additives was demonstrated in a number of Army and Navy guns. A multitude of systems consisting of talc-polyurethane, talc-in-combustible cartridge case, talc-wax, and others have been developed and used in this country and abroad. As previously stated, dimethyl silicone shows improved anti-erosion properties in the 75mm and 90mm systems.

In the case of small arms ammunition, (due to the small chamber volume) propelling charge-liner cannot be used to counteract erosion. By necessity, the additives must be formulated within the propellant. Some excellent results have been obtained with TiO_2 or Talc at concentration levels of 1-2%, but a great deal remains to be done in this area.

VII. Conclusion

Barrel erosion is an extremely complex area where all the disciplines of Chemistry, Physics and Materials Science interact at the bore surface of the gun to effect reproducible ballistic performance and a high degree of accuracy.

Although over simplified thermo-mechanical and thermo-chemical models have been proposed, no reliable comprehensive model capable of predicting barrel life has, as yet, been developed. No one refutes, however, that the combined effort of the propellant chemist and metallurgist will eventually lead to a successful solution.

Boundary layer coolants, like polyurethane foam, TiO_2-wax and talc-wax, dimethyl silicone, low flame temperature propellants, and plastic rotating bands represent a number of control measures developed and which demonstrate significant improvements. The lack of adequate understanding of the mechanisms involved is a deterrent factor in achieving maximum effectiveness in every gun barrel.

The challenge of using chemistry, physics, and materials science to resolve this age-old problem and to establish a greater cooperation between the users, Industries, and the R&D Community does exist.

In view of the above considerations, the conclusion is that more work is required to realize and perpetuate past years' effort. The necessity of further in-depth investigation of the above is well justified by the scenario of Air Land Battle 2000, for which successful materialization of advanced concepts, such as ICAS, DSWS, hypervelocity light weight guns (MPGS), rapid fire (DIVAD), and aircraft guns, etc. must be developed in the 1990's. It is easy to visualize that every increment in muzzle velocity, rate of fire, or range will result in increase in erosion. Therefore, it is imperative that every program aimed at developing an advanced system must include early in the development cycle, some provision to investigate effects related to bore erosion. Furthermore, a steady RDTE activity must be maintained to continue improving the techniques of erosion control and overcoming the adverse side effects of erosion on the performance of future weapons.

REFERENCES

1. I. Ahmad, J. P. Picard, Proceedings of the Tri-Service Technical Meeting on "Gun Tube Erosion and Control", Watervliet Arsenal, Watervliet, NY, Feb. 1970.

2. J. P. Picard, I. Ahmad, Proccedings of the Tri-Service Gun Tube Wear and Erosion Symposium, Dover, NJ, March 1977.

3. Thornhill, C. K., Some Theoretical Considerations of the Problem of Gun Erosion, December 1943 (AD 42 526).

4. Cullinan, R. L., et al, "Study of Erosion Resistant Materials for Gun Bores - Part II: Tantalum Coated Liners, " ARLCB-TR-81911, Benet Weapons Laboratory, Watervliet, NY, April 1981.

5. Dicerson, D. A. et al, "Improvement of Firing Accuracy and Test Effectiveness of Gases through the Use of Urethane Foams," J. Cellulose Plastic 189, (1968).

6. Joseph W., et al, Picatinny Arsenal Technical Report 2520, June 1958 and 2710, March 1961.

7. S. Y. Ek and D. E. Jacobsen, U.S. Pat. 3148620, September 1966, U.S. Pat. 3363438, January 1968 and U. S. Pat. 3397636, August 1968, also "Engineering Study of Barrel Wear Reducing Additive", Wegematic Corp. Report Pt A, May 1962.

8. J. P. Picard, Erosion Reducer, U.S. Patent No. 3,392,669, July 1968.

9. J. P. Picard, Erosion Reducer, U.S. Patent No. 3,397,637, August 1968.

SESSION II

PHENOMENOLOGY AND CHARACTERIZATION

CHAIRMAN: Dr. Joseph A. Lannon

GAU-8/A BARREL LIFE IMPROVEMENT PROGRAM

- MICROFLASH PHOTOGRAPHY
- POST TEST METALLOGRAPHIC RESULTS

by:

S.R. DUKE, D.P. PERRIN, M.A. BLAIR
General Electric Company
Burlington, VT 05402
Phone No. (802) 657-6000

ABSTRACT

The GAU-8/A Barrel Life Improvement Program was an Air Force sponsored program to determine low cost barrel modifications which would improve barrel life and ammunition performance. The project entailed designing, building, and testing several modified barrels. The significant modifications to these barrels involved changes to rifling twist, bore coating, and number of lands. The following discussion concerns two aspects of the program: 1) microflash photography, and 2) metallographic results of selected barrels.

INTRODUCTION

Microflash photography and metallography of sections from worn barrels are two essential means of evaluating barrel and bore coating performance, respectively, which this paper will discuss. More details regarding the overall program are covered in the paper entitled GAU-8/A Barrel Life Improvement Program by (1) Messr's Jenus, Perrin, and Duke. Microflash photography is especially useful for the GAU-8/A barrel, because the GAU-8/A barrel does not exhibit significant velocity drop throughout its useful life. This characteristic deprives the evaluator of a relatively simple and straightforward parameter by which to judge barrel performance or condition. Instead, attention must be given to the condition of the rotating band, the degree of body engraving on the projectile, the spin rate of the projectile, the magnitude of the projectile yaw, and the projectile's general appearance or structural soundness. Microflash photographs of individual projectiles during firing provide this information and were used extensively during the GAU-8/A Barrel Life Improvement Program.

Post life metallography of barrel cross sections was also used during this program to examine the behavior of the different coatings. After all fire testing was complete on the experimental barrels, each barrel was sectioned at several locations and micrographs were made. These micrographs were beneficial in illustrating the strengths and weaknesses of the particular coatings, providing a good supplement to the general appearance appraisal made with the borescope.

MICROFLASH PHOTOGRAPHY

Microflash photographs can be taken during single shot firing, where long burst firing can be simulated by preheating the barrel to a high temperature, or during burst firing to guarantee authenticity of the operating environment and the resulting projectile behavior. Burst fire microflash photography is of greatest value when studying an infrequent or intermittent failure, such as windscreen losses. Both single shot and burst fire techniques were used during the program.

Briefly, microflash photography, whether single shot or burst fire is accomplished in the following manner. Two cameras, polaroids for single shot and movie cameras for burst fire, are mounted to the side of the projectile path in a partitioned box. The box provides the dark enclosure necessary to allow the camera shutters to be kept open as the projectiles pass. Two flash units, one for each camera, provide the light necessary for photographing the projectiles. The box partition acts as a light shield isolating each camera. A scale is stretched between the cameras to allow the photographs to show projectile displacement between the successive photographs. A ballistic screen which acts as a triggering mechanism is mounted in the front of the box. This arrangement is depicted schematically in Figure 1. Figure 2 provides a flow chart showing the sequence of events in the microflash photographic process. The main points are when the trigger is depressed, the shutters open and the gun fires. As the projectile passes the ballistic screen it initiates a signal which fires each flash unit at the appropriate time when the projectiles pass in front of the cameras. The motion of the projectile is stopped by the very short duration of the flash.

Figures 3 through 8 provide examples of the types of information available. These particular examples are from single-shot firing, but similar data can be obtained during burst firing, however, in the form of a movie instead of snapshots. Figure 3 shows an example of how the microflash photographs can be used to determine rotating band condition. This particular photograph shows band chunking of a Honeywell rotating band. However, such photographs are also useful in showing the severity of band wear or indicating if the projectile is fully spun as shown by Figure 4. Figure 5 illustrates body engraving which was

one of the particular areas of concern addressed during the program. Figure 6 shows a projectile which has lost its windscreen. A severe yaw caused by failure to be fully spun is shown in Figure 7. The method of determining spin rate is depicted by Figure 8. This figure shows two photographs of the same projectile taken a number of inches apart. The lines painted on the projectile can be used to determine the amount of rotation which has taken place. Knowing the amount of rotation which has occurred in a certain distance allows for the determination of actual spin rate. Actual spin rate when compared to the spin rate which should exist, is the most valuable indicator of GAU-8/A barrel condition.

Such detailed projectile behavior and condition data obtained both through single shot and burst fire microflash photography is necessary to the determination of GAU-8/A barrel performance. This performance data can then be related to the extent of GAU-8/A barrel erosion. This correlation has formed the basis of a recommended replacement criteria based upon borescope inspection.

METALLOGRAPHIC RESULTS

Several internal modifications were tested during the GAU-8/A Barrel Life Improvement Program. Primary variations among those tested were as follows:

1) Incoloy 903 barrel steel,
2) Nitriding and high contraction (HC) chromium plate,
3) Additional lands,
4) Low contraction (LC) chromium plate,
5) Duplex chromium plate (a 2 mil layer of LC chromium under 5 mils of HC chromium),
6) Thick HC chromium plate.

Figures 9 through 28 are intended to provide an indication of the relative success and salient failure modes of each variation. However, before these details are discussed, it may be illustrative to compare Figures 9, 10 and 11. Figure 9 shows the extensive erosion which is experienced in a 20-mm M61 barrel while still functional. Figures 10 and 11 show the relatively minor amount of erosion at the initiation of rifling and down barrel, respectively, which requires barrel replacement in a GAU-8/A weapon. A GAU-8/A projectile with plastic rotating band can tolerate much less erosion; fortunately, it also causes less erosion, at least with a mild firing schedule.

Figures 12 and 13 provide graphic evidence of the poor performance of the unplated Incoloy 903 barrel after only 400 barrel rounds. Figure 12 is a view near the initiation of rifling showing how the rifling has been nearly entirely removed with only rounded, slightly raised lands remaining. The surface also exhibits extensive grain boundary cracking. Figure 13 shows in detail this mode of deterioration, intergranular cracking. IN 903 is known to be quite sensitive to grain boundary oxygen embrittlement, and this is believed to be the primary motivator leading to the barrel's early failure.

The nitrided and HC chromium plated barrel exhibited some interesting results also. These results included:

1) Absence of groove pitting,
2) Large spots of chrome plating flaking off,
3) Deeper barrel steel cracking,
4) Relatively severe erosion at the initiation of rifling.

Groove pitting is a common occurrence in GAU-8/A barrels, as shown in Figure 14; however, there was a noticeable lack of such pitting in the nitrided and HC chromium plated barrel as seen by Figure 15. Down barrel (about 30 inches) large areas of chromium plate loss did occur in the grooves. This is shown in Figure 16. It is believed that less than optimum surface activation prior to plating was the cause for this failure. All barrels experience cracks which penetrate the plating into the barrel steel. The cracks in the nitrided barrel like those shown in Figure 17 were about twice as deep as in the unnitrided barrels. Erosion at the intiation of rifling was also more severe due perhaps to the brittleness of the nitrided steel. A land which has completely cracked away is shown in Figure 18.

One general observation made during the program was that adding additional lands generally led to greater erosion. Figure 19 illustrates this behavior.

LC chromium plate appeared to demonstrate at least one real positive feature--extremely tenacious adherence to the underlying barrel steel. Unfortunately, the LC chromium also allowed land flattening to occur. Figures 20 and 21 compare sections taken at the same location of two barrels--one plated with LC chromium and the other with HC chromium. The barrels were in the same firing cluster which insures identical firing treatment. As evident in the figure, the rifling with HC chromium plating did not distort and the rifling with LC chromium plating did distort. Softening of the LC chromium was also measured down barrel. Prefiring hardness was about 55 R_C and post-life hardness was measured at about 35 R_C. Softening of the HC chromium is not usually detected in GAU-8/A barrels.

The duplex coating of LC and HC chromium also showed promise. Figure 22 shows the relative thickness of the two layers. However, it suffered from the same drawbacks as the lone LC chromium coating; primarily, land swaging and chrome softening. Figure 23 provides another example of this. It did, however, also exhibit the same tenacious adherence as the other LC coatings. Frequently when chrome loss occurred, separation took place in the barrel steel, not at the steel chrome interface. This is illustrated in Figure 24. Another unique feature of this coating was the crack blunting which occurred when the cracks in HC chromium reached the LC chromium as shown in Figure 25. This duplex plating ranked second best of the coatings tested, second to thick HC chromium plate.

The thick HC chromium plate was nothing more than an increase from a standard 4 mils of HC chromium plating to 10 mils of HC chromium plating. Generally, it remained on the rifling longer and protected the rifling better by preventing land swaging. Throughout the program barrels with HC chromium plate consistently evidenced less erosion at the initiation of rifling and less down barrel edge chromium loss. For instance, compare Figure 26 with Figure 27. These sections were taken at 20 inches from the breech in two barrels fired in the same cluster. Figure 26 shows the thick HC chromium plating and Figure 27 shows a barrel with standard thickness chromium plating. One negative feature of the thick chrome which didn't appear to have any functional affect is shown in Figure 28. Down barrel many large spots of chromium plating were missing from the groove surface.

CONCLUSIONS

1) Both burst fire and single shot microflash photography are useful and essential to GAU-8/A barrel performance evaluation.

2) Thick HC chromium provides the best erosion protection for the GAU-8/A barrel of the variations tested.

BIBLIOGRAPHY

1. "GAU-8/A Barrel Life Improvement Program", Paper presented at Tri-service Symposium on Gun Tube Wear and Erosion, 25-28 October 1982, by J. Jenus, D. Perrin, and S. Duke.

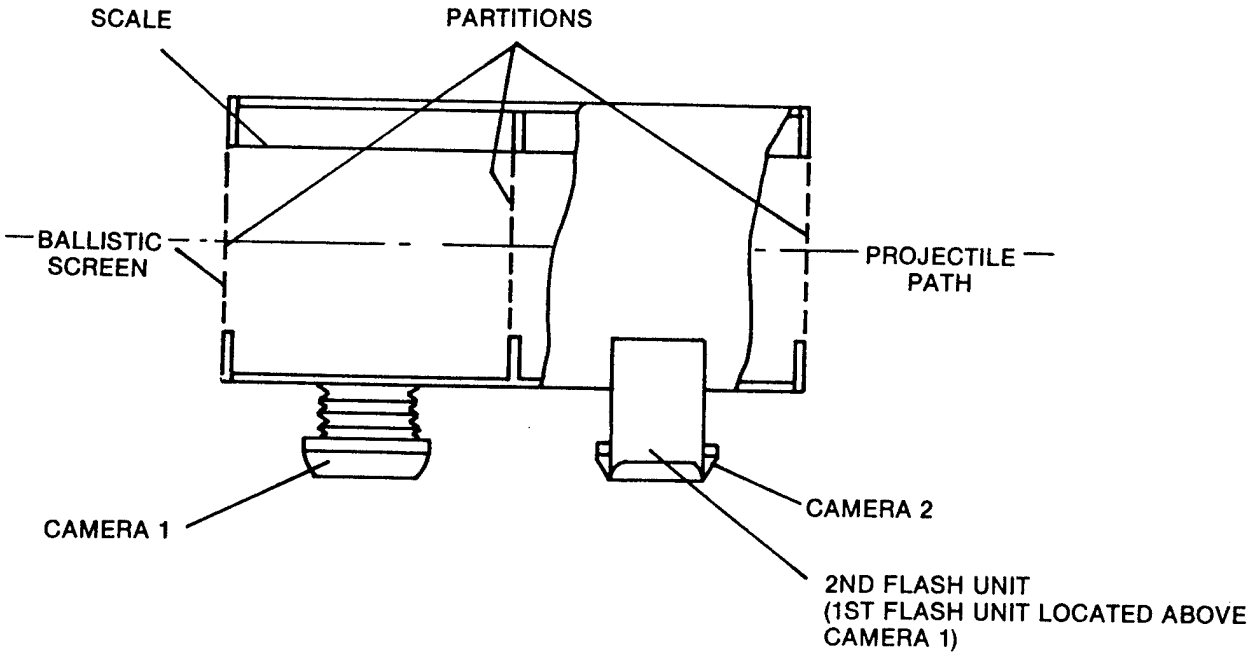

Figure 1. Schematic arrangements of photographic box.

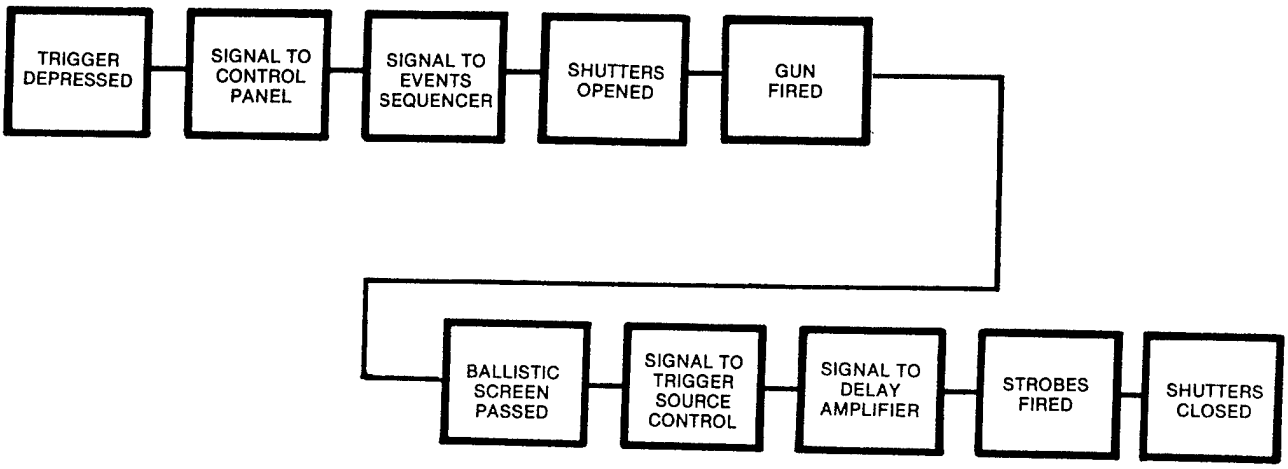

Figure 2. Sequence of events for microflash photographic process.

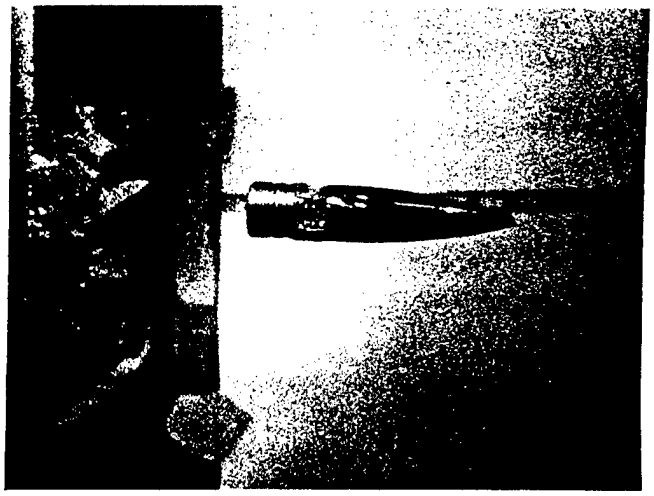

Figure 3. Chunking of a Honeywell Rotating Band.

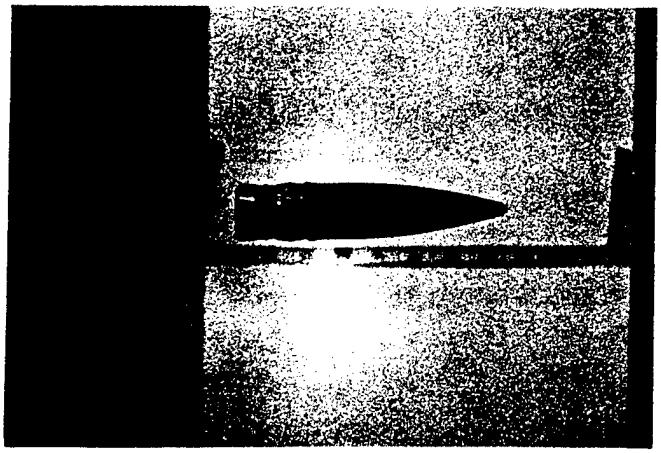

Figure 5. Substantial Body Engraving on Aft Portion of Projectile.

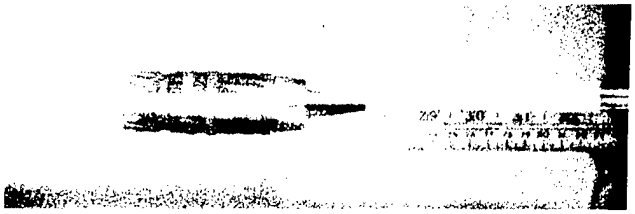

Figure 6. Projectile with Windscreen Missing.

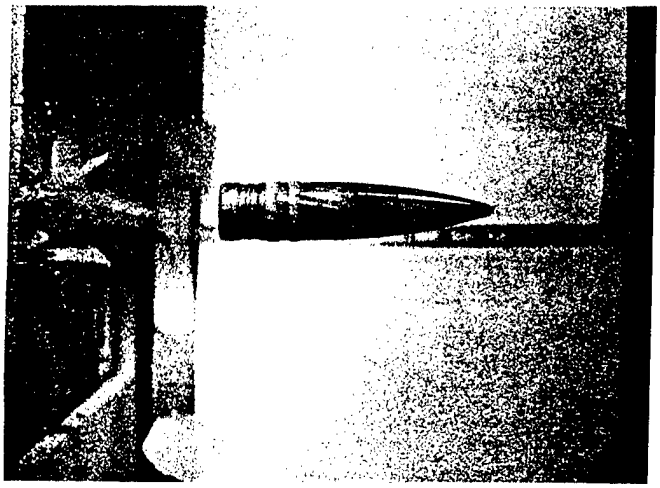

Figure 4 . Fully Spun Projectile; Evident from Intact Grooves in the Rotating Band.

Figure 7. Yawed Projectile.

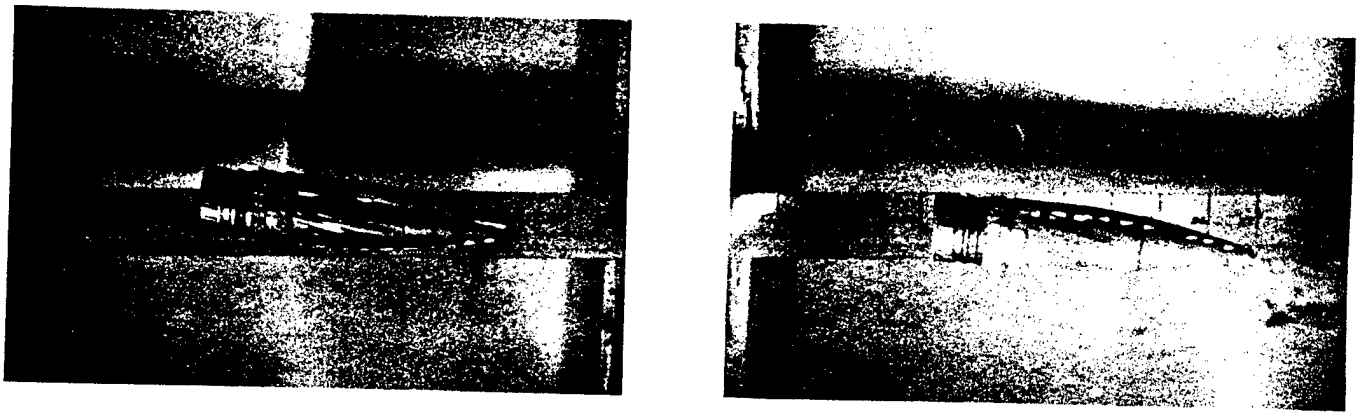

Figure 8. Successive Photographs Used to Determine Spin Rate.

Figure 9. Typical M61A1 Barrel Erosion.

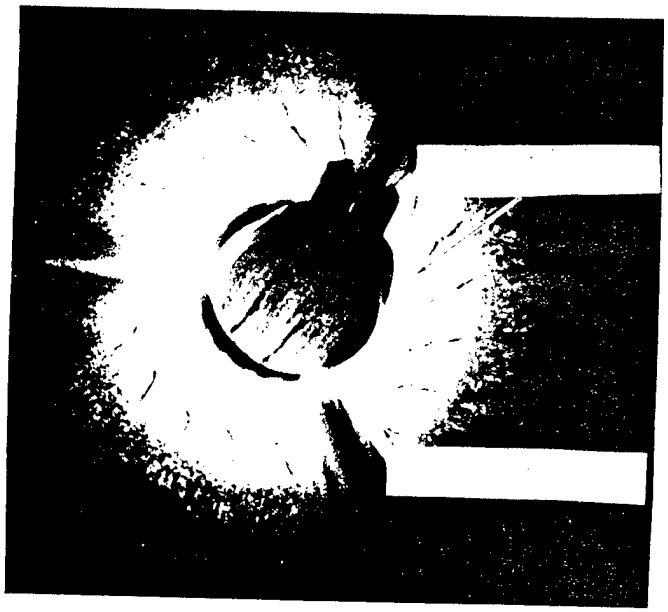

Figure 10. Typical GAU-8/A Initiation of Rifling Erosion.

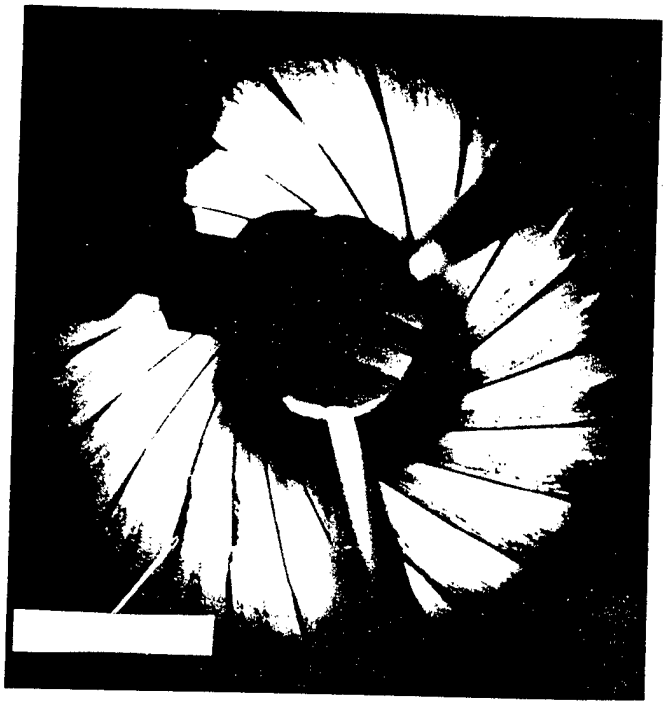

Figure 11. Typical GAU-8/A Down Barrel Erosion.

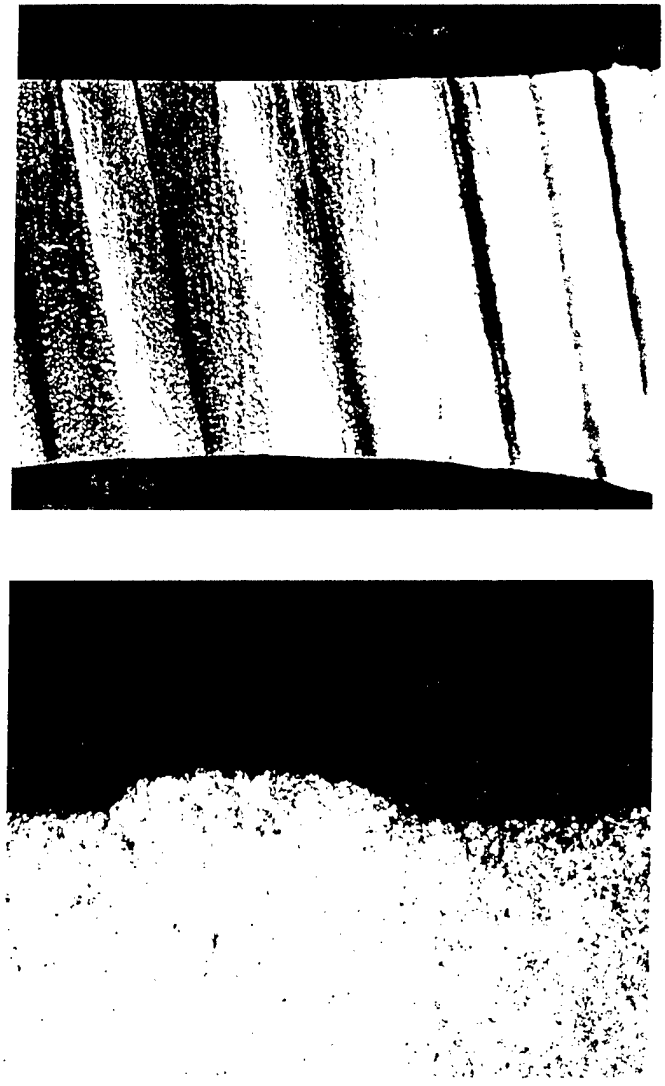

Figure 12. Two Views of Section Near Initiation of Rifling of Inconel 903 Barrel Showing Cracked Surface and Rounded Rifling.

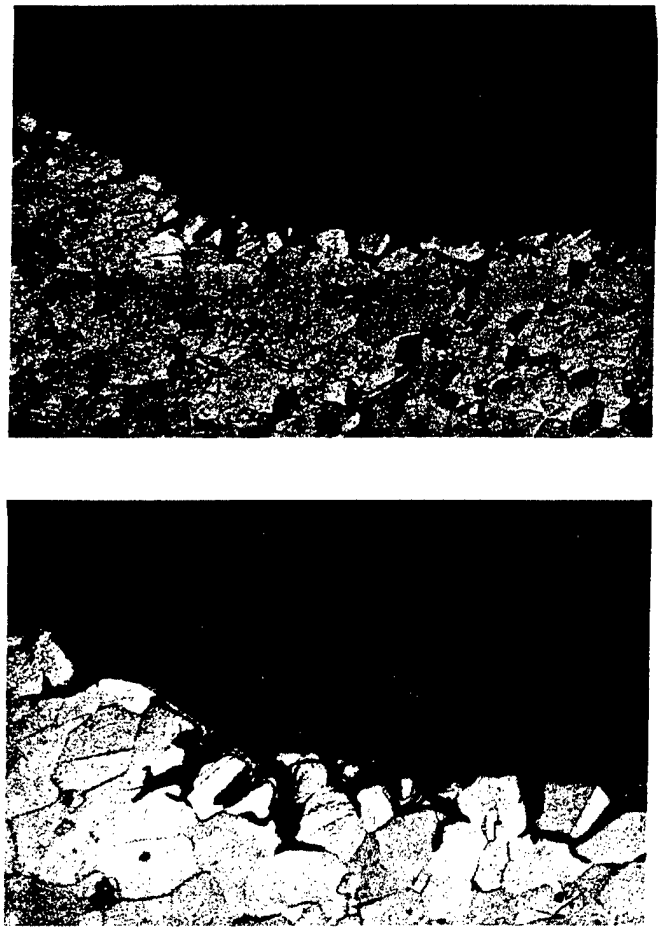

Figure 13. Cross-section Taken 12'' from Breech End of Inconel 903 Barrel Showing Grain Boundary Attack.

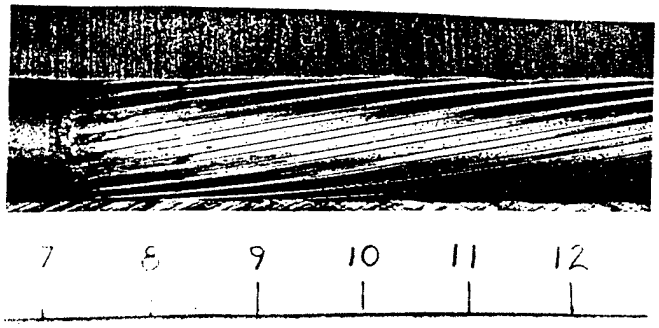

Figure 14. View of a Barrel Exhibiting Typical Chrome Plate Pitting in the Grooves.

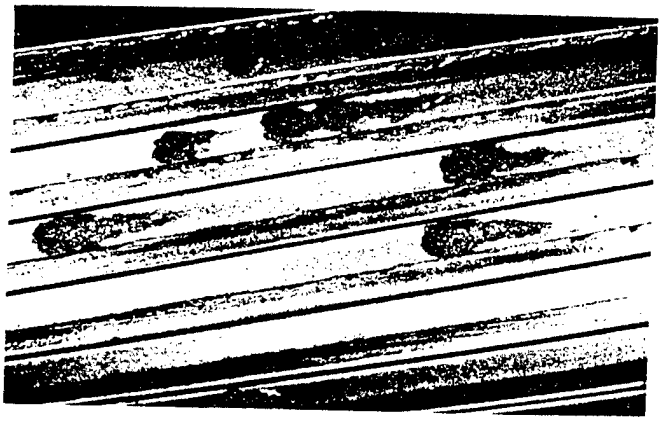

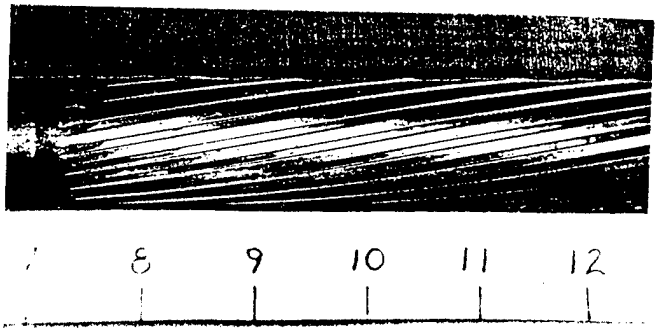

Figure 15. View Similar to that of Figure 12 Showing Absence of Pitting in the Grooves of Nitrided Barrel.

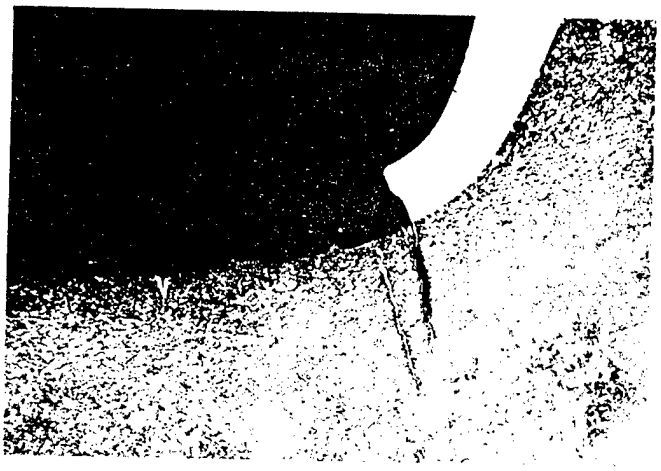

Figure 16. Top, Macrograph of Groove Plating Failure in Nitrited Barrel 33'' from Breech End; Middle & Bottom, Cross-sections Showing Closer Detail of Chrome Plate Failure.

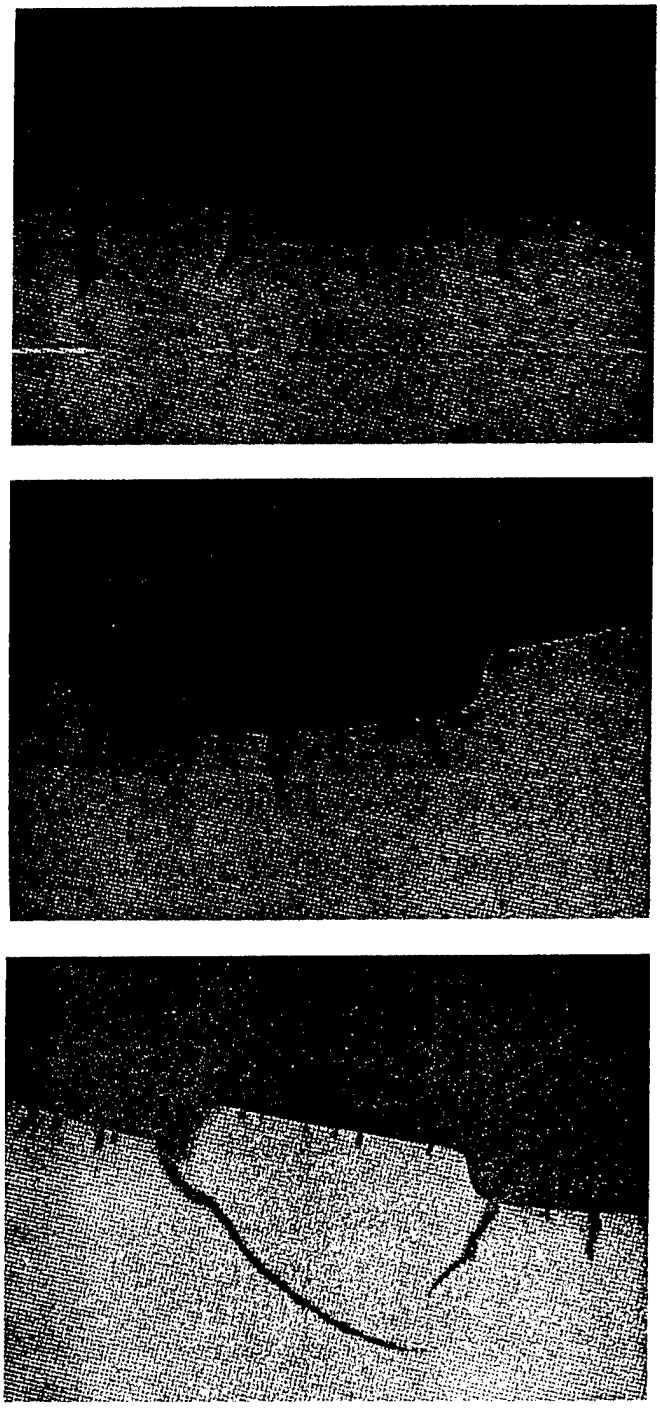

Figure 17. Top, Typical Crack Pattern at 7'' from Breech; Middle, Typical Crack Pattern in Rifling Groove. Crack Length Reflects Total Radial Penetration; Bottom, Large Crack Under Rifling Land, Drive Side, Growing In Circumferential Direction.

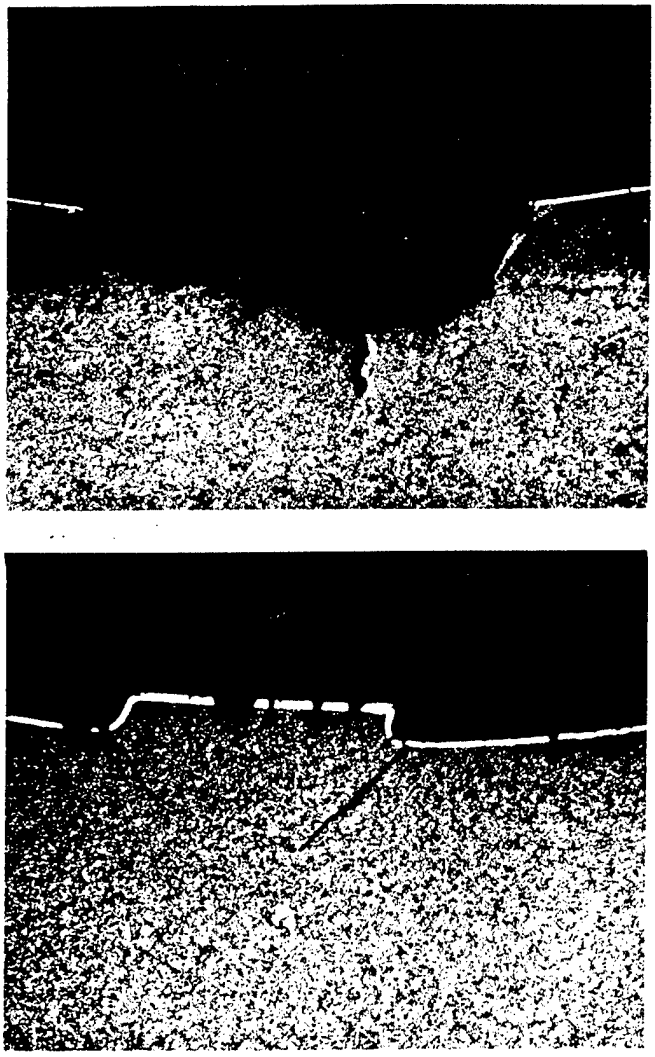

Figure 18. Cross-section at Initiation of Rifling 7.5'' from Breech End in Nitrided Barrel.

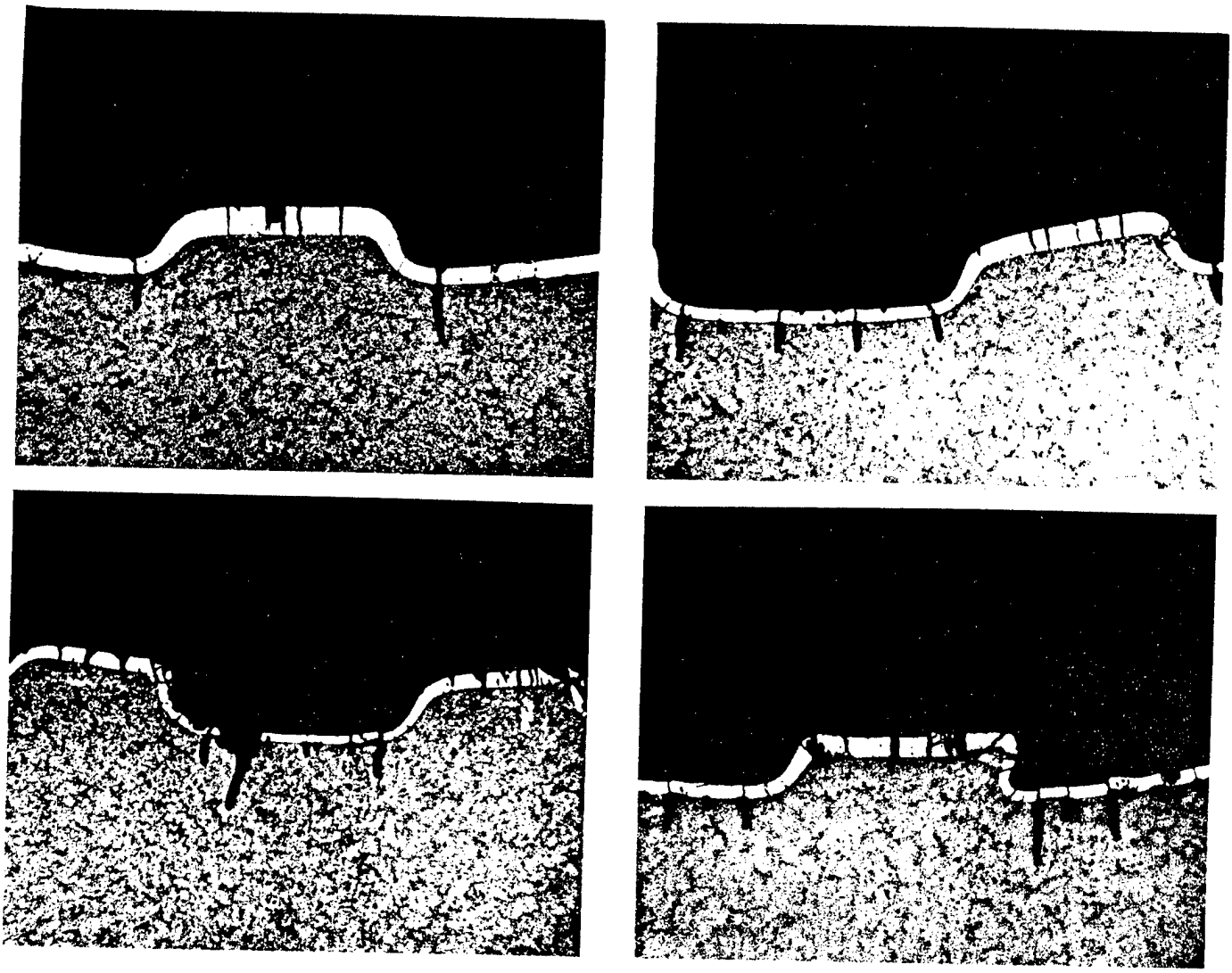

Figure 19. Cross-sections Taken at 20'' from Breech End of 4 Barrels Fired Together. Number of Lands Varies, going clockwise, by 20, 22, 24, and 28.

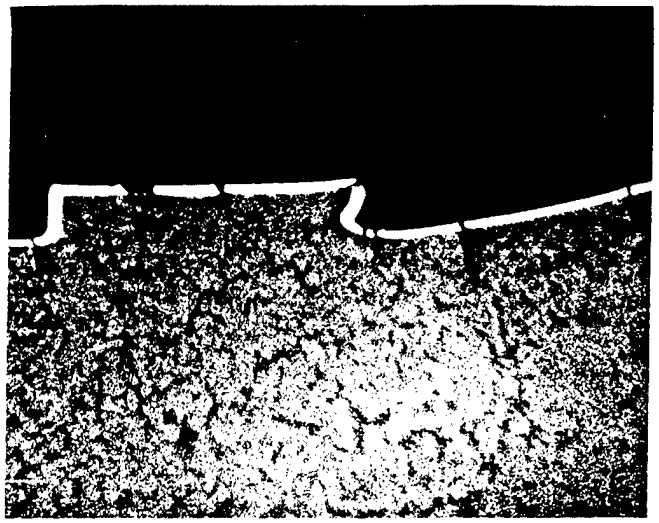

Figure 20. Cross-section Taken at 30'' from the Breech End of LC Chromium Plated Barrel.

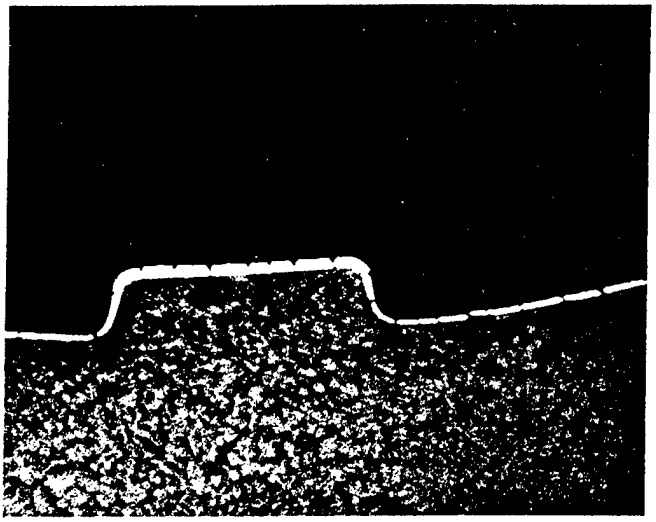

Figure 21. Cross-section Taken at 30'' from the Breech End of HC Chromium Plate Barrel.

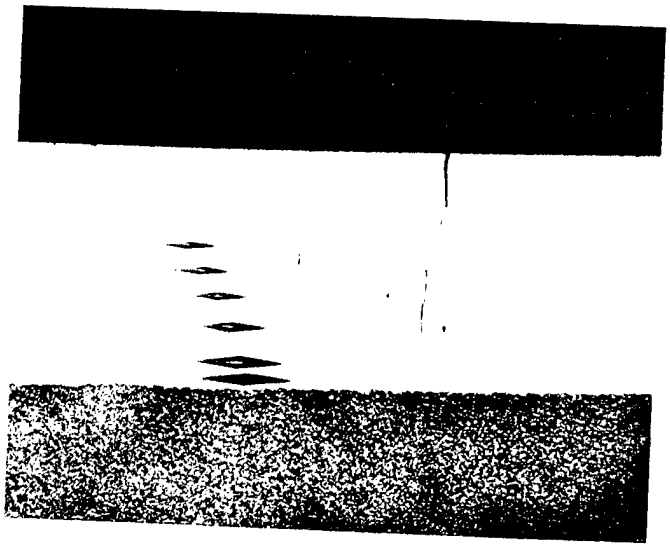

Figure 22. Cross-section Taken Near Initiation of Rifling of Duplex Plated Barrel Showing Relative Thicknesses of LC and HC Plating Layers.

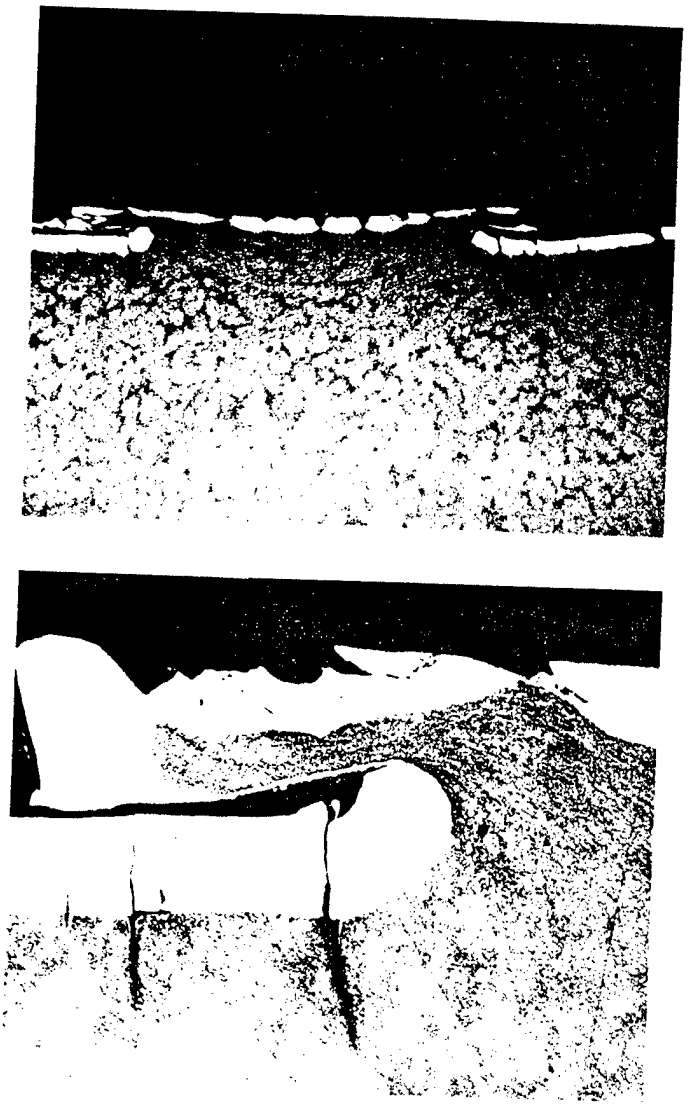

Figure 23. Cross-section Taken at 30'' from Breech of Duplex Chrome Barrel.

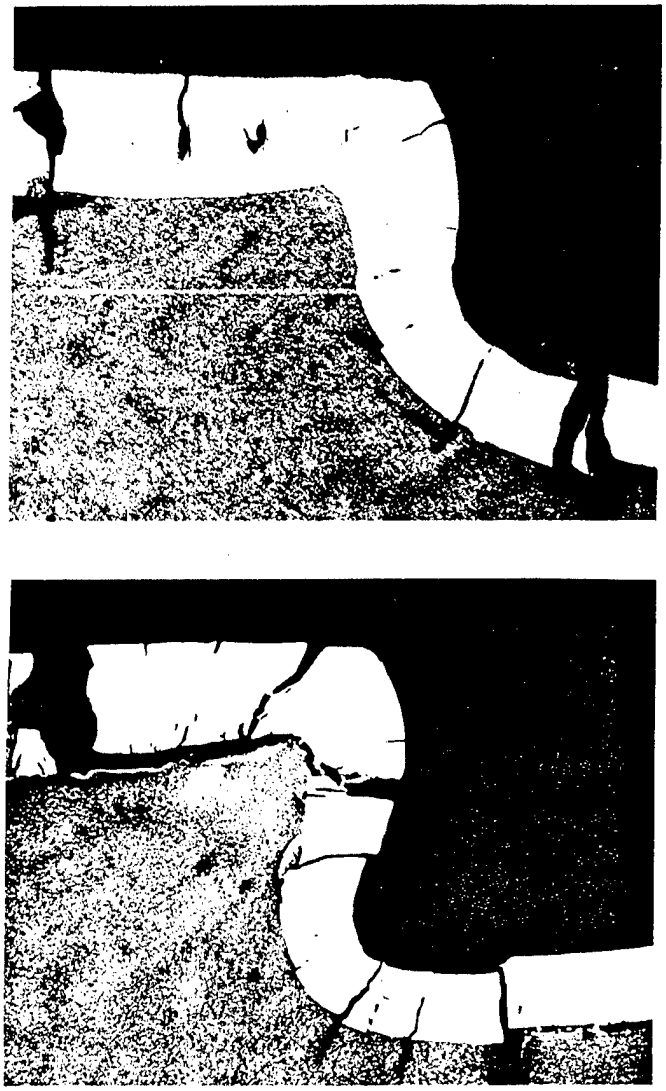

Figure 24. Top, Example of Erosion Parallel to Bore Surface in the Barrel Steel Instead of at the Chrome/Steel Interface; Bottom, Example of Typical Attack at Chrome/Steel Interface.

Figure 25. Example of Crack Blunting Which Occurred as Cracks in HC Chromium Reached the LC Chromium Layer.

Figure 26. Cross-section Taken at 20'' from Breech End of a Thick HC Chromium Plated Barrel.

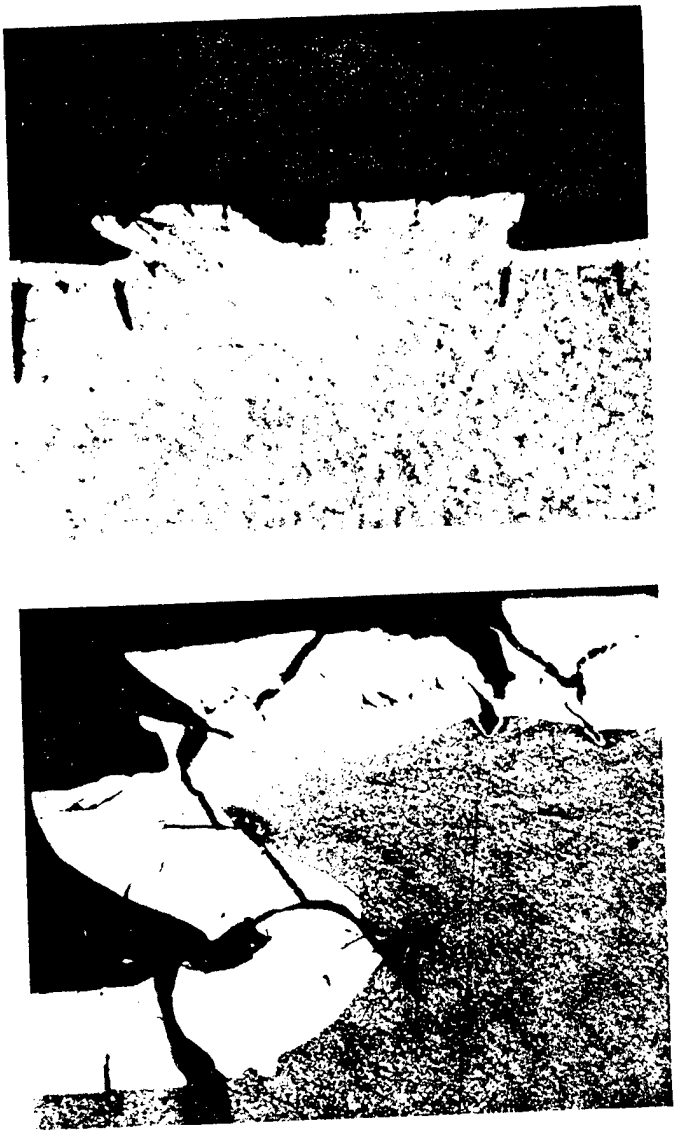

Figure 27. Cross-section Taken at 20'' from Breech End of a Standard Barrel.

Figure 28. Top, Macrograph Showing Typical Down Barrel Groove Chrome Plating Loss; Bottom, Cross-section Through Typical Groove Chrome Plating Loss Area.

(U) WHITE LAYER DEVELOPMENT ON GUN STEEL IN BALLISTIC COMPRESSOR TESTS

R. J. Arnott
W. J. Croft
L. A. Shepard
AMMRC
Watertown, Massachusetts 02172

ABSTRACT

Short, bored gun steel cylinders were fired in the Calspan ballistic compressor using gas mixtures of argon with either N_2, CO plus N_2, or CO. Firing temperatures and pressures matched actual gun propellant detonation. Cylinder sections were studied by microprobe, microscope and X-rays.

Specimens fired in CO containing atmospheres exhibited a multiphase outer white layer and an austenitic inner white layer over the heat affected zone. The alloy content of the outer white layer was the same as the steel. However, the chromium and manganese content of the inner white layer was reduced to less than 10% of the original values. Speculation as to the cause and effect of the changes are offered.

INTRODUCTION

This is a study of the surface effects of hot gas erosion on gun tube steels. The samples were tested in the Calspan ballistic compressor (1) a unit designed to simulate gun barrel erosion under controlled atmosphere, pressure and heat flux. The compressor design was modeled to match the pressure-time curve of an eight inch howitzer over a range of firing conditions.

The processes and effects by which hot gases cause gun tube erosion were summed very succinctly by Ahmed (2). To paraphrase his review for single based propellant gases, the heat and pressure cycling produces:

a. The thermally altered layer (heat affected zone) cycled through the austenite-martensite transition.

b. The austenitic inner white layer, stabilized by carbon and nitrogen, and occasionally partially melted.

c. The multiphased outer white layer consisting of carbides, nitrides, austenite and martensite.

The inner white layer forms before the outer. Dissolved carbon lowers the melting point of the steel and molten products are swept away.

The studies of Kamdar, Campbell and Brassard (3) simulating gun erosion effects and the careful and sophisticated examination of their samples by Fisher and Szirmae (4) brought additional insight to the erosion process. The outer white layer (formed under carbonaceous gas) proved to be a solidified melt layer of cementite dendrites with pools of partially transformed austenite. The inner white layer was coarse grained austenite with cementite in the grain boundaries. Between that and the heat affected zone was a lower carbon austenite-martensite

Approved for public release; distribution unlimited

layer. Thus, the outer white layer, the melt layer is reasonably formed after the inner austenitic white layer.

In both of the above studies the surface effects in actual gun barrels were compared with the simulated erosion samples. Fisher and Szirmae (4) concluded that both melt and wipe-off and the cracking caused by surface intrusion of the low melting, high carbon iron are responsible for the erosion.

The Calspan ballistic compressor studies (5,6,7) are a series of well designed and controlled tests to relate gas chemistry and thermodynamics to gun tube erosion. The samples studied here were tested in an investigation of the role of carburization on erosion, reported by Morphy and Fisher (6). They were fired in gas mixtures containing argon and either N_2, CO plus N_2 or CO.

Specimens were 60 degree segments of the Calspan Shock Tube Gun Samples, cylinders 1-1/2 inches long and 1-1/4 inches in diameter with a 1/2 inch drilled bore and a polished radius inlet (Fig 1). They were prepared from hardened and tempered 4340 steel, and kindly provided by Dr. Joseph A. Lannon, Chairman, AARADCOM Erosion and Wear team.

One might wonder, in view of our present knowledge of surface effects in gun tube erosion, whether there is more to be learned from this type of study. From the questions that arose in the present work, the answer appears to be "yes".

EXPERIMENTAL PROCEDURE

Examples of the four basic types of sample erosion conditions investigated in the Calspan tests (6) were selected for study. The remaining gas in each case was argon.

(1) 45.5% N_2, considered chemically inert.
(2) High temperature and/or considerable mass loss, 10% CO
(3) Carburizing gas mixtures containing either 45.5% CO or 45.5% (CO plus N_2) in several ratios
(4) Carburizing gas mixture with slightly increased pulse duration (45.5% CO plus 4% He).

The temperature, pressure and mass loss for the fifteen specimens tested are given in Table I.

The bore surfaces were first studied at low magnification and then examined in the microprobe at 1mm intervals. Variations of nickel, chromium and manganese content along the surface were measured. Surface phases were determined by X-ray. Then the samples were mounted and polished for microscopic study of the bore edge, further microprobe study and microhardness measurements of prominent features.

Because surface curvature reduces the microprobe count, measurements were initiated at 4 to 5 mm from the polished radius inlet end and followed the bore centerline. Counts of iron, nickel, chromium and manganese were made, as much as possible, at the same spot. A pure standard was counted each time the specimen was traversed. Each reading is an average of two or more values. The measurement error was estimated to be $\pm$ 5%, increasing somewhat for very small values.

Table I. Calspan Shock Tube Gun Test Conditions for Specimens Examined (Reference 6)

Spec. No.	Active Gas	Peak Gas Press. (MPa)	Peak Gas Temp. (K)	Mass Loss (mg)	Heat Input (J/mm^2)
30	10%CO, 5%N_2	224	5007	630	1.29
35	10%CO, 5%H_2	232	3352	694	1.17
39a	30.5%CO, 15%N_2	288	3660	166	1.05
40	45.5%N_2	208	3355	3(incr)	1.12
41	"	285	3678	112	1.26
42	"	335	3865	267	1.23
43	45.5%CO	277	3588	226	1.31
44	"	245	3462	124	--
45	"	213	3322	2	--
48	10%CO, 35.5%N_2	296	3711	123	--
50	20.5%CO, 25%N_2	287	3665	244	1.12
52	45.5%CO, 4%He	250	3479	110	1.12
54	"	236	3422	98	1.15
55	"	219	3351	97	1.10
57	"	210	3268	20	1.14

The microprobe measurement of the standard composition of the 4340 steel used for these samples, averaged over 20 readings, is:

Table II.

Element	Ni	Cr	Mn
Atom %	1.52±.05	0.95±.05	0.83±.05

Too little molybdenum is present to measure compositional variations, and this probe cannot read the lighter elements.

EXPERIMENTAL RESULTS

Low magnification study of the bore surfaces, Fig. 1, shows that surface melting occurred in all specimens examined. Specimen 40, for example, one of the samples showing the least mass loss, exhibits a melt smoothing near the inlet and a decrease in the number and depth of drill grooves. At intermediate temperatures, some of the machining grooves were deepened by erosion, and high temperature and large melt loss produced a completely smooth surface.

Microprobe measurements of nickel, chromium and manganese content along the bore surfaces of five representative samples are shown in Fig. 2. The normal content of each element is shown at the ordinate.

Specimen 40 is typical of samples fired in N_2. The Ni, Cr and Mn contents remained constant along the entire bore, within experimental error, and unchanged from the nominal composition.

Note also that the Ni content of all samples, whether in N_2 or CO atmospheres, remained essentially constant and unchanged. A Ni decrease of as much as 12% was

often recorded on the first reading.

In a CO atmosphere, the bore surface concentrations of Cr and Mn exhibited considerable variation. Measurements fluctuated from the nominal Cr-Mn contents down to as low as 5% of those values. In general, low values were recorded for first readings at 4 or 5 mm from the inlets concentrations increased in the 7 to 12 mm region, and then declined again toward 20 mm . Concentration peaks were frequently recorded as in sample 57 at 16 and 20 mm.

The only exception to this general trend in CO was Specimen 54. The Cr-Mn concentration was almost uniformly high, and close to the nominal composition.

Microexamination of the surfaces on edge showed the expected differences between samples fired in N_2 and CO gas. For N_2 gas, the heat affected zone extended right to the bore surface. For CO gas, both a continuous white layer of varying thickness, and a discontinuous melt layer covered the heat affected zone.

In most cases, for CO containing gases, the white layer was about 1μm thick near the inlet, 1/2 μm in the 7 to 12 mm region and increasing to 1 to 2μm beyond. For samples 52 to 57, the 4% He addition in the gas increased the pulse length and raised the surface temperature. These samples exhibited a 10 to 20μm thick white layer, starting 3 mm from the inlet, extending roughly 2 mm and thinning rapidly thereafter, Fig. 3.

The melt layer, blown down the tube, deposited over the white layer in machining grooves and irregularities, Fig. 4a. The deposit is porous and dendritic, Fig. 4b, and probably consists of the mixture of carbides, austenite and martensite noted by Ahmed (2) and Fisher (4). At the highest temperature and pressure (eg. sample 30) no melt layer was retained. Usually, however, it was found in grooves beyond 10 mm, and often as a continuous layer beyond 30 mm.

The mystery of the varying surface composition was unraveled when it was realized that a point by point correlation exists between the Cr-Mn variation and the white layer - melt layer distribution. Where the white layer is 1-2μm or thicker, the Cr-Mn content of the surface decreases toward zero. However, the microprobe beam has a penetration depth of about a micrometer. Therefore, for a 1/2 μm white layer thickness, the beam penetrates to the heat affected zone resulting in a higher average Cr-Mn reading. This behavior is seen in Specimen 30, Fig. 2 where the white layer thins in the 4 to 8 mm region and thickens beyond, and to a lesser extent, in Specimen 50.

Where the melt layer covered the white layer, the surface concentration of Cr-Mn approached that of the steel. For example, in Specimen 57, pools of melt formed in the grooves at 15.4 and 19.3 mm, and an increased Cr-Mn concentration is observed at these points. Specimen 54 is an unusual case where a well developed white layer is covered by a melt layer from 6.6 mm on, resulting in an almost uniformly high Cr-Mn surface content.

Microprobe measurements of composition of the white and melt layers in edge section corroborated these conclusions. Because of the beam width, observations were confined to selected areas over 5μm thick; the thick white layer near the inlets of samples 54, 55 and 57, and the melt layer groove pools and a large melt bead on sample 45. However, the presumption that these results are also valid for

thinner layers is in keeping with the overall observations.

The white layer was found to contain less than 10% of the original Cr and Mn content of the steel. The Ni content was unchanged. The alloy content of the melt layer, on the other hand, was the same as the steel (but the carbon content was probably much greater).

The white layer from X-ray and microhardness measurements, proved to be a comparitively soft, stabilized austenite, in keeping with previous observations (2,3,4). The hardness of the melt layer matched that of the heat affected zone; both were greater than the tempered in artensite interior.

Surface X-rays of samples fired in both N_2 and CO showed a roughly 50-50 mixture of austenite and martensite. Thus, within the penetration depth of the X-rays, about 5μm, austenite is stabilized by the diffusion of either N_2 or CO.

DISCUSSION

Explanation of the experimental results should allow the rationalization of the following points:

a. How are Cr and Mn depleted in the white layer while the Ni content remains constant?

b. Why are Cr and Mn lost in the white layer but not in the melt layer?

c. Since surface austenite is stabilized in both CO and N_2 atmospheres, why isn't a white layer observed on samples tested in N_2?

A most attractive solution to the problem of white layer formation fulfills the above criterion and is in agreement with Ahmed's review (2) cited in the introduction. It is proposed that both the white and melt layers grow from the high carbon surface melt with partitioning of the solutes. The thick white layer portion of Specimen 54 which seems to have been caught in this growth process, Fig. 5, is offered as evidence. The stout austenite dendrites grow from the surface, and the randomly nucleated melt is frozen above.

In sequence, the temperature-pressure pulse produces a liquid phase with a high dissolved carbon content. The austenitic heat affected zone offers the source for austenite nucleation from the molten surface layer. Closely spaced, thick dendrites grow rapidly into the melt due to the large temperature gradient. The carbide formers, Cr and Mn are rejected into the high carbon, low melting point liquid; Ni, the austenite stabilizer is retained in solution in the growing dendrites. The liquid is blown down the tube.

The white layer forms in CO because of the large melting point depression associated with dissolved carbon. Solution of nitrogen in steel does not, as far as can be determined, greatly lower the melting point.

If the above explanation were correct in every detail, an elevated Cr-Mn content would be found in the melt layer. This is not generally true, although occasional spots, high in Mn were observed beyond 10 mm.

CONCLUSIONS

White layer development was studied in 4340 steel ballistic compressor specimens fired above the surface melt temperature in CO containing gases. Phase and composition changes were identified by microscope, microprobe and X-rays. The following conclusions were reached from the study.

1. The austenitewhite layer which covers the heat affected zone contains the normal Ni content but less than 5% of the original Cr and Mn content of the steel.

2. The high carbon, dendritic melt layer which solidifies discontinuously over the white layer contains the same Ni, Cr and Mn content as the steel.

3. The composition difference between the two layers probably arises from the partitioning of the Cr and Mn into the lower melting carbide liquid. The austenite retains the Ni in solution as it solidifies.

ACKNOWLEDGEMENTS

The authors wish to thank Dr. Paul J. Ahearn for his helpful advice, and the staff of the metallography lab, Ray Middleton, Andrew Zani and Carolyn Jones for their competent assistance and patient tolerance.

REFERENCES

1. Vassalo, F. A. "The Shock Tube Gun" PII 268, Proceedings of the Tri-Service Gun Tube Wear and Erosion Symposium, March 1977, J. P. Picard and I. Ahmed, editors.

2. Ahmed, I. "The Problem of Gun Barrel Erosion, An Overview", PI-1, Proceedings of the Tri-Service Gun Tube Wear and Erosion Symposium, March 1977.

3. Kamdar, M. H., Campbell, A. and Brassard, T. "A Metallographic Study of White Layers in Gun Steel", Report No. ARLCB-TR-78012, Benet Weapons Lab., Watervliet Arsenal, August 1978.

4. Fisher, R. M. and Szirmae, A. "Characterization of White Layer Formations on a Fired Cannon and on Laboratory Simulation Samples", Preliminary Report on Contract DAAA22-81-C-0121, AARADCOM, U. S. Steel Research Laboratory, March 1981.

5. Fisher, E. B. and Morphy, C. C. "The Role of Oxygen in Gun Barrel Erosion and Cracking", Calspan Corp., Contract Report ARBRL-CR-00427, April 1980.

6. Morphy, C. C. and Fisher, E. B. "The Role of Carburization in Gun Barrel Erosion and Cracking", Calspan Corp., Contract Report ARBRL-CR-004, September 1980.

7. Morphy, C. C. and Fisher, E. B. "Gas Chemistry Effects on Gun Barrel Erosion, A Shock Tube Gun Investigation", Calspan Corp., Contract Report ARBRL-CR-00481, June 1982.

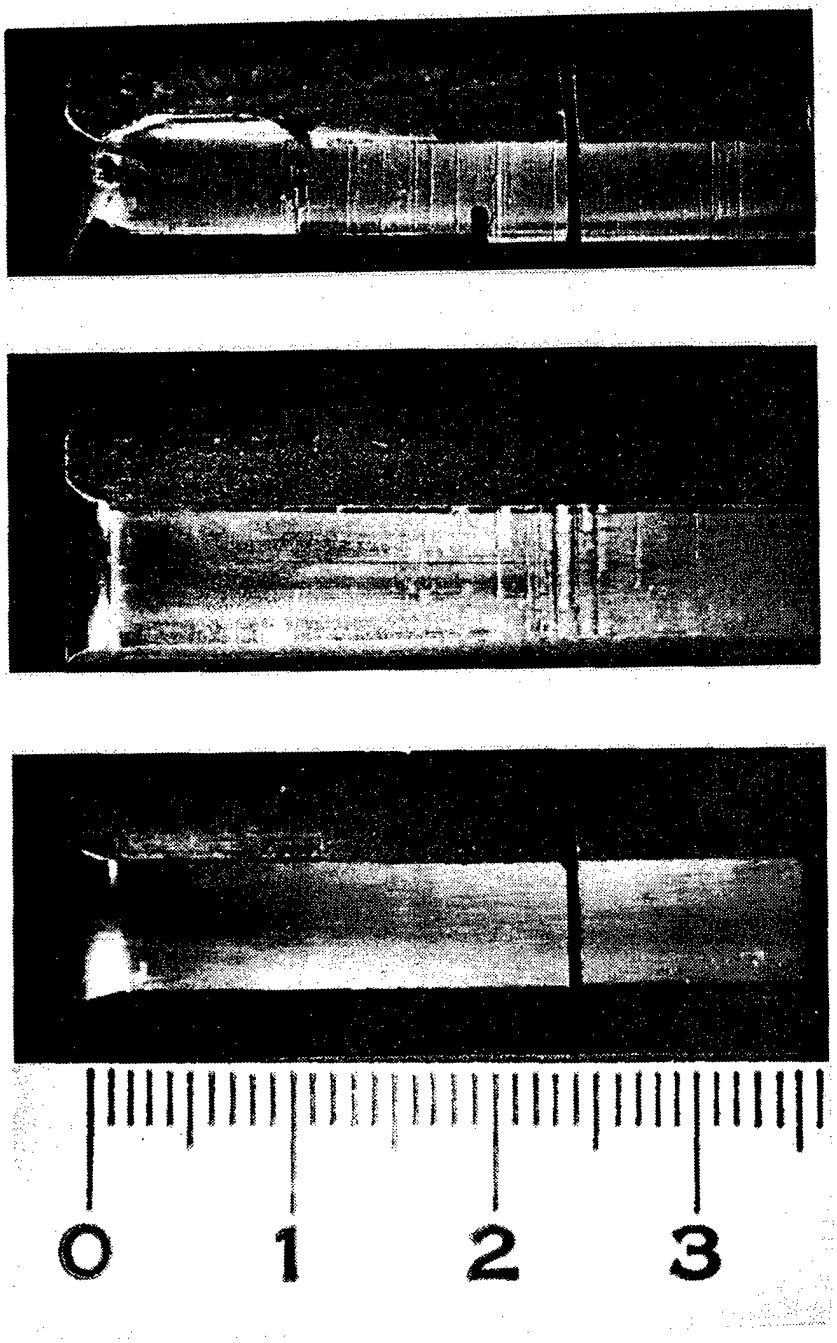

Figure 1. Macrographs of specimens 40 (top), 44, and 30 showing progressive erosion with increasing temperature.

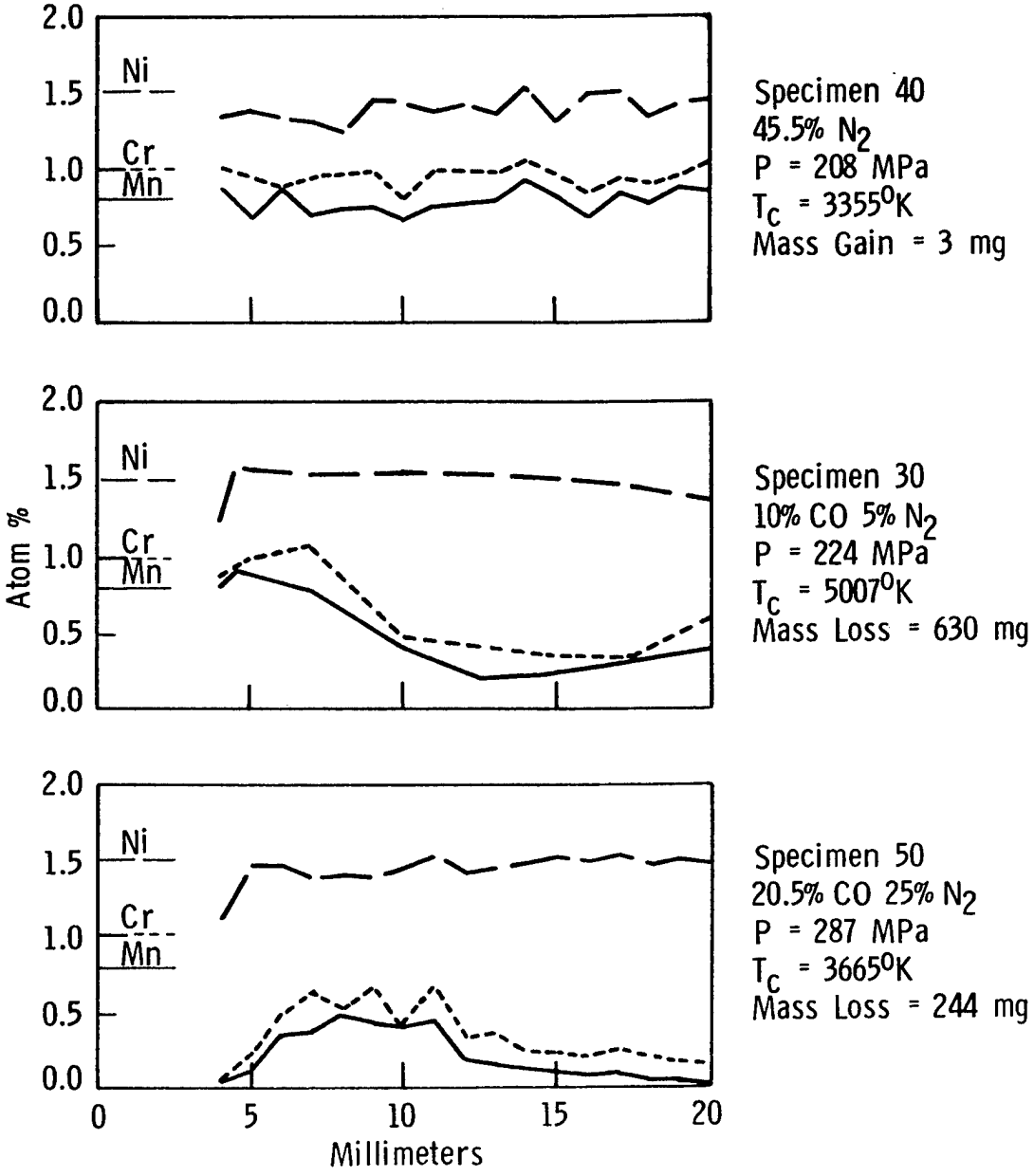

Figure 2a. Variation in surface concentration of Ni, Cr, and Mn simulated gun tube erosion samples.

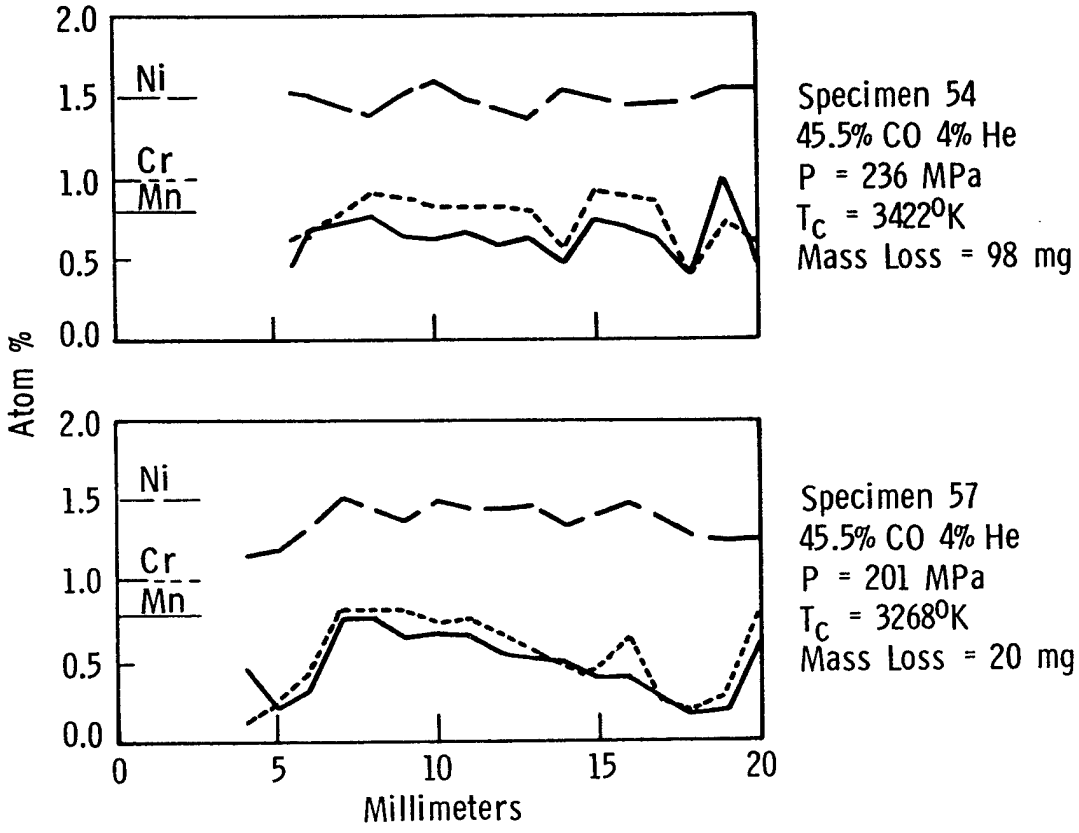
2.0
1.5
1.0
0.5
0.0
Ni
Cr
Mn
Atom %
Specimen 54
45.5% CO 4% He
P = 236 MPa
T_C = 3422°K
Mass Loss = 98 mg
Specimen 57
45.5% CO 4% He
P = 201 MPa
T_C = 3268°K
Mass Loss = 20 mg
0
5
10
15
20
Millimeters

Figure 2b.

Figure 3. Thick white layer near inlet specimen 55. Mag. 1000X

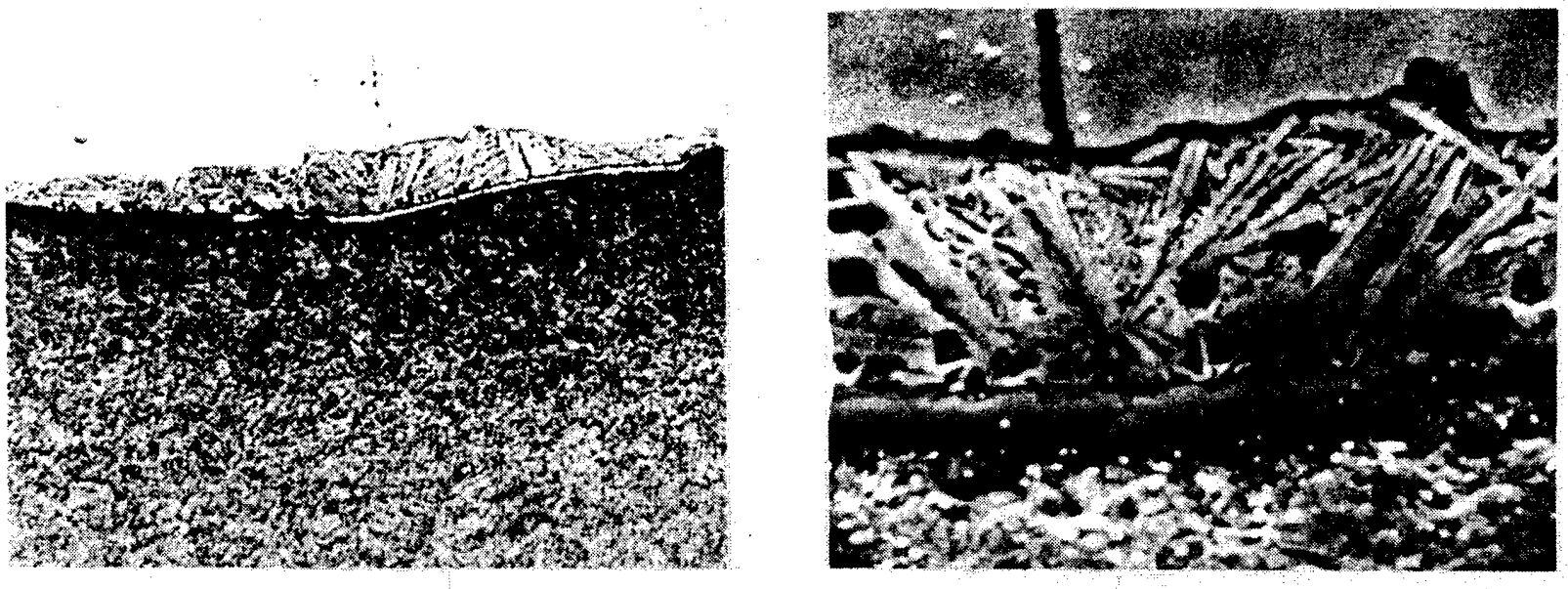

Mag. 1000X

Mag. 5000X

Figure 4. Melt layer deposit over white layer specimen 45.

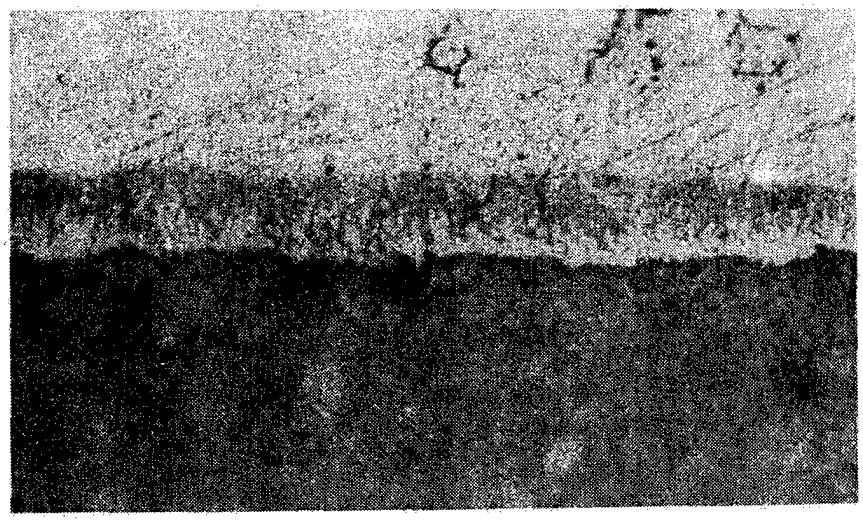

Mag. 800X

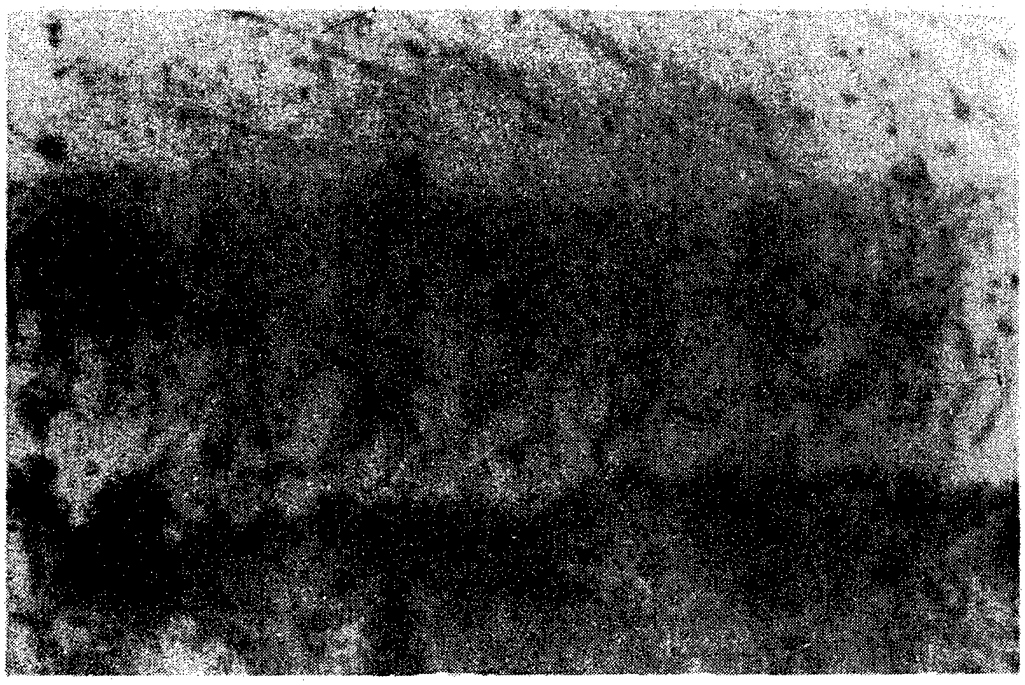

Mag. 2400X

Figure 5. Thick austenite dendritics growing from heat affected zone.

METALLURGICAL CHARACTERIZATION OF THE ERODED BORE SURFACE OF A HIGH PERFORMANCE BARREL

K. Iyer
Metallic Materials Branch
Materials and Manufacturing Technology Division
Fire Control and Small Caliber Weapon Systems Laboratory
US Army Armament Research and Development Command
Dover, New Jersey 07801

and

A. Schumacher and H. Weiss
Fraunhofer-Institut fur Angewandte Materialforschung (IFAM)
Lesumer Heer Str 36
2820 Bremen, West Germany

ABSTRACT

The bore surface region around the gas ports of test fired rapid fire 27mm caliber gun barrels was metallographically examined by the tapered section technique. Unique metallographic features were recorded by optical microscopy. Scanning electron microscopy was also employed wherever edge rounding precluded clear focusing by optical microscope and wherever greater clarity could be obtained at high magnifications. Notwithstanding conditions of nonequilibrium rates of heating and cooling and dissimilarities in the degree of attack between regions of bore surface near the breech end and gas port, generalized hypotheses on temperature effects at the bore surface and mechanisms of material removal in unplated high performance cannons are presented. Suggestions for future work are indicated.

INTRODUCTION

The bore surface of a rapid-fire gun barrel, especially near the breech end, is exposed to high temperatures, stresses and chemically aggressive environment. Rapid heating and cooling, repetitive loading and the chemical reaction of propellant gases with the barrel material contribute to severe erosion of the barrel. Metallurgical examination of test-fired barrels by visual examination of the eroded surface, macroscopic and microscopic observations on fractures as well as polished and etched sections, microhardness measurements and x-ray and elctron diffraction techniques have been used in the past to identify the transformation products of the barrel material in the eroded region of the barrel (1) and (2)*.

The erosion in test-fired, 27 mm, MRCA barrels were metallographically examined. The barrel had no surface treatment before test firing and was made of low alloy steel (containing about 0.35% C, 3% Cr, 1% Mo and 0.3% V) in the quenched and tempered condition. The thin bore surface region is unetchable in the presence of the base material and is entirely too thin and gets a bit rounded during polishing to allow metallographic characterization. The thickness of this region is about 10 microns. The numerous and complex variables,all simultaneously in action at and near the bore surface make it extremely difficult to characterize the damage in this region. The small thickness available for conventional

* Numbers in parenthesis indicate references at the end.

metallographic preparation does not help the situation. And yet, this is the most interesting region because, this is the layer of material which is presented to the following round.

Tapered section metallography of the bore surface to enlarge artificially the bore surface region is an improvement over conventional sectioning and polishing. A location in the barrel which experiences severe erosion is where the hot gases enter the gas ports. Gas flow patterns and stream velocities are different in this region from those near the breech and heat flow and temperatures attained are bound to be different: yet the erosion pattern, though more severe, is not unlike pockets of erosion found near the breech end. These erosion pockets are usually initiated by an inhomogeneity of one kind or another which results in partial lack of obturation followed by streaming of hot gases past the projectile. This accentuates erosion in these pockets. Hence for reasons of understanding erosion the bore surface region near the gasport was metallographically examined by the tapered section technique.

EXPERIMENTAL TECHNIQUE

Figure 1 is a photograph of the gas port regions of two barrels of the 27mm Gun, one of which had experienced a lot less number of rounds than the other. The gas port region of a barrel which had experienced number of rounds somewhere in between those of Figure 1 was subjected to detailed metallography. A longitudinal specimen containing the bore surface and a portion of the gas port was lightly polished without mounting in plastic. The rounding effect customary in metallography was enough to remove the oxide film on the curved surface around the gas port. This specimen, when etched, allowed an examination of a few locations by scanning electron microscope. Then the specimen was mounted and progressively polished and etched to reveal microstructural details around the gas port. The region immediately ahead of the gas port turned out to be most interesting. Standard procedures of metallography were employed to record the details. Wherever optical focussing was limited by edge rounding or when higher magnification was necessary for clarification scanning electron microscopy was employed. A schematic to illustrate the application of tapered section technique is shown in Figure 2.

METALLOGRAPHIC OBSERVATIONS

Figure 3 is a macrograph of the highly polished and etched surface of the unmounted specimen. The curvature of the specimen around the gas port precluded optical metallography. Figure 4 is a low magnification SEM picture which shows from right to left the unpolished surface with oxide, the transition and the surface from which the oxide had been polished away and the bare metal etched. Figure 5 shows two SEM photographs of the latter region at higher magnifications. Melting at the grain boundary and contraction and separation from the grain are recognizable. Also noticeable are needles of martensite within the grains and microfissures in some of the needles.

Firuge 6 is a macrograph of the surface of a mounted, polished and etched specimen of the bore surface around the gasport. The direction of the projectile travel is shown to clarify orientation. Figure 7 is a photomicrograph at 100X of the region indicated by a rectangle in Figure 6. The top edge of the banded

region shows no sign of grain coarsening. When curvatures and magnifications are accounted for, the depth location of the top of the banded region is only 8-10 microns. The material at this depth reacted as if it experienced heating up to complete austenitization of this steel and cooling at a rate rapid enough to cause complete martensite to form in the alloy-rich bands (light) and lower bainitic transformation in the alloy-poor bands (dark).(3). Figures 8 and 9 are micrographs of this region at a higher magnification. Micro hardness values of VPN 835 and 685 were measured for the light and dark bands respectively. No further analysis of this region was made. The rest of the analysis will deal with the area between the top of the banded region and the gasport edge of the specimen.

Figures 8 and 9 are good examples of the near bore surface region which, under conventional transverse sectioning metallography would have appeared as the unetchable bore surface layer of about 8-10 micron thick. Four distinct layers or subregions can be identified. The region closest to the bore surface shows severe grain boundary rupturing and a network of precipitates within the grains. Figure 10 shows two SEM photographs of this layer at high magnifications. The absence of any other detail in this layer is noteworthy. A similarity with the microstructure of sensitized austenitic stainless steels is indicated. (4).

The second layer is similar to the first with the exception of the presence of streaks of about 0.8 micron in width and several grain diameters in length. These streaks or needles were not noticeable in the unetched specimen. The needles were completely unetchable. They run through grain boundaries without changing direction. Figure 12 is a photomicrograph of these needles when the specimen was etched with an etchant containing hydrogen peroxide. This was the only etchant (5) which showed any detail at all inside the needles other than their clear boundaries. Figures 13 and 14 are SEM photographs which show the behavior of these needles when a shear or a rupture runs across them. Signs of deformation (lips) in the needles indicating ductility are noticeable. The needles are not wide enough to make a microhardness indentation. No difference in the chemical compositions of the needles from the surrounding material could be found by the microprobe.

In an attempt to identify the needles, the specimen was treated in vacuum to 520°C, maintained at temperature for 10 minutes and furnace cooled. The specimen was repolished and etched with picral. Figure 15 is photomicrograph after "tempering". The fact that after "tempering" the needles are etchable by picral is interesting. An SEM photograph after gold deposition of the specimen surface is shown in Figure 16.

The third layer is a necklace of carbide precipitation clearly noticeable in Figure 9 (Sodium Carbonate Solution etching) and the next layer is a carbon depleted layer, again clearly recognizable in Figure 8 (picral etching). Microhardness measurementw with 25 gms load show a hardness of about 530VPN between the bore surface and the top of the banded region.

DISCUSSION

Heat transfer calculations for the 27mm cannon show that the bore surface temperatures could easily exceed the melting point of the steel. The thick barrel wall acting as a heat sink and the exposure of the thin bore surface layer to the ambient during pauses cause rapid cooling. Analysis of propellant gases and

examination of the bore surface for the identification of chemical elements have shown the possibility of diffusion of nitrogen into the bore surface (6). Based on these facts an explanation of the observed metallographic features will be attempted.

The grain boundary melting is caused by the lowering of the melting point of steel by either the diffusion of elements like nitrogen and carbon or segration of minor alloying elements (impurities, S, P etc.,). If one remembers that the time interval between rounds is of the order of a tenth of a second whereas the passage of a projectile through the barrel takes only a couple of milliseconds, one can appreciate how the molten grain boundary region can cool rapidly enough to contract and separate from the grain. It is also clear how this phenomenon would facilitate the next stream of gases to pull grains of material from the bore surface. The acicular features within the grains show microfissures in them. They are identified as martensitic needles formed by rapid cooling during which autotempering could not have taken place. It is not surprising that such a region was a rare find because it is to be expected that such regions would have been washed out.

The top of the banded region in Figure 8 is deemed significant. Because of the absence of grain growth and the presence of quenched transformation products an estimate of about 900°C at a depth of 8-10 microns from the bore surface is hypothesized. Equilibrium rates of heating and cooling are not experienced by the cannon during firing. The temperature estimates are based on material reaction to an environment. Only statements such as "the material reacted as if it was exposed to" are possible. Such estimates are significant to the barrel material developer.

The region between the top of the bands and the bore surface is a layer of steep thermal gradient from about 900°C to the melting point. The high temperature facilitates diffusion of nitrogen and dissolution rather than the formation of nitride. Upon cooling the high concentration of nitrogen stabilizes austenite. The material damage appears as typical sensitization with the alloy carbides segregating to the grain boundaries and subgrain boundaries. The formation of unetchable needles with their observed characteristics is difficult to explain without further study. Based on the fact that tempering rendered them etchable by simple picral it is tempting to identify them as martensite of some form. The sequence in which the reaction products formed may explain why grain boundaries are discernible within these needles.

The formation of a layer rich in carbides followed by a layer of ferrite rich region near the bore surface suggests the possibility of uphill diffusion of carbon. This layer is bounded on one side by a nitrogen rich layer and on the other a martensitic layer. The diffusion kinetics in this region is complex, to say the least. Diffusion kinetics under dynamic conditions need to be understood before an explanation can be offered. Auger analysis and high resolution microscopy of longitudinal fracture in this region will go a long way toward answering several questions.

SUMMARY AND CONCLUSIONS

Tapered section technique was applied to the bore surface region around the gasport of a 27mm cannon toward metallographically identifying erosion damage at and very near the bore surface. The technique provided an enlarged area for examination. Based on a knowledge of the service environment of the cannon, an explanation of the

observed metallographic features has been offered. Material removal by grain boundary melting at the surface and sensitization in the subsurface is postulated and an effective temperature of about 900°C at a depth of 8-10 microns below the bore surface is estimated.

RECOMMENDATIONS FOR FUTURE WORK

1. Similar work must be carried out on specimens from cannons which have experienced different number of rounds of fire, but at the same schedule, to determine the sequence of formation of the phases.

2. Auger electron microscopy and fractography of a longitudinal fracture of the region between the bore surface and the top of the bands will be useful.

3. Laboratory controlled experiments in which steel surface could be heated and cooled repetitively and rapidly, followed by careful metallography will assist the understanding of diffusion kinetics in the bore surface region.

ACKNOWLEDGEMENT

The work was performed during K. Iyer's tenure at IFAM as an exchange scientist from ARRADCOM, USA. The authors wish to acknowledge with gratitude Frau Vogel's assistance in taking the scanning electron micrographs and the discussions with many colleagues in IFAM Germany and ARRADCOM USA.

REFERENCES

1. Hyper Velocity Guns. Summary Technical report of NDRC (1946). Chap. 12.

2. K.Iyer and W. Ebihara "Metallurgical Characterization of Eroded Gun Barrels". Paper presented at the Wear and Erosion Symposium (1977) at Dover, NJ.

3. A. Schrader and A. Rose. De Ferri Metallographia, Verlag Stahleisen m.b.H, Dusseldorf 1966.

4. Atlas of Microstructures. Metals Handbook. Vol. 7. Page 133. Plates 1071, 1072 and 1073. American Society for Metals, Cleveland, Ohio.

5. M. Beckert and H. Klemm. Handbuch der metallographischen Atzverfahren, VEB Deutscher Verlag Fur Grundstoffindustrie, Leipzig 1962.

6. Private Communications with Dr. V. Schlett. IFAM, Bremen, Germany.

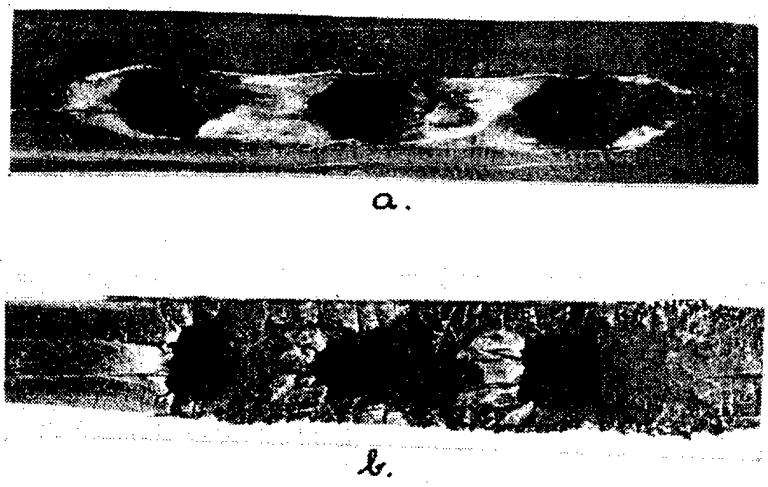

Figure 1. Appearance of the gas port region of two test fired 27mm barrels.

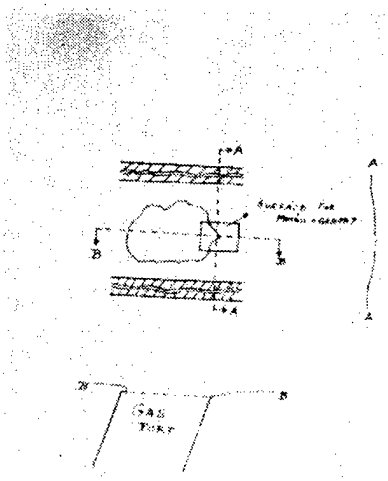

Figure 2. Schematic illustration of tapered section technique.

Figure 3. Macrograph of gas port region, polished and etched.

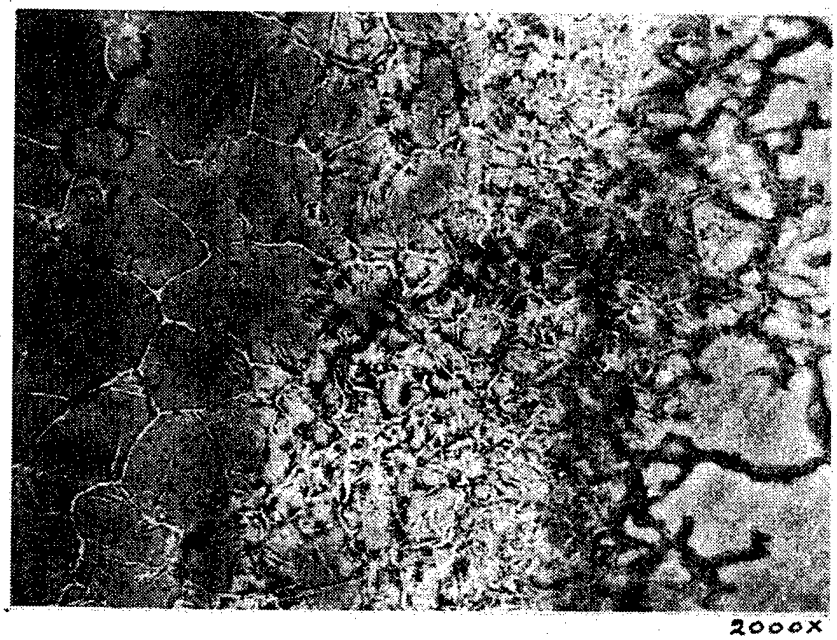

Figure 4. SEM Photograph of region A in Figure 3.

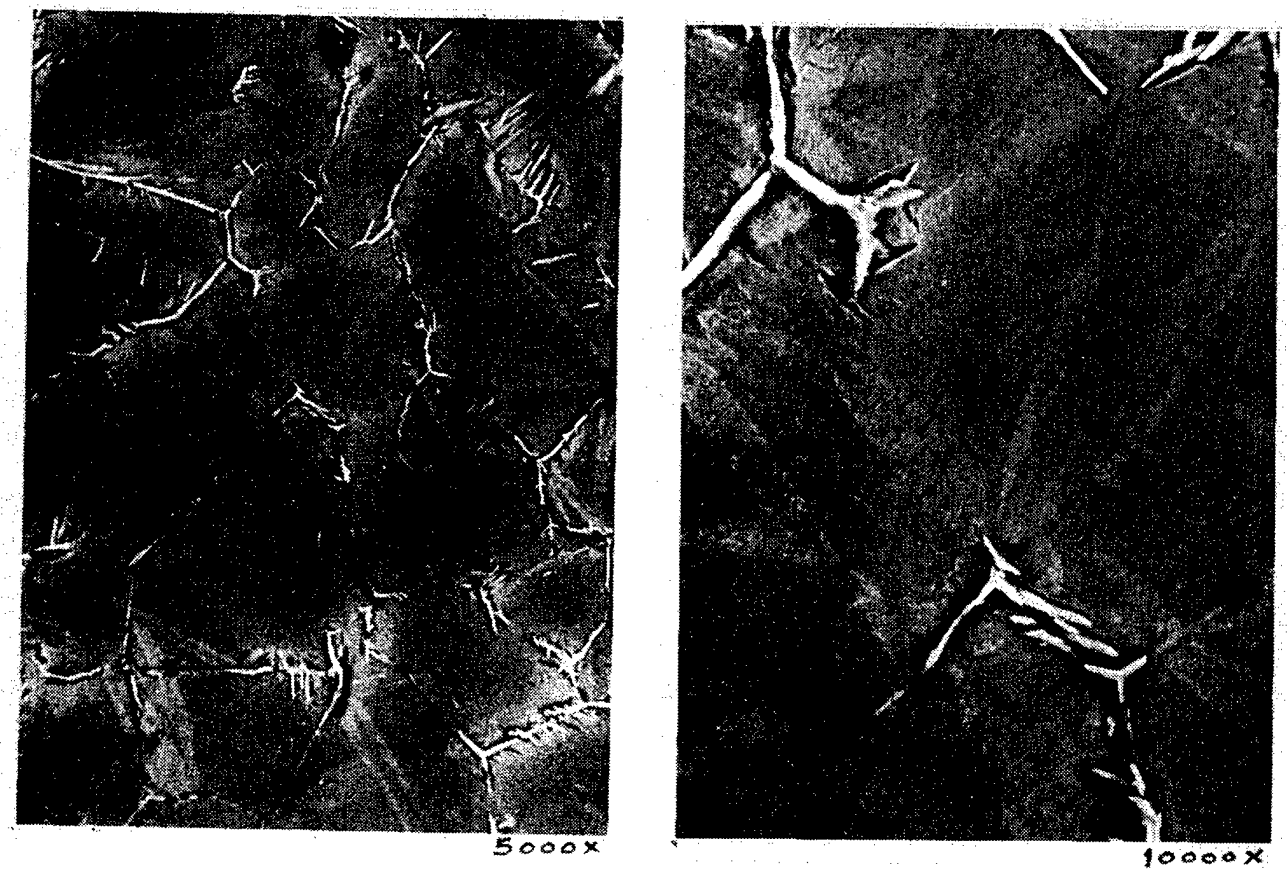

Figure 5. Scanning electron micrographs of the edge region of a gas port.

Figure 6. 8X

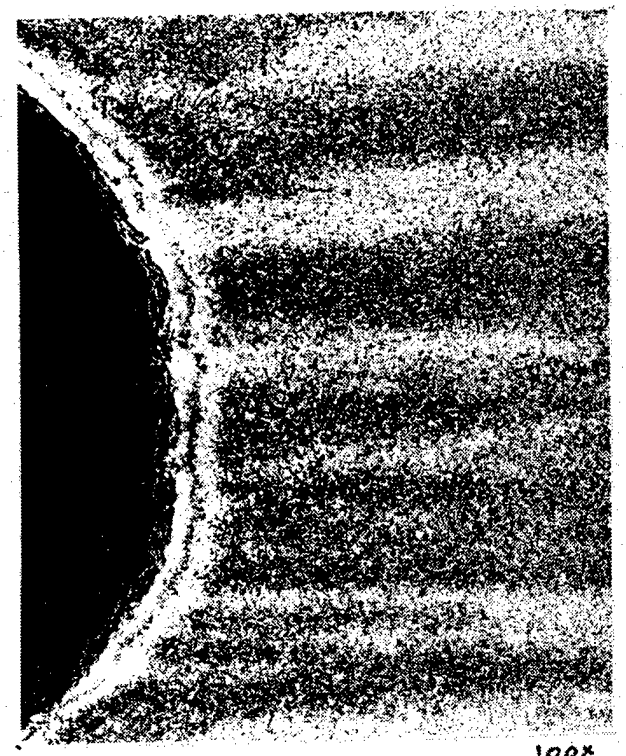

Figure 7. 100X

Figure 8. 1000X

Figure 9. 250X

Optical metallography of the forward edge region of the gas port.

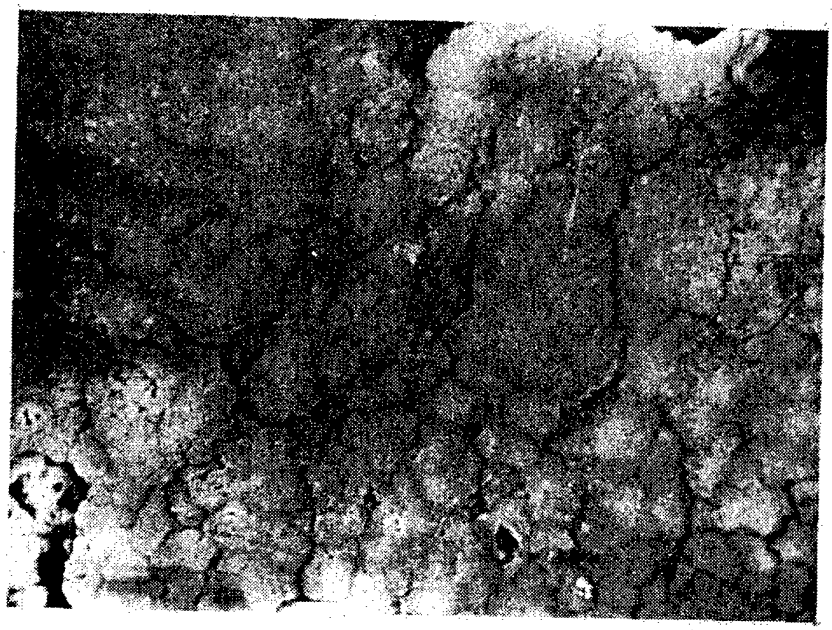

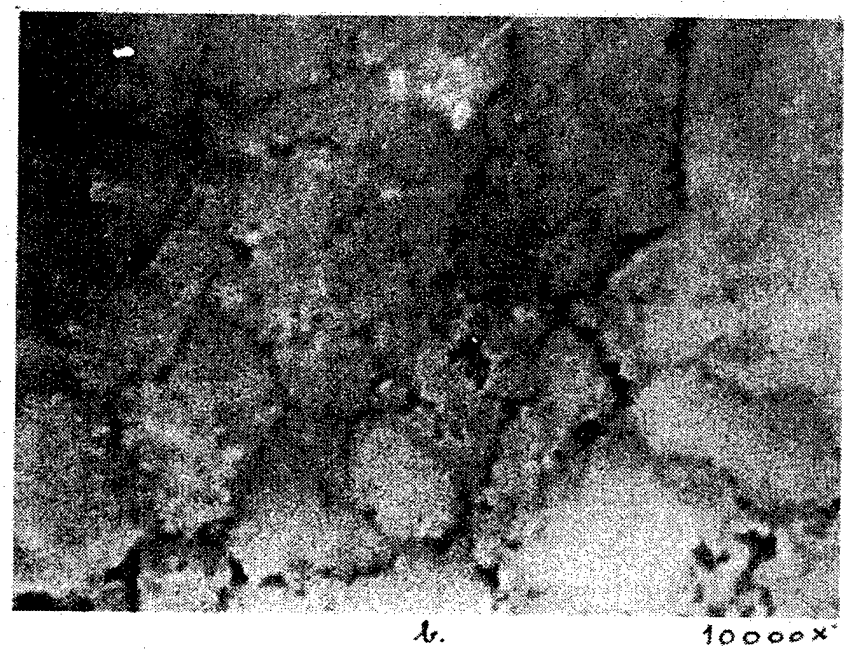

Figure 10. Scanning electron micrograph of the "ruptured grain" layer.

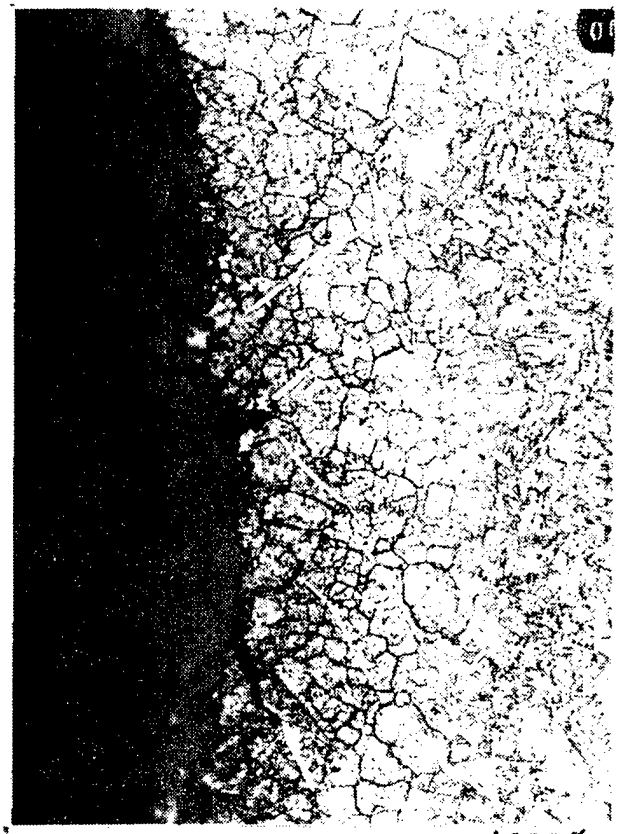

Figure 11. 1000×

Figure 12. 1000×

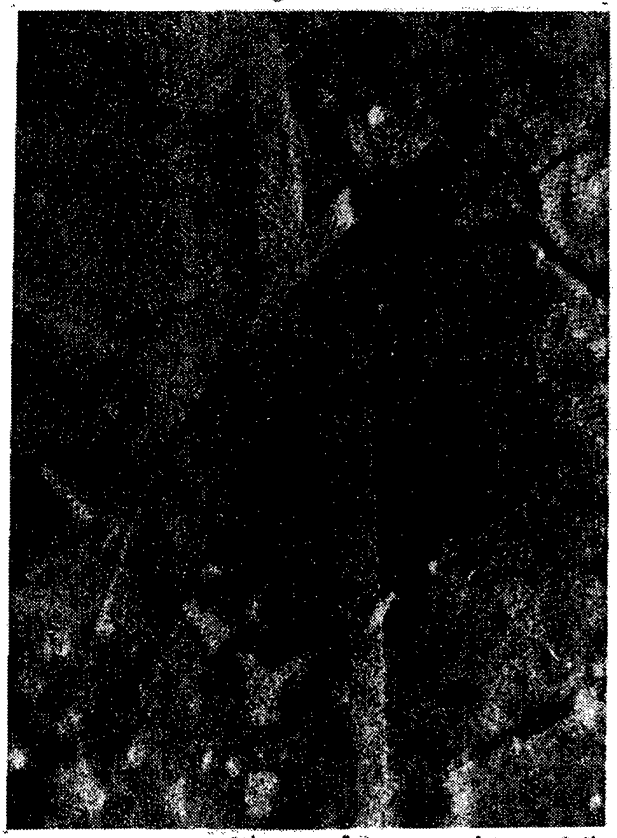

Figure 13. 10,000×

Figure 14. 10,000×

Optical and scanning electron micrography of the "NEEDLES".

Figure 15. Appearance of the needles after tempering.

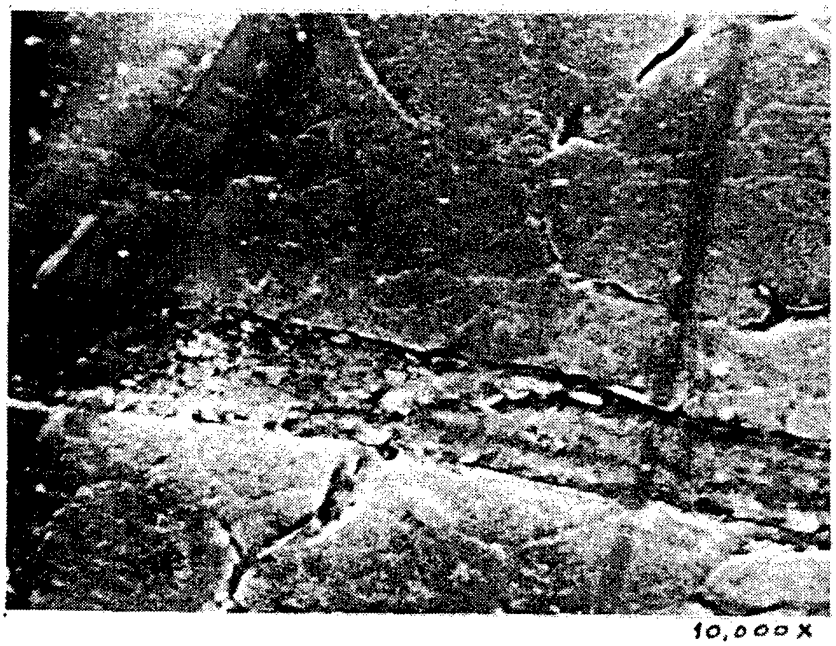

Figure 16. Same as above in SEM. (Specimen sputtered with gold)

AUGER ELECTRON SPECTROSCOPIC ANALYSIS ON GUN TUBE EROSION

Sin-Shong Lin
Materials Characterization Division
Organic Research Laboratory
Army Materials & Mechanics Research Center
Watertown, Masschusetts 02172

ABSTRACT

The eroded surface of three gun tubes, 20, 47 and 105 mm calibre, have been examined with the surface analytical technique of Auger electron spectroscopy. The instrument used was PHI model 548 ESCA/AES manufactured by Physical Electronic Industries. The chemical compositions of the surface as well as sub-surface layers were determined semi-quantitatively from the Auger peaks in the spectra. The depth profiling of the eroded surface was accomplished either by argon ion sputtering or by mechanically tapering a cross-section of the gun tubes.

The chemical elements present on the top surface layer depend largely on the ammunitions used in firing. Two groups of chemical elements were detected from these analyses. The first group, which consisted of Ba, Be, P, Pb, Cl, Cu and Zn(not in 105 mm), is deposited with no depth penetration into the gun body. They are believed to be less corrosive and easily blown away by exploding propellant gases. The second group of chemical elements such as S, K, C, Ca, N(in 47 mm), O, Fe(in 105 mm) and Zn(in 105 mm) is the elements which participated in the erosion of the gun tube by processes such as oxidation(O), carburization(C), nitridation(N), sulfurization(S), and alloying(K,Ca,Fe,Zn). The depth profiles of these elements illustrate the extent of chemical interaction between these elements and the bore surface. The physical feature of surface cracking may be derived partially from the chemical interactions.

INTRODUCTION

The technique of Auger electron spectroscopy (AES) has become one of the most widely used analytical techniques for obtaining chemical information on solid surfaces during past ten years. The Auger spectrum provides reliable semi-quantitative elemental compositions and in many cases the binding status of chemical constituents. The basic advantages

ACKNOWLEDGEMENT The author would like to thank Dr. Lawrence A. Shepard and Dr. Ronald J. Arnott for their assistance and discussions. The GS3 specimen was obtained from Dr. Iqbal Ahmad, Benet Weapons Laboratory, Waterveliet Arsenal through Dr. Shepard.

APPROVED FOR PUBLIC RELEASE

of this technique are a high sensitivity for chemical analysis in the near surface region of the materials, a rapid data aquisition, and the ability to detect all atomic elements heavier than helium. The technique is especially suitable for the analysis of light elements such as carbon, nitrogen and oxygen.

The application of AES to gun tube erosion[1] is not very different from other applications. The AES technique could be used for elemental composition analyses of eroded gun surfaces. Although the technique is sensitive only from the surface region to a depth of 20 ^{o}A, the combination of inert gas ion sputtering and ion milling with AES can be used to study the compositions of the sublayers below the eroded surface. In the study of gun tube erosion, the information obtainable from the sublayers is more valuable than that from the surface for the characterization of erosion behavior and the extent of corrosion. In most cases of eroded gun tubes, the thermal cracks and the altered erosion sublayers are unique features of the erosion. These cracks and layers usually extend into the subsurface a few tens to hundreds of microns deep. Thus the depth profiling by ion sputtering and ion milling becomes a time comsuming procedure for the analysis. The currently available method of obtaining the chemical information for such a depth range is by a mechanically tapered cut of the cross-section of the gun or by cratering the eroded surface by ball grinding. From this the AES analysis can be performed on the exposed sublayers in the usual manner.

In a brief description, the fundamental mechanism involved in AES is the ionization of atomic core levels by an incident electron beam, followed by the radiationless Auger transition and the capture of Auger electrons escaping from surface by an electron spectrometer. Since the signal from Auger electrons are weak and barely distingusihable from background noises, it is necessary to improve the singal/noise ratio by electronic differentiation. The addition of a field modulation during the electron detection removes the signal from large backscattered primary electrons and inelastic scattered Auger electrons. Thus the chemical information can be derived from the energy distribution of Auger electrons characteristic of the atomic configurations.

EXPERIMENTAL

Specimen preparation

The surfaces of three gun tubes have been examined. These guns have been fired extensively but their usages have never been recorded, and the propellants employed in firing are not known. All guns were believed to be fabricated from Type 4330 steel but were not made from the same batch of ingots. The surfaces of the eroded guns, as received, were heavily soiled and coated with hydrocarbons or greases. In some instances, attempts have been made to remove these coatings by a mild detergent solution or by direct heating in vacuum. The area near the forcing cone at the entrance to the chamber was so heavily coated that argon ion sputtering for a period of 60 minutes, equivalent to removal of a 0.6 μm layer, could not reach the

underlaying metal surface. For specimen preparation, the corroded bore surface was first sliced from the gun body to about 2 mm thickness, then the sliced surface was cut into pieces of an approximate size 1 cm x 2 cm which could be mounted directly on the sampling carousel of the Auger analytical instrument.

The physical appearance of these gun tubes, designated as GS1, GS2 and GS3 are shown in the microphotographs of Figure 1. The topographic views as well as the cross-sectional views of eroded surfaces are shown. The descriptions of these surfaces and the preparation of individual specimens are as follows:

GS1: The specimens were cut fron the bore surface of a 20 mm gun extending from the chamber end 15 cm along the length of the tube. A total of 15 specimens were prepared for surface analyses. The eroded surface was grey to black in appearance with no metallic luster. This surface was so severely etched and cracked that no rifling pattern, land and groove, was distinguishable at the chamber end of the gun tube as shown in Figure 1a. The majority of the large cracks spaced about 1 mm apart, are propagated along the circumference of the tube and are also interconnected by smaller cracks running along the tube. Originally the surface was electroplated with Cr to about 20-25 μm thick, and most of the Cr layer had been depleted by erosion as shown in the cross-section of the surface Figure 1b. The cracks about 100 μm long are found to penetrate into the surface at an angle, and some of them are interconnected below the surface so that a portion of the surface surrounded by cracks is loosened and removed. A few small chunks are missing from the surface as indicated in Figure 1a.

GS2: Four specimens were prepared from a 47 mm gun 10 cm from the edge of the chamber. The gun was still serviceable and was not badly damaged as shown in Figure 1c. To the naked eye, the rifling pattern of the gun tube is well preserved, and no crack or pebbling of the bore surface is visible. This gun has no coating as shown by the microphotograph of the surface cross-section in Figure 1d. Two white reaction layers of 0.5 and 18 μm thickness are clearly observable.

GS3: Four specimens were obtained from the bore surface of a 105 mm gun, from the muzzle end(designated as Section 101) after 600 rounds of firing. The surface is severely cracked, but the rifling pattern is still in good condition. The cracks are randomly propagated and are concentrated more on the groove portion of the rifling. The surface holes and pits formed by cracks are found to dominate the topology of the groove area as shown in Figure 1e. The cross-section of the bore surface shown in Figure 1f, reveals that the bore surface was electroplated with chrominum to a thickness of about 200 μm. All the large cracks are found to propagate normal to the surface through the Cr layer and to extend some distance into the underlying steel. These cracks are wider and larger than those observed in the GS1 specimens.

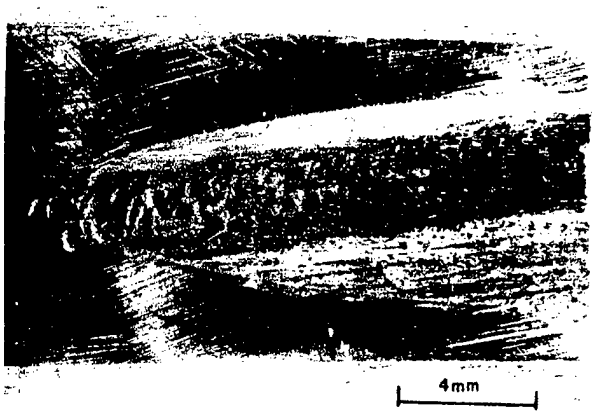

Figure 1a Top view of specimen GS1 (20 mm gun), 10X Actual size of specimen is 1.25 x2.55 cm. This specimen is tapered cut at the edge for depth profile examination.

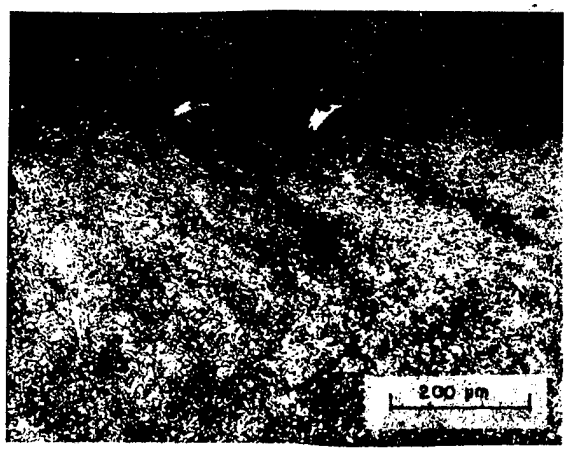

Figure 1b Cross-section of bore surface GS1(20 mm gun), 200X, Cracks are penetrated into surface about 200 µm long. White materials on the top of the surface are Cr residues

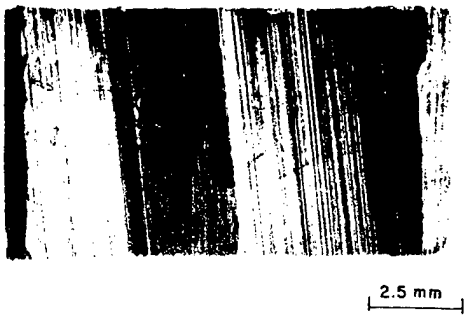

Figure 1c Top view of specimen GS2(47 mmgun), 10X, Rifling pattern is well preserved. Specimen size is 0.68 x 1.25 cm and the width of land is 0.25 cm. Scratches are from mishandling of specimen.

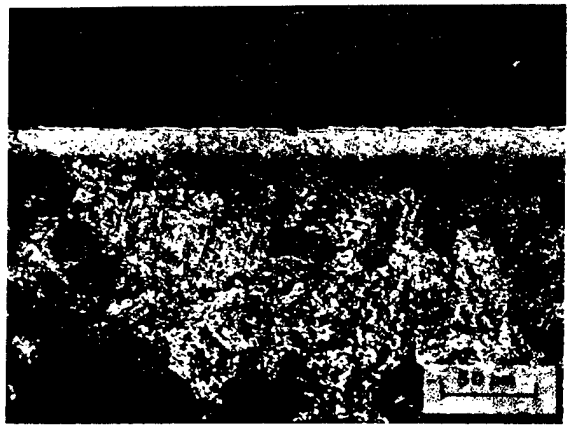

Figure 1d Cross-section of bore surface GS2(47 mm gun), 500X, Taken from the land area of the rifling pattern. Two thermally altered white layers, 0.5 and 18 µm thickness, are visible on sub-surface.

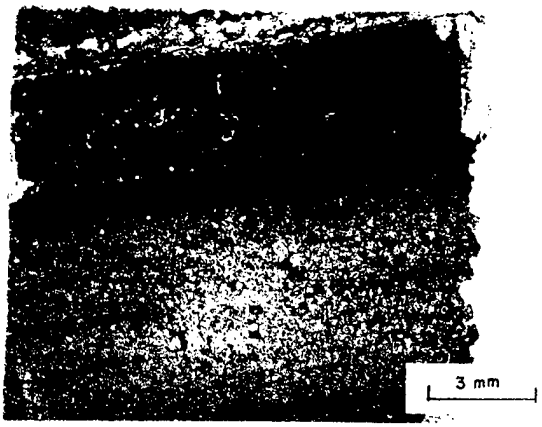

Figure 1e Top view of specimen GS3(105 mm gun), 10 X. The surface is badly cracked and some debris are missing. Pits are 0.2 mm in an average size. The width of the land in the rifling pattern is 3.4 mm.

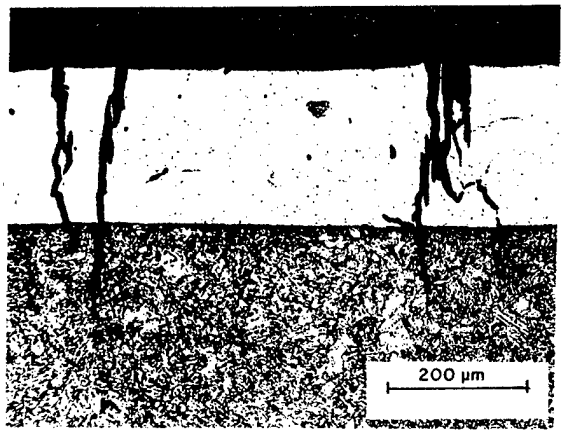

Figure 1f Cross-section of bore surface GS3(105 mm gun), 200X, The surface is coated with Cr about 220 µm thick. Cracks are penetrated into surface approximately 300 µm long and 20 µm wide.

Instrument

A PHI ESCA/AES instrument model 548 with a precision electron energy analyzer Model 15-255 was used throughout the present investigation. The specimen was loaded onto the carousel of the manupulator, and the vacuum maintained at a pressure of 10^{-9} torr or less. Auger electron spectra were obtained with a primary focussed electron beam of 5 kV and 10 μA with a beam diameter of approximately 50 μm and a peak-peak modulation voltage of 3 ev. The electron multiplier for signal detection was set at 1.75 kV. Several Auger electron spectra were taken from each specimen. The spectra were recorded at electron energy ranges 0-1000 and 0-2000 ev, at scan speeds of 1 and 2 ev per second respectively The atomic fractions of the elements present on the surface were calculated semi-quantitatively from these spectra using the technique outlined in the Handbook of Auger electron Spectroscopy[2].

In the ion sputtering, the chamber is filled with argon of purity 99.998 % at a static pressure of 5×10^{-5} torr. The output current of the ion sputtering is 6 μA at the 5 kV, 30 mA filament power setting. The depth profile of surface is accomplished either by ion sputtering or by mechanical tapering of specimen surface. The tapering of the specimen is made first by rough grinding the surface at a shallow angle then sanding the exposed cross-section with a fine grit SiC paper. The prepared specimen is then washed in a detergent solution followed by rinsing twice in distilled water before loading into the vacuum chamber. The cross-section is subjected to ion sputtering before the spectroscopic analysis.

RESULTS

GS1 Specimen: Numerous AES spectra were obtained from each of the 15 specimens prepared from a 20 mm gun. Since some elements on the surface are not homogeneous distributed but are clustered on prefered locations, only a statistical description will be presented here. In general, the elemental constituents on the surface are similar except for a wide variation in localized distribution. At the chamber end of the gun tube, where no erosion is visible, only signals of oxygen and carbon were detected. The hydrocarbon coating on this area is so thick that metal signals from the underlying surface could not be detected even after a prolong period of argon ion sputtering.

In addition to the commonly observed contaminants C and O, and the major constituents of steel, Fe, the foreign elements found on the surface in order of increasing Auger electron energy are Ba, S, Ca, P, Cl, Cr and Zn. Not all of these elements are present in all spectra and a typical Auger electron spectrum is shown in Figure 2. The element Ba is found throughout the sampling surface but it is distributed unevenly. This element is not detected after cleaning and rinsing the specimen by an ultrasonic vibrator. The presence of Ba seems to be associated with S and O. Presumably $BaSO_4$ is precipitated on the top layer of the bore surface.

The distributions of Cl and P on the eroded surface are very uneven. They are observed only in a few spectra, and are absent on the specimen after cleaning and rinsing. It might be that the chlorides and phosphates on the eroded surface are quite soluble in water and are accumulated sparsely on the top surface layer.

A weak signal of N is detected occasionally. Although N is one of trace constituents of gun steel, the N content in steel is below the limit of the present detector. Therefore the N signal detected presumably is the result of surface deposition of nitrates and nitrites from propellant gases.

Significant amounts of K and Ca are observed in almost all spectra. These two elements are found to exist to a considerable depth below the eroded surface. Perhaps surface migration and diffusion of these two elements along micro-cracks and grainboundary interfaces during repeated heat cycling might lead to the observed depth penetrations. It is well known[3,4] that the K ion can diffuse rapidly along grain boundary interphases to the sputtering surface . However the simultaneous disappearance of K and Ca after a period of sputtering indicated that this was not the case. It also suggests that the migration of both atoms into the interior may occur by the same diffusion mechanism.

The element Zn is observed mostly on the land portion of the rifling pattern, but near the chamber end, the land and groove of the rifling pattern are hardly distinguishable. Cu and Zn are the principle alloying elements of gilding metals for the rotating band of projectiles. These elements are left on the surface from friction with the projectile.

Chrominum is a minor constituent of gun steel, about 1-3 wt %. This concentration is at the edge of the detection limit of the present Auger electron spectroscopic technique. The unexpected high concentrations of Cr observed in some spectra occurred because the gun was originally electroplated with a 20-25 μm thick Cr layer. Since the gun was severely damaged and the Cr layer depleted at some spots, the element was not observed in all spectra. The cross-sectional view of the surface as shown in Figure 1b confirms the AES observation.

Oxygen and carbon, the most abundant elements on the eroded surface, are always detected together with metal signals. Both elements are well known contaminants of residual gases in the vacuum system. Their existence is found to extend far into the bore surface as indicated by Ar ion sputtering. The large oxygen concentration near or on the surface other than from the vapor contamination suggests that the metal is highly oxidized. The presence of a carbon signal deep into the surface also implies that the formation of stable metal carbides is the most probable process.

The depth profile by a tapered cross-section of the gun tube surface is shown in Figure 3. The bore surface is severely cracked and altered as seen in Figure 1b. The focused primary electron beam diameter of the Auger electron spectrometer is about 50 μm, and the width of cracks is in the range of 10 μm. During the measurement across the tapered surface,

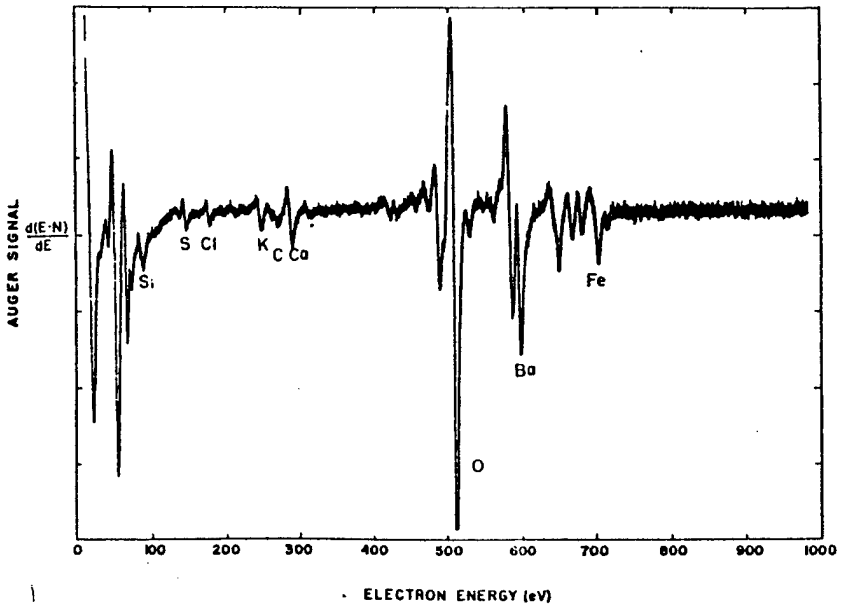

Figure 2 Auger electron spectrum obtained from GS1 specimen
Bright Land surface, After sputtering for 15 min. Chart 111881-1000 GS1-6
E_p= 5kV, I_p= 5 μA, V_{mod}= 3 eV, V_{mult}= 1.75 kV, RC= .01 sec. P=3x10^{-9}

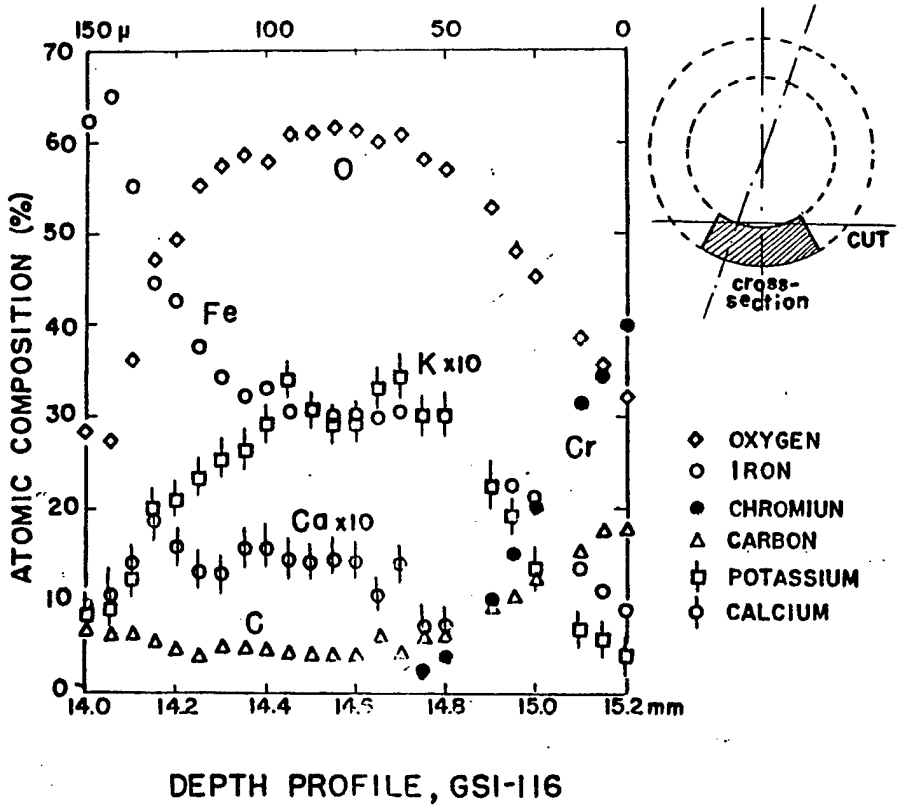

Figure 3 Depth profile by tapering cross-section of bore surface, Specimen GS1-116, Coordinate is the movement of specimen in mm, the equivalent depth in μm is also shown. Abscissa is the atomic composition calculated semi-quantitatively from Auger electron spectra.

the spectrometer may have recorded the compositions of both tapered surface and interior surfaces of cracks. Therefore, good agreement between the depth profile by mechanical tapering and ion sputtering is not expected. . .

As shown in Figure 3, the major elements detected on the surface in order of decreasing magnitudes are Cr, O, C, and Fe. In the depth range 0-50 μm, Cr is found to diminish while oxygen and iron increase, and carbon drops to a steady concentration of a few atomic percent. The depletion of oxygen in this region may be caused by the presence of Cr and C. Between 50-100 μm, the concentrations of oxygen , carbon and iron are constant. This probably indicates the formation of stable chemical compounds such as FeC and Fe_2O_3 in this depth range. After 100 μm depth, the iron signal increases and approaches that of the steel composition and the concentrations of all other elements fall to insignificant amounts. It is surprising to note that K and Ca have depth profiles similar to oxygen although the oxygen concentration is much higher. Perhaps K and Ca exist as oxides along the sampling path.

GS2 Specimens: The elemental analyses of four specimens reveal that except for a few elements, the constituents of the eroded surface are similar to those observed in GS1 specimens. Those elements detected are S, Cl, K, Ca, C, N, O, Fe, Cr, Ni, Cu and Zn. Pb is observed in a few spectra. A typical Auger electron spectrum from this moderately eroded surface is shown in Figure 4. Fe, Cr, and Ni are the metal components of

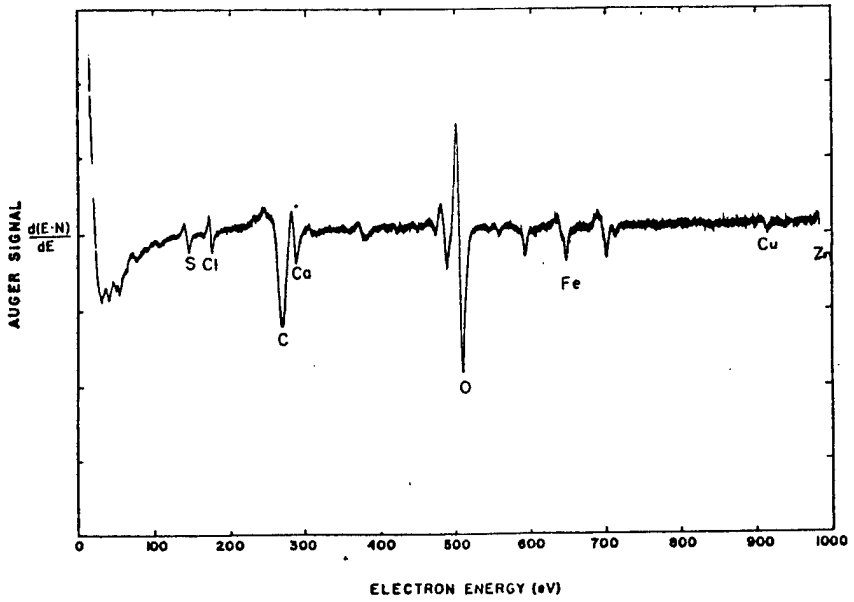

Figure 4 Auger electron spectrum obtained from GS2 (47 mm gun) specimen. Groove surface, after heating. Chart 120981-950 GS2-1
E_p= 5 kV, I_p= 5 μA, V_{mod}= 3 eV, V_{mult}= 1.75 kV, RC=.01 sec. P=4×10^{-9}

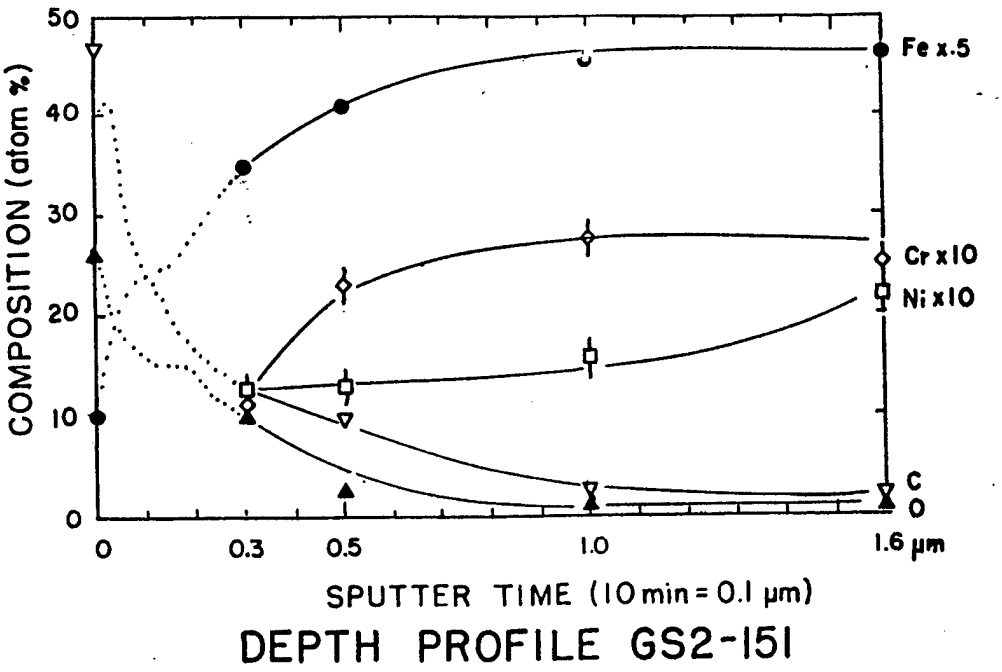

Figure 5a Depth profile by argon ion sputtering
Specimen GS2-151 from 0.3 to 1.6 μm. Gun at 5 kV, 30 mA

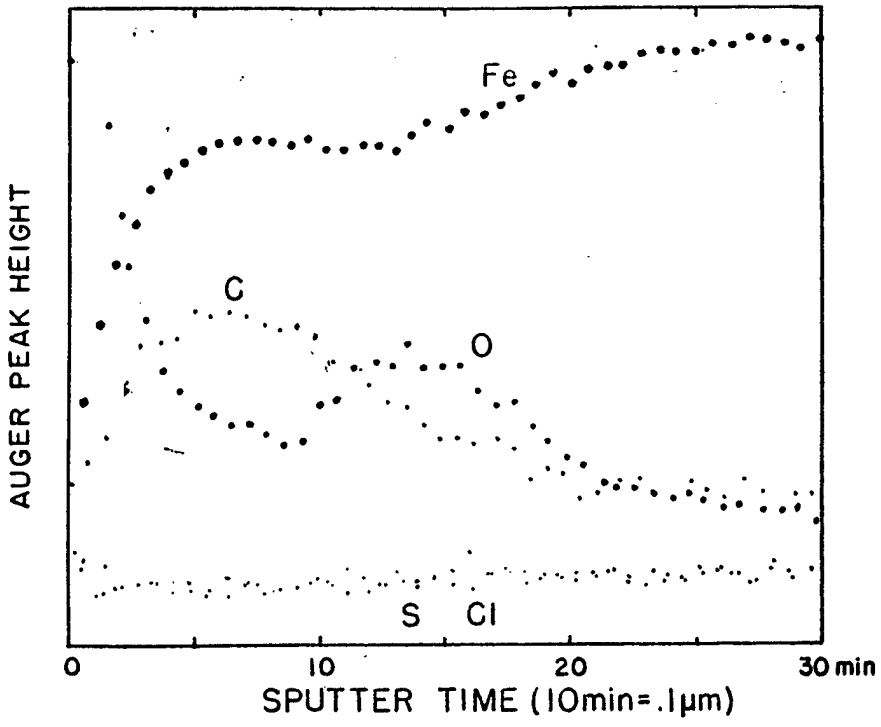

Figure 5b Depth profile by argon ion sputtering
Specimen GS2-151 from 0 to 0.3 μm. Gun at 5 kV, 30 mA.
Taken directly from Auger peak multiplexer.

gun steel and S, K, Cl and Ca are derived from chemicals in the propellants. Cu and Zn are from gilding metals in the rotating band of the projectile and they are scraped away during firing.

The elements S, and K are found to exist in sublayers of the surface, and they are not precipitated on the top layer surface. The signals of N and C are comparatively larger than those observed in GS1 specimens. Nitrogen is found imbedded in the interior not far from the surface. The formation of FeN_x might be the source of this signal. As expected, the top layer of the surface is extensively oxidized and carburized. This is demonstrated by the presence of large oxygen and carbon signals in the spectra.

The depth profile by ion sputtering is shown in Figure 5. In the first 0.5 μm below the surface, the composition of steel had been significantly altered by the presence of large amounts of oxygen and carbon. The metal oxides, carbides and nitrides are believed to be the major components of this layer. Two distinct layers are visible in the microphotograph of surface cross-section as shown in Figure 1d. The first white layer about 0.5 μm thick is a reacted layer consisting of high proportions of oxygen and carbon, and the second white layer about 18 μm thick, is a thermally altered and recrystallized layer containing increasing amounts of oxygen and carbon. Below 18 μm depth, the original tempered martensite phase of gun steel exists.

The semi-quantitative chemical analysis calculated from Auger electron spectra along the depth profile is tabulated in Table 1. The depth of 0-0.5 μm is the approximate location of the first white layer observed in Figure 1d. The composition at 1.6 μm depth is representative of the second white layer. The depth penetrations of K, S, and N seem to be limited to the first 0.5 μm, that is, within the first white layer.

TABLE 1 Chemical Compositions of Sublayers from 47 mm Gun, GS1-151 032382-1530

Sublayer	Chemical composition in atomic percents[a]											
depth(μm)[b]	C	N	O	S	Cl	K	Ca	Fe	Cr	Ni	Cu	Zn
surface	47.	2.4	25.9	2.5	1.9	0.5	2.9	10.2	-	-	2.0	4.7
0.3	12.5	3.5	10.5	0.2	-	0.8	-	70.0	1.2	1.3	-	-
0.5	9.7	1.7	2.5	-	-	0.8	-	81.7	2.3	1.3	-	
1	3.0	-	1.0	-		-	-	91.5	2.8	1.6	-	
1.6	2.7	-	0.9	-			-	91.7	2.5	2.2	-	

Note(a): Calculated semi-quantitatively from Auger spectra, see Ref(2)
Note(b): Argon ion sputtering at 5kV, 6μA power output. 10 minutes sputtering is equivalent to 0.1 μm depth.

GS3 Specimens: The elements detected in these specimens are P, Be, Cl, S, K, Ca, C, Cr, O, Fe, Cu, Zn and Al. Two typical spectra taken from the specimen are shown in Figures 6a and 6b. Not all elements listed are observed in one sampling area. The first three elements, Be, P and Cl are found only in a few specta, and their magnitudes decrease drastically with Ar ion sputtering depth. The absence of these elements in specimens after washing suggested that they are probably precipitated from propellant gases on the surface and are sparsely distributed. The elements K, S, and Ca are observed in all spectra, and these elements exist not only on the surface but also below the surface. Carbon and oxygen signals are largest in the spectra taken on the surface and they are contaminants from residual vapors as well as from surface oxides and carbides. As shown in Figure 1f, the specimen surface is electroplated with Cr, thus the observed Fe and Al signals could only be derived from engraving of the projectile onto the bore surface. Zn and Cu derived from the rotating band of the projectile, are concentrated on the land portion of the rifling pattern. In Figure 7a, the depth profile by the tapered GS3 specimen cross-section is given. Zn and Fe are found to have unexpectedly high penetration depths extending 50 μm below the surface. Since the Cr layer was 200 μm thick, Fe could not diffuse from the underlaying steel. The oxygen content in the depth profile of the Cr layer is distinctly lower than that of gun steel without a chrominum coating.

In Figure 7b, the depth profile by Ar ion sputtering is shown. The figure is obtained directly from the Auger peak multiplexer. It is obvious that Zn, S, O, C and Al have high depth penetrations into the Cr layer.

DISCUSSION

Three gun surfaces have been examined with the analytical technique of Auger electron spectroscopy. Although these guns have varying degrees of service length and have been subjected to different ammunitions, their erosion behaviors have many similarities. In particular, the erosion characteristics resulting from repeated firing cycles are identical. In physical appearance, all bore surfaces have been severely cracked and/or corroded. The metal luster of the original surface has been transformed into a grey charcoal colored appearance, and some materials loosened from the surface have been removed by hot propellant gases.

The elements identified in the Auger electron spectra common to these three gun surfaces are S, K, C, Ca, O, Cr, Fe, and Zn. Some elements are charactertistics of a special ammunition used in firing, such as Ba, P, Cl, N in GS1(20 mm gun), Cl, Pb, N, Cu in GS2(47 mm gun), and Be, P, Cl, Cu in GS3(105 mm gun). Thus from the surface analsis, the elements existing on eroded surfaces could be used to trace back the ammunition employed in firing. The major chemical transformations observed on the eroded surfaces of gun tubes are oxidation, carburization, and to lesser extents nitridation and sulfurization as evidenced by the presence of O, C, N and S.

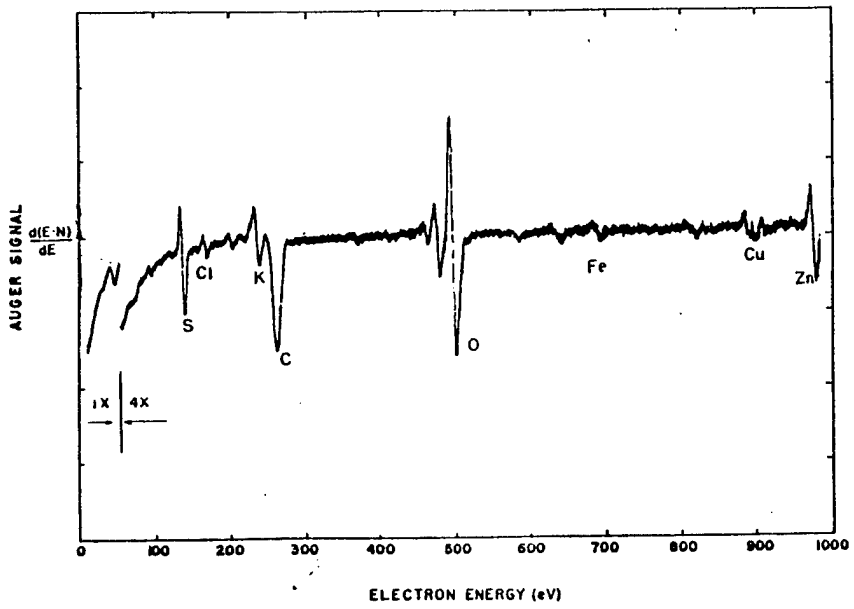

Figure 6a Auger electron spectrum obtained from GS3(105 mm gun) specimen Land surface Chart 021082-900 GS3-1
E_p= 5 kV, I_p= 10 μm, V_{mod}= 3 eV, V_{mult}=1.75 kV, RC=.01 sec

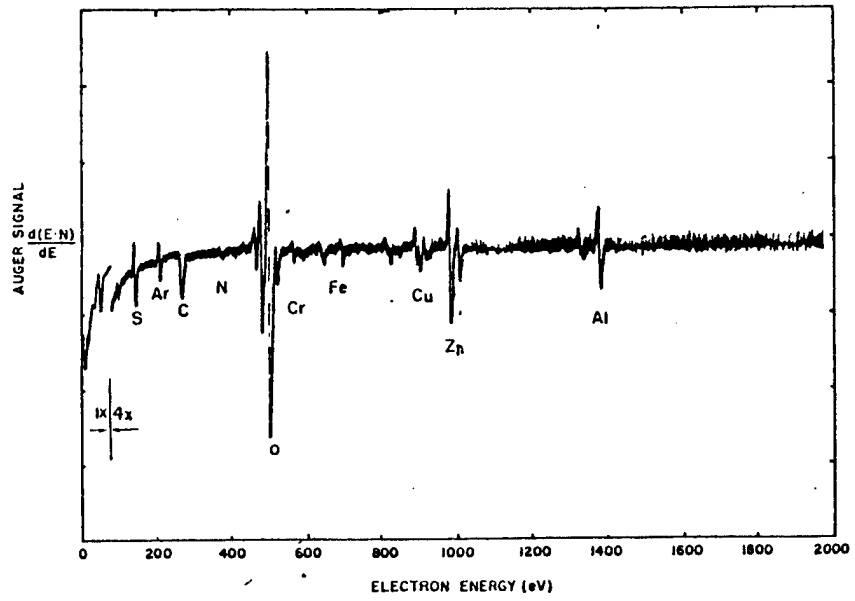

Figure 6b Auger electron spectrum obtained from GS(105 mm gun) specimen Land surface after 90 min sputtering, Chart 021082-1110 GS3-2
E_p= 5 kV, I_p= 10 μA, V_{mod}= 3 eV, V_{mult}= 1.75 kV, RC=.01 sec.

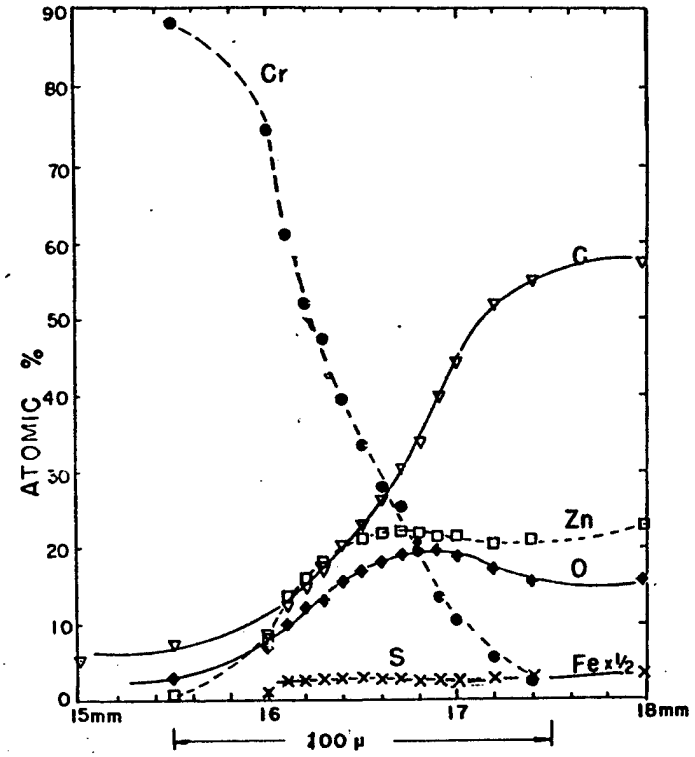

Figure 7a Depth profile of specimen GS3 by tapering cross-section
The atomic compositions are calculated semi-quantitatively from Auger spectra. The coordinate shows the movement of the specimen and the equivalent depth in μm

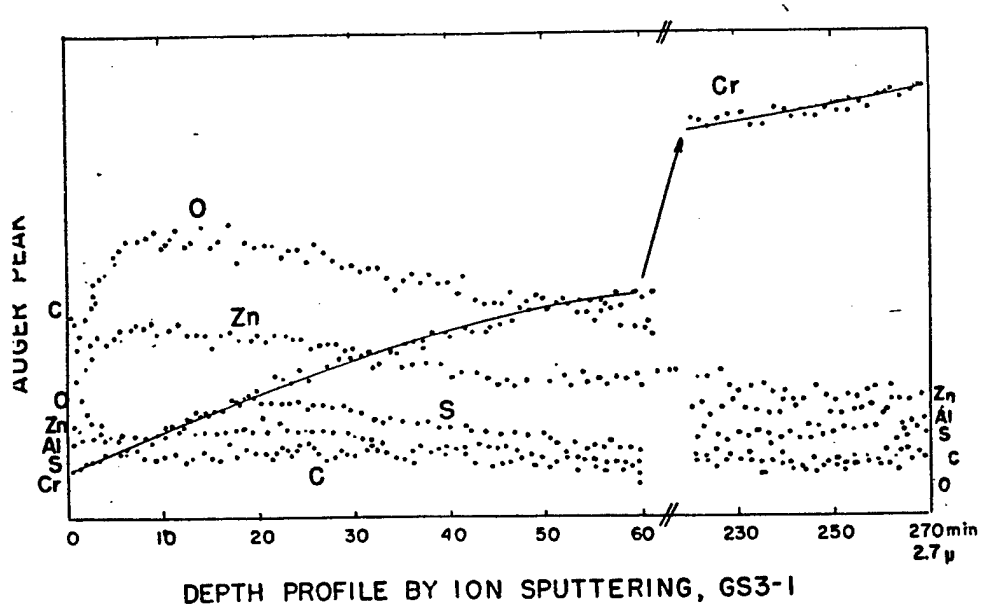

Figure 7b Depth profile by argon ion sputtering
Taken directly from Auger peak multiplexer, Specimen GS3-1
Gun at 5 kV, 30 mA.

The large concentrations of oxygen and carbon present on eroded bore surfaces could be explained by assuming high temperature chemical reactions between the metal surface and the hot propellant gases containing large amounts of oxygen and carbon. Although nitrogen containing molecules constitute a large proportions of the propellant gas, the formation of metal nitride on the bore surface is limited and is observed only in iron. It could be that nitrogen-rich explosives are less corrosive than those containing oxygen and carbon resulting in limited amounts of nitrogen observed on eroded surfaces.

The elements found on the top layer of the surface as deposits and precipitates are considered to be less corrosive than those elements which penetrate deep beneath the bore surface. Such elements, Ba, Be, P, Pb, Cl, Cu and Zn(not in GS3) have no depth penetration, and they are probably derived from condensates of hot propellant gases and from engraving of the projectile onto bore surfaces. The interactions of these elements with metal surfaces in the form of diffusion, dissolution, combination and alloying are believed to be less important than the removal processes of these elements by evaporation, blowby and scraping during the pulsed cycling of high temperatures and pressures. Thus there is no appreciable accumulation of these atoms on bore surfaces.

The atomic elements S, K, C, Ca, N(in GS2), O, Fe(in GS3) and Zn(in GS3) are found to have depth penetrations varying from a few tenths to several μm into the bore surface of gun tubes. This could result from the fact that high temperature interactions of these elements with gun steel are more favorable processes than the removal processes by exploding gases. Therefore, they may be sources of gun tube erosion and corrosion at high temperatures. The absence of one or more elements in this group might have reduced the crack formation, and consequently might have prolonged the useful life of the gun.

The major component of the gilding metal, Cu, is reported[1] to form alloys on the bore surface of gun tubes. However the so-called "coppering" was not clearly observed in the present investigation. Copper is found usually deposited on the surface layer, and no depth penetration is observed. It might be that the high temperature duration in the firing cycle is too short for the formation of copper alloys in these guns. But the second component of the gilding metal, Zn, is found to have a considerable depth penetration into the Cr layer of the GS3 specimen.

Gun tube erosion is a highly complex and multiple component phenomenon. Numerous factors and parameters are involved in the optinum design and the maximum performance of a gun. Any changes in structural materials, composition of propellants, presumably intended to prevent erosion, may lead to adverse effect on the useful life of a gun. The present investigation has identified the elements involved in gun tube erosion. Some characteristics of the erosion behavior of these elements have been obtained from the depth profile technique. Although the major elements C, O and N have been known for many years, the effects of the minor elements K, S, Ca and Zn are not well understood. Thus information provided from the Auger surface analytical technique could be very useful in the understanding of gun tube erosion phenomena.

REFERENCES

1. Iqbal Ahmad, The Probelm of Gun Barrel Erosion - An Overview, Proceeding of the Tri-service Gun Tube Wear and Erosion Symposium, ppl, March 29-31, 1977

2. L. E. Davis, N. C. McDonald, P. W. Palmberg, G. E. Raich & R. E. Weber, Handbook of Auger Electron Spectroscopy, Physical Electronics Industries, Eden Prairie, 1976

3. J. I. Walter, P. Rao & R. R. Russel, Impurity segregation to Voids in Doped Tungsten Ribbon Filaments, Metallurgical Transaction A, 6A, 1775 (1975)

ELECTROCHEMICAL STUDIES OF CHROMIUM IN MOLTEN LIF-NAF-KF

R. A. Bailey and T. Yoko
Department of Chemistry, Rensselaer Polytechnic Institute
Troy, New York 12181

ABSTRACT

Cyclic voltammetry and chronopotentiometry show that Cr(III) is reduced in two quasi-reversible steps in the LiF-NaF-KF eutectic over the temperature range 600-1000°C. The product of the first step, $Cr(III) + e^- \rightarrow Cr(II)$, is insoluble below about 900°C, and the details of the reduction mechanism are clearly variable with temperature. Only above 900°C can non-dendritic deposits be obtained. Anodization of chromium metal, and disproportionation of Cr(II), lead to an average oxidation state in the melt of about 2.6 at equilibrium.

INTRODUCTION

Electroplating of refractory metals from fused salts has been of interest for many years. Notable is the work of Senderoff and Mellors in the early 1960's using fluoride melts[1]. There has been renewed interest in this area in more recent years, not only for those refractories such as Ta that cannot be plated from aqueous media; but also for chromium[2]. Melt electrodeposits of this metal potentially have some desirable properties not obtainable from aqueous plates. The electrochemistry of Cr(III) reduction in FLINAK melts, although initially investigated some time ago[3], remains not totally clear. In this report, we discuss some voltammetric and chronopontentiometric studies of Cr(III) reduction, and correlate these with properties of the deposit.

EXPERIMENTAL

Melts were made up from reagent grade salts, vacuum dried at 160°C for over a week, melted under argon in a nickel crucible and filtered through a platinum screen. The melt was pre-electrolyzed at 1.5 V using a vitreous carbon anode and a steel cathode to a cathodic current density of less than 0.3 mA cm^{-2}. Chromium was added as K_3CrF_6. Electrodes were a vitreous carbon auxillary, a platinum plate quasi-reference, and a fine (0.12 mm diameter) Pt working electrode for voltammetry, or a Pt cylinder working electrode for chronopotentiometry. At the temperatures involved, no satisfactory insulator could be found. The voltammetric electrode area was controlled only by depth of immersion, about 5 mm, and consequently the area in use was only known approximately.

The melt was contained in a Ni crucible in a Hasteloy-X container fitted with a gate-valve, sliding O-ring seals for electrode adjustment, and provision for evacuation or for an argon atmosphere. All work was done under a slight positive pressure of argon.

This work was supported by the Army Research Office, Contract No. DAAG29-79-C-0035

RESULTS AND DISCUSSION

Cyclic voltammograms and chronopotentiograms were run over a temperature range of about 600°C to 1000°C and a Cr(III) concentration of 0.07 to 0.13 mole l^{-1}. Typical results are shown in Fig. 1. Two reduction and two oxidation steps are observed, as is expected from other work. These are expected to be due to the processes

$$Cr(III) + e^- \rightarrow Cr(II)$$

and

$$Cr(II) + 2e^- \rightarrow Cr(0)$$

on chemical grounds and previous work[3]. This is confirmed from the ratio of the chronopotentiometric transition times of the two waves, which should be 8 for a 1 electron reduction followed by a 2 electron reduction (the alternative is 1.25). The values found are given in Table I. At high temperatures the value found is 8;

Table I. Temperature dependence of the ratio of the transition time of the first to the second reduction step, τ_{2r}/τ_{1r} (concentration of Cr(III) = 0.09 mol.l^{-1}).

Temp (°C)	983	893	804	716	612
τ_{2r}/τ_{1r}	8.0	8.6	9.3	11.3	13.4

at lower temperatures a larger value is found that results from the fact that the first reduction step is not a simple diffusion controlled process. Ratios of the forward to reverse transition times for the first wave given in Table II are consistent with a soluble product above 893°C, but with an insoluble product at lower temperatures. (A ratio of 3 holds for a soluble product, while a value of 1 holds if the product is insoluble.)

The shape of the first reduction wave in cyclic voltammetry also suggests that this is not a simple reversible process, as it does not show a peak except at very high scan rates. On the other hand, the relationship of $i_o\tau^{\frac{1}{2}}/C$ vs C at different temperatures are essentially linear and the transition time constant $i_o\tau^{\frac{1}{2}}/C$ is constant with temperature; $i_o\tau^{\frac{1}{2}}$ is essentially constant at high currents and short times. Voltammetry shows that i_p varies linearly with $V^{\frac{1}{2}}$ at fast scan rates, although for the second peak this is non-linear at very fast scan rates also. The peak current i_p is linear with concentration. These various relationships rule out coupled chemical reactions. Other trends, Tables 3 and 4, include variation of E_p and $E_{\tau/4}$ with concentration and scan rates; both shift cathodic with increasing scan rate and current density, and anodic with increasing concentration. These overall criteria fit a quasi-reversible mechanism. These are summarized in Table 5.

Table II. Ratio of the forward to the reverse transition time for the first wave at different temperatures (Concentration of Cr(III) = 0.13 mol.ℓ^{-1})

Temp. (°C)	Current Density (10^2.mA.m^{-2})	Forward τ_f(sec)	Reverse τ_r(sec)	τ_f/τ_r
983	51.0	0.102	0.039	2.6
	40.8	0.156	0.047	3.3
893	46.0	0.067	0.071	0.93
	35.8	0.110	0.098	1.1
804	30.7	0.157	0.126	1.2
	25.6	0.201	0.193	1.0
716	25.6	0.114	0.112	1.0
	20.5	0.186	0.169	1.1
612	20.6	0.119	0.123	0.97
	18.0	0.158	0.150	1.1

Table III. Scan Rate Dependence of Peak Potentials (voltammetry) and Current Density Dependence of Quarter-Wave Potential (chronopotentiometry). Concentration of Cr(III), 0.11 mol l^{-1}, 983°C

Scan Rate, V sec^{-1}	Ep/V		Current Density mAm m^{-2}	$E\tau/4/4$	
	1st wave	2nd wave		1st wave	2nd wave
1.0	-0.126	-0.738	33.2	-0.135	-0.610
2.0	-0.152	-0.749	35.8	-0.145	-0.616
5.0	-0.162	-0.786	38.4	-0.156	-0.628
8.0	-0.173	-0.796	40.9	-0.178	-0.637
10.0	-0.186	-0.815	43.5	-0.194	-0.646
20.0	-0.234	-0.857	46.0	-0.244	-0.656

Table IV. Concentration Dependence of Peak Potentials and Quarter-Wave Potentials. Scan Rate (voltammetry) 2.0V sec^{-1}; Current Density (chronopotentiometry) 45.9 x 10^2 mAm^{-2}; Temperature 983°C

Concentration of Cr(III), mole l^{-1}	Ep/V		$E_{\tau/4}$/V	
	1st wave	2nd wave	1st wave	2nd wave
0.07	-0.86	-0.774	-	-
0.08	-0.164	-0.762	-0.32	-0.782
0.10	-0.156	-0.746	-0.259	-0.792
0.11	-0.192	-0.734	-0.202	-0.764
0.12	-	-	-0.206	-0.752

The overall mechanism for reduction of Cr(III) in FLINAK is

$$Cr(III) \xrightarrow[e^-]{\text{slow}} Cr(II) \xrightarrow[2e^-]{\text{slow}} Cr(0)$$

insoluble
below 893°C

The changes in electrochemistry with temperature shown in Fig. 1 are reflected in a qualitative fashion in the nature of the electrodeposit, which at lower temperatures is highly dendritic. Dendrite formation decreases and essentially disappears at temperatures exceeding 900°C.

It is supposed that dendritic electrodeposits are favored by mass transfer limited processes, while smooth deposits require kinetic limitations[4]. This, in turn, would be favored by the formation of stable complexes of the metal ion in the melt. Chromium(III) reduction may very well involve the formation of complex or cluster intermediates. At any rate, the steps are not simple diffusion controlled processes. The stability of complexes or clusters is dependent on other cationic species that may be present, with small or highly charged cations having a destabilizing influence, presumably through competition for the fluoride ions. Plating from NaF-KF melts showed qualitatively less dendrite formation, while addition of AlF_3 increased dendrite formation under otherwise identical conditions. Changes in electrochemistry under these conditions have not yet been explored.

A complicating feature of the chemistry is the disproportionation of Cr(II) to Cr(III) and metal. The rate of this process is slow compared to the time scale of the electrochemical measurements, but rapid enough to be in equilibrium before measurements can be made if Cr(II) is added to the melt. Thus, electrochemistry of Cr(II) added as CrF_2 to FLINAK was qualitatively identical to that of Cr(III), although not with the same relative voltammetric current or chronopotentiometric transition times for the two waves. Chromium metal was deposited on the crucible. It follows that in electroplating or with a chromium anode, a mixture of Cr(III) and Cr(II) is present in the melt. Initial attempts to form plates from Cr(III) melts are always unsuccessful until Cr(II) has built up in the melt. The average oxidation state of chromium in the melt used for electroplating was about 2.6

over the range 950-1050°C. Thus, nearly half the total chromium present is Cr(II). Current efficiency of the anodic dissolution of chromium in FLINAK also indicated this value.

REFERENCES

1. G. W. Mellors and S. Senderoff; J. Electrochem. Soc. 112, 266 (1965); 113, 60, 66 (1966); 114, 556, 586 (1967); G. W. Mellors, S. Senderoff and W. J. Reinhart, J. Electrochem. Soc. 112, 840 (1965).

2. James F. Smith, private communication.

3. G. W. Mellors and S. Senderoff, Application of Fundamental Thermodynamics to Metallurgical Processes, G. R. Fitterer, ed., Gordon and Breach, N. Y., 1967, p. 81.

4. D. Inman and S. H. White, J. Appl. Electrochem., 11, 291 (1978).

Table IV. Comparison of the results obtained for the first reduction step with the diagnostic criteria for typical electrode processes

Electrode process	$i_p/V^{\frac{1}{2}}$ vs. V	$i.\tau^{\frac{1}{2}}$ vs. i	ipa/ipc vs. V	Ep vs. V	$E\tau/4$ vs. i	$E\tau/4$ vs. C	τ_f/τ_r vs. i
Observed	const.	const.	incr.	cathodic	cathodic	anodic	1 a) 3 b)
Reversible	const.	const.	1 c) > 1 d)	const.	const.	const.	1 c) 3 d)
Quasi-rev.	const.	const.	———	cathodic	cathodic	anodic	1 c) 3 d)
Irrev.	const.	const.	0	cathodic	cathodic	anodic	0 or 1 c) 0 or 3 d)
Cr.Er.	decr.	decr.	incr. from 1 at low V	anodic	———	———	3
Er.Cr.	const.	const.	decr. from 1 at low V	cathodic	cathodic	anodic	incr.
Catalytic	*	incr. from 1	*	anodic or const.	anodic	———	———

Cr.Er.: Reversible chemical reaction preceding a reversible charge transfer.

Er.Cr.: Reversible charge transfer followed by a reversible chemical reaction.

* : Decreasing at low V and constant at high V.

a) : At 983°C; b): Below 893°C.

c) : Insoluble product; d): Soluble product.

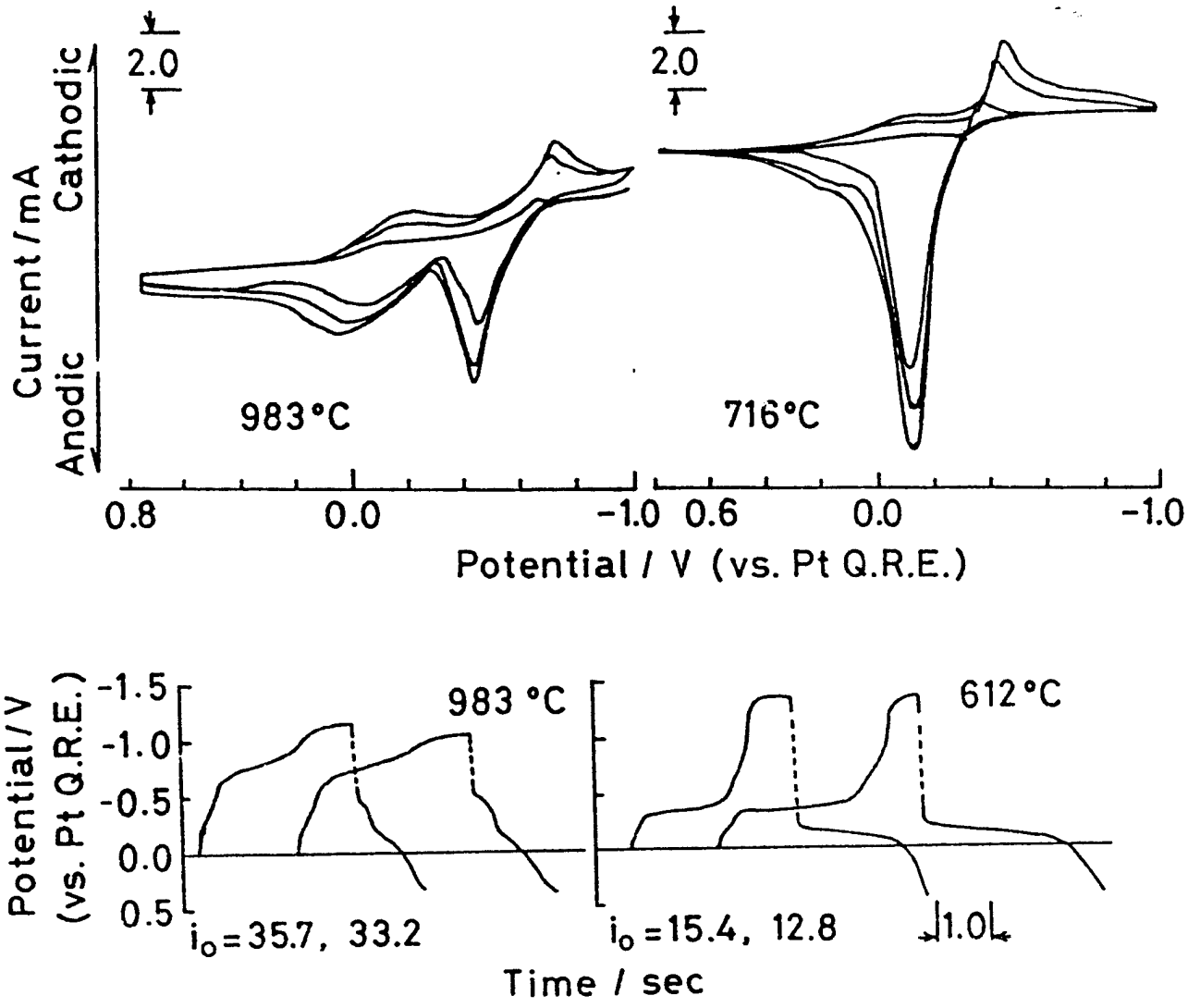

Figure 1. Cyclic voltammograms (upper) and chronopotentiograms (lower) for the reduction of Cr(III) in molten FLINAK.

MONITORING INTERIOR SURFACE CONDITIONS OF LARGE CALIBER GUN BARRELS AT ABERDEEN PROVING GROUND

R. A. GILLEY
Materiel Testing Directorate
Aberdeen Proving Ground, MD.

This paper does not contain anything revolutionary. It is a summary of the method, instrumentation and information used and generated by the Nondestructive Test Section of the Materiel Testing Directorate of Aberdeen Proving Ground, MD. for monitoring the interior condition of large caliber gun barrels.

One of the responsibilities of the Materiel Testing Directorate is conducting tests on ammunition and large caliber gun barrels. Often, these tests are concerned with erosion phenomena and the effect materiels, new propellant formulations, anti-erosion additives, barrel design, rotating bands, etc. have on the erosion of gun barrels. To assist this Directorate in this phase of its mission, the Nondestructive Test Section is responsible for measuring the interior dimensions and identifying the interior surface conditions of these barrels. The data generated is forwarded to the Test Director (an individual assigned by this Directorate for managing a particular test program) to aid him in generating information for evaluating his program. This information is often forwarded to the developing agency to aid them in improving or modifying their designs.

The "variation from original diameters" is the most common measurement of interior dimensions of gun barrels. Information gained from this measurement reveals the effect ammunition, rotating bands, etc., have on the interior surface of the barrel. One of the oldest methods of obtaining these interior dimensions is using the mechanical stargage. The stargage is used to measure interior dimensions of barrels where abnormal amounts of wear, erosion, scoring and other interior surface conditions occur due to the number and type of rounds fired.

Two types of mechanical stargages used to measure wear in large caliber barrels are: the 2 inch gage with a range of 75mm to 155mm and the 5.75 inch gage with a range of 155mm to 16 inches, see figure 1. These stargages consist of three major assemblies:

1. Measuring head: one with three movable measuring points (used mainly in measuring smooth bore barrels, see figure 2a) and a four point head with two movable measuring points (used mainly for rifled barrels, see figure 2b).
2. Operating handle: equipped with a vernier, see figure 3.
3. Stave: a graduated rod used to connect the head to the operating handle, see figure 4.

When the stargage is assembled and its vernier adjusted to coincide with the selected size ring (a precisely machined metal ring that is the size of the gun barrel being gaged, see figure 5), it is possible to measure the interior diameter, at any given point, for the entire length of the gun barrel.

Approved for public release; distribution unlimited

Before stargaging a rifled cannon barrel, a vertical land is established as a reference. All stargage measurements are taken relative to the vertical land which is the 6:00 o'clock land in the commencement of rifling area. When stargaging a cannon with a four point measuring head, measurements are taken on the vertical and horizontal land and groove for the entire length of the barrel. The horizontal position is located 90° from vertical. On some occasions, a three point measuring head is used in a rifled cannon barrel. A set of Y-up and Y-down measurements are taken on the lands and grooves using the vertical land as a reference along with a guide plate*, see figure 6.

In cannon barrels with heavy wear, erosion and scoring at the commencement of rifling area, see figure 7, the driving edge of the lands (this is the left edge of the lands as seen from the breech end of the barrel) is worn away. This causes the land to become sloped, see figure 8. The stargage operator is able to "feel out" this condition by locking the stargage measuring head in respect to its staves. He then turns the stargage handle, this causes the measuring head to rotate and the measuring points to follow the slope of the land to its highest point (minimum diameter). The grooves are felt out to their deepest point (maximum diameter).

Another method used to measure wear in gun barrels is the use of an air gage, see figure 9. Because of its limited range of measuring bore diameter changes of approximately 0.014 of an inch, it is used only on production weapons (these are new cannon barrels that have little if any wear).

The air gage consists of a measuring head with two measuring points, staves, and graduated columns on which the measurments are read. The measuring head has a built-in rifling guide that keeps the measuring points on the desired land and groove. The air gage is adjusted to coincide with a calibrating master (a precisely machined metal device that is the size of the gun barrel being measured, see figure 10) before each gaging operation.

Measurement intervals vary for each barrel. Normally measurements start 0.10 of an inch forward of commencement of rifling and end 0.10 of an inch from the muzzle. Measurements are taken approximately every five inches between commencement of rifling and muzzle. In the commencement of rifling area where the greatest amount of wear and erosion occur, measurements are taken in 0.10 to 1.00 inch intervals, see figure 11. The time required to stargage the entire length of a cannon barrel is approximately three hours.

Some examples of interior surface conditons monitored with these stargages are: out of roundness; bulges; stripped, flattened or gouged lands; and restrictions which are caused by the build-up of copper and/or other deposits. Figure 12 shows an example of stripped, flattened and gouged lands. The majority of the above conditions can cause loss of velocity and accuracy of projectiles fired from a gun barrel and may be hazardous to operating personnel.

---

*A guide plate is a device that is machined to fit on the measuring head of the mechanical stargage and into the rifling of the barrel. When the guide plate is attached to the measuring head and placed into the bore, it keeps the measuring points on the appropriate land and/or groove.

In lieu of stargaging the entire length of a gun barrel, a quick check method of determining remaining wear life of the barrel is to use the pullover vernier gage, see figure 13. Wear tests performed on gun barrels show that "pullovers" taken at a single distance slightly forward of the commencement of rifling can be correlated with remaining life. The pullover gage consists of a body with a movable slide at the top, a non-movable rest at the bottom and a vernier scale. The pullover head is attached at both ends to graduated rods. The bottom rod has a bore stop attached to it. This bore stop rests against the rear face of barrel and is used to set the distance where the pullover gage stops in the bore. By moving the top rod of the pullover gage forward, the pullover body is in a forward tilt position. The pullover is inserted into the barrel to the prescribed distance set by the bore stop. Then by pulling the top rod rearward, the pullover body is moved to the rearward tilt. This operation causes the "gage slide", which is set (pulled out past the gage body) to exceed the diameter of the bore being measured, to be forced into the gage body. This sets the bore land diameter on the gage.

Measurements obtained from all these gages, added to the basic diameter of the cannon barrel, are the actual diameters. The accuracy of these gages is $\pm$.001 of an inch.

An instrument used to visually detect any adverse interior condition of gun barrels such as: heat checking, erosion, scoring, coppering, damages, etc., is a white light borescope, presently a Watervliet supplied M2 scope, see figure 14. When any of these conditions are found, they can be permanently recorded by:

1. Interior photographs taken with the aid of a white light borescope (see figure 7).
2. RTV silicon rubber impressions, see figure 15.
3. Low temperature metal casts.

The information generated by the Nondestructive Test Section and passed on to the Test Director in the form of data sheets and laboratory reports is often the only information available to reveal what occurs during testing to the interior surface of the gun barrel.

REFERENCES

1. TM 9-1000-202-14, Evaluation of Cannon Tubes, November 1976.

2. TOP 3-2-802, Measurements of Cannon, November 1976.

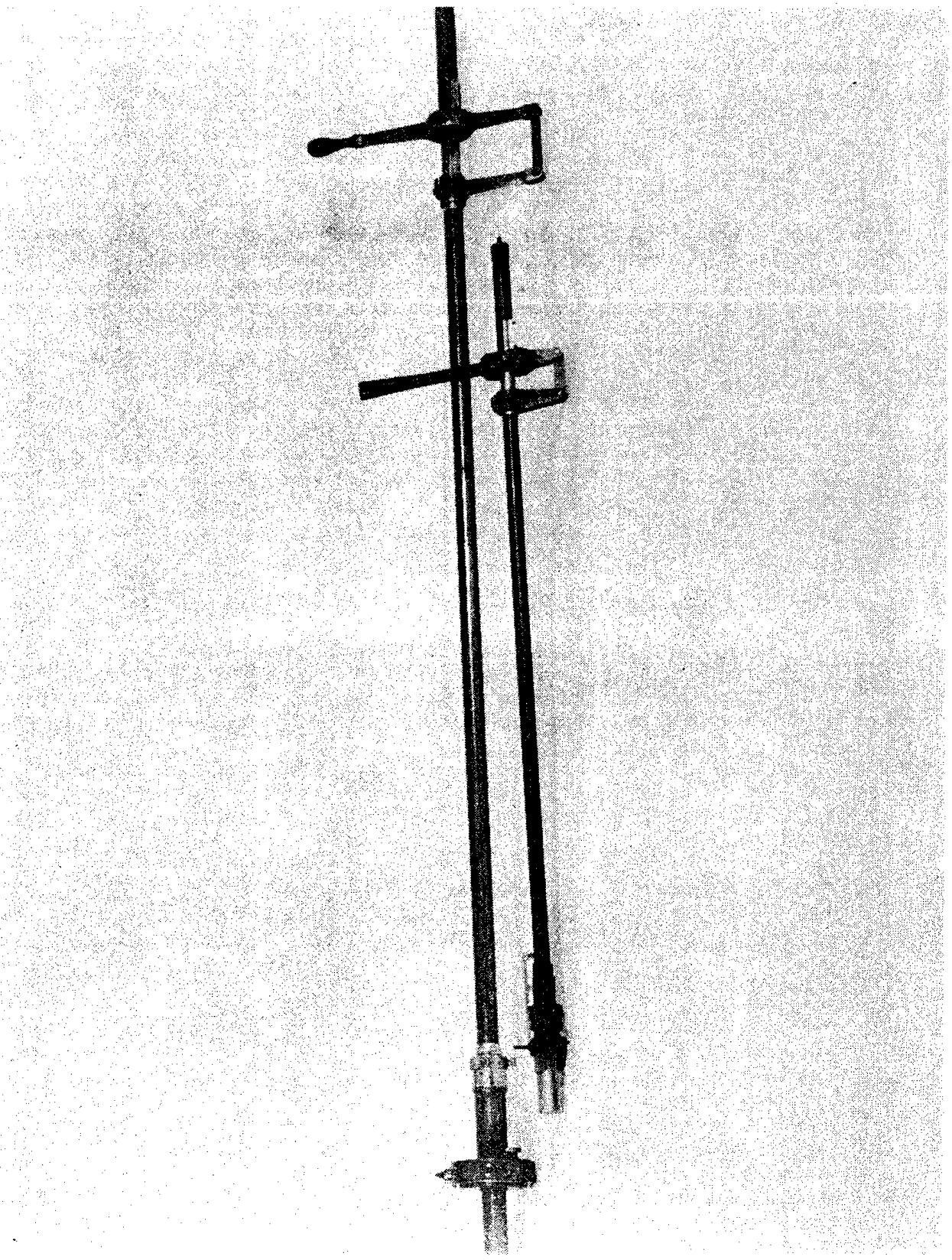

Figure 1. Mechanical Stargages

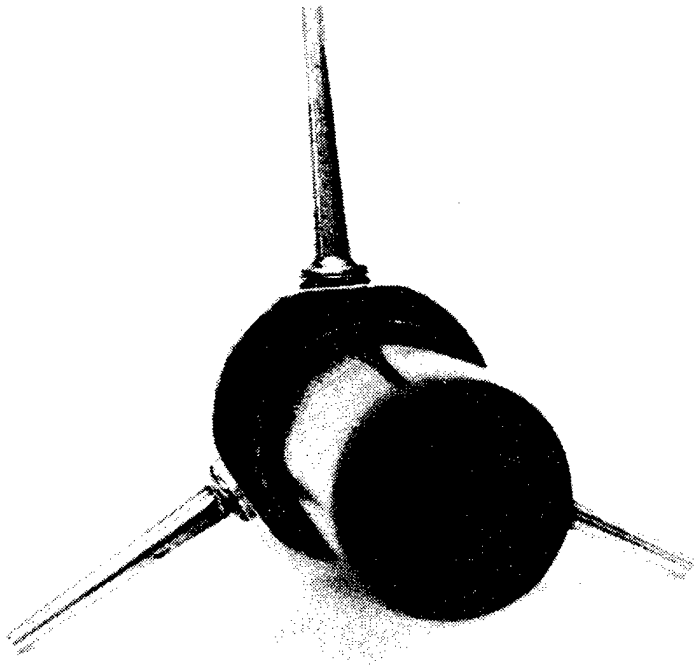

Figure 2a: Measuring Head with Three Movable Measuring Points.

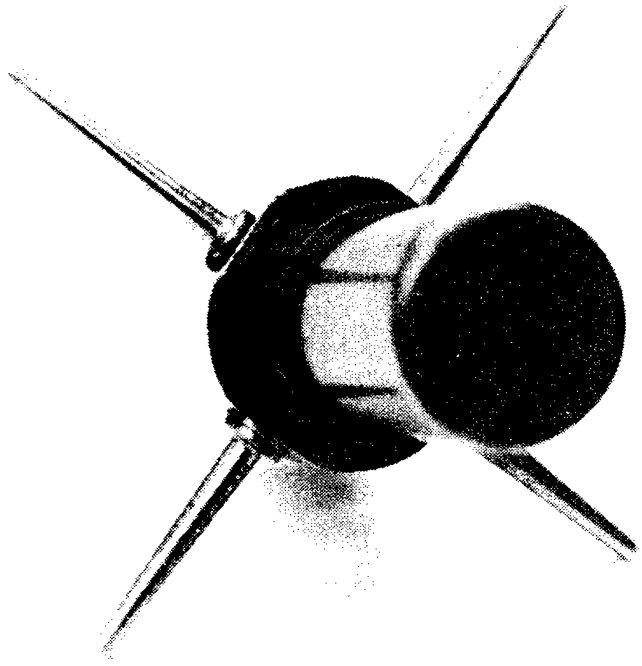

Figure 2b: Four Point Measuring Head with Two Movable Measuring Points

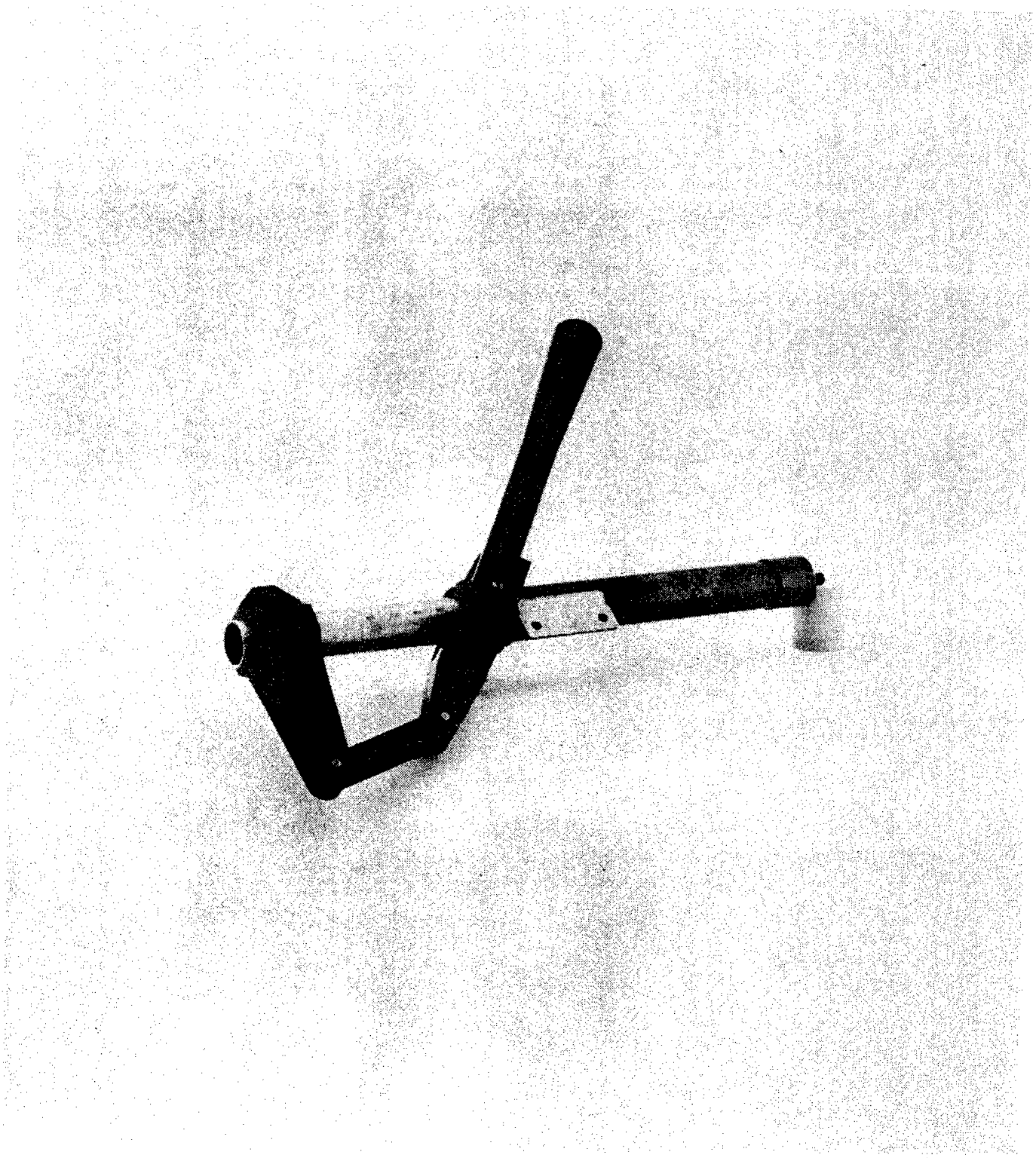

Figure 3. Operating Handle

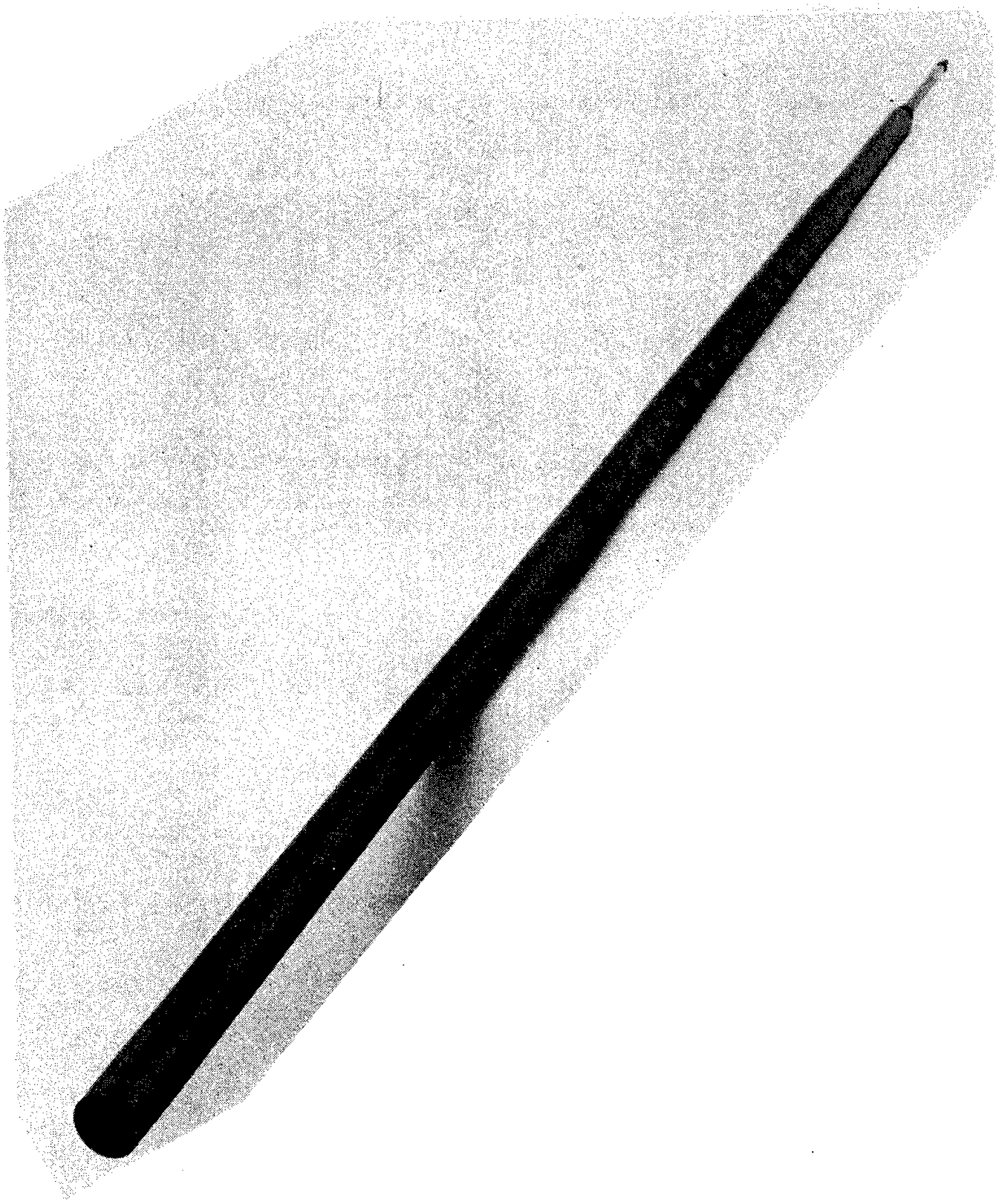

Figure 4. Stave

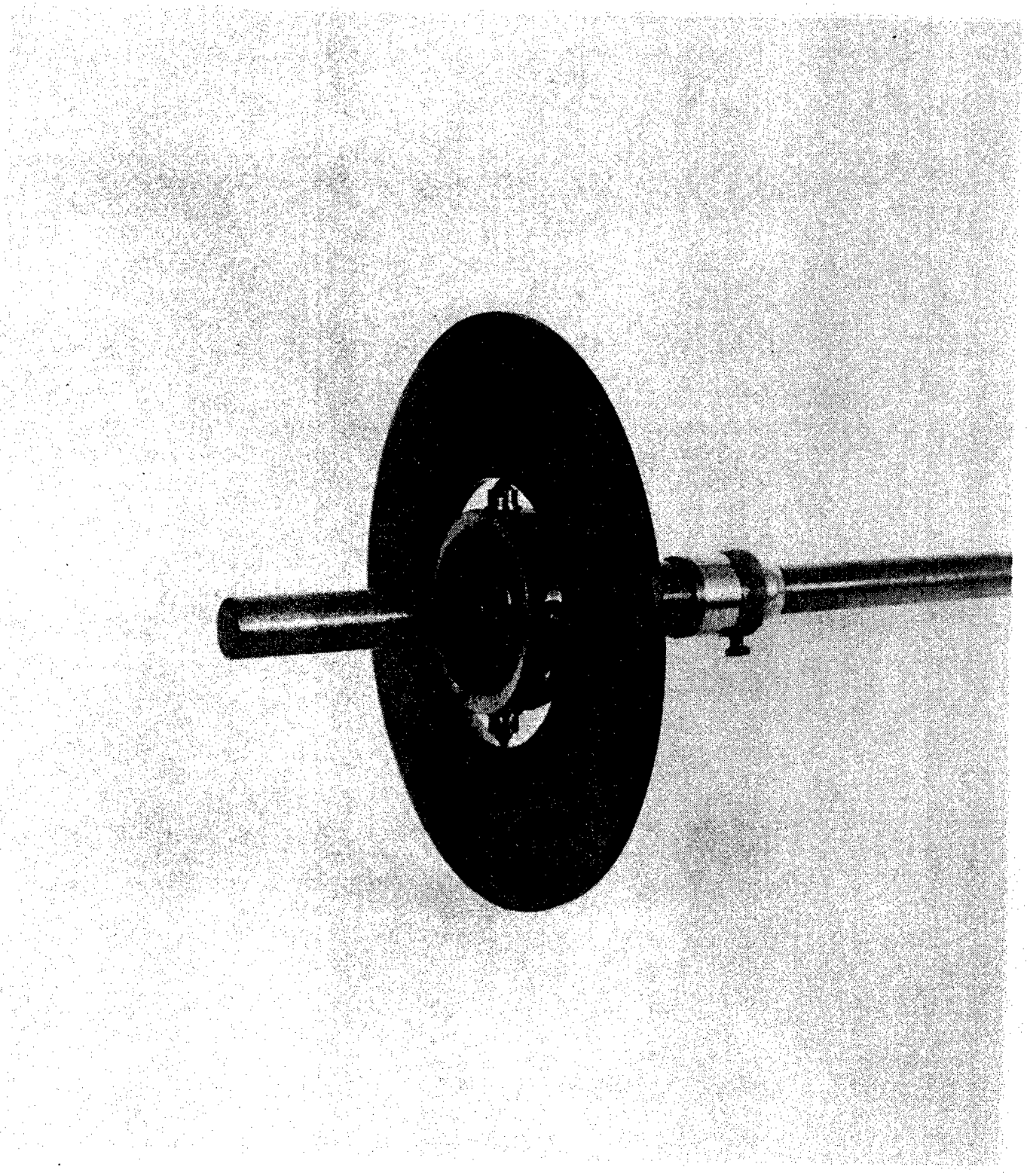

Figure 5. Size Ring

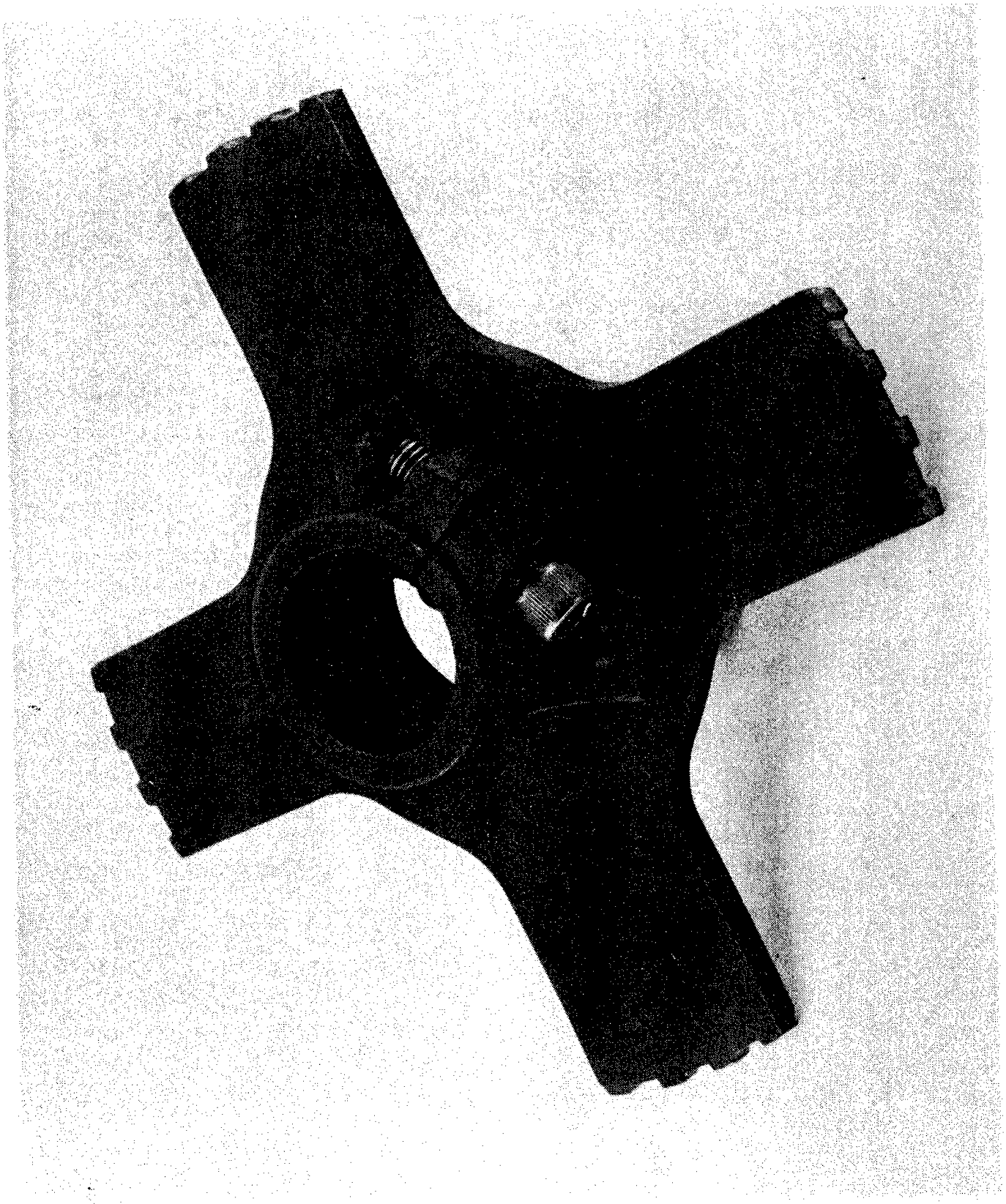

Figure 6. Guide Plate

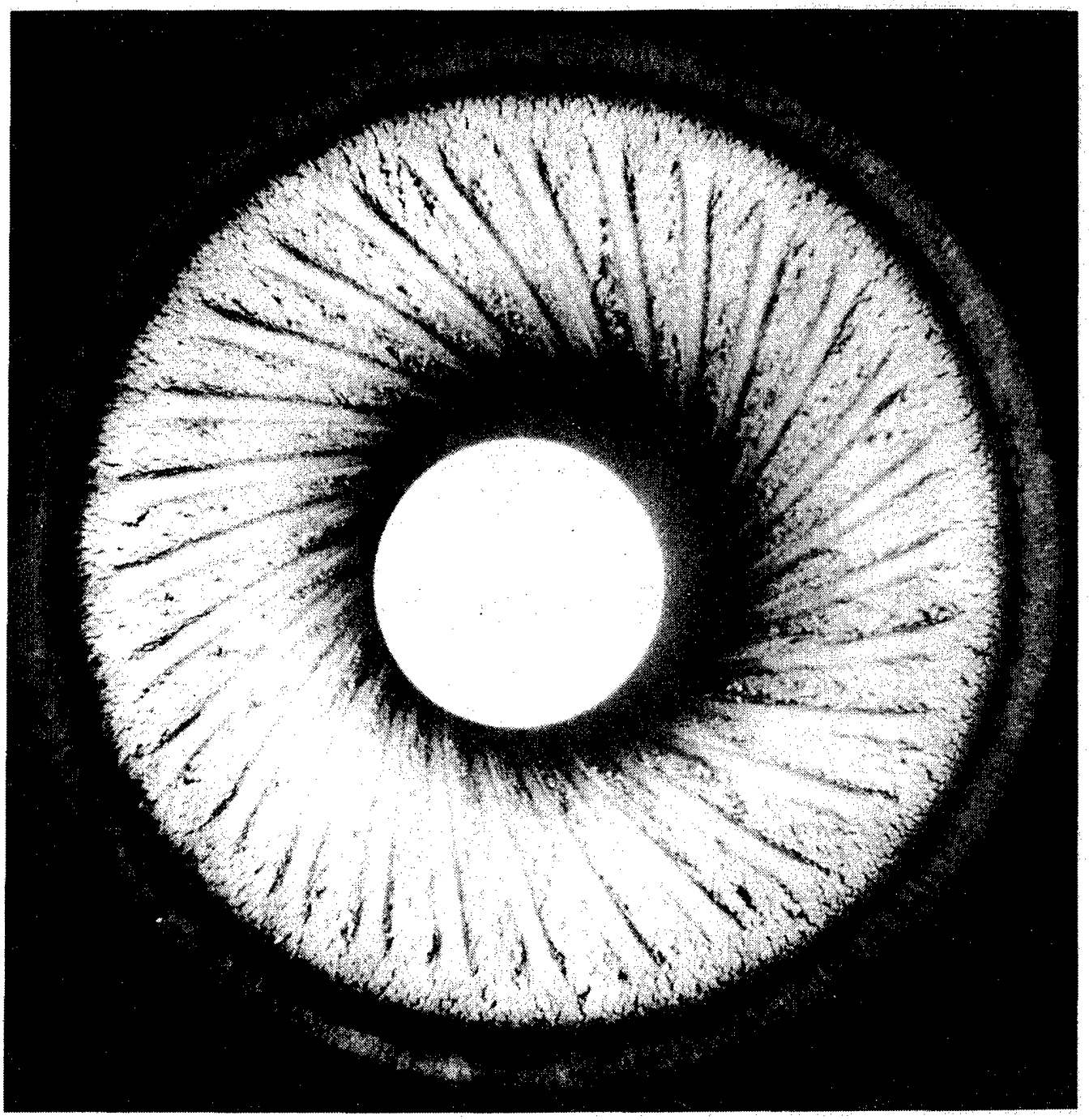

Figure 7. Heavy Wear, Erosion, Scoring

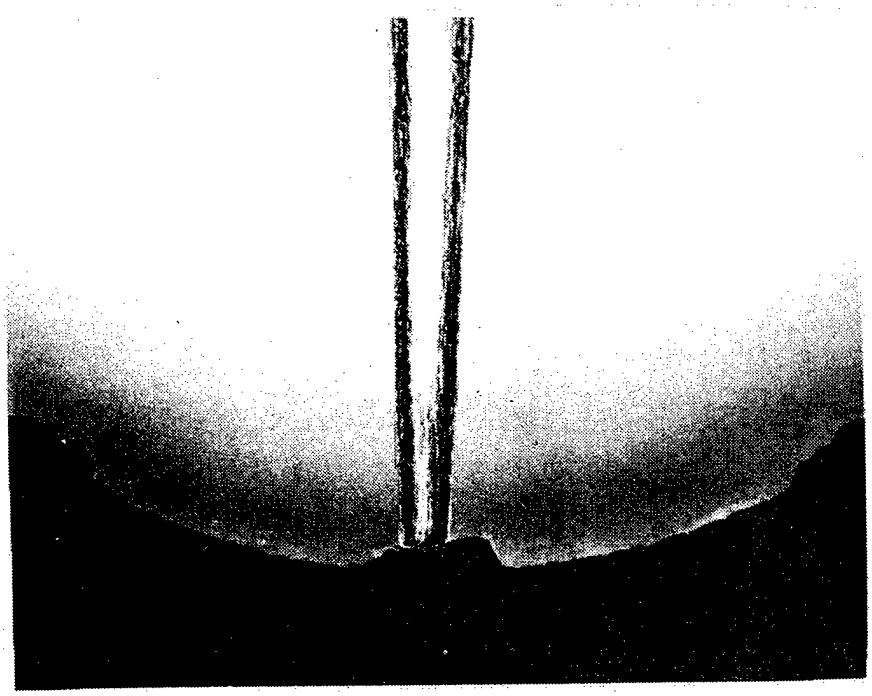

Figure 8. Worn Driving Edge of Land

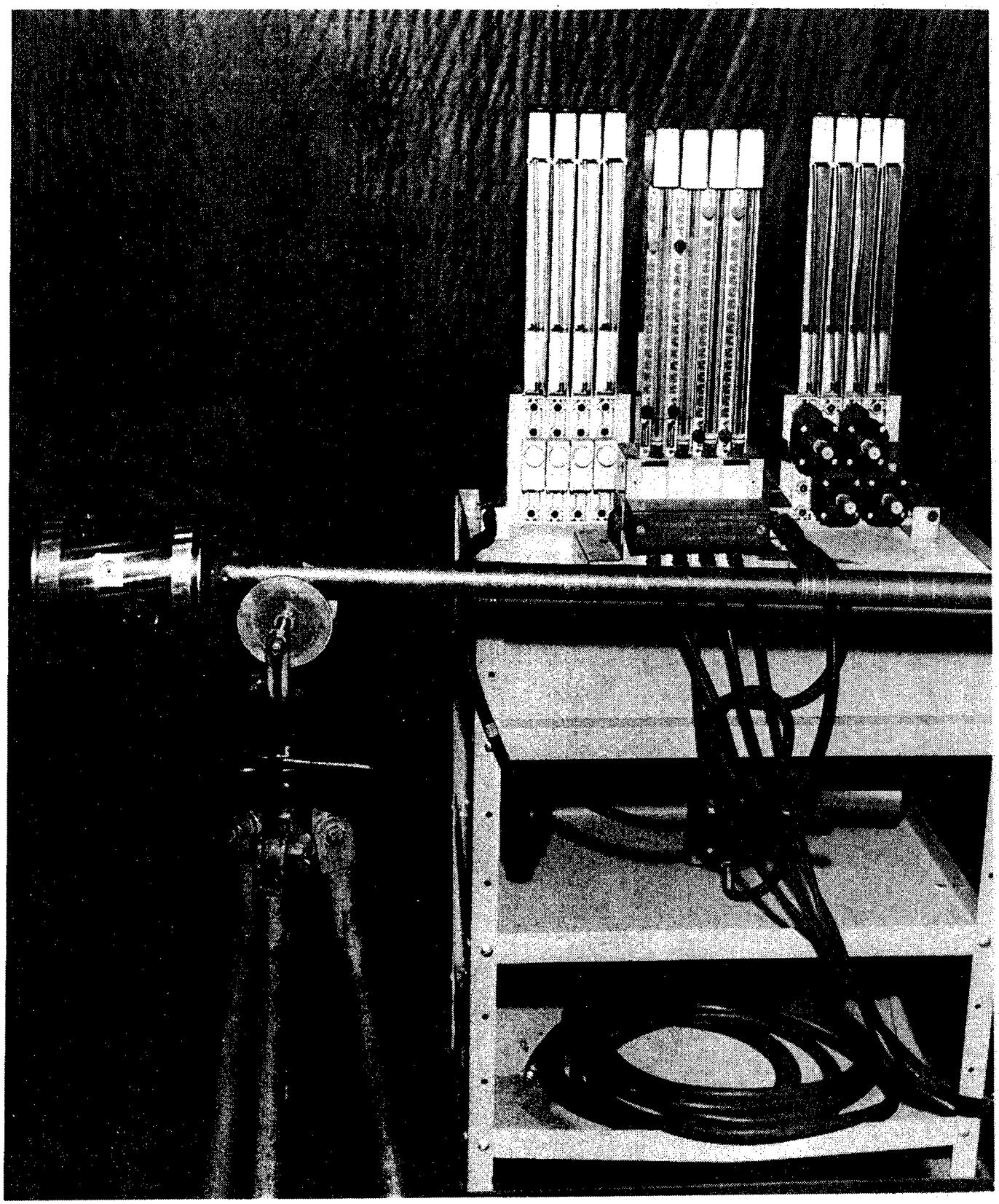

Figure 9. Air Gage

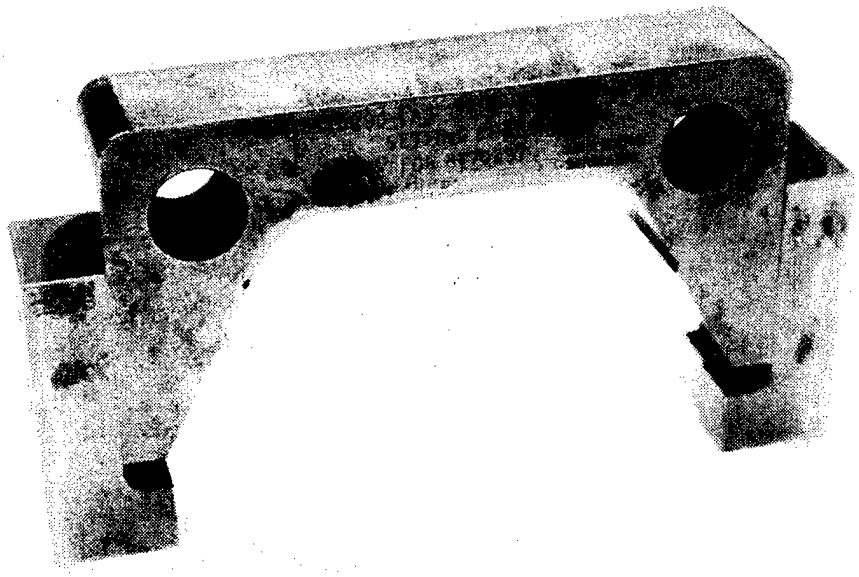

Figure 10. Calibrating Master

MULTIPLE STARGAGE MEASUREMENT & INSPECTION DATA FORM (PT-IOP 750-1

105 MM Tube, M68

Main Bore - 24.9" to 210.50"

Gage Head, Indicated in 1/1000 of an inch

CASTING NUMBER	MANUFACTURER	MODEL	NUMBER	PROOF ACCEPTANCE	PROOF OFFICER W.O.	NUMBER OF ROUNDS	FIRING STATUS (Check One) AFTER	FIRING STATUS (Check One) BEFORE	Distances (Inches) From Rear Face of Breech	Distances (Inches) From Muzzle Face	Distances (Inches) From Rear Face of Tube	LANDS 4.134" Basic Diameter Vert.	LANDS 4.134" Basic Diameter Hor.	GROOVES 4.224" Basic Diameter Vert.	GROOVES 4.224" Basic Diameter Hor.
	WVT. ARS.	M68							218.25	.25	210.25				
									217.00	1.50	209.00				
									215.00	3.50	207.00				
									213.00	5.50	205.00				
									208.00	10.50	200.00				
									203.00	15.50	195.00				
									198.00	20.50	190.00				
									193.00	25.50	185.00				
									188.00	30.50	180.00				
									183.00	35.50	175.00				
									178.00	40.50	170.00				
									173.00	45.50	165.00				
									168.00	50.50	160.00				
									163.00	55.50	155.00				
									158.00	60.50	150.00				
									153.00	65.50	145.00				
									148.00	70.50	140.00				
									143.00	75.50	135.00				
									138.00	80.50	130.00				
									133.00	85.50	125.00				
									128.00	90.50	120.00				
									123.00	95.50	115.00				
									118.00	100.50	110.00				
									113.00	105.50	105.00				
									108.00	110.50	100.00				
									103.00	115.50	95.00				
									98.00	120.50	90.00				
									93.00	125.50	85.00				
									88.00	130.50	80.00				
									83.00	135.50	75.00				
									78.00	140.50	70.00				
									73.00	145.50	65.00				
									68.00	150.50	60.00				
									63.00	155.50	55.00				
									58.00	160.50	50.00				
									53.00	165.50	45.00				
									48.00	170.50	40.00				
									45.25	173.25	37.25				
									43.00	175.50	35.00				
									41.25	177.25	33.25				
							X		38.00	180.50	30.00				
									37.00	181.50	29.00				
									36.00	182.50	28.00				
									35.00	183.50	27.00				
									34.00	184.50	26.00				
									33.50	185.00	25.50				
								X	33.25	185.25	25.25				
									33.10	185.40	25.10				

Figure 11. Data Sheet

Figure 12. Damaged Interior Surface of a Rifled Barrel

Figure 13. Pullover Gage

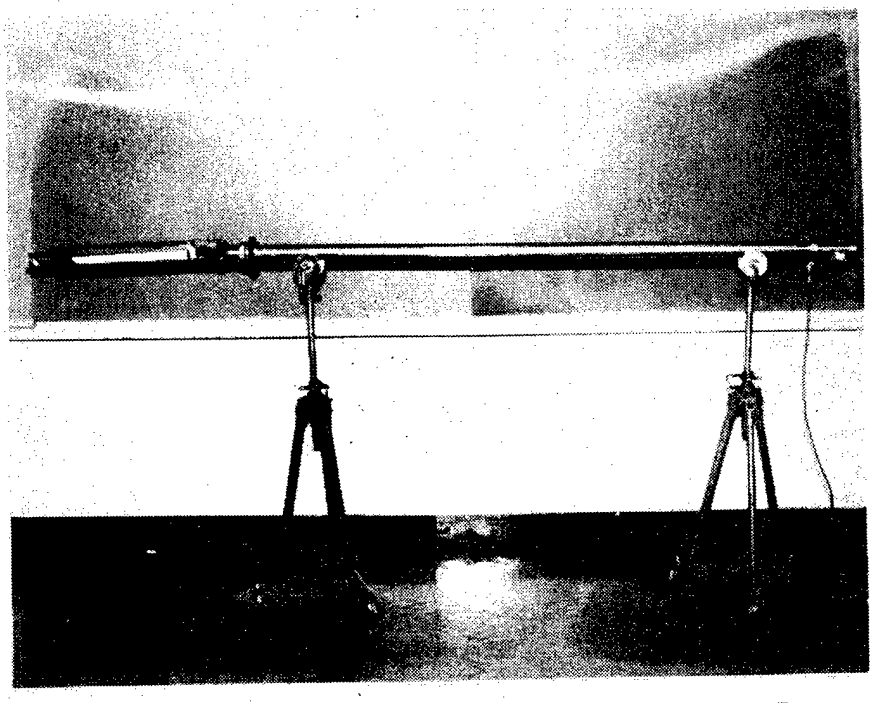

Figure 14. White Light Borescope

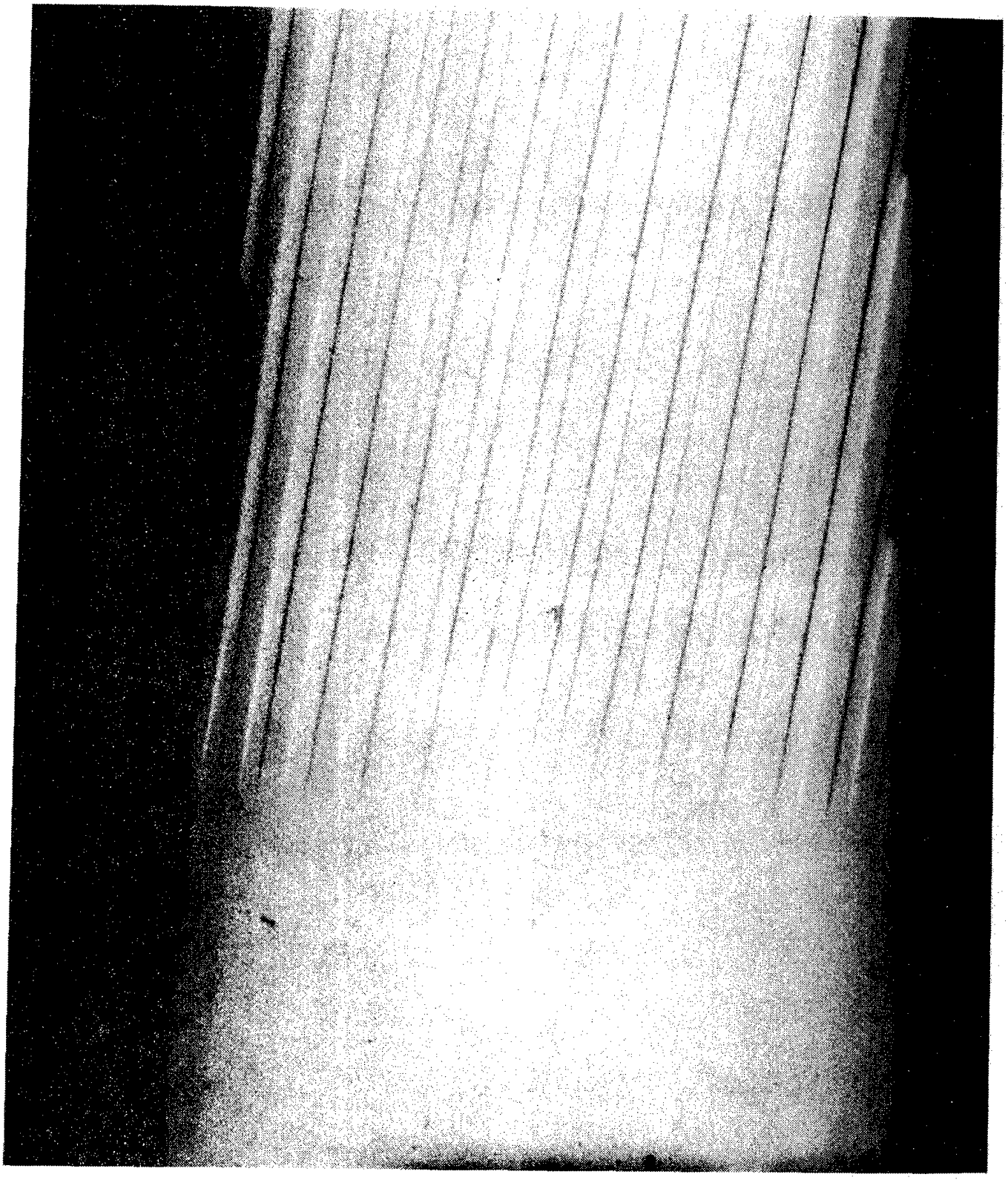

Figure 15. RTV Silicon Rubber Impression of Origin of Rifling in a 155-MM M199 Barrel.

METALLOGRAPHIC STUDIES OF EROSION AND CRACKING OF CANNON TUBES

R.M. Fisher and A. Szirmae
U.S. Steel Corporation, Research Laboratory
Monroeville, PA 15146

and

M.H. Kamdar
Department of the Army
U.S. Army Armament Research and Development Command
Benet Weapons Laboratory, Watervliet Arsenal
Watervliet, NY 12189

ABSTRACT

The characteristic erosion features of fired cannons and the closely related surface alterations on laboratory simulation samples have been examined with a variety of electron optical and other analytical techniques. The results suggest that the heat-checking pattern is caused by the large differential thermal contraction between surface austenite and subsurface tempered martensite, the deep longitudinal cracks result from liquid-solid metal embrittlement primarily by copper, and the subsurface microstructural alterations are a consequence of intense carburization by the explosion gases. The observations could provide the basis for thermomechanical modeling of the erosion and cracking of cannon tubes.

INTRODUCTION

The continuing studies at Watervliet Arsenal of the erosion of cannon tubes during firing have been described in keynote and contributed papers at previous Tri-Service Conferences and in the fracture mechanics and metallurgical literature.[1-5] The results of visual inspection and metallographic examination of the bore surfaces of fired cannon tubes have clearly established the occurrence of three rather distinct features, namely, (1) a corncob-like heat-checking pattern, (2) a series of deep cracks nearly aligned parallel to the tube axis, and (3) several etch-resistant "white layers" and a region of "thermally altered ferrite" with microstructures and hardness values very different from the tempered martensite steel base. As mentioned in the forementioned papers and as discussed in detail in this paper, these three erosion features appear to result from (a) thermal stresses, (b) fatigue crack propagation with the added influence of an embrittling agent, and (c) chemical reaction with the bore surface, namely, carburization.

Recently, the optical metallographic studies have been augmented and extended by the application of a variety of electron-beam instruments and other analytical equipment to develop a more detailed description of the major erosion features.

Because of the very limited number of cannon tubes that are available, especially with a complete record of firing history, the program has also utilized simulation samples prepared in the laboratory by capacitance-discharge pulse heating.

EXPERIMENTAL MATERIALS METHODS

All samples examined were of 4340 steel and included sections cut from the breech area and bottom of the rifling of fired cannon tubes and from flat sheet tensile specimens heated by capacitance discharge as listed below.

Description of 4340 Steel Samples

Cannon Tubes (105 mm)
- 6826
- 7544 (Cr-plated prior to firing)
- T-45 (additive used)

Simulation Samples
- pulse heated in 3000 psi methane
- Cu-plated and pulse heated in vacuum

Selected specimens were examined by optical microscopy, scanning (SEM), and high-voltage-transmission electron microscopy (HVEM) to study the surface and subsurface microstructures at high magnification and by energy dispersive X-ray spectroscopy (EDXS), Auger spectroscopy, Mossbauer spectroscopy, and secondary ion mass spectroscopy (SIMS) to determine the surface and near-surface chemical composition. The pulse-heating apparatus has made it possible to produce chemical alterations to the surface that simulate the effects of propellant gases.

The results of the investigation are illustrated with representative examples obtained with the various samples examined and techniques employed.

EXPERIMENTAL RESULTS

The characteristic heat-checking pattern and deep cracks parallel to the rifling are illustrated in Figure 1 (a,b). The bright areas are abrasion marks from the rotating Cu band on the projectile. The appearance of this surface in the SEM is shown in Figure 2, along with an EDX spectrum showing that the surface is covered with Ti and lesser concentrations of Al, S, K, and Cu. Point-to-point probing revealed that the Fe signal from the steel base largely came from the spaces between the hillocks and that the Cu was associated with the abrasion marks.

A Ni-plated, polished and lightly etched cross section of sample T-45, illustrating the alternating pattern of shallow, deep and very deep cracks that is typical of fired cannons, is shown in Figure 3.

The near-surface structure of this sample can be seen in more detail in the optical micrograph of a 15° taper section shown in Figure 4a. EDXS analysis of this same area in the SEM revealed that a considerable amount of Cu, and some S and Al were present in cracks extending in to the altered ferrite region.

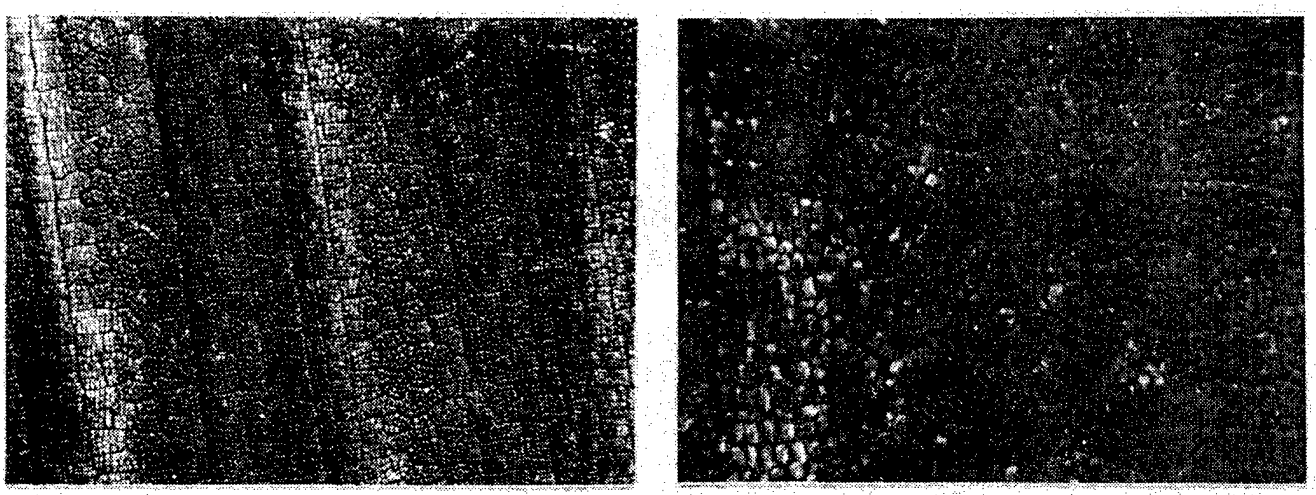

(a) 3X (b) 10X

Fig. 1. Optical micrographs of the bore surface of Cannon Tube T-45.

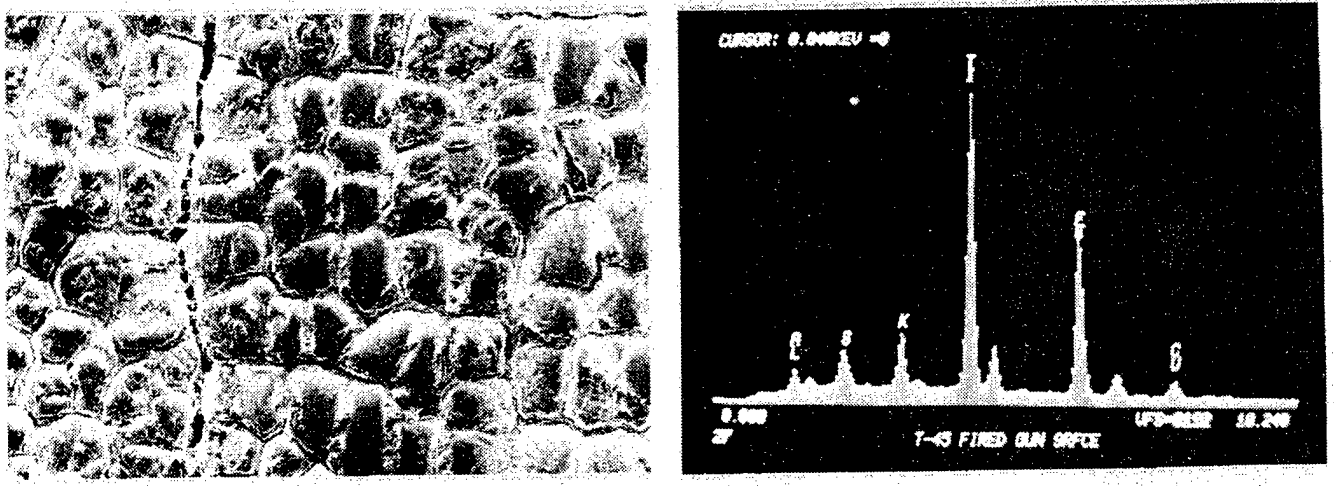

(a) SEM 60X (b) Whole Surface EDXS

Fig. 2. Cannon Tube T-45, bore surface.

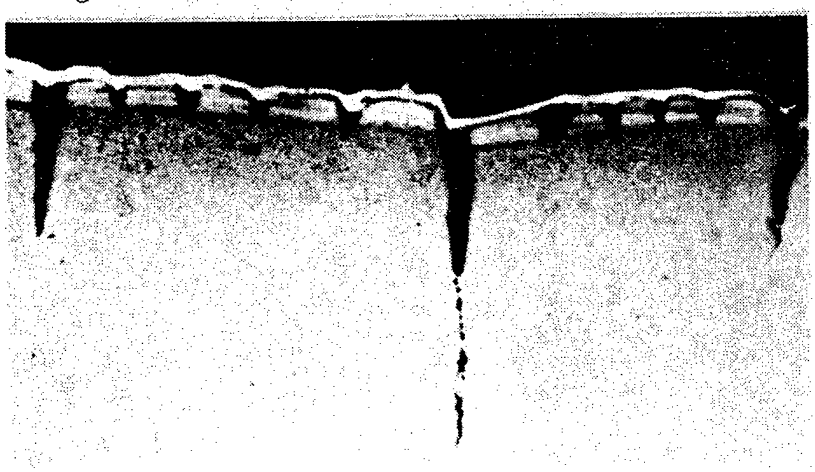

Fig. 3. Cannon Tube T-45, cross section 50X

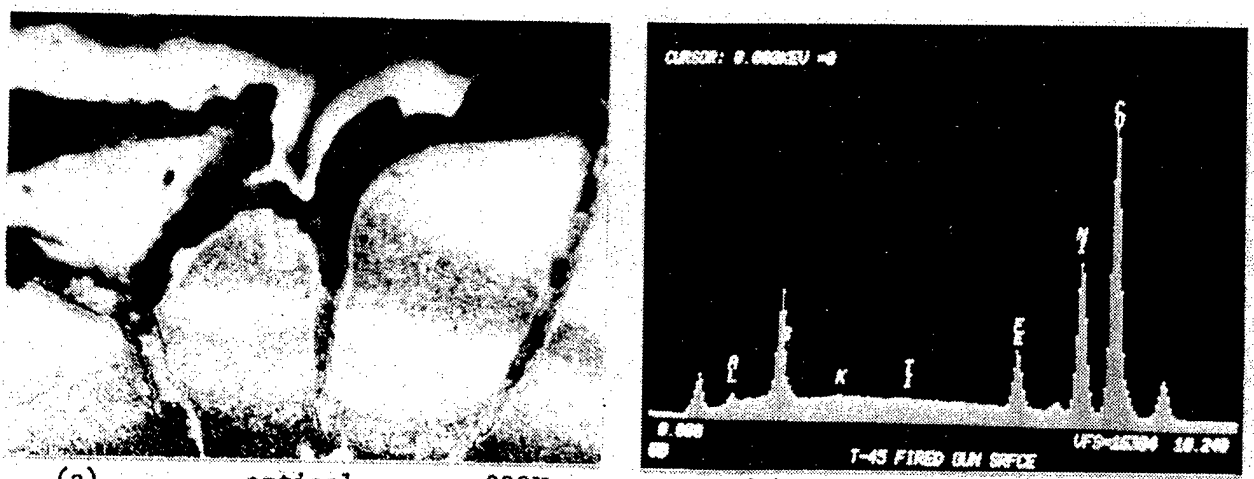

(a) optical 200X (b) EDXS

Fig. 4. EDXS of Ni-plated taper section of Cannon Tube T-45 (arrow in (a)) shows Cu penetration.

Penetration of Ni during plating demonstrates that these cracks were open to the bore surface.

Examination of the bore surface of cannon tube 6826 (no additive in the propellant) in the SEM revealed a rather different appearance, as illustrated in Figure 5. The small crystals visible on the surface at higher magnification were suspected to be cementite (Fe_3C). This opinion was confirmed by subsequent Auger, Mossbauer, and SIMS analyses of the surface, and by stripping the surface film and obtaining direct electron diffraction evidence for Fe_3C.

The carbon concentration in the altered region was determined by several techniques including a Mossbauer surface analysis method, depth profiling by Auger

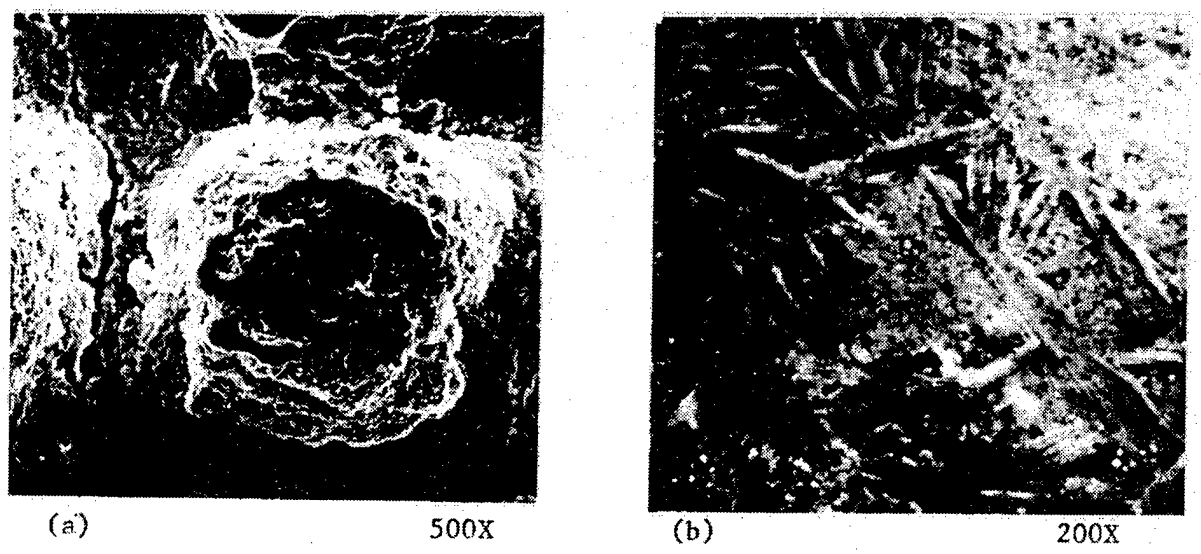

(a) 500X (b) 200X

Fig. 5. SEM of bore surface of Cannon Tube 6826, showing fine Fe_3C crystals (b).

and SIMS, and profiles on cross sections by electron probe analysis using a special light element detector. All of these methods indicated the presence of 0.25 to 0.5 μm of Fe_3C on the surface and a subsurface layer of about 2 to 10 μm of austenite containing 2 percent carbon near the surface and about 1 percent carbon in the interior. The very rough surface of eroded cannon tubes precludes obtaining more than an estimate of the thicknesses of the white layer constituents by profiling. The SIMS depth profiles for carbon in Figure 6 were obtained in two different laboratories.

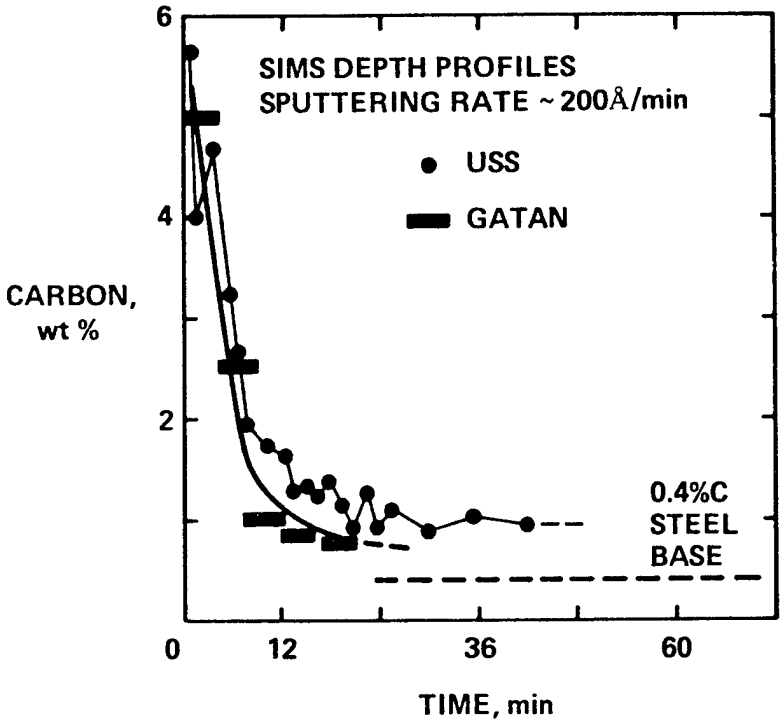

Fig. 6. Cannon Tube 6826, bore surface.

The effects of chemical alteration of the surface of 4340 steel during pulse heating in high pressure methane are illustrated in Figure 7. Polished and etched 6° taper sections reveal the appearance of the surface eutectic structure (with pools of austenite) and the grain boundary carbides in the subsurface austenite. The very fine scale of the eutectic suggests an extremely rapid solidification rate. An example of transformation of a surface austenite pool to martensite is illustrated in Figure 7a.

Transmission electron micrographs illustrating the lamellar structure of the surface carbide film and an example of the high carbon plate martensite which formed in the subsurface austenite region are shown in Figure 8. The electron diffraction pattern from this film confirmed that it was Fe_3C, i.e., identical to that observed for fired cannon specimens.

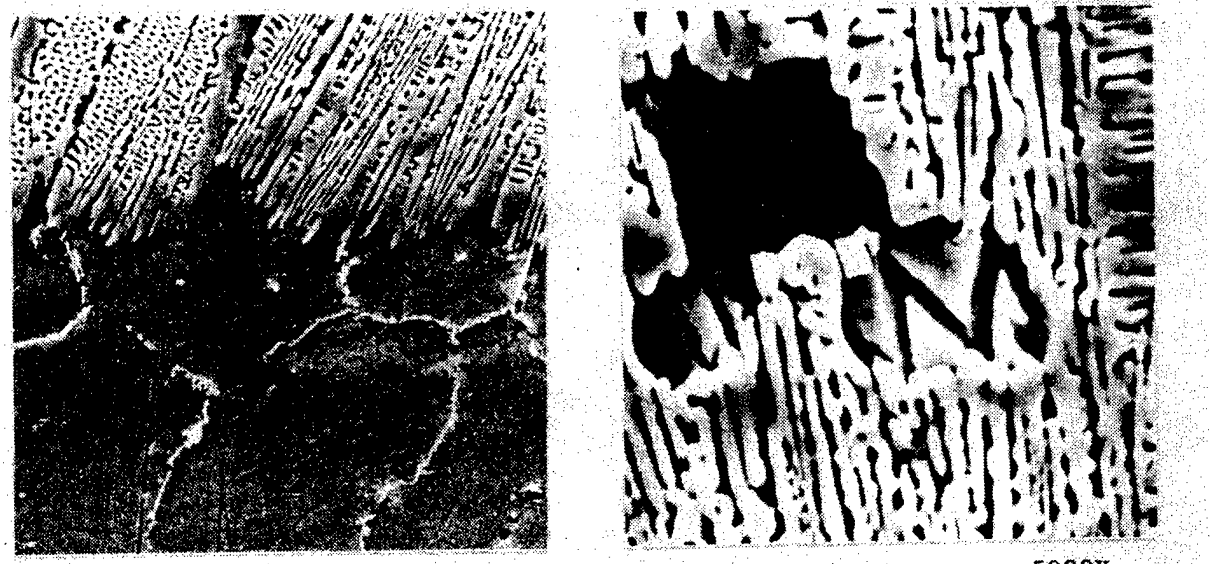

(a) SEM 2000X (b) SEM 5000X

Fig. 7. SEM of a taper section of a simulation specimen pulse-heated in methane showing Fe_3C at the surface [top (a)] and in grain boundaries in austenite [bottom (a)]; pools of austenite and martensite formation are shown in (b).

(a) HVEM 16,000X (b) HVEM 21,500X

Fig. 8. Thin foils of simulation specimen pulse-heated in methane showing lamellar carbide (a) and subsurface austenite and martensite (b).

and SIMS, and profiles on cross sections by electron probe analysis using a special light element detector. All of these methods indicated the presence of 0.25 to 0.5 μm of Fe_3C on the surface and a subsurface layer of about 2 to 10 μm of austenite containing 2 percent carbon near the surface and about 1 percent carbon in the interior. The very rough surface of eroded cannon tubes precludes obtaining more than an estimate of the thicknesses of the white layer constituents by profiling. The SIMS depth profiles for carbon in Figure 6 were obtained in two different laboratories.

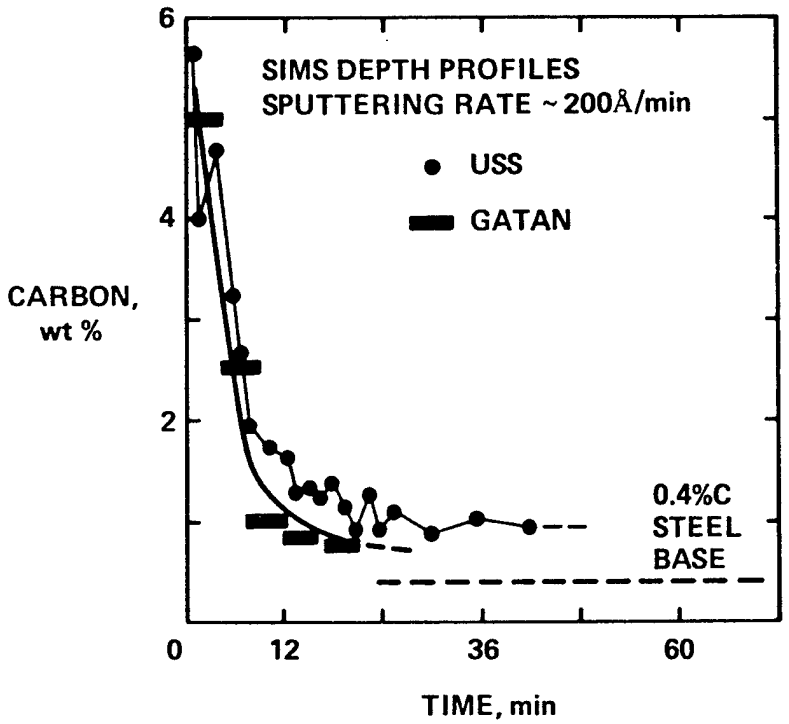

Fig. 6. Cannon Tube 6826, bore surface.

The effects of chemical alteration of the surface of 4340 steel during pulse heating in high pressure methane are illustrated in Figure 7. Polished and etched 6° taper sections reveal the appearance of the surface eutectic structure (with pools of austenite) and the grain boundary carbides in the subsurface austenite. The very fine scale of the eutectic suggests an extremely rapid solidification rate. An example of transformation of a surface austenite pool to martensite is illustrated in Figure 7a.

Transmission electron micrographs illustrating the lamellar structure of the surface carbide film and an example of the high carbon plate martensite which formed in the subsurface austenite region are shown in Figure 8. The electron diffraction pattern from this film confirmed that it was Fe_3C, i.e., identical to that observed for fired cannon specimens.

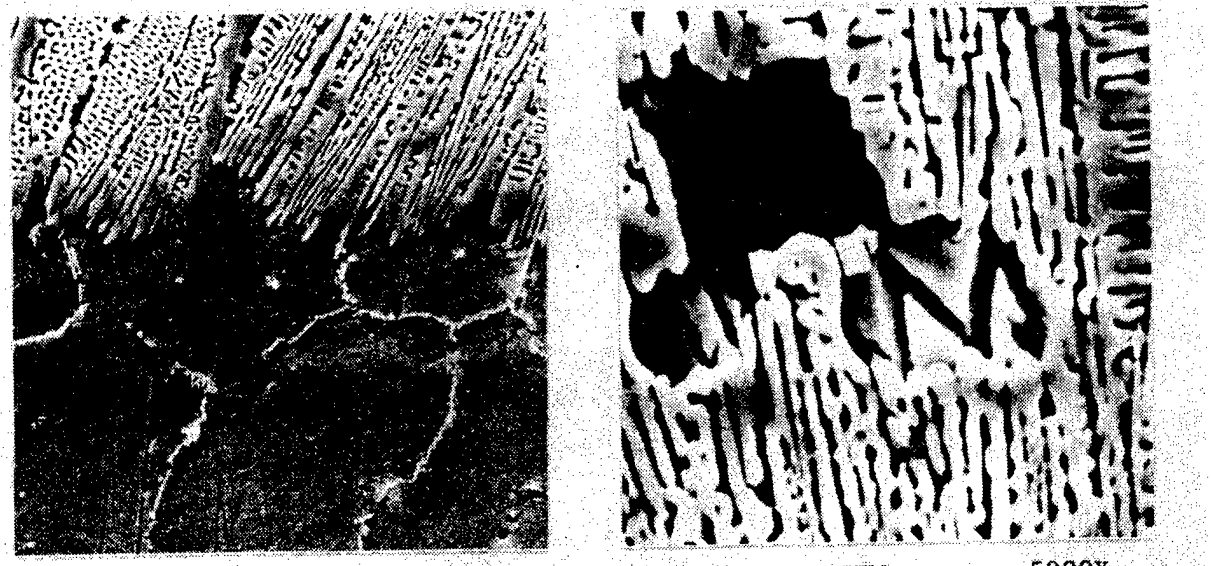

(a) SEM 2000X (b) SEM 5000X

Fig. 7. SEM of a taper section of a simulation specimen pulse-heated in methane showing Fe_3C at the surface [top (a)] and in grain boundaries in austenite [bottom (a)]; pools of austenite and martensite formation are shown in (b).

(a) HVEM 16,000X (b) HVEM 21,500X

Fig. 8. Thin foils of simulation specimen pulse-heated in methane showing lamellar carbide (a) and subsurface austenite and martensite (b).

The observations of Cu penetration deep into the longitudinal cracks prompted some analogous experiments to pulse heat specimens that had been Cu-plated. An example of the cracks that developed at the root of the notch (used to localize the heating) is shown in Figure 10. The presence of Cu could be detected by EDXS in the cracks but penetration to their tips did not occur in any of the pulse-heated specimens.

SUMMARY OF OBSERVATIONS

The three major microstructural characteristics of eroded cannon barrels, mentioned in the Introduction to this paper, are described below in order of their probable detrimental effects on the useful life of cannon barrels. General discussion of the factors that appear to determine erosion rate and suggestions for future work are presented in a separate section.

White Layer - The explosion gases are extremely carburizing to the extent that carbon-saturated liquid iron forms on the surface and solidifies rapidly after the firing cycle to form a thin layer of very fine eutectic of Fe_3C and Fe with a considerable amount of retained austenite. Carbon diffusion into the steel results in the formation and retention of a layer of relatively soft austenite and an altered ferrite region hardened by the precipitation of alloy carbides. No white layer forms on surfaces protected by chrome plating.

Heat Checking - Rupture of the surface results from rapid thermal expansion and contraction of the surface during each firing cycle. The expansion coefficients of ferrite and austenite are very different so that the presence of a surface layer of high-carbon austenite (with a very low M_S) can result in very large tensile strains, as illustrated qualitatively in Figure 11. Because of the large mass of the cannon tube, cooling of the heat-affected zone is relatively rapid and the effective strain rate fairly high, resulting in the formation of "quenching cracks." The occurrence of coarse and fine networks suggests that the stresses relieved by an initial stage of crack formation recur during further cooling and cause secondary cracking. This is analogous to the familiar paint-crazing or mud-flat crack patterns and fire cracking on work rolls.

Longitudinal "Fatigue" Cracks - Sharp cracks, 0.2 to 1 mm deep, form parallel to the rifling with a spacing of about 1 mm (the very deep cracks are spaced about 10 mm apart). These cracks are associated with regions of Cu transfer from the rotating band. The cracks contain easily detectable Cu, some S (presumably from the propellant), and Al (which may be a contaminant from metallographic polishing), to very near the crack tips. Propagation of the deep cracks during each firing cycle is presumably enhanced by the enbrittling agents (Cu, S, Al?) which may be forced into the cracks by the explosion pressure.

The chemical activity of pure methane is probably greater than that of the explosion gases, and there is little turbulence so that the carbide layer tends to be thicker and more uniform. Because no quenching is used, the pulse-heated specimens cool more slowly than the thick cannon tubes resulting in the formation of grain boundary carbides in the austenite.

The deep penetrating cracks in fired cannon tubes were found to contain Cu, and lesser amounts of Al and S right to the tip of the crack, i.e., more than 400 μm in some cases. The results of all of the various observations and analyses of eroded bore surfaces from two cannons are summarized schematically in Figure 9.

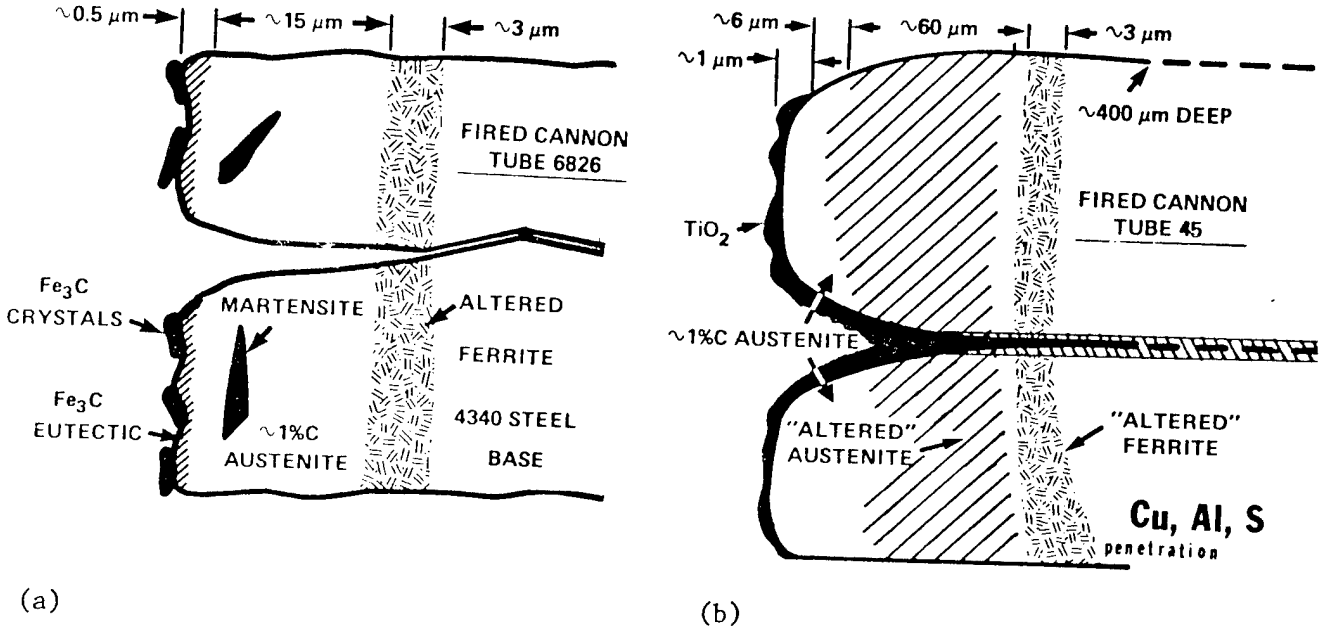

Fig. 9. Schematic illustration of cannon bore surface.

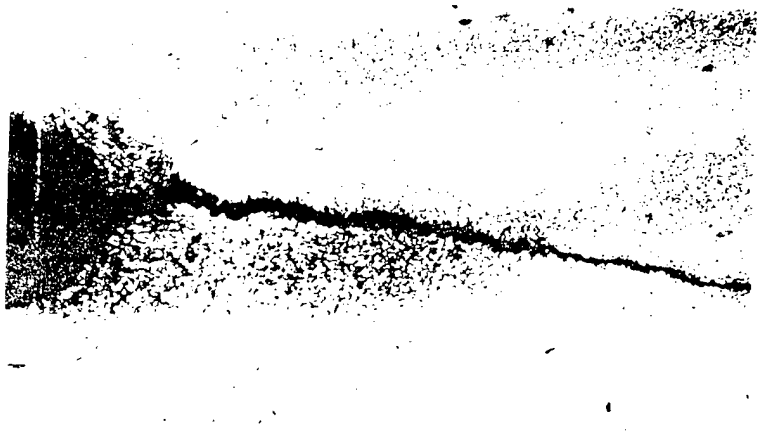

Fig. 10. Optical micrograph of crack at the root of a notch in a Cu-plated and pulse-heated 4340 steel sample. 50X

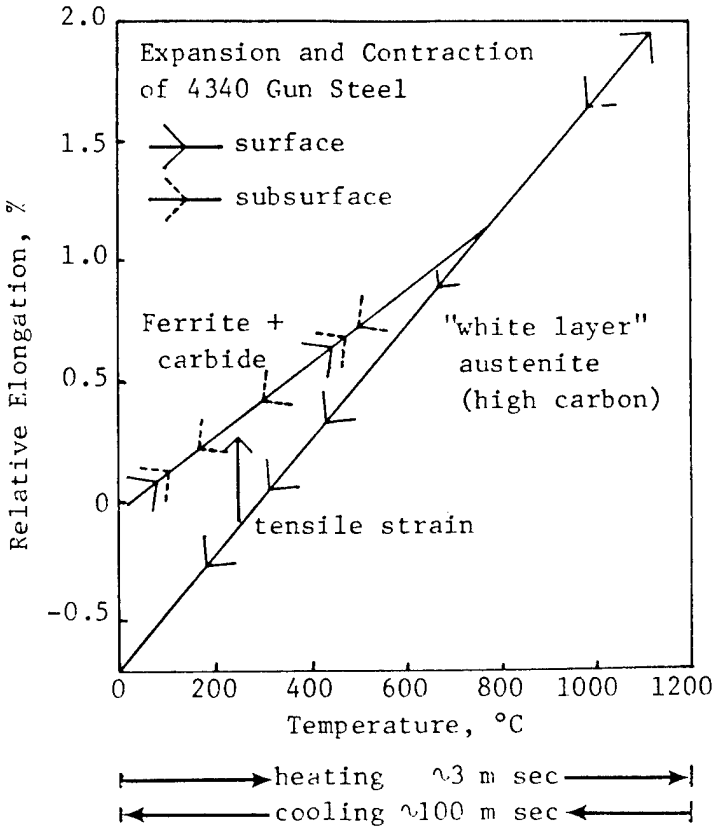

Fig. 11. Illustration of origin of heat checking due to differential contraction.

DISCUSSION AND RECOMMENDATIONS

The results of this study confirm many of the observations of previous investigators, particularly with respect to carbide formation[5] and to deleterious effects of Cu.[4] The new or more quantitative information provides the basis for a more detailed understanding of cannon-barrel erosion due to white layer formation and cracking due to heat checking.

Several metal-removal mechanisms must be involved in the erosion and wear of cannon barrels. The average wear rate is about 25 μm per round unless an additive is used in the propellant. This is comparable to the depth of the crevices between the "kernels" of the heat-check pattern so that it is reasonable to presume that they are largely removed during each firing cycle. This could occur if the proturbances are converted to liquid metal and swept away by the explosion. The reduced erosion resulting from lower firing temperatures, the application of Cr-plating or use of TiO_2 additive in the propellant support this view.

The heat-checking cracks expose the subsurface of the bore to the carburizing atmosphere and enhanced formation of low-melting carbide and "cast iron." In addition, on occasion, some cracks link up below the surface causing the

formation of large pits when the metal "plug" is forced out leading to accelerated erosion. Fatigue cracks, due to Cu embrittlement when Cu rotating bands are used, may become a significant factor if erosion control measures succeed in extending tube life appreciably.

FURTHER WORK

The results of this study suggest further experiments or analyses of both fired cannon samples and laboratory simulation specimens as outlined below.

Field Studies - Attempts to replicate a particular section of the bore surface of a cannon before and after firing could determine the persistence of the heat-check pattern. Techniques for obtaining surface replicas of industrial machinery such as large steel rolls in the field are available. Detailed examination of debris particles collected from the breech area or from the ambient air using air sample monitors could also yield important information about erosion mechanism.

Laboratory Studies - Some further analytical work on cannon samples with known firing history is needed to establish the effect of additives on white layer formation more quantitatively. The surface and near-surface (0-1 mm depth) heating and cooling temperature cycles (especially after considerable erosion has occurred) should be measured and calculated. This information is required in order to develop a model for heat checking due to differential thermal contraction as illustrated in Figure 11. Further laboratory studies of the effects of peak pulse heating time and temperature on carbon pickup, and the reduction afforded by the use of protective coatings and thin layers of additive are needed to develop reaction rate parameters to apply to actual firing conditions in order to predict erosion rate. Controlled studies of the embrittling effects of Cu are required using both pulse-heating methods and slow hot-tensile tests with special apparatus such as a Gleeble.

REFERENCES

1. Ahmad, I., I-1-50, Proc. Tri-Service Gun Tube Wear and Erosion Symposium, ARRADCOM, Dover, NJ, March 29-31, 1977. Eds. Jean-Paul Picard and Iobal Ahmad.
2. Albright, A.A., Friar, G.S. and Morris, S.L., reference cited above.
3. Griffin, R.B., Pepe, J. and Morris, C., Metallography 8, 1975, pp. 453-471.
4. Davidson, T.E., Throop, J.F. and Underwood, J.H., 3.9.1-13, Case Studies in Fracture Mechanics, AMMRC Conf. Report 77-5. Eds. Rich and Cartwright.
5. Kamdar, M.H., Campbell, A. and Brassard, T., ARRADCOM Technical Report ARLCB-TR-78012, "A Metallographic Study of White Layers in Gun Steel," August 1978.

The material in this paper is intended for general information only. Any use of this material in relation to any specific application should be based on independent examination and verification of its unrestricted availability for such use, and a determination of suitability for the application by professionally qualified personnel. No license under any United States Steel Corporation patents or other proprietary interest is implied by the publication of this paper. Those making use of or relying upon the material assume all risks and liability arising from such use or reliance.

SESSION III

MECHANISM AND MODELING

CHAIRMAN: Dr. Austin Barrows

A BALLISTIC COMPRESSOR FOR STUDIES OF CORROSION AND EROSION OF METALS EXPOSED TO A HOT, DENSE GAS

M. Takeo, J. Dash and C.E. Sanford

Department of Physics, PSU
Portland, Oregon

ABSTRACT

This report describes the use of a free-piston gas compressor for studies of crystal structure and chemical changes which cause corrosion and erosion of metals due to its exposure to hot, dense gases. The compressor at Portland State University can produce a gas at more than 2000 atmospheres pressure and 6000 K, though only for about 0.5 msec. Small samples are mounted on the piston head and the compressor may be fired without opening repeatedly as many times as desired. Preliminary observations were made with samples of pure metals and an alloy. Microhardness tests showed no significant effects on the bulk of a copper, gold, or aluminium rod when used as a sample with nitrogen gas. However, an electrolytically thinned austenitic stainless steel became slightly magnetic after exposure to hot, dense argon containing a trace of oxygen. The optical and TEM micrographs and the electron diffraction patterns before and after the exposure to a hot, dense gas show some changes in structure and additional chemical compounds.

INTRODUCTION

When metals are exposed to reactive gases corrosion often occurs. If the temperature and pressure of the gases change rapidly with time there may be thermal and mechanical stresses over the surface. If hydrogen molecules are present at elevated temperatures, they may easily diffuse into the metal, introducing microcracks and plastic deformation during the course of cooling. If there is locally a strong flow of a hot, dense gas, erosion may be expected. History of corrosion and erosion research is very long[1], but such research seems not to cover the case of exposure to a gas at high temperatures and high pressures, except for explosive bonding of metals.[2] The purpose of this paper is to show that research with a ballistic compressor can fill some of this gap.

In contrast to a shock wave produced, for instance, by an explosion, the compressed gas in a compressor can be at very high density, comparable to the density of liquid. Thus, high density chemistry may become important in interpreting the effects of a hot, dense gas. However, traditional approaches seem to apply to the results obtained thus far.

In corrosion processes, oxidation is important. But stress-corrosion and hydrogen embrittlement[3] are also mechanisms leading to functional failure of otherwise well-designed metallic structures. The rate of these processes may become faster or types of reactions may change if metals are exposed to gases at higher temperatures and pressures. It is well known in flame research[4] that important

Approved for public release; distribution unlimited

types of chemical reactions can change depending on the pressure and temperature of the system.

A ballistic compressor can also be helpful in determining whether microcracks develop on a metallic surface when the metal is exposed to a moderate hydrogen pressure at an elevated temperature and then rapidly cooled. Hydrogen as well as oxygen are important reactants leading to undesirable modification of the physical properties of a metal. These gases are dangerous to use in the compressor without being diluted. They were added by 1% or less by volume to helium before firing.

For preliminary observations, pure metals and an alloy were used as samples. Because of complicated phase diagrams, alloys might give more interesting observations compared to pure metals. A thin metallic film prepared by electrolytic thinning of bulk Fe18%Cr12%Ni alloy gave a good example. The film, originally in γ phase, became slightly magnetic after the exposure to a hot, dense argon with a trace of oxygen. The optical and TEM micrographs and the electron diffraction patterns of the sample on the exposure clearly shows the structural difference.

DESCRIPTION AND OPERATION OF THE PSU BALLISTIC COMPRESSOR

The ballistic compressor at Portland State University is a modification of the original structure, which has already been fully described elsewhere.[5] The following is therefore limited to a brief description of the present device.

As shown in Fig. 1, the compressor consists of the horizontally-mounted 2.90m (9.51 feet) long, 5.72cm (2.25 inches) inner diameter tube (A) attached on one end to the driving gas reservoir (B) and on the other to the high pressure head (C). With a 52.6cm (20.7 inches) long, 9.63kg (21.23 lb.) piston in prefiring position, the volume of the driving gas reservoir is 9.30 liters (2.46 gallons), and the volume of the test gas chamber is 7.5 liters (1.98 gallons). The maximum possible stroke is 2.77 m (9.09 feet).

The high pressure head (Fig. 1-b) is made from ARMCO17-4 PH stainless steel 25 cm (9.84 inches) in outside diameter, which is able to withstand a gas pressure of 6000 atmospheres. The driving gas reservoir (Fig. 1-C) contains the piston holding and release mechanism. In the prefiring position, the tail of the piston engages in the mechanism, which opens and pushes the piston slightly forward at firing by cranking the handle (D).

The piston is shown in Fig. 1-d. The piston head (E) has a diameter of .05 mm (0.002 inches) less than the bore of the tube, and is made from the same material as the high pressure head. The short piece of 2mm diameter lead rod (F) attached to the front of the piston head is used for determination of the closest approach of the piston to the end wall.

In operation, with the piston in prefiring position, the test gas chamber is filled to an absolute pressure of less than 1 atmosphere. Next, the driving gas reservoir is filled with the same gas to a predetermined pressure. Then, using the releasing mechanism, the piston is fired.

Various modifications have been made to the original construction. One example is as follows. Small size copper pipes were used originally for the vacuum system. But they have been replaced by larger sized ones (4 cm (1.6 inches) in diameter) for faster operation of the vacuum system. This replacement has made it posssible to return the piston to its prefiring position without disassembling the device after each firing, so that repeated firing is now possible without disassembly.

The output of the pressure transducer is recorded on an oscilloscope (Tektronix RM35A) with a polaroid camera. The peak pressure at each firing can thus

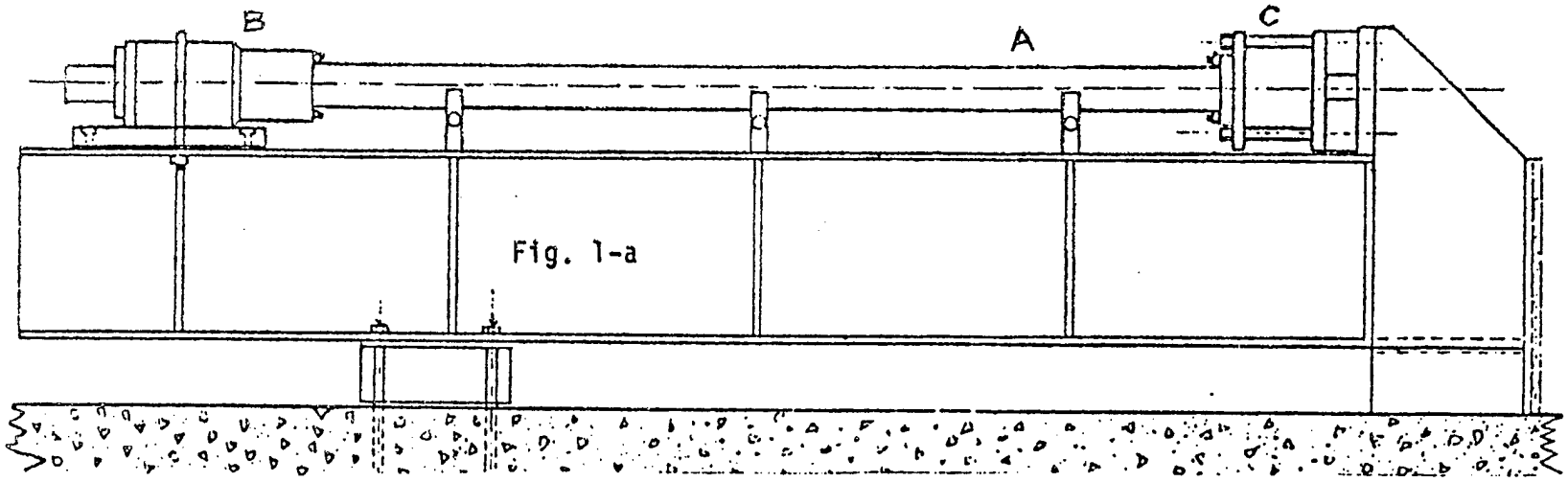

Fig. 1-a

Fig. 1-c

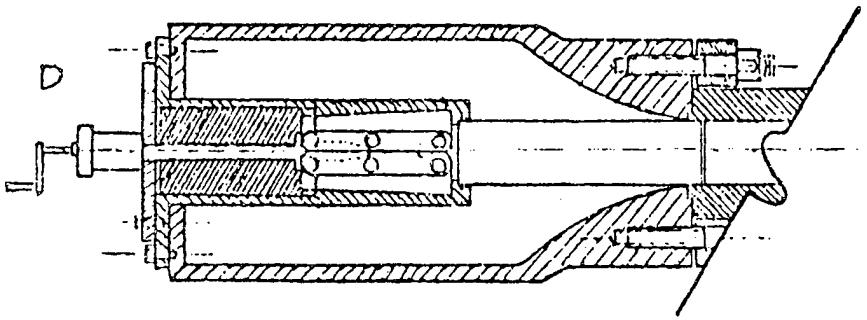

Fig. 1-b

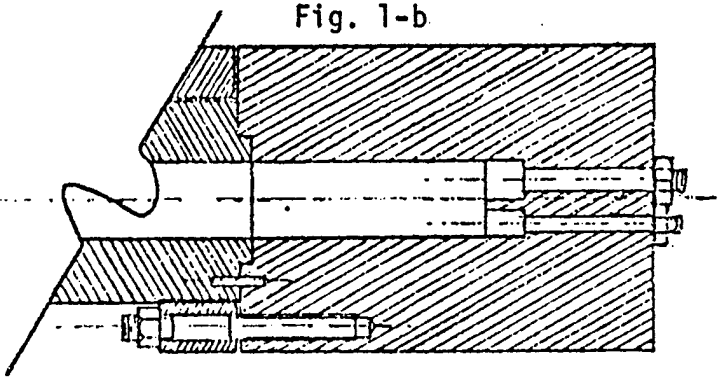

Fig. 1-d

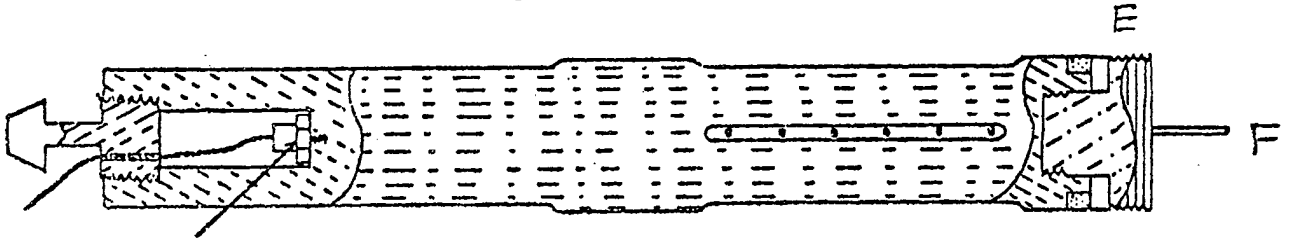

Accelerometer, presently not in use.

Fig. 1 Diagrams of PSU Ballistic Compressor and the piston.

be easily read on the oscillogram, but the gas temperature is found by using a computer program as described in detail elsewhere.[5,6] The program is to solve the equation of motion for the piston by allowing heat loss of the test gas by conduction through the compressor wall and gas leakage through the piston gap under the assumption of thermal equilibrium in both test and driving gases at any time during the compression and expansion of the gas systems.

A simple examination of the gas leakage can be made by observing the pressure profile at the instant of maximum radiation intensity.[7] The leakage rate of the test gas in the compressor may be as large as 10 moles/sec near the peak pressure. If the piston gap is made small in order to reduce the leakage, the mechanical friction becomes too large and unpredictable, thus destroying the reproducibility of gas compression. If the gap is as large as that of the present compressor, the piston is full floating inside the horizontal cylinder bore. Thus, the force on the piston due to the leaking viscous gas is solely the frictional force against the motion of the piston. Then the frictional force is given by

$$F = \pi r_0(r_0-r_p)(P-P_r)+2\pi\eta v L r_0/(r_0-r_p). \qquad (1)$$

The piston gap, r_0-r_p, is small, so that the first term can be neglected and the frictional force becomes proportional to the velocity of the piston. But the proportionality constant changes because the viscosity depends on temperature:

$$\eta=AT^B. \qquad (2)$$

For monatomic gases at the temperature attained in the ballistic compressor, the majority of gas molecules are in the ground state. Therefore, it is justified to use the van der Waals' equation of state

$$(P+a/V^2) \cdot (V-b) = n \cdot R \cdot T \qquad (3)$$

for the gas systems.

The equation of motion for the piston is conveniently written in the form of the energy equation. For a time interval dt, the piston makes a displacement of dx. Then, the energy changes satisfy

$$mvdv = \delta q+\delta q_\ell-dU-dU_r-Fdx, \qquad (4)$$

where dU is the internal energy change of the test gas during dt due to a heat flow δq into the gas, due to the work on the piston and due to work $P\frac{V}{n}dn$ which causes dn moles of leaking gas to flow, and due to gas leakage which carries away a part of the internal energy, dU_ℓ. From the first law of thermodynamics,

$$dU = \delta q-PdV-PVn^{-1}dn-dU_\ell. \qquad (5)$$

Similarly for the reservoir gas, for which an adiabatic process can be assumed,

$$dU_r = -P_r dV_r+P_r V_r n_r^{-1}dn+dU_{\ell r}. \qquad (6)$$

The rate at which gas leaks though the piston gap is governed by the pressure difference between the test and driving gases. It is given by

$$\frac{dn}{dt} = \pi P(m_a)^{-1} r_0(r_0-r_p) \cdot \left[\frac{P-Pr}{8\eta L} \cdot (r_0-r_p)^2+v\right]. \qquad (7)$$

The gas leaks from the reservoir to the test gas system at the beginning of the first stroke, but the direction is reversed in the course of compression.

The heat flow δq into the test gas is obtained by solving the well-known equation of thermal conduction applied to the compressor walls, by assuming that the gas systems are uniformly at their respective temperatures, and that the heat flow at the boundary is proportional to the difference of the temperatures of the gas and the inner surface of the walls. The proportionality constant is adjustable in the computation. Another adjustable parameter is the piston gap. At each firing, the minimum volume of the test gas is measured by the deformed length of the lead rod mounted at the piston head and the peak pressure is found with the pressure transducer. By assigning various values to the two adjustable parameters, the computer program is run until the computed minimum volume and peak pressure agree with observed ones. Then, the gas temperature profile as a function of time and the density in the test gas system are found. Usually, a few trial runs on the computer are good enough to uniquely determine the thermodynamic conditions of the gas systems.

A test of the accuracy of the computed temperature was made at the melting point of tungsten.[8] There was a discrepancy of about 3%. The program has been used with the NOR ballistic compressor at the University of Florida to determine the equation of state of UF_6. The results of measurements of the van der Waals' constants are acurate to about 10%.

For attaining temperatures above 4000 K, the quasi-adiabatic compression of a gas with the compressor must be combined with some other means of feeding extra energy to the gas. A condenser of 60 μF charged to 10kV serves the purpose. An electronically-timed ignitron switch is used to discharge the charged capacitor through a spark plug on the side wall of the high pressure head. If two such capacitors are used, the maximum gas temperature may be boosted to 7000 K. The discharge current and voltage are measured at the spark plug as a function of time, so that the instantaneous energy input to the gas system can be obtained and used in the computation of the gas condition. Since the peak discharge current can be as high as 1000 ampares, falling off to zero in about 100μsec, care has been taken in the design of the measurements to minimize the effect of the induced e.m.f. In the preliminary observations where rather thin samples were used, the gas temperature was limited to a lower value (less than 3000 K) in order to minimize the specimen damage.

EXPERIMENTAL PROCEDURE

Commercially pure copper wire and aluminum wire of 2mm (0.079 inches) diameter were heated in a Bunsen burner to red heat and then air cooled. Gold rods of the same size were also annealed in the same way. Each rod was exposed separately in the ballistic compressor. The rods were mounted, like the lead rod used for the measurement of the miniumum test gas volume, on the piston head and the compressor was fired with nitrogen gas. The rods were observed to have been bent by hitting the end wall of the compressor. Avoiding the portion where the rods were bent, they were cut with a hacksaw and the sections were embedded, ground, and polished. Microhardness tests were made at various places on the cross-sectional areas.

Some copper and aluminum rods were mounted differently from the above so that no portion of the rod could hit the end wall. After firing, the rods were examined

with the microhardness tester.

Samples in the form of thin sheets were also used. In order to mount the sheets on the piston head, in such a manner that the sheet is fully exposed to a compressed hot gas, an area of 9mm X 28mm (0.35 inches X 1.10 inches) is recessed to the depth of 6mm (0.24 inches) on the flat surface of the piston head and a block of steel is made to fill the recessed volume, so that the sheet sample can be clamped in the gap between the two. (See Fig.2). Thus, thin sheets (about 0.1 mm (0.04 inches)) of aluminum, iron, tungsten were prepared and exposed to hot, dense gases.

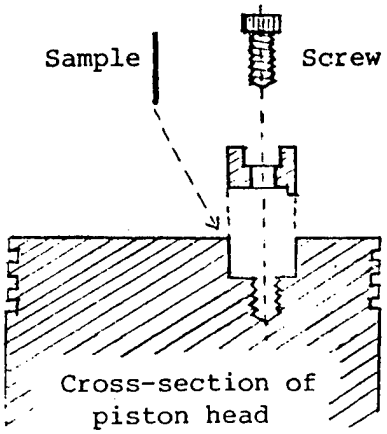

Fig. 2 Sample Mounting Mechanism

Another experiment utilized a specimen 0.2 mm(0.079 inches) thick and an electrolytically thinned film of the Fe18%Cr12%Ni stainless steel, which was used previously by one of the present authors in investigations of the martensite transformation.[9] These specimens had been heated at 1200°C in vacuum for one hour and cooled to room temperature in ten minutes, and then cooled to 77 K.The microstructure then contained about 10% ferromagnetic BCC martensite in non-ferromagnetic FCC austenite matrix. The 0.2 mm thick specimen was cut to a size of 4 mm X 10 mm (0.16 inches X 0.39 inches) heated to a red heat in vacuum and air cooled. This specimen was then non-ferromagnetic. It was then mounted on the piston head using the above-mentioned mounting mechanism and the compressor was fired. The sample was examined on an optical microscope before and after exposure to a hot, dense argon gas. The electrolytically thinned stainless steel film was also exposed to a hot, dense argon gas. Since its thickness is about 0.1 μm (3.9×10^{-6} inches) it could be observed with TEM (one MV electron microscope at Lawrence Berkeley laboratory and 100 kV electron microscope at PSU), and electron micrographs and diffraction patterns were obtained.

RESULTS AND DISCUSSION

After exposure of copper, aluminum, and gold rods of 2 mm (0.079 inches) in diameter to a hot, dense nitrogen gas at about 1300 atmospheres and 2000 K in the ballistic compressor, Knoop Hardness Numbers were observed at various places in the cross-sectional areas of the exposed pieces on Tukon Microhardness Tester and

compared with those numbers obtained with unexposed rods. There were no significant differences between the two observations. Thus, a hot, dense gas seems to give under the above conditions no effect on the bulk hardness of these pure metals.

One of the interesting observations with the rods exposed to the hot, dense gas is that if the rods were bent by hitting the end wall of the compressor they became extremely stiff and hard so that they could hardly be deformed by hand. It is not clear at present if this is simply due to work-hardening.

The most significant effect of exposure to a hot, dense gas occurs near the surface of the sample. Since the gas pressure attainable by the compressor is at most a few thousands atmospheres, the gas temperature may be more important in affecting metals. Thus, samples were shaped to a form of a sheet or a film. The shaping could also reduce the heat conduction to the piston body compared to the shape of a rod.

Iron, tungsten, aluminum, low-carbon steel, and non-magnetic stainless steel specimens were exposed to helium or argon gas at about 1000 atmospheres and 2200 K. There was no obvious difference between the effects due to argon or helium, when they were observed with a scanning electron microscope. A trace of oxygen must always be expected in the gas, but hydrogen was sometimes added to helium before firing the compressor. The scanning electron microscope did not show any significant difference betweeen effects of gases with or without hydrogen. The typical scanning electron micrograph is shown in Fig. 3, which was made with a low-carbon steel specimen. In the figure, the bright part corresponds to the part of the metal which was visually brownish due to oxidation during exposure to the hot gas. The dark part (visually shiny) was the part where the sample clamped in the piston head.

The non-magnetic stainless steel specimen became slightly ferromagnetic after the exposure to argon gas at 1000 atmospheres and 2200 K with a trace of oxygen. It was observed under the optical microscope before and after the exposure . The micrographs are shown in Figs. 4 and 5. The figures show that a new structure, possibly martensite was developed in a single crystal, but there is no change in the grain boundaries (other than grooving) during the exposure to the hot, dense gas. It is not quite clear why the new structure has appeared, but it may be noted that the cooling rate is extremely rapid (about 5×10^4 °C/sec).

The electrolytically thinned film of stainless steel was exposed to argon gas at about 160 atmospheres and 1800 K. The original shiny surface became brownish. This was then examined by TEM. Fig. 6 is a micrograph taken with a 1 MV electron microscope and Fig. 7 shows the polycrystalline diffraction pattern obtained from the region in Fig. 6. The original austenite crystal size was about 100 μm, so all of the bands in Fig. 6 are believed to have formed within one austenite crystal during exposure in the compressor. A single band in Fig. 6 gives a single crystal electron diffraction pattern, such as that shown in Fig. 8. The orientation relationship between adjacent bands has not yet been determined. The complicated patterns of Figs. 7 and 8 may suggest formations of chemical compounds during exposure.

ACKNOWLEDGEMENTS

Electron micrographs at 1 MV were obtained with the high voltage electron microscope at Lawrence Berkeley Laboratory. The present authors are grateful to D. Ackland for his assistance. Thanks are also due to C. Lopez and D. Beard for performing the hardness tests, and to C. Tam, who took the optical micrographs.

1mm

Fig. 3 Scanning electron micrograph of a low-carbon steel specimen after exposure

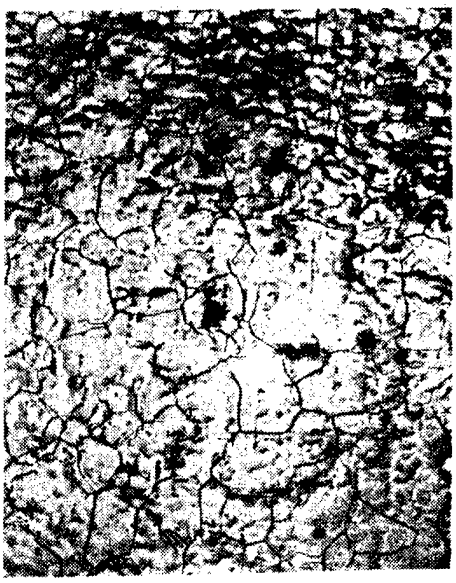

100μm

Fig. 4 Optical micrograph of a sheet of stainless steel before exposure.

25μm

Fig. 5 Optical micrograph of the arrow portion of Fig. 4, after exposure.

Fig. 6 TEM micrograph of a thin film of stainless steel exposed to a hot, dense gas.

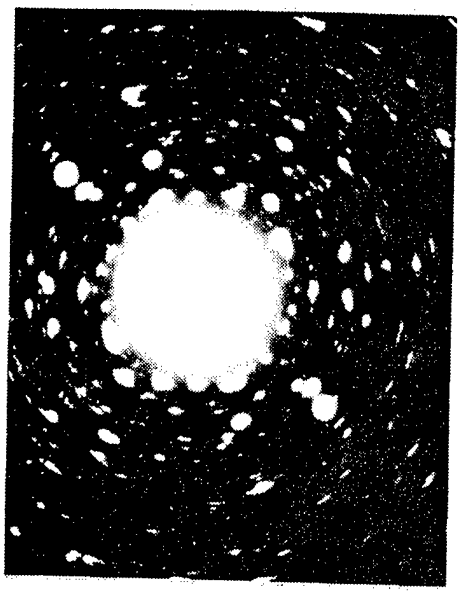

Fig. 7 Electron diffraction pattern of the region of Fig. 6.

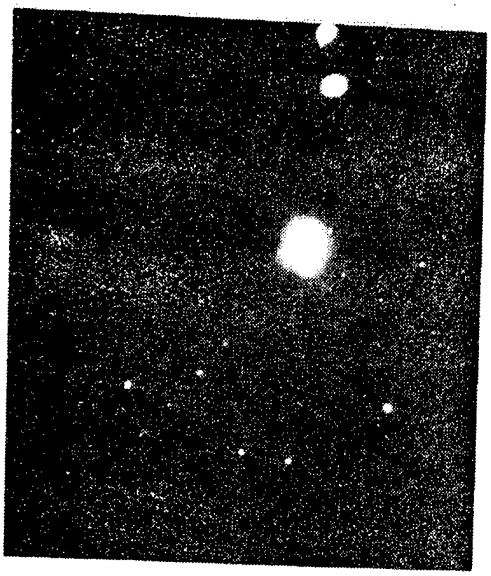

Fig. 8 Electron diffraction pattern of a single band in Fig. 6.

REFERENCES

1. "Metallurgy at High Pressures and High Temperatures", sponsored by Physical Chemistry of Steel Making Committee, Feb 1963.
2. W.C. Leslie, E. Hornbagen, and G.E. Dieter, J. Iron Steel Inst. 200, 622(1962).; T. Yamashita and T. Onzawa, J. Electron Microsc. 29, 32(1980).
3. C.D. Beachem, ed., "Hydrogen Damage", American Society of Metals, Metals Park, Ohio, 1977.
4. Irvin Glassman, "Combustion", Academic Press, N.Y., 1977, pp. 23-55.
5. M. Takeo, O.A. Holmes, and S.Y. Ch'en, J. Appl. Phys. 38 3544(1967).
6. D.E. Sterritt, G.T. Lalos and R.T. Schneider, Special Report, University of Florida, to NASA (NGL-10-005-089), March 1973; G.T. Lalos and G.L. Hammond, Experimental Thermodynamics of Non-Reacting Fluids, Ch. 25, 1975, pp. 1193-1218.
7. M. Takeo, Bull. Am. Phys. Soc. 9, 712 (1964).
8. S.Y. Ch'en, Univ. of Oregon, private communication (1976).
9. J. Dash and H.M. Otte, Acta Met. 11, 1169(1963).

LIST OF SYMBOLS

A: viscosity constant.
a: van der Waals' "a" constant. T-dependent.
B: viscosity constant.
b: van der Waals' "b" constant, T-dependent.
F: frictional force against the piston.
L: length of the piston.
m: mass of the piston.
m_a: molecular weight of the leaking gas.
n: the total number of moles of the test gas.
dn: number of moles of the leaking gas in dt.
n_r: the total number of moles of the reservoir gas.
P, P_r: pressure of the test , reservoir gas, respectively.
δq: heat flow to the test gas in dt.
δq_ℓ: heat flow to the leaking gas in dt.
R: gas constant.
r_0: diameter of the bore.
r_p: diameter of the piston.
T: absolute temperature.
t: time.
U, U_r: internal energy of the test, reservoir gas, respectively.
U_ℓ: internal energy carried by the leaking gas from the test to the reservoir gas.
$U_{r\ell}$: internal energy carried by the leaking gas from the reservoir to the test gas.
V, V_r: volume of the test, reservoir gas, respectively.
v: velocity of the piston.
x: position of the piston measured from the prefiring position.
η: viscosity of the leaking gas.
ρ: density of the leaking gas.

CALIBRATION OF THE NORDHEIM-SOODAK HEAT TRANSFER MODEL TO THE LARGE CALIBER ARTILLERY TUBE HEATING PROBLEM

by

John E. Kovacs

U. S. Army Armament Research and Development Command
Requirements and Analysis Office
Dover, New Jersey 07801

ABSTRACT

This paper presents a comparison of two methods for calculating the heat transfer coefficients to the gun barrel wall, and the calibration of the Nordheim[1] defined friction factors against the present experimental values for the bore heat input, as a function of position along the tube for the 8 inch, 155mm and 105mm artillery cannon systems, firing their respective charges with and without wear reducing additive. Also, the bore heat transfer coefficients, propellant gas temperatures, and bore surface temperatures as calculated by both the Nordheim and Calspan[2] methodologies, are presented for a conceptual 155mm system.

The technique used to calibrate the Nordheim friction factors was to iterate the friction factor until the value of the calculated heat input came within 0.5 percent of the Calspan experimental value. All calculations supporting this manuscript were performed by computer programs written by the author.

Tube wear life has been correlated fairly well with the maximum bore surface temperature at the origin of rifling, and the potential for propellant cook-off can be avoided by knowledge of the chamber temperatures.[1] The effort initiating this investigation has been a continuing one to support the capability to assess the improvements to the large caliber tube wear technology, and to make reasonable estimates of tube life and cook-off potential for new conceptual weapon systems.

The resulting calibrated friction factor profiles can be used to reasonably predict heat input values for conceptual systems providing the concepts are designed using the same propellants and are within the same calibers.

---

(1) Refers to investigation of gun barrel heating by Nordheim, Soodak and Nordheim, Ref. 2.

(2) Refers to Thermal Research Center activities of Calspan Corporation, Buffalo, New York.

Distribution limited to U. S. Government agencies only; test and evaluation; October 1982. Other requests for this document must be referred to ARRADCOM, ATTN: DRDAR-TSS, Dover, New Jersey 07801.

NORDHEIM-SOODAK THEORY

The Nordheim theory assumes the following form for a forced convective heat transfer coefficient (h) between the high temperature gas and the gun barrel wall.

$$h = 0.5 \lambda C_p \rho v \qquad (1)$$

where λ = dimensionless friction factor

C_p = specific heat of propellant gases at constant pressure

ρ, v = density and velocity of gases, respectively

Further, defining a reduced ballistic system, and using the classical equations of interior ballistics, and assuming that the unburnt propellant is uniformly distributed in the gas, the following expression for h was derived by Nordheim.[2/]

$$h_{s,t} = \sqrt{\alpha K C_s \rho_s / 2} \left(\chi_s / \chi_0\right) L f(\tau) \qquad (2)$$

where α = reduced time coefficient

K, C_s, ρ_s = thermal conductivity, specific heat, and density of steel, respectively

χ_s = coordinate of position in the gun tube at a definite point s, calculated as tube volume up to point s, U_s, divided by the cross-sectional area of the bore, A

χ_0 = coordinate of position at beginning of projectile travel, calculated as chamber volume, U_0, divided by cross sectional area of the bore, A

L = fundamental parameter for heat transfer, given by

$$L = \frac{43.1 \lambda C_p C^{3/4} p_{max}^{5/4}}{\sqrt{K C_s \rho_s}\, m^{1/4} A^{1/2} F} \left(\frac{1 - \Delta/\rho_p}{\Delta}\right)^{3/4} \qquad (3)$$

where Δ, ρ_p, F = bulk density, density and impetus of propellant, respectively

C, p_{max}, A = charge weight, maximum chamber pressure, and barrel cross-sectional area, respectively

m = reduced projectile mass, calculated as $m = 1.04\ (m_0 + C/3)$ where m_0 = projectile mass

$f(\tau)$ = time dependency, given as a function of the reduced travel ratio, (y_s/y_0), given as, (before burnout)

$$f(\tau)=\frac{\left[1-(y_0/y_s)^{\frac{\gamma-1}{2}}\right]^2}{(1-\Delta/\rho)\left[y_s/y_0+\frac{\Delta}{E(1-\Delta/\rho)}\left\{1-\left(\frac{y_0}{y_s}\right)^{\frac{\gamma-1}{2}}\right\}\right]\left(\frac{y_s}{y_0}+\frac{\Delta/\rho}{1-\Delta/\rho}\right)} \quad (4)$$

and, (after burnout)

$$f(\tau)=\frac{E^{3/2}\left[1-\frac{1}{1-E}\left(\frac{y_0}{y_s}\right)^{\gamma-1}\right]^{1/2}}{(1-\Delta/\rho)\left[y_s/y_0+\frac{\Delta/\rho}{1-\Delta/\rho}\right]^2} \quad (5)$$

where E = burning parameter, given as, $E=0.18F/j\phi^2$

where j = ratio, m/C

ϕ = reduced burning constant, given as, $\phi=\left[\frac{1-\Delta/\rho}{j\Delta}(3.45P_{max})\right]^{1/2}$

γ = ratio of specific heat of propellant gases, a value of $\gamma = 1.36$ has been used in all calculations and equations

The reduced travel ratio, y_s/y_0, is given in integral form as, (before burnout)

$$I_1(\eta)=\int_{1.05}^{\eta}\frac{d\eta}{(1-\eta^{-.18})}=\tau \quad (6)$$

and, (after burnout)

$$I_2(\xi)=\int_{1.4}^{\xi}\frac{d\xi}{(1-\xi^{-.36})^{1/2}}=E^{1/2}(1-E)^{\frac{1}{\gamma-1}}(\tau-\tau_b) \quad (7)$$

where η = reduced travel ratio, y_s/y_0

ξ = ratio, $\eta/\eta_b^{1/2}$

η_b = reduced travel ratio, at all burnt, y_b/y_0

y_b = all burnt position, given as

$$(y_b/y_0)=(1/1-E)^{2/\gamma-1}$$

τ, τ_b = dimensionless time, and time at all burnt position. τ_b given as a function of y_b/y_0 2/

y_o = reduced travel at beginning of projectile motion given as

$$y_o = x_o - (C/A\rho_p)$$

y_s = reduced travel coordinate describing the projectile's motion, given as

$$y_s = x_s - (C/A\rho_p)$$

t = time of travel, related to τ as, $\tau = \alpha t$, where $\alpha = \phi/(.18\, y_o)$

The temperature of the gas T_g, is given as a function of the reduced travel y_s, and the adiabatic flame temperature, T_A, of the gas,

$$T_g = T_A\left(y_o/y_s\right)^{(\gamma-1)/2}, \qquad T_g = T_A\left(\frac{y_b}{y_o}\right)^{\frac{(\gamma-1)}{2}}\left(\frac{y_o}{y_s}\right) \tag{8}$$

before, and after burnout, respectively.

After muzzle exit, the following expressions are used to calculate the heat transfer coefficient and gas temperatures.[7]

$$H = H_m\left(1 + b(\tau - \tau_m)\right)^{-2} \tag{9}$$

$$T_g = T_m\left[\frac{1 - nC/Ax_m}{1 - nC/Ax_m + b(\tau - \tau_m)}\right]^{\gamma-1} \tag{10}$$

where τ_m, V_m, x_m = dimensionless time, velocity and coordinate of position at the muzzle, respectively

$b = V_m/\alpha x_m$

H = reduced heat transfer coefficient given as $H = \sqrt{2}h/\sqrt{\alpha K C_s \rho_s}$

H_m, T_m = values of H, and T_g, respectively, at the muzzle

The friction factor λ, must be determined empirically. Based on the experiments of R. C. Machler, the following expression for the friction factor, as a function of the bore diameter, D, has been derived.[2]

$$\lambda = (Z + 4\log_{10} D)^{-2} \tag{11}$$

A value for $Z = 13.2$ has been determined to fit Machler's .50 caliber machine gun firings, based on a heat input measurement of 11.1 cal/cm^2 at a point just before the forcing cone.[2]

Given values for all the parameters, previously defined, a convective heat transfer coefficient history can be calculated during gun firing, at any position along the barrel, and using a numerical finite element type of analysis as described in reference 3/, a complete temperature time history can be calculated for the tube wall.

CALSPAN METHODOLOGY

According to tubular flow theory,[4] the convection coefficient is,

$$h_g(t) = \frac{C K_g}{D}\left(\frac{V_g \rho_g D}{\mu_g}\right)^n \tag{12}$$

where V_g, ρ_g, μ_g, K_g = gas velocity, density, viscosity and conductivity

D = tube diameter

C, n = empirical constants

P_g = gas pressure

Simplifying and combining yields

$$h_g(t) = B\left(\frac{V_g P_g}{T_g}\right)^n \tag{13}$$

where $$B = C K_g D^{n-1}/\mu_g^n \quad , \quad \rho_g = P_g/T_g$$

By definition, the convection coefficient is,

$$h_g(t) = \frac{q(t)}{(T_g - T_w)} \tag{14}$$

where $q(t)$ = heat flux rate to the surface

T_g, T_w = propellant gas and barrel wall temperatures, respectively

The value of B, at specific stations for a given weapon firing a given charge can be calculated as follows[3], i.e. equating equations (13) and (14) and integrating:

$$B = \frac{\int q(t)\,dt}{\int \left(\frac{V_g P_g}{T_g}\right)^n (T_g - T_w)\,dt} \tag{15}$$

The integral in the numerator represents the total heat input, Q_{in}, at the station in question, and is determined from actual temperature data obtained from in-wall thermocouples.[4]

The gas temperature is calculated by applying the equation of state for the propellant gas to the following energy equation[4]

$$\text{Heat Loss to Walls} + \text{Work Done on Projectile} + \text{Energy in Gas} = \text{Total Heat Available} \tag{16}$$

The gas temperature is assumed to decay as a function of the pressure decay beyond the muzzle time, where the pressure is considered to decrease exponentially with time.

An initial value for the temperature of the tube wall, T_w, is assumed, and a first estimate of B is made using equation (15), then h_g is calculated according to equation (13). The h_g history is then applied to a .24 inch plane homogeneous "slab", and the temperatures and total heat input, Q_{calc}, calculated using a finite element analysis, as described in reference 3/. The value of B is varied according to the ratio Q_{calc}/Q_{in}; a new h_g history calculated, and the "slab" calculations repeated. When the value of Q_{calc} falls within 5 percent of Q_{in}, the resulting h_g history is assumed to be correct.

The heat loss to the wall, Q_{loss}, is a function of the barrel radius, station of interest, the measured heat input Q_{in}, and the time to reach each respective station of interest.

The work done on the projectile W_K is calculated by integrating the pressure-travel function obtained from the calculated interior ballistics data for the weapon considered. The velocity of the gas, V_g, and the gas pressure, P_g, is obtained from interior ballistic calculations.

Reference 3/ presents a full description of the above formulations and complete equations.

PROCEDURE

The Nordheim-Soodak (N-S) model has been computerized by the author, incorporating the "slab" routine to calculate the temperatures and resulting heat flux into the tube wall. Additionally, an iterative procedure allows for the calculation of the "friction factor", λ, which reproduces any given value of the total heat input, Q_{in}, within any specific tolerance. The program, then, has the capability to calculate heat transfer coefficients for a given value of λ, and also to calibrate λ to reproduce given values of total heat input.

Using this program, the friction factor has been calibrated, as a function of reduced position down the bore, against the Calspan experimental values of the heat input for the 105mm, 155mm, and 8 inch artillery weapons firing their respective charges.

Also, the heat transfer coefficient history, and subsequently the bore surface temperatures and gas temperatures were calculated for a conceptual 155mm weapon using both the N-S model and the Calspan methodology.

WEAPON SYSTEMS DATA

ARTILLERY HEATING DATA

Table I gives a description of each of the artillery systems, considered in this study, and the respective values of the measured heat input Q_{in}, and the distance from the rear face of the tube (RFT) at which the thermocouples were placed.4/ 5/ 6/

MUNITIONS/PROPELLANT/GUN DATA

Table II gives the values of the required design parameters relating to the weapon systems. Table III gives the values of the propellant constants used for this study.

HEAT TRANSFER THERMAL CONSTANTS

The following average values for gun steel were used: C_s = 0.156 btu/lb_m-^oF, K = 0.007 btu/ft-sec-^oF, ρ_s = 490.0 lb_m/ft^3; and $(1/\sqrt{KC_s\rho_s})$ = 2.80 ^oC-cm^2-$sec^{-\frac{1}{2}}$/cal.[2/]

155MM CONCEPT DATA

The conceptual 155mm system consists of a tube design similar to that of the M185 cannon, but 5 percent greater in wall thickness, overall; a chamber volume of 1400 cubic inches, a 235 inch shot travel, and an M203 propelling charge of 26.1 lbs. containing 17.5 oz. of TI-02 wear reducing additive.

The friction factors used to calculate the heat inputs for this concept were estimated from the calibrated values for the M199 cannon firing the M203 charge, system 4, Table I.

RESULTS

CALIBRATED FRICTION FACTORS

Figures 1, 2, 3, and 4 present plots of the reciprocal calibrated friction factor as a function of reduced position along the bore for each of the systems listed in Table I. Table IV gives the same data in tabular form.

ESTIMATED HEATING

The estimated values for the total heat input, as a function of position along the bore, the heat transfer coefficients, gas temperatures, and bore surface temperatures as calculated from the respective methodologies, as a function of time, for the conceptual 155mm system, are presented in figures 5, 6, 7, and 8, respectively.

CONCLUSIONS

It is worthwhile to remember that the methodologies presented assume that the equations of heat transfer for steady, fully developed flows in pipes can be applied, instantaneously, over the time domain involved, despite the lack of such a flow in gun tubes. However, both the Nordheim and Calspan methodologies provide a technique for calculating gun barrel heat transfer coefficients which do not differ significantly from each other; and because of the impulsive nature of the heating, it would not be expected that the calculated residual temperatures would be different.

The Calspan technique and methodology is based on actual firings, and calibrates the calculated heating values against the measured data, and thus provides the best approach for calculating gun barrel temperatures.

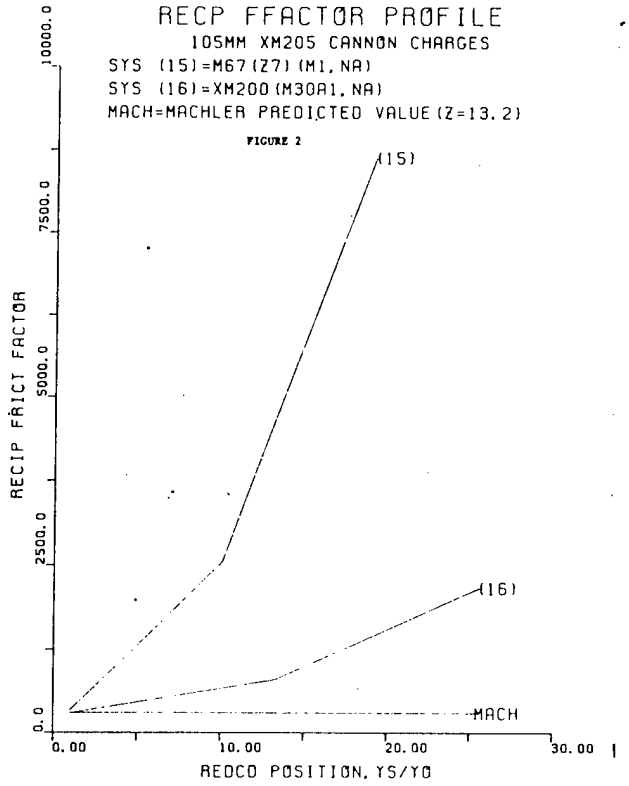
RECP FFACTOR PROFILE
105MM XM205 CANNON CHARGES
SYS (15)=M67(Z7)(M1, NA)
SYS (16)=XM200(M30A1, NA)
MACH=MACHLER PREDICTED VALUE(Z=13.2)
FIGURE 2
RECIP FRICT FACTOR
10000.0
7500.0
5000.0
2500.0
0.0
(15)
(16)
MACH
0.00
10.00
20.00
30.00
REDCD POSITION, YS/YO

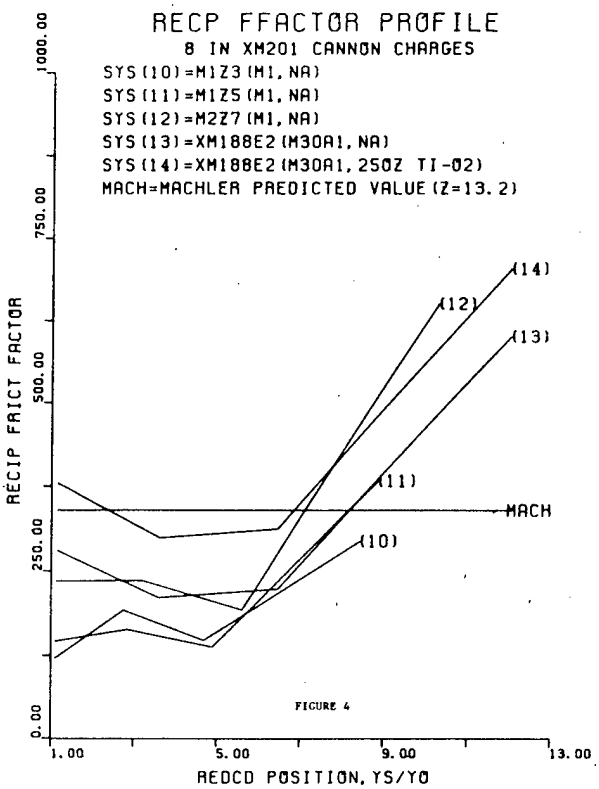
RECP FFACTOR PROFILE
8 IN XM201 CANNON CHARGES
SYS (10)=M1Z3(M1, NA)
SYS (11)=M1Z5(M1, NA)
SYS (12)=M2Z7(M1, NA)
SYS (13)=XM188E2(M30A1, NA)
SYS (14)=XM188E2(M30A1, 250Z TI-02)
MACH=MACHLER PREDICTED VALUE(Z=13.2)
RECIP FRICT FACTOR
1000.00
750.00
500.00
250.00
0.00
(14)
(12)
(13)
(11)
MACH
(10)
FIGURE 4
1.00
5.00
9.00
13.00
REDCD POSITION, YS/YO

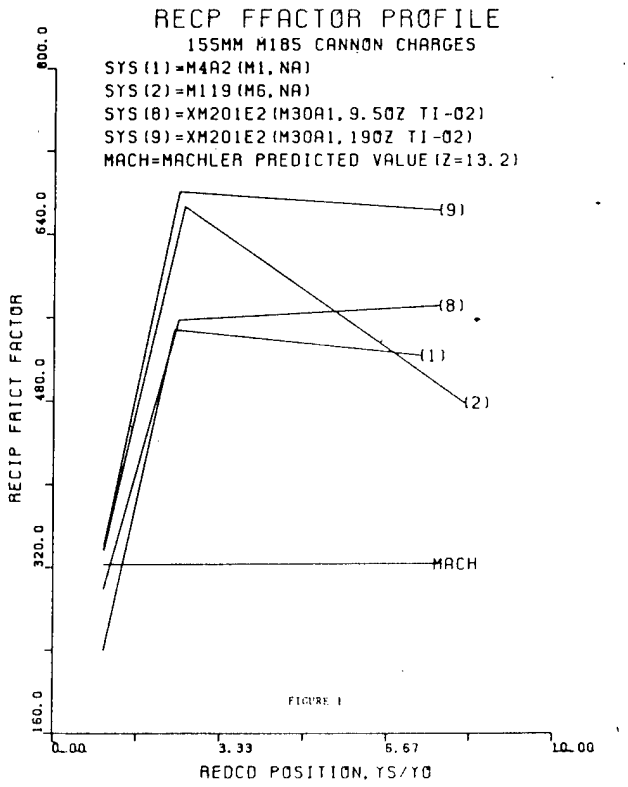
RECP FFACTOR PROFILE
155MM M185 CANNON CHARGES
SYS (1)=M4A2(M1, NA)
SYS (2)=M119(M6, NA)
SYS (8)=XM201E2(M30A1, 9.50Z TI-02)
SYS (9)=XM201E2(M30A1, 190Z TI-02)
MACH=MACHLER PREDICTED VALUE(Z=13.2)
RECIP FRICT FACTOR
800.0
640.0
480.0
320.0
160.0
(9)
(8)
(1)
(2)
MACH
FIGURE 1
0.00
3.33
6.67
10.00
REDCD POSITION, YS/YO

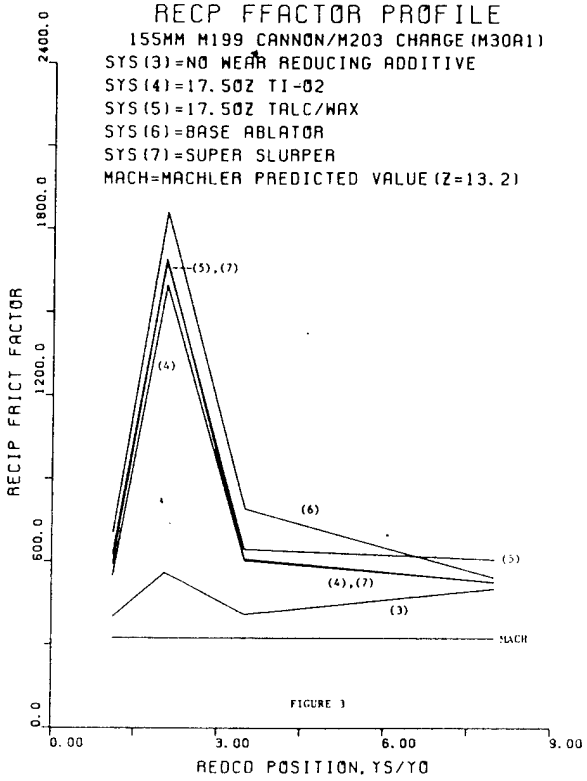
RECP FFACTOR PROFILE
155MM M199 CANNON/M203 CHARGE(M30A1)
SYS (3)=NO WEAR REDUCING ADDITIVE
SYS (4)=17.50Z TI-02
SYS (5)=17.50Z TALC/WAX
SYS (6)=BASE ABLATOR
SYS (7)=SUPER SLURPER
MACH=MACHLER PREDICTED VALUE(Z=13.2)
RECIP FRICT FACTOR
2400.0
1800.0
1200.0
600.0
0.0
(5),(7)
(6)
(6)
(5)
(4),(7)
(3)
MACH
FIGURE 3
0.00
3.00
6.00
9.00
REDCD POSITION, YS/YO

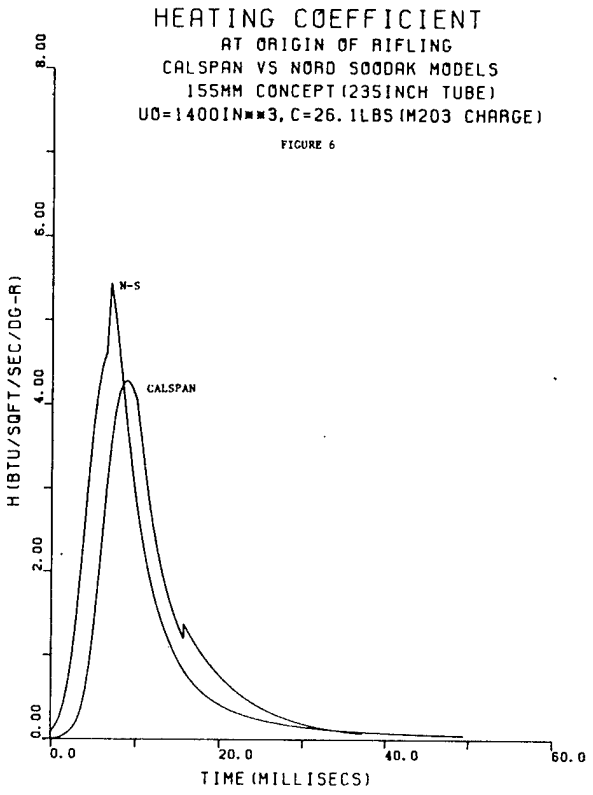
HEATING COEFFICIENT
AT ORIGIN OF RIFLING
CALSPAN VS NORD SOODAK MODELS
155MM CONCEPT (235INCH TUBE)
U0=1400IN**3, C=26.1LBS (M203 CHARGE)
FIGURE 6
H (BTU/SQFT/SEC/DG-R)
8.00
6.00
4.00
2.00
0.00
N-S
CALSPAN
0.0
20.0
40.0
60.0
TIME (MILLISECS)

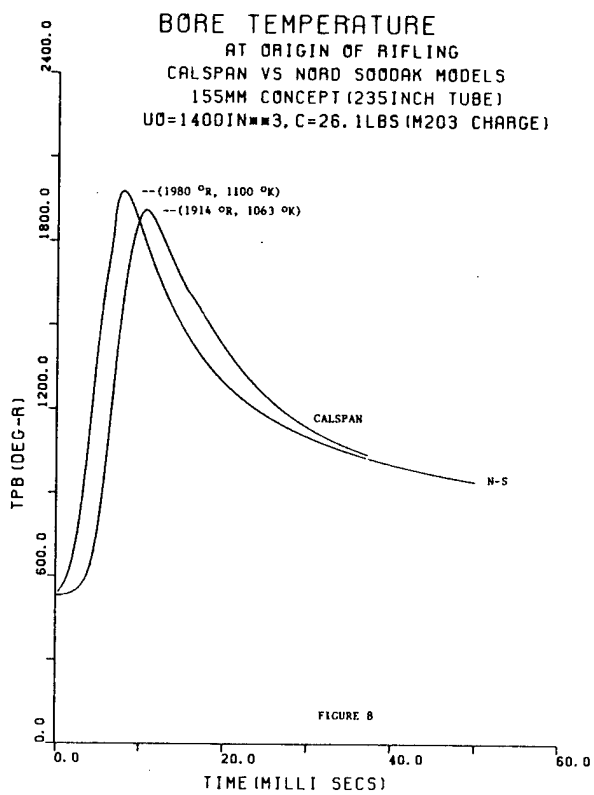
BORE TEMPERATURE
AT ORIGIN OF RIFLING
CALSPAN VS NORD SOODAK MODELS
155MM CONCEPT (235INCH TUBE)
U0=1400IN**3, C=26.1LBS (M203 CHARGE)
--(1980 °R, 1100 °K)
--(1914 °R, 1063 °K)
TPB (DEG-R)
2400.0
1800.0
1200.0
600.0
0.0
CALSPAN
N-S
FIGURE 8
0.0
20.0
40.0
60.0
TIME (MILLI SECS)

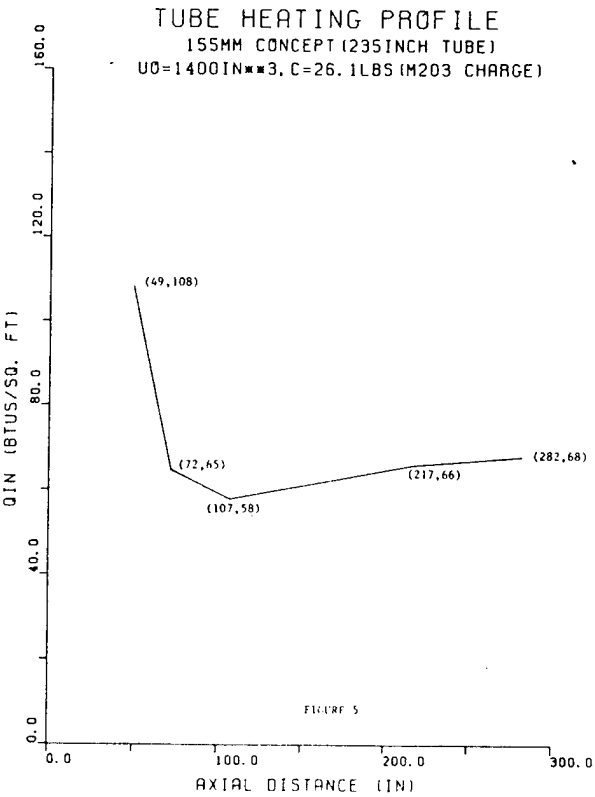
TUBE HEATING PROFILE
155MM CONCEPT (235INCH TUBE)
U0=1400IN**3, C=26.1LBS (M203 CHARGE)
QIN (BTUS/SQ. FT)
160.0
120.0
80.0
40.0
0.0
(49,108)
(72,65)
(107,58)
(217,66)
(282,68)
FIGURE 5
0.0
100.0
200.0
300.0
AXIAL DISTANCE (IN)

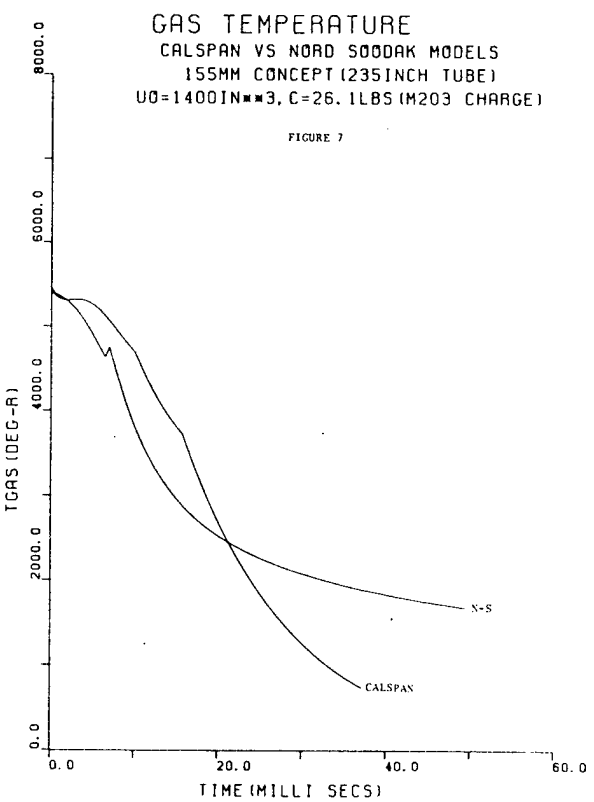
GAS TEMPERATURE
CALSPAN VS NORD SOODAK MODELS
155MM CONCEPT (235INCH TUBE)
U0=1400IN**3, C=26.1LBS (M203 CHARGE)
FIGURE 7
TGAS (DEG-R)
8000.0
6000.0
4000.0
2000.0
0.0
N-S
CALSPAN
0.0
20.0
40.0
60.0
TIME (MILLI SECS)

TABLE II. MUNITIONS/GUN DATA.

System	C (lb_m)	Δ (gm/cc)	P_{max} (K-lb_f/in^2)	V_m (ft/sec)
1	13.5	.3249	25.7	1845
2	20.0	.4836	28.0	2240
3	26.1	.6282	46.3	2765
4	26.1	.6282	44.6	2683
5	26.1	.6282	44.4	2672
6	26.1	.6282	46.0	2741
7	26.1	.6282	45.7	2715
8	17.3	.4164	31.9	2239
9	17.3	.4164	32.7	2241
10	7.5	.1065	12.0	1010
11	13.2	.1874	14.3	1474
12	28.2	.4003	30.1	1980
13	43.6	.6189	41.4	2590
14	43.6	.6189	40.7	2549
15	2.83	.4161	38.8	1699
16	4.6	.6764	43.9	2125

	D (cm)	m_o (lb_m)	U_o (in^3)	X_m (in)
155mm	15.5	96	1150	240
8 in	20.3	200	1950	316
105mm	10.5	33	153	152

TABLE I. ARTILLERY HEATING DATA.

System	Caliber, Cannon, Charge (Prop)	(Q_{in}(btu/ft^2), RFT (inches))			
1	155mm, M185, M4A2, NA, (M1)	(84,39.6)	(44,83.0)	(26,236.5)	
2	155mm, M185, M119, NA, (M6)	(96,39.6)	(67,83.0)	(45,236.5)	
3	155mm, M199, M203, NA, (M30A1)	(124,41.85)	(108,65.0)	(100,100.0)	(66,210.0)
4	155mm, M199, M203, 17.5 oz $Ti0_2$, (M30A1)	(101,41.85)	(51,65.0)	(82,100.0)	(66,210.0)
5	155mm, M199, M203, 17.5 oz Talc/Wax, (M30A1)	(92,41.85)	(49,65.0)	(79,100.0)	(60,210.0)
6	155mm, M199, M203, Base Ablator, (M30A1)	(85,41.85)	(45,65.0)	(66,100.0)	(63,210.0)
7	155mm, M199, M203, Super Slurper, (M30A1)	(97,41.85)	(49,65.0)	(80,100.0)	(65,210.0)
8	155mm, M185, XM201E2, 9.5 oz $Ti0_2$, (M30A1)	(114,39.6)	(69,83.0)	(42,236.5)	
9	155mm, M185, XM201E2, 19 oz $Ti0_2$, (M30A1)	(103,39.6)	(62,83.0)	(38,236.5)	
10	8 in, XM201, M1(Z3), NA, (M1)	(62,42.36)	(36,102.36)	(32,171.86)	(9,307.86)
11	8 in, XM201, M1(Z5), NA, (M1)	(87,42.36)	(66,102.36)	(58,171.86)	(15,307.86)
12	8 in, XM201, M2(Z7), NA, (M1)	(102,42.36)	(84,102.36)	(75,171.86)	(21,307.86)
13	8 in, XM201, XM188E2, NA, (M30A1)	(156,42.36)	(143,102.36)	(117,171.86)	(49,307.86)
14	8 in, XM201, XM188E2, 25 oz $Ti0_2$ (M30A1)	(131,42.36)	(124,102.36)	(100,171.86)	(43,307.86)
15	105mm, XM205, M67(Z7), NA, (M1)	(47.5,11.4)	(23,81.4)	(9,151.4)	
16	105mm, XM205, XM200(Z8), NA, (M30A1)	(71,11.4)	(44,81.4)	(23,151.4)	

NA means that no wear reducing additive included in charge.

TABLE IV. CALIBRATED FRICTION FACTORS.

System	($1/\lambda$, y_m/y_o)			
1	(239.5,1.01)	(548.1,2.40)	(523.2,7.32)	
2	(336.3,1.01)	(666.6,2.60)	(478.1,8.21)	
3	(398.5,1.10)	(559.9,2.05)	(408.3,3.48)	(502.5,7.98)
4	(547.0,1.10)	(1597.0,2.05)	(603.6,3.48)	(526.8,7.98)
5	(626.7,1.10)	(1683.4,2.05)	(643.1,3.48)	(606.0,7.98)
6	(703.6,1.10)	(1860.5,2.05)	(790.9,3.48)	(541.4,7.98)
7	(589.6,1.10)	(1690.8,2.05)	(608.4,3.48)	(523.1,7.98)
8	(299.1,1.01)	(557.4,2.48)	(571.2,7.69)	
9	(340.2,1.01)	(680.7,2.48)	(663,7.69)	
10	(121.1,1.10)	(192.7,2.76)	(147.8,4.68)	(294.7,8.44)
11	(146.3,1.10)	(163.8,2.86)	(137.9,4.89)	(383.9,8.87)
12	(235.6,1.12)	(236.5,3.20)	(192.7,5.60)	(651.6,10.31)
13	(280.2,1.15)	(210.5,3.61)	(223.4,6.47)	(601.5,12.05)
14	(379.8,1.15)	(298.6,3.61)	(312.5,6.47)	(704.9,12.05)
15	(334.0,1.0)	(2559.8,10.11)	(8626.2,19.22)	
16	(291.6,1.0)	(797.3,13.30)	(2168.9,25.61)	

TABLE III. PROPELLANT CONSTANTS

	$\mathcal{M}$ (in^3/lb_m)	C_p(cal/gm-°C)	ρ_p(lb_m/in^3)	F(K-ft-lb_f/lb_m)	T_A(°K)
M1	30.57	.435	.0567	305	2417
M6	29.92	.440	.0571	317	2570
M30A1	29.13	.449	.060	359	3025

REFERENCES

1. John E. Kovacs, "Computer Methodology for Large Caliber Artillery Cannon Heating and Cooling," TR ARSED-TR-80001, U. S. Army Armament Research and Development Command, Dover, New Jersey, December 1980.

2. L. W. Nordheim, Harry Soodak and G. Nordheim, "Thermal Effects of Propellant Gases in Erosion Vents and in Guns," NDRC Armor and Ordnance Report No. A-262 (OSRD No. 3447), March 1944.

3. F. A. Vassalo, "Mathematical Models and Computer Routines Used in Evaluation of Caseless Ammunition Heat Transfer," Calspan Report No. GM 2948-Z-1, Calspan Corporation, Buffalo, New York, June 1971.

4. F. A. Vassalo, "Development of Tube Instrumentation and Shock Tube Gun Techniques for Investigation of Heat Transfer and Erosion in Large Caliber Guns-Eight Inch Howitzer Studies," Calspan Report No. VL-5337-D-2, Calspan Corporation, Buffalo, New York, December 1976.

5. F. A. Vassalo, "An Evaluation of Heating and Erosion in the 105mm XM204 Howitzer and 155mm M185 Cannon," Calspan Report No. VL-6050-D-1, Calspan Corporation, Buffalo, New York, April 1977.

6. G. A. Sterbutzel, D. E. Adams, and F. A. Vassalo, "Minimizing Heating and Erosion in the 155mm M199 Tube Using Modified M203 Charges," U. S. Army ARRADCOM Contractor Report ARLCD-CR-81008, Dover, New Jersey, October 1981.

7. "Interior Ballistics of Guns," AMCP 706-150, Headquarters, U. S. Army Materiel Command, February 1965.

ROLE OF SURFACE OXIDE ON GUN BARREL WEAR

I.C. Stobie and J.R. Ward
USA Ballistic Research Laboratory
Aberdeen Proving Ground, MD

ABSTRACT

Earlier analysis of gun tubes and steel nozzles exposed to propellant combustion gases showed that a tenacious oxide layer is left on the surface after firing. The thickness of the oxide layer was inversely proportioned to the flame temperature of the propellant. Experiments were performed in a 37-mm blow-out gun to determine whether the oxide layer influences wear. The experiments were performed with a nozzle that had been conditioned with M1, M30, M5, or M8 propellant. The results showed the oxide layer insulates the steel and reduces erosion. The wear with M8 propellant decreased as the flame temperature of the propellant used for the previous shot decreased. Conversely, the wear with M1 propellant increased as the flame temperature of the propellant from the previous shot increased.

These results show the Effective Full Charge (EFC) factors determined from standard wear tests may not predict total wear when rounds with different propellants are fired in combination. These results also suggest that if propellants with comparable flame temperatures produce different oxide thicknesses, the wear could be significantly greater for the propellant with the thinner oxide layer.

The oxide layer effect was shown in imbedded thermocouple tests in a 105-mm tank gun. The heat transfer was higher in a M392A2 round preceeded by an M490 without a liner than an M392A2 preceeded by an M467. The M467 conditions the barrel with a thicker oxide layer. A similar trend was shown with M490 rounds with conditioning rounds that had different oxide thicknesses.

The oxide layer effect was used to explain abnormally high wear in a study where M392A2 rounds and M467 rounds were fired alternately. The total wear was twice as great as predicted by the correlation of heat transfer from the M392A2 and the wear from a wear test of M467 TP-T rounds.

INTRODUCTION

Earlier analysis[1,2] of steel nozzles exposed to propellant combustion gases showed that a tenancious oxide layer is left on the surface. The thickness of the oxide layer was inversely proportional to the propellant's flame temperature as illustrated in Table 1. If this oxide layer affects the subsequent round, it is conceiveable that wear produced from firing rounds with different propellants will be much different than that expected from EFC factors determined from wear tests where rounds with a given propellant are fired continuously.

Approved for public release;
distribution unlimited

TABLE 1. OXYGEN CONCENTRATION PROFILES ON STEEL EXPOSED TO PROPELLANTS WITH DIFFERENT FLAME TEMPERATURES

Propellant	Flame Temperature, K	Oxygen, atoms/cm^2, x 10^{-16}
M2	3,375	9
M30	2,994	17
M1	2,480	34

In order to determine if wear was influenced by firing combinations of propellants with different flame temperatures, tests were run in a 37-mm blowout gun with M1, M30, M5 and M8 propellants. In one set of tests, M8 was fired alternately with another propellant to see the effect when the nozzle had a thin oxide coating. A second set of tests was run with M1 propellant to see the effect when the nozzle had thick oxide deposit. The wear in these sets of tests was compared with wear from repeated shots with M8 or M1 propellant.

EXPERIMENTAL

The compositions of the four propellants used in the wear tests are listed in Table 2. Thermochemical properties computed by the BLAKE code[3] are listed in Table 3 where

T = flame temperature,
F = impetus,
η = co-volume,
M = molecular weight,
C_p = specific heat,
γ = ratio of specific heats.

The wear measurements were done with a 37-mm blowout gun described earlier.[4] Wear was determined by weighing a contoured steel nozzle after each shot. In these experiments, the nozzle's throat diameter was 12.5 mm which gave a rupture pressure of 262 MPa (38 kpsi) with two 1.6 mm thick shear disks. Propellant charge masses were adjusted to give a closed bomb pressure of 306 MPa (44.4 kpsi) to insure shear disk rupture.

Baseline wear was determined by repetitive firings in which each propellant was fired alternately with M8, and then each propellant was fired alternately with M1 to test the effect of oxide layer on wear.

RESULTS AND DISCUSSION

Table 4 summarizes the effect on wear of M8 propellant as the propellants with progressively lower flame temperatures at thicker oxide coatings are fired alternately. One can see that the oxide acts as an insulator with the greatest difference in M8 when M1 propellant is the conditioning round.

Table 5 summarizes the reverse experiment in which one examines the effect on M1 wear as propellants leaving thinner oxide coatings are fired alternately. Again,

the trend shows that the oxide insulates the steel, the difference in wear being greatest with M8. These results are plotted in Figures 1 and 2.

Tables 6 and 7 show the results for M5 propellant and M30 propellant illustrating that there is no significant difference in wear regardless of the propellant used on the previous round. This suggests that there is a threshold thickness in the oxide which must be exceeded before measurable differences in wear are obtained, and the thicker the oxide the more protection provided. This is entirely analogous to the role TiO_2 plays in wear-reducing additives[5].

TABLE 2. COMPOSITIONS OF PROPELLANTS

	M5	M8	M1	M30
Nitrocellulose (Percent Nitrogen)	81.95 (13.25)	52.15 (13.25)	85.00 (13.25)	28.0 (12.6)
Nitroglycerine	15.00	43.00	-----	22.5
Nitroguanidine	-----	-----	-----	47.7
Ethyl Centralite	0.60	0.60	-----	1.5
Barium Nitrate	1.40	-----	-----	-----
Potassium Nitrate	0.75	1.25	-----	-----
Diethylphthalate	-----	3.00	-----	-----
Dinitrotoluene	-----	-----	10.0	-----
Dibutylphthalate	-----	-----	5.00	-----
Cryolite	-----	-----	-----	0.3
Diphenylamine, Added	-----	-----	1.00	-----
Ethyl Alcohol, Residual	2.30	0.40	0.75	0.2
Water, Residual	0.70	-----	0.50	-----
Graphite	0.30	-----	-----	-----

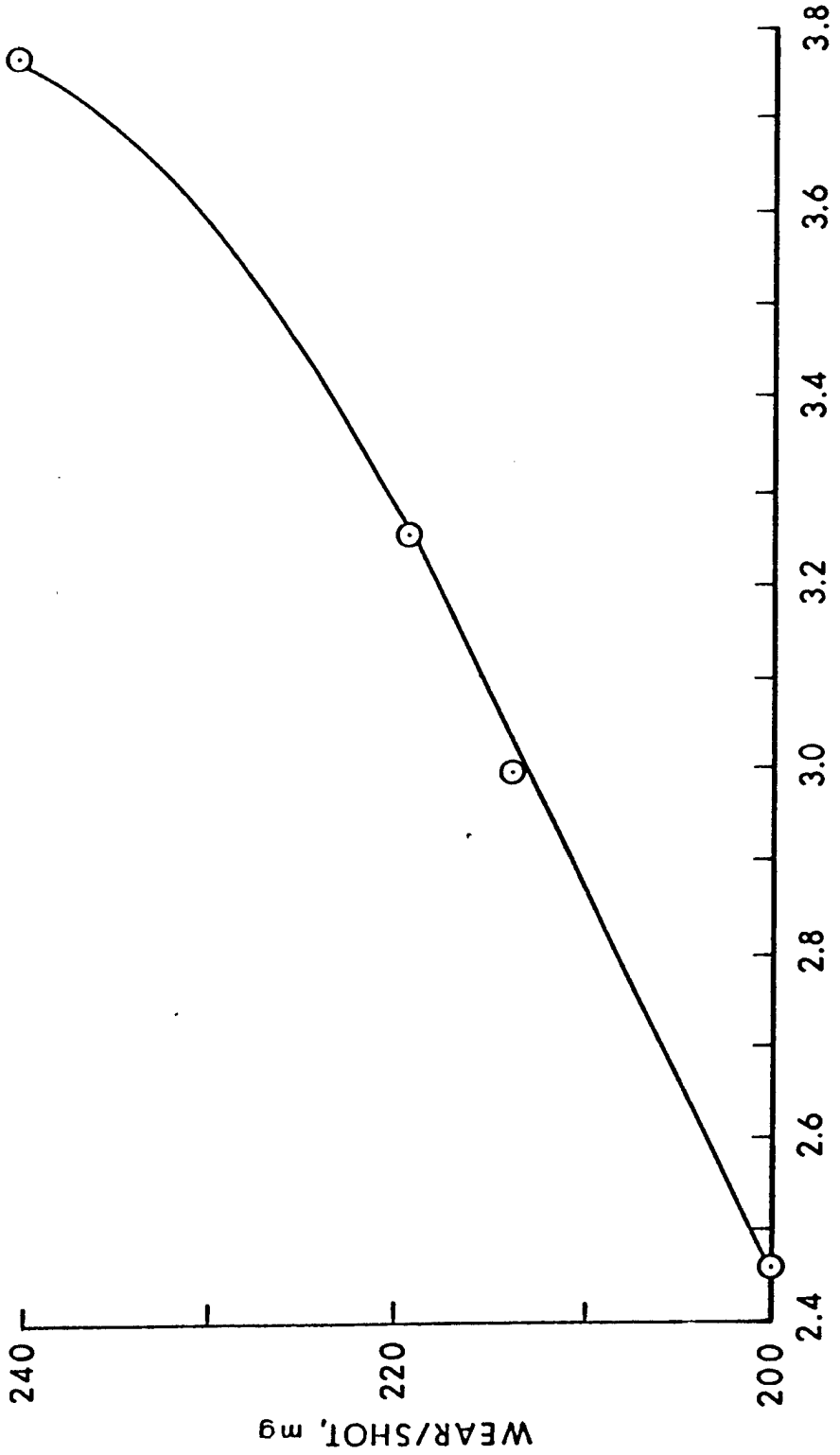

Figure 1. M8 Propellant Wear Vs the Flame Temperature of the Preceeding Round

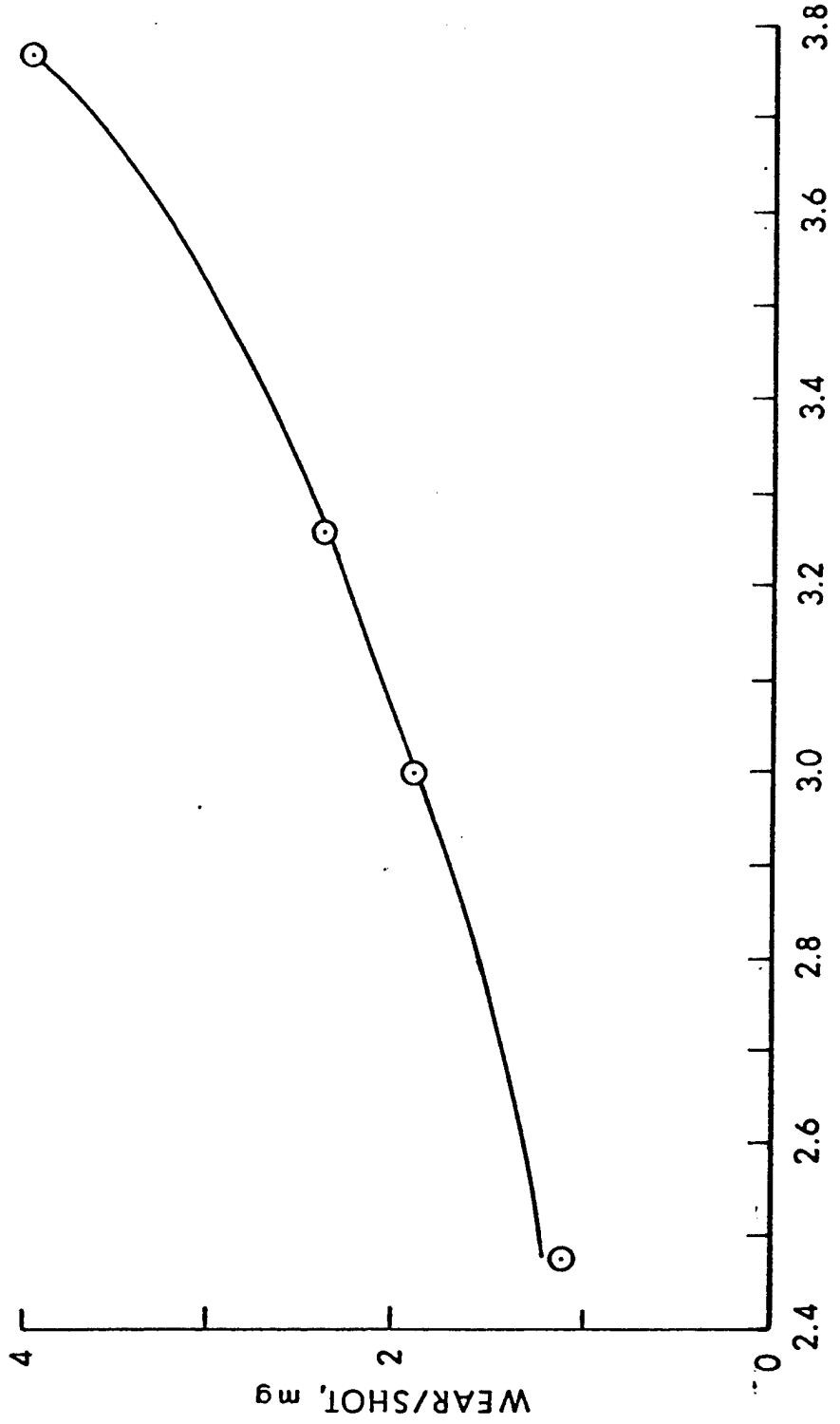

Figure 2. M1 Propellant Wear Vs the Flame Temperature of the Preceeding Round

TABLE 3. SUMMARY OF THERMOCHEMICAL PROPERTIES AND COMBUSTION GASES OF PROPELLANTS

Prop	Temp K	Force J/g	η cm^3/g	M g/mole	CO*	CO_2*	H_2O*	H_2*	N_2*	C_p J/mole	γ
M8	3,716	1,178	0.970	26.2	13.0	6.4	10.2	2.4	5.4	47.7	1.22
M5	3,264	1,079	1.003	25.1	16.5	4.9	9.3	4.0	4.9	45.5	1.23
M30	3,021	1,078	1.050	23.3	11.8	3.0	10.5	5.5	11.9	41.1	1.24
M1	2,480	928	1.108	22.2	22.8	2.4	6.1	9.1	4.5	41.0	1.27

**Moles of gas/kg of propellant.*

TABLE 4. EFFECT OF SURFACE OXIDE ON WEAR OF M8 PROPELLANT

Conditioning Propellant	Flame Temp K	Charge Mass, g	No. Shots	M8 Mass Loss mg/shot*
M8	3,716	68.4	6	240.5 ± 15.0
M5	3,264	72.8	3	219.3 ± 5.0
M30	3,021	72.2	2	219.5 ± 8.1
M1	2,480	80.09	3	199.6 ± 14.4

**Error expressed as sample standard deviation.*

TABLE 5. EFFECT OF SURFACE OXIDE ON WEAR OF M1 PROPELLANT

Conditioning Propellant	Flame Temp K	Charge Mass, g	No. Shots	M1 Mass Loss mg/shot*
M1	2,480	80.09	5	1.1 ± 0.4
M30	3,021	72.2	4	1.9 ± 1.7
M5	3,264	72.8	4	2.4 ± 1.7
M8	3,716	68.4	4	4.0 ± 0.8

**Error expressed as sample standard deviation.*

TABLE 6. EFFECT OF OXIDE COATING ON WEAR WITH M5 PROPELLANT

Conditioning Propellant	Flame Temp, K	No. Shots	M5 Mass Loss, mg/shot*
M8	3,716	3	48.6 ± 3.7
M5	3,264	5	50.7 ± 6.0
M1	2,480	3	44.2 ± 3.1

**Error expressed as sample standard deviation.*

TABLE 7. EFFECT OF SURFACE OXIDE ON WEAR OF M30 PROPELLANT

Conditioning Propellant	Flame Temp, K	No. Shots	M30 Mass Loss, mg/shot*
M8	3,716	3	12.3 ± 5.8
M30**	3,021	7	10.8 ± 3.1
M30**	3,021	6	3.9 ± 1.1
M1	2,480	4	5.5 ± 1.3

**Error expressed as sample standard deviation.*

***Different M30 lots used in alternate firings with M1 and M8.*

Some evidence for the insulation by low-flame temperature propellants in guns may be found by examining heat input with different "clean-out" rounds. If the heat input for the M392 round (M30 propellant) with an M467 cartridge (M1 propellant) as cleanout round reflects the contribution from the oxide deposit left by the M467 round, then the M392 cartridge should have higher heat input if the cleanout round were an M392 round without additive or an M392 round with polyurethane foam. Each of these rounds is more erosive than the M467 cartridge, hence each should leave a thinner oxide. The first experiments to measure heat input of 105-mm tank rounds did use M392 rounds minus TiO_2-wax additive as cleanout rounds, but the thermocouples were not in the same axial location as in the second test.[6] One can use data from rounds common to both tests to estimate heat input. Table 8 summarizes the heat transfer results where one first notes that total heat input decreases as one goes downbore. One would expect the heat input from an M392A2 round following an M392 round (no additive) to be higher than a M392A2 following an M467. The heat input for the M392 clean-out round heat input for the M392 round is higher at 641mm RFT.

TABLE 8. EFFECT OF CLEANOUT ROUND ON HEAT INPUT FROM M392 CARTRIDGE*

Cartridge	Additive	Cleanout Round	Heat Input, J/mm 641mm**	667mm***	1,010mm***
M392A1	none	none	449	426	359
M392A2	polyurethane foam	none	416	401	342
M392A2	TiO_2-wax	M392 no additive	---	380	321
M392A2	TiO_2-wax	M467TP-T	381	---	---

* *Axial distances measured from rear face of tube*
** *Reference 3*
*** *Reference 5*

Another opportunity to test the effect of previous rounds on heat input was in the evaluation of wear-reducing additives for the 105-mm tank cannon[7] where rounds without wear-reducing liners were used as "clean-out" rounds along with M467 TP-T cartridges. The pertinent data are listed in Table 9 where the heat input effect is reflected as the peak temperature of the thermocouple nearest the bore surface. The peak temperature for both the M392A2 and the M490 cartridges, both with M30 propellant, was higher following a "no liner" cleanout round vs the M467 TP-T (M1 propellant) cartridge.

TABLE 9. EFFECT OF "CLEAN-OUT" ROUND ON HEAT INPUT

Round	Temperature Rise, K	Clean-out Round, Propellant
M392A2	157	M490 (no liner), M30
M392A2	150	M467, M1
M490	182	M490 (no liner), M30
M490	174	M490 (no liner), M30
M490	167	M467, M1

The failure to see any change in wear for M5 and M30 propellants regardless of the propellant used on the previous shot implies the difference in thickness between the oxide left by repetitive firing and by firing M1 or M8 is not sufficiently thick to change the heat transfer rate to affect wear measurably in the blow-out gun. An analogous situation illustrating this point involved a Navy experiment in which rounds were shot with three propellants having flame temperatures ranging from 2,100 to 3,000 K.[8] Charge weights were adjusted to give equivalent interior ballistics. Rounds were fired without wear-reducing additive and repeated with additive. Presumably, the oxide layer deposited was equivalent for each propellant, yet the

change in wear was most dramatic for the 3,000 K propellant and not even measureable for the 2,100 K propellant.

Heat input could be used to determine which combination of rounds produces the most wear. For rounds with a wear reducing additive depositing an insulating residue, the combination would appear to be the alternate shots, since the insulating residue from repeated firings of either TiO_2-wax additive of M1 propellant is not formed. Niiler, et al[9], recently showed the oxide from M1 propellant builds on repeated firing much like the residue from the TiO_2-wax liner.

CONCLUSIONS

1. Gun barrel wear from propellant combustion gases is affected by the oxide left on the surface by the previous shot. The oxide acts as an insulator. Since the oxide thickness varies inversely with propellant flame temperature, wear increases following a shot with a higher flame-temperature propellant and decreases following a shot with a lower flame-temperature propellant.

2. The EFC factors determined from conventional gun wear tests where a given round is fired repeatedly will not predict wear when rounds with different flame temperatures are fired in combination.

3. Limited analysis of heat transfer results in the M68 tank cannon suggests the heat input is sensitive to the previous round. This suggests that the oxide layer influences wear in guns and heat input measurements can be used to determine what combination of rounds produces the worst wear.

REFERENCES

1. A. Niiler, J.E. Youngblood, S.E. Caldwell, and T.J. Rock, "An Accelerator Technique for the Study of Ballistic Surfaces", BRL Report No. 1815, August 1975.

2. A. Niiler and R. Birkmire, "Composition Changes in Gun Steel Surfaces Due to Erosive Propellant Burn", Proceedings of the Tri-Service Gun Tube Wear and Erosion Symposium, Dover, NJ, March 1977.

3. E. Freedman, "BLAKE-A Ballistic Thermodynamic Code Based on TIGER", Proceedings of the International Symposium on Gun Propellants, Picatinny Arsenal Dover, NJ, October 1973.

4. J.R. Ward and R.W. Greene, "Erosivity of a Nitramine Propellant with a Flame Temperature Comparable to M30 Propellant", BRL Memorandum Report No. 02926, June 1979.

5. J.R. Ward and T.L. Brosseau, "Role of the Insulating Layer form TiO_2-Wax Liner in Reducing Gun Tube Wear", Proceedings of the 1980 JANNAF Propulsion Meeting, CPIA Publication 315, March 1980.

6. T.L. Brosseau and J.R. Ward, "Reduction of Heat Transfer in 105-mm Tank Gun by Wear-Reducing Additives", BRL Memorandum Report No. 2698, November 1976.

7. I.C. Stobie, T.L. Brosseau, and R.P. Kaste, "Heat Transfer Measurements in 105-mm Tank Gun With M735 Rounds", Technical Report ARBRL-TR-02265, September 1980.

8. M.C. Shamblen, "Overview of Erosion in US Naval Guns", Proceedings of the Tri-Service Gun Tube Wear and Erosion Symposium, Dover, NJ, March 1977.

9. A. Niiler, et al, report in preparation.

TWO-DIMENSIONAL, TURBULENT, TWO-PHASE INTERIOR BALLISTIC FLOWS USING AN IMPLICIT NUMERICAL ALGORITHM

N. E. Banks
U.S. Army Ballistic Research Laboratory
Aberdeen Proving Ground, MD

H. J. Gibeling and H. McDonald
Scientific Research Associates, Inc.
Glastonbury, CT

ABSTRACT

A two-dimensional implicit interior ballistic computer code (ALPHA) has been developed to solve the turbulent two-phase flow in a gun tube beginning with primer discharge and ending with the projectile exiting the tube. The detailed prediction of flow properties in a gun barrel during firing would aid in the understanding and prevention of both gun barrel erosion and catastrophic gun failures. The governing partial differential equations were formulated in strong conservation form by application of a Jacobian transformation to the equations in cylindrical polar coordinates. The formulation includes the following constitutive models: Noble-Abel gas equation of state, molecular viscosity and thermal conductivity, turbulent viscosity and length scale, intergranular stress relation, interphase drag and heat transfer relations, and a burning rate correlation for solid phase combustion. One-dimensional heat conduction models are utilized to obtain both the barrel wall surface temperature and the average solid particle surface temperature. An axisymmetric time-dependent adaptive coordinate system for interior ballistics flow field calculations is utilized, and distinct filler elements and the projectile are treated using a quasi-one-dimensional lumped parameter analysis. The governing equations, constitutive relations and the time-dependent coordinate system have been incorporated into an existing computer code which solves the multi-dimensional time-dependent compressible Navier-Stokes equations using a consistently split, linearized, block-implicit numerical procedure developed by Briley and McDonald.

Results have been obtained for the two-dimensional, two-phase flow in a gun tube with a noncombusting particulate phase. The initial conditions for this case were uniform except for a small gas phase region near the projectile base, and spherical particles with 100μm diameter were considered. Results are also presented utilizing 5μm diameter spherical particles with two different tube wall boundary conditions on the solid phase tangential velocity component. These calculations demonstrate the importance of the particle-wall interaction. The computed results obtained demonstrate the feasibility of making two-dimensional, two-phase predictions for the flow in a gun tube. This procedure also provides a framework for the development and evaluation of two-phase flow turbulence models and constitutive relations which are appropriate for a multi-dimensional prediction scheme.

---

*This work was supported by the U.S. Army Ballistic Research Laboratory under Contract DAAK11-79-C-0098.

Approved for public release; distribution unlimited.

INTRODUCTION

A detailed understanding of the phenomena occurring within a gun tube during firing would aid in the development of modern high muzzle velocity gun systems. In particular, the reliable prediction of flow properties in the gun tube would aid in understanding and prevention of both gun barrel erosion and catastrophic gun failure. The ballistic cycle which we wish to simulate begins with the ignition of the solid propellant particles, and ends with the projectile exiting the gun tube and the discharge of hot gases and any unburned propellant. The ignition of the propellant particles is normally initiated by a hot gas-particle flow from a primer consisting of an igniter and a black powder charge. The hot primer gas glows into the propellant bed and heats the propellant particles via conduction, radiation and convection. As the propellant burns gas pressure and temperature rise, thereby promoting the flame spread through the propellant bed. Pressure waves propagate through the chamber, and after the pressure becomes large enough to overcome frictional resistance to motion the projectile will accelerate down the tube. At some point in the cycle the propellant bed will fluidize, and interaction between particles will diminish. As the projectile moves down the tube several processes may occur which are not considered in the present analysis; these are projectile instability and tube vibration, and leakage of propellant gases past the projectile. The former two phenomena would not normally have a significant influence on the two-phase flow in the tube. While leakage of propellant gases may influence the flow, especially near the projectile-tube wall juncture, its consideration has been deferred until a later stage of the program development.

Until recently, most other efforts in modeling the flow phenomena in guns have been limited to quasi-one-dimensional, inviscid two-phase flow analyses[1-4]. Portions of the ballistic cycle can now be modeled with two-dimensional analyses by assuming cylindrically symmetric flow. Gough[5] has developed an inviscid, two-dimensional analysis for the ignition phase of the ballistic cycle. The present analysis and computer code ALPHA[6,7] were developed by Scientific Research Associates under Ballistic Research Laboratory sponsorship. A previous paper[8] present the initial one-phase flow applications of the ALPHA code to the ballistic cycle. These included laminar flow-adiabatic wall, turbulent flow-adiabatic wall and laminar flow-isothermal wall simulations.

This paper presents the initial two-dimensional two-phase, nonreacting viscous flow simulation for an idealized ballistic cycle with 100μm diameter spherical particles. These two-phase results are compared with a one-phase simulation of the cycle to illustrate the influence of solid particles on the flow development in the tube. Two additional two-phase flow calculations with 5μm diameter spherical particles and two different tube wall boundary conditions are compared in order to assess the importance of the particle-wall interaction mechanisms.

GOVERNING EQUATIONS

The governing equations for a two-phase, two-dimensional flow in a gun tube have been presented previously[6,7]. Since the large number of propellant particles present precludes treating each individually, the present formulation considers averaged flow properties. These equations[6,7] were obtained using the formal averaging procedure presented by Gough[9,10] and Gough and Zwarts[1], with extensive

reference to the time-averaging approach of Ishii[11]. In this approach an averaged variable is the space-time integral of the product of the microscopic variable and a weighting function which reflects the influence of remote points on the average values. The microscopic equations are replaced by a set of averaged equations in the averaged variables for each spatial position and time. The two phases are treated distinctly in this so-called two-fluid model with momentum, mass and energy exchange terms between the two phases being replaced by appropriate constitutive relations.

The governing equations in the ALPHA code were formulated in conservation form by application of a Jacobian transformation to the equations in cylindrical-polar coordinates[6]. An axisymmetric time-dependent adaptive coordinate system for interior ballistics flow field calculations is utilized, with the projectile and any distinct filler elements treated using a quasi-one-dimensional lumped parameter analysis. The governing equations, constitutive relations, and the time-dependent coordinate system have been incorporated into an existing computer code which solves the multidimensional time-dependent compressible Navier-Stokes equations using a consistently split, linearized, block-implicit numerical scheme (LBI) developed by Briley and McDonald[12,13]. Since the LBI algorithm is well-documented in Refs. 12 and 13, it will not be discussed further here.

TWO-PHASE FLOW MODEL PROBLEMS

Because of the complex nature of the multidimensional, two-phase flow phenomena occurring in a gun tube, an idealized two-phase flow in a Lagrange gun has been simulated. This problem permits verification of the two-phase equation system in the ALPHA code, and provides an understanding of some basic two-phase flow mechanisms which occur in a real gun. The Lagrange gun is a smooth tube of constant radius which is closed at one end by the breech. The model combustion chamber is bounded by the breech, a flat based projectile, and the tube wall. The chamber is filled initially with a high pressure, high temperature gas-particle mixture with a small gas-phase region adjacent to the projectile base. In the first case (Case A), the particles were chosen to be spherical with a constant 100μm diameter throughout. No combusion of the particles is permitted in these calculations, so that this simulation of the ballistic cycle approximately represents that of a real gun if the propellant combustion ceases before the projectile begins moving at time t = 0. As in prior one-phase Lagrange gun simulations[8], frictional forces between the projectile and the tube wall are neglected. For this initial two-phase simulation the flow is assumed to remain laminar throughout the cycle, and an adiabatic wall condition is applied. Even though the actual flow in a gun tube is turbulent and the heat transfer to the walls influences the flow field, the present simulations provide insight into the effects of solid particles on the viscous flow development in the tube. The required governing equations are the gas and solid phase continuity and momentum conservation equations, gas phase energy conservation equation and the solid phase heat conduction equation. Heat transfer between the gas and solid phases is accomplished by the interphase heat transfer coefficient model with the particle surface temperature advanced in time after the coupled solution of the gas and solid phase continuity and momentum equations, and the gas phase energy equation. However, the test cases were run with thermally insulated particles, i.e., no heat transfer between the gas and solid phase was permitted and the particle internal energy remained constant throughout the cycle. The particle size is assumed to remain constant, and the gas phase specific heat (at constant

pressure) and mixture molecular weight are also assumed to remain constant throughout the cycle. The Noble-Abel equation of state, Sutherland's laws for viscosity and thermal conductivity, and the Fourier heat conduction relation are employed for the gas phase.

The following coupled boundary conditions are utilized for the two-phase calculation: at the breech, projectile and tube wall, no-slip conditions are imposed on the gas phase velocities and the gas phase density is determined from the normal momentum equation. At the solid surfaces, the adiabatic condition of zero normal derivative of gas temperature is applied. At the breech and tube wall, the normal component of solid phase velocity is assumed to be zero, while the tangential component is determined by assuming that there is no solid phase momentum decrease due to interaction with the wall. This latter condition is approximated by assuming a zero normal derivative of the solid phase tangential velocity component. The solid phase partial density (related to void fraction) at the breech and tube wall is obtained by application of the solid phase continuity equation. At the projectile base, the solid phase velocity and partial density are set to zero (unit void fraction) since there is only gas present at that location. At the tube centerline the symmetry conditions of zero normal velocity and zero normal derivative of all other variables are imposed.

The computational mesh employed in the calculations consists of 61 uniformly spaced mesh points in the axial direction, and 19 nonuniformly spaced mesh points in the radial direction. The mesh points are concentrated near the tube wall in the radial direction in order to resolve the gas phase boundary layer. The gun tube configuration, gas and solid phase properties, and initial conditions for the calculation are given in Table I.

Table I. Two-Phase Lagrange Gun Paremeters (Case A)

Bore Diameter	20mm
Combustion Chamber Length	0.175m
Total Bore Length	1.290m
Projectile Mass	0.120kg
Gas Molar Mass	23.8g/mole
Covolume	$1.08 \cdot 10^{-3}$ m^3/kg
Ratio of Gas Specific Heats	1.271
Solid Particle Diameter	0.1mm
Particle Density	1500 kg/m^3
Initial Gas Pressure	$300 \cdot 10^6$ Pa
Initial Gas Temperature	3000 K
Initial Void Fraction; $0m \leq Z \leq 0.169m$	0.94
$0.169m < Z < 0.175m$	1.0

A one-phase flow Lagrange gun simulation was computed with nearly the same computational mesh (19 x 49) for comparison with the two-phase calculation. The additional grid points in the axial direction were used in the two-phase calculation because of the large void fraction gradient occurring near the projectile base. The one-phase simulation has the same parameters as Table I except, of course, that the void fraction is unity throughout. As previously reported by Schmitt, et al[8], the one-phase Lagrange gun results compare favorably with both a one-dimensional analytic isentropic solution[14] which is valid for early times in the cycle, and the

numerical calculation of Heiser and Hensel[15]. A one-phase calculation run with the present computer code was compared to an identical calculation run with the code utilized by Ref. 8 in order to verify the present one-phase results. These results give confidence that the numerical procedure is capable of capturing the pressure waves propagating in the gun tube, as long as the spatial and temporal resolution remain adequate.

The two-phase calculation was started with a time step of 2.0μs, and the time step was permitted to increase to maintain a predetermined maximum change in the solution over each time step. The maximum time step reached in this case was about 4.3μs. The one-phase calculation was run with a constant time step of 5.0μs, so that temporal accuracy in the two cases should be comparable. The calculations were both terminated at muzzle exit time. The results are compared shortly before muzzle exit time with the projectile speed, position, and problem time of 580 m/s, 1.267m, and 2.550 ms, respectively, for the one-phase simulation; and 557 m/s, 1.268 m, and 2.635 ms, respectively, for the two-phase simulation.

The comparison of the boundary layer development in the one-phase and two-phase cases shows some interesting results. The boundary layer axial velocity profiles are shown in Fig. 1, for a representative axial position, from which it is seen that the gas velocities are smaller in the two-phase case than in the one-phase case, reflecting the energy expended to accelerate the solid particles. The solid phase lags behind the gas in the core flow as expected; the particle velocity decreases very little near the wall because of the relatively large particle size and the assumption of no particle momentum loss at the wall. The character of the tube wall boundary-layer is noticeably different in the one- and two-phase cases, as seen in Fig. 1. The axial distribution of boundary layer displacement thickness (Fig. 2) gives another indication of the influence of solid particles on the wall boundary layer. Here, the displacement thickness (δ*) is defined for the gas phase as

$$\delta^*(z,t) = \int_0^R \left[1 - \frac{\rho(r,z,t)\, w(r,z,t)}{\rho_c(z,t)\, w_c(z,t)} \right] \frac{r}{R}\, dr \qquad (1)$$

where the subscript c denotes the centerline value, w is the axial gas velocity, ρ is the gas density, and R is the tube radius. It can be seen that the displacement thickness is larger in the two-phase case for most of the distance from the projectile to the breech. Furthermore, the wall shear stress is larger in the two-phase case (Fig. 1). If the thermal boundary layer for a flow with wall heat transfer exhibits similar behavior, an increase in wall heat flux would be expected due to the presence of solid particles of the present size. Since the particle size is comparable to the gas boundary layer thickness, the interphase correlations must be examined to include near-wall effects and a particle-wall interaction model should be developed to account for particle momentum transfer to the wall.

In order to further assess the importance of near wall interaction phenomena two additional cases were calculated using 5μm diameter spherical particles. Particles of this size are expected to follow more closely the gas motion, and thus the influence of the particle velocity boundary conditions along the tube wall may be studied easily. These calculations were initiated with a completely uniform particle distribution (void fraction 0.94) and no gas zone adjacent to the projectile

base, and with the other conditions as specified in Table I. The first case (Case B) was computed using the condition of no solid phase momentum loss at the tube wall, which is approximated by a zero normal derivative of the solid phase tangential velocity component as in Case A. The second case (Case C) was computed using a no-slip condition on the solid phase tangential velocity component. In both cases the particles at the projectile base were assumed to move at the projectile speed, and all other boundary conditions were the same as those for Case A. These two cases represent the extreme limits of the actual physical behavior which is expected as a result of particle-wall and particle-gas interaction.

The boundary layer axial velocity profiles and the axial distribution of boundary layer displacement thickness for Cases B and C are compared in Figs. 3 and 4, respectively. The large difference between the results for Cases B and C indicates the significant influence of the wall boundary condition, and demonstrates a need for experimental information concerning the particle-wall interaction for particle sizes and flow conditions of interest in interior ballistic problems.

CONCLUSIONS

The present two-phase, averaged Navier-Stokes analysis has been applied to the two-phase flow in a Lagrange gun. A consistently split, linearized, block implicit numerical procedure has been employed to solve the governing partial differential equations. This initial two-phase flow application has been restricted to laminar flow and adiabatic wall conditions; however, the ability of the computer code to solve the governing equations has been demonstrated.

It has been noted that the interphase correlations must be examined to include near wall effects, and the influence of particle-wall interaction must be determined. These areas will require more detailed experimental measurements than are presently available, and to this end benchmark experiments in a simulated ballistic environment have been designed by BRL personnel and J. Whitelaw of Imperial College. The resulting data will be used in future modeling efforts for both improvement of the interphase correlations and verification of turbulence models for two-phase flows in gun tubes.

REFERENCES

1. Gough, P.S. and Zwarts, F.J., "Modeling Heterogeneous Two-Phase Reacting Flow," AIAA Journal, Vol. 17, No. 1, 1979, pp. 17-25.

2. Kuo, K.K., Koo, J.H., Davis, T.R., and Coates, G.E., "Transient Combustion in Mobile Gas-Permeable Propellants," Acta Astronautica, Vol. 3, 1976, pp. 573-591.

3. Fisher, E.B., Graves, K.W., and Trippe, A.P., "Application of a Flame Spread Model to Design Problems in the 155 mm Propelling Charge," 12th JANNAF Combustion Meeting, CPIA Pub. 273, Vol. I, December 1975, pp. 199-219.

4. Krier, H. and Gokhale, S.S., "Modeling of Convective Mode Combustion Through Granulated Propellant to Predict Detonation Transition," AIAA Journal, Vol. 16, No. 2, 1978, pp. 177-183.

5. Gough, P.S., "A Two-Dimensional Model of the Interior Ballistics of Bagged Artillery Charges," PGA-TR-81-1, 1981, Paul Gough Associates, Inc., Portsmouth, NH.

6. Gibeling, H.J. and McDonald, H., "Development of a Two-Dimensional Implicit Interior Ballistics Code," ARBRL-CR-00451, March 1981, US Army ARRADCOM/Ballistic Research Laboratory, Aberdeen Proving Ground, MD.

7. Gibeling, H.J. and McDonald, H., "An Implicit Numerical Analysis for Two-Dimensional Turbulent Interior Ballistic Flows," Final Report, Contract DAAK11-79-C-0098, US Army ARRADCOM/Ballistic Research Laboratory, Aberdeen Proving Ground, MD, September 1982.

8. Schmitt, J.A., Banks, N.E., Zoltani, C.K., Gibeling, H.J., and Mann, T.L., "Two-Phase Viscous Flow Modeling of Interior Ballistics, Algorithm and Numerical Predictions for an Idealized Lagrange Gun," Proceedings of the ASME Symposium on Computers in Flow Predictions and Fluid Dynamic Experiments, Edited by K.N. Ghia, T.J. Mueller, and B.R. Patel, 1981, pp. 181-190.

9. Gough, P.S., "Derivation of Balance Equations for Heterogeneous Two-Phase Flow by Formal Averaging," ARO Workshop on Multiphase Flows, Ballistic Research Laboratory, February 1978, pp. 71-80.

10. Gough, P.S., "The Flow of a Compressible Gas Through an Aggregate of Mobile, Reacting Particles," Ph.D. Thesis, Department of Mechanical Engineering, McGill University, Montreal, 1974.

11. Ishii, M., "Thermo-Fluid Dynamic Theory of Two-Phase Flow," Eyrolles, Paris, 1975.

12. Briley, W.R. and McDonald, H., "Solution of the Multidimensional Compressible Navier-Stokes Equations by a Generalized Implicit Method," Journal of Computational Physics, Vol. 24, No. 4, 1977, pp. 372-397.

13. Briley, W.R. and McDonald, H., "On the Structure and Use of Linearized Block Implicit Schemes," Journal of Computational Physics, Vol. 34, No. 1, 1980, pp. 54-73.

14. Love, E.H., and Pidduck, F.B., "Lagrange's Ballistic Problem," Phil. Trans. Roy. Soc., Vol. 222, 1921-22, pp. 167-226.

15. Heiser, R. and Hensel, D., "Berechnung der Gasströmung in einen Waffenrohr mit Hilfe des Zweidimensionalen AMI-Modells," E1/81, January 1981, Ernst-Mach-Institut, Abteilung Für Ballistik, Weil am Rhein, West Germany.

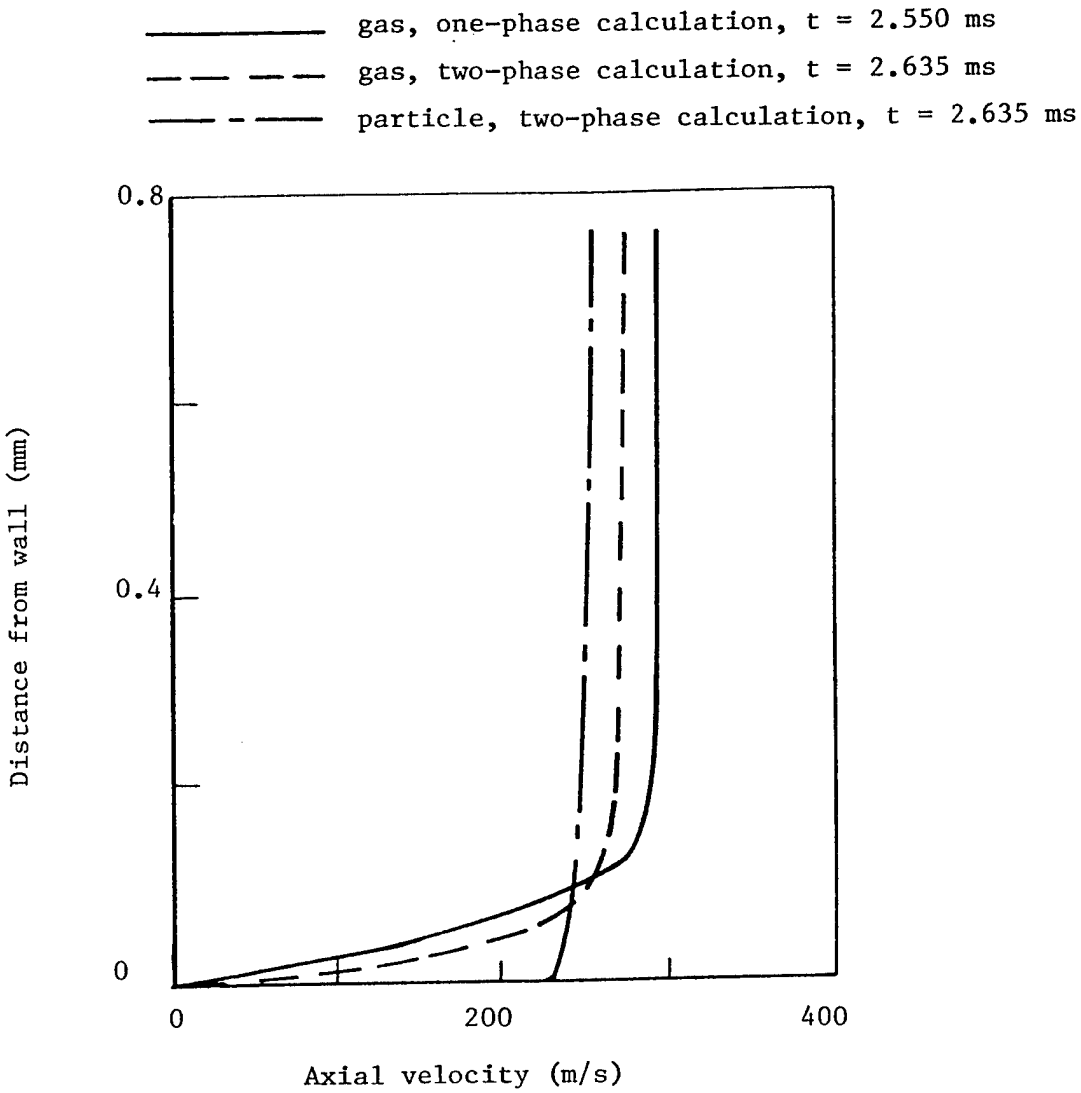

Fig. 1 - Comparison of one and two phase tube wall boundary layer profiles near muzzle exit time at z = 0.634 m; 100 μm diameter particles (case A); projectile position, 1.27 m.

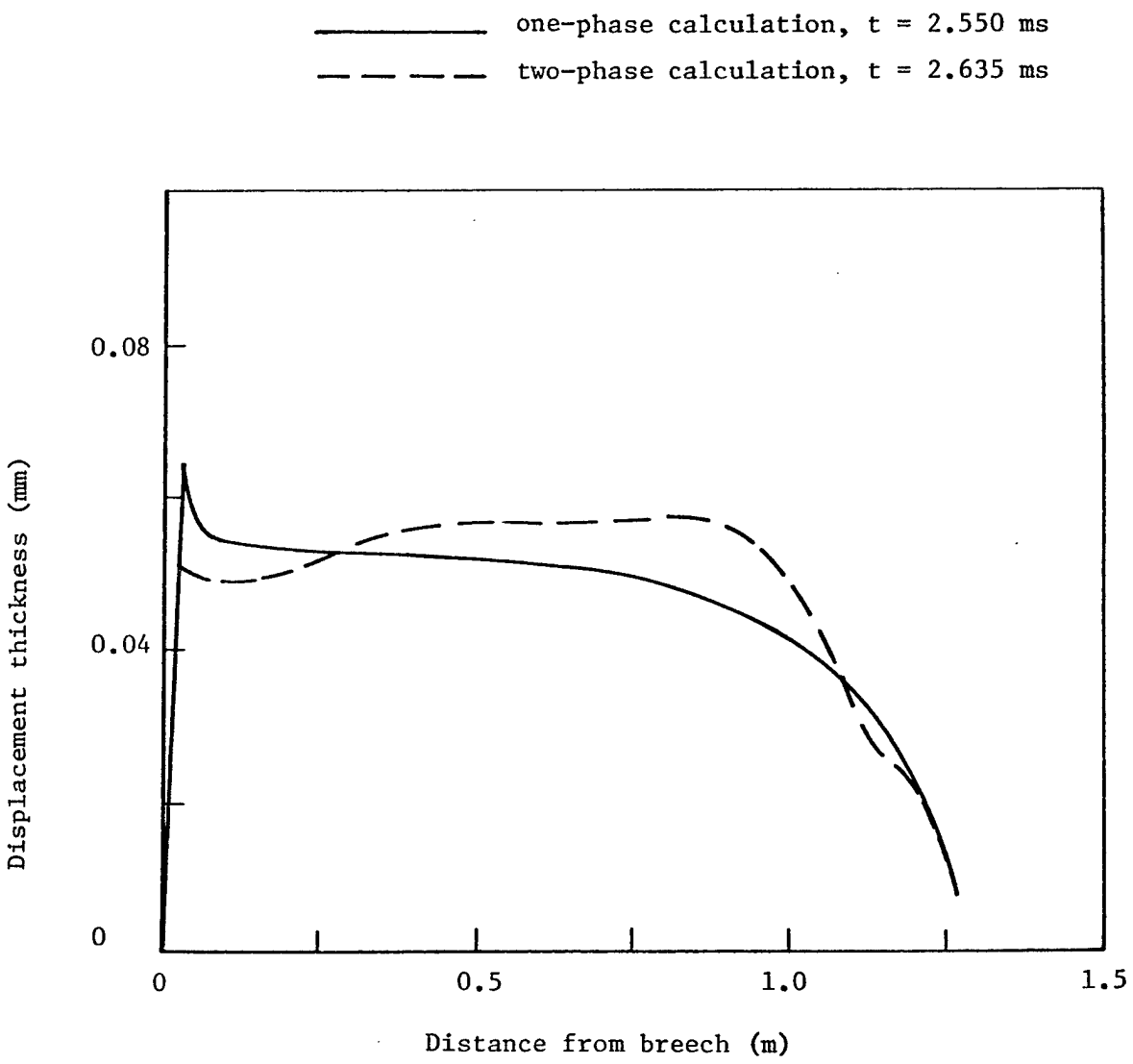

Fig. 2 - Comparison of boundary layer displacement thickness for one and two phase calculations near muzzle exit time; 100 μm diameter particles (case A); projectile position, 1.27 m.

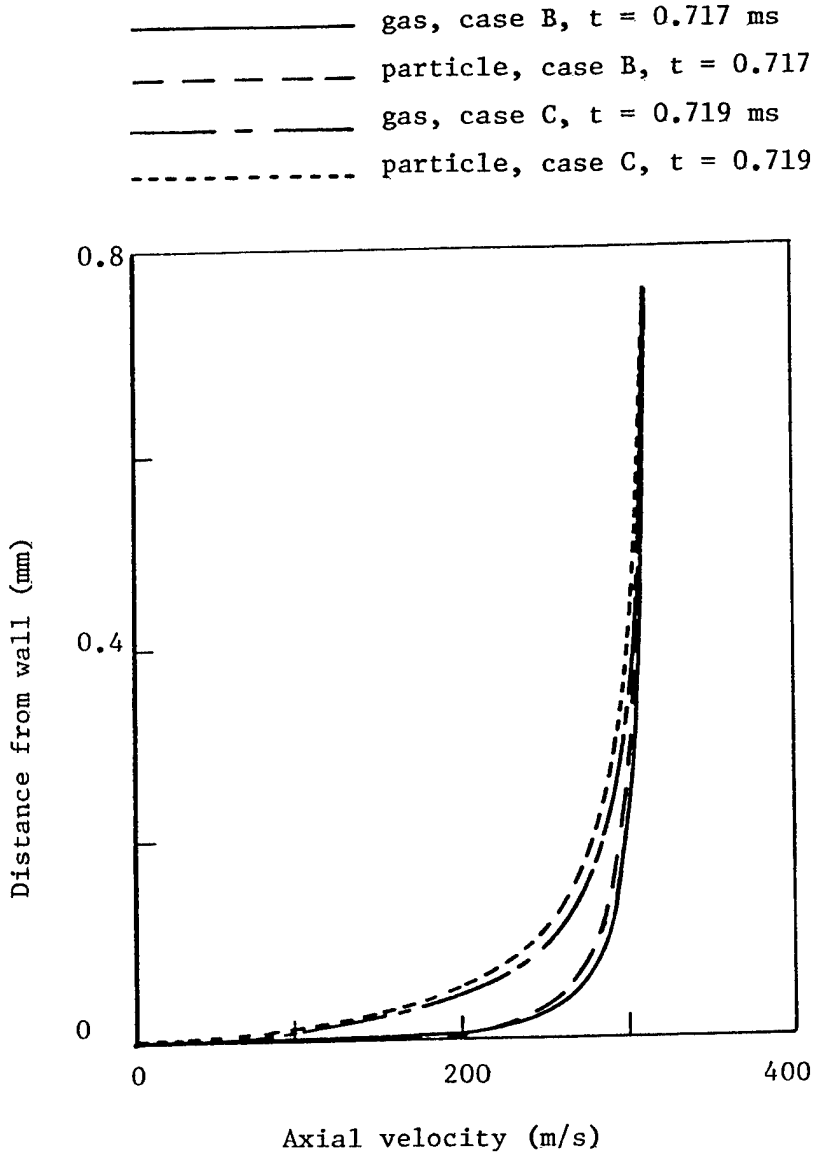

Fig. 3 - Comparison of tube wall boundary layer profiles for two phase calculations with full slip particle wall velocity (case B) and no-slip particle wall velocity (case C) at z = 0.28 m; 5μm diameter particles; projectile position, 0.33 m.

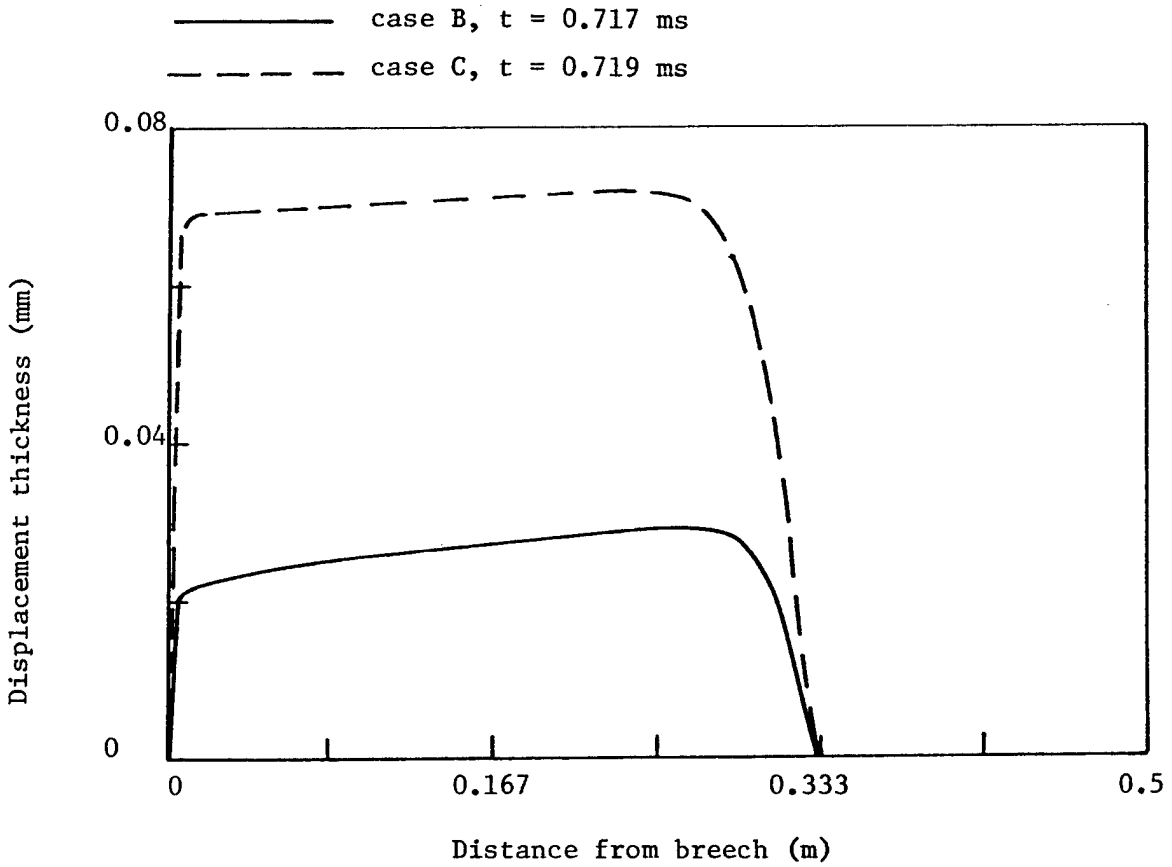

Fig. 4 - Comparison of boundary layer displacement thickness for two phase calculations with full slip particle wall velocity (case B) and no-slip particle wall velocity (case C); 5 μm diameter particles; projectile position, 0.33 m.

MODELED HEATING AND SURFACE EROSION COMPARING MOBILE (GAS BORNE) AND STATIONARY (SURFACE COATING) INERT PARTICLE ADDITIVES*

A. C. Buckingham and W. J. Siekhaus
University of California, Lawrence Livermore National Laboratory
Livermore, California 94550

ABSTRACT

The unsteady, non-similar, chemically reactive, turbulent boundary layer equations are modified for gas plus dispersed solid particle mixtures, for gas phase turbulent combustion reactions and for heterogeneous gas-solid surface erosive reactions. The exterior (ballistic core) edge boundary conditions for the solutions are modified to include dispersed particle influences on core propellant combustion-generated turbulence levels, combustion reactants and products, and reaction-induced, non-isentropic mixture states. The wall surface (in this study it is always steel) is considered either bare or coated with a fixed particle coating which is conceptually non-reactive, insulative, and non-ablative. Two families of solutions are compared. These correspond to: (1) consideration of gas-borne, free-slip, almost spontaneously mobile (motile) solid particle additives which influence the turbulent heat transfer at the uncoated steel surface and, in contrast, (2) consideration of particle-free, gas phase turbulent heat transfer to the insulated surface coated by stationary particles. Significant differences in erosive heat transfer are found in comparing the two families of solutions over a substantial range of interior ballistic flow conditions. The most effective influences on reducing erosive heat transfer appear to favor mobile, gas-borne particle additives.

INTRODUCTION

In a recent publication[1] we summarized the findings of our research over the last four years on fundamental mechanisms of erosion. One of the questions emphasized in our studies of erosive environments is the identification and evaluation of the influence of erosion reducing additives. We want to understand if they work, how they work and how effective they are. Many of the questions about the use of additives for erosion reduction such as their active or catalytic influence on gas phase reactions or their influence on the gas-to-solid surface reactions with thermal radiation remain. These questions form a major part of our present or future experimental and theoretical investigations. Here, however, it is useful to apply some theoretical tests to the issue of whether inert solid particle additives are more effective if introduced as gas-borne and free to disperse or if fixed to the wall as an insulative coating.

*Work performed under the auspices of the U.S. Dept. of Energy by Lawrence Livermore Natl. Lab. under contract #W-7405-Eng-48 and supported by the Dept. of the Army, U.S. Army Research Office, Research Triangle Park, NC and ARRADCOM, LCWSL, Dover, NJ, under contract #15812-MS.

Approved for public release. Distribution unlimited.

Either introducing additives as a freely dispersed phase or applying them as a semi-stationary liner or coating at the metal surface appear to be effective in reducing erosion. Experiments and firing tests seem to support the view that at least some types of additives significantly reduce erosion and extend the useful life of the working container surface (whether it is a cylindrical barrel or a contoured convergent divergent rocket propellant nozzle). However quantitative consistency and definitive information on the sensitivity of the additive influence with respect to size, material composition and state, concentration, placement and the manner in which the additives are introduced seem to be lacking. A goal of our current and on-going investigations is to shed some light on these questions and to provide some quantitative results in evaluating their influence on solid propellant combustion, flow, and erosion processes.

In-situ firing tests and laboratory based combustion generated erosion simulators provide the majority of the data available for erosion analysis. However, unfolding the influence of any single mechanism and, indeed, even the evaluation and analysis of the data for consistency and trends is difficult, if not impossible. Some simplification of the experimental configuration and implementation of prescribed, specific controls on the experimental conditions and process evolution throughout its test duration is needed. Appreciation of some of the interpretation difficulties may be derived from reading descriptions of the substantial recent efforts of Army scientists.[2,3] These efforts aim at evaluating the heat transfer to gun tubes and attempting to interrelate the different conditions based on (integrated over time) heat load or heat input. Direct effects of material micro-structural response and resultant characterization are intangibly lost, since the integral of the heat flux is a non-unique characterization of the heat transfer environment. Addition of a change in test configuration[4,5] only adds to the difficulty of relating the heat transfer information to erosion to any real system, in the absence of information on all scale factors (including time) which may control the evolution of the process.

It is apparently difficult to unfold the sensitivity of the unsteady influences, and account for configuration effects and scale effects even in a systematic data scatter and error analysis.[6] Evaluating more subtle influences such as one anticipates with additives as to their size, composition, and concentration influences is, we judge, even more difficult.

In view of this we adopt a different approach. We attempt to decompose the more complicated physical system into a set of simpler, more controllable, experiments. We further develop our investigations by devising and conducting both the experimental and theoretical investigations coincidentally and in parallel.[7,8,9] In our view it is encouraging to observe the development of similar joint theoretical and experimental efforts through Army collaboration with West German scientists over the past two years.[10,11] These efforts together with the basic shock tube research in Great Britain on reduction of turbulent wall heat transfer in particle laden flows represent a potentially major new source of appropriately controlled fundamental and useful information on the mass laden turbulent erosive heat transfer process.[17]

The questions that appear, theoretical considerations and experimental observations necessitate forming a global view (from wall to wall) of the combustion

chamber. We analyze the combustion process from its instigation until a substantial portion of the combustion generated impulse wave has decayed (usually an e-fold decay, relative to the maximum pressure pulse). Necessarily, however, systematic study of the erosion process requires that our final attention must be placed on a very much smaller portion of the global flow field. This is the wall boundary layer region consisting of the steepest flux gradients and the corresponding maximum erosion activity.[13,14,15]

PROCEDURE AND DISCUSSION

In the interest of spatial compactness in this article we will avoid extensive mathematical development and limit our illustrations to a minimum of figures necessary to support the discussion. We will cite, wherever necessary, the several open literature references in which more of the detail, omitted here, is available.

Perhaps the two most revealing factors pertinent to the stage of our investigation discussed here are first, the presence of a continuous distribution of turbulence energy (from combustion generated free core turbulence to wall generated boundary layer turbulence) and second, the existence of a threshold of inert particle size (about 1 micron) below which particles act to reduce erosion and above which particles act, in general, to enhance it.

In our study we preserve the continuity of turbulence from core to wall throughout the chamber by using two overlapping (asymptotically matched) solution procedures. One is a generally three-dimensional Navier-Stokes plus Lagrangian particle field solution procedure.[7,8,9] This extends, conceptually from the bounding chamber (or tube) walls throughout the combustion core in the mixed phase flow field region which grows between the relatively slowly expanding propellant bed and the more rapidly moving projectile it accelerates. The second solution procedure magnifies the all-important boundary layer region for further detailed study. It is computationally efficient to match the unsteady, chemically reactive multi-component turbulent boundary layer solutions at selected small intervals of time to the core solutions. The chosen intervals are those which we judge to be critical phases in the combustion flow evolution, boundary layer structure evolution and corresponding changes to heat, mass and momentum (wall shear stress) transport.[13,14,15]

Figure 1 illustrates the experimentally observed continuous distribution of turbulence intensity which extends from a combustion generated mixing region (in this case a combustion mixing free shear layer emanating from the splitter plate dividing a two channel rectangular combustion tube) to the chamber walls. The turbulence intensity is defined as the localized (space and time resolved) root mean square of the statistical velocity fluctuations ratioed to the local mean flow velocity. The distribution of values in mean flow velocity are shown in the upper frames at several designated streamwise locations, measured downstream of the splitter plate trailing edge. The lower frames illustrate values of the turbulence intensity measured with non-intrusive laser Doppler anemometer (LDA) techniques in our University of California, Berkeley combustion test facility.[8,9] The two channel rectangular combustion tube facility is a propane combustion flow tube with provision for a variation in flow speeds from about 10 to 20 m/s, for variation of air-fuel mixture ratios at the splitter plate, and for introduction

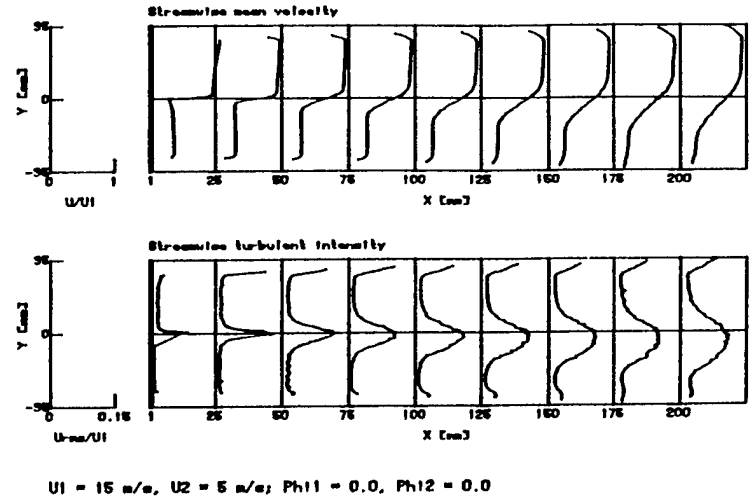

Fig. 1 LDA traces of mean two channel velocity profiles (above) and turbulent intensities (below) at listed stations.

of a range of concentrations of arbitrarily sized inert solid particles in the free shear layer. The experimental configuration is shown in Fig. 2.

The basic ingredients of the particle field plus time evolving but mean averaged (with respect to high frequency fluctuating velocity components) computational model include three interactive phases. One phase is an axially symmetric or plane two dimensional finite difference procedure for numerical integration of the time dependent Reynolds and Favre' averaged compressible Navier-Stokes equations. This also includes a volumetric node-to-node averaging for particle plus gas mixtures, and provision for finite rate kinetics with up to twenty matrix reaction equations.

The second computational phase includes both two- and three-dimensional time-dependent Lagrangian center-of-mass particle trajectory, momenta, and energy expectancy computations. The third phase is, conceptually, a statistical overlap between the other two fields. This third phase is basically a Monte-Carlo stochastic mixing phase which randomly samples the turbulent velocity expectancies and applies these in discrete time steps to the particle field through a set of self-consistent, velocity fluctuation dependent, particle-gas and particle-particle force laws.[7,8,9]

Using this procedure we compute turbulent intensity distributions in the rectangular geometry and under the experimental conditions previously described with respect to Fig. 1. The computed, predicted distributions, shown in Fig. 3, display, qualitatively, the same continuous profiles of intensity as those shown experimentally for the corresponding combustion test case in Fig. 1. Here, in Fig. 3, we also predict the influence of small particle mass loading, $K_m = 0$ (no particles) and $K_m = 0.002$ (about 1.3×10^4 cm^{-3} of 0.5 micron T_iO_2 particles). The mass loading parameter, K_m, is defined as the ratio of the mass of the particles in a unit volume to the sum of the mass of the gas and particles in the same volume. We see that even for very modest particle concentrations, the level of

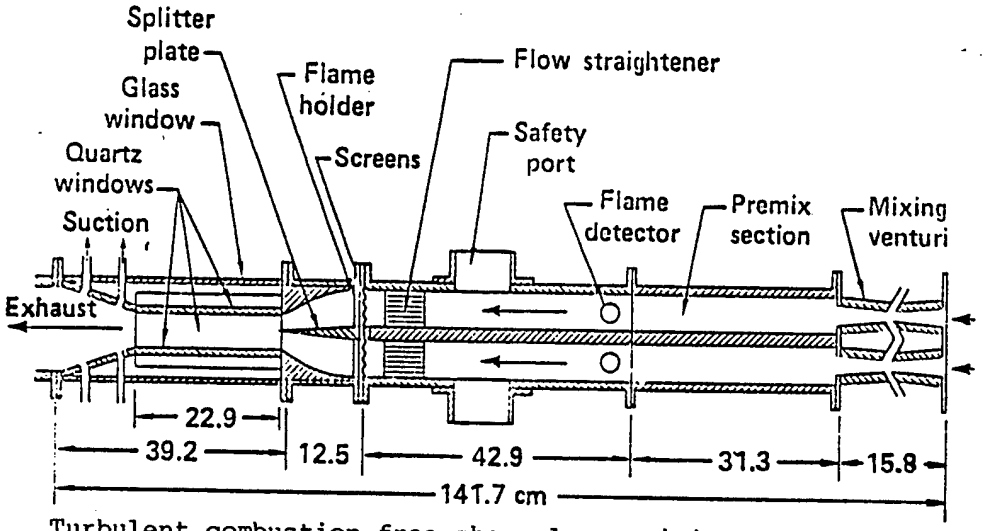

Fig. 2 Turbulent combustion free shear layer mixing two channel combustion tube for vapor phase and particle laden experiments. Dimensions shown are in cm.

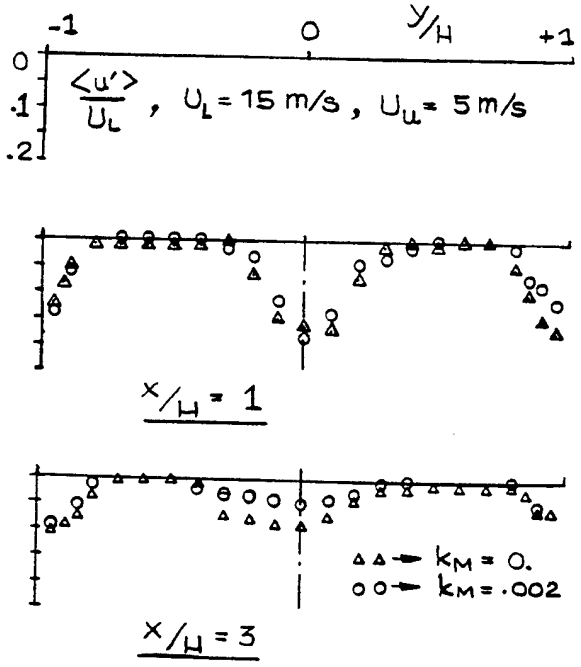

Fig. 3 Computer predictions of two-channel turbulent intensity profiles at listed stations, for the experimental flow conditions in Fig. 1. Particles are 0.5 μm diameter.

turbulence as measured by its local turbulence intensity is predicted to be significantly reduced. This is the potential, dominant, inertial mechanism for reduction of turbulent mixing, transport and consequent reduction of erosive heat, mass and momentum transfer. It results from addition of small (submicron) particles which relax almost instantaneously to the local mean gas field velocity.

Next we investigate a theoretically magnified view of the wall boundary layer region and alterations to its structure when even minute concentrations, $\mathcal{O}(10^5\ cm^{-3})$, of small inert particles are entrained. In order to simulate boundary layer structure changes in the presence of such particle mass loadings we asymptotically match the turbulent, finite-rate reactive, multi-component mixed phase boundary layer solution procedure to the previously described global mixture phase and particle field computations. The asymptotic matching procedure and results of parametric tests with boundary layer structure and altered flow conditions have been developed and described in previous articles.[13,14] Here, we summarize.

Let $\kappa(\vec{r},t)$ and $\varepsilon(\vec{r},t)$ be the space and time distributions of turbulence kinetic energy and turbulence dissipation rate, respectively. The transformed turbulent boundary layer stream function is represented by f, so that the parallel velocity is given by f' and its gradient with respect to the normal-to-the-wall distance is given by f", where primes denote differentiation with respect to this normal distance. The asymptotic outer edge position for the matching is then designated with the symbol ∞.

The conventional boundary layer matching conditions for a reacting ($\partial C_J/\partial t \neq 0$ where C_J is a species component), non-isentropic ($\partial s/\partial t + f' \partial s/\partial x \neq 0$) mixed conditions are expressed as,

$$\frac{\partial C_J}{\partial t} = \frac{\partial C_J}{\partial t}\ (\infty),\ \frac{\partial s}{\partial t} + f' \frac{\partial s}{\partial x} = \frac{\partial s}{\partial t}\ (\infty),\ \kappa(\infty),\ \varepsilon(\infty),\ f''(\infty) = 0. \qquad (1)$$

For the modified overlap region in our matching procedure they are identical to eq. (1) except that the vanishing turbulence kinetic energy and dissipation are replaced by local minima constraints,

$$\kappa'(\infty),\ \varepsilon'(\infty) = 0\ . \qquad (2)$$

The molecular gas transport coefficients are computed locally in the mixture boundary layer once the local particle dispersal and mass loading distribution is determined,

$$\kappa_p(x, y, t) = \kappa_m(x, y, t) + 1\ .$$

The space, time distributions of viscosity, conductivity and self diffusion, μ, κ_T, D_J are then computed from an elementary application of Enskog theory which results in a first approximation for the two phase mixture for light particle loading (neglecting <u>instantaneous</u> changes to intermolecular cross sections and collision frequencies),

$\mu = \mu^0/\kappa_p$, D_J^0/κ_p and κ_T from the renormalized Prandtl No., N_{PR}, (3)

$$N_{PR} = \left(\frac{\mu c_p}{\kappa_T}\right)^0 \cdot \left[\frac{1 + \kappa_m c_s^0/c_p^0}{\kappa_p}\right].$$

In the foregoing relations, superscript (0) refers to the locally computed pure gas thermal or transport properties while c_s and c_p are the solid particle heat capacity and gaseous specific heat respectively.

To compare our gas borne additive effectiveness with a fixed particle-in-binder coating layer as an insulative wall coating such as examined by Russell,[16] we make the following initial assumptions. First, the coating of particle-plus-binder (phenolic or glue) possesses a very low equivalent thermal conductivity (say equal to a graphite layer) and is uniformly applied and remains throughout at a depth of 5 mm as a coating around a cylindrical barrel-like container. We consider a streamwise wall segment 1 cm long, axially. An equivalent number density of uniformly distributed 0.5 micron particles in the central core of a 15.5 cm diameter cylinder (neglecting convection velocity distribution) is found to be about 6×10^{10} cm^{-3}. With a conservative estimate of the convective entrainment (ignoring boundary layer capture and particle concentration buildup) we estimate that a minimum of 6×10^5 cm^{-3} uniformly distributed particles populate the boundary layer wall region. Actually, using more detailed entrainment and statistical average dispersion calculations we have estimated that the boundary layer mixture may yield concentrations of particles about two orders of magnitude higher than those used here for our comparisons.[13,14] However, even applying these seemingly pessimistic concentration estimates to our analysis we predict the encouraging results shown in Fig. 4. Here the open circles represent a range of (peak) heat flux values delivered to the bare surface, while the filled circles and filled squares represent the modulated heat flux actually sensed through (i) the fixed coating layer and (ii) the gas-borne additive distribution, respectively. Either of the particle additive situations: the optimistically invariant, non-degrading liners, or the pessimistically sparse gas borne particles yield about the same level of reduction in heat transfer flux delivered at the wall surface. These heat flux data are plotted against the Reynolds' No., R_e^*, based on the chamber diameter, the mean flow density, and mean velocity at the peak of the gas phase heat pulse.

While direct measurement of the particle laden wall boundary layer shear and heat transfer are not yet available from our University of California, Berkeley experiments, the collaborative University of Southampton dusty gas shock wave driven turbulent boundary layer measurements (to date)[12] have indicated convincingly similar reductions in wall heating with particle entrainment (15%-30%).

SUMMARY

It appears that within the next few years we will have a useful understanding about particle additives and particle residue interaction in solid propellant

combustion erosion. Experimental verification and guidance is beginning to accumulate. The importance of this topic in erosion studies is evident on reflecting that the gas borne particles significantly influence not only the erosion but also the basic propellant combustion process itself by viscous and eddy damping, catalytic or reactive interaction with the kinetics, and scattering and absorption in the closely related thermal radiation transport processes. It is also encouraging to view the interest and emphasis placed on this area of research by our European colleagues in active collaboration with the Army efforts.

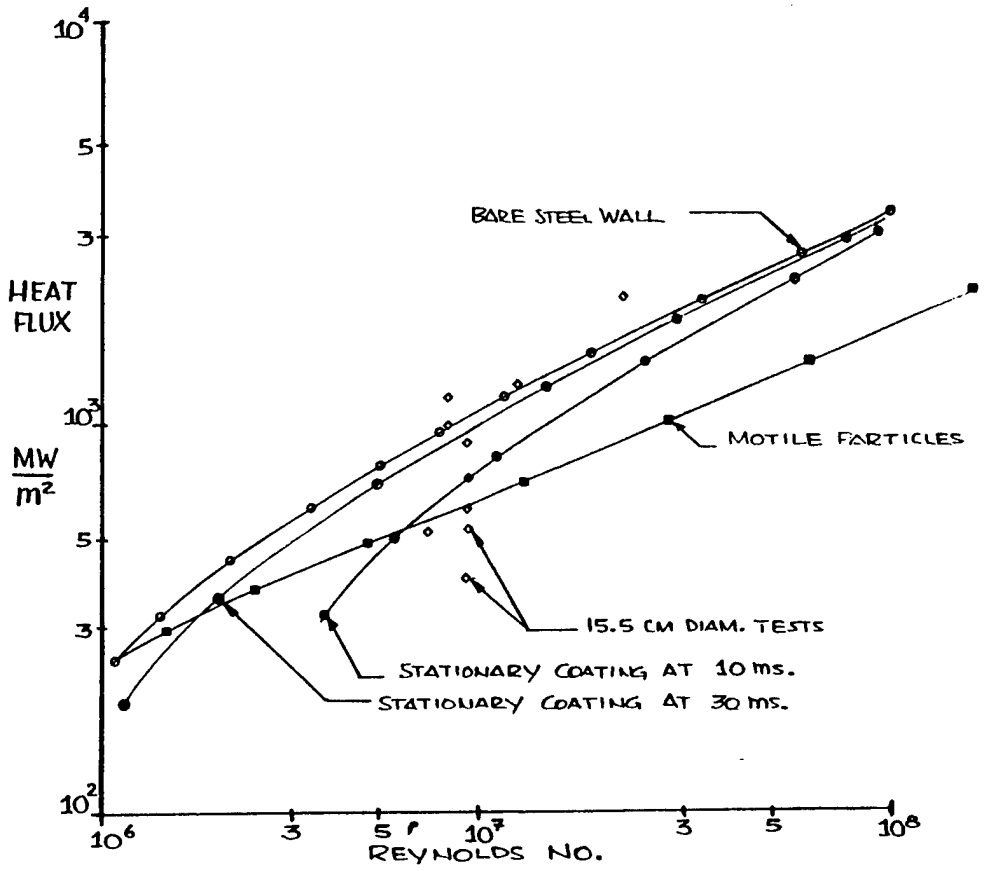

Fig. 4 Heating sensed at a steel surface: (1) directly exposed (2) coated semi-permanently with a 5 mm particle-plus-binder layer and (3) dispersed gas borne inert, non-reactive particles.

REFERENCES

1. A. C. Buckingham, W. J. Siekhaus, C. W. Price, "Erosion Mechanisms" in Proc. 29th Annual Sagamore Army Materials Conference, eds. V. Weiss and J. Mescall (Lake Placid, NY, July 19-23, 1982).

2. C. W. Nelson, J. R. Ward, Calculation of Heat Transfer to Gun Barrel Walls, U. S. Army, BRL, Aberdeen Proving Ground, MD, Report No. ARBRL-MR-03094 (March, 1981).

3. J. R. Ward, T. L. Brosseau, B. B. Grollman, Heat Transfer in Guns-Determination of Friction Factor from Heat Input Measurements, U. S. Army, BRL, Aberdeen Proving Ground, MD, Report No. ARBRL-MR-02366 (Sept., 1981).

4. R. Greene, B. Grollman, A. Niiler, A. Rye, J. R. Ward, Nitromine Propellant Erosivity III, U. S. Army, BRL, Aberdeen Proving Ground, MD, Report No. ARBRL-MR-02278 (Dec., 1980).

5. A. J. Bracuti, L. Bottei, J. L. Lannon, L. H. Caveny, Evaluation of Propellant Erosivity with Vented Erosion Apparatus, U. S. Army, LCWSL, Dover, NJ, Report ARLCO-TR-80017 (March, 1981).

6. J. R. Ward, I. C. Stobie, Comparison of Scatter in Wear Measurements of Large Calibre Guns with Nozzles, U. S. Army, BRL, Aberdeen Proving Ground, MD, Report No. ARBRL-MR-03168 (April, 1981).

7. A. C. Buckingham, W. J. Siekhaus, "Simulating Interactions between Turbulence and Particles in Erosive Flow and Transport", in Numerical Methods in Laminar and Turbulent Flow, eds. C. Taylor and B. A. Schrefler (Pineridge Press, Swansea, U.K., 1981) pp. 929-940.

8. A. C. Buckingham, W. J. Siekhaus, J. O. Keller, J. Ellzey, G. Hubbard, J. W. Daily, "Computed and Experimental Interaction between Eddy Structure and Dispersed Particles in Developing Free Shear Layers", AIAA paper 82-0965 in AIAA/ASME 3rd Joint Thermophysics, Fluids, Plasma and Heat Transfer Conf. (St. Louis, MO, June 7-11, 1982).

9. A. C. Buckingham, W. J. Siekhaus, J. O. Keller, J. Ellzey, G. Hubbard, J. W. Daily, "Computations and Experiments on Interactions between Inert Particles and Turbulence in Developing Free Shear", in Proc. Ninth U.S. National Congress of Applied Mechanics (Cornell University, Ithaca, NY, June 21-25, 1982).

10. G. Klingenberg, N. E. Banks, Review on Interior and Transitional Ballistic Research: State of the Art Computational and Experimental Efforts, Fraunhofer-Gesellschaft, Ernst-Mach-Institut, Abteilung für Ballistik, Weil-am-Rhein, FRG Report No. E12/81, in collaboration with N. E. Banks, U. S. Army BRL, Aberdeen Proving Ground, MD (December 1981).

11. H. Mach, U. Werner, H. Masur, Measurement of the Unsteady Velocity Field in the Muzzle Exhaust Flow of a 20 mm Rifled Gun Using a Laser Doppler Interferometer", Deutsch-Französisches Forschungsinstitut (ISL) Saint-Louis, France Report R128/81, in collaboration with N. E. Banks, U. S. Army BRL. Aberdeen Proving Ground, MD (December 1981).

12. G. T. Roberts, A Shock Tube Investigation of the Heat Transfer from a Non-Steady Boundary Layer in Two Phase Flow, (supv.) R. A. East and N. H. Pratt, Dept. of Aero and Astro, University of Southampton, UK Report ERC/9/4/2040/0223/RARDE (April 1980).

13. A. C. Buckingham, "Dusty Gas Influences on Transport in Erosive Propellant Flow", AIAA Journ. 19 (4) 501-510 (1981).

14. A. C. Buckingham, "Additive Erosion Reduction Influences in the Turbulent Bondary Layer" in Proc. 1981 JANNAF Propulsion Meeting (New Orleans, LA, May 26-28, 1981).

15. S.-W. Kang and J. L. Levatin, "Surface Heating due to a Turbulent Boundary Layer Flow" in Numerical Methods in Thermal Problems, Vol. II, eds. R. Lewis, K. Morgan, B. Schrefler (Pineridge Press, Swansea, UK, 1981) pp. 1235-1245.

16. L. H. Russell, Simplified Analysis of the Bore Surface Heat Transfer Reduction in Gun Barrels as Achieved by Using Wear Reducing Additives, U. S. Navy, Naval Surface Weapons Center, Dahlgren, VA, Report NSWC/DLTR-3378 (October 1975).

ks

CONSIDERATION OF SOME FUNDAMENTAL EROSION PROCESSES ENCOUNTERED IN HYPERVELOCITY ELECTROMAGNETIC PROPULSION*

A. C. Buckingham and R. S. Hawke
University of California, Lawrence Livermore National Laboratory
Livermore, California 94550

ABSTRACT

Experimental and theoretical research has been conducted jointly at the Livermore and Los Alamos National Laboratories on dc electromagnetic railgun Lorentz accelerators. Pellets weighing a few grams to tens of grams have been launched at velocities up to better than 11 km/s. The research is addressed to attaining repeated launches of samples at hypervelocity in target impact experiments. In these experiments, shock-induced pressures in the tens of megabars range are obtained for high pressure equation-of-state research. Primary energy sources of the order of several hundred kJ to a MJ and induction currents of the order of 1 or more MA are necessary for these launches. Erosion and deformation of the conductor rails and the accelerated sample material are continuing problems. We are examining the heating, stress, and erosion resulting from simultaneous imposition of rail induction current, dense plasma (armature) interaction, current distribution, magnetic field stresses and projectile/rail contact friction. We find that while frictional heating and consequent sliding contact erosion are minor contributors to the overall erosion process, the same cannot be said for plasma impingement, penetration, and almost simultaneous induction current (Joule) heating.

INTRODUCTION

The following discussion pertains to collaborative studies conducted at Lawrence Livermore National Laboratory (LLNL) and the Los Alamos National Laboratory (LANL). While we will refer to some of the previous results of our joint efforts at higher velocity, most of the present discussion will emphasize recent material and launch dynamics tests at LLNL conducted with more massive projectiles (tens of grams) at lower speeds. This emphasis enables us to concentrate on the materials issues, plasma interaction and rail erosion, which are prominant in our current work. Most of the material here is abstracted from current publications[1,2] or from another, currently unpublished, report on recent results and experimental interpretations by the second author.[3]

As a foundation for this discussion, we condense some previous descriptions of the railgun electromagnetic accelerator,[4,5] other related electromagnetic (EM) accelerators, principles of operation, and distinctions between related EM acceleration devices.

---

*Work performed under the auspices of the U.S. Department of Energy by Lawrence Livermore National Laboratory under contract #W-7405-Eng-48.

Approved for public release. Distribution unlimited.

Interest in research and development of electromagnetically (EM) driven projectile accelerators has increased dramatically in the past decade. This interest results from advances in energy storage and pulsed power technology combined with the growing requirements for launch velocities in excess of those obtainable with gas, powder and explosively driven launchers. At the LLNL the need is stimulated by limitations in the speeds achievable using two stage light gas guns for equation of state impact experiments.

The magnetic railgun accelerator is essentially a linear dc motor consisting of a pair of rigid, field-producing conducting rails and a movable conducting armature. The armature is accelerated by the Lorentz force produced by the current, I, in the armature (which may be a moving plasma layer) interacting with the magnetic field B associated with the rail current circuit (Fig. 1). In this discussion we consider a plasma arc armature which impinges on and is trapped at the rear of the projectile it accelerates.

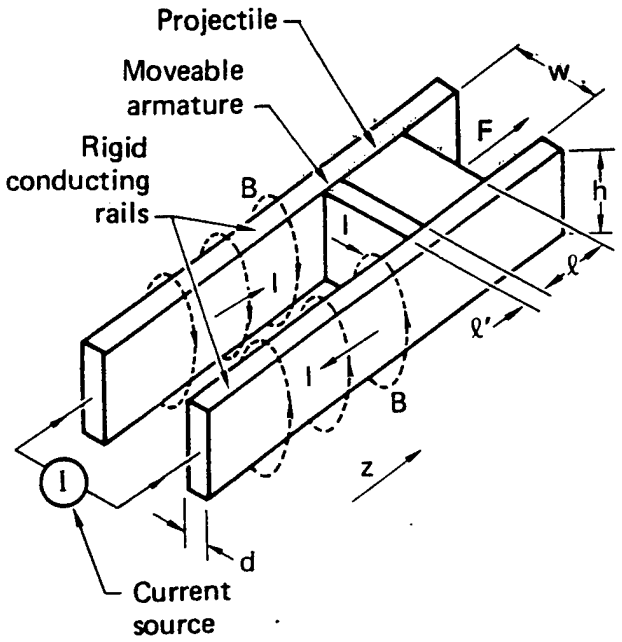

Fig. 1 Diagram of the elements of a railgun accelerator.

Accelerating mass with a plasma arc has several advantages over a sliding metallic armature. First the plasma easily maintains continuous contact with the rails. Of course, the resulting direct plasma material impingement and interaction is found to be the primary source of conduction rail erosion. On the other hand, a solid armature, necessarily a conductor, is also vulnerable to current heating, melt, ablation and erosion. In addition, a sliding solid armature that is not tightly constrained by the sidewalls is subject to sidewall collisional impact stresses. If, on the other hand, it is tightly constrained it may be subjected to excessive contact erosive drag forces. In addition, a solid armature

has not been found which can maintain electrical continuity with the rails at velocities greater than about 2 to 3 km/s. Our investigations, then, center on use of plasma arcs.

DISCUSSION

In previous descriptions of the erosion and material loss processes, we have studied the individual problems contributing to in-launcher rail/projectile erosion and failure[6] and post-launch hypervelocity atmospheric projectile degeneration.[7] We studied friction, stress, and thermally generated erosion processes by themselves, in the absence of the plasma interaction. However, our results have shown that the other factors exert minimal influence during the launch cycle on the overall erosion process except as possible coincident contributors with the plasma impingement and interaction mechanisms. Plasma impingement and distribution factors dominate among the material heating and erosive loss processes, particularly at the start of the projectile acceleration when an almost stagnant, thick, non-uniform plasma acts on the rails.

In effect the conducting launcher rails and projectile are severely tested by at least four interactive phases leading to material loss and potential system failure, or at least denial of re-use capability. These are:

1) contact erosion and ablation at the highly sheared interface between projectile and conducting rails;

2) exposure to radiating hot dense plasma heating and rail surface impingement and penetration, elevating and altering the projectile/rail surface state and phase;

3) induction current (Joule) heating and non-uniform current flow;

4) stresses associated with the plasma pressures on projectile, rail and dielectric and substantial magnetic field stresses associated with the high induction currents that are set up.

Figure 2 schematically illustrates this combination of influences on the launch process.

Experimentally determined factors relating to plasma arc behavior[3] have provided the information and incentive for conducting our current line of investigation. Contemporary railgun plasma arc behavior is important in two ways: (1) energy loss from the system and (2) erosion damage to the launcher.

Our LANL and LLNL experiments cover a purposely broad range of launch conditions. The projectile masses, which ranged from 1 to 47 g, were accelerated by square and round bore launchers ranging from 9.5 to 50 mm diameter or bore measure. Launch velocities studied were on the order of tens to hundreds of km/s for the larger masses while we have achieved in excess of 11 km/s for the smaller masses. The launchers were powered by both a capacitor bank and magnetic flux compression generator (MFCG) with dc currents in the range of 0.3 to 2 MA.

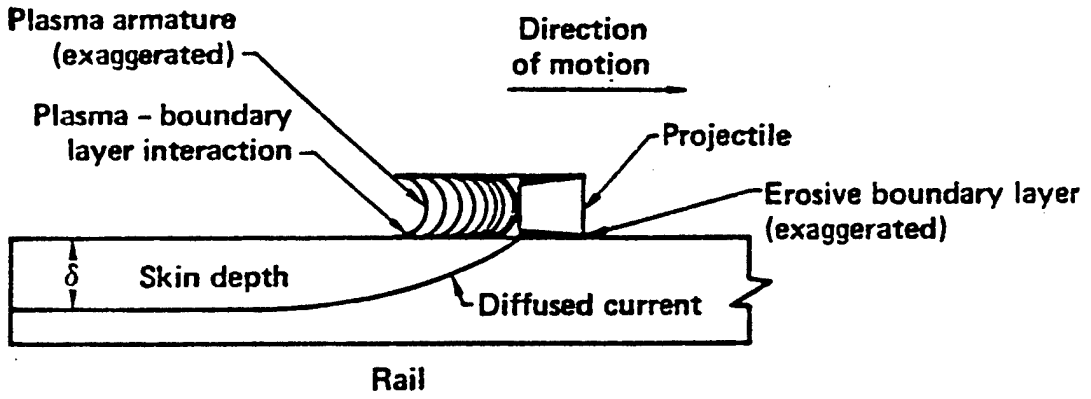

Fig. 2 Combined influences of current diffusion, non-uniform plasma interaction and projectile-wall friction on rail erosion.

The power source at the LANL launch site uses the MFCG with a 25 kV, 3 mf capacitor bank to provide the initial current. The MFCG system, as a whole, typically supplies average currents ranging from 0.5 to 1 MA and peak currents of 1-2 MA with pulse lengths of about 500 μs.

The capacitor bank used at LLNL for the majority of the erosion studies reported here consists of 24 capacitors with a total capacitance of 30 mf and stores 375 kJ at 5 kV. The maximum peak current input to a railgun was 1 MA with a quarter cycle rise time of 100 μs and a half cycle of about 300 μs.

Theoretically we are modifying the one-dimensional thin, uniform plasma heating and impingement calculations of More[8] to include thick spatial non-uniformity implied by the rail erosion patterns outlined in Fig. 3. This is a typical erosion pattern representing a composite of the many test cases for which photographic traces were prepared. These photographic data will be presented at the conference for which the present discussion is prepared. Space requirements do not permit their publication together with this discussion. The first calculations on the plasma interaction are made with a two dimensional, steady, stagnating, plasma at the start of launch. Unsteady plasma effects will be combined with accelerating motion and the viscous-shearing projectile-wall friction influences using the model previously developed.[6,7]

In More's one dimensional calculations, the temperature rise and resistance of the rails are computed simultaneously. First, the current density, j, in the rails is given by,

$$j = \frac{\partial \vec{H}}{\partial y} , \qquad (1)$$

where $\vec{H}$ is the magnetic field and y is the dimension normal to the rail surface. The diffusion of $\vec{H}$ into the conductor is given by

$$\mu_0 \frac{\partial \vec{H}}{\partial t} = \frac{\partial}{\partial y} [\eta \frac{\partial \vec{H}}{\partial y}] , \tag{2}$$

while, simultaneously, heating due to thermal and field penetration takes place according to,

$$\rho C_v \frac{\partial T}{\partial t} = \frac{\partial}{\partial y} [k \frac{\partial T}{\partial y}] + \eta [\frac{\partial \vec{H}}{\partial y}]^2 , \tag{3}$$

where μ_0 is the permeability, η is the resistivity, C_v is the specific heat, k is the thermal conductivity and ρ the nominal mass density of the rails, assumed constant in these calculations. Both conductivity, k, and resistivity η are generally nonlinearly coupled through temperature dependence. While More's calculations assumed constant conductivity, the more general temperature variation is assumed with no additional difficulty. The functional form is,

$$\phi = \phi_0 + \alpha_{k,\eta} T , \tag{4}$$

where ϕ represents k or η, the subscript zero denotes the assumed initial value, and the coefficient $\alpha_{k,\eta}$ is the respective, corresponding temperature coefficient. The non-linearity and coupling of eqs. (2) through (4) suggested the implicit finite difference solution procedure, that was applied. Results included temperature profiles and resistance as functions of time, rail dimensions, and current.

From these previous results for the one-dimensional model we see that the maximum temperature rise occurs on the surface of the rails. This is shown in Fig. 4, as a function of current concentration.

For these estimates we need to know rail resistivity, specific heat and thermal conductivity. All are functions of temperature and are reasonably well defined (at least when neglect of dense plasma interaction is possible) for standard conductors such as Cu and Al. However, fundamental property and property change investigations are necessary on other materials and composites such as refractory metal coatings or inserts which could be used in fabricating erosion-resistant rails. Two initial temperatures, T_0, are used in this illustration. The lower one refers to a condition attained, perhaps by cryogenic cooling. Rail heat dissipation during the cooling cycle remains another research issue.

We briefly summarize the results of current experiments which are guiding our development of a theoretical model for the interactive erosion process. Five different materials were used as rails under identical conditions at LLNL. The degree of erosive rail damage can be ranked from worst to best in the following order: 100% copper, 70% tungsten-30% copper, 98% tungsten-2% thorium, 90% tungsten-6% copper-2% nickel-2% iron, and 90% tungsten-10% silver. In all cases, even the best, the degree of erosion was greater than desired in a multishot launcher. The rail erosion occurred at a current concentration far less than the predicted limit due to Joule heating ($\sim$40 kA/mm). Multi-shot plasma armature launchers

will require even lower current concentrations in the breech region and/or other techniques, such as injection of the projectile with a gas gun in order to reduce the time that the plasma dwells in each region of the rails. Figure 3 outlines the erosion patterns that resulted from these tests. Due to the massiveness of the projectile, only 5 mm of motion occurred during the current pulse. Hence the majority of the eroded area experienced the total arc duration. The average charge transfer density was $\sim$7.5 Coulombs/cm^2 (assuming the transfer occurred primarily in the "rough" region).

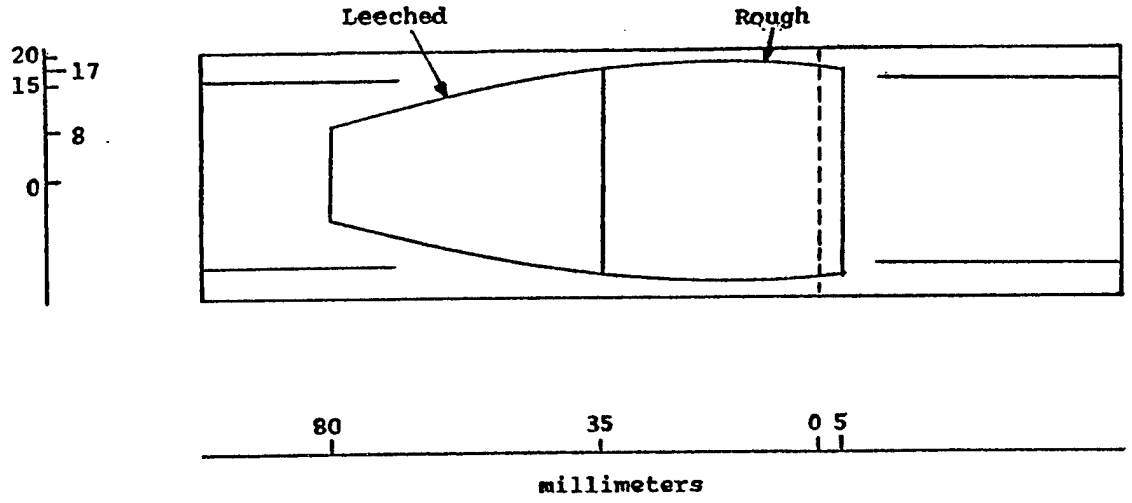

Fig. 3 Rail erosion patterns suggest plasma arc distributions.

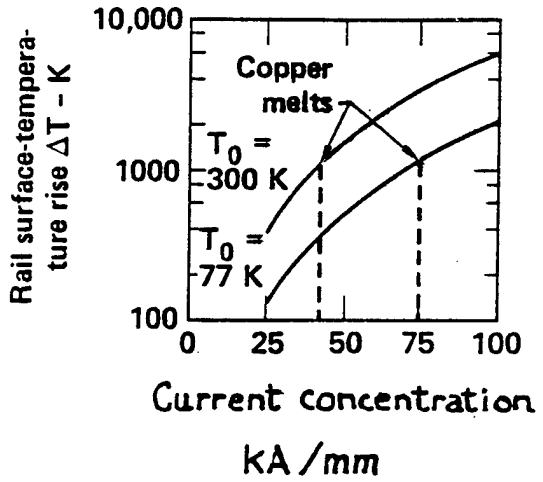

Fig. 4 Maximum temperature rise occurs on surface of rails.

Assuming the "rough" region area represents the arc cross section, and the saturated arc resistance is ~ 0.7 mΩ, the equivalent arc resistivity is $\sim 1.4(10^{-5})\Omega$m.

In the same tests two dielectric (rail separator) materials were tested for their resistance to arc erosion, Delrin and Polyimide. The degree of damage to both materials was far less than that experienced by the rails and later was found to be nearly unchanged. This helps confirm that the erosion seen in the rails is primarily a function of plasma and current interaction in conducting materials.

The erosion of the back side of the polycarbonate projectiles was surprisingly small. An intensified test used one projectile, clamped in place for 10 consecutive arc discharges. Approximately 85 mg of material, representing a mean erosion depth of about 80 μm were lost. The peak current was 390 kA. The charge transfer was estimated at 450 Coulombs for each of the discharges.

We also observed, from our experiments, that during acceleration of a projectile from rest (the static start) we obtain maximum erosion. The rail material and fuse material (for the arc) probably should be the same, initially. Al fuses used with Cu rails result in very high plasma augmented erosion with no counter source for material replenishment or vapor phase ablation buffering. Also we find that the projectile should be in motion when the arc is struck and electromagnetic acceleration begins. At LLNL tests with up to 200 m/s preinjection velocity result in a marked reduction in rail erosion although indications are that about 600 m/s initial velocity will be needed to eliminate plasma augmented erosion.

SUMMARY

This discussion placed emphasis on the following factors and questions which appear to dominate in-launcher material erosion. Study is necessary on:

1) Dense plasma and high current density influences on changes in microstructure and properties of conventional rail conductors such as Cu, Al, and W alloys or composites,

2) The influences described in (1) on more advanced high temperature, microstrain resistant, materials such as amorphous tungsten,

3) Location, description and temporal evolution of current, magnetic field, and losses during intense plasma-current field interactions with conductors,

4) Composite materials and sequentially sectioned structures for more efficient EM dc launcher configuration.

REFERENCES

1. A. C. Buckingham and R. S. Hawke, "Configurations, Materials and Performance Considerations for Railguns in Space Propulsion", Lawrence Livermore National Laboratory, Livermore, CA Report UCRL-87002 (Feb. 1982) to appear in AIAA Advances in Aeronautics and Astronautics: Space Propulsion, L. H. Caveny, ed. (approximate publication date, Fall 1982).

2. A. C. Buckingham and R. S. Hawke, "Some Preliminary Views of Plasma Interaction: Electromagnetic Launch Systems", in Proc. 29th Annual Sagamore Army Materials Research Conf., eds. V. Weiss and J. Mescall (Plenum Press, NY, 1982).

3. R. S. Hawke, A. L. Brooks, C. M. Fowler, D. R. Peterson, "Plasma Behavior in Arc Driven Railguns", University of California, Lawrence Livermore National Laboratory, Livermore, CA, to be published (1982).

4. R. S. Hawke and J. K. Scudder, "Magnetic Propulsion Railguns: Their Design and Capabilities", in Megagauss Physics and Technology, ed. P. J. Turchi, Plenum Publishing Co., New York (1980) pp. 297-311.

5. R. S. Hawke, "Devices for Launching 0.1-g Projectiles to 150 km/s or More to Initiate Fusion", Atomkernergie, Kerntechnik Bd. 38 (1981) pp. 35-46.

6. A. C. Buckingham, "Electromagnetic Propulsion: Drag and Erosion Modeling", in AIAA Journ. 19 (11) 1422-1428 (1981).

7. A. C. Buckingham, "Projectile and Rail Launcher Design Analysis for Electromagnetic Propulsion to Velocities Exceeding 10 km/s", AIAA Paper #81-0750 in AIAA/JSASS?DGLR 15th International Electric Propulsion Conf. (Las Vegas, NV, April 21-23, 1981).

8. R. More, Lawrence Livermore National Laboratory, Livermore, CA, private communication (1979).

GUN WEAR: AN ACCOUNT OF RECENT UK RESEARCH AND NEW WEAR MECHANISMS

D C A Izod BSc, PhD
R G Baker

RARDE
Fort Halstead, Sevenoaks, Kent, United Kingdom

ABSTRACT

This paper outlines some of the existing theories of gun barrel wear, describes their inadequacy in explaining gun wear patterns in modern UK tank guns. It highlights the main features of the research programme undertaken to obtain a better understanding of the processes, particularly in respect to talc, impregnated combustible cartridge cases. Finally, a number of additional wear mechanisms are proposed.

© Crown Copyright Reserved

1. INTRODUCTION

Following the application of talc impregnated combustible cartridge cases to charge construction, barrel wear in tank and artillery guns has been important but not dominant factor affecting charge development. There has been a concern, however, to determine the limits to wear reduction by this method and it is necessary to understand why it works in order to do this. Oval barrel wear has also been a notable feature of recent APFSDS ammunition. It is required to understand also why this occurs.

For these reasons UK gun barrel work has concentrated upon the experimental and theoretical development of wear mechanisms, mostly on the fluid dynamical aspects of heat transfer.

The aim of this paper is to present the evidence derived from the above work, to support the postulation of some additional wear mechanisms. These, under particular circumstances, become the dominant contributors to the heat transfer and hence the wear process.

To achieve this aim, a brief review of the present theories are presented in section 2, section 3 lists the weaknesses in present theories, section 4 outlines wear reduction methods whilst section 5 describes the activities of RARDE and its various contractors.

2. WEAR MECHANISMS

It is generally accepted that there are three main causes of barrel wear, although in our view they are all intimately interrelated. These are, ranked in probable order of importance, thermal, mechanical and chemical.

2.1 Thermal Mechanisms

A convenient starting point for a discussion of thermal wear mechanisms is the phase diagram for steel which is shown in figure (1).

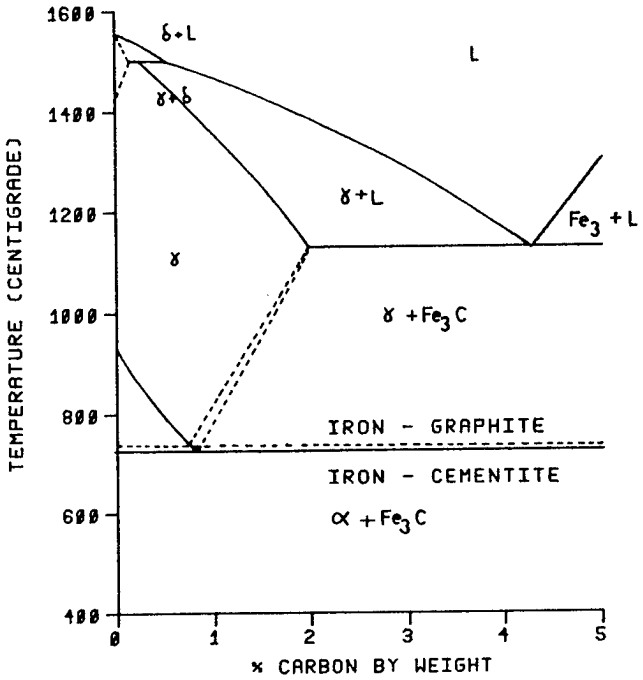

FIGURE 1 PHASE DIAGRAM FOR STEEL (TEMP vs CARBON CONTENT)

The carbon content for gun steels is typically about 1/3%. The phase diagram shows that there are two or three important temperatures which should be considered; at about 725°C there is the first of several solid state phase changes from α-iron plus Fe_3C (cementite) to a mixture of γ-iron and α-iron crystalline states, above about 825°C to γ-iron, and finally at 1500°C the formation of mixed liquid and solid phases. There are volume changes associated with the changes in the crystalline state and this is thought to result in the characteristic "heat craze cracking" which is commonly observed in gun bores.

The rate of wear per round observed in a wide range of guns against predicted bore surface maximum temperature rise has been plotted by Thornhill (Ref 1). Here it is seen, shown in figure (2), that there are three regions of interest. Below 660°C there is no wear, whilst between 660°C and 1050°C wear takes place relatively slowly. Above 1050°C wear takes place at an accelerated rate. There is apparently no correlation between the phase diagram and wear pattern so far as the temperature at which certain events take place.

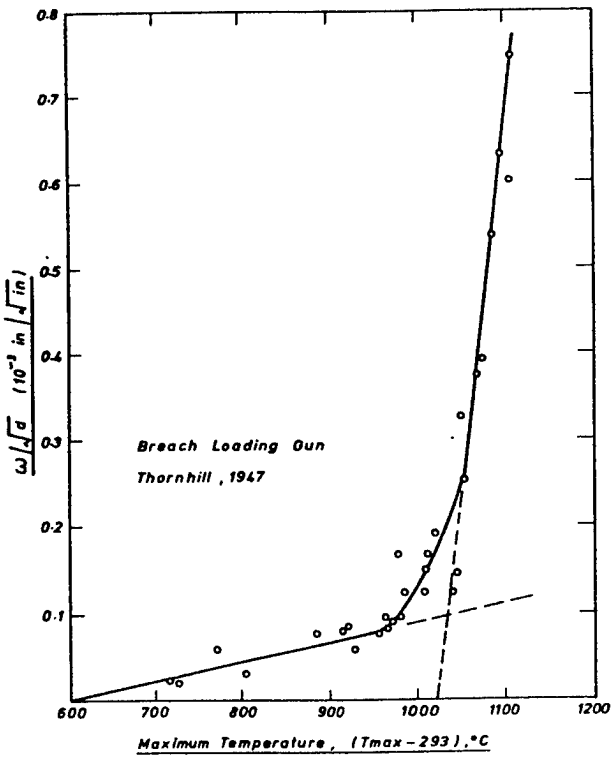

Fig 2·3 CORRELATION OF WEAR / ROUND AND MAXIMUM TEMPERATURE

FIGURE 2 CORRELATION OF WEAR/ROUND AND MAXIMUM TEMPERATURE

Visual examination of the bore shows that it is rare to observe the characteristic surface associated with the mett-wipe wear process, therefore attention has turned to the hot gas erosion process.

Lawton (Ref 2) applies Finnie's equation for hot gas erosion (Ref 3) to the gas flow around the shot assuming that it is choked to derive a bore surface wear rate:

$$\frac{dw}{dt} = K.F(\alpha) \cdot g(\gamma) \frac{b}{a} Pg \frac{\sqrt{RTg}}{H^{1.5}} \quad .. \qquad (1)$$

where $\frac{dw}{dt}$ = the rate of wear on the bore diameter, m/s.

K = a constant depending on the propellant gases.

$F(\alpha)$ = a function of the angle of incidence of the gas upon the bore.

$g(\gamma)$ = a function of the ratio of gas specific heats.

b,a = windage past shot, and erosion zone width, m (see figure 3).

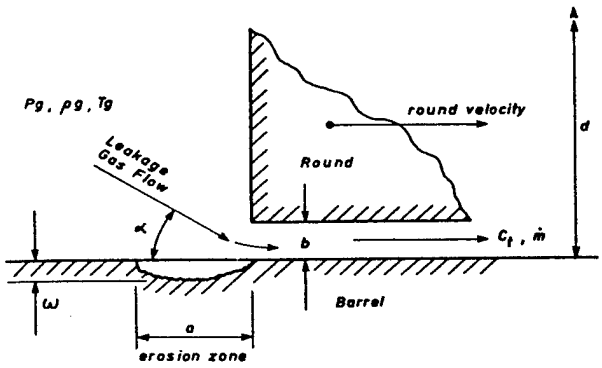

FIGURE 3 ASSUMED EROSION ZONE ASSOCIATED WITH GAS LEAKAGE PAST A ROUND

P_g = gas pressure, MPa

t_g = gas temperature, K

R = Universal Gas Constant

H = hardness of gun barrel.

It is pointed out that the hardness of steel is a function of temperature and this is presented in figure (4) for a 0.2% content steel and pure iron.

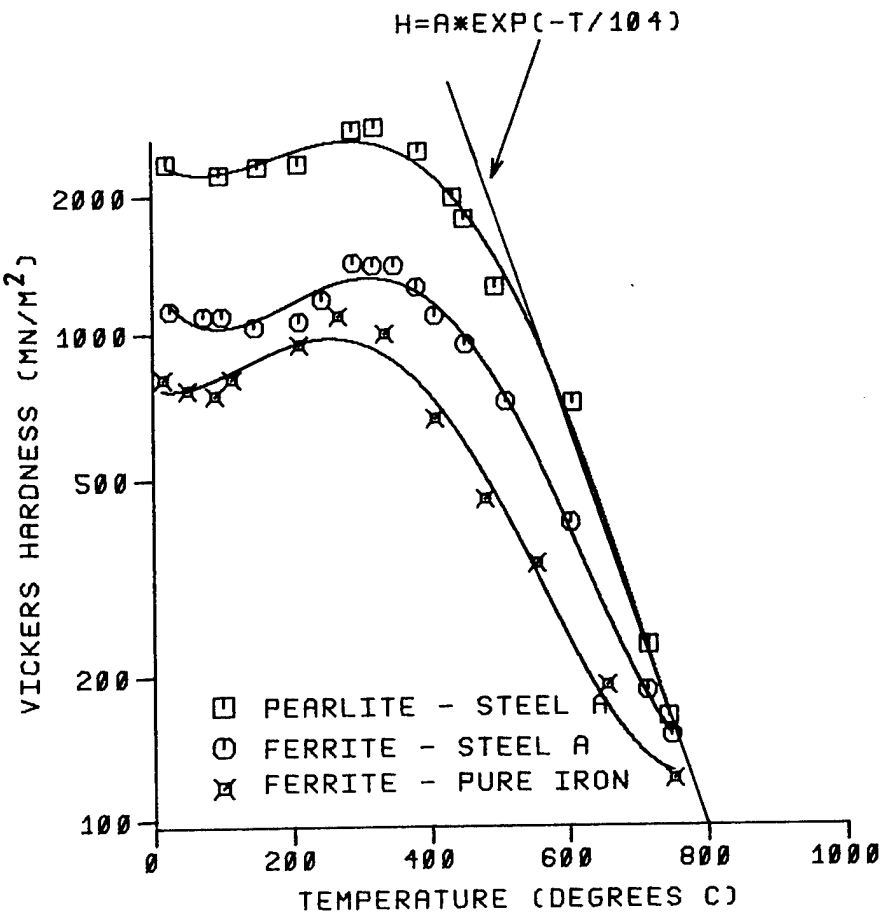

FIGURE 4 HARDNESS OF FERRITE AND PEARLITE IN A 0.2 % STEEL AND OF FERRITE IN A NOMINALLY PURE IRON

In the temperature region of interest to those concerned with wear, the hardness varies as:-

$$H = A \cdot \exp\left(-\frac{T}{104}\right) \qquad (2)$$

This may be substituted into (1) to give

$$\frac{dw}{dt} = K' \cdot \frac{b}{a} \cdot P_g \sqrt{RT_g} \cdot \exp\left(\frac{1.5\ T_w}{104}\right) \qquad (3)$$

where K = a lumped constant
T_w = bore surface temperature

Lawton makes some simplifying assumptions concerning the time independence of some of the variables during the erosion process an integrates equation (3) to obtain:

$$w = A.\exp(T_{max}/B) \quad (4)$$

where T_{max} = maximum bore temperature

and A,B = constants (B = 104/1.5 = 69 from (hot hardness data)

Comparison of this equation with Thornhill's data and with more recent US data measured by Ward et al (Ref 4) shows that the correlation is good with B = 68 and 62 respectively. This gives confidence that, in the temperature region T_{max} 800°C, hot gas erosion resulting from gas leakage past the shot is a dominant wear mechanism. Data for the hot hardness of gun steels above 800°C is needed to confirm this conclusion for higher maximum bore temperatures. Whilst the hot gas erosion gives an apparently satisfactory temperature dependence for wear, greater confidence in the theory would be achieved if the absolute wear (ie a knowledge of the value of A) could be predicted from physical parameters. This aspect is being studied further.

When the data from Thornhill (Ref 1) is sorted into propellant type and replotted, an interesting result is obtained which may be seen in figure (5).

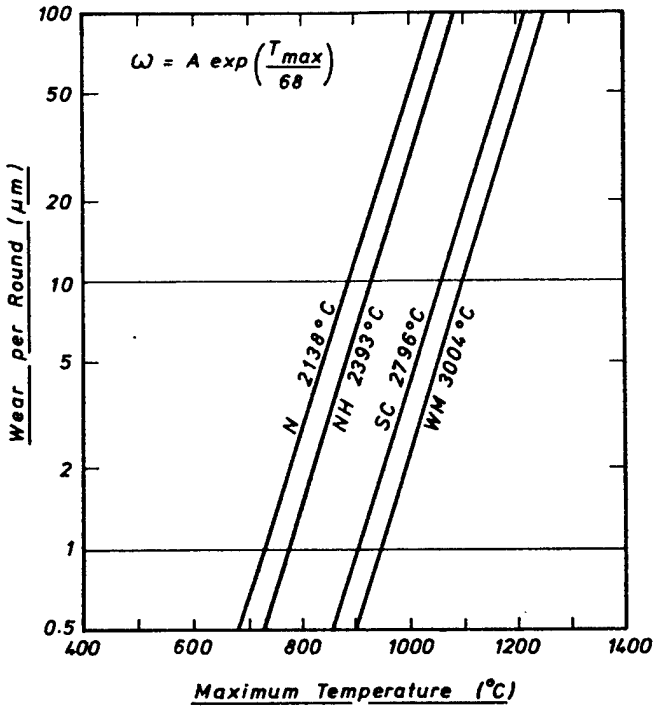

FIGURE 5 COMPARISON OF THE WEAR CHARACTERISTICS OF FOUR PROPELLANTS

It may be seen that the value of B is independent of propellant type, and that the greatest wear is observed with the lower flame temperature propellants. It should be borne in mind that the Thornhill data is based on guns ranging from the 0.303 inch rifle to 16 inch naval guns. This result would appear to be contrary to this empirical equation generated by lumping all the data together which is given below:

$$T_{max} = \frac{900}{\sqrt{C_m}} \cdot \frac{(T_f - T_w)}{1.7 + \frac{670\ d}{m^{0.86}}^{2.22}} \ ^\circ C \qquad (5)$$

where T_f = the adiabatic flame temperature of the propellant

d = bore diameter, m

m = charge mass, kg

C_m = muzzle velocity, m/s.

The results from experimental wear tests in a 30mm RARDE gun seem to confirm that this equation may not be valid and are presented later in the paper.

Equation (5) has a semi-empirical basis upon heat transfer in a pipe. The usual heat transfer processes are conduction, convection and radiation from the hot propellant gas to the surface, and a few simple calculations shows that the convetive one will predominate. Radiative heat transfer is about 0.5% of the total heat transfer.

Many theories are based upon steady state heat transfer in a pipe using the Nusseltt equation where the heat transfer coefficient, h, is given by

$$\frac{hD}{k} = 0.23 \left(\rho\frac{uD}{\eta}\right)^{0.8} \left(\frac{C_p\eta}{k}\right)^{0.4} \qquad (6)$$

where D is the pipe diameter, k, ρ, u, η, C_p are the thermal conductivity, density, free stream velocity, viscosity and specific heat respectively. The heat transfer rate, Q, is then presumed to be given by

$$\dot{Q} = h\ A\ (T_f - T_w). \ldots. \qquad (7)$$

This type of approach has been adopted by Heiney et al in reference (5).

The steady state inviscid gas flow approach is unsatisfactory because it ignores the presence of the boundary layer and its effect on heat transfer. This has been addressed by a number of authors notably Shelton et al (Ref 6) who solve the continuity and conservation equations for the propellant gas generation and flow. Unfortunately there does not appear to be a satisfactory validation of the model against experimental data nor any attempt to relate wear to heat transfer. Nevertheless, this type of approach has been adopted in the UK by CHAM Ltd under RARDE contract and is reported in Section (3). The results of the model have been compared with experiments carried out by the University of Southampton's 5 inch Shock Tube to determine the effect of wear additives such as talc on the heat transfer rate behind a shock. Agreement between theory and this experiment is now good both for clean and dusty gas conditions. This work has been reported at references 7 and 8.

2.2 Chemical Mechanisms

There are two main mechanisms which can be described as chemical wear. Recombination reactions between the products of combustion can take place preferentially on the barrel surface because of a higher collisional probability due to the adsorption process. If the reaction is exothermic, then the heat transfer to the barrel wall is increased. The second mechanism arises from the formation of compounds or different crystalline structures by surface reactions between the propellant gas and steel. The work of Squire (Ref 9) has shown that the top black surface layer is mainly zinc sulphide but there may also be free sulphur diffused into the steel causing embrittlement. Sulphur and sulphides presumably come from the gunpowder igniter. There are two thin white layers usually formed underneath; the first layer probably consisting of ε-Fe_3C, austenite and α-Fe which is mechanically weak, whilst the second white layer contains austenite and free carbon. The white layers have the effect of reducing the temperature at which the mixed liquid phases appear and possibly the hot hardness.

2.3 Mechanical Mechanisms

The passage of the projectile over the bore surface can remove mechanically weakened material. In addition, there are significant frictional heating effects during the engraving process. In data to be presented later in this paper, frictional heating contributes about 8% of the total heat transfer in a 40mm RCL gun test.

The pressure gradient causes the acceleration and impact of burning propellant grains against the bore causing increased heat transfer and ablation of material from the wall.

3. WEAKNESSES IN PRESENT THEORIES

The major weaknesses in present theories are summarised as follows:-

(i) They fail to account satisfactorily for the differences in wear rates of charges conditioned and fired at elevated and reduced temperatures. In Table 1, wear results for an experimental charge firing the L23 APFSDS

	Wear mm/rnd x 10^{3}		
	Horizontal	Vertical	Mean
-40°C	1.8	0	0.9
21°C	7.3	10.9	9.1
52°C	9.1	18.1	13.6

TABLE 1 WEAR RATES FOR EXPERIMENTAL CHARGE FIRING L23 PROJECTILE

projectile show a 15 fold increase for only a 82°K temperature rise of a propellant whose flame temperature is 3580K. Thornhill's equation predicts only a 24% increase in wear rate.

(ii) They fail to account for the well known fact that the use of separated ammunition results in oval barrel wear. This is not due to the asymmetry of the charge lying in the chamber. Further as the mean wear rate has been reduced so the magnitude of ovality has increased suggesting that there is another wear mechanism which becomes a larger factor. The gas leakage mechanism is hypothesised as being the major cause of oval wear. Table 2 shows some wear results for fixed and separated ammunition obtained over the past two decades showing how the ovality has increased although the mean wear rate has been considerably diminished.

Gun/Ammunition	Mean Wear mm/rnd x 10^{-3}	Ovality %
105 mm L7/APDS fixed	14	0
120 mm L11 /APDS bag	21	1(Vert)
120 mm L11/APDS CCC	8	7 (Hor)
120 mm M13a/APDS CC fixed	21	0
110 mm /APDS CCC	13	18 (Vert)
120 mm L11/F APFSDS CCC	4	50 (Vert)

TABLE 2 MEAN WEAR RATES AND OVALITY IN TANK GUNS

(iii) They fail to correlate the observed wear with the observed or predicted heat transfer. In particular the wear profile along the barrel length is localised in the region of the commencement of rifling, whereas heat transfer to the barrel wall is predicted from steady state convective heat transfer to be much more uniform down bore. The localised nature of wear observed in chrome plated and unplated 120mm L11 barrels firing APDS projectiles is presented in figure (6).

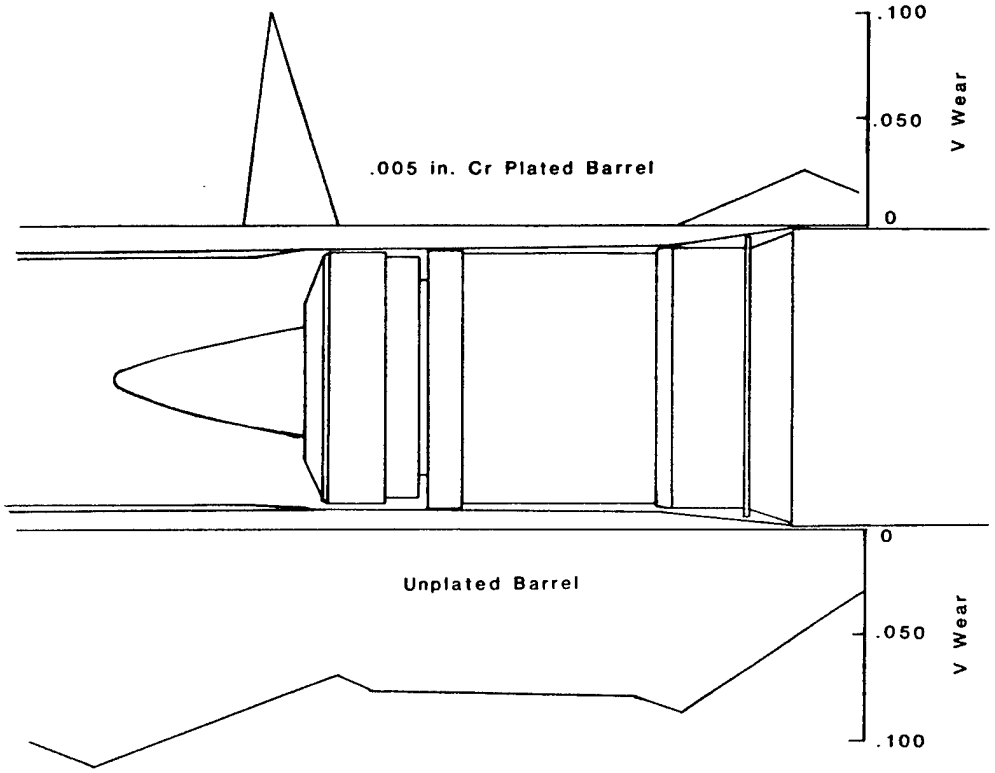

FIGURE 6 APDS ROUND IN CHAMBER L11

4. METHODS OF REDUCING WEAR

There are two types of method of reducing barrel wear; by increasing the bore surface melting points, its hot hardness or its resistance to chemical attack by the application of refractory coatings, or by reducing the amount of heat transferred usually by changing the characteristics of the boundary layer. In this section, the common methods of reducing wear are discussed briefly.

4.1 Coatings

Chromium, applied by electro-plating, has been used for many years. With a melting point of 1900°C, high hot hardness, and its chemically inert nature it would appear to be an ideal material. Unfortunately, it has a tendency to chip or flake away from the steel substrate. Wear then takes place at an enhanced rate in this region, probably due to increased turbulence in the boundary layer leading to increased mixing with core flow. This is because the amount of wear is comparable to the boundary layer thickness. It is noticeable that wear in a plated barrel seems to exhibit the melt-wipe process rather than the usual heat craze cracking observed in unplated barrels and this may be seen in figure (7).

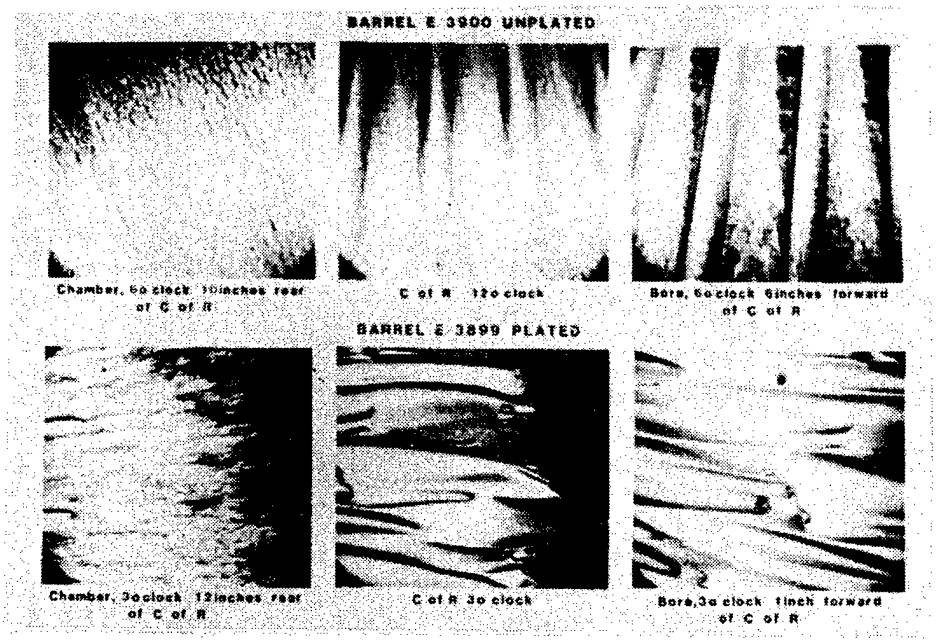

FIGURE 7 COMPARISON OF PLATED AND UNPLATED BARRELS

A problem, which is a consequence of this localised wear, is that the forces required to engrave the projectile increase, leading to a larger maximum chamber pressure. This may limit the increase in the number of rounds which can be fired.

In the absence of fatigue cracking, barrel life is determined by the amount of degradation in accuracy which can be tolerated and this is usually correlated with the observed wear near commencement of rifling. Data from LCWSL/ARRADCOM obtained for 155mm ordnance suggeests that chromium plate degrades accuracy. However, UK experience with the 120mm L11 tank gun firing APDS bagged charge ammunition shows no statistically significant difference in accuracy between the standard ordnance and 0.13mm (0.0005 inch) chromium plated barrels. Nor has the accuracy shown any statistically significant correlation with the amount of wear at the 25.4mm (1 inch) forward of commencement of rifling (CoR) position, provided that its effect on muzzle velocity is compensated for.

In general, chromium plating offers about a doubling in the wear life of barrels, which is useful but not sufficiently great as to make its adoption mandatory.

There has therefore been increased effort to develop alternative coating techniques and materials both in the UK and the US. By carefully controlling the plating bath temperature and rate of deposition a so-called "low contractile" chromium plate can be deposited. This is relatively free from micro-cracks and seems to offer improved resistance to flaking from the steel substrate. Longer term research involves barrel coating by tungsten, molybdenum or their alloys using chemical vapour deposition or the more promising plasma vapour deposition. The major problem with the former process is that the high temperature employed tends to degrade the mechanical properties of the substrate, whilst the problem with the latter process is the extremely slow coating rate. Tungsten and molybdenum offer much improved room temperature hardness and melting points even over chromium and would therefore appear to offer improved wear characteristics.

The thickness of the coating required is determined by its thermal diffusivity. It is assumed that it is necessary to have a sufficient thickness of coating so that the maximum temperature rise of the steel substrate is less than 725°C, the first of the solid state phase changes (see figure 1). The thickness required can be simply calculated by solving the 1-D heat conduction diffusion equation assuming that the heat is applied as a delta function to the boundary. This yields:

$$y = \sqrt{\frac{2}{\pi e}} \cdot \frac{H}{\rho C_v T_{max}} \qquad (8)$$

where,

H = total heat transfer

ρ = density

C_v = specific heat

T_{max} = maximum permissible temperature rise.

For chromium, the thickness required in a 120mm barrel firing CX propellant (the UK RDX based gun propellant) is 0.10mm (0.004 inch), but there is considerable uncertainty in the thermal diffusivity of chromium at elevated temperatures. Arbitrarily increasing the thickness much further probably results in flaking problems due to differences in the strain and the temperature coefficient of linear expansion with the steel.

It has also been proposed that one effect of introducing materials such as talc or "Swedish additive" is to build up a layer along the bore surface which exhibits a low thermal diffusivity. Calculations based upon estimates of the thermal diffusivity indicate that this could be significant in reducing heat transfer.

4.2 Boundary Layer Effects

In the early 1950s it was discovered by the Canadians that cartridge case liners made from polyurethane foam increased the barrel life by a factor of about four and this was attributed as being due to the injection of relatively cool gas from the liner into the boundary layer. It was found that the cellular nature of the foam was necessary to its efficacy which suggests that the effect is not solely due to the gaseous decomposition products.

By 1961 the so-called Swedish additive, comprising of a mixture of titanium dioxide and wax impregnated into a rayon cloth had appeared. Brosseau and Ward (Ref 10) have shown that these additives reduce heat transfer by up to 20% and increase barrel wear life by up to 25 times.

The UK practice since the late 1960s has been to employ combustible cartridge cases (CCC) impregnated with talc. Table 2 shows the effect of replacing a bag charge comprising of cotton by a CCC comprising of nitrocellulose, Kraft paper and a Latex binder only and indicates a $3\frac{1}{2}$ to 4 fold reduction. When talc is added at the 10-15% by weight level, a wear reduction of the order of 25 fold is experienced.

Experimental work has indicated that a mean particle size of talc of about 5 microns results in maximum wear reduction. The reasons for the reduction in heat transfer and wear are probably two fold. Firstly, there is a transient effect due to the thermal capacity of the particles. Secondly, the particles affect the boundary layer characteristics through slip between them and the gas flow and this provides a longer term effect. The interaction of the particles with the boundary layer is the subject of study by the University of Southampton using a 5 inch Shock Tube and is discussed in section 5.5.

A promising technique is the so-called silicone smear which was thought to work by sweat cooling. In its original concept, it was contained in a plastic cup within the charge. Unfortunately, if the silicone fluid escapes from its cup, the propellant is catastrophically degraded. An alternative form of packaging was developed by LCWSL/ARRADCOM by adding dimethyl silicate to produce a high viscosity "grease". Later a water impregnated gel based on the proprietary material "Super-Slurper" was utilised. In the UK, talc and silica were added to the silicone fluid to increase its viscosity. The reason why these materials work is probably through their effect on the initial gas leakage around the projectile and as a result their effectiveness is crucially dependent on their early release into the gas leakage path. Packaging is thus critical.

5. UK RESEARCH PROGRAMME ELEMENTS

The UK gun barrel wear research programme has tended to concentrate on the solid particle/gaseous boundary layer interaction and upon transient phenomena, particularly early in the ballistic cycle. In this section, the main elements of the programme and the results are presented.

5.1 RARDE

RARDE is responsible for co-ordinating all barrel wear research activities and undertakes research in 30mm and 120mm calibre guns.

A high speed cine photography trial was carried out on 120mm proof shot representing APDS and APFSDA (see figures 8 and 9) in which a retro-reflective material was fitted

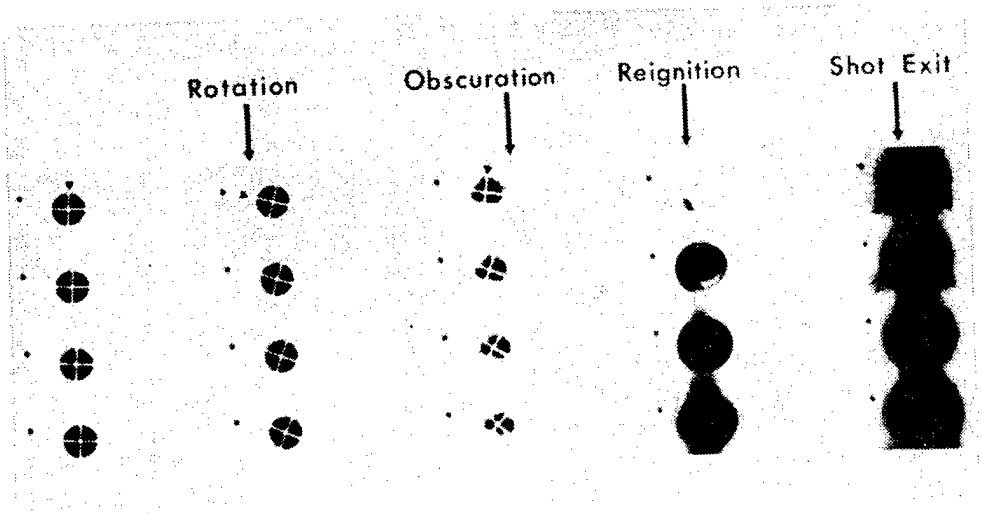

FIGURE 8 IN BORE PHOTOGRAPHY OF APDS SHOT

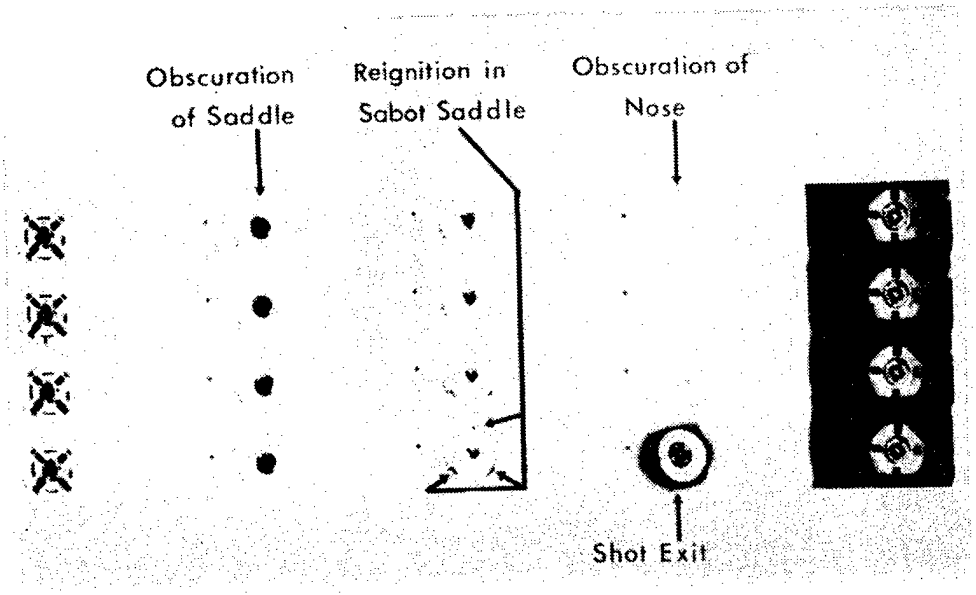

FIGURE 9 IN BORE PHOTOGRAPHY OF APFSDS SHOT

to the front face of ths hot, illuminated by a xenon arc lamp and the in-bore motion was recorded on a 20,000 flame per second camera via mirrors. The ammunition was separately loaded. There were clear indications that the projectiles experience considerable vibration at two times; at charge ignition and immediately before and during shot engraving. Early in the ballistic cycle, cool, non-luminous gas leaks past the projectiles prior to engraving and is pushed along with the shot. Later, this gas mixes with the air in the barrel and is compressed by the motion of the shot so that there is reignition in the bore. For the APDS projectile the magnitude and duration of this event is much greater than for the APFSDS projectile. Projectile motion was determined using microwave interferometry and related to cine events and the measured pressure time curve. This experiment has indicated the importance of gas leakage in the heat transfer process. It has led to the idea that when rammed separately, the projectile is not aligned with the barrel axis due to the chamber diameter being larger than the bore diameter and the forcing cone region. The cine film showed, in some cases, the projectile "pitching" into alignment during the engraving process. It has also been observed that the amount of oval wear depends upon the ramming technique employed. Tests to study the rammed position and orientation of shot using Linac X-Ray equipment are in hand. It is postulated that due to the pitch of the projectile in the vertical plane, gas leakage, heat transfer and hence wear tend to predominate in this plane. An experiment to measure heat transfer in the vertical and horizontal planes will be conducted when fast response thermocouples have been developed.

Bore surface thermocouples are being developed for 30mm and 120mm gun experiments using machineable glass ceramic technology and a junction formed by sputtering a thin layer of tungsten onto Pt/Pt Rh wires. They are designed for an operational pressure of 600MPa. Figure 10 shows how the surface harmonic temperature is attenuated by the depth of steel between the bore surface and the thermocouple. In order to record temperature fluctuations of 10kHz the thermocouple must be within 0.02mm (0.8 thou) of the bore surface.

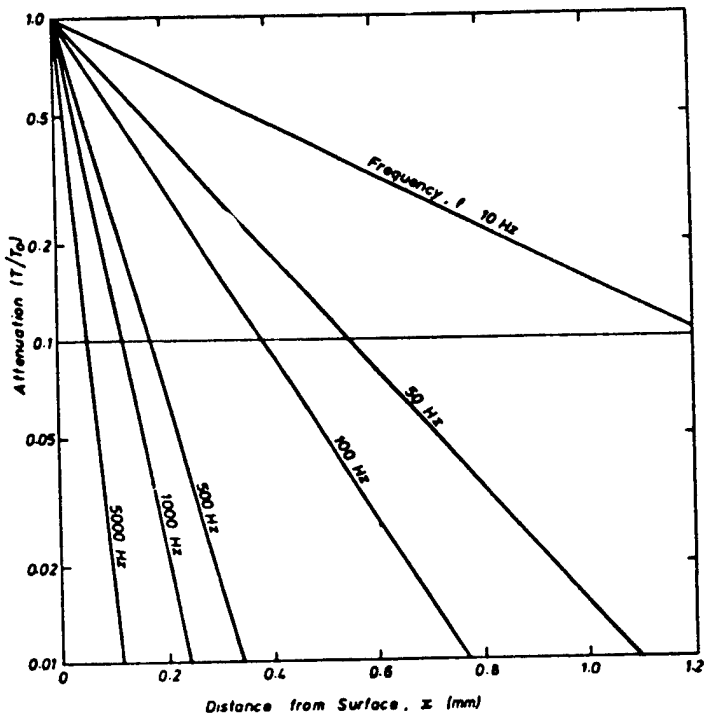

$$\frac{T}{T_0} = \exp\left(-x\sqrt{\pi f/K}\right) \; ; \; K = 8.9 \times 10^{-6}\ m^2/s \ \text{(Steel)}$$

FIGURE 10 ATTENUATION OF A SURFACE HARMONIC TEMPERATURE (T_O)

The radioisotope technique in which a region of the barrel or small probes are irradiated by a neutron beam to produce Co_{56} from Fe in the steel is being used to study wear in 30mm barrels and will be extended to 120mm barrels. It permits wear measurements with a resolution of better than 1 micron compared with conventional mechanical methods of about 25 microns.

This measurement technique has been employed to attempt to validate Thornhill's equation. Propellants, based upon the RDX/NG/NC formulation, having flame temperatures ranging from 3102K to 3574K were manufactured with various ballistic sizes to give the same muzzle velocity in the 30mm test gun. The compositions are given in Table (3).

FLAME TEMP °K	FORCE MJ/KG	PERCENTAGE			
		RDX	NG	NC	PICRITE
3102	1.174	44.2	18.5	18.5	8.4
3195	1.170	32.0	20.0	20.0	21.0
3299	1.172	21.8	25.8	25.8	20.7
3397	1.172	9.8	34.8	34.8	14.4
3574	1.181	-	46.3	46.3	-

TABLE 3 PROPELLANT MAIN CONSTITUENTS

Figure 11 shows the wear measurements obtained from the irradiated spot on the barrel (in a groove, 1 inch forward CoR) as a function of round number and propellant type. The wear per round was obtained by least squares fitting of a line through the data and the determination of its slope. The ammunition fired was of a fixed nature, and the charge weight was kept constant at 139 grams.

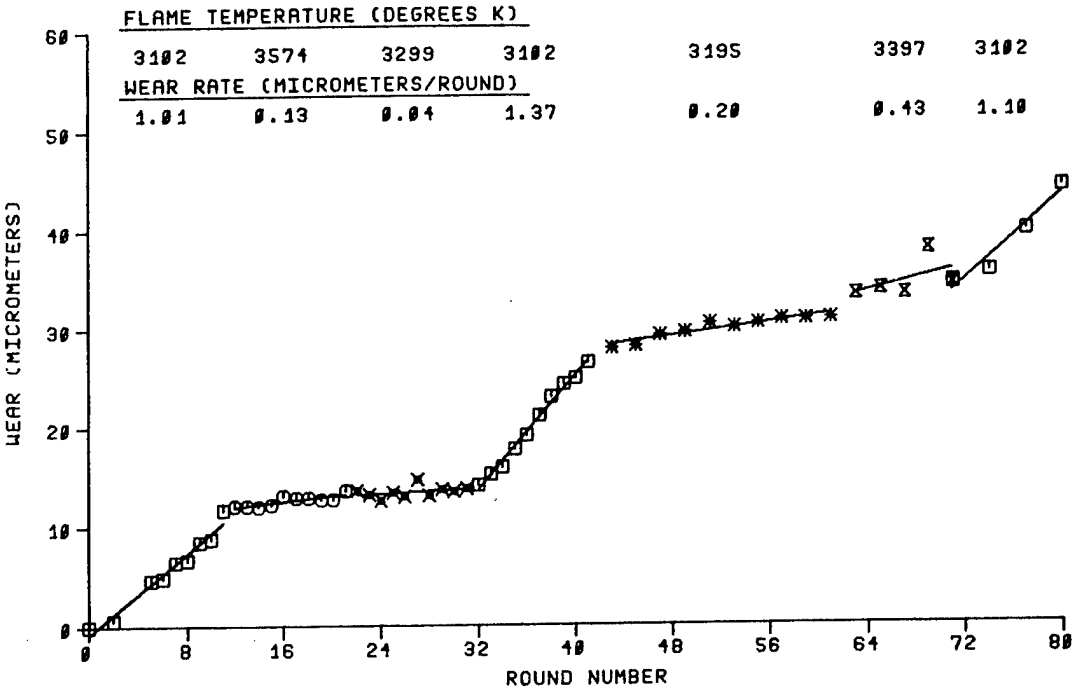

FIGURE 11 WEAR RATE OF 5 DIFFERENT FLAME TEMP PROPELLANTS

Table 4 is a summary of results and compares the observed wear with the Thornhill prediction. Clearly, although the prediction is of about the right magnitude for the low flame temperature propellant it is incorrect for the others. The approximate bore surface temperature rise in this experiment is calculated as 950C and the data from figure (5) has been reworked to obtain wear rates for the same value. These are plotted in figure (12) together with the experimental results and reveal an impressive consistency. It seems to appear that the rule of thumb that the hotter the flame temperature, the more severe the wear is incorrect, when the shot performance and bore surface temperature are kept constant.

Further work is in hand to study the effects of a wide range of combustible cartridge case formulations on heat transfer and wear rate using an experimental stub RARDEN ammunition.

FLAME TEMP °K	PMAX MPA	VELOCITY M/S	PREDICTED		WEAR/RND		
			TMAX °C	WEAR (THORNHILL)	BARREL (MICROMETERS)	PROBE	KNOOP
3182	429.4	1244.4	891	2.83	1.16	3.34	5.2
3195	358.3	1206.8	919	2.29	0.28	0.66	0.68
3299	381.5	1230.2	952	2.54	0.84	1.88	1.98
3397	401.9	1245.5	983	2.79	0.43	1.28	0.98
3574	346.8	1212.8	1037	3.85	0.13	1.48	2.98

TABLE 4 SUMMARY OF RESULTS

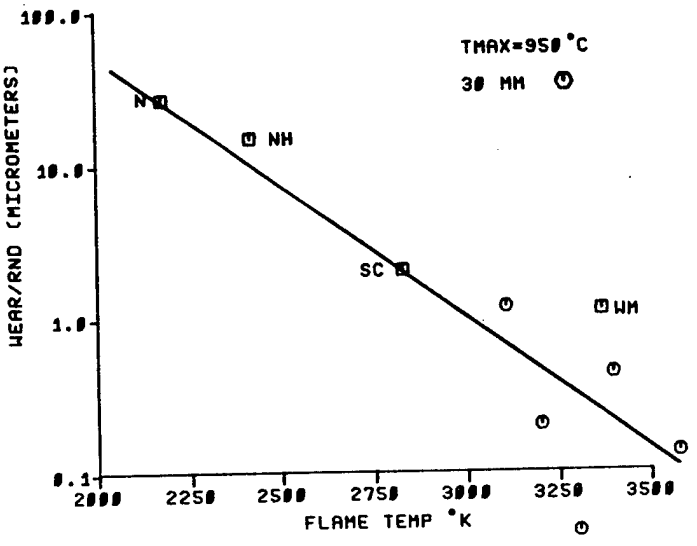

FIGURE 12 EFFECT OF PROPELLANT FLAME TEMPERATURE ON WEAR RATE

5.2 Royal Military College of Science

RMCS have been working under RARDE contract to measure the heat transfer in a 40mm reccoilless gun and a 0.5 inch General Purpose Machine Gun (Ref 2), using bore surface thermocouples of the ASEA type, having a maximum pressure limit of 60MPa and giving a high frequency response. Figure 13 shows a typical result from a 40mm RCL gun firing and it may be noted that some of the transient rises in temperature at 1 inch CoR contain frequencies of about 15kHz.

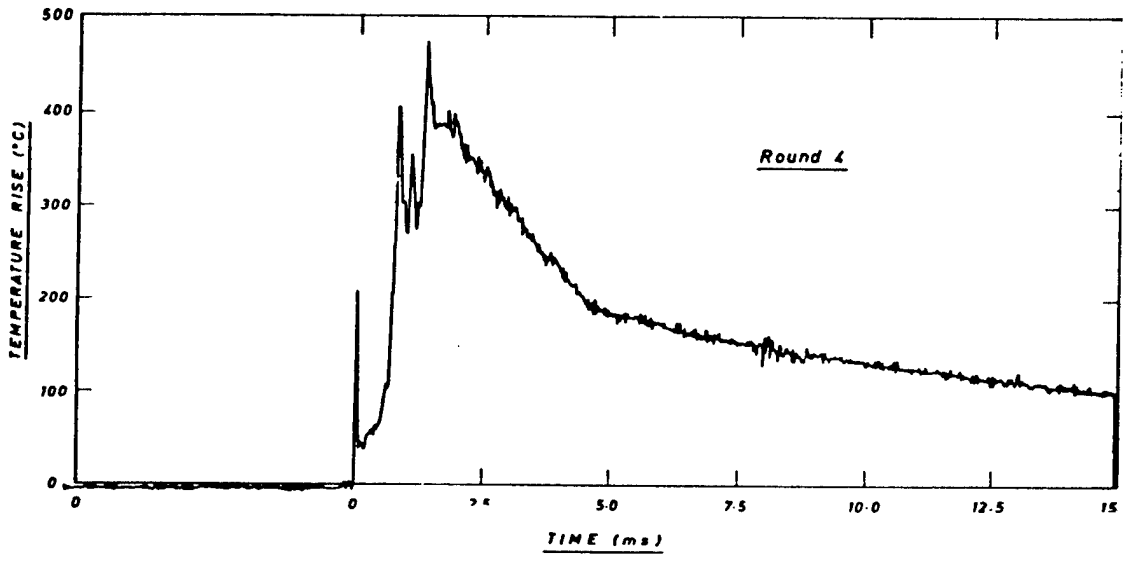

FIGURE 13 SURFACE TEMPERATURE RISE AT 1 inch C of R 40mm RCL GUN

This data can be converted into a heat flux, q, and by integration the total heat transfer, H, can be deduced. This may be seen in figure 14. Round by round variations are small in terms of the total heat transferred to the barrel wall after shot exit as may be observed in figure (15).

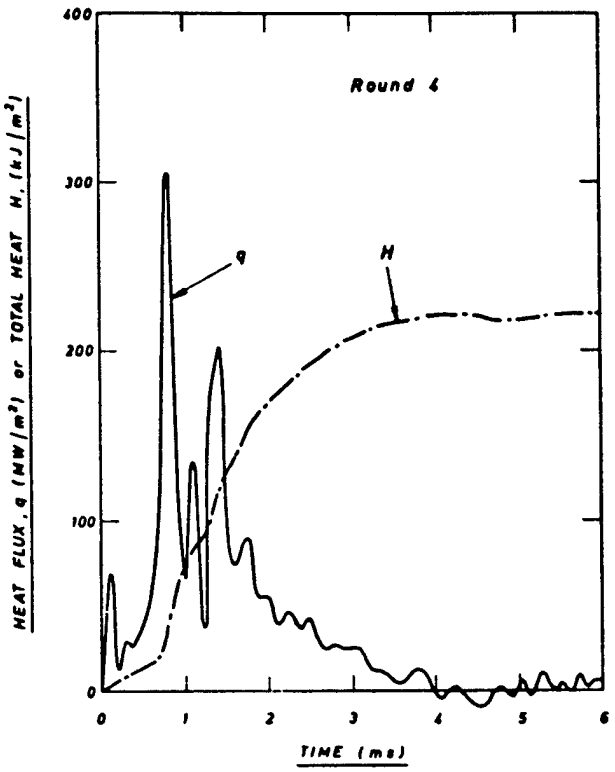

FIGURE 14 INSTANTANEOUS HEAT FLUX & TOTAL HEAT TRANSFER AT THE BORE OF A 40mm RCL GUN 1 inch C of R

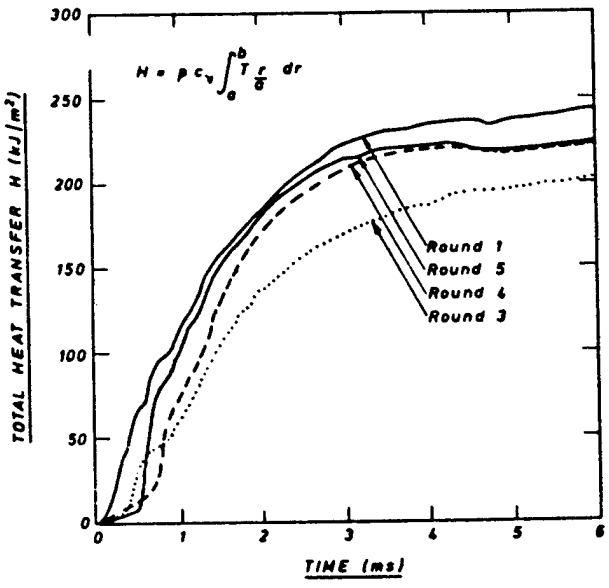

Mean Heat Transfer after 6ms = 224kJ/m^2
90% Rise Time = 2.5ms

Maximum Pressure at 1.5ms
Shot Ejection at 4.5ms

FIGURE 15 TOTAL HEAT TRANSFER AT 1 inch C of R 40mm RCL GUN SHOWING ROUND BY ROUND VARIATIONS

The projectile has three positions of interest (see figure 16), 1 is the commencement of the driving band, 2 the end of it and 3 the base of the shot.

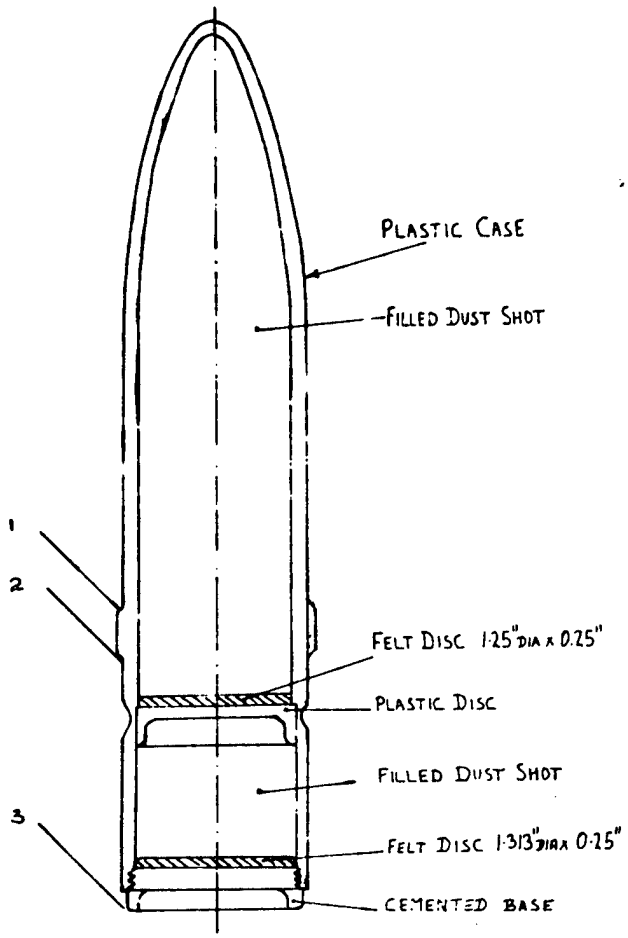

FIGURE 16 40mm Mk 10/1 BREAK UP SHOT

Figure 17 shows the bore surface temperature, total heat transfer and pressure time curve. The projectile motion is deduced, ignoring the effect of engraving forces, from the latter and the time at which the three positions of interest on the projectile pass the thermocouple measuring station are marked. It is postulated that the first large temperature excursion is due to gas leakage, whilst the second corresponds to frictional heating during engraving, and the convective heat transfer from pipe flow conditions occurs only relatively late in the ballistic cycle. Indeed, 60% of the total heat transfer in this case occurs before the projectile has "uncovered" the thermocouple.

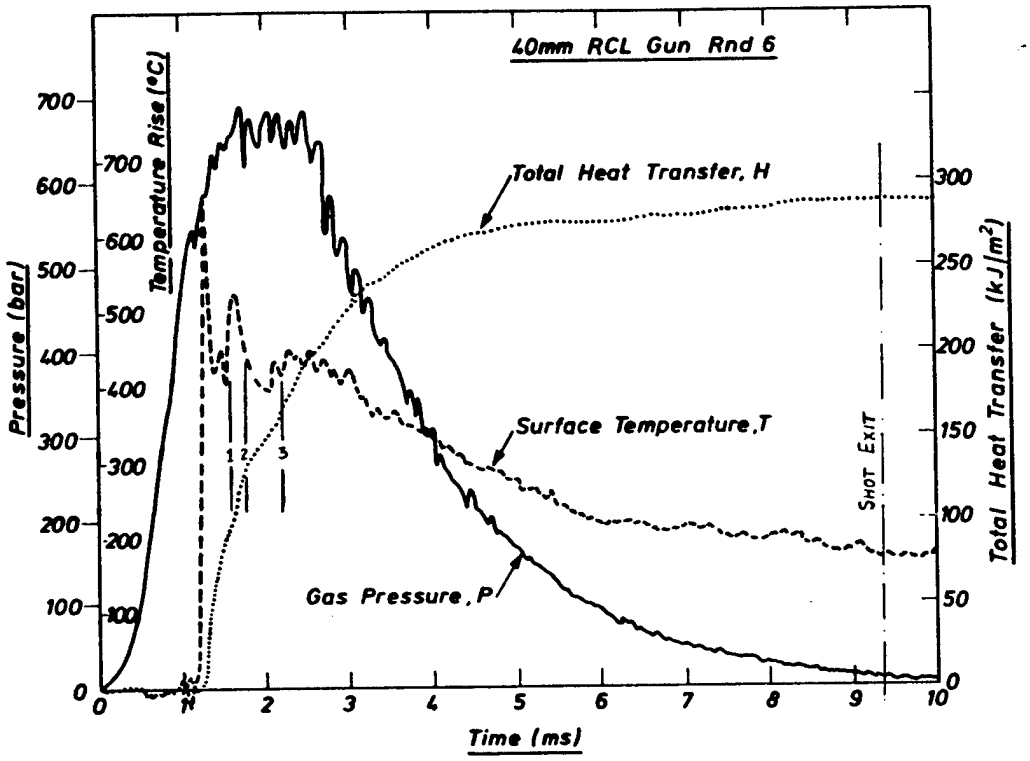

FIGURE 17

5.3 Concentration, Heat and Momentum Ltd

CHAM have been computing solutions to the Navier-Stokes equations using PHOENICS, a general three dimensional hydrodynamics and heat transfer code. A turbulence model based on the high Reynolds Number k-ε approach is used and wall shear stress and heat transfer are computed using a wall function method (1/7th power law). The boundary conditions corresponding to the 120mm gun firing APFSDS ammunition are used. Propellant gas, combustible case gas and talc are injected into the spatial mesh across an arbitrary inlet plane according to previously generated data obtained using a conventional "lumped parameter" internal ballistics code.

The code has also been applied to the conditions appertaining to the University of Southampton 5 inch shock tube. Good agreement was immediately obtained for the case of clean argon "driven" gas, but only when allowance was made for slip between the particles and the gas in the boundary and an appropriate source function governing the lift of particles from the shock tube wall was good agreement obtained for the dusty case.

Some initial results for the 120mm gun case are presented here for two instants in time, 2.5ms and 4.5ms after the start of projectile motion. Figures (18) and (19) show the isotemperature contours and talc distribution between the inlet plane and the simplified geometry of the rear end of the shot. The adiabatic flame tempera-

ture of the propellant was 3580K. It will be noted that local temperatures are in excess of this due to compression heating of propellant gas formed early in the ballistic cycle by that formed later. The talc, injected near the boundary layer, remains close to the bore wall, does not mix with the core flow and reduces the temperature at the edge of the boundary layer by 200C.

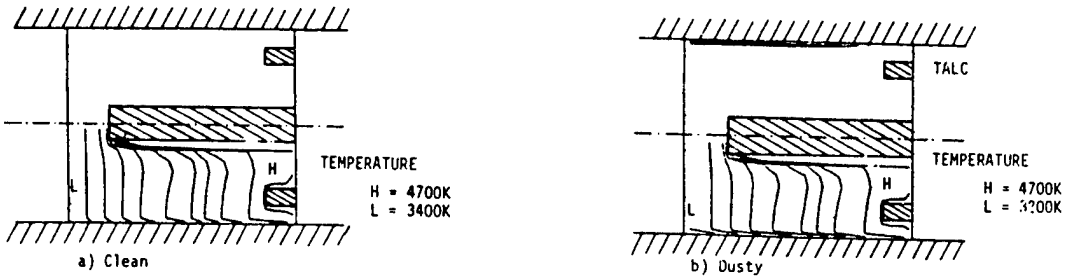

- INCREASE IN TEMPERATURE DUE TO EXPANSION
- LOWER TEMPERATURE NEAR WALL IN 'DUSTY' CASE.

FIGURE 18 2.5msec. CONTOURS OF TALC DISTRIBUTION AND TEMPERATURE

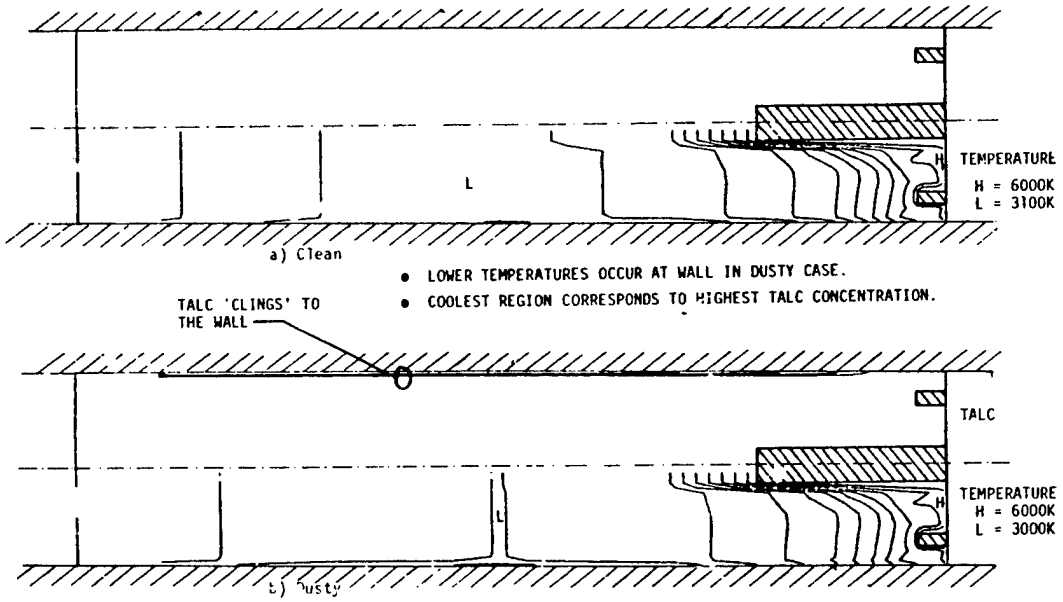

FIGURE 19 4.5msec. CONTOURS OF TALC DISTRIBUTION AND TEMPERATURE

Gas velocities and streamlines are shown in figures 20 and 21. Note the formation of eddy rotation at the base of the projectile, which coupled with the high temperature of the gas may cause localised regions of high heat transfer as the base of the projectile passes across, particularly when the velocity is low. Some experimental support for this may be deduced from figure 6 for the chrome plated barrel at the base of the shot.

This work is being extended to include the effect of gas leakage past the shot together with improved methods of handling particle motion and injection. The results so far indicate that particle size is not too important and that the greater the amount injected, the larger the heat transfer reduction.

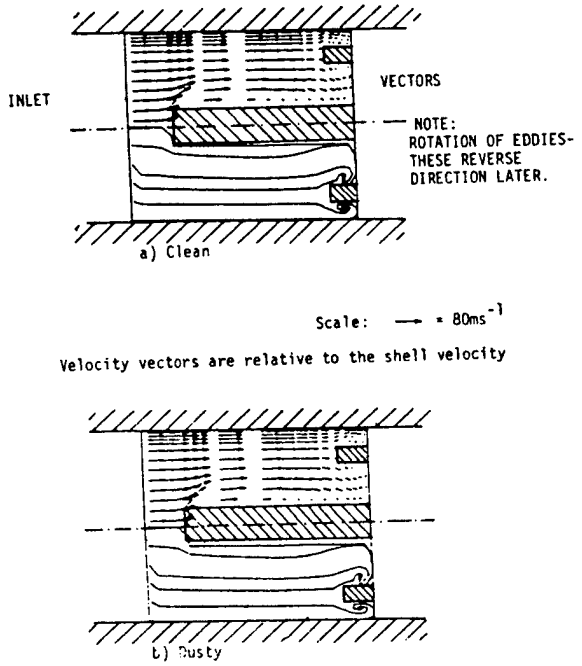

FIGURE 20 2.5msec. VECTORS AND STREAMLINES. VELOCITIES RELATIVE TO PROJECTILE

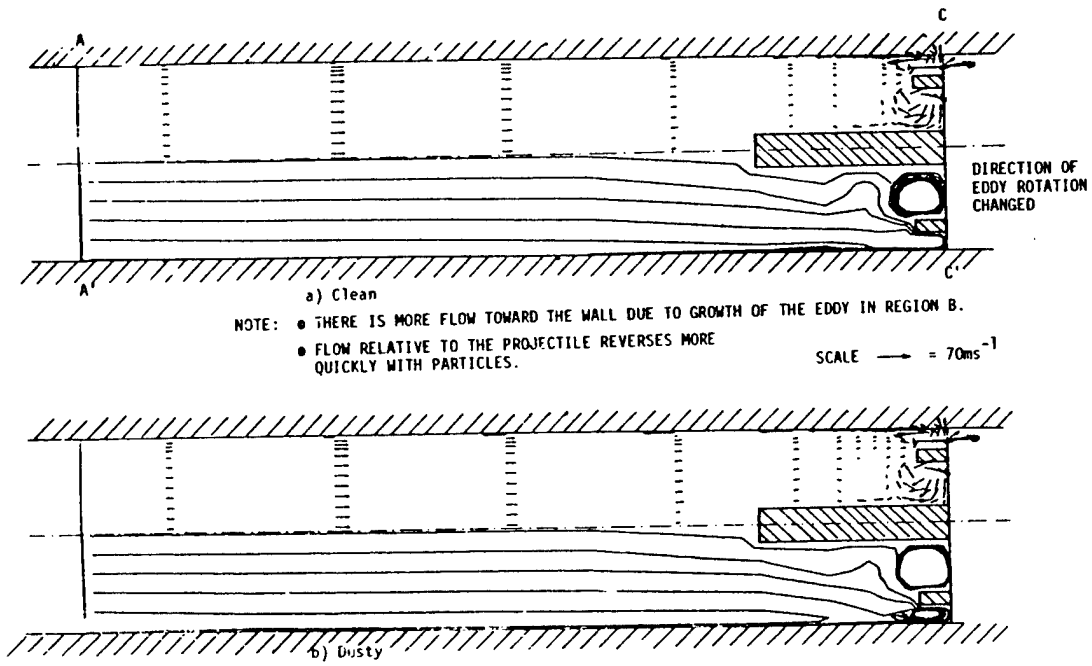

FIGURE 21 4.5msecs. VECTORS AND STREAMLINES. VELOCITIES RELATIVE TO PROJECTILE

5.4 Combustion and Particle Flow Research Ltd

Because it was thought that the effect of the particles on heat transfer was through its action on the turbulent intensity [eg see Saffman (Ref 11)] it was thought desirable to set up an experiment to measure the turbulent KE in the boundary layer using the laser Doppler anemometry technique. This work is being undertaken in several gun test fixtures including a 30mm RARDEN barrel using a modified Diehl LDA interferometer and a 4 watt argon laser at a newly developed test site 25 miles south of Manchester, England. Progress has been delayed due to the inadequate performance of the LDA system, vibration effects on the Doppler signal and the need to refine further the sapphire window in the gun. However, experimental results will shortly become available.

5.5 University of Southampton

Measurements of heat transfer during and after the passage of a shock wave across a Pt thin film gauge mounted initially in the side wall, but later in a flat plate insert in the centre of a shock tube have been carried out in the presence and absence of a uniform dust layer of talc, and other additives (Ref 8). An attempt has also been made to measure the dust loading in the boundary layer by means of an extinction experiment using a He-Ne laser. The schematic layout of the experiment is shown in figure (22).

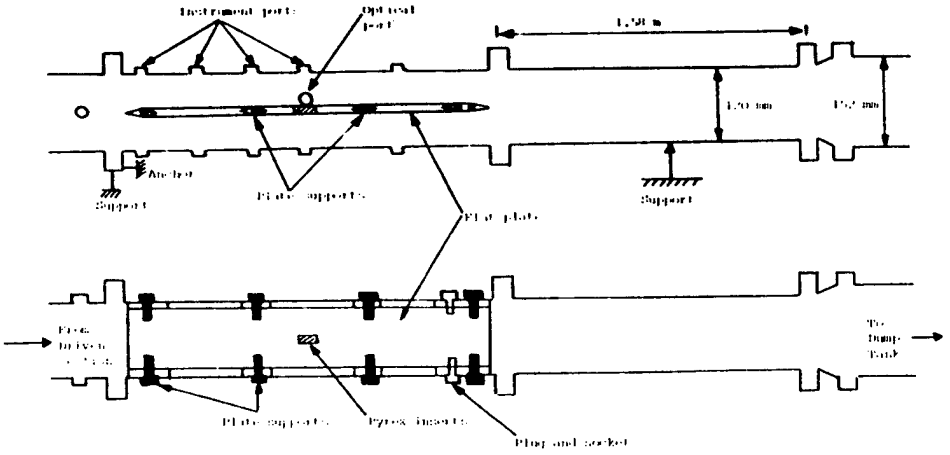

FIGURE 22 GENERAL ARRANGEMENT OF THE FLAT PLATE WORKING SECTION

Results to date have shown that there are no major differences in the reduction of heat transfer for dusts composed of talc (mean size 4.5 micron), aluminium hydroxide FRF 40 (4.5 microns), zinc borate (0.67 microns) and copper II ethylene diamine tetra-acetate (7.4 microns). The dust has a very very large effect on the heat transfer as may be seen in figure 23, increasing as the mass loading is increased,

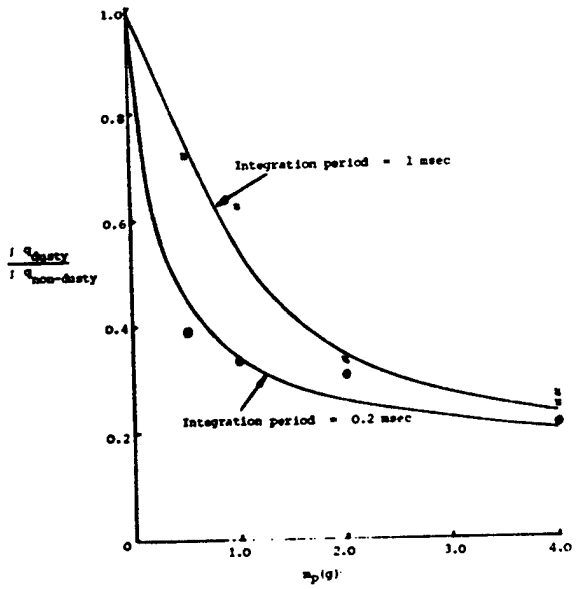

FIGURE 23 HEAT TRANSFER REDUCTION VS. MASS OF PARTICLES

so that the value of the heat transfer is reduced to as little as 20% of that observed in the clean gas case. The transition from the laminar to the turbulent boundary layer is delayed in the dusty case. When dust is placed over the heat transfer gauge then the response time is increased significantly confirming the effect that the thermal diffusivity of the particles on the bore surface can be important under certain circumstances. A comparison of the observed heat transfer for clean and dusty cases may be seen in figure 24, showing that the major reduction is during the formation of the turbulent boundary layer, and that dust induces high frequency variations in heat transfer (~20kHz) which are not observed in clean conditions. This effect has not yet been satisfactorily explained.

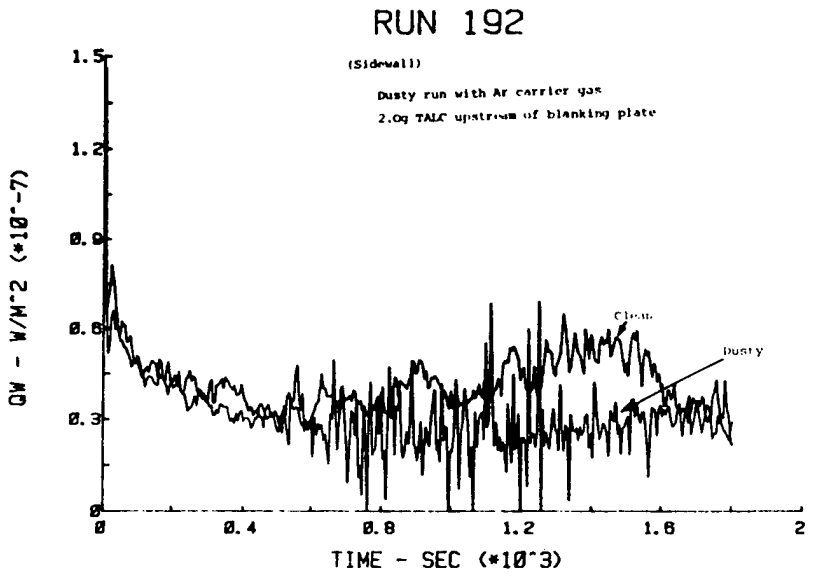

FIGURE 24 HEAT TRANSFER HISTORY - RUN 192

The work has recently been extended to include a "driven" gas mixture roughly corresponding to propellant gas as a replacement for argon. The effect of the dust is even greater in this case (up to 90% reduction in heat transfer) and some effects due to gas chemical kinetics are being observed.

In the next few months a rifled section of 120mm barrel will be inserted into the shock tube with side wall mounted gauges to determine the effect of the rifling. This should be significant since it is of a comparable dimension to the boundary layer thickness.

6. CONCLUSIONS

Other heat transfer mechanisms, in addition to that of convection from the propellant gas, are important in determining barrel wear. these are likely to be gas leakage past the shot early in the ballistic cycle, frictional heating, eddy rotation of propellant gas at the base of the shot.

Gas leakage past the shot may be responsible for oval barrel wear in separated ammunition. It may be controlled by the appropriate design of driving band and by the silicon smear technique provided it is in the region of the shot base at the beginning of the ballistic cycle. Chromium plating or other coatings in this region would be beneficial in reducing wear.

The nature of dust additives such as talc, molybdenum trioxide, titanium dioxide etc does not seem to be important. They seem to work primarily by their effect on the turbulent boundary layer producing reductions in heat transfer of up to 80%. More additive produces more heat transfer reduction.

The above techniques appear to be extremely promising in controlling heat transfer in still higher performance guns than available at present.

REFERENCES

1.	C K Thornhill	An Analysis of Gun Erosion ARD Report 38/47
2.	B Lawton	Heat Transfer and Wear in Gun Barrels, 2nd Year Report RMCS Tech Note TN/108
3.	I Finnie, A Levy and D H McFadden	Fundamental Mechanisms of Erosive Wear or Ductile Metals by Solid Particles, ASTM, STP 664, pp 36-58, 1979
4.	J R Ward and T L Brosseau	Role of the Insulating Layer from TiO_2-wax Liner in Reducing Gun Tube Wear, JANNAF Propulsion Meeting, Minterey, CA, 1980
5.	O K Heiney, R J West and W H Stone	Gun Propellant Heat Transfer and Barrel Temperature Measurement. Proceedings of Tri-Service Gun Tube Wear and Erosion Symposium, March 1977
6.	S Shelton, A Bergles and P Saha	Study of Heat Transfer and Erosion in Gun Barrels, AFATL-TR-78-69, dated March 1973, AD 912519
7.	J C Ludwig and N Rhodes	Gun Barrel Erosion Studies, CHAM Ltd Rpt No 2440/2, presented at ARO "Hot Gas Erosion Conference", LLL April 1981
8.	G T Roberts, R A East and N H Pratt	Heat Transfer in Two Phase Flow, University of Southampton, ASSU Memo 80/6, ibid
9.	J D Squire	Characterisation of the Bore Surface in Large Gun Barrels. Martin Marietta report
10.	J R Ward and T L Brosseau	Reduction of Heat Transfer to High Velocity Gun Barrels by Wear Reducing Additives. Trans ASMR, Aug 1977
11.	P G Saffman	On the Stability of Laminar Flow of a Dusty Gas, J Fluid Mechanics, Vol 13, 1962, pp 120-123.

SESSION IV

COATINGS

CHAIRMAN: Dr. Iqbal Ahmad

The Tri-Services Symposium, "Gun Tube Wear and Erosion" GAU-8/A Barrel Life Improvement Program

Authors:

David Perrin, Advance Design Engineer
General Electric Company
Burlington, Vermont 05402
Tel: 802-657-7102

Steven Duke, Advance Design Engineer
General Electric Company
Burlington, Vermont 05402
Tel: 802-657-7123

Abstract

The 30-mm GAU-8/A gun system is the first operational medium caliber gun designed to fire only ammunition with plastic rotating bands. The GAU-8/A Barrel Life Improvement Program was directed toward improving barrel life for projectiles with plastic rotating bands and optimizing performance of all types of current GAU-8/A ammunition. This project included building and testing 63 barrels and firing 165,000 rounds of GAU-8/A ammunition including target practice (TP), high explosive incendiary (HEI) and armor piercing incendiary (API). Sets of seven barrels were produced consisting of six special barrels and a standard barrel for a base line. Thus all barrels in a set were subject to the same duty cycle, enabling direct comparisons of ammunition performance and barrel condition resulting from the various barrel designs.

Introduction

The program was structured to evaluate low cost modifications to the GAU-8/A barrels with promise of increasing barrel life and to evaluate modifications which would minimize projectile body engraving and windscreen losses in hot gun barrels. After preliminary screening iterations, consisting of building and testing various barrel designs, optimized barrels were designed and qualified.

Two types of tests were used during this program:

1. Single-shot heated barrel tests were used to simulate the rounds fired toward the end of long bursts (Figure 1).
2. Burst fire tests were used to determine barrel life and evaluate ammunition performance throughout the life of the barrels. (Figure 2).

This program used extensive instrumentation to insure that a realistic assessment of barrel condition and ammunition performance was obtained. Table 1 shows instrumentation used during tests.

For the purposes of this study, a barrel was considered to be worn out when:

1. Projectile spin was inadequate to ensure gyroscopic stability (Table 2).
2. Safe fatigue life was exceeded.

The GAU-8/A barrel also has a 10% muzzle velocity drop limit, however, in actual usage projectiles exhibit very little velocity drop at the muzzle prior to the barrel reaching one of the above two limits. Constant velocity throughout the life of the barrel is probably the most important benefit of plastic rotating bands in the GAU-8/A gun.

The program also compared performance of ammunition fired from hot thermally expanded barrels with ammunition fired from barrels at ambient temperature with oversized bores. The purpose was to determine if oversize barrels could be beneficially applied to check ammunition performance under realistic operational conditions.

Improved Barrels:

Bore Coating and Material Changes to Reduce Erosion

Long life is achieved with GAU-8/A barrels firing ammunition with plastic rotating bands because of much longer chrome plate retention than with copper bands. Once the chrome plate is lost erosion progresses relatively quickly. Since the plastic bands can tolerate relatively little erosion and still meet projectile spin requirements, chrome plate retention is essential. Testing has shown that chrome retention is very sensitive to firing schedule as shown in Figure 3. This probably explains why plastic bands have not performed very well in some large caliber weapons where single shot heat inputs are very high. This program was oriented toward low cost modifications which would improve barrel life. Several bore coatings were tested in an attempt to find coatings more resistant to erosion than the standard 4 mil HC chrome plate. Modifications tested and life test results are summarized in Table 3. More details on coating performance are contained in a paper on that topic by Messrs Duke, Perrin, and Blair.(1) Thick HC chrome or a duplex coating of a thin layer of LC chrome covered by a thick layer of HC chrome gave the best results.

Design Changes to Reduce Body Engraving

One of the most interesting phenomenon about which relatively little information has been presented in barrel conferences is projectile down barrel yawing (balloting) which can result in body engraving of the projectile (Figure 4). Figure 5 shows the effect of thermal expansion of the muzzle on clearance between the projectile and the barrel when firing a long continuous burst. Plastic rotating bands tend to increase yaw because the plastic does not center the aft end of the projectile as well as copper or iron. After exit from the barrel, the projectiles may yaw severely. Figure 6 shows clearance between the barrel and the projectile including body engraving versus first maximum yaw. If the projectiles are fully spun, they are stable and the yaw damps out. An example of damping is shown in Figure 7. Figure 8 shows an example of the effect of yaw of a fully spun round on target velocity. The current GAU-8/A barrels are constant twist. Gain twist was not used initially because it was not known where erosion would occur first and it was felt to be very important to reduce torque down barrel where rapid wearing of the plastic rotating band was expected because of high velocities and hot rotating bands. Gain twist was evaluated in this improved barrel for a unique reason; to minimize body engraving of projectiles. Gain twist was used as a means of changing the contact point between a tipped (balloted) projectile and the rifling and thus reducing engraving of the projectile body. Barrels with five different gain twist designs were produced and tested. The torque versus travel curves for these barrels are shown in Figure 9.

This study showed that conventional gain twist barrels starting with straight rifling were not satisfactory because as a result of band wear out, they did not always fully spin projectiles even when the barrels were new. Adding lands helped, however, projectile body engraving was found to increase as the number of lands was increased (due to reduced width of the top of the land). The best combinations tested had an initial constant twist ranging from 5.4° to 7° with a gain twist after peak chamber pressure was reached. Exit angle in all cases was 9.9° which is required for API projectile stability. The maximum projectile yaw of API rounds fired from hot gain twist barrels was about 50% less than rounds fired from constant twist barrels (Table 4). Improvement in HEI rounds was less, however, target velocity of API rounds is the prime concern in the A-10 aircraft due to the fact that armor penetration capability is significantly affected by target velocity. Current TP's have no body engraving problem due to their favorable mass properties.

Design Verification Tests

The improved barrels incorporating gain twist and thick chrome were evaluated by testing conducted at Eglin AFB. Tests were conducted firing the Tactical Air Command (TAC) combat firing schedule shown in Table 5. Tests were conducted with sets of seven barrels including one standard barrel, 3 improved barrels with 20 lands, and 3 improved barrels with 22 lands. Primary testing was conducted firing combat ammunition on one set, and firing target practice ammunition on another set. Firing history and estimated life are shown in Table 6. Firing the TAC schedule, the barrel life was increased from the range of 12,000 to 15,000 gun rounds to a range of 20,000 to 25,000 gun rounds. Training life with both current and improved barrels will typically be limited to 36,000 gun rounds by fatigue; however, if long bursts are fired during training the 36,000 limit will not be reached by either barrel but the improved barrel will have a longer life. Dispersion of the current barrel firing API ammunition was about twice as large as with improved barrels due to projectile body engraving. Less, but significant, improvement was made in HEI ammunition. All TP rounds had low dispersion because they do not body engrave. Figure 10, 11 and 12 show an example of dispersion of individual barrels firing API, HEI, and TP ammunition.

After completion of life testing at Eglin, the barrels were returned to GE for single shot evaluation. Single shot tests were run with ammunition conditioned at temperatures between -65° and 160°F and with barrel temperatures up to 1000°F. The HEI round was found to limit barrel life. HEI rounds failed to reach their 67% spin required for stability prior to the time that the API round fails to reach its 91% stability criteria. Figure 13, 14, and 15 show spin rates obtained during these tests. It is interesting to note that in barrels with relatively slight erosion, the failures to fully spin occurred first in hot barrels; however, after significant erosion occurred, there was little difference in spin rates with hot versus cold gun barrels.

Selected Design of Improved Barrels

The design changes made in the improved barrel are shown in Table 7. The new barrel design includes changes which have little effect on production costs but improve life and performance very significantly when firing severe schedules. Primary among the changes are thicker chrome and gain twist rifling.

Oversize Barrel Evaluation:

Oversize barrels were also tested in this program to determine if an oversized barrel at ambient temperature could be used to simulate a hot thermally expanded barrel. The results were very favorable showing that:

- .01'' oversized bore simulates a new hot barrel including:
  - Projectile body engraving with resulting yaw
  - Increased rotating band losses
- .014'' oversize bore simulates a very hot barrel or a worn barrel including:
  - Reduced spin
  - Windscreen losses (Figure 16)

These results indicate that it would be practical to adopt oversized barrel tests as a standard method of showing ammunition compatibility with thermally expanded barrels. Tests with oversized barrels should be conducted during ammunition development and lot acceptance tests. This is a simple alternative to adequately instrumented burst fire tests.

Summary

1. Optimized GAU-8 barrels with .009'' ± .002'' thick HC chrome, a 6° to 9.9° gain twist rifling and 22 lands significantly improve GAU-8/A weapon effectiveness.
2. Oversized barrels should be used during ammunition development and acceptance tests for all ammunition which will be used in weapons with barrels which experience significant thermal growth.

Bibliography

1. "GAU-8/A Barrel Life Improvement—Microflash Photography and Post Test Metallographic Results", Paper presented at Tri-Service Symposium on Gun Tube Wear and Erosion, 25-28 October 1982, by S. Duke, D. Perrin and M. Blair.

Table 1
Instrumentation Used During Tests

Instrumentation	Purpose	Single Shot	Burst Fire	
			GE	Eglin
Photographs of each projectile 26 and 27 ft. from muzzle	• Spin Rate • Projectile Yaw • Rotating Band Condition • Wind Screen Condition	X	X	
High Speed movie of projectile in flight	• Projectile Flight • Rotating Band Loss			X
Velocity	Check for Velocity loss (caused by drag of yawed projectile)	X	X	X
X-Y Projectile Position (Electronic Target)	Dispersion and mean point of impact		X	X
Paper Targets	Maximum Yaw of Fully Spun Rounds	X		
Moving Targets	Projectile Yaw and Windscreen Loss			X
Projectile Recovery in sawdust	Evaluate Body Engraving	X		
Barrel Temperature	Bore Expansion	X	X	

Table 2
Barrel Life Criteria

1. Adequate spin to insure gyroscopic stability

Ammunition	Spin Required to Ensure Stability % of Full Spin	
	70°F, Still Air	-65°F, 350 Knots
Aerojet HEI	49%	66%
Honeywell HEI	49%	66%
Aerojet API	67%	91%
Honeywell API	65%	88%
Aerojet TP	37%	49%
Honeywell TP	42%	56%

2. Safe fatigue life (36,000 Gun Rounds)

3. Projectile muzzle velocity drop of 10%
(10% drop was never approached, 1% is typical)

Table 3

Designs Evaluated in Barrel Sets "A" and "B"

Design Modifications	Gun Rounds Fired	Erosion
Standard Barrel*	17,800	Moderate
5.4 to 9.9° Gain Twist	17,800	Moderate
24 Lands	17,800	Worst
Gas Nitride Prior to Chrome Plate	17,800	Moderate
.007" Cr	17,800	Best
Modified Initiation of Rifling	17,800	Moderate
Extra Material Where Down Barrel Erosion Occurs	17,800	Moderate
Inconel 903 Barrel Material w/o Cr Plate	3,178	Very Severe
Standard*	20,600	Worst
.01" Cr	20,600	Best
.007" Cr; 12.5° Forcing Cone	20,600	Best
.007" Cr; Band Stripper at Muzzle	20,600	Best
.007" Cr; 22 Lands	20,600	Best
.007" Cr; 24 Lands	20,600	Worst
.007" Cr; 28 Lands	20,600	Moderate

Designs Evaluated in Barrel Sets "C" and "D"

Standard Barrel*	18,800
.01" HC Cr; 9.5° Constant Twist	26,600
.002" LC Cr + .005" HC Cr	23,200
Shot Peened and Increased Groove Radius	18,800
.004" LC Cr	16,600
.007" LC Cr	16,600
Wide Lands	18,800
Standard Barrel*	14,700
.007" HC Cr; NO 1.192 Bore Diameter	26,000
.007" HC Cr; 7 to 9.9° Gain Twist	26,000
.007" HC Cr; 7 to 9.9° Gain Twist 24 Lands	26,000
.007" HC Cr; 5.4 to 9.9° Gain Twist 22 Lands	26,000
.007" HC Cr; 5.4 to 9.9° Gain Twist 24 Lands	21,300
0 to 9.9° Gain Twist: 24 Lands; Saw Tooth Rifling	9,600 **

*Standard Barrel Has

20 Lands
.004" Minimum HC Chrome on Lands
9.9° Constant Twist Rifling
1.192" Bore Diameter at Initiation of Rifling

**Severe Chrome Loss. Plating History is Unknown

Table 4

Tactical Air Command (TAC) Firing Schedule

Burst Length (Gun Rounds)	Cooling Time (Seconds)	
	In-Flight	Ground Simulation
150	45	90
150	45	90
150	45	90
150	180	480
150	45	90
150	45	90
150	Long Cool	Long Cool

Table 5

Design Verification Tests of Improved Barrels

	Gun Rounds Fired	Estimated Life* (Gun Rounds)
Set 1		
Fired with Combat Ammo		
Current Barrel	23,368	12,000 to 15,000
Improved Barrel with 20 Lands	34,753	18,000 to 23,000
Improved Barrel with 22 Lands	34,753	20,000 to 25,000
Set 2		
Fired with TP Ammo		
Current Barrel	24,200	12,000 to 15,000
Improved Barrel with 20 Lands	35,512	18,000 to 23,000
Improved Barrel with 22 Lands	35,512	20,000 to 25,000

* Estimated life is based on 67% projectile spin required to stabilize HEI rounds fired from a 350 knot aircraft with a -65°F Ambient Temperature.

Table 6
Comparison of Optimized Barrel Design with Standard Design

Feature	Standard Barrel Dwg. No.	Optimized Barrel Dwg. No. 211F954	Benefit Of Change
Number of Lands	20	22	Full spin with greater erosion
Chrome Thickness on Lands	.004" Minimum	.009" ± .002"	Longer chrome plate retention and less land swaging
Rifling	9.9° Constant Twist	6 to 9.9° Gain Twist	Reduced body engraving of API projectiles
Relief for Projectile	1.192 ± .002	1.186 ± .001	Reduced blowby and lower potential for windscreen losses in a hot, worn barrel.
Chrome Plating	Per QQ-C-320	Per Spec A10357	Improve control of chrome plate process

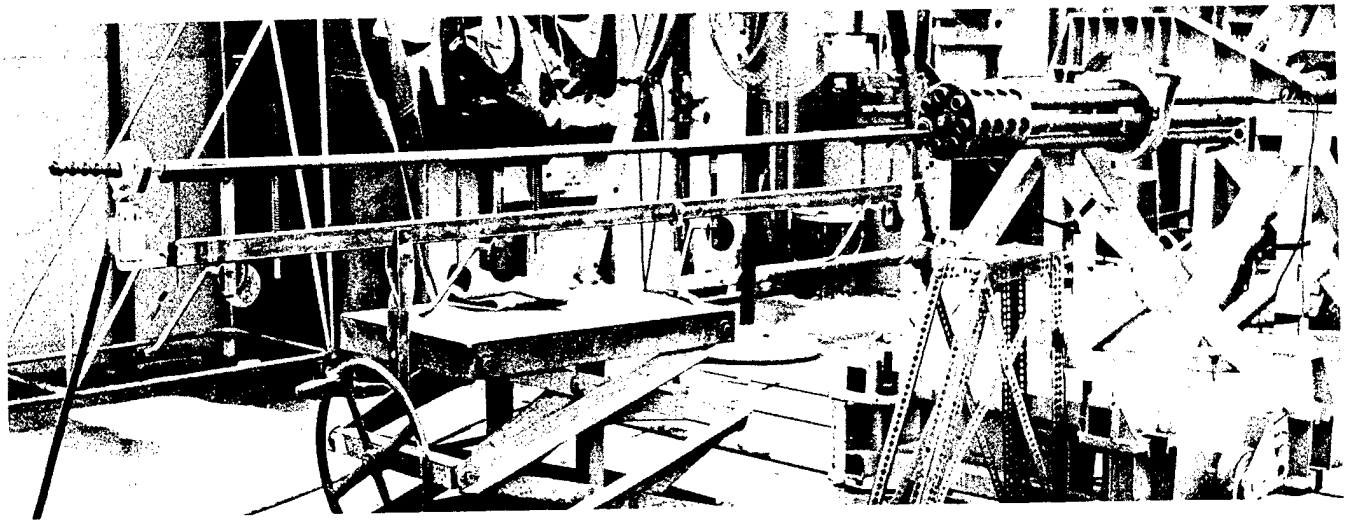

Figure 1. Test Set-up for Single Shot Heated Barrel Test. Simulates a Hot, Thermally Expanded Barrel.

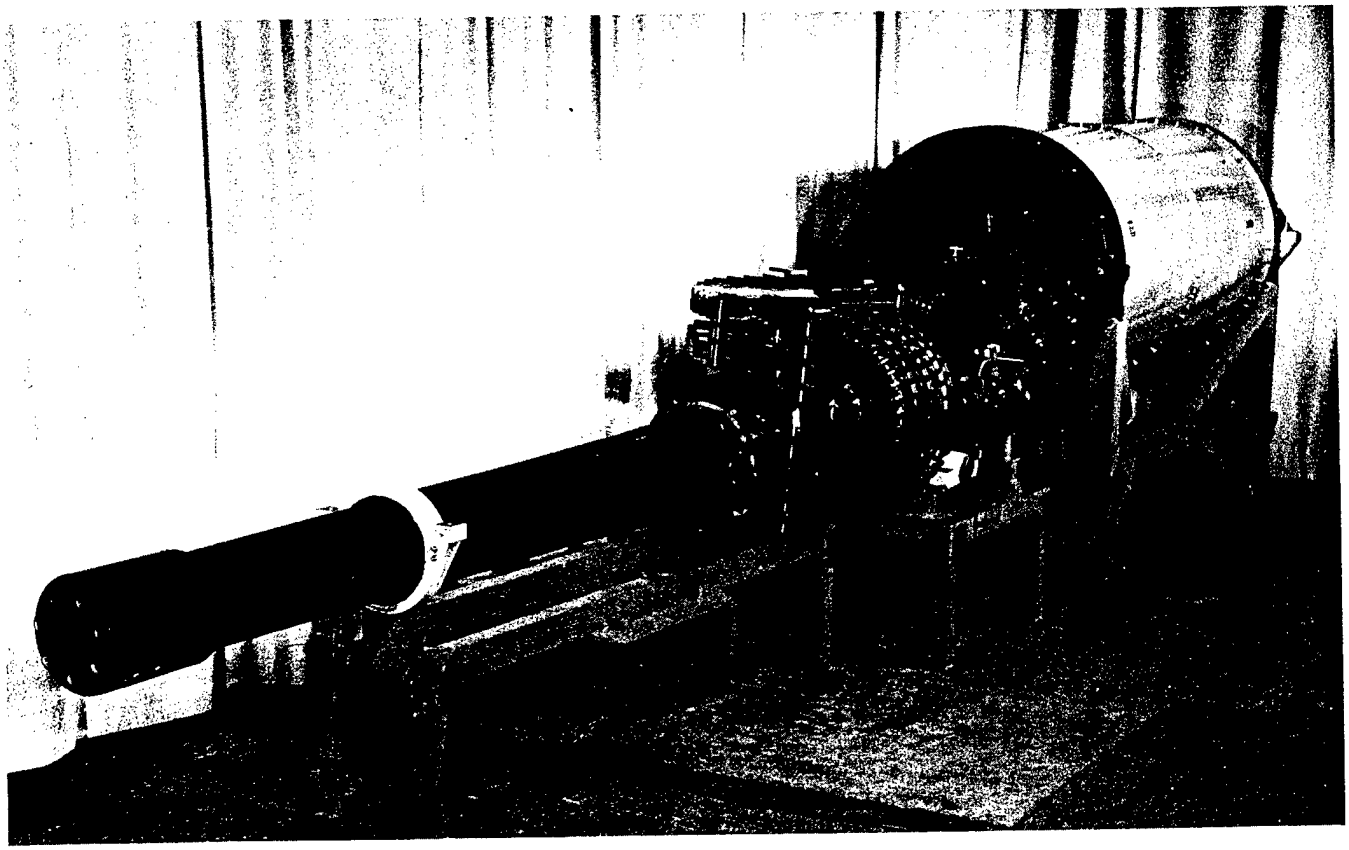

Figure 2. Burst Fire Testing Used to Determine Barrel Life.

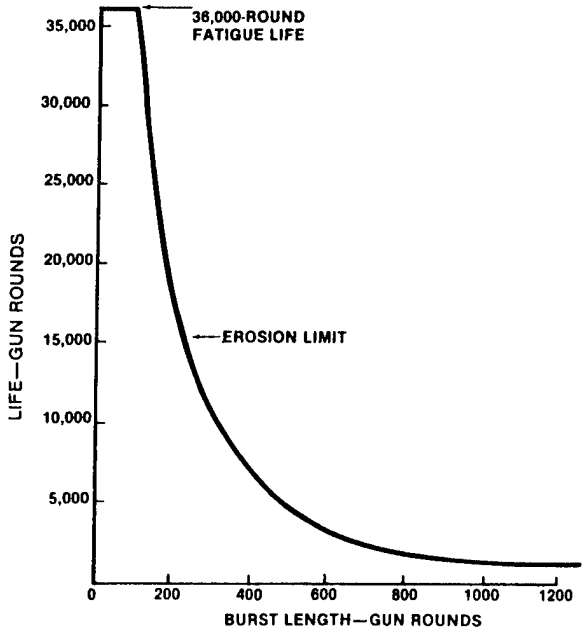

Figure 3. Effect of Burst Length on Life of GAU-8/A Barrels.

Figure 4. Severe Projectile Yaw Caused by Body Engraving. 25 Feet from Muzzle, -65°F Ammunition, 1000°F Barrel

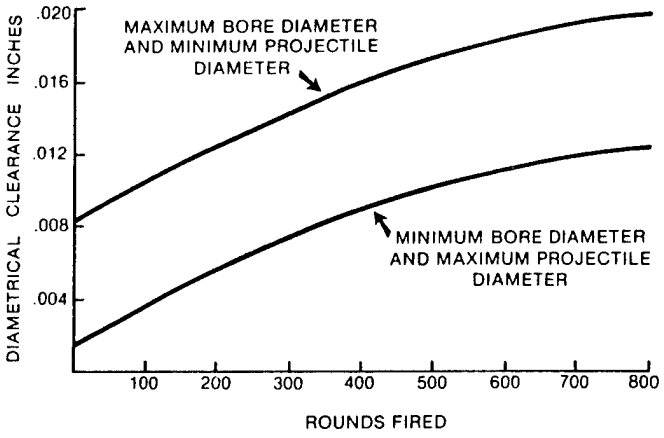

Figure 5. Clearance Between Projectile and Bore Vs. Rounds Fired in a Continuous Burst.

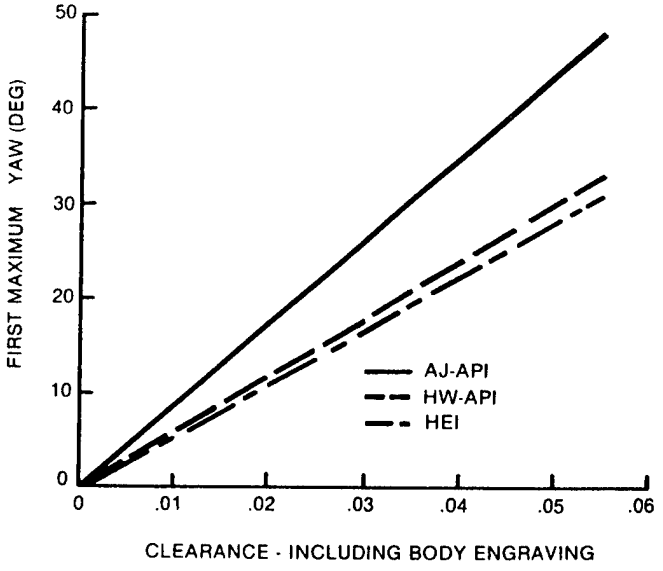

Figure 6. Effect of Clearance Between the Projectile and the Bore on Projectile Yaw After Exit.

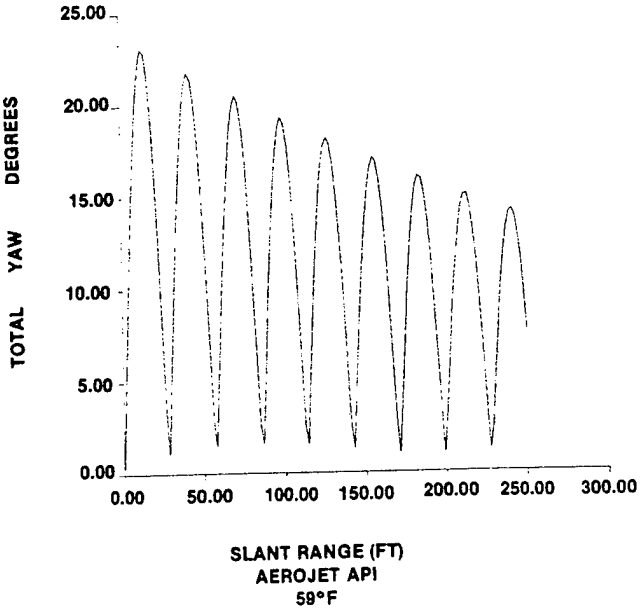

Figure 7. Total Yaw Vs. Range

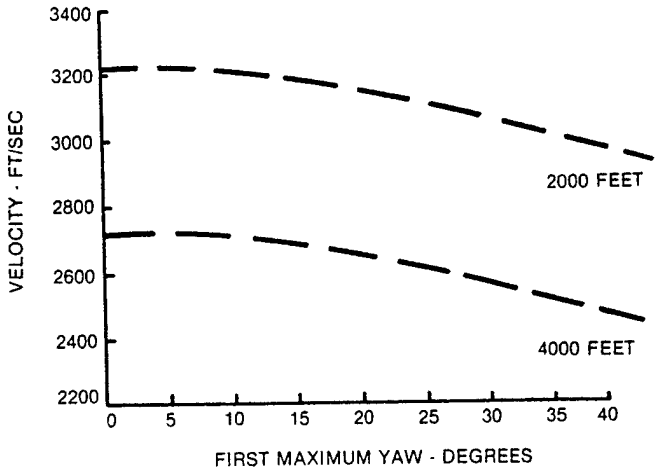

Figure 8. Effect of Yaw of a Fully Spun API Round on Target Velocity.

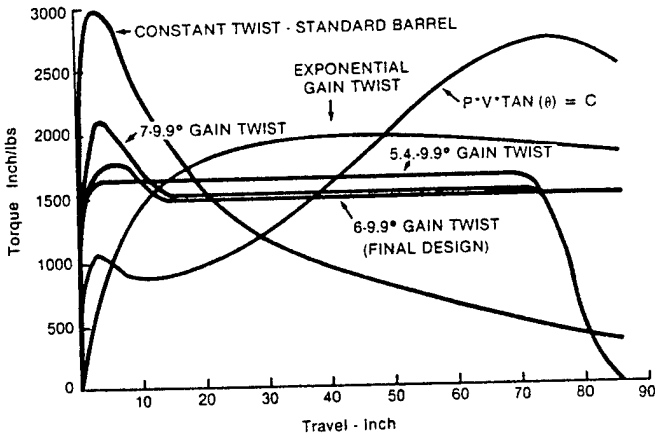

Figure 9. Gain Twist Designs Which Were Tested.

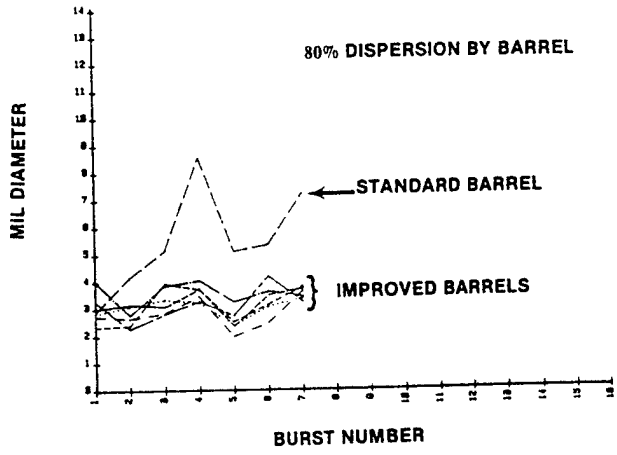

Figure 10. First Complement of API Fired on Set 1 at Eglin.

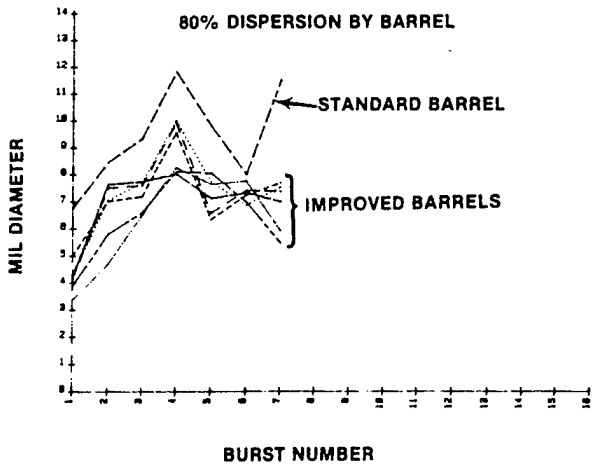

Figure 11. First Complement of HEI Fired on Set 1 at Eglin.

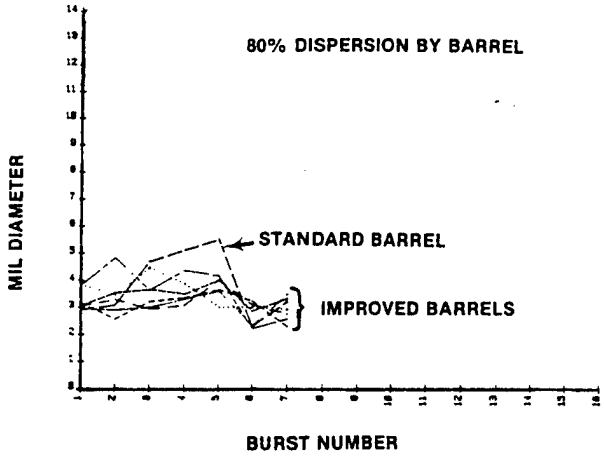

Figure 12. First Complement of TP Fired in Set 2 at Eglin.

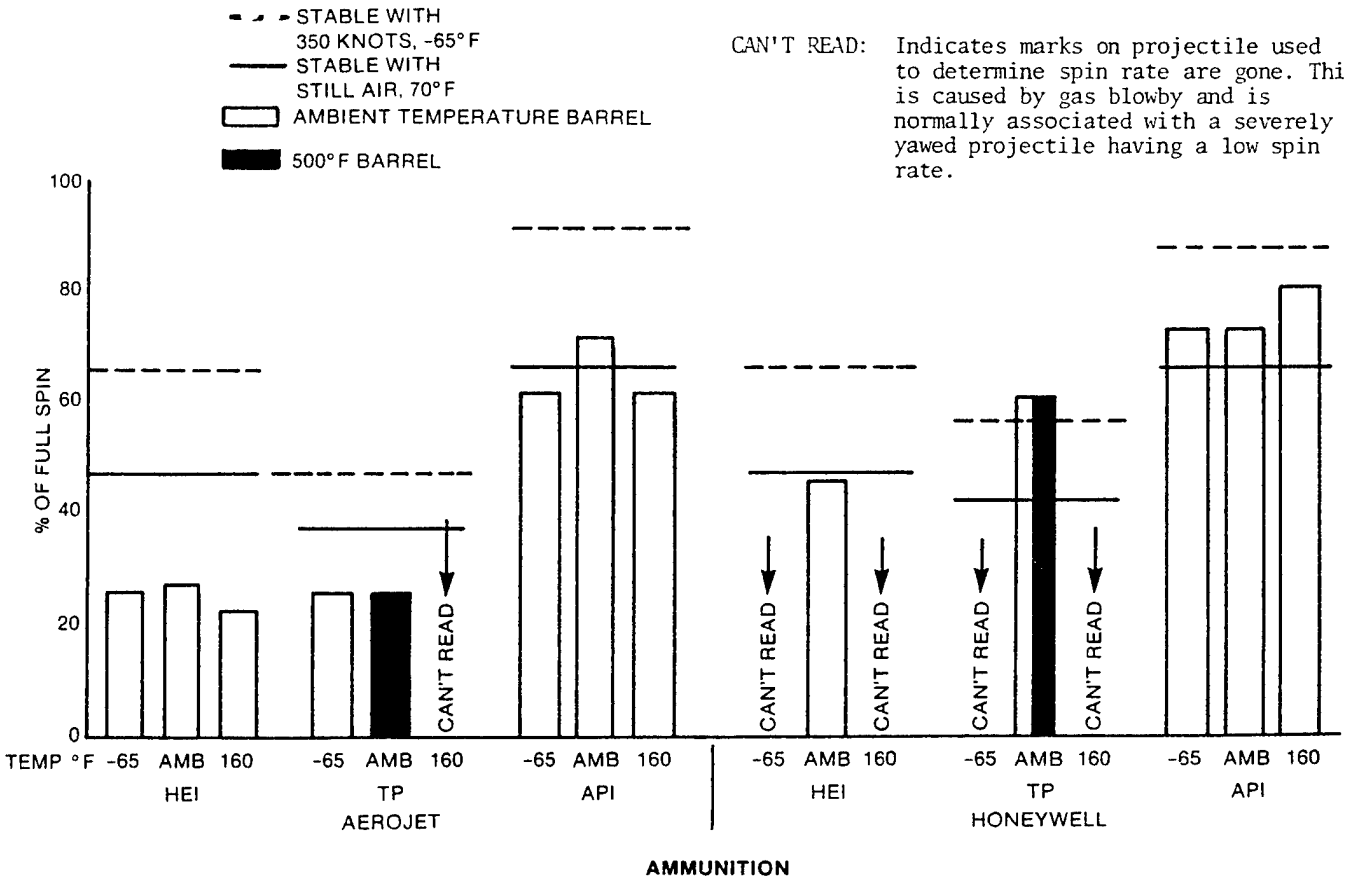

Figure 13. Barrel 201F158 S/N1004772 (Standard) Firing History 23,368 Rounds with TAC Firing Schedule.

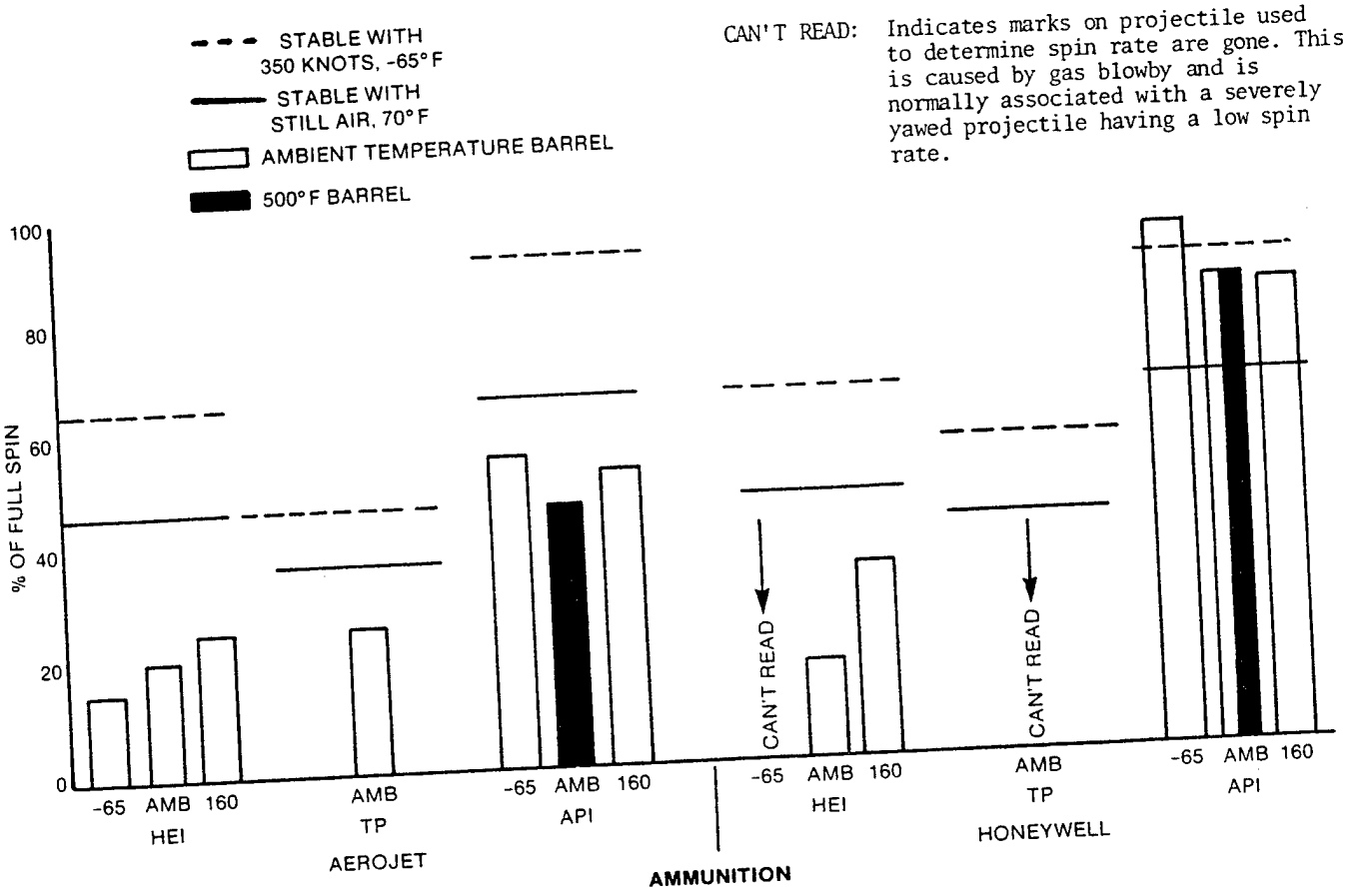

Figure 14. Barrel 211F954-2 S/N1000001 Improved—20 Lands Firing History 34,753 Rounds with TAC Firing Schedule.

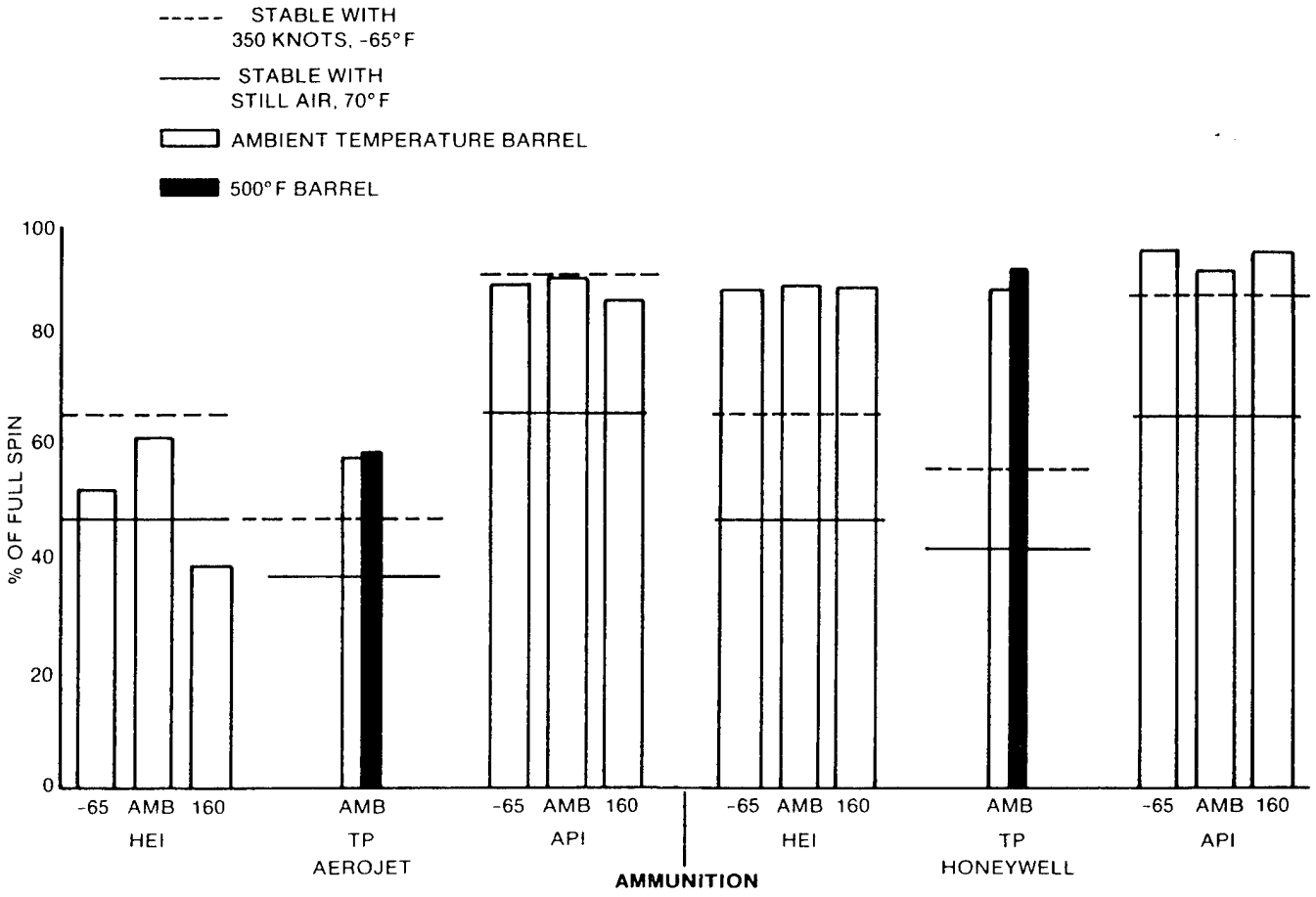

Figure 15. Barrel 211F954-1 S/N1000001 Improved—22 Lands Firing History 34,753 Rounds with TAC Firing Schedule.

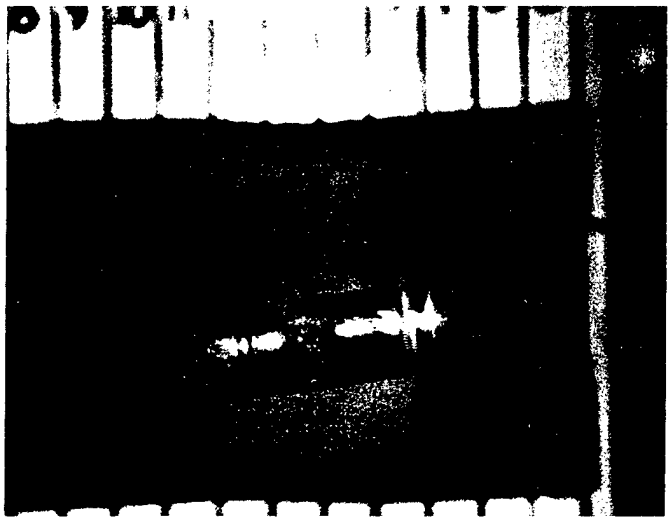

Figure 16. Projectile Windscreen Loss When Fired From a .014" Oversized Barrel. (6 of 29 Honeywell Projectiles Fired Lost Windscreens).

EVALUATION OF DIFFUSION COATINGS ON GUN BARREL MATERIALS

G. R. Lakshminarayanan and W. T. Ebihara
Materials and Manufacturing Technology Division
Fire Control and Small Caliber Weapon Systems Laboratory
US Army Armament Research and Development Command
Dover, New Jersey 07801

ABSTRACT

In this program erosion resistance characteristics of candidate gun barrel materials have been evaluated. Both chromized coating and chromium plating have been applied to these materials and tested with a double base WC846 propellant in an erosion test apparatus. The results show that chromized coatings improved erosion resistance of nickel base alloy Inconel 718, while chromium plating provided better protection than the chromized coating for an iron base alloy, CG-27; hot work tool steel, H-11; and chromium-molybdenum-vanadium (Cr-Mo-V) gun steel.

INTRODUCTION

Since gun tube wear and erosion continue to be the concern of weapon technologists, methods are constantly being sought to improve gun tube service life by utilizing improved materials and applying suitable coatings which provide effective erosion-resistant surfaces. To date,chromium plating is the method most widely used both in large and small caliber gun barrels to combat erosion because it is a cost effective method and chromium has many favorable properties such as a high melting point (1930^{o} C), high hardness, low coefficient of friction, and resistance to thermal and chemical attack by propellant gases.

With the increasing demands for high muzzle velocity and rapid rate firing weapon systems and the need to replace liners made from cobalt, a critical strategic material, weapon technologists visualize improved coating systems as a solution to the problem of providing gun tubes with the required level of performance. Work at Rock Island Arsenal[1] on heat-resistant superalloys and H-11, a hotworkedtool steel, showed considerable promise in combating erosion problems for small caliber weapon systems. For example, using CG-27 in the 25mm Bushmaster gun system resulted in a considerable increase in barrel service life over steel gun tubes. The work also indicated that breech-end erosion resistance in superalloy 7.62 mm systems had definitely improved over chromium-plated steel, but that muzzle-end erosion was still a problem in need of resolution. Chromium plating of superalloy material did not improve the situation because of its poor adhesion to the base metal. However, it was expected that diffusion coating will generally improve adhesion to these superalloy materials because the coating becomes an integral part of the base material. Diffusion coating (chromizing) is usually applied by a chemical-vapor-deposition technique using a gaseous-flow or static pack (cementation) process. In this program, the chromizing technique, a process in which a chromium rich surface is developed, was applied to various gun barrel materials and evaluated for their erosion-resistant characteristics in a simulated gun barrel environment.

EXPERIMENTAL PROCEDURE

The candidate materials selected for this study were: an iron-nickel base alloy (CG-27); a nickel-base alloy (Inconel 718); medium strength AISI H-11 steel, and Chromium-Molybdenum-Vanadium (Cr-Mo-V) gun steel. Chromized coatings for the erosion test specimens were provided by the Chromalloy Corporation located at Orangeburgh, NY. These were treated in the temperature range of 925 to 1094°C (1700 to 2000°F) for 20 to 70 hours. The samples were post-heat treated according to the requirements with cooling taking place in a vacuum or argon atmosphere rather than air to prevent oxidation.[3,4] Erosion tests were conducted using a closed bomb type apparatus[2] where a simulated gun-type environment was obtained by firing the double base WC846 ball propellant which has a flame temperature of about 2587°C (2860°K). Metallographic analyses were performed using these samples both prior to and after testing.

RESULTS AND DISCUSSION

Photomicrographs of chromized coatings of Inconel 718, CG-27, H-11, and Cr-Mo-V steel are shown in figure 1. The maximum concentration increases of chromium (percent by weight) near the surface for various samples by electron microproble analyses are as follows: from 19 to 38.7 percent for Inconel 718, from 13 to 50.6 percent for CG-27, from 5 to 84.1 percent for H-11 and from about 1 to 70.6 percent for Cr-Mo-V steel. Chromizing[5] generally takes place, for iron base systems, both by interchange reactions of iron and chromium and reduction reactions of chromium halides, while, for the nickel base system, it occurs only be reduction reactions. The very high chromium concentration near the surface, particularly for the H-11 and Cr-Mo-V samples was mainly due to the formation of chromium carbide (during the chromizing process) which acts as a barrier for further chromium diffusion into the core of the substrate, thus allowing the build up of a higher chromium concentration at the surface. In the case of nickel-rich Inconel 718, where mutual solid solubility of chromium/nickel exists, a smooth chromium concentration gradient is established through the surface region which is governed by diffusion kinetics at the treatment temperature. The observed diffusion zones (Figure 1) confirm this rationale. Figure 1 shows a primary coating depth of 0.005mm (0.2 mil) with up to a 0.05 mm (2.0 mil) total diffusion zone for Inconel 718 and a primary coating of 0.038 mm (1.5 mil) with about 0.013 mm (0.5 mil) diffusion zone for CG-27. A total diffusion zone of 0.038 mm (1.5 mil) for Cr-Mo-V and 0.019 mm (0.75 mil) primary coating with about 0.011 mm (0.4 mil) diffusion zone for H-11 are seen in figure 1.

The results of erosion test analysis are summarized in table 1 for chromized samples, uncoated samples and chromium-plated samples. Erosion or erosivity is represented as the weight loss of material per shot during firing. As seen in table 1, erosivity is reduced for Inconel 718 from 50.3 mg for the uncoated specimens to 25.9 mg for the chromium plated specimens; and further reduced to the 0.9 to 4.2 mg range for specimens with the chromized coating. Poor adhesion of chromium plate to Inconel 718 is mainly responsible for the loss of chromium plate and reduced erosion resistance. For CG-27 specimens, erosivity is reduced from 12.7 mg for the uncoated sample to the 1.2 to 5.0 mg range for chromized samples and reduced to the 1.2 to 1.7 mg range for chromium plated samples. However, for both H-11 and Cr-Mo-V materials chromizing resulted in an increase in the loss of

material. Erosivity ranged from 2.2 to 3.7 mg for the chromized samples compared to 1.6 mg for uncoated H-11. Similarly, erositivity ranged from 1.7 to 6.0 mg for the chromized samples compared to 1.3 mg with uncoated Cr-Mo-V steel. However, chromium plating these samples provides the best protection. No measurable weight loss was observed for the chrome plated H-11 samples and only 0.8 mg loss per shot was observed for chrome plated Cr-Mo-V steel. In fact,the chrome plated H-11 samples are better than even Cr-Mo-V steel. The results agree favorably with those observed in actual test firing results[1] of M134, H-11, and Cr-Mo-V (7.62 mm) barrels where the service life of the chrome plated H-11 barrel was nearly doubled when compared with that of the chrome plated Cr-Mo-V barrel.

Table I

EROSION RESULTS OF VARIOUS COATING/MATERIAL COMBINATIONS

Coating	Erosivity (mg/shot)*		
Material	No Coating	CR Plate	Chromized
Inconel 718	50.3	25.9	4.2 - 0.9
CG-27	12.7	1.2 - 1.7	1.2 - 5.0
H-11	1.6	0	2.2 - 3.7
CR-MO-V	1.3	0.8	1.7 - 6.0

*Ball powder WC846 propellant; results are the average of up to six inserts and 3 shoots per insert.

The photomicrographs of test fired samples are shown in figures 2 through 4. For Inconel 718 (figure 2) the chromized sample, after the test exhibited a strong diffusion zone with a thin coating while the chrome plated sample shows very little coating, if any, indicating poor adhesion of chrome plate to the substrate material. For CG-27 (figure 3), the chromium plate is still intact with only cracks appearing while loss of material is indicated for the chromized sample after test firing. Figure 4 represents typical chrome plated and chromized samples of H-11 and Cr-Mo-V samples after erosion test. In both cases it can be seen that only cracks appear in the chrome plated samples after testing, while the chromized samples show loss of material and severe erosion. This result might be attributed to the brittle chromium carbide formed at the surface layer and its subsequent removal during the erosion test.

The erosion test analyses indicated that chromized coatings decreased the erosivity of Inconel 718 considerably. However, chromium plating provided better protection for CG-27, H-11 and Cr-Mo-V steel than chromized coating. It must be pointed out that erosion tests in an enclosed chamber of this type is much different than the situation that is developed in an actual test firing of a gun tube. The duration of each single thermal pulse,or shot,was much longer than encountered in gun tests. The effects of wear and swaging introduced by a projectile in a gun test were absent in the erosion test. In view of these and other factors, it is recognized that the erosion test analyses provide qualitative information on the performance and endurance of coatings in a high-temperature propellant gas stream. Application of chromized coating on Inconel 718 and CG-27 liners and their

evaluation for uniformity, dimensional variation and test firing of the liners would provide additional information on the integrity of the coating.

CONCLUSIONS

1. Chromizing of gun barrel materials provide chromium concentrations of fifty percent or less at the surface for CG-27 and Inconel 718, a chromium rich surface of up to eighty-four percent for H-11, and up to seventy percent for Cr-Mo-V steel.

2. Chromizing Inconel 718 reduced erosivity considerably compared to uncoated or chromium plated samples. Chromizing also reduced the erosivity of CG-27 compared to the uncoated sample. However, chromium plating of CG-27 provide better protection than chromized coating.

3. Chromium plating is more erosion-resistant for both H-11 and Cr-Mo-V steel than chromizing.

REFERENCES

1. W.T. Ebihara, "Erosion Analysis and Control Studies at Rock Island Arsenal - A Review", Proceedings of the Tri-Service Gun Tube Wear and Erosion Symposium, ARRADCOM, Dover, N.J., pp 580-595, March 1977.

2. C. Lenchitz et al., "Some Aspects of Erosion Reducing Characteristics of the TiO_2 - Wax Additive:, PA Tech Memo 1768, Picatinny Arsenal, Dover, N.J., November 1965.

3. K.R. Iyer and W.T. Ebihara, "Metallographic Characterization of Eroded Gun Barrels", Proceedings of the Tri-Service Gun Tube Wear and Erosion Symposium, ARRADCOM, Dover, N.J., pp 150 - 177, March 1977.

4. Dr. R.P. O'Shea, G.S. Allison, J.D. DiBenedetto, and Dr. K.R. Iyer, "Improved Materials and Manufacturing Methods for Gun Barrels (Part 1)", U.S. Army Weapons Command Technical Report SWERR-TR-72-54, U.S. Army Weapons Command, Rock Island, IL, August 1972.

5. R.L. Samuel and N.A. Lockington, "The Prediction of Metallic Surfaces by Chromium Diffusion", Metal Treatment and Drop Forging, pp 407-415, September 1951.

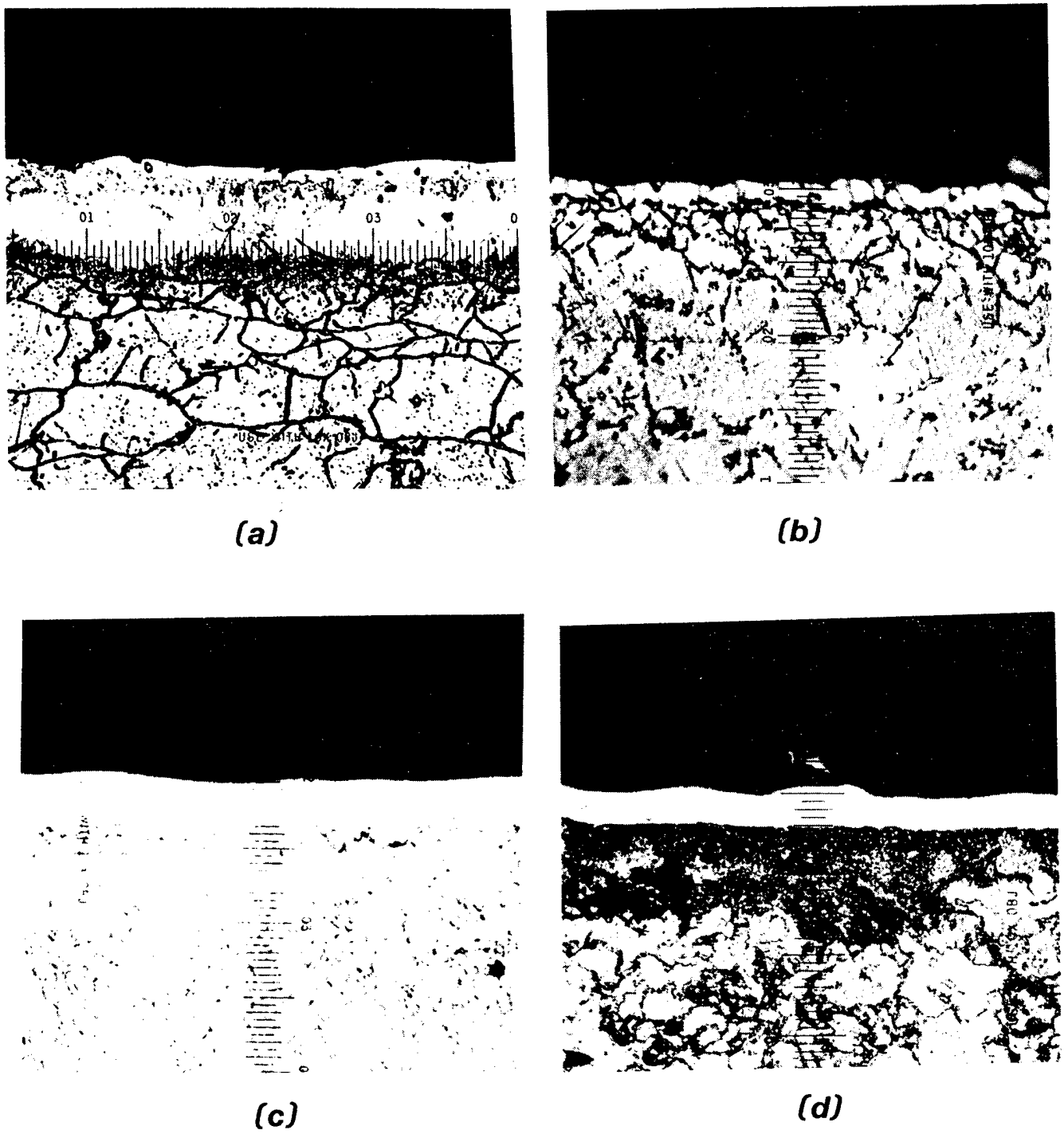

Figure 1. Photomicrograph of chromized samples (a) CG-27 (b) Inconel 718 (c) H-11 and (d) Cr-Mo-V gun steel

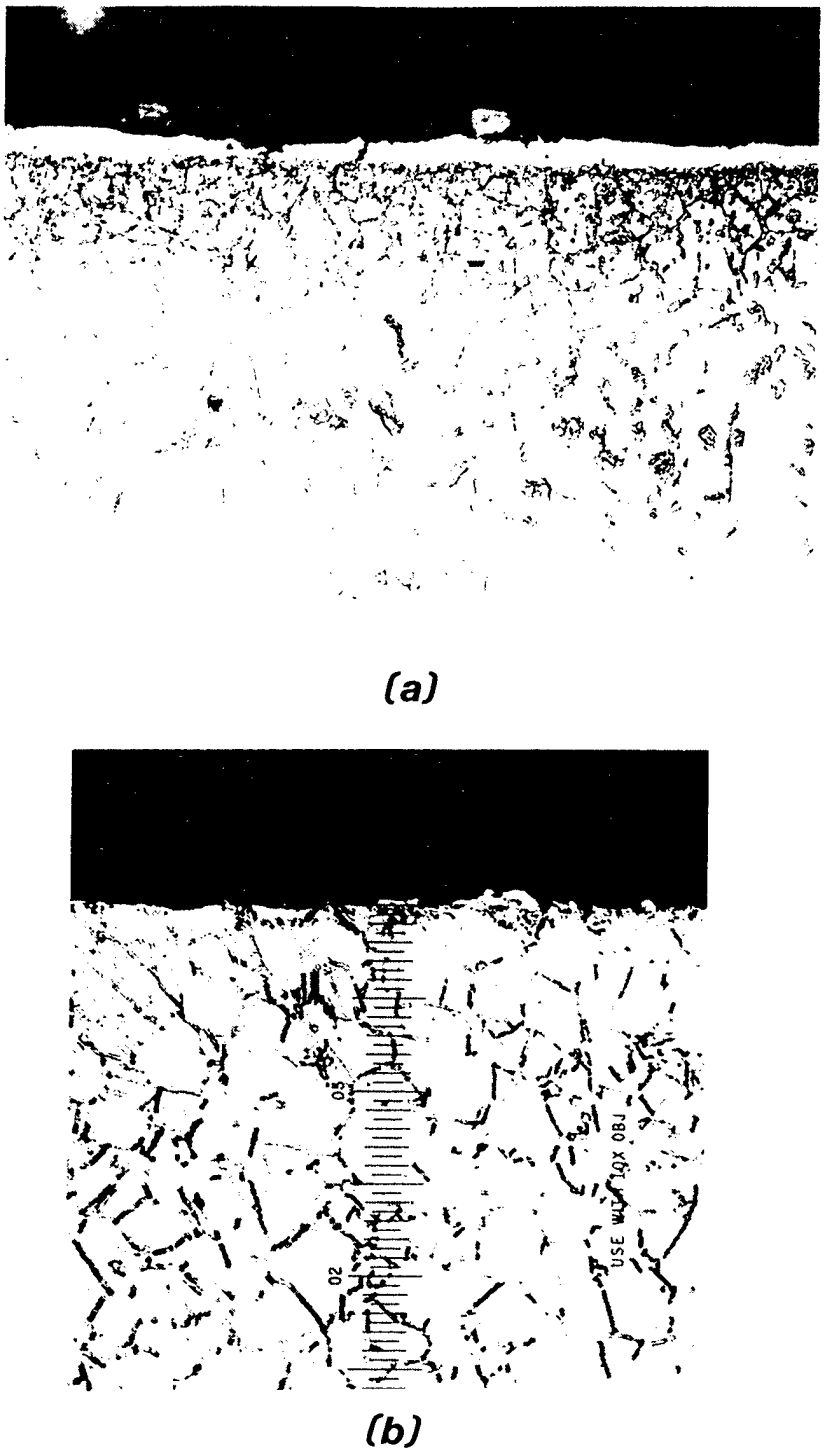

Figure 2. Photomicrographs of Inconel 718 after erosion test with WC846 ball propellant (a) chromized and (b) chromium plated samples

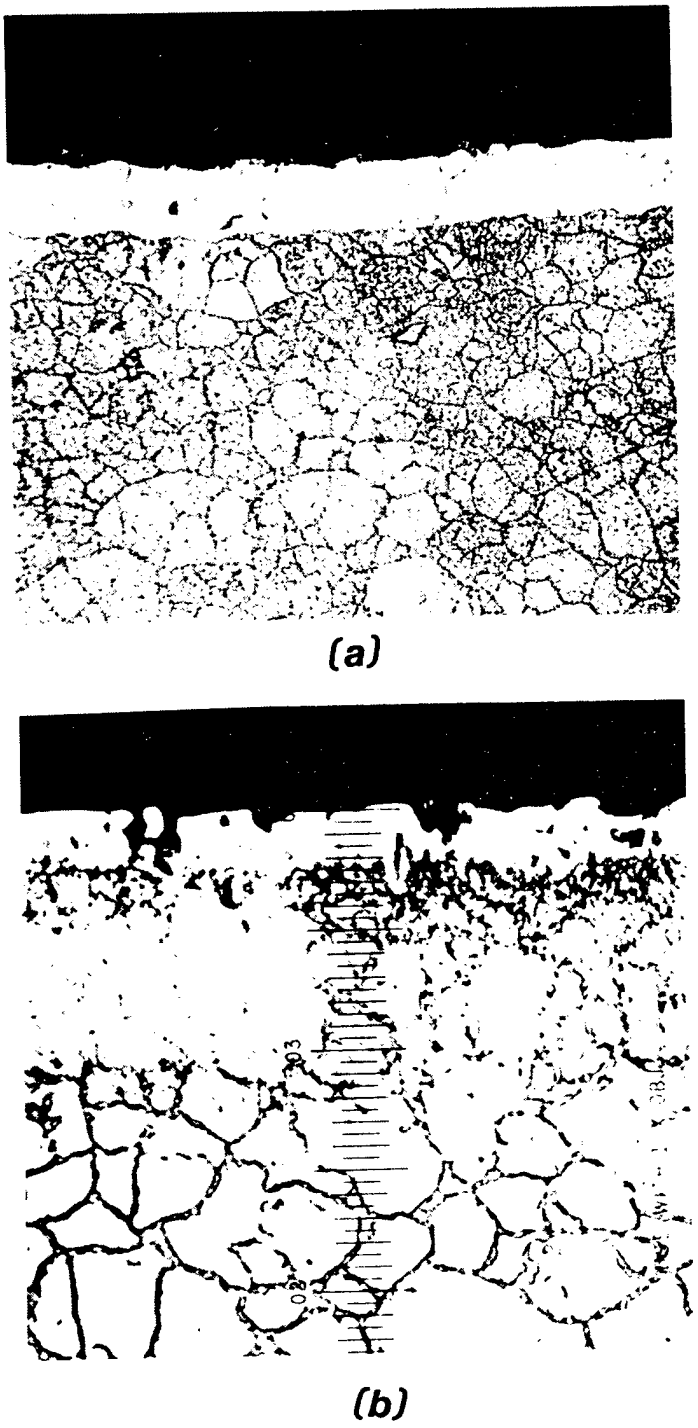

Figure 3. Photomicrographs of CG-27 after erosion test with WC846 ball propellant (a) chromium plated and (b) chromized samples

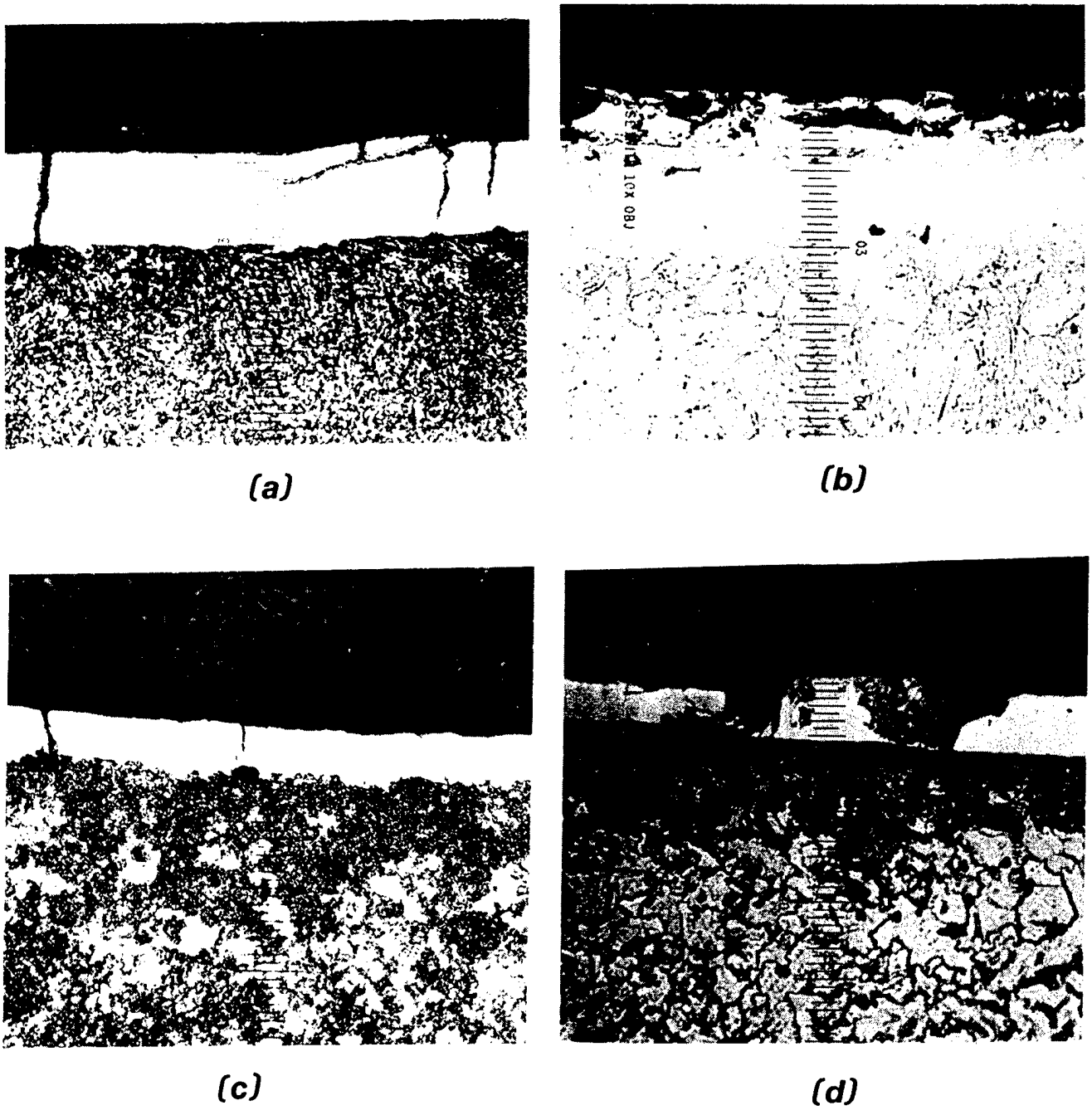

Figure 4. Photomicrographs of samples after erosion test with WC846 ball propellant (a) chromium plated H-11 (b) chromized H-11 (c) chromium plated Cr-Mo-V gun steel and (d) chromized Cr-Mo-V gun steel.

HIGH RATE SPUTTERING OF TANTALUM ONTO GUN STEEL

J. F. Cox
US Army Armament Research and Development Command
Large Caliber Weapon Systems Laboratory
Benet Weapons Laboratory
Watervliet, NY 12189

E. D. McClanahan
Battelle Pacific Northwest Laboratories
Richmond, WA 99352

ABSTRACT

The useful life of various gun tubes is increased by protecting the internal gun tube surface with electrodeposited chromium. The properties of refractory metals such as tantalum, molybdenum, niobium, and tungsten indicate that these materials should exhibit superior resistance to erosion processes which occur at gun tube surfaces. In this paper the results of a study of the application of high rate sputtering to the preparation of tantalum coated gun steel surfaces is presented. The sputtering conditions required to obtain tantalum coatings about 125 micrometers thick on flat surfaces, are discussed and physical properties of the tantalum deposits such as hardness, microstructure, crystal structure, and composition are presented. Results from similar studies carried out on smooth bore 120 mm diameter cylinders and rifled 20 mm diameter cylinders are also discussed.

INTRODUCTION

As the demands for improved performance of modern gun systems escalate, it becomes increasingly necessary that the bore surface of gun tubes be protected from erosion. At the present time the useful life of several weapon systems has been increased by protecting the gun barrel surface with electrodeposited chromium. The properties of refractory metals such as tantalum, molybdenum, niobium, and tungsten indicate that these materials should exhibit superior resistance to the erosion processes which occur at gun tube surfaces.[1] The results of a recent testing program[2] clearly show that the average erosion rate for tantalum coated steel liners test fired in a 20 mm gun is substantially less than the erosion rate of all other tested liners including chromium coated liners. The technique used to coat the 20 mm liners with tantalum, electrodeposition from molten salts, involves heating the substrate to about 800°C. At this temperature gun steel undergoes undesirable changes in mechanical properties. To avoid degradation of the gun tube mechanical properties, tantalum coatings are applied to liners which are shrunk fit into the breech end of the gun tube. This last step in the process could be eliminated if the protective coating could be applied directly to the gun tube surface at temperatures less than about 500°C. High rate sputtering is a technique which can be used to deposit thick metallic coatings in reasonable time intervals at substrate temperatures significantly below 500°C.

Distribution limited to US Government Agencies only because of test and evaluation; September 1982. Other requests for this document must be referred to Commander, ARRADCOM, ATTN: Benet Weapons Laboratory, DRDAR-LCB-RP, Watervliet, NY 12189.

In this paper the results of a study of the application of high rate sputtering to the preparation of tantalum coated gun steel surfaces is presented. The sputtering conditions required to obtain tantalum coatings about 125 micrometers thick on flat surfaces are be discussed and physical properties of the tantalum deposits such as hardness, microstructure, crystal structure, and composition are presented. Results from similar studies carried out on smooth bore 120 mm i.d. and rifled 20 mm i.d. cylinders are also presented.

EXPERIMENTAL

A schematic diagram of the Battelle Pacific Northwest Laboratories thermionically supported glow discharge sputtering apparatus used to deposit tantalum on the face of disc shaped specimens is shown in Figure 1.[3] The stainless steel, water cooled sputtering chamber is evacuated to an unbaked base pressure of about 10^{-7} torr (1.3×10^{-5} Pa) with a liquid nitrogen trapped oil diffusion pump. Prior to each run the surfaces of all system components contained within the vacuum chamber are carefully degreased and cleaned. After assembly the system is pumped to its base pressure, helium leak checked, and the system outgassing rate is measured. When the outgassing rate is sufficiently small, a leak of 99.99 percent krypton is established to produce a dynamic vacuum at an automatically controlled pressure of about 3×10^{-3} torr (0.4 Pa). The composition of the atmosphere in the sputtering chamber is continually monitored with a residual gas analyzer.

Both the pure tantalum target and the steel substrates are water cooled. The substrate temperature is monitored with a thermocouple which penetrates the rear surface of the 2.54 cm diameter by 0.62 cm thick disc shaped specimen and is embedded in close proximity to the surface being coated. The cooling water flow rate to the substrate holder is adjusted to provide temperatures ranging from 70°C to 450°C. The substrates, which had been lapped through No. 600 paper, are ion etched before tantalum deposition is initiated. The effect of electrical bias on the deposits was determined by producing coatings at bias voltages of -35 volts (floating) and -50 volts.

A schematic diagram of the apparatus used to coat the internal surfaces of cylinders is presented in Figure 2. In this configuration the tantalum target, the steel substrate, and the close fitting water cooled copper thermostat are coaxial. The substrate temperature is monitored with a thermocouple embedded in or in intimate contact with the exterior surface of the cylindrical substrate. Substrate temperature is controlled by adjusting the cooling water flow to the copper thermostat. The two substrate configurations used with this apparatus were a smooth bore 120 mm i.d. by 200 mm long cylinder and a rifled 20 mm i.d. by 100 mm long barrel insert. The internal diameter of the 20 mm insert had been increased by electropolishing to compensate for the addition of the 0.127 mm thick tantalum deposit. The 120 mm diameter cylinder was machined from a section of a 105 mm gun tube.

The apparatus is operated using essentially the same procedure used to prepare the planar specimens. The cylindrical substrates were vapor degreased and cleaned ultrasonically. In addition to routine cleaning procedures, it was found necessary to subject the 120 mm cylinders to an overnight vacuum bake at about 500°C. When the 120 mm cylinders were not baked, the residual gas analyzer indicated the presence of high hydrogen concentration in the sputtering chamber.

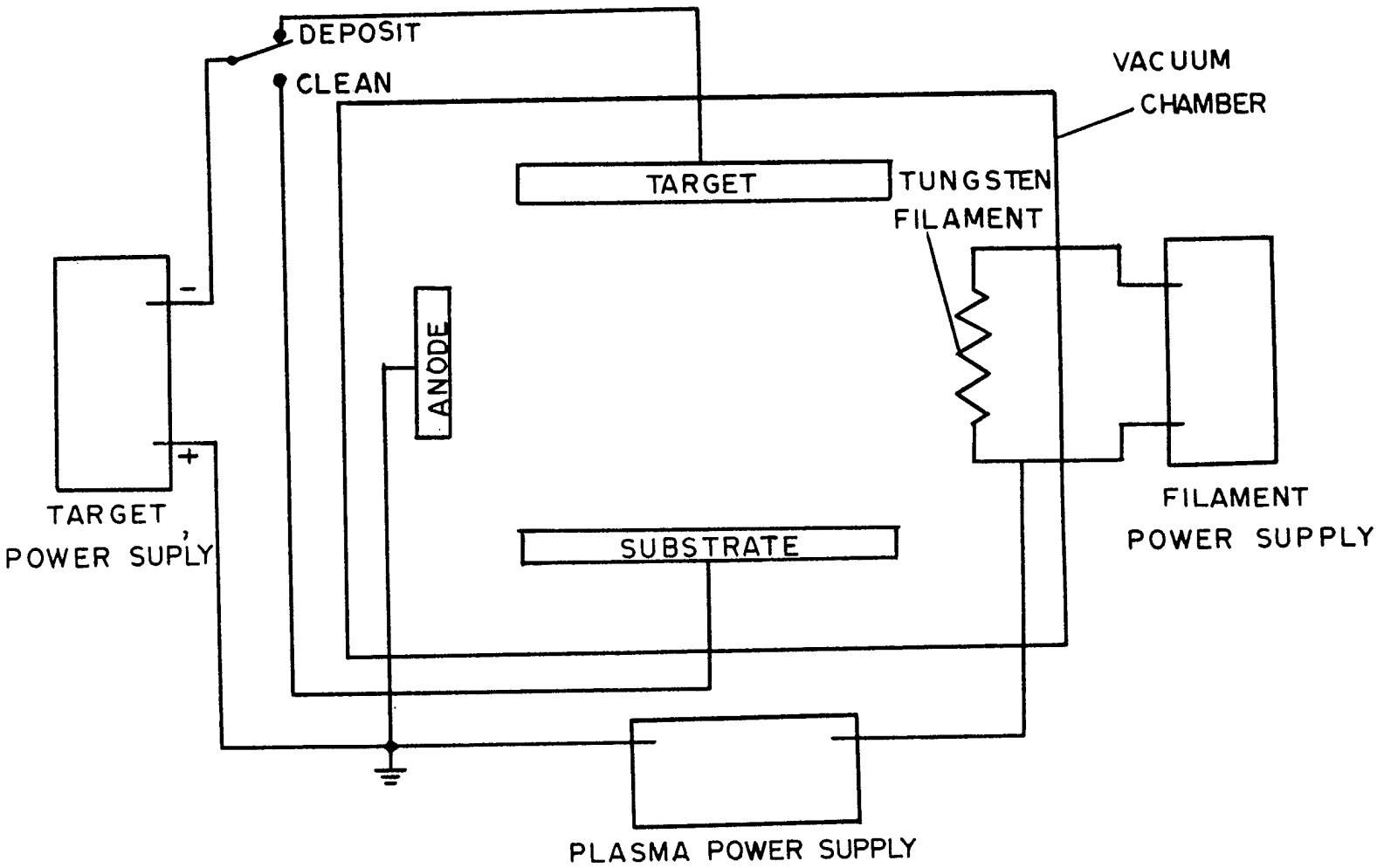

SCHEMATIC DIAGRAM OF TRIODE SPUTTERING APPARATUS
FOR COATING PLANAR SUBSTRATES

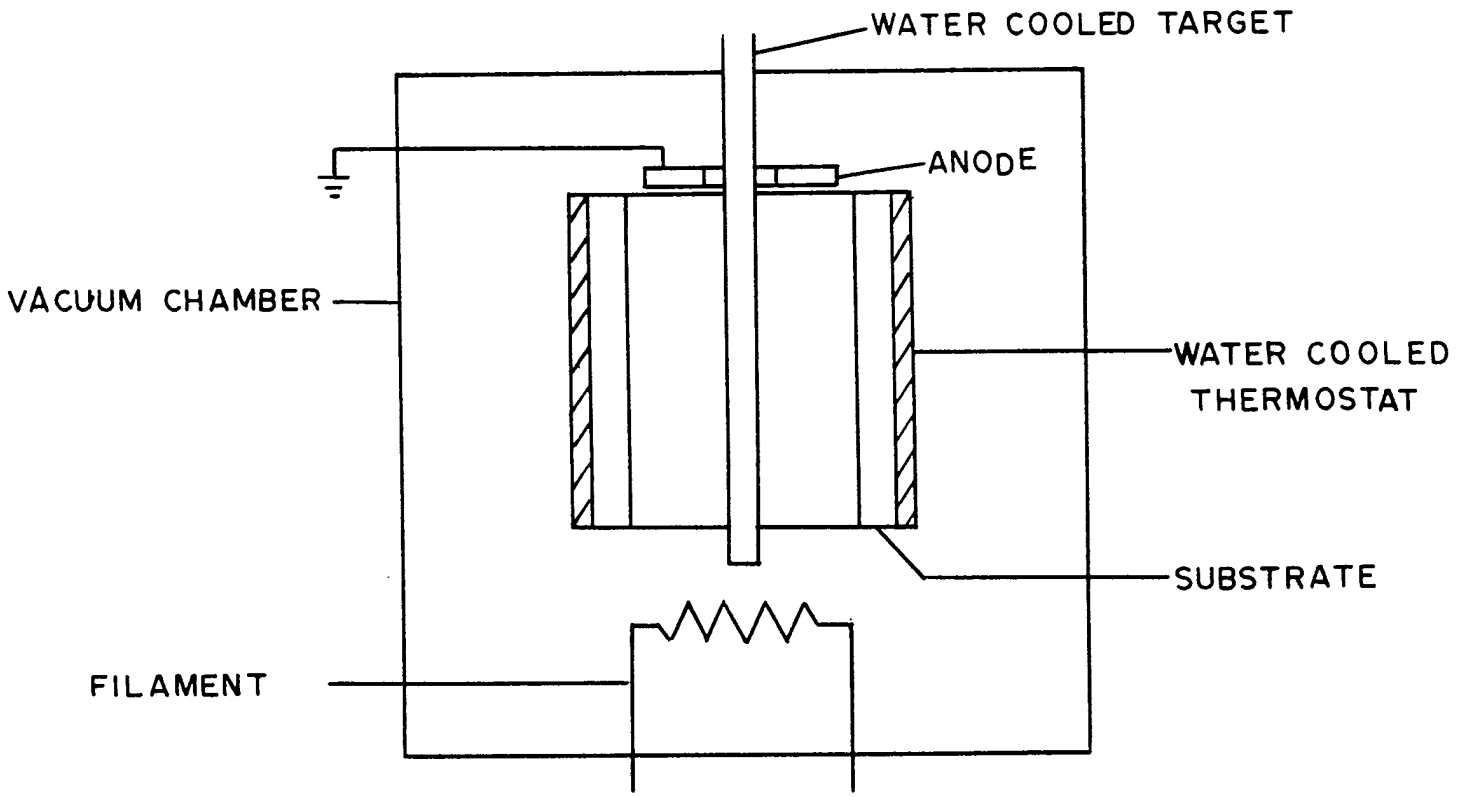

SCHEMATIC DIAGRAM OF TRIODE SPUTTERING APPARATUS FOR COATING THE BORE SURFACE OF CYLINDRICAL SUBSTRATES

Data on the structure of both the tantalum deposits and the gun steel substrates were obtained using x-ray diffractometry, optical microscopy, and scanning electron microscopy. Chemical composition of the deposits was investigated using x-ray fluorescence and electron microprobe analyses.

The microhardness of the growth surfaces and transverse sections was measured using both diamond pyramid and Knoop indentors. The microhardness of the tempered martensitic gun steel was determined using a Knoop indentor only.

Adhesion of the tantalum to the gun steel was evaluated using a recently developed technique[4] for classifying the degree of adhesion between electrodeposited chromium and a variety of alloy substrates. In this technique a carbide tool moving at a speed of 75. cm/sec is used to cut a series of parallel grooves into a specimen surface. Experience with the technique has shown that reproducible results are obtained when the grooves are cut with a spacing of 1 mm with a depth that extends 175 micrometers below the coating-substrate interface. The adhesion, as determined by optical microscopy, is rated as excellent, good, poor, or nil depending on the presence and/or location of fracture surfaces.

RESULTS AND DISCUSSION

PLANAR SUBSTRATES

The experimental data for high rate sputtering of tantalum onto the surface of disc shaped specimens are presented in Table I. The data are not sufficiently complete to establish a precise relationship between hardness and either substrate bias or temperature. The tantalum deposited onto substrate two is much thinner than all the other deposits. If the hardness data for specimen two are not considered then the hardness of tantalum deposited at a substrate bias of -50 volts is independent of substrate temperature, increasing by 5 DPH_{500} units as the substrate temperature is increased from 69°C to 350°C. The decrease in hardness in going from substrate condition of -50 volts and 350°C to -35 volts (floating) and 450°C, then indicates that deposit hardness is more dependent on substrate bias than on substrate temperature. Regardless of the details of the relationship between deposit hardness and operating parameters, the data show that both growth surface and transverse section hardnesses (which have ranges of 387 to 446 DPH_{500} and 380 to 413 KHN_{50} respectively) are relatively insensitive to substrate bias and substrate temperature.

A photomicrograph of tantalum deposited at 69°C and -50 volts bias is shown in Figure 3. In addition to the expected body centered cubic phase of tantalum the deposit contains a second phase which has been tentatively identified with x-ray diffractometry as the metastable tetragonal beta tantalum phase. The existence of this phase has been well documented in the thin film literature.[5,6]

As shown in Figure 4, the beta phase is present at the tantalum-steel interface in deposits prepared at 450°C and -35 volts (floating). Both Figures 3 and 4 show that there is intimate contact between the coating and the substrate and that there is no discernible interfacial reaction layer formed during sputtering.

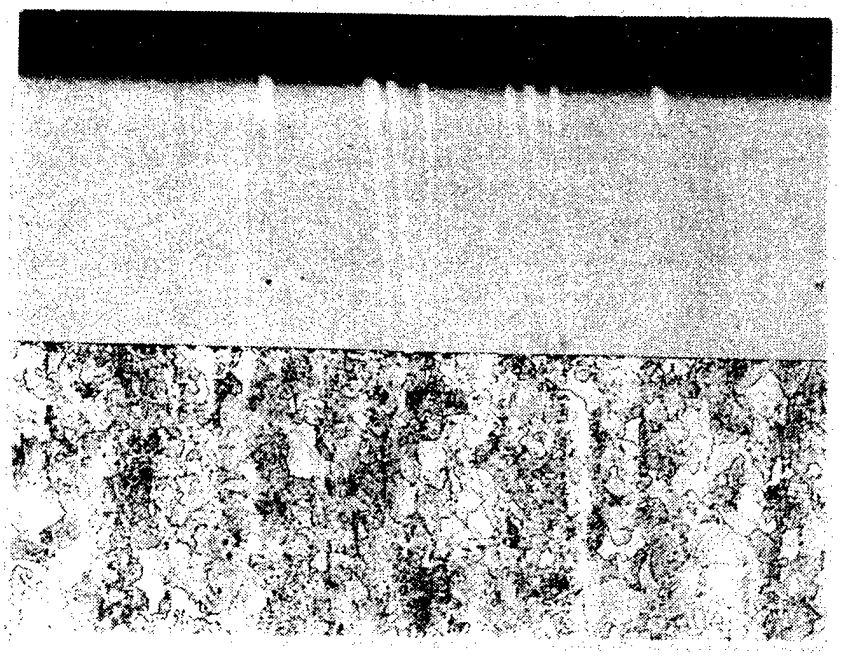

Fig. 3. Photomicrograph of Ta sputtered onto steel substrate held at 69°C. (250X)

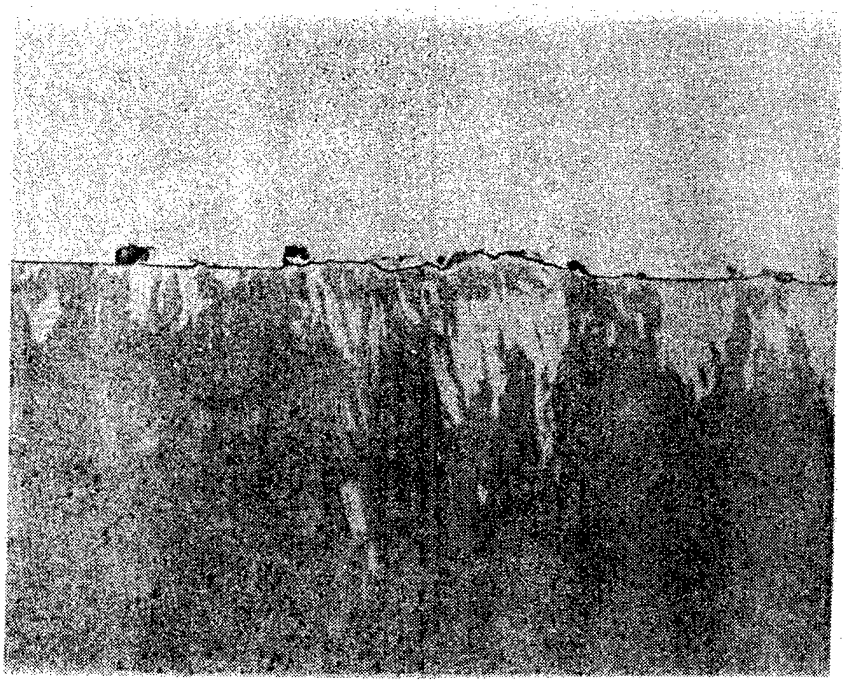

Fig. 4. Photomicrograph of Ta sputtered onto steel substrate held at 450°C.(1000X)

An additional tantalum deposit, the data for which is not included in Table I, was prepared under inadequately defined conditions. During the run errant material in the sputtering chamber shorted the specimen to a shield. As a result of the shorting, the specimen bias changed from -50 volts to -35 volts (floating) while the substrate temperature remained at 70°C. Metallographic examination of this specimen showed the deposit to be a reflecting deposit with a microhardness of about 1200 KHN_{50}. Wide film Debye-Scherrer diffraction patterns of this deposit showed the tantalum to be almost pure (> 95 percent) beta-tantalum. A more detailed discussion of the formation of beta-tantalum is in preparation.

X-ray fluorescence analysis and electron microprobe analysis of the body-centered-cubic and the beta phases of tantalum did not indicate the presence of either interstitial or substitutional impurity elements. If foreign elements are present in either of the phases, their concentrations are less than ten to one hundred parts per million by weight for all elements except hydrogen (which has not been analyzed for), carbon, nitrogen, and oxygen which cannot be present in concentrations greater than about five to ten atom percent.

CYLINDRICAL SUBSTRATES

The results from the experiments with planar substrates were used to select deposition parameters for coating the bore surface of the 120 mm cylinders. To minimize the possibility of beta phase formation the deposit was prepared at a substrate bias of -51 volts and a substrate temperature of 370°C. A photograph of the coated cylinder showing the smooth and essentially defect free deposit is shown in Figure 5. Longitudinal and radial sections were removed from the cylinder and prepared for metallographic examination. A photomicrograph showing both the tantalum deposit and the steel substrate is presented in Figure 6. The section has been etched to show the microstructure of the steel substrate. The steel substrate retains the original tempered martensite of the gun steel. The microhardness of the tantalum deposit was determined to be about 460 KHN_{50} and the steel substrate to be about 425 KHN_{50} (unchanged from the hardness of the uncoated steel). The metallographic samples were also used to determine longitudinal and radial variations in coating thickness. The thickness of the tantalum deposit in the longitudinal direction varied from a low of 76 to a high of 180 micrometers. The thickness of the deposit in a 12 cm long central portion of the cylinder varied from 112 to 140 micrometers. Similar measurements in the radial direction showed a variation in thickness of less than 25 micrometers. These variations in coating thickness can be reduced by careful design and positioning of the target relative to the substrate.

The photomicrograph in Figure 6 of a section from the 120 mm diameter specimen shows the presence of beta tantalum at the tantalum-steel interface. The SEM image of a tantalum fracture surface presented in Figure 7 shows that the beta tantalum fractures in a brittle manner thus indicating that the tantalum may show poor adherence to the steel substrate.

Figure 8 shows two of ten adherence test tracks cut into samples removed from the 120 mm cylinder. The absence of cracks in the coating and of spalling of the coating from the substrate establishes the excellent quality of the tantalum-steel adherence.

TABLE I. SUMMARY OF DATA FOR HIGH RATE SPUTTERING OF Ta ONTO PLANAR STEEL SUBSTRATES

Specimen	Deposition Rate (cm/hr)	Deposit Thickness (cm)	Substrate Bias (volts)	Substrate Temperature (°C)	Deposit Hardness Growth Surface (DPH-500)	Deposit Hardness Transverse Section (KHN-50)
1	0.0030	0.015	-34 (Floating)	450	394	397
6	0.0033	0.012	-38 (Floating)	450	396	383
2	0.0029	0.008	-50	350	387	380
5	0.0048	0.017	-50	350	441	411
4	0.0035	0.014	-50	69	446	413

Sputtering Conditions:

Atmosphere: Research grade krypton @ 3×10^{-3} torr
Target Bias: -1500 volts
Target and Current: 200 ma

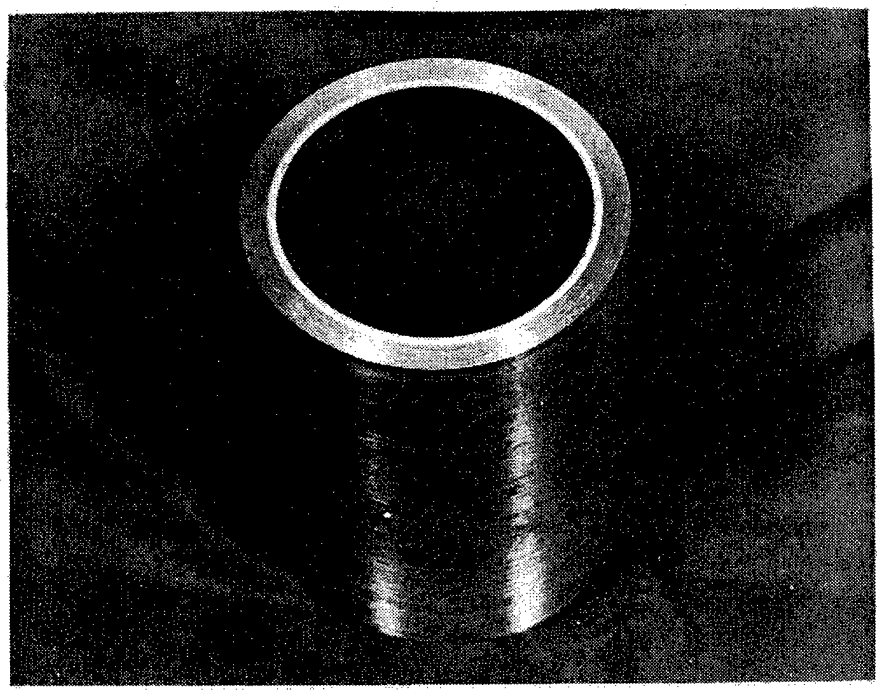

Fig. 5. Smooth bore 120 mm x 200 mm cylinder coated with 0.015 cm thick Ta.

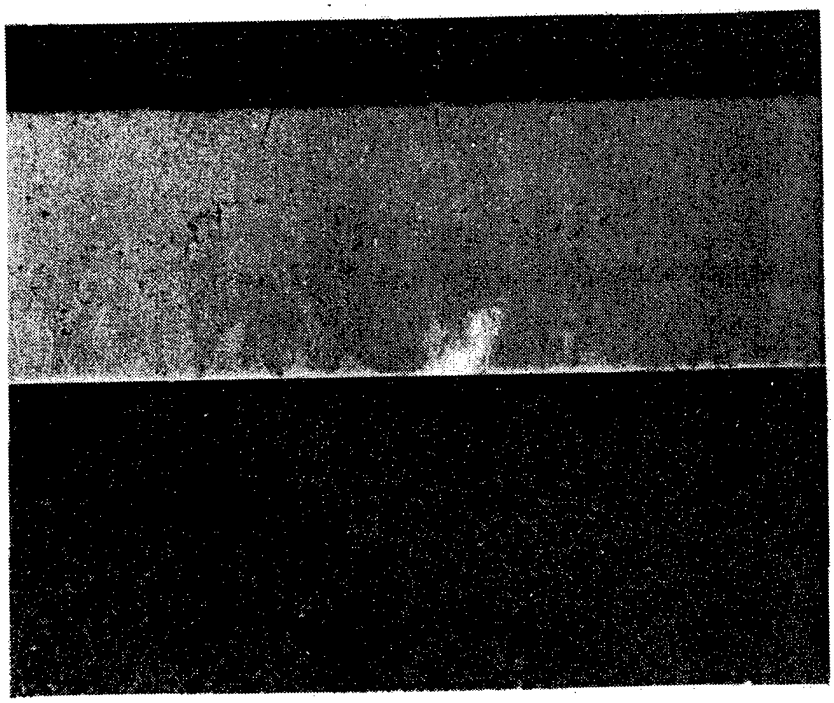

Fig. 6. Photomicrograph of Ta coated gun steel etched to show unaffected steel microstructure. (200X).

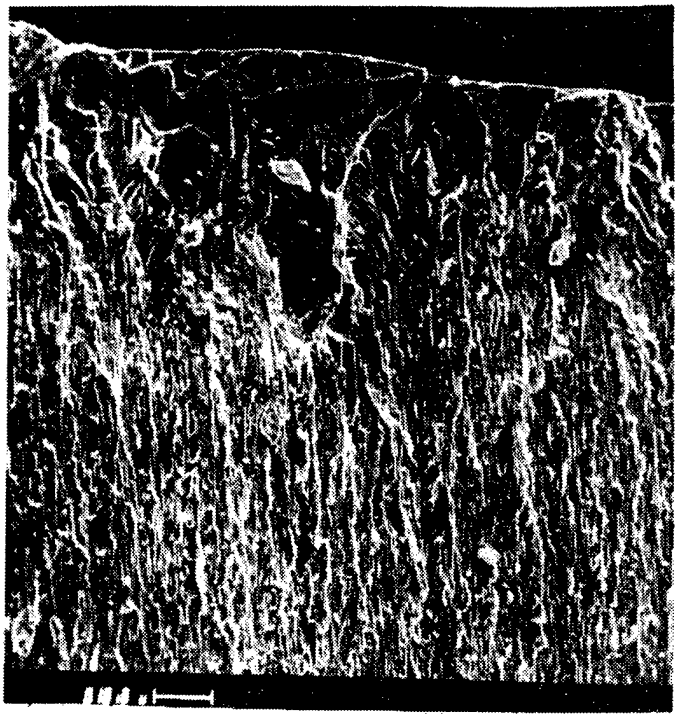

Fig. 7. SEM image of Ta fracture surface. (750X).

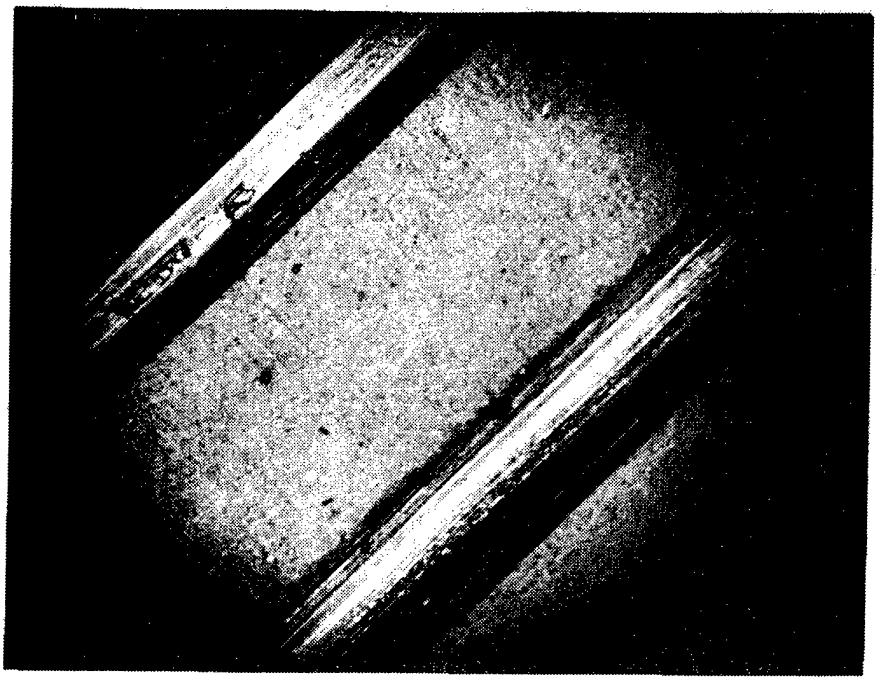

Fig. 8. Test for adherence of sputtered tantalum to bore of 120 mm substrate. (30X).

The ability of the sputtering processes to successfully coat a rifled surface was evaluated with rifled 20 mm barrel inserts. A photomicrograph of a section from a tantalum coated rifled insert is shown in Figure 9. The tantalum is about 76 micrometers thick on the lands and in the grooves and has a minimum thickness on the vertical land faces of 46 micrometers. The tantalum deposit, which was prepared at a substrate bias of -50 volts and a temperature of 405°C had a hardness of about 450 KHN_{50} and contained the beta phase.

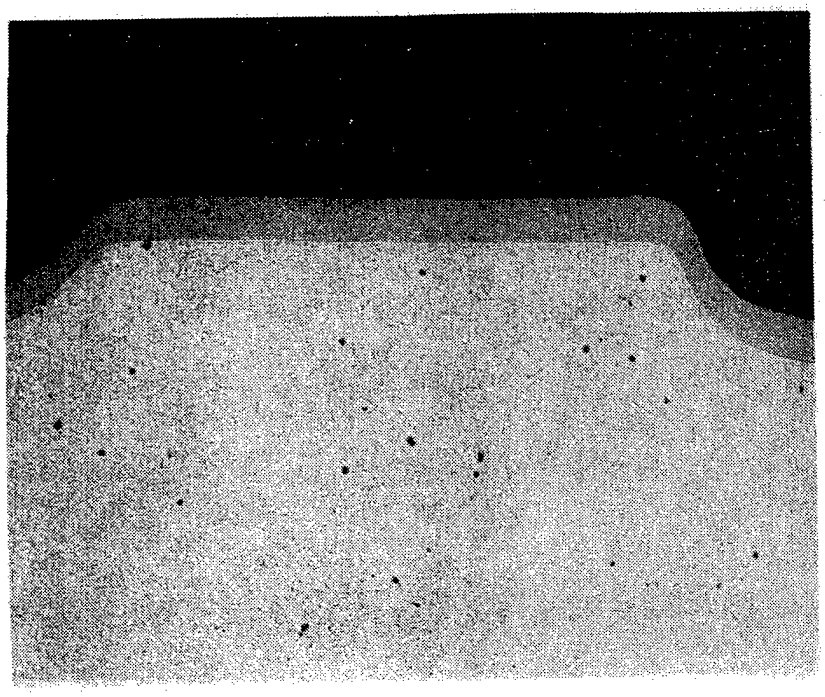

Fig. 9. Photomicrograph of sputtered Ta coating on rifled 20 mm insert. (50X).

CONCLUSIONS

1. The microhardness of sputtered tantalum is relatively insensitive to substrate temperatures from 70° to 450°C and to substrate bias of -35 volts (floating) to -50 volts.

2. The beta phase of tantalum, which previously has only been observed in thin (< 5000Å) films, can be produced in bulk quantities.

3. The high rate sputtering process can be used to produce adherent, defect free and relatively uniformly thick tantalum coatings on smooth bore 120 mm i.d. cylinders.

4. The high rate sputtering process coats all the surfaces, including the vertical land faces, of rifled 20 mm liners.

REFERENCES

1. Ahmad, I., et al, "Potential Erosion Resistant Refractory Alloy Coatings for Gun Tubes," Proceedings of 1978 Triservice Conference on Corrosion, p. 203, Battelle Memorial Institute, Columbus, OH.

2. Cullinan, R. L., D'Andrea, G., and Croteau, P., "Study of Erosion Resistant Materials for Gun Tubes - Part I: 20 MM Liner Technology," ARLCB-TR-80027, December 1980, "Part II: Tantalum Coated Liners," ARLCB-TR-81011, April 1981; Part III: Low Contraction (LC) Chromium Plated LIners," ARLCB-TR-81046, December 1981, Benet Weapons Laboratory, Watervliet, NY.

3. McClanahan, E. D., et al, "State-of-the-Art for High Rate Sputter Deposition," BN-SA-772, October 1977.

4. Chen, E. S. and Baldauf, W., "Activation of Superalloys and Stainless Steels for Chromium Plating," ARLCB-TR-81035, August 1981.

5. Maissel, L. and Glang, R., Eds., Handbook of Thin Film Technology, Chapters 4 and 18, McGraw-Hill Book Company, NY (1970).

6. Perry, R. W., et al, Thin Film Technology, D. Van Nostrand Company, Inc., NY (1968), pp. 221-233.

A NEW CONCEPT FOR DEPOSITION OF CHROME COATINGS IN TUBES

A. Niiler, W.F. Henshawt and J. R. White
ARRADCOM/Balllistic Research Laboratory
Aberdeen Proving Ground, MD 21005

ABSTRACT

Improved protection of bore surfaces against erosion is a major Army concern for modern, high performance gun tubes. High temperature materials such as chrome have been strongly bonded to tubes by ion plating and have high potential for providing improved erosion protection. A metal vapor source capable of vaporizing chromium and operating in the cylindrical confines of the inside of a tube has been designed and built. This device consists of a multiply shielded, water cooled hollow cathode discharge (HCD) gun made of tantalum tubing and loaded with Cr pellets. The high temperature generated within the HCD vaporizes the Cr and the Argon gas flowing through the HCD carries these vapors through an end constriction into the plating region. The tube to be plated, positioned concentrically about the cathode, is biased to several hundred volts and is swept past the HCD opening. The bias on the tube is necessary to produce ion plating by which a graded interface of about 1 μm thickness is produced between the tube and coating. This interface is essential to the established strong adhesion properties of ion-plated coatings to substrates. This HCD source has been used to ion-plate smooth and rifled tubes with l/d of 10, providing uniform Cr coatings at a rate of 10μm per hour. The discussion will include a description and operating characteristics of this HCD gun, the parameters found to produce the coatings and the description of the coating characteristics.

INTRODUCTION

During the firing of a gun, the high temperature, high velocity propellant gases cause a melt and blow-off condition which erodes the tube. Improved protection of the bore surfaces against such erosion is a major challenge in the design of modern, high-performance gun tubes. It has been found that a high melting temperature coating can reduce the wear rate considerably. HC chrome coatings deposited in the gun tube by electro-deposition (ED) will extend the gun tube life but also will fail unpredictably and catastrophically, often resulting in the tube being more damaged than an uncoated one[1]. LC deposited chrome coatings, on the other hand, have shown substantial improvement in protecting 20mm barrels[2].

High temperature coatings such as chromium can be ion-plated with strong bonding to tubes and as such are good candidates to provide erosion protection to gun tubes. Ion plating is a PVD process whereby a negative voltage is applied to the object being coated (substrate) in the presence of a working gas such as Argon[3]. The negative voltage ionizes the working gas, causing some material to be sputtered off the substrate during deposition. Initially, an intermixing of the deposition material with the substrate material occurs, but later the deposition material mixes

† NRC Research Associate. Present address:Naval Research Lab, Washington,D.C.

Approved for Public Release; Distribution Unlimited.

only with the previously deposited material. When the deposition rate is greater than the sputtering rate, a coating is produced which has a graded film-substrate interface instead of the sharp interface characteristic of other plating processes. The graded interface is typical of ion plating and is generally thought to be instrumental in the observed excellent adhesion of the film to the substrate[4]. Ion plating is generally done at pressures where the mean free paths of ions are small, resulting in a high throwing power. Throwing power, the ability to uniformly coat surfaces shadowed from the vapor source, is especially important when coating a surface which has lands and grooves. Therefore, the ion plated coating with its graded interface and uniform thickness should be an excellent method of protecting gun tubes against erosive wear.

Conventional ion plating methods work well when coating flat or outside surfaces but fail when attempting uniform coatings on the inside surfaces of tubes having a large length to diameter ratios. Consequently, a high current hollow cathode discharge chromium vapor source has been developed to allow ion plating in a cylindrical geometry.

EXPERIMENTAL APPARATUS AND PROCEDURE

The details of the gas fed hollow cathode discharge (HCD) gun are shown in figure 1 and are fully described in references 5 and 6. The cathode assembly consists of a thin walled Ta tube, two additional concentric, tubular Ta radiation shields and a thick walled Cu outer shield, all coaxially mounted in a water-cooled holder. In these experiments, a hollow cathode 30 cm in length was used. At a given gas flow rate, cathode diameter (d), and pressure (p), a pressure gradient is developed along the tube. The cathode wall temperature has a maximum where the condition pd=constant is satisfied. The material to be evaporated, Cr pellets, are centered at the position of this maximum temperature for the gas flow rate desired and the vapors are removed from the cathode through atomic collisions with the working gas.

The experimental set-up, shown in figure 2, consists of a moveable cylindrical substrate, a stationary cathode and anode, and their associated power supplies. After the discharge is started with a high voltage, low current supply, the temperature rises, causing a drop in the cathode voltage and a low voltage, high current (50Amp) supply takes over. Typical operating parameters are: a) cathode to anode current of 15 Amps, b) gas flow rate of 4ml/min, which for our particular vacuum system results in a pressure of 20 millitorr, and c) a negative substrate bias of 250 Volts. The low substrate bias of 250V and low pressuree of 20 millitorr are major points of departure from the conditions in conventional ion plating. Due to the shorter mean free paths at operating pressures of 100 millitorr in conventional systems, the average energy of the atoms striking the substrate is approximately five percent of the bias voltage, typically several kilovolts. The average energy of the atoms at the lower pressures used in this experiment is closer to the bias voltage since fewer gas collisions occur due to the longer mean free path. In addition, the higher pressures in conventional ion-plating geometries cause some of the atoms sputtered from the substrate to be returned to it through gas collisions to form the graded film-substrate interface. The confined nature of

the cylindrical geometry, however, guarantees a high probability that a sputtered atom returns to the substrate to form the graded interface desired.

Radiation from both the cathode and anode is the major source of heat generated in this plating process. In order to keep this radiation from raising the substrate temperature above the austentite/martensite transformation temperature of about 600 deg C, both the anode and cathode were water cooled. The resulting temperature profiles in the substrate, as measured by embedded thermocouples, are shown in figure 3. From this figure it can be seen that the maximum temperature does indeed stay below the critical value. The small temperature increase from 15 to 80 millitorr pressures was the result of increased ion current heating of the substrate.

RESULTS AND DISCUSSION

A series of experiments was conducted to determine the pressure dependence of various parameters using the HCD vapor source. Plating efficiency, throwing power and substrate power were measured and plating uniformity was subjectively evaluated.

The plating efficiency was determined by measuring the film thickness and mass of Cr evaporated. The ratio of the film thickness to the mass of Cr evaporated was then plotted as a normalized thickness. The throwing power was determined by using a 20mm by 40mm microscope cover-slide facing the Cr vapor source. After being coated, the Cr thicknesses were measured on the front and rear surfaces, their ratio being reported as the throwing power. As would be expected, the Cr coating on the rear of the cover glass was not uniform but still provided information about the pressure range for operation of the vapor source. The power dissipated in the substrate was determined from the measurement of the ion current (I) and the substrate bias voltage (V). Since the ions lose some energy in gas collisions, the substrate bias voltage is not an exact measure of the ion energies. Consequently, the substrate power (IxV) is only a relative measure of the average temperature of the substrate. The results of these tests, as shown in figure 4, indicate that the pressure range of 25 to 50 millitorr was best for ion plating with the HCD vapor source. These pressures are approximately a factor of three lower than are normally used in planar ion plating geometries.

The subjective aspect of these tests was performed by ion plating 3/4" x14 TPI brass nuts at various pressures. The plated nuts were sectioned and a visual appraisal of the coatings was performed whereby plating thickness and throwing power were noted. These evaluations were in good agreement with the above, more quantitative measurements.

Typical plating rates of 1 μm/min per centimeter of tube length were observed at a 20 millitorr pressure. This rate decreased at higher pressures due to increased sputtering.

The ion plated chromium films were characterized by Ion Beam Analysis (IBA), electron microscopy and a number of subjective tests.

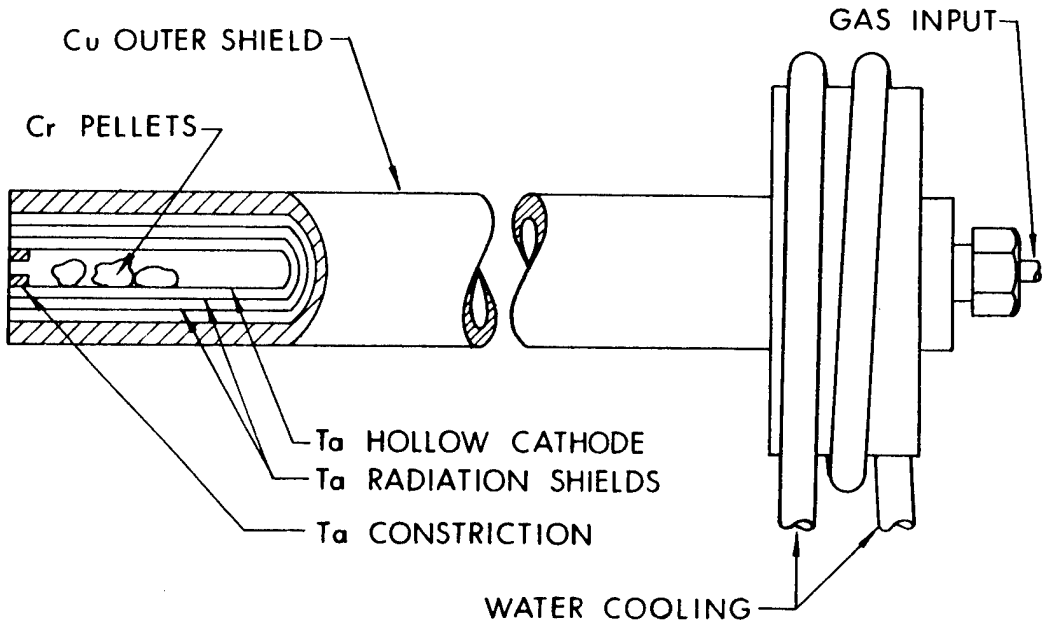

Figure 1. Hollow Cathode Metal Vapor Source.

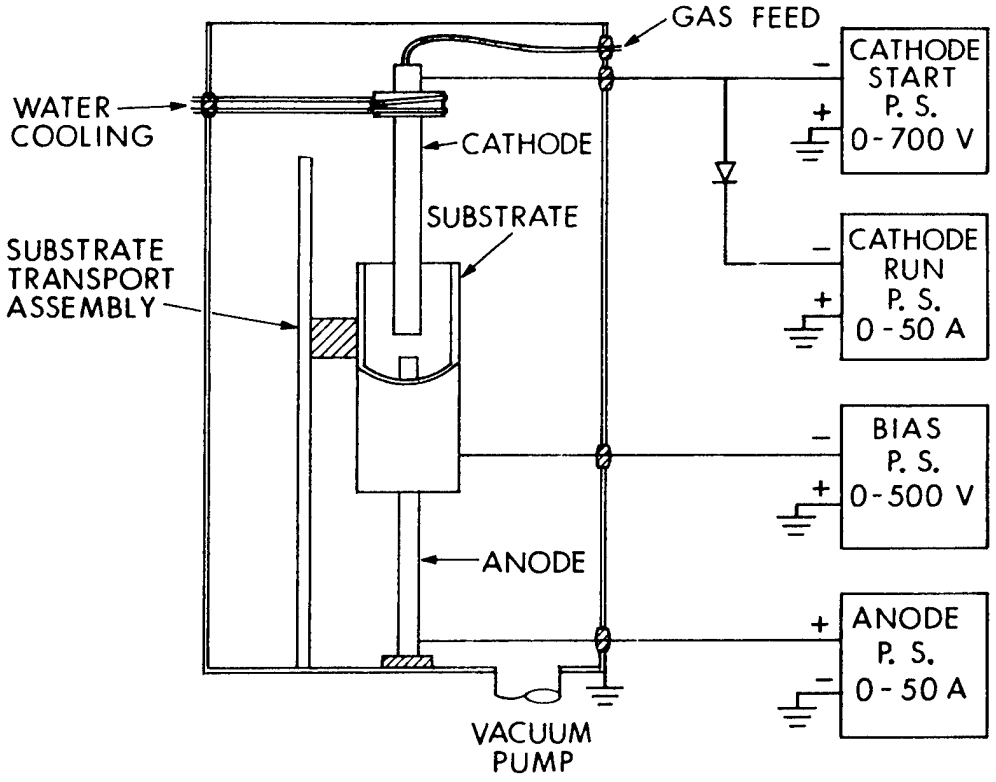

Figure 2. Schematic of the Plating Apparatus.

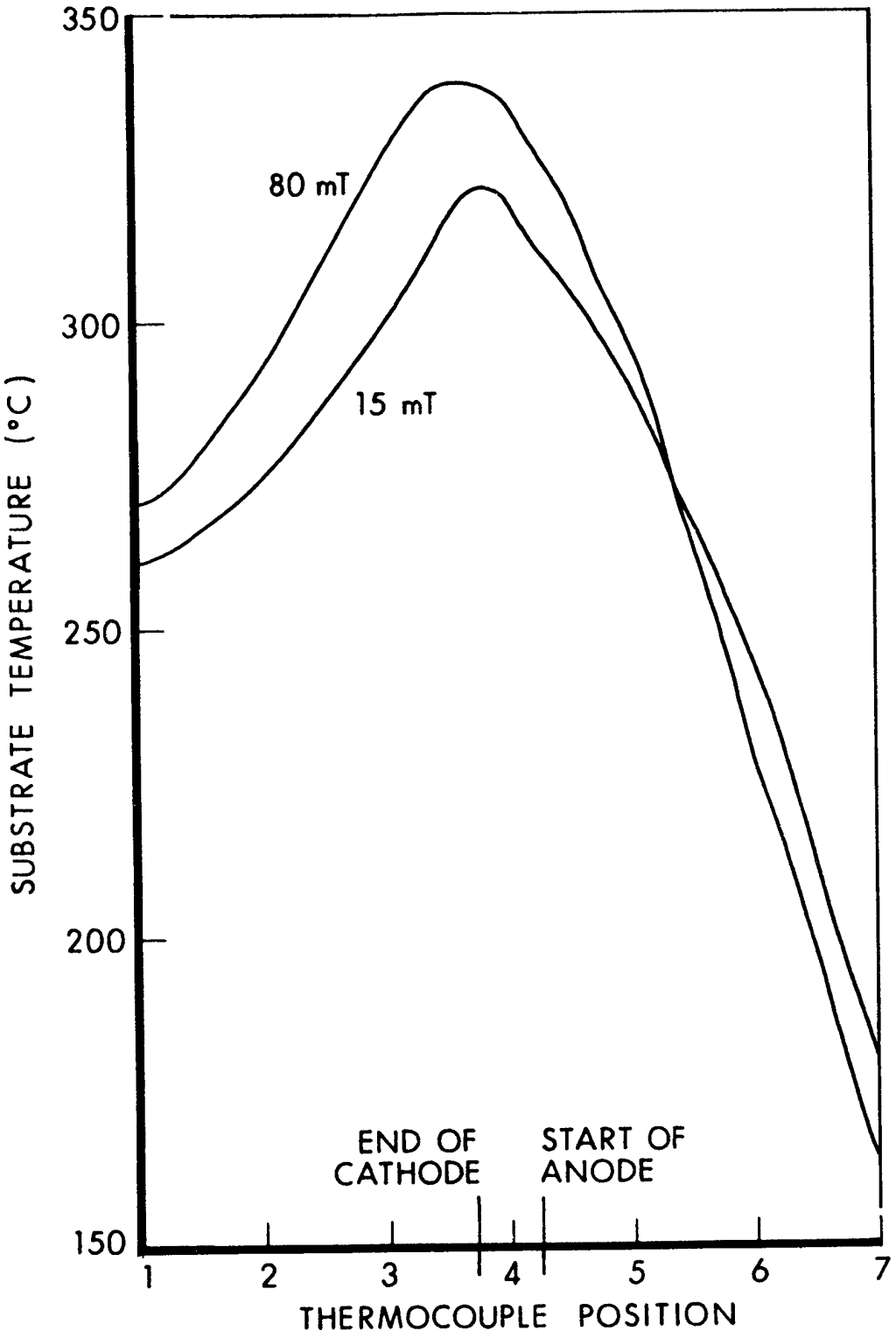

Figure 3. Substrate Temperature Profile with Cathode-Anode Cooling.

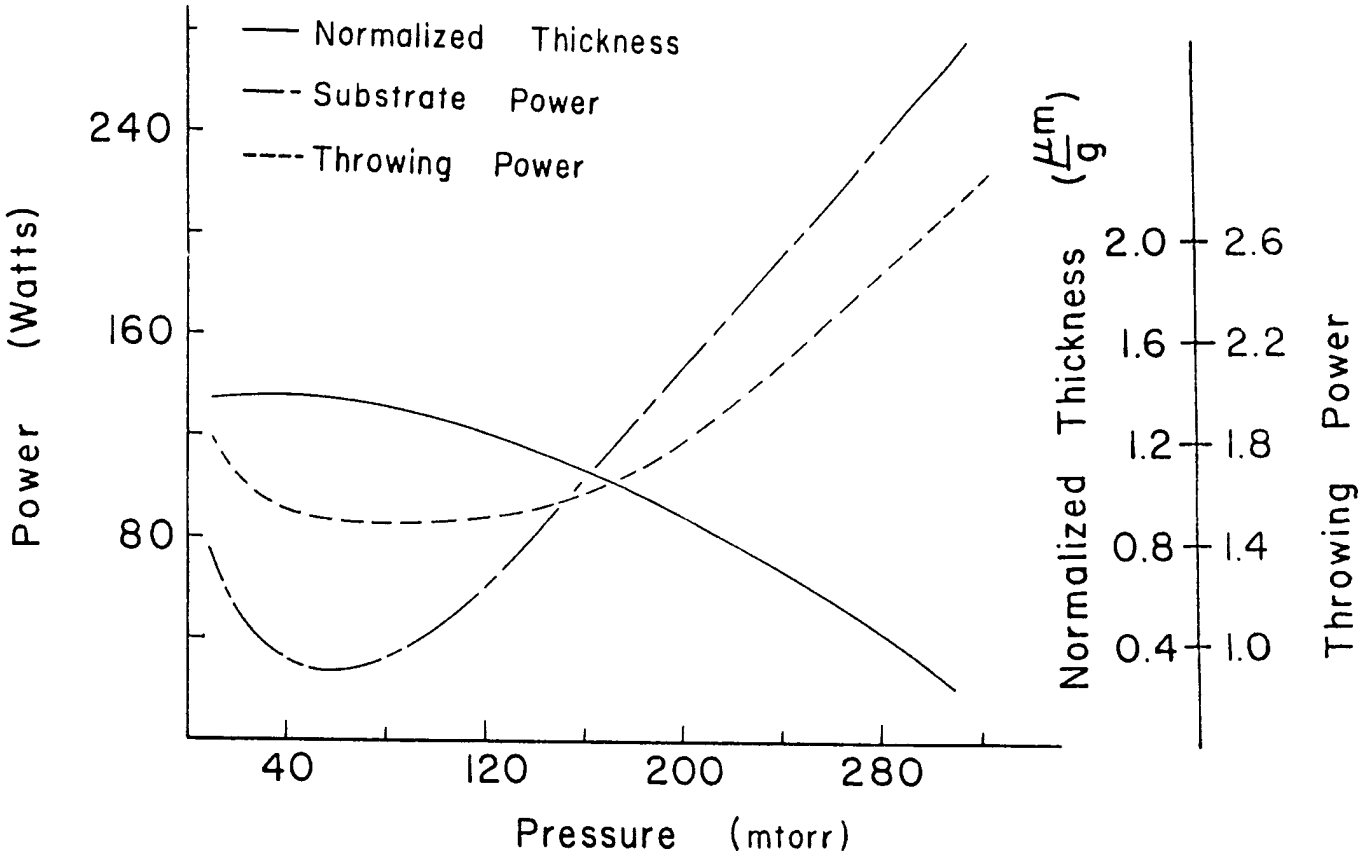

Figure 4. Working Gas Pressure Effects on Ion Plating.

IBA has been found very useful in depth profiling of the various elemental constituents of a surface[7]. The feature of ion plated films which lends itself ideally to such IBA is the expected graded interface between the film and substrate. To study this feature, a roughly 1 μm thick film of Cr was plated onto Cu. Cu rather than Fe was chosen as the substrate because thermal diffusion between Cr and Cu is minimal while Cr diffuses readily into Fe. Consequently, the effect of the ion plating mixing mechanism can be measured in the Cu/Cr system with no ambiguity. The thickness of the Cr film could not exceed about 1 μm for this study because IBA cannot probe deeper into the surface with accuracy. The results of this measurement are shown in figure 5 where the concentrations of Cr and Cu are shown as a function of depth. 1mg/cm^2 of Cr and Cu translates to approximately 1.3 μm. As can be seen, the Cr and Cu are intermixed over a depth of more than 1 μm. The structure that is seen is real and is due to the fact that the substrate was swept past the cathode opening three times. It is expected that this type of broad interface will provide for very strong bonding between the film and substrate.

The next phase of the experiment was the investigation of plating uniformity over lands and grooves as would be found in gun tubes. To this end, grooves were cut in the inside of a 30mm dia. by 15cm long Cu tube. The tube was swept past the plating region 10 times in 30 minutes. Micrographs, figure 6, show a 5 μm, uniform plating thickness on the 'lands', and plating which is continuous with approximately a factor of two difference between the thickest and thinnest portions of the film, with the thin sections lying in regions on the wall shadowed from the HCD source. The factor of two difference between the thick and thin sections of the coating can be decreased by plating at a higher pressure with the only disadvantage being a slightly lower plating rate.

A series of highly subjective tests on these and other plated samples, consisting of scratch tests, scouring with abrasive material, bending of substrate with plate and polishing all were consistent with a strongly adhering, hard film.

CONCLUSIONS

We have developed a method which is capable of ion plating the inside surfaces of gun tubes with little restriction on their length. The films produced by this process have large graded film-substrate interfaces even for materials such as chrome and copper in which thermal diffusion is negligible. The extended interface is a result of utilizing the confining geometrical nature of a tube to contain and intermix the deposition and substrate atoms. The present experiments have also shown that the plating is uniform over simulated lands and grooves. These results show that the process is a feasible method of protecting gun tubes against erosion.

ACKNOWLEDGEMENTS

The authors wish to acknowledge the efforts of the following without whom this work would not have been successful: Drs. D. Eccleshall, K.A. Jamison, and T. Leete and Mr. P. Yunker.

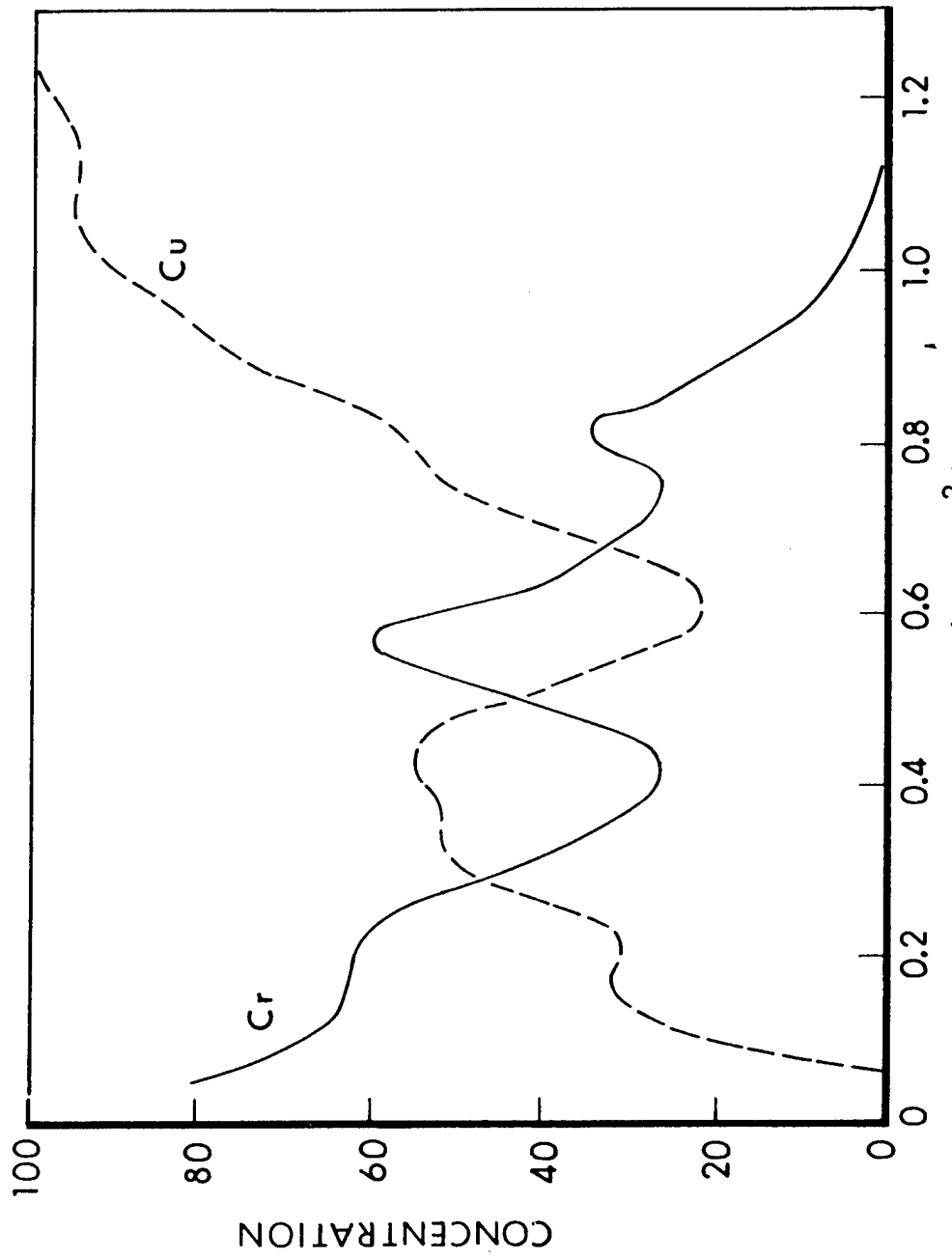

Figure 5. Concentration Depth Profiles of a Chrome Film on a Coppper Substrate.

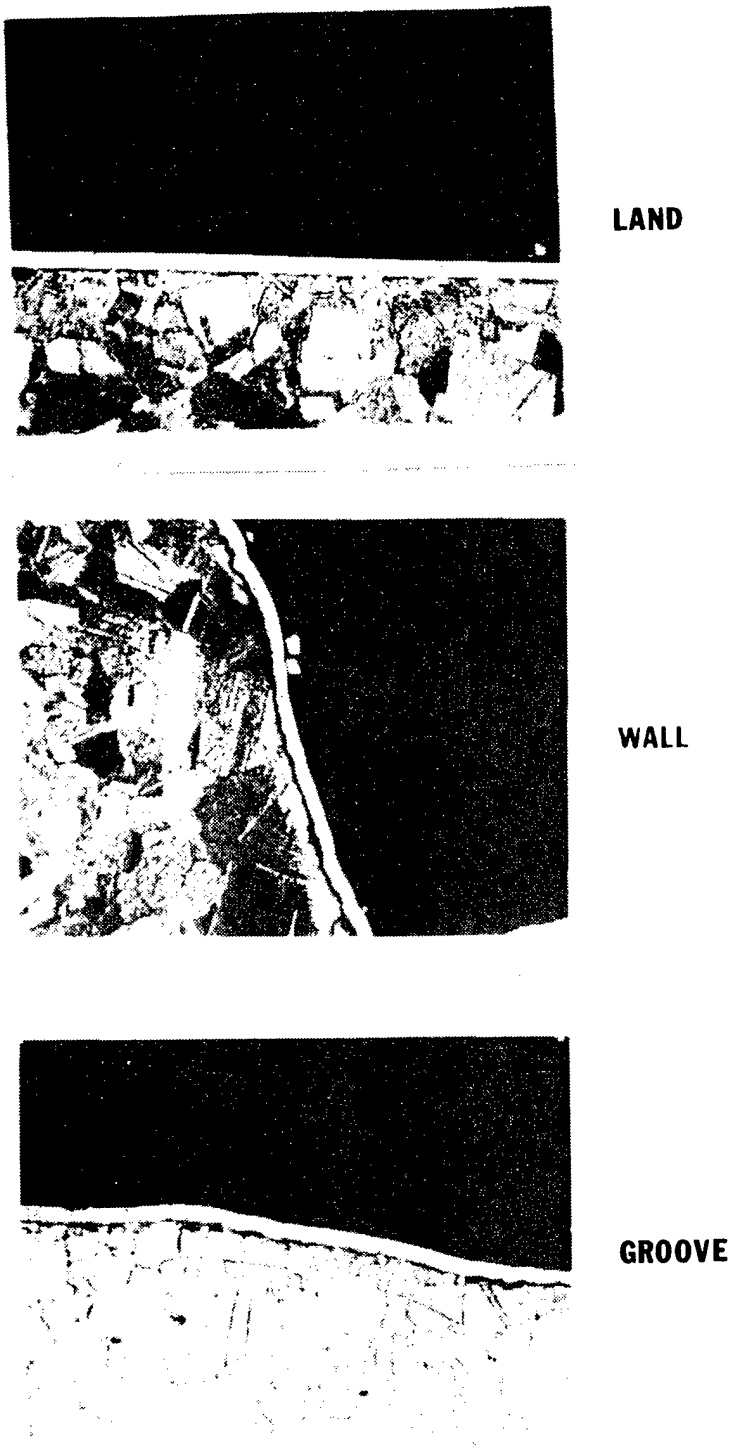

Figure 6. Photomicrographs of a Chrome Coated Copper Substrate with Simulated Rifling.

REFERENCES

1. C.R. Musick, Final Report Product Improvement Test of Cannon, 105mm (10-mil Chrome Plate), APG-MT-5516, May 1981.

2. R.L. Cullinan et al., Study of Erosion Resistant Materials for Gun Tubes, Part I, ARLCB-TR-80027, December 1098.

3. D.M. Mattox, Fundamentals of Ion Plating, J. Vac. Sci. Tech., 10, No.1, Jan/Feb 1973.

4. D.G. Teer, Adhesion of Ion Plated Films and Energies of Deposition, J. Adhesion, 8, 289 (1977).

5. W.F. Henshaw, J.R. White and A.Niiler, A Hollow Cathode Discharge Source of Metal Vapor, ARRADCOM Patent Application Docket 53-81, September 1981.

6. W.F. Henshaw, J.R. White and A. Niiler, Ion Plating Chrome Coatings in Tubes, BRL Report in press.

7. A. Niiler, R. Birkmire and J. Gerrits, PROFILE: A General Code for Fitting Ion Beam Analysis Spectra, BRL Technical Report ARBRL-TR-02233, April 1980.

ELECTRODEPOSITION OF REFRACTORY METAL COATINGS (TANTALUM AND COLUMBIUM) FROM FUSED SALT ELECTROLYTES

I. Ahmad, G. J. Janz*, J. Spiak*, and E. S. Chen
US Army Armament Research and Development Command
Large Caliber Weapon Systems Laboratory
Benet Weapons Laboratory
Watervliet, NY 12189

INTRODUCTION

One of the important measures to control erosion in gun barrels used for the last 50 years is the application of coatings. However, chromium is the only one which has been applied in both small and large caliber guns with various degrees of success. It can be easily applied from aqueous electrolytes at a reasonable cost. Unfortunately, even the best of conventional chromium coating as plated is highly stressed, very brittle, and invariably full of microcracks (Figure 1). It chips and spalls off at various stages of firing unpredictably. This weakness of chromium coating has not yet been brought under control.

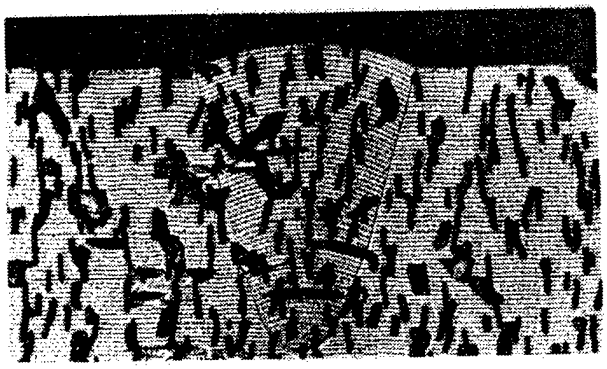

Fig. 1. Conventional chromium coating (from 120 mm M256 tube plated by "pump thru" process. Heavily etched X500).

At Benet Weapons Laboratory, we therefore decided to explore[1] other erosion resistant refractory metals which are not as brittle as chromium, are available at a reasonable price, and can be plated in gun barrels with relative ease. On the basis of these criteria the potential metals are shown in Table I. Those not in the shaded area are either too reactive and expensive or are scarce. Of those in the shaded area, tantalum and columbium were selected for the first phase study, as they are ductile, have low ductile to brittle transition temperatures (Figure 2), and have lower elastic modulus (27×10^6 and 15×10^6 psi respectively) than steel (therefore their coatings could easily transfer load to the substrate without being overstressed). Molybdenum and tungsten have high elastic modulii (55×10^6 and 42×10^6 psi respectively) and high DBTT. Therefore, in order to use them effectively they will have to be placed under a compressive stress state; otherwise they will have the tendency to fracture on pressure cycling during firing.

*G. J. Janz and J. Spiak are from Rensselaer Polytechnic Institute, Troy, NY.
Distribution limited to US Government Agencies only because of test and evaluation; September 1982. Other requests for this document must be referred to Commander, ARRADCOM, ATTN: Benet Weapons Laboratory, DRDAR-LCB-RP, Watervliet, NY 12189.

TABLE I. POTENTIAL EROSION RESISTANT ELEMENTS AND THEIR m.p. °C.

IVA	VA	VIIA			VIII
Ti	V	Cr			
1668	1890	1875			
Zr	Cb	Mo	Tc	Ru	Rh
1852	2468	2670	2140	2250	1960
Hf	Ta	W	Re	Os	Ir
2150	2996	3410	3180	3000	2410

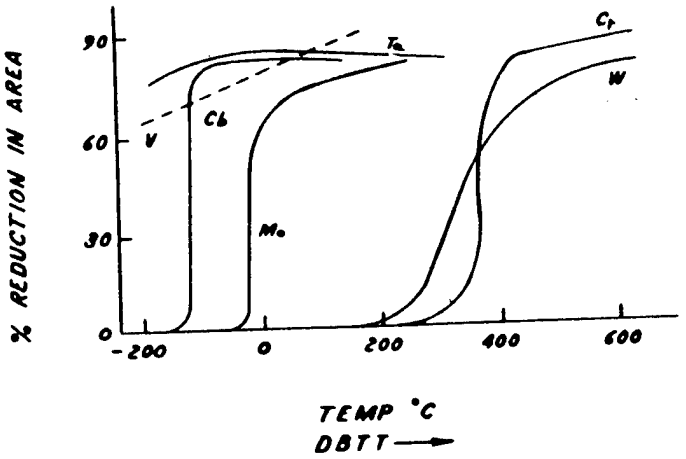

Fig. 2. Ductile to brittle transition temperatures of some refractory metals.

Unlike chromium, as shown in Table II, none of these metals can be electroplated from an aqueous electrolyte. In the initial studies chemical vapor deposition was investigated. However, because of difficulty of controlling the impurity pick up and the very high temperature (1000-1100°C) of deposition required, it was given up. Sputtering has an advantage that the substrate temperature does not exceed 300-400°C, but, it requires expensive set up. Also, it is a line of sight deposition process and therefore could present difficulty, if used for coating rifled barrels. In view of the advantage of the low deposition temperature however, this process is being investigated as a part of the long range program at BWL. Results obtained thus far will be reported by Mr. Cox.

TABLE II. METHODS OF APPLYING COATINGS OF REFRACTORY METALS

Processes	Materials	Limitations
Vapor Deposition		
Chemical		High Temperature, Impurities
Sputtering	Cr Ta Cb Mo W	Line of Sight, Impurities
Plasma Spray		Porosity, Impurities
Electrodeposition		
Aqueous Electrolyte	Cr	Stresses, Cracks
Fused Electrolyte	Cr Ta Cb Mo W	High Temperature
Diffusion		
Metalliding	Alloys & Compounds	Only thin coatings

The process which yields very pure ductile refractory metal coatings at moderate temperatures (700-850°C) is the electrodeposition from fused salt electrolytes. Although electrodeposition of metals from fused salt baths has been studied for more than 50 years, it was in 1964, that Senderoff and Mellor[2] reported a general process for the deposition of pure, coherent coatings of IVA, VA, and VIA group metals from a solution of the fluoride of the metal to be deposited in the eutectic mixture of KF-LiF-NaF (also called FLINAK). The conditions found to be the best for the electrodeposition of these metals are summarized in Table III. It was established that for the maximum anodic and cathodic efficiency (which in most cases approach 100 percent) the salts must be free of moisture, oxides, and other halogens, and the atmosphere used in the cell - usually argon, must be of high purity. In addition to the temperature, the oxidation state of the metal in the solution was critical. According to Senderoff, for coherent deposits it is necessary that the electrolyte contained a complex with correct thermodynamic stability. Insufficient amounts of stable complex ion will make available dissociated cations in high concentration and will hence give powdery or dendritic deposits. Too stable a complex will require high deposition potential, which could result in codeposition of alkali metals from the electrolyte. Presence of K^+ was also found to be important. Fordyce and Baum,[4] by infrared analysis showed that $[TaF_7]^{-2}$ was the main complex in the electrolyte in which K_2TaF_7 was added as a source of tantalum. By using the chronopotentiometric technique, Senderoff et al[5] deduced that the reduction of this complex took place in two steps.

$$[TaF_7]^{-2} + 3e \rightarrow TaF_2 + 2F^- \quad (1)$$

$$TaF_{2(s)} + 2e \rightarrow Ta^o{}_{(s)} + 2F^- \quad (2)$$

The first step is diffusion controlled and highly reversible, while in the second step reduction of both the solid and dissolved TaF_2 to Ta^o is irreversible. Likewise in columbium deposition, CbF formed is either solid or in solution and is reduced to Nb^o irreversibly. Probably the formation of the insoluble phase (TaF_2 or CbF) may be responsible for providing additional nucleation sites and hence promoting the formation of smooth coherent coating rather than dendrites.

TABLE III. CONDITIONS OF PLATING REFRACTORY METALS FROM FUSED FLUORIDE BATHS

Metal	Salt	Temp°C	Current Density Ma/cm^2	Oxidation State	Remarks
Tantalum	K_2TaF_7	725-775	5-100	+5	Process Well Developed
Columbium	K_2CbF_7	725-775	5-100	+4.2	Good Coating
Chromium	K_3CrF_6	775-850	5-50	+3	Process Less Developed
Molybdenum	K_3MoF_6	700-750	5-100	+4	
Tungsten	WF6 (Bubble)	700-750	5-100	+4.5	

The currently used gun steel is a tempered martensite, with a room temperature yield strength in the range of 160-180 ksi (hardness 30-35 RC). This steel is known to lose its temper and hence its strength when heated above about 500°C. The deposition temperature for Ta and Cb from their respective electrolytes, as mentioned earlier is 700-850°C. Therefore as such, these coatings could not be applied in the gun barrel directly, without damaging the mechanical properties of the gun steel.

This problem was overcome by applying the coating in a suitable liner, which was then shrink fitted in the gun barrel. For the initial studies M24A1 gun barrel was selected as a test vehicle. The liner used for this gun is shown in Figure 3.

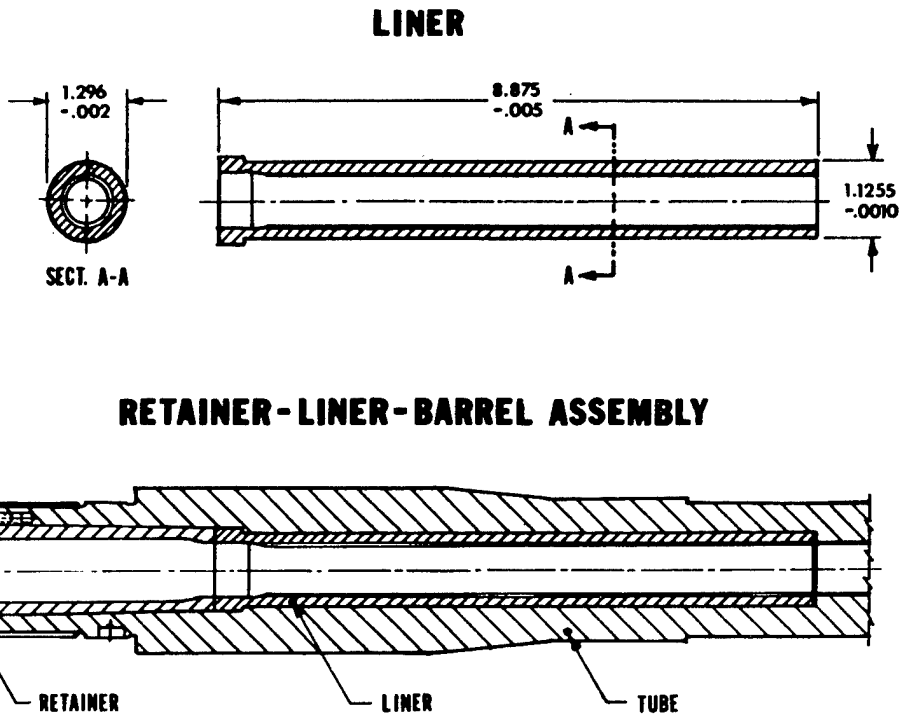

Fig. 3. Sketch of the 20 mm liner and the retainer-liner-barrel assembly.

Because of their size, it was not possible to apply tantalum/columbium coating in the liner in the laboratory. They were plated by GMTC, Richmond, VA, the only outfit in US with the facility to plate tantalum and columbium from fused salts. In this paper results of both the lab studies on the electrodeposition of Ta, Ta-Cr, and columbium alloys and the evaluation of the coated liners before and after test firing is summarized.

ELECTROPLATING CELL

The electrodeposition cell used in the lab was essentially similar to the one described by Senderoff and Mellor,[3] and is illustrated in Figure 4. The cell used by GMTC is also similar in design, albeit is large enough to plate objects up to 22 inches long, and 12 inches in diameter.

Anhydrous LiF, KF, and NaF salts are mixed in the ratio 26.2:10.5:47.0 by weight and premelted in a graphite crucible in order to remove residual moisture and oxygen. (Binary eutectic mixtures can also be used, for which higher deposition temperature is required.) The solidified slug is then transferred to the nickel crucible. Dried K_2TaF_7 (10-15 wt. %) is added. The crucible containing these salts is placed in the reactor. The anode is a single rod or a bundle of rods of tantalum positioned carefully with respect to the cathode (i.e. a flat coupon or the liner).

Prior to actual plating the system is evacuated and thoroughly purged with high purity argon. All precautions are taken to exclude moisture or air. The electrolyte is melted and equilibrated at 800°C. It is then preelectrolyzed to remove residual oxide, moisture, and other impurities such as Fe. Completion of preelectrolysis is indicated by smooth coating on the test coupon. The electrode assembly is then withdrawn in the air lock. The gate valve is closed. After the electrodes have cooled down, they are removed. The item to be plated, appropriately fixed at the cathode is positioned with respect to anode. The assembly is then returned to the air lock, which is then purged with argon. The gate valve is opened and the electrode assembly then lowered in the region just above the electrolyte for preheating. After 0.5-1 hour, it is then immersed in the electrolyte. For a smooth coating of high quality 5-10 ma/cm^2 is preferred. For a 5 mil coating 14-16 hours of plating time is required. A typical coating obtained is shown in Figure 5. A similar set up and condition are used for columbium coating with K_2CbF_7 as the source of columbium.

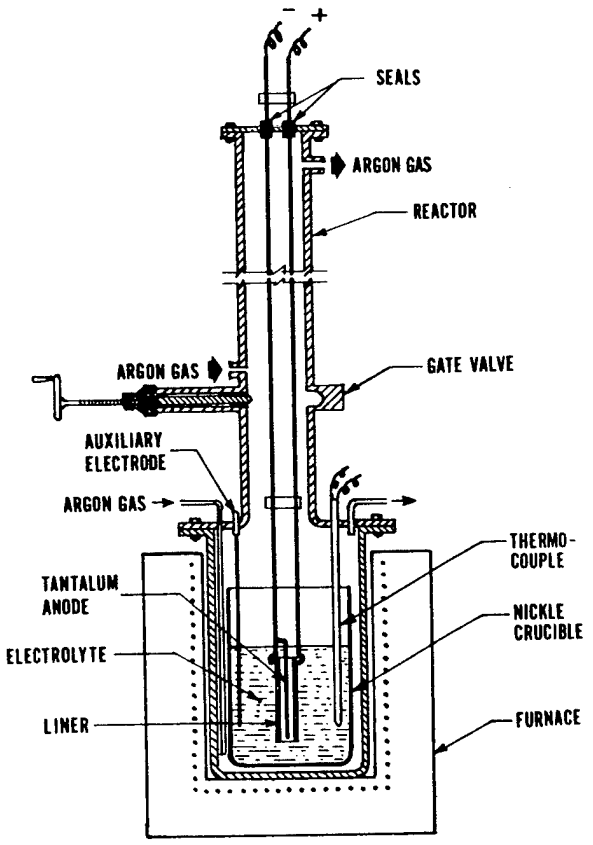

Fig. 4. Electroplating cell.

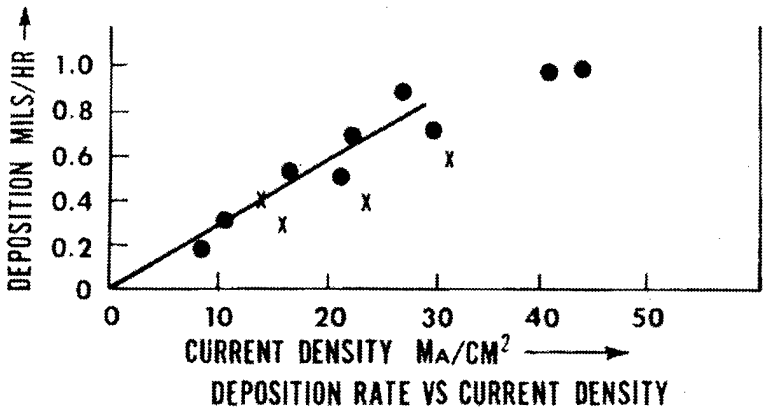

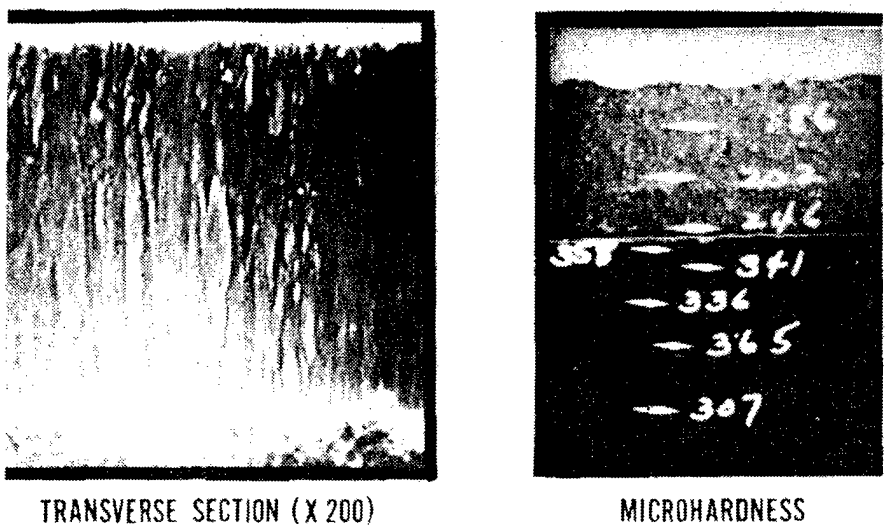

Fig. 5. A typical tantalum coating deposited from fused fluoride bath.

EVALUATION OF Ta IN 20 MM LINERS

Figures 6(a) and (b) show a 20 mm liner coated with 5 mil tantalum. Note the uniformity of the thickness and absence of any nodules and gross surface roughness. Such a liner coated with 5 mil tantalum was shrink fitted in a 20 mm M24A1 barrel which was test fired. The details of this test are described by Cullinan et al.[5] In the first liner, excessive deformation of lands was noticed which was traced to the slow cooling of the liner after withdrawing of the melt. The hardness of the liner had decreased to RC 20. In the second liner, steps were taken to achieve faster cooling which resulted in the recovery of the hardness of the substrate to about 30 RC. This liner when test fired, although showed some deformation, gave excellent erosion protection as is shown by Figure 7, in which the bore enlargement at 0.5 inches from the origin of the rifling as a function of number of rounds fired is plotted. For comparison, an unplated liner and a conventional HC chromium plated liner were also test fired under the same conditions and their data are included in this figure.

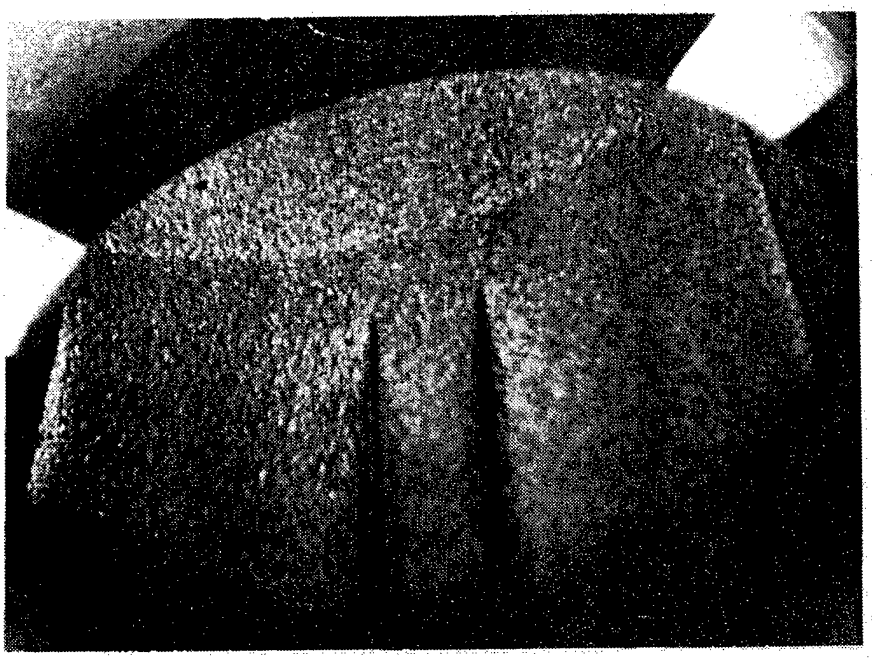

(a) Coated surface in the origin of rifling area.

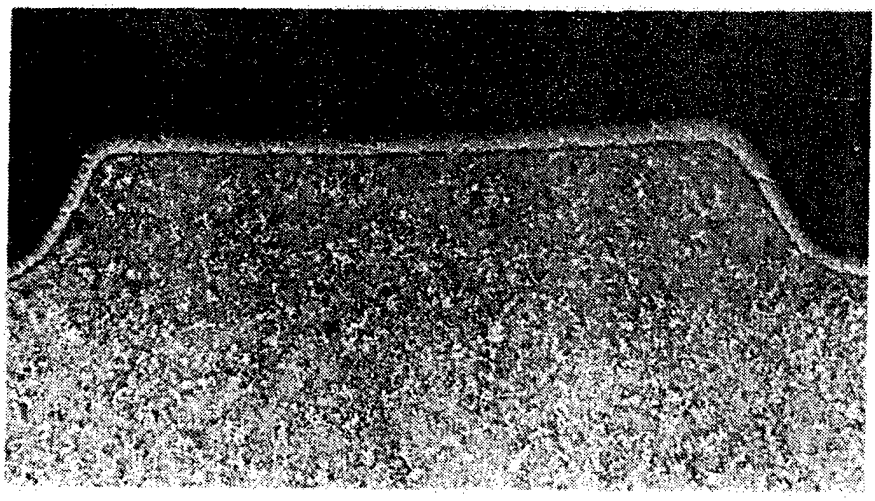

(b) A transverse section of the coated tube.

Fig. 6. Tantalum coating in a 20 mm liner.

The liners were sectioned after test firing and examined metallographically (Figure 8). While the chrome plated liners showed loss of the plating and considerable erosion in the origin of rifling area and down bore, the tantalum coating remained intact even after 5000 rounds.

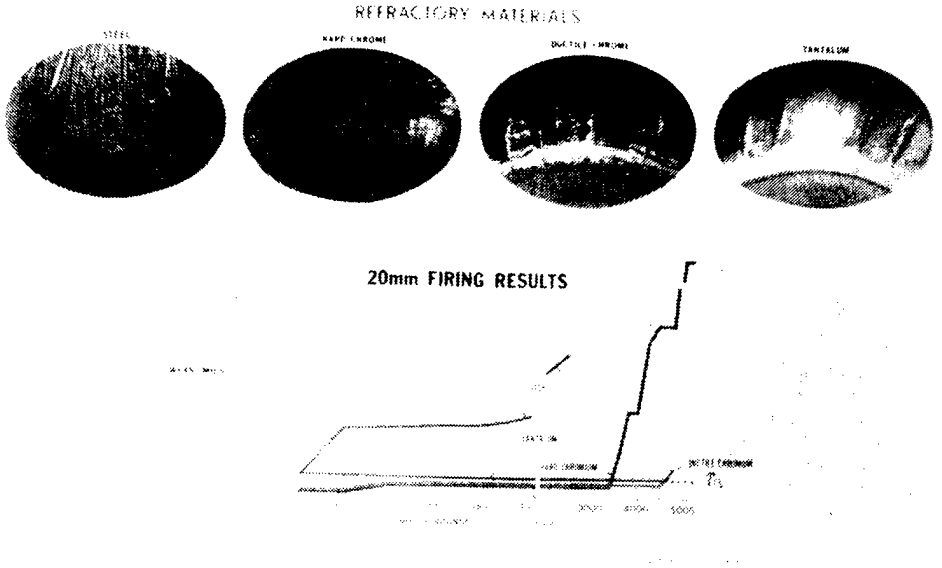

Fig. 7. Firing data of tantalum liners. Erosion vs. number of rounds. Inset are the borescope views of O.R. of unplated steel, chrome plated and tantalum plated steel liner.

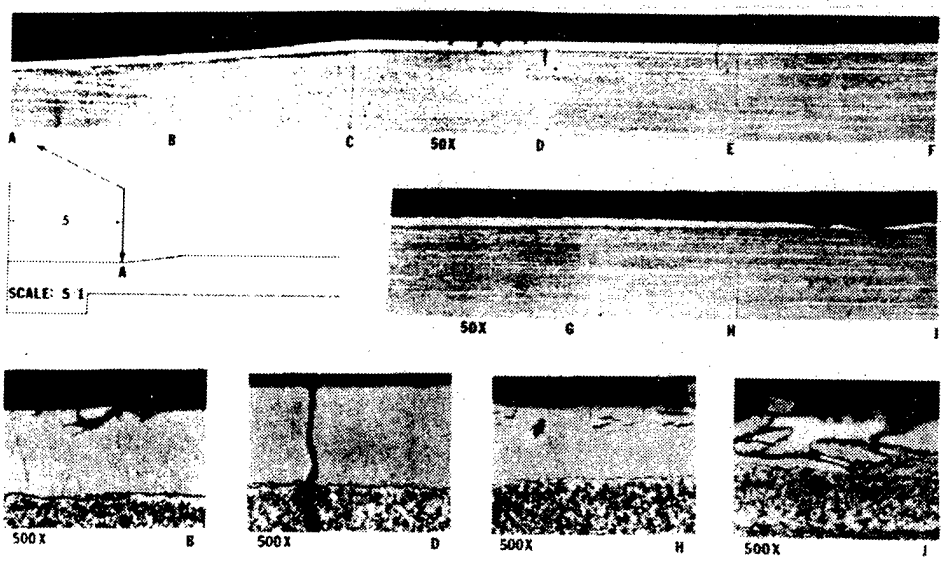

Fig. 8. Longitudinal section of a 20 mm liner after 4923 rounds. Cracking in area J could be due to the presence of β-tantalum at the interface.

Encouraged from these results, investigations were made to plate 105 mm liners (Figure 9). Details of this work will appear in another technical report. The main conclusion of this study was that by this technique it was possible to coat these larger liners at affordable cost, e.g., $600-900 per liner. The shrink fitting of these liners in a full scale gun and test firing results will be described by Aalto in this symposium. The dimensional stability of the liner and uniformity of coating, are some of the areas which are being presently investigated. The effect of the coating on the mechanical properties such as yield strength, hardness, Charpy impact strength are summarized in Table IV. It shows that the room temperature properties of gun steel used in 105 mm M68 are not adversely affected by tantalum coating process. The hot hardness of steel is still of concern, because it could swage by the engraving stress of the round. This prompted investigation of other substrate alloys such as Pyrotool V, CG27, etc. which are known to retain their hardness at elevated temperatures (see Figure 10). Two other problems became apparent in this study.

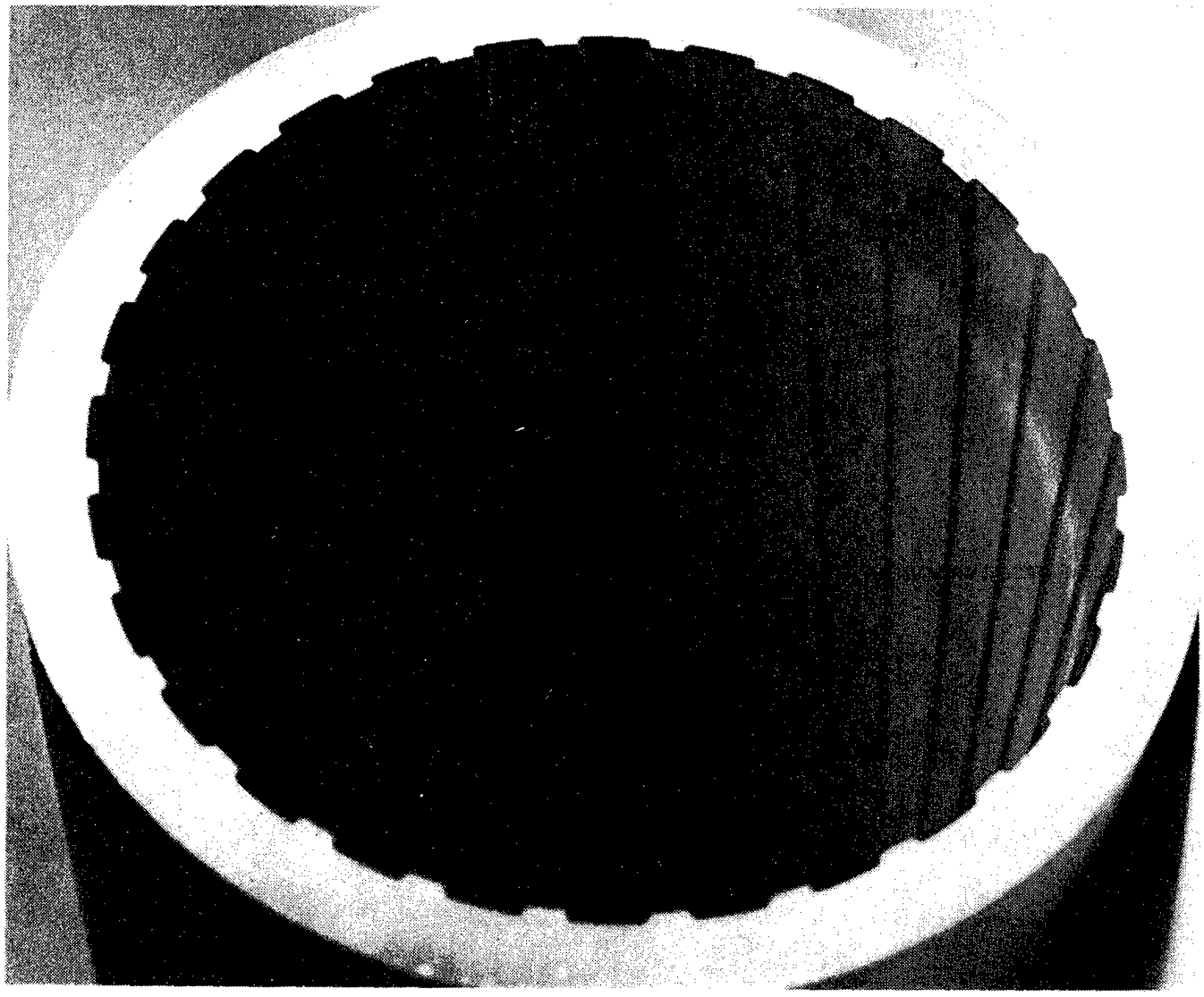

Fig. 9. A view of 105 mm liner coated with tantalum by GMTC.

TABLE IV. EFFECT OF PLATING CONDITIONS ON THE MECHANICAL PROPERTIES OF GUN STEEL (105 MM M68)

	UTS KSI	0.1% YS KSI	ε%	RA%	Hardness RC
As Received	193	178		41.6	40.5
After Exposure to 800°C for 12 hrs	193	119-136	10.3	27.0	40.0
Tantalum Plated	180	98.8	12.3	37.5	40.0

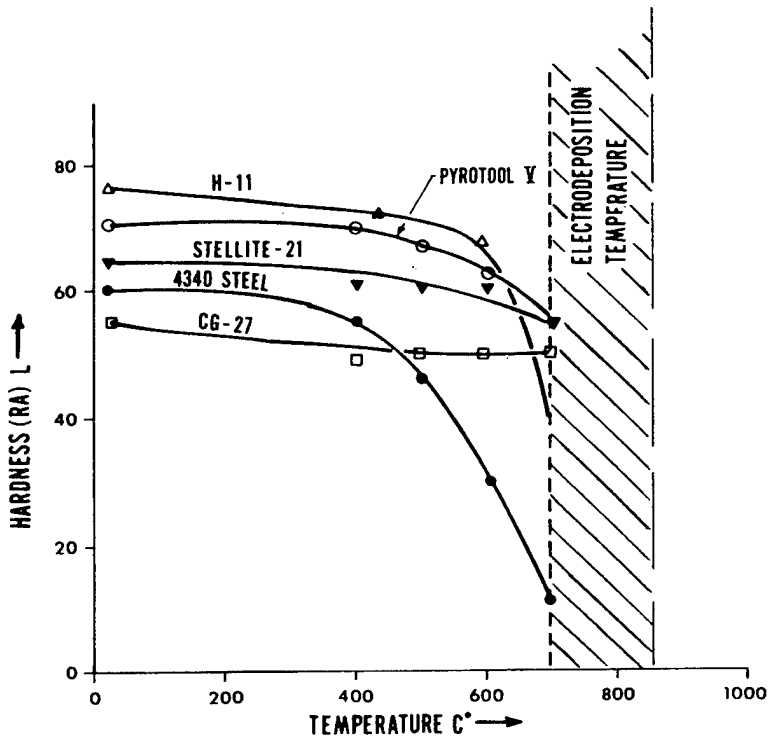

Fig. 10. High temperature hardness of some alloys.

a. Metallographic examination of some tantalum coated liners (both 20 mm and 105 mm) showed that in some regions (particularly at the land corners) a very hard phase nucleated at the coating substrate interface (Figure 11). It was identified by x-ray diffraction analysis to be β-tantalum.[6] It is slightly brittle and can be a cause of debonding of the coating during firing. In fact, it was observed that in a liner made of Pyrotool V, the coating did debond, as shown in Figure 12. This may also be a cause of some chipping of tantalum in Figure 8 (area H). Details of this work will be reported elsewhere. Briefly the formation β-phase, which may be impurity (probably oxygen) stabilized phase, is considered to be due to high current density in areas which are closer to the anode (due to asymmetric positioning of the anode or the rifling profile). This condition was eliminated in 105 mm liners by carefully redesigning the anode. Instead of using a bundle of tantalum bars, the anode was a copper tube on which tantalum was electroplated uniformly. This anode was then concentrically positioned in the liner.

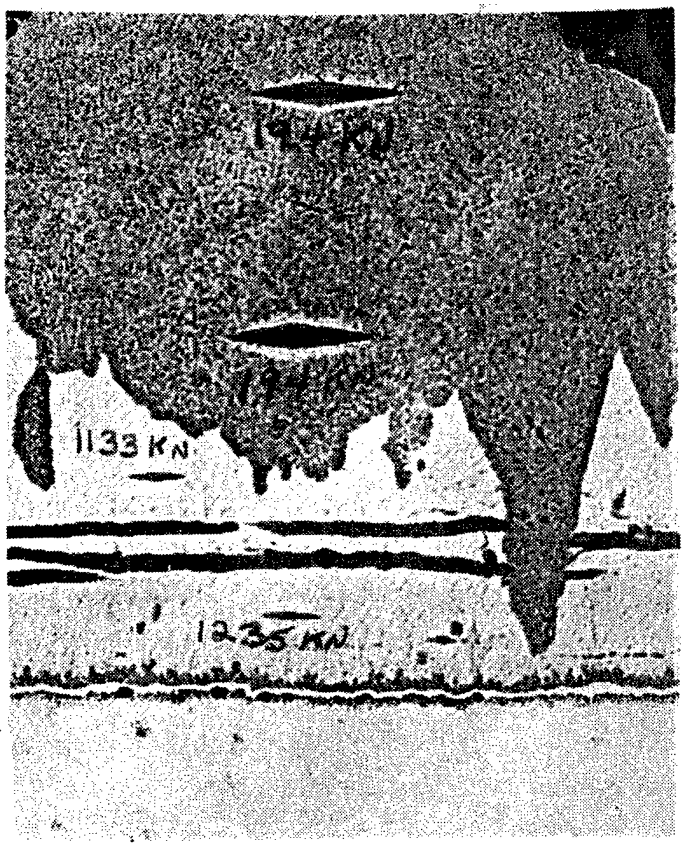

Fig. 11. β-Tantalum at the interface of tantalum coating and the land of the liner.

Fig. 12. Tantalum coating debonded from the substrate on firing. Notice β-tantalum at the interface.

b. As mentioned earlier, not only that the liner material has a tendency to become soft because of the exposure to 750-850°C for 14-16 hours, but the coating itself is very soft. Hence in the origin of rifling area, the lands and the coating tend to swage (Figure 13). So, as has already been stated, while other iron alloys with better elevated temperature properties such as CG27, Pyrotool V, H11 are being investigated, a systematic study was also made to improve the hardness of tantalum. This was accomplished by the codeposition of chromium with tantalum. Chromium was added in the electrolyte as K_3CrF_6. This did not effect the deposition rate of tantalum. The microstructure was slightly refined (Figure 14). The hardness was found to increase with the increase of the concentration of chromium as shown in Figure 15. The details of this work have already been reported.[7]

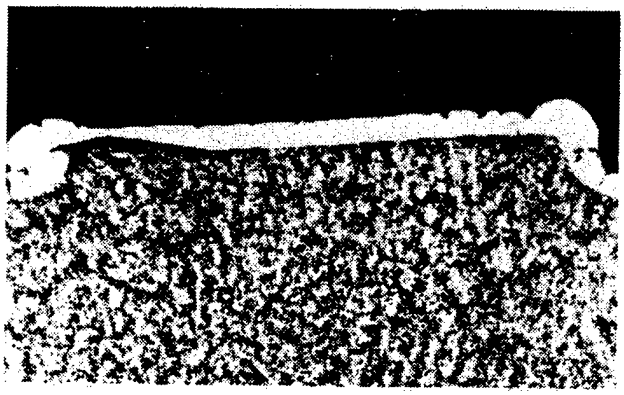

Fig. 13. Swaged lands and coating of tantalum coating liner fired in M24A1.

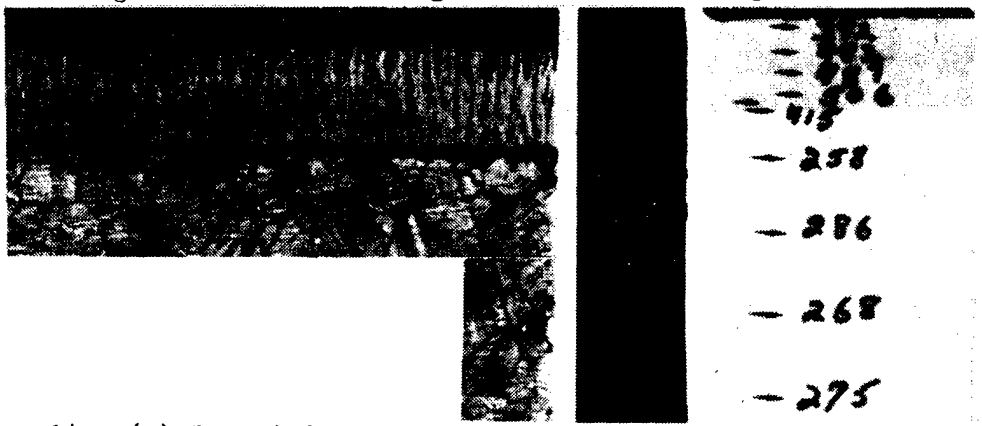

Fig. 14. (a) Deposition rate vs. current density.
(b) Microstructure and hardness of a deposit coating 0.5

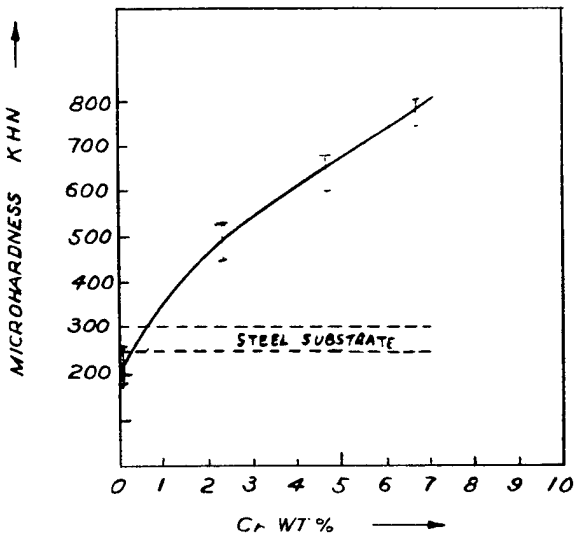

Fig. 15. Hardness vs. chromium content in tantalum.

COLUMBIUM

Using the same type of electrolyte cell as shown in Figure 4, columbium was also successfully coated (at GMTC) in 20 mm liners made of gun steel and Pyrotool V alloy (Figure 16). They are awaiting test firing.

A systematic laboratory study was made at improving the hardness of columbium by codepositing chromium. K_3CrF_6 in the quantities varying from 0.5-6.0 percent was added to the electrolyte. But in none of the compositions chromium codeposited with columbium.

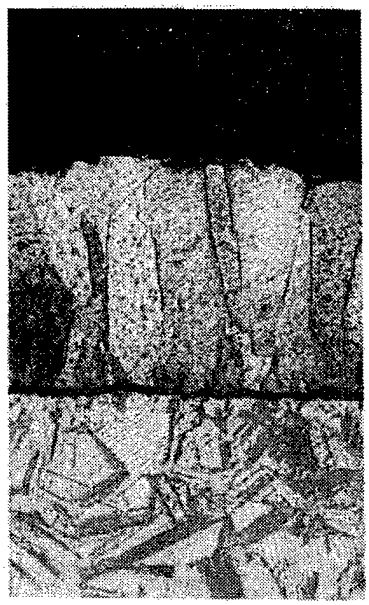

Fig. 16. Transverse section of a columbium plated specimen.

SUMMARY

1. The feasibility of plating tantalum and columbium in 20 mm liners has been demonstrated.

2. Firing tests have shown that tantalum did not chip off or crack even after 5000 rounds fired in 20 mm M24A1 gun barrels.

3. Tantalum has also been successfully applied in 20 inch long 105 mm liners, and the influence of the coating conditions on the mechanical properties has been determined.

4. The formation of β-tantalum at the coating-substrate interface has been identified. Also, conditions to eliminate this phase have been worked out.

5. Hardness of tantalum can be predictably increased (from 200 to 700 KHN) by codepositing 1-6 wt. % chromium. Alloying with chromium did not have undesirable effects either on the current efficiency or the microstructure of the deposit.

6. Columbium has also been coated in 20 mm liners of gun steel and Pyrotool V liners. Chromium could not be codeposited with columbium.

ACKNOWLEDGEMENTS

Thanks are due to Mrs. T. Brassard and Mr. L. McNamara for the metallography and scanning electronmicroscopic examination of the coatings, respectively. We also appreciate GMTC, particularly Mr. John Perry for coating the 20 mm and 105 mm liners, and openly discussing the problems encountered in developing the process parameters for improved coatings.

REFERENCES

1. Ahmad, I., et al, "Potential Erosion Resistant Refractory Metal Coatings for Gun Barrels," Proceedings of the Triservice Conference on Corrosion, AMMRC, Watertown, MA, 1978.

2. Senderoff, S. and Mellor, G. W., "Electrodeposition of Refractory Metals," U.S. Patent 3444058, May 13, 1969, Canadian Patent 658,456 (1964).

3. Senderoff, S., "Electrodeposition of Refractory Metals," Met. Rev., 11, 97-112 (1966).

4. Fordyce, J. S. and Baum, R. L., J. Chem. Phys. 44, 1159 (1966).

5. Cullinan, R. L., D'Andrea, G., and Croteau, P., "Study of Erosion Resistant Materials for Gun Tubes - Part I: 20 MM Liner Technology," ARLCB-TR-80027, December 1980; "Part II: Tantalum Coated Liners," ARLCB-TR-81011, April 1981, Benet Weapons Laboratory, Watervliet, NY.

6. W. D. Westwood and F. C. Livermore, "Thin Solid Films," 5, 407 (1970); L. G. Feinstein, Appl. Phys. Letters, 19, 137 (1971).

7. Ahmad, I., Spiak, J., and Janz, G. T., "Electrodeposition of Tantalum and Tantalum-Chromium Alloys," J. Appl. Electro-Chemistry II, pp. 291-999 (1981).

8. Ahmad, I., et al, "Studies of Erosion Resistant Refractory Metal Coatings for Advanced Gun Barrels," under preparation.

CHARACTERIZATION OF CRYSTALLOGRAPHIC STRUCTURE AND INTERNAL STRESS OF CHROMIUM COATINGS PLATED UNDER CURRENT INTERRUPTIONS

G. P. Capsimalis and E. S. Chen
U.S. Army Armament Research and Development Command
Large Caliber Weapon Systems Laboratory
Benet Weapons Laboratory
Watervliet, NY 12189

ABSTRACT

The effect of interrupted current (IC) plating on the visual crack morphology, crystallography, and residual stresses of electrodeposited chromium has been investigated. Varying the process parameters such as the on/off plating cycle and current density resulted in changing the crystallographic fiber texture of the deposit from the conventional <111> orientation to a combination of <211>, <111> and a small fraction of randomly oriented crystallites. Under these plating conditions, it was also found that (i) lower amounts of chromium hydride (CrH_x) occur in the deposit, (ii) a large decrease in the microcrack density of the deposit occurs, and (iii) the deposits tend to become compressively stressed.

INTRODUCTION

For over 30 years HC chromium has been used to extend the wear and erosion life of gun barrels. Its attractiveness results from its oxidation resistance and retention of hardness at elevated temperatures and its excellent resistance to friction and wear. The acceptance of electrolytically deposited HC chromium as a good protective coating is limited however, by the large tensile stresses and the well-known crack networks which are always present in the deposit. These two limiting factors being dependent upon the deposition conditions, proved to be the target of numerous investigations. The idea of plating conventional HC crack-free chromium has been reported by Saiddington and Hoey[1] and others.[2-4] Based on the observation that cracks do not form in chromium deposits until a critical thickness of about 0.5 um is reached, they have demonstrated[1] that by means of controlled current interruptions the microcracks can be effectively reduced or eliminated. Although there is no simple theory to explain the presence of stresses in electrodeposits, a number of comprehensive reviews[5,6] suggest that their origin is due to the crystal lattice defects which are trapped in the deposit during the electrocrystallization process. Likewise, the evidence from these articles and others suggest that the various plating parameters are the critical factors that control the residual stress of the deposit.

On the basis of the above evidence, the current work was undertaken to investigate the crystallography and residual stresses in electrodeposited chromium produced as a function of plating variables, as a means of formulating the direction towards property improvements. In particular, the investigation was aimed at the effect of interrupted current (IC) chromium plating at various current densities on

Approved for public release; distribution unlimited.

the visual crack morphology, crystallographic structure, and residual stress state of the deposit.

EXPERIMENTAL

A standard plating system was set up in which a Flexopulse periodic current-interruptor made by Rapid Electric was placed in series with the D.C. power supply to allow IC plating using several preselected on/off cycles. All of the IC chromium deposits for this study were prepared using a conventional chromic acid solution which has been aged for 250 A-hr/ℓ and maintained at the composition of 250 g/ℓ CrO_3 and 2.5 g/ℓ H_2SO_4 and a temperature of 55°C. The coatings were deposited on a polished flat sheet of annealed brass substrate and to a total chromium thickness of 75 μm which is optimum for x-ray diffraction analysis.

DETERMINATION OF OPTIMUM ON/OFF DUTY CYCLE

As was discussed in the introduction the effective interruption of current during plating can produce crack-free deposits. This current interruption is responsible for disrupting the cathode film during chromium plating and thus can lead to changes in the deposit properties. The nature of this disruption during IC plating was investigated through polarization measurements using the same type of conventional chromic acid electrolyte at 55°C. The resulting current-voltage relationships shown in Figure 1 indicated that a current interruption of 15 sec duration was necessary to disrupt the cathode film completely. On the basis of these measurements, the on/off duty cycles of 30/5, 30/15, and 30/30 seconds were selected for studying the IC chromium deposits. Additionally, for each of the duty cycles indicated above, IC chromium deposits were prepared at current densities of 30, 45, and 60 A/dm^2.

STRUCTURAL RESULTS AND DISCUSSION

APPEARANCE AND MECHANICAL PROPERTIES

A comparison of some of the properties of IC and HC chromium is shown in Figure 2. The surface morphology of this IC chromium deposits was examined by means of a low magnification stereo microscope. The crack pattern of these deposits varied from a crack-free structure to one of heavy crack density. Corresponding to this structure, the hardness was found to vary between 770 and 1100 KHN and the tensile strength between 30.0 and 0 ksi. While a wide range of properties can be attained with IC chromium plating, the better results are obtained from deposits plated at the higher current densities and longer interruption time.

TEXTURE

The x-ray diffraction spectra shown in Figures 3 through 5 have been obtained by means of a diffractometer scan using molybdenum monochromatic radiation. For the sake of convenience these spectra have been organized in Figures 3 through 5 to reflect the changes which occur in the deposited structures as a result of the longer current interruption times and also the higher current densities. It is clearly seen that for the case of no current interruption, all three current density deposited structures are characterized by the expected and well known <111> fiber texture. When, however, the current interruption time is increased, distinct

found that increasing the current density to 60 A/dm^2 and the interruption interval to 30 sec have resulted in deposits with lower microcrack densities and improved mechanical properties. It is also found that uninterrupted deposits have a very strong <111> fiber texture while for high interruption times and 60 A/dm^2 current density, the <111> fiber texture is diminished considerably and the <211> orientation becomes dominant. Additionally, our measurements show that along with these changes there is a decrease in the chromium hydride retained in the deposit. The above evidence suggest a mechanism in which the crystallites with growth cones in the <111> direction preferentially trap the chromium hydride during coalescence. As the deposit becomes more random or tends towards the <211> texture less of the hydride phase is retained. The chromium hydride phase has a larger unit cell than bcc chromium and is unstable and its decomposition has been considered for a long time as being responsible for the presence of cracks in electrodeposited chromium.

Finally, the residual stresses measured were found to correlate best with electrodeposition rate due to current density and the orientation textures due to interruption cycle.

ACKNOWLEDGEMENTS

The authors wish to express their appreciation to Dr. I. Ahmad for his encouragement and technical support throughout the course of this project.

REFERENCES

1. J. C. Saiddington and G. R. Hoey, Plating, 61, p. 923 (1974).

2. H. Chessin and E. J. Seyb, Jr., Plating, 55, p. 821 (1968).

3. H. Fry, Trans. Inst. Met. Finishing, 32, p. 107 (1955).

4. W. Blum, Plating, 48, p. 613 (1961).

5. R. Weil, Plating, 57, p. 1231 (1970).

6. J. B. Kushner, Plating, 60, p. 1248 (1973).

7. G. P. Capsimalis, R. F. Haggerty, and K. Loomis, "Computer Controlled X-Ray Stress Analysis for Inspection of Manufactured Components," WVT-TR-77001, Watervliet Arsenal, Watervliet, NY, January 1977.

differences in structure among the three current densities is found. For the case of the low current density of 30 A/dm^2 as seen in Figure 3, increasing the current interruption interval does not affect the characteristic (111) preferred orientation of the deposits. As shown in Figure 4 at 45 A/dm^2 a noticeable disturbance of the (111) preferred orientation occurred as the current was interrupted at the various duty cycles. As a result of the changes in intensities of the x-ray lines observed in Figure 4, it was deduced that a small fraction of the chromium crystallites grown in these deposits have departed from the common <111> direction to random orientations and favored especially the <211> direction. As shown in Figure 5 at 60 A/dm^2 the current interruption produced deposits with a dual <211> and <111> fiber texture. Again from a comparison of the intensities observed the <211> texture of these deposits was stronger than the <111> texture, implying that a larger number of crystallites with the (211) rather than the (111) preferred orientation have competitively grown parallel to the deposit surface. Also, a comparison of intensities of Figures 4 and 5 showed that a greater fraction of the crystallites have become random as the current density was increased from 45 to 60 A/dm^2.

RESIDUAL STRESSES

Residual stresses in the IC chromium deposits have been measured by means of an automated computer controlled x-ray diffraction system we developed and reported earlier.[7] Typically, the chromium deposit stresses varied from tensile stresses of 15 ksi to compressive stresses of 30 ksi. Regarding the stress measurements however, it should be noted that for the deposits with large microcrack densities the results were scattered and not always meaningful. Also, the x-ray stress data had to be carefully interpreted to eliminate the effects of texture and of high stress gradients that are present across the thickness of the deposits. In general, the high compressive stresses were measured from practically crack free samples that were deposited at the high interruption cycles and the current density of 60 A/dm^2.

CHROMIUM HYDRIDE PHASE

As a consequence of the x-ray residual stress measurements it was found that an additional non-equatorial reflection occurred which did not belong in the bcc chromium structure but satisfied the angular position of chromium hydride in the form CrH_x. Assuming that the chromium hydride phase has a preferred orientation as most other electrodeposits, this peak found off the equatorial direction provided a way of measuring qualitatively the retained chromium hydride in the IC chromium deposits. On the basis of the above findings our x-ray measurements on the IC chromium deposits show that CrH_x is almost always present at low current densities and no current interruption, and decreases significantly as the interruption time and current density reach their high values.

SUMMARY AND DISCUSSION

Several of our results are similar to those previously reported. In particular, the deposition of crack-free chromium by means of current interruptions is well documented.[1-4] The present study extends these earlier findings in providing more specific information on the effect of current interruption cycles and current density on the crystal structure and internal stress of the chromium deposits. While varying the on/off duty plating cycle and current density deposits with very different structures and properties have been observed. As a rule we

Figure 1

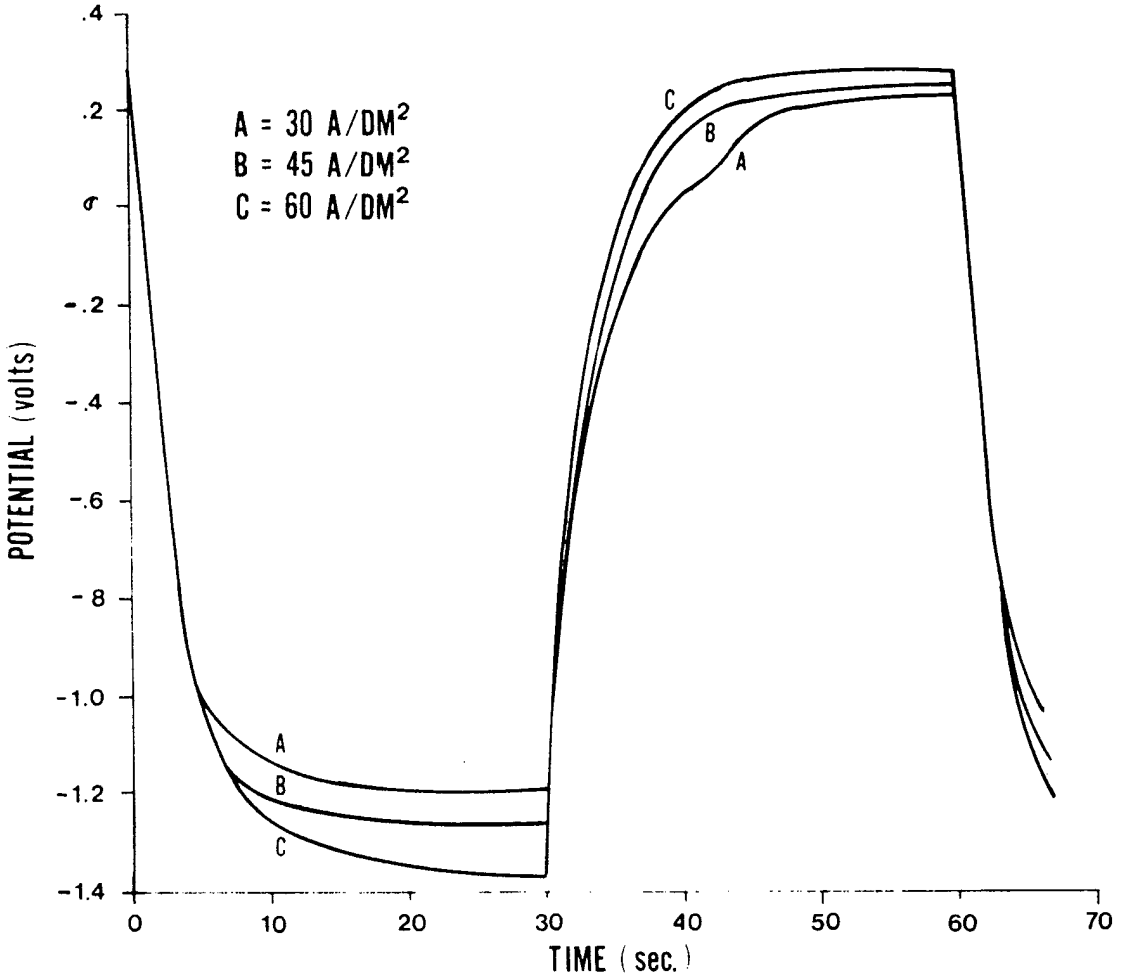

CATHODE POTENTIAL (WITH RESPECT TO STANDARD CALOMEL ELECTRODE)
VS. TIME (CHARGING/OFF TIME)

STANDARD HARD CHROME (HC)

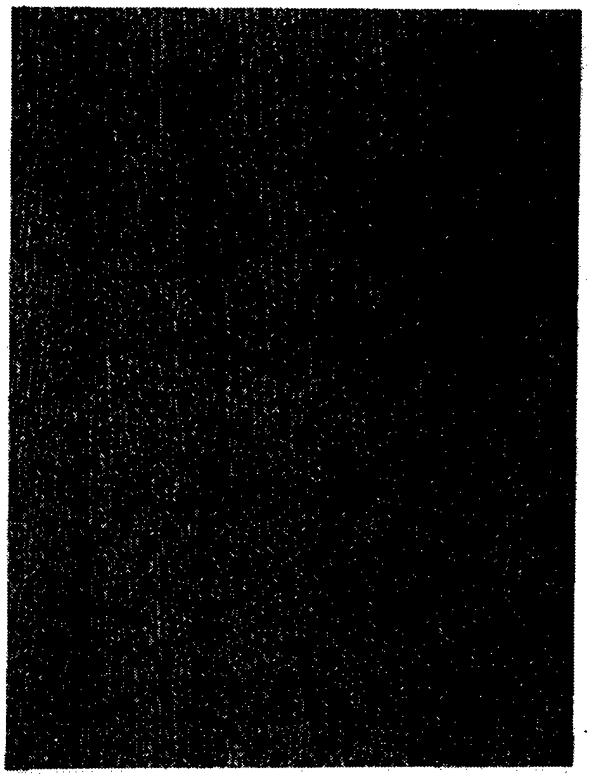

1000X

INTERRUPTED PLATED CHROME (IC)

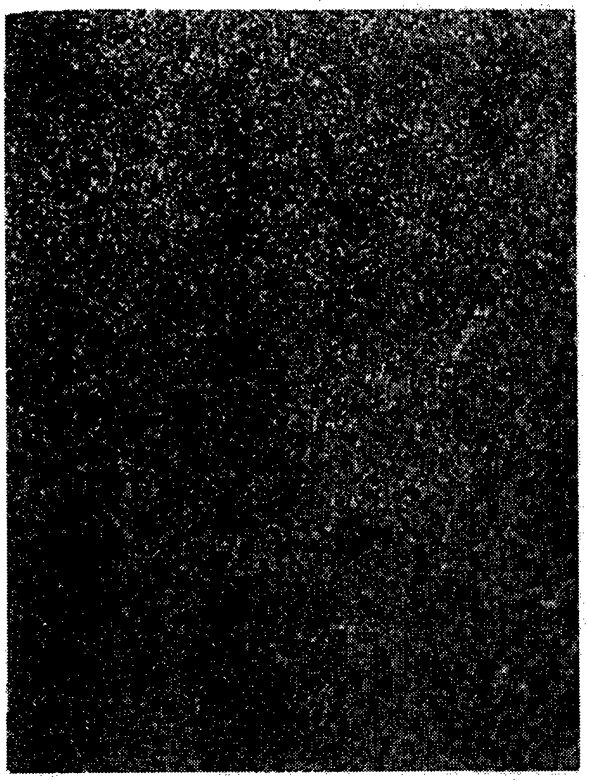

1000X

	HC Chrome	IC Chrome
Bath Temperature °C	55	55
Current Density (A/dm^2)	30	35
Plating Rate (Mils/Hrs)	1	0.5
Hardness (KHN)	940	790
UTS (Psi)	15,000	30,000

Fig. 2. Comparison of Microstructure and Some Other Properties of HC and and IC Chromium.

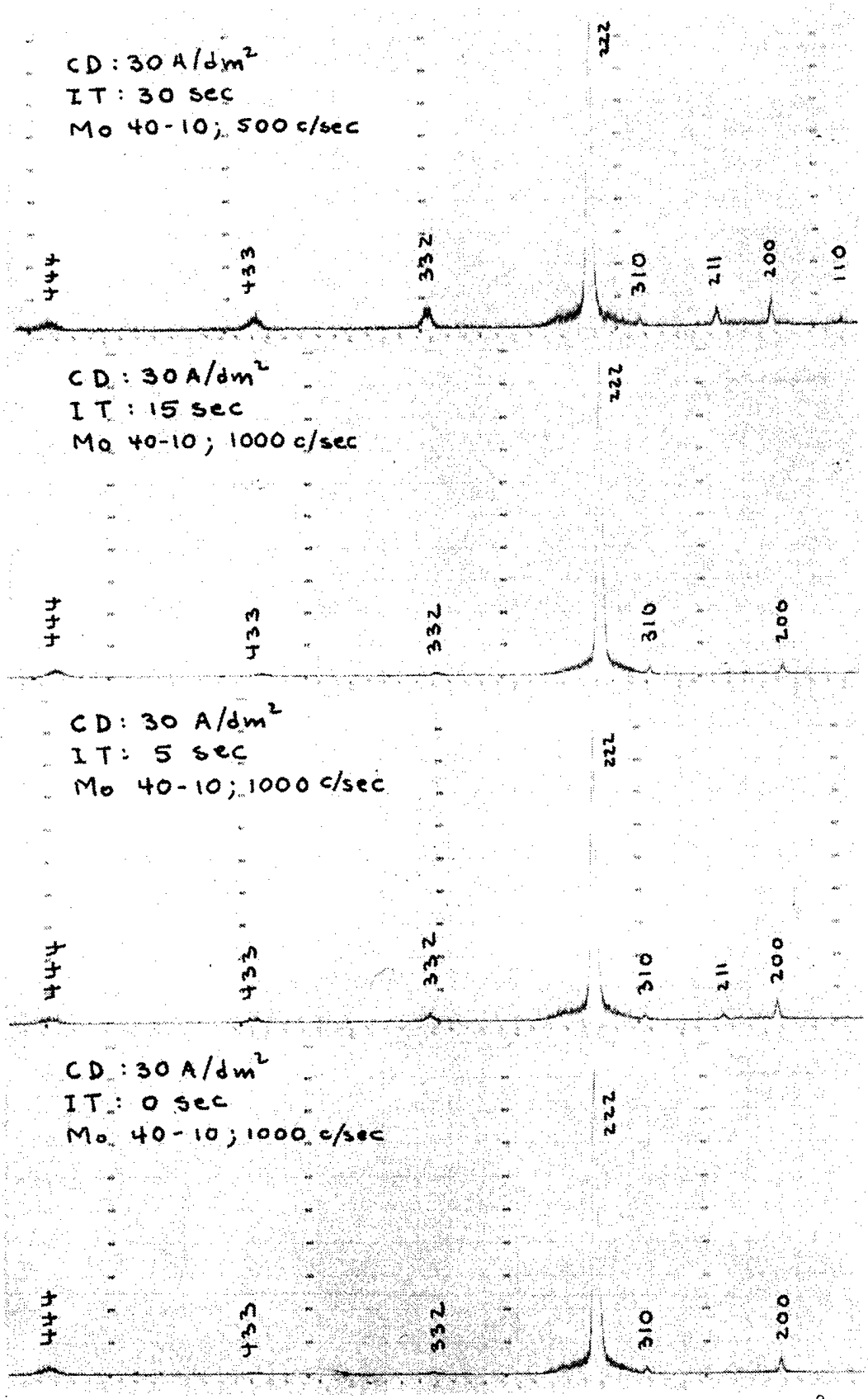

Fig. 3. X-Ray Diffraction Spectra of IC Chromium Plated at 30 A/dm^2 and Various Interrupt Time (IT) Intervals.

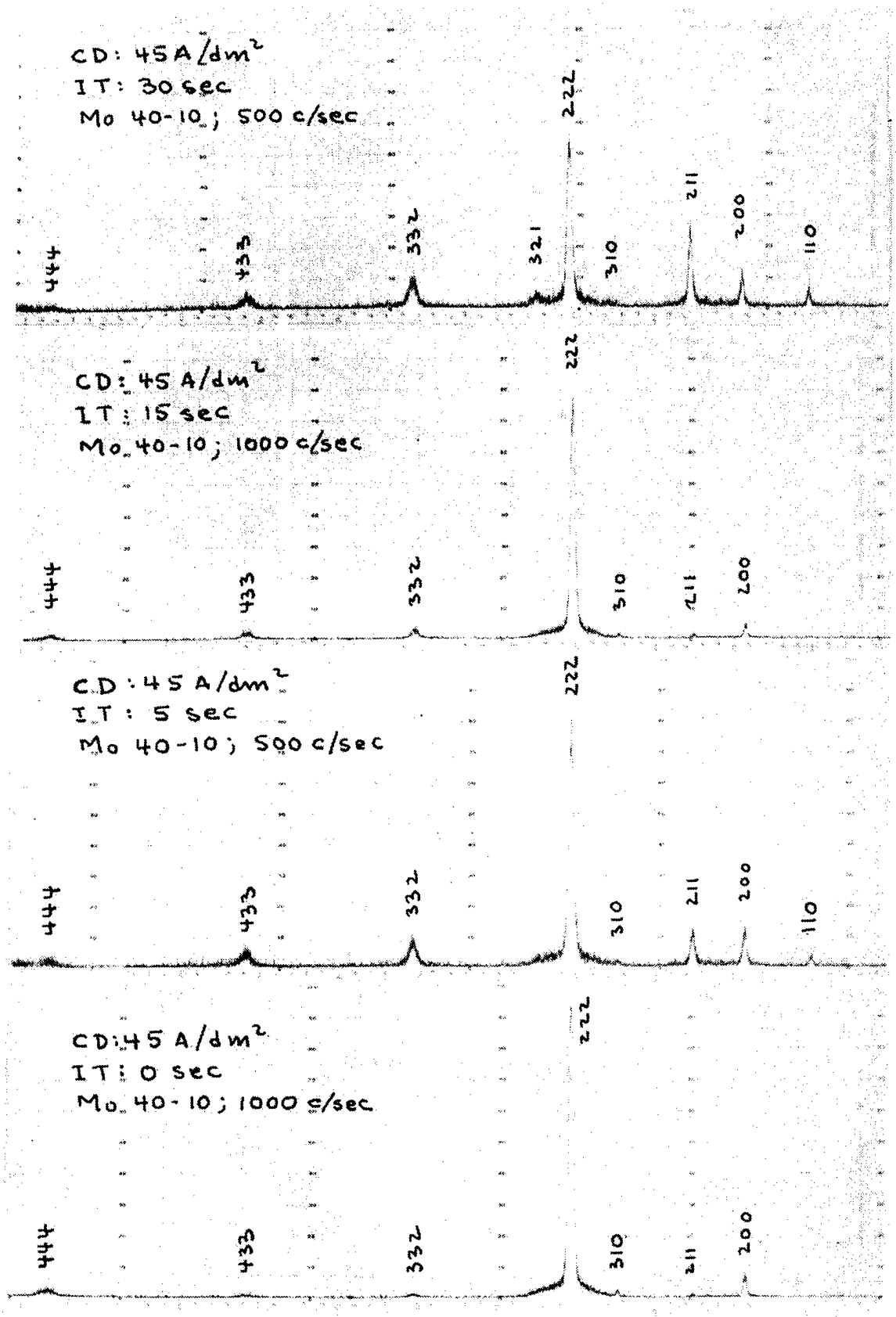

Fig. 4. X-Ray Diffraction Spectra of IC Chromium Plated at 45 A/dm^2 and Various Interrupt Time (IT) Intervals.

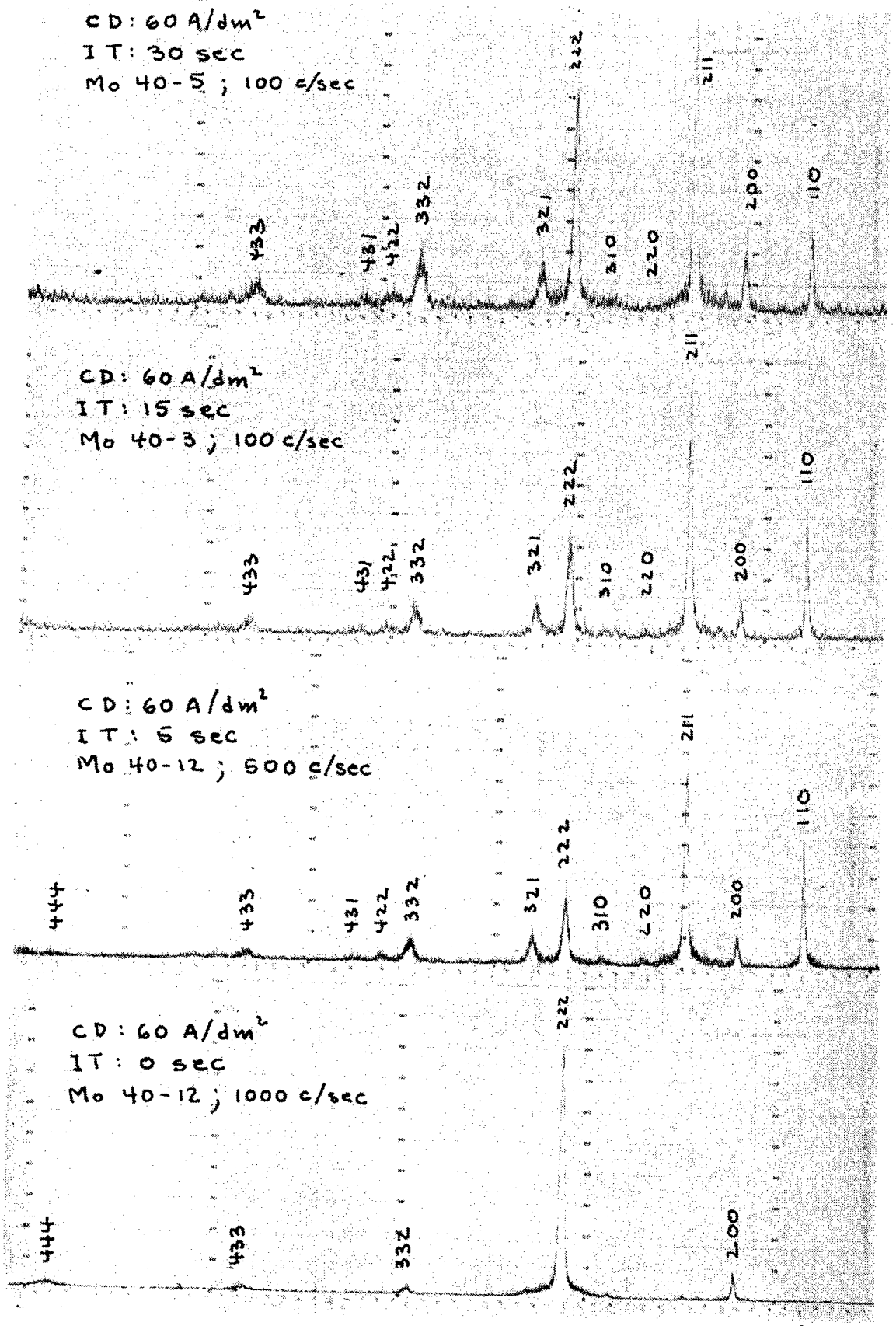

Fig. 5. X-Ray Diffraction Spectra of IC Chromium Plated at 60 A/dm^2 and at Various Interrupt Time (IT) Intervals.

RECENT FINDINGS AND DEVELOPMENTS IN CHROMIUM PLATED GUN TUBES

V. P. Greco, G. D'Andrea, and J. Walden
U.S. Army Armament Research and Development Command
Large Caliber Weapon Systems Laboratory
Benet Weapons Laboratory
Watervliet, NY 12189

ABSTRACT

The shortcomings encountered with conventional (high contraction) chromium coatings in gun bores during past investigations are reviewed. Changes in the application of chromium for improving its performance during firing are proposed. Recent developments on the application of low contraction chromium with a new plating process, effects of partially plated bores on accuracy, and the effects of rifling profile on the wear of chromium coatings are discussed.

INTRODUCTION

The present day measures to minimize erosion in gun bores are the application of electrodeposited chromium coatings and the use of ammunition additives. The major shortcoming of chromium is its brittleness and inherent crack pattern which makes it susceptible to spalling and flaking during firing.[1-2] The disadvantages with additives are their relatively high cost and limited effectiveness in some weapon systems, due to difficulties in preparing or properly positioning the material in the propellant system.[3-5]

At the present time, both measures of retarding erosion (i.e., chromium and additive) are incorporated in full length bores of 8" howitzers, 120 mm M256, and 90 mm M41 cannons with satisfactory results. The combined use of these retardants is the best protection against erosion and wear of bore surfaces exposed to severe environments. However, the use of chromium has not been considered for all gun systems. Due to the success reported with ammunition additives[5-12] in the 60's, efforts to improve chromium were abandoned. In the case of studies with coatings, attention was primarily given to refractory metals for protection against severe high temperature gaseous environments.

While the search for new erosion resistant coatings continued for more than three decades, chromium still remains as the only acceptable coating for increasing the wear life of our present day weapons. In view of this, researchers have taken a closer look at the behavior of chromium in gun bores in recent years.

This paper reviews some of the shortcomings encountered with conventional (high contraction) chromium coatings in gun bores during past investigations. These experiences are leading to new changes in the application of chromium for meeting the demands of future weapons.

Some of the problems encountered in the 105 mm, 120 mm, and 155 mm, and recent developments to solve these problems are presented next.

Distribution limited to US Government Agencies only because of test and evaluation; September 1982. Other requests for this document must be referred to Commander, ARRADCOM, ATTN: Benet Weapons Laboratory, DRDAR-LCB-RT, Watervliet, NY 12189.

TARGET DISPERSION

The first change which was attempted in the application of electrodeposited chromium was prompted by two separate occurrences reported in the 105 mm M68 gun.

1. Chromium Plated Tubes - Chromium plated bores showed a 2-3 fold increase in tube life but unacceptable target dispersion with discarding sabot ammunition.[3] This was due to excessive downbore chipping and spalling of chromium occurring during early stages of firing.

2. Unplated Tubes - Firing of M456E HEAT projectile (with ammunition additive) caused the formation of secondary erosion characterized by a second region of bore enlargement forward of the primary wear region at the commencement of rifling. This new erosion pattern also caused unacceptable target dispersion with discarding sabot ammunition.[4,5,12-15] Secondary wear is believed to be caused by the loss of effectiveness of the wear-reducing additive as the projectile advanced downbore.[5]

An extensive wear test was conducted comparing partially chromium plated bores with full length plated bores. Results showed that partially plated bores eliminated the downbore chipping and flaking of chromium and successfully retarded primary and secondary erosion without degradation in target dispersion.[16-18]

The accuracy behavior of a 10 mil full length and partial length plated gun tube can be observed by the target impacts shown in Figure 1. The impacts from each tube at the start of the test show an acceptable value of dispersion. However, as firing continued, the full length tube showed a significant increase in dispersion, whereas the partial length plated tube showed little change in dispersion throughout the 1000 round test.

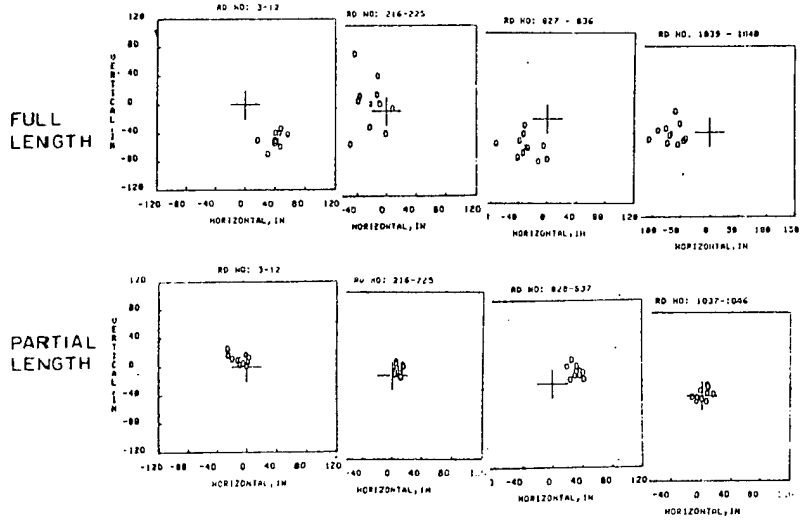

Fig. 1. Target Impact Data for the M392A2 Projectile/105 mm M68 Gun at the 1000 Meter Range During the 1000 Round Test.

BEHAVIOR OF THICK CHROMIUM DEPOSITS

Thick chromium deposits increase the protection of the bore surface against erosion and heat checking. However, increasing the deposit thickness decreases the strength due to defects and the lack of support for the brittle deposit. Therefore, one must compromise between the thermal protection of the surface and the endurance level at which chipping and spalling of the deposit takes place thereby exposing the substrate.

An example of thicker deposits experiencing a greater amount of spalling and downbore wear during firing can be seen in Figure 2.

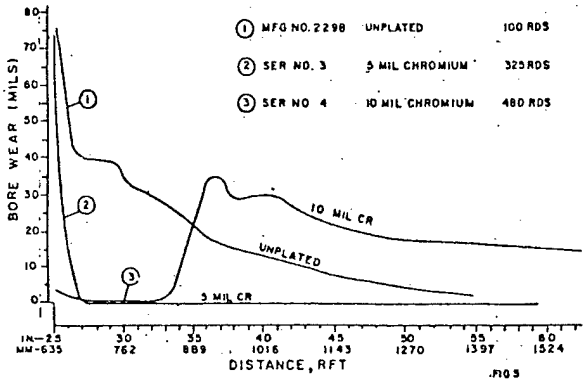

Fig. 2. 105 MM M68 Bore Wear Profiles (Showing Effect of Chromium Thickness in Full Length Plated Bores). Heat Rds. M490 W/O Additive.

120 MM M256 CANNON

BEHAVIOR OF THICK CHROMIUM DEPOSITS

Excessive downbore spalling was also experienced with 10 mil thick deposits in 120 mm XM256 gun tubes during early stages of firing. When 5 mil thick deposits were applied, spalling of the deposit was significantly reduced.

MIDBORE WEAR

Testing of 120 mm M256 gun tubes firing super slugs and heat rounds have resulted in the formation of a midbore wear pattern as shown in Figure 3. The wear in this region is smooth and increases with chamber pressure and rate of fire.

Metallographic examination of some gun tube cross-sections have shown the wear to be eccentric and predominantly in the 9-3 o'clock position (Figure 4).

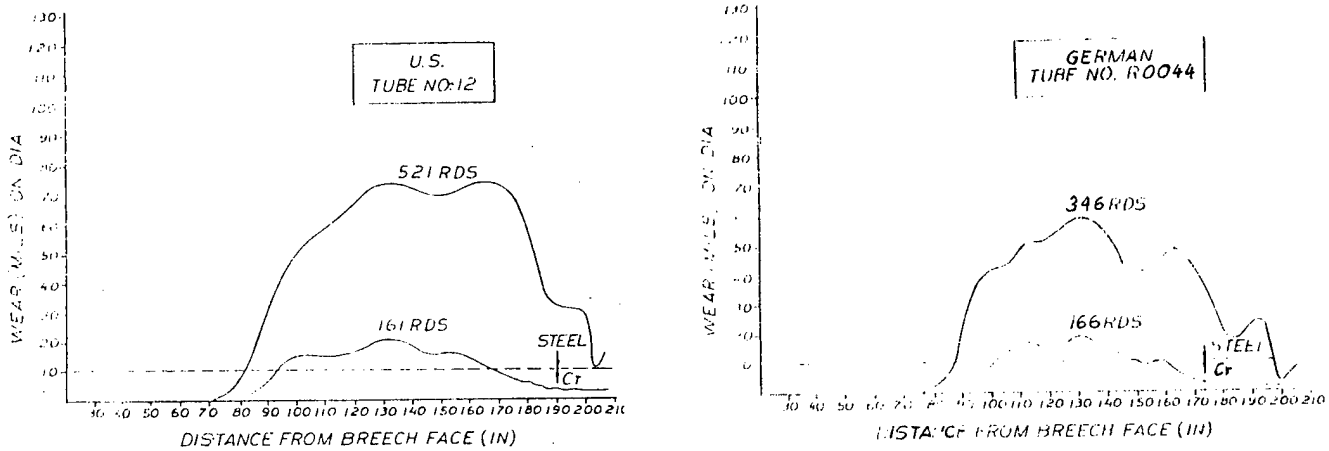

Fig. 3. Progressive Bore Wear Profiles of Fired 120 mm M256 Gun Tubes with 5 Mil Chromium Deposit. (Super Slugs Fired in 60 Rd. Groups at Same Rate of Fire.)

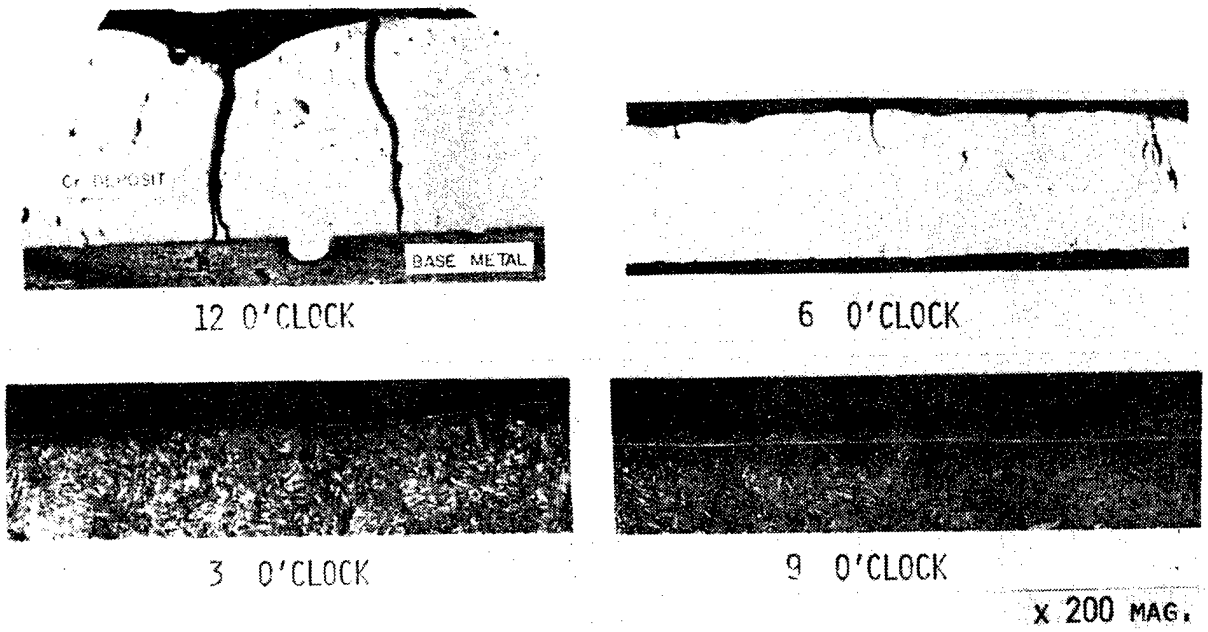

Fig. 4. Bore Surface Cross-Sections of 120 mm M256 (Tube No. 6) at 132 in. From RFT After 297 Super Slug Rds.

MUZZLE WEAR

A chromium plated 155 mm tube (No. 83) showed little wear at the origin of rifling and superior ballistic performance compared to unplated tubes after 1800 rounds.[19] However, the plated tube experienced a significant amount of muzzle wear during the latter rounds and was reported to be related to the irregular body engraving found on the M549 projectiles.

It was speculated that the cause of irregular engraving on the M549 projectile is related to the wear pattern at the bore origin. In the case of unplated tubes, irregular projectile engraving was not reported as a problem.

HIGH TORSIONAL IMPULSE

Another problem of concern was the relatively high torsional impulse readings which were recorded during the later stage firing of a chromium plated tube.[20] It has also been speculated that the high torsional impulses are related to the irregular erosion pattern that develops at the origin of rifling in plated tubes. Investigators have proposed the theory that the latter erosion pattern causes a free run for the projectile during firing which produces the high torsional impulse.

Because of these findings and the associated higher chamber pressures, the incorporation of chromium in 155 mm production tubes was not previously considered.

RECENT DEVELOPMENTS

Regardless of the uncertainties in relating wear with the projectile behavior in large caliber systems, investigations are currently underway which will have a significant effect on the performance of chromium in cannon tubes. These investigations, which are aimed at improving the properties of chromium, include three significant process changes:

1. The modification of the rifling profile at the bore origin prior to plating.

2. The application of low contraction chromium.

3. The use of a new plating process.

BORE ORIGIN OF RIFLED BORES

The most critical area in which shearing and spalling of chromium occurs during firing is at the sides of the lands at the commencement of rifling (C.R.). Once spalling is initiated, the hot propellant gases undermine the edges of the remaining coating and the substrate is rapidly eroded away. Figure 5 shows how such surface damage progresses from an early to a final stage of firing at the C.R. of a rifled gun tube.

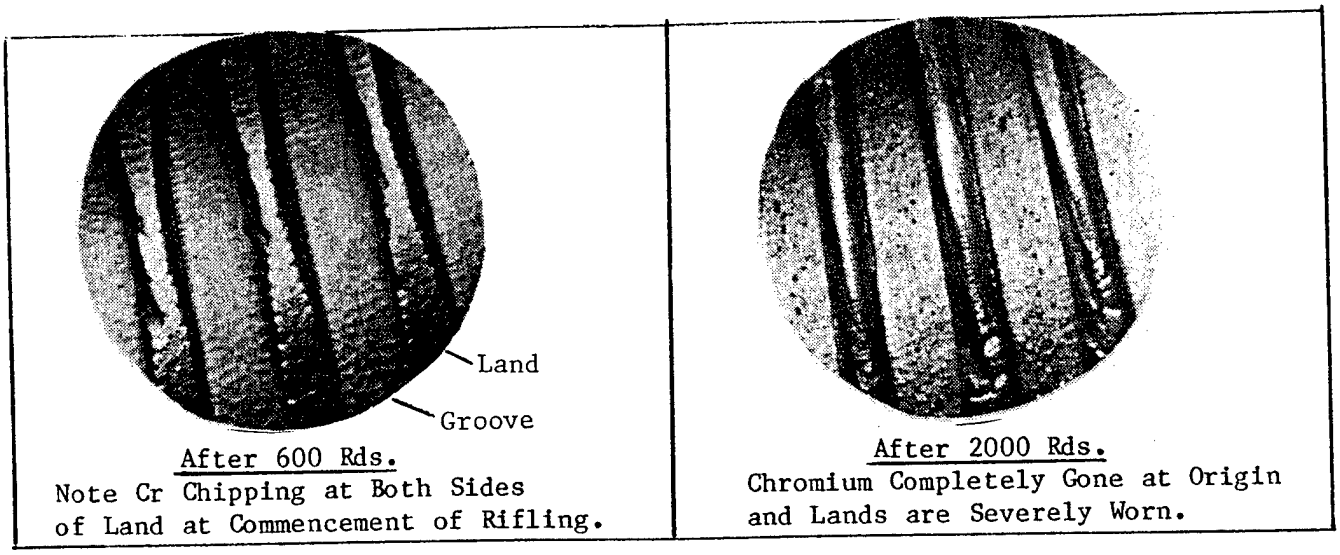

After 600 Rds.
Note Cr Chipping at Both Sides of Land at Commencement of Rifling.

After 2000 Rds.
Chromium Completely Gone at Origin and Lands are Severely Worn.

Fig. 5. Views of Progressive Bore Damage in a 155 mm M199 Howitzer Tube.

Cause of Chromium Breakthrough at C.R. - The primary factor which causes the brittle chromium deposit to be more susceptible to shearing and spalling at the C.R. is the sharp corners of the land run-up (i.e., forcing cone) which is unavoidably formed during the rifling operation. Figure 6 shows a sectional surface view of the origin of rifling which represents the specified machined surface of a gun bore prior to chromium plating. Surfaces with sharp corners promote high current density gradients during electrolysis which leads to excessive build-up and weak chromium in rifled bores as shown in land cross-sections in Figure 7.

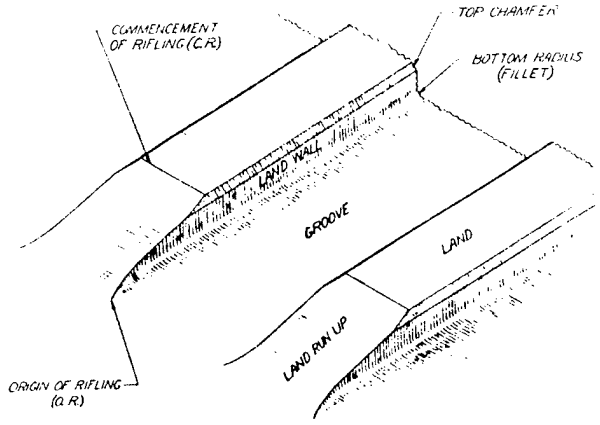

Fig. 6. Sketch of Rifling at Origin of Bore.

Optimum Rifling Profile at the O.R. - A recent study for minimizing the shearing and spalling of chromium at the C.R. have been undertaken. The rounding off of sharp corners at the bore origin was a "difficult task" due to the remote location and small area of the land run-up at the bore origin. A significant accomplishment has been achieved in a recent study in which special tooling and a process has been developed to successfully produce an optimum rifling profile at the bore origin. The results of these efforts with 155 mm M199 test cylinders is shown in Figure 7.

Conventional | Chipped Corner After Firing | Optimum

Fig. 7. Cross-Sections of Chromium Plated Lands at the C.R. of 155 MM M199 Howitzer Tube.

LOW CONTRACTION CHROMIUM

In comparison to the present day high contraction (HC) chromium, low contraction (LC) chromium is softer and less brittle, contains less stress cracks, and experiences less shrinkage after heating. The concept of applying LC chromium in gun tubes was considered and tested in small caliber barrels in the 1950's.[21-23] LC chromium showed great promise against erosion in small arms. However, studies were discontinued because the coating showed a tendency to swage with the steel lands at high projectile velocities and during extended firing when the bore surface of machine gun barrels approached very high temperatures.

As a result of the above, LC chromium was never previously considered for application in large caliber barrels. However, large caliber barrels are not subjected to sustained firing and the heating of the bore surface is not the same as in machine gun barrels. Furthermore, swaging of a 5 mil thick coating in a large barrel (if it occurs at all) should have little effect on a large caliber land as compared to a 5 mil thick coating on top of a 6 mil land height in a 20 mm barrel.

IMPROVED LOW CONTRACTION CHROMIUM

Recent efforts have been undertaken to upgrade the LC chromium plating process to improve coating performance in gun bores.[24] Major emphasis has been placed on the effects of current density, solution aging, and bath additives on the mechanical properties of the deposit. The results show deposits with higher tensile strengths, lower micro-hardness values, and primarily crack-free compared to the conventional HC deposits produced. The latter studies are significantly more extensive than those found in the earlier literature.[1]

LC chromium deposits produced with the new plating process have been evaluated through 20 mm test firing[25] and are currently being evaluated in 120 mm M256 gun tubes (Figure 8). Plans have also been made to apply the coating in 105 mm M68 and 155 mm M199 cannon bores for evaluation through extensive firing tests.

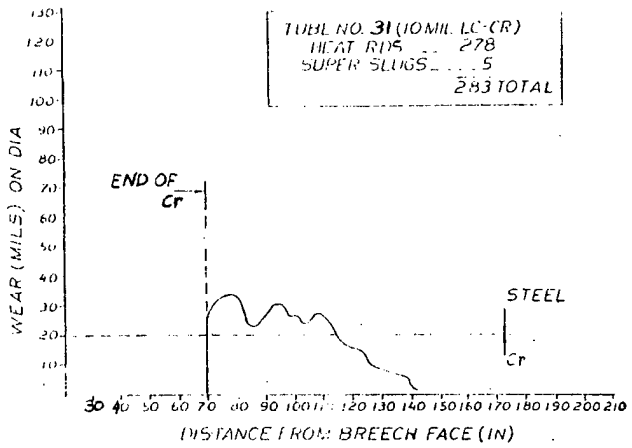

Fig. 8. Longitudinal Wear Pattern of a Partially Chromium Plated 120 mm M256 Tube.

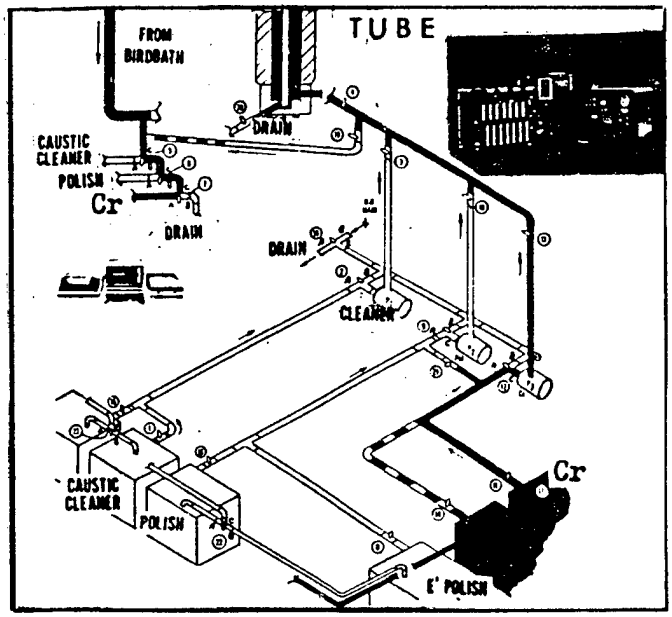

Fig. 9. A "Pump Thru" Plating System for Plating Long Cylinder Bores.

PLATING PROCESS

The conventional method of plating gun bores in production includes the immersion of gun tubes in the plating solution which is contained in large open tanks requiring deep pits and high cranes. Another method for plating cylinder bores involves the pumping of the process solution through the bore from a small storage tank. This method offers considerable advantage over the "immersion" technique for controlling the solution temperature and current density distribution.

In view of the above, a prototype "pump thru" plating facility has been constructed for the surface treatment and plating of gun bores using a computer aided system to control the process parameters (Figure 9).[26,27]

The various surface treatments are accomplished by the "pump thru" plating method using a series of tanks, pumps, valves, and associated piping to direct and control the flow rate of the process solutions. The facility is especially suitable for the deposition of LC chromium which requires high solution temperature, high current densities, and a high rate of solution flow to control deposit distribution.

Recent studies have been conducted on the structural characteristics of HC chromium deposits produced with the "pump thru" method of plating bores.[27] X-ray examination of these deposits have shown that increasing the linear flow of the electrolyte produces two significant changes in the deposit:

1. Crystal growth changes from a preferred to a random orientation.

2. Residual stresses change from tensile to a compressive type.

Preliminary tests have shown that deposits produced with the "pump thru" system are significantly stronger than those produced by the immersion process.

ANODES FOR CHROMIUM PLATING GUN BORES

The "pump thru" process is currently being employed to deposit higher density and higher purity lead alloy coatings for producing chromium plating anodes. The conventional anodes are produced by a lead burning process which results in coatings with a high percentage of porosity and impurities. Chromium plating anodes have a significant effect on the quality of the deposits in gun bores.

CONCLUSIONS

Partial length plated tubes produce acceptable target dispersion with discarding sabot type projectiles.

An optimum rifling profile at the bore origin will result in less tendency for chromium to chip and flake off from the base metal. This, in turn, will prevent the formation of the irregular erosion pattern which occurred in 155 mm M199 tests.

LC chromium deposits will possess greater strength and less brittleness than HC deposits.

The "pump thru" plating process will produce deposits with improved properties.

REFERENCES

1. Lamb, V. A. and Young, J. P., Summary Report 5797, NBS, Jan 1946 - Dec 1955.
2. Burlew, J. S. (Ed), Summary Technical Report of NDRC, Div. 1, Vol. 1, Washington, DC, 1946.
3. USA TECOM Report No. DPS-469, APG, Aberdeen Proving Ground, MD, 1962.
4. Ward, J. R., BRL IMR No. 402, Aberdeen Proving Ground, MD, June 1975.
5. Ward, J. R., BRL MR 2557, Aberdeen Proving Ground, MD, Nov 1975.
6. Wolff, R., Picatinny Arsenal Technical Report No. 3069, Part I, Dover, NJ, May 1963.
7. Wolff, R. O., Picatinny Arsenal Technical Report No. 3096, Part II, Dover, NJ, August 1963.
8. APG Report No. DPS-768, Aberdeen Proving Ground, MD, January 1963.
9. APG Report No. DPS-838, Aberdeen Proving Ground, MD, March 1963.
10. APG Report No. DPS-1520, Aberdeen Proving Ground, MD, December 1964.
11. Lenchitz, C., Velicy, R. W., Bottei, L. A., and Silvestro, G., Picatinny Arsenal Technical Memo No. 1768, Dover, NJ, November 1965.

12. Ward, J. R. and Brosseau, T. L., Tech. Report ARBRL-TR-02238, Aberdeen Proving Ground, MD, April 1980.

13. Albright, A. A. and Friar, B. S., WVT-TR-75047, Watervliet Arsenal, Watervliet, NY, July 1975.

14. Albright, A. A., Coppola, E. E., and Friar, G. S., ARLCB-TR-77034, USA ARRADCOM, Benet Weapons Laboratory, Watervliet, NY, July 1977.

15. Albright, A. A., Friar, G. S., and Morris, S. L., WVT-TR-76037, Watervliet Arsenal, Watervliet, NY, September 1976.

16. Musick, Clyde, R., APG-MT-5516, Aberdeen Proving Ground, MD, May 1981.

17. Lannon, J. A., Ahmad, I., Greco, V. P., Stobie, I. C., and Ward, J. R., "The Wear and Accuracy of 105 MM M68 Tank Cannons Electroplated With 0.25 mm (10 mil) and 0.38 mm (15 mil) Thick Chrome Plating," USA ARRADCOM, 15 May 1981.

18. Greco, V. P., ARLCB-TR-82025, USA ARRADCOM, Benet Weapons Laboratory, Watervliet, NY, August 1982.

19. Lannon, J. A., Vallado, A. C., USA ARRADCOM, 155 MM M199 Chrome Plated Cannon Tube, S.N. 83 Wear Test, Dover, NJ, January 1979.

20. Lannon, J. A. and Vallado, A. C., ARLCD-TR-80018, Dover, NJ, February 1981.

21. Lamb, V. A. and Young, J. P., NBS Technical Note 46, May 1960.

22. Young, M. P., NBS Report No. 3B101, 1 August 1954.

23. Wolfe, R. H., Rock Island Arsenal Technical Report No. 57-2498, 15 October 1957.

24. Chen, E. S. and Baldauf, W., ARLCB-TR-80008, USA ARRADCOM, Benet Weapons Laboratory, Watervliet, NY, March 1980.

25. D'Andrea, G., Cullinan, R., Croteau, P., ARLCB-TR-81046, USA ARRADCOM, Benet Weapons Laboratory, Watervliet, NY, December 1981.

26. D'Andrea, G., Greco, V. P., and Walden, J., ARLCB-TR-81033, USA ARRADCOM, Benet Weapons Laboratory, Watervliet, NY, October 1981.

27. Walden, J., ARLCB-TR-81036, USA ARRADCOM, Benet Weapons Laboratory, Watervliet, NY, September 1981.

28. Capsimalis, G., USA ARRADCOM, Private Communication (to be published), USA ARRADCOM, Benet Weapons Laboratory, Watervliet, NY.

perpendicularly to the crack planes in the tensile test while it acts parallel to the crack planes in the adhesion test. Two additional parameters, crack length and plating stress, are important to the strength of HC chromium. It is suggested that the observed increase in strength with increasing crack density is due to the presence of smaller cracks and the reduced plating stress in the deposits.

The addition of $H_2C_2O_4$ to produce Cr^{+3} ions has little effect on HC chromium below a Cr^{+3} ion concentration of 40 g/ℓ. Above this concentration, up to 50 g/ℓ, an increase in tensile strength of 51 percent is observed. The observed increase in strength is attributed to the formation of Cr^{+3} complex ions. This in effect reduces the concentration of the chromic acid in the plating solution.

In the electrodeposition of chromium, the plating temperature has a pronounced effect on deposit properties. At a temperature of 85°C, low contraction (LC) chromium is deposited with a crack-free structure which is softer and stronger than conventional HC chromium. In LC chromium plating, parameters other than temperature are known to have a large influence on the soundness and strength of the deposits.[8] Aging the solutions to 250 A-hr/ℓ by pre-electrolysis prevented spallation. The use of pre-electrolyzed solutions together with higher current densities is also beneficial to deposit strength. For unaged solutions, raising the current density from 60 to 150 A/dm^2 increases the strength of LC chromium from 7.1 to 29.1 ksi. With pre-electrolyzed solutions at the same current density range, the increase is between 32.8 and 48.2 ksi. The addition of an electroactive chemical such as V_2O_5 at a concentration of 10 g/ℓ improves the deposit strength to between 54.1 and 56.3 ksi. The improvement in deposit strength is believed to be the result of lower plating stresses associated with the reduction of codeposited hydrogen.

Figure 5 shows a bar graph of the different types of chromium deposits and their characteristic strengths. In this graph, the spread of the tensile strength for each type of chromium reflects on both data reproducibility and effects of current density. Essentially, the strength of HC chromium can be changed significantly by several procedures. The first is to use current modulation such as interrupted current (IC) in the chromium plating process. Depending on the on/off duty cycle selected, the IC chromium deposits can have hardness values between 700 and 900 KHN and tensile between 8 and 32 ksi. However, the reproducibility of the strength data is unpredictably poor. The better procedure for increasing the strength of HC chromium is by raising the plating temperature from 55° to 85°C. This change in plating temperature will favor the formation of a soft crack-free deposit that is characteristic of LC chromium. Additional requirements through the use of solution aging, high current densities, and vanadium additions can produce optimized LC chromium deposits.

CONCLUSIONS

1. The presence of Cl^- ions in chromic acid plating solutions favors the formation of smaller cracks and increases the crack density. An improvement in tensile strength is obtained.

2. Using a CrO_3/H_2SO_4 ratio below 100/1 is preferable to using higher ratios. HC chromium plated at high catalyst ratios show poorer adhesion and lower tensile strength.

3. Cations have different effects on the strength of HC chromium. Fe^{+3} ions in the chromic acid plating solutions tend to reduce the crack density and lower the tensile strength. The presence of Cr^{+3} ions has the opposite effect of increasing the tensile strength.

4. LC chromium with optimum properties can be obtained by aging the plating solution through pre-electrolysis, the use of high current densities, and the addition of vanadium in the plating solution.

REFERENCES

1. J. D. Greenwood, Heavy Deposition, Robert Draper LTD, Teddington, 1970, p. 137.

2. J. B. Mohler, Electroplating and Related Processes, Chemical Publishing Co. Inc., New York, 1969.

3. Plating Engineering Handbook, Ed. A. Kenneth Graham, Van Nostrand Reinhold Co., New York, 1971.

4. W. H. Safranek, NBS Special Publication 452, Proceedings of the 23rd MFPG Meeting, September 1976.

5. E. S. Chen and W. Baldauf, "Improved LC Chromium For Gun Tube Applications," USA ARRADCOM Technical Report ARLCB-TR-80008, Benet Weapons Laboratory, Watervliet, NY, March 1980.

6. D. E. Neimer, Metal Finishing, Vol. 89, March 1959.

7. W. H. Dancy, UVA/ORL-504-12RD-59 QPR No. 1, March 1959.

8. E. S. Chen, "Improved Electrodeposited LC Chromium," to be published in the Proceedings of the 82nd SUR/FIN Technical Conference.

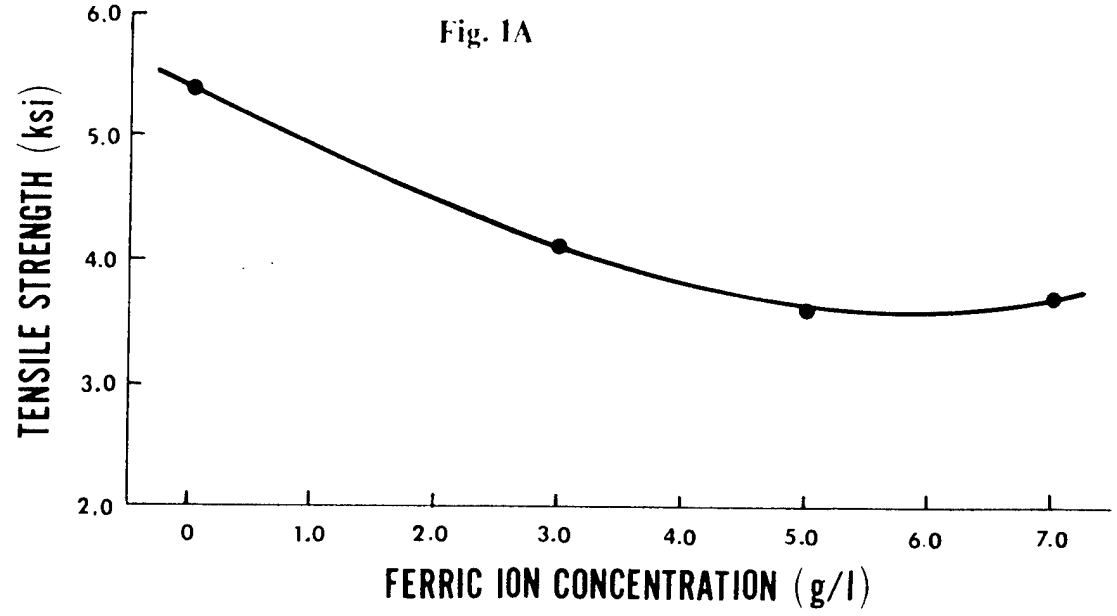

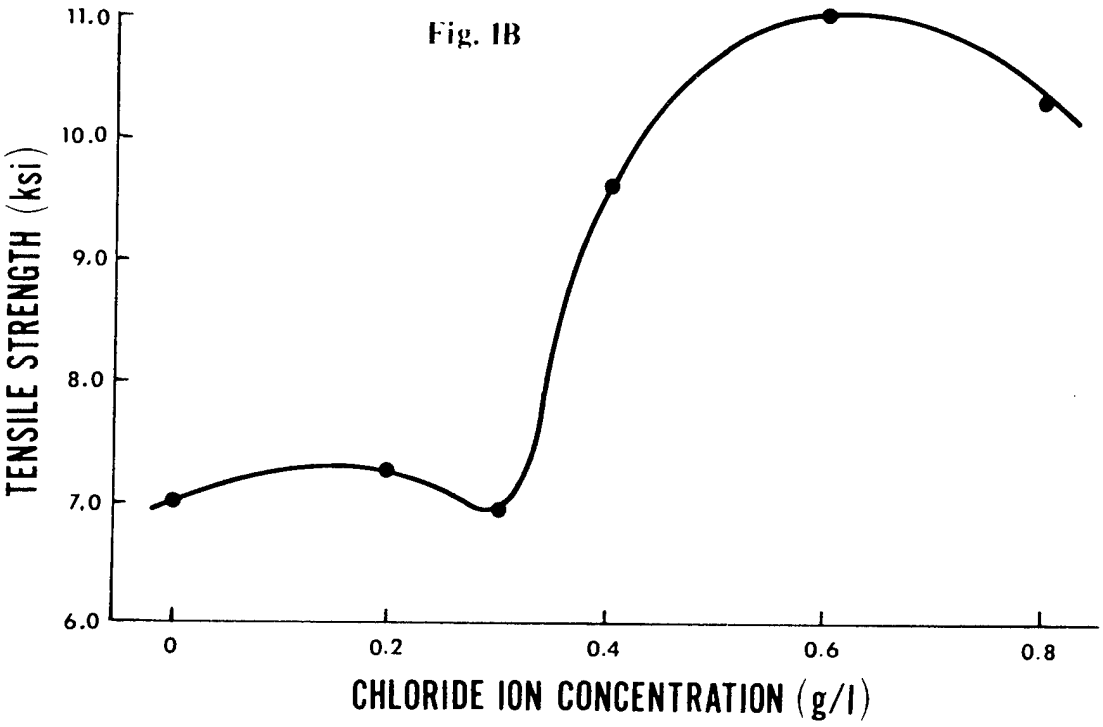

Fig. 1(a). The Effect of Fe^{+3} Ion Concentration on the Tensile Strength of HC Chromium.

Fig. 1(b). The Effect of Cl^{-} Ion Concentration on the Tensile Strength of HC Chromium.

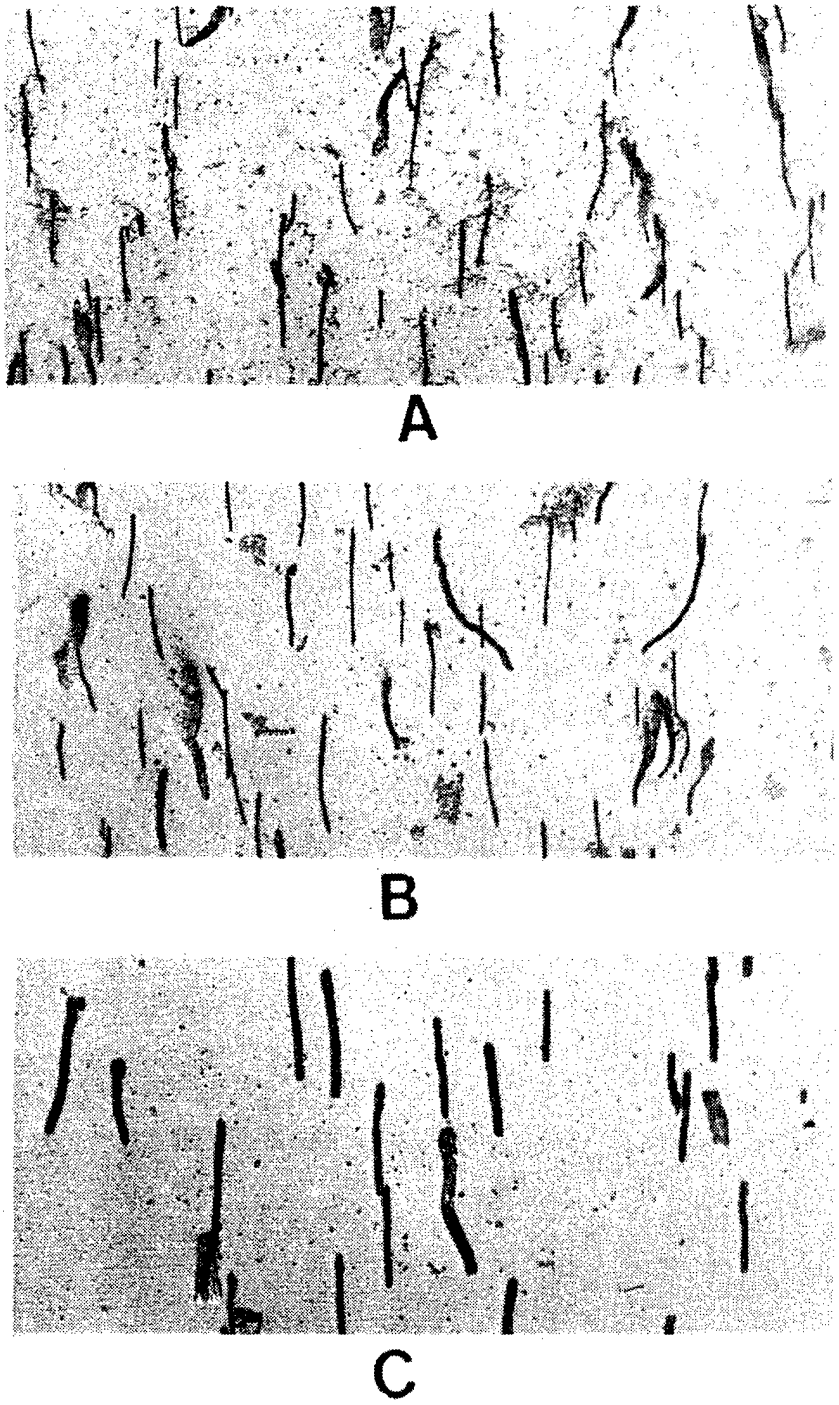

Fig. 2. Microstructure of HC Chromium Showing the Effect of Fe^{+3} ions. Deposits Plated at 55°C and 30 A/dm^2 Using Solutions Containing CrO_3/H_2SO_4 at 250/2.5 g/ℓ and Fe^{+3} Ion Concentrations of (a) 3.0 g/ℓ (b) 5.0 g/ℓ, and (c) 7.0 g/ℓ. 500X Magnification.

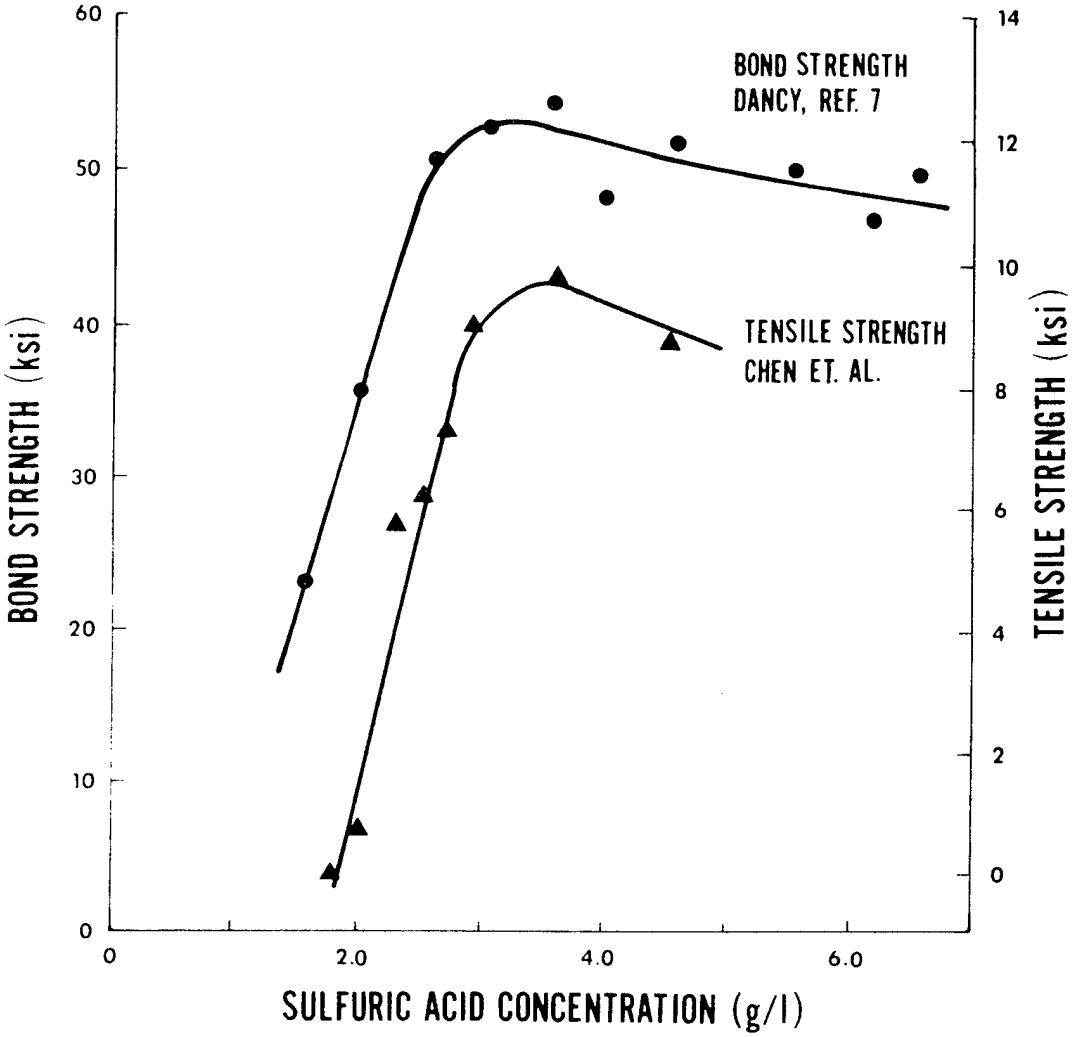

Fig. 3. The Influence of H_2SO_4 Catalyst on the Tensile Strength and Bond Strength of HC Chromium.

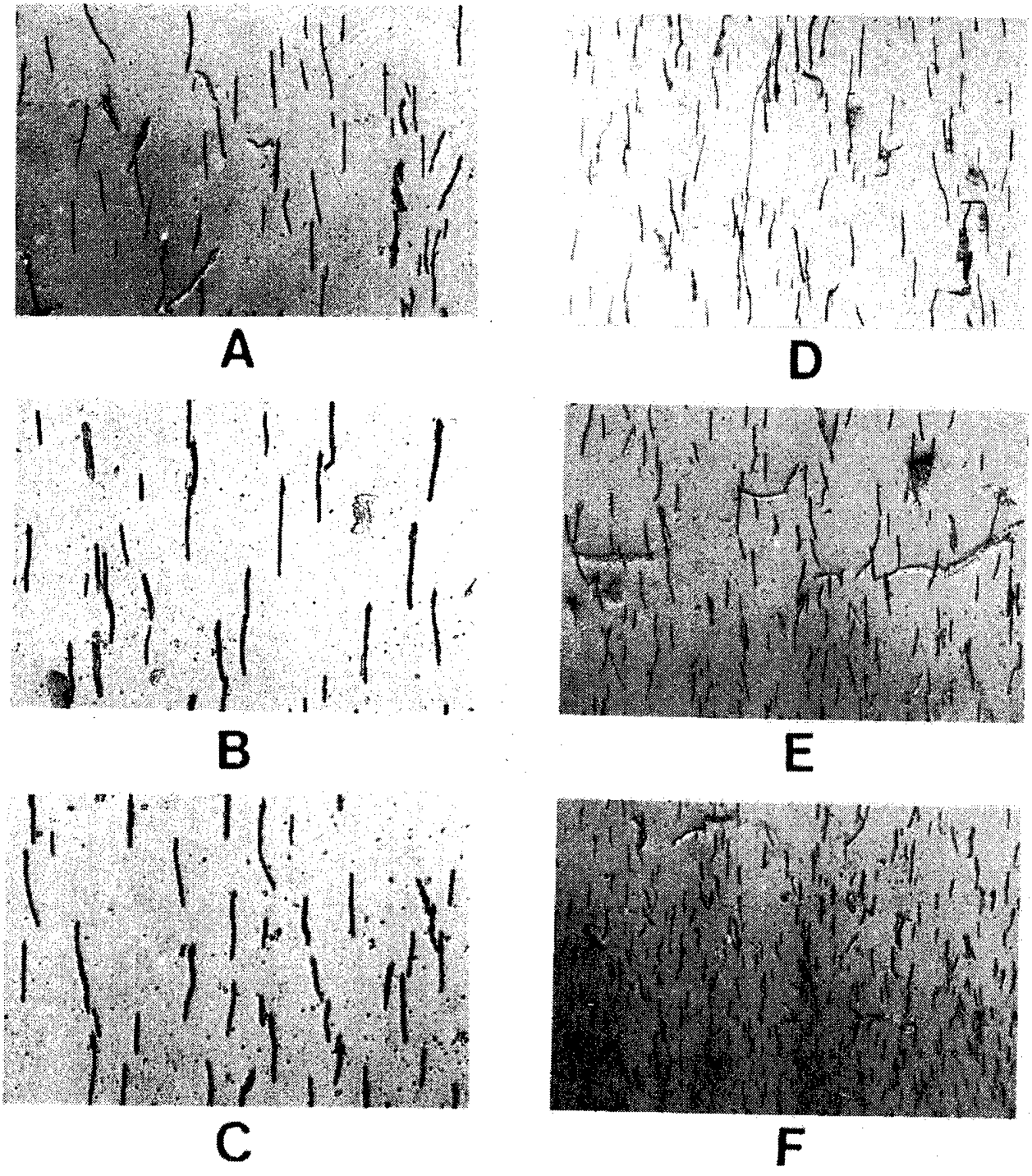

Fig. 4. Microstructure of HC Chromium Showing the Effect of Cl^- Ions. Deposits Plated at 55°C and 30 A/dm^2 Using Solutions Containing $CrO_3H_2SO_4$ at 250/2.5 g/ℓ and Cl^- Ion Concentrations of (a) 0.0 g/ℓ, (b) 0.2 g/ℓ, (c) 0.3 g/ℓ, (d) 0.4 g/ℓ, (e) 0.6 g/ℓ, and (f) 0.8 g/ℓ. 500X Magnification.

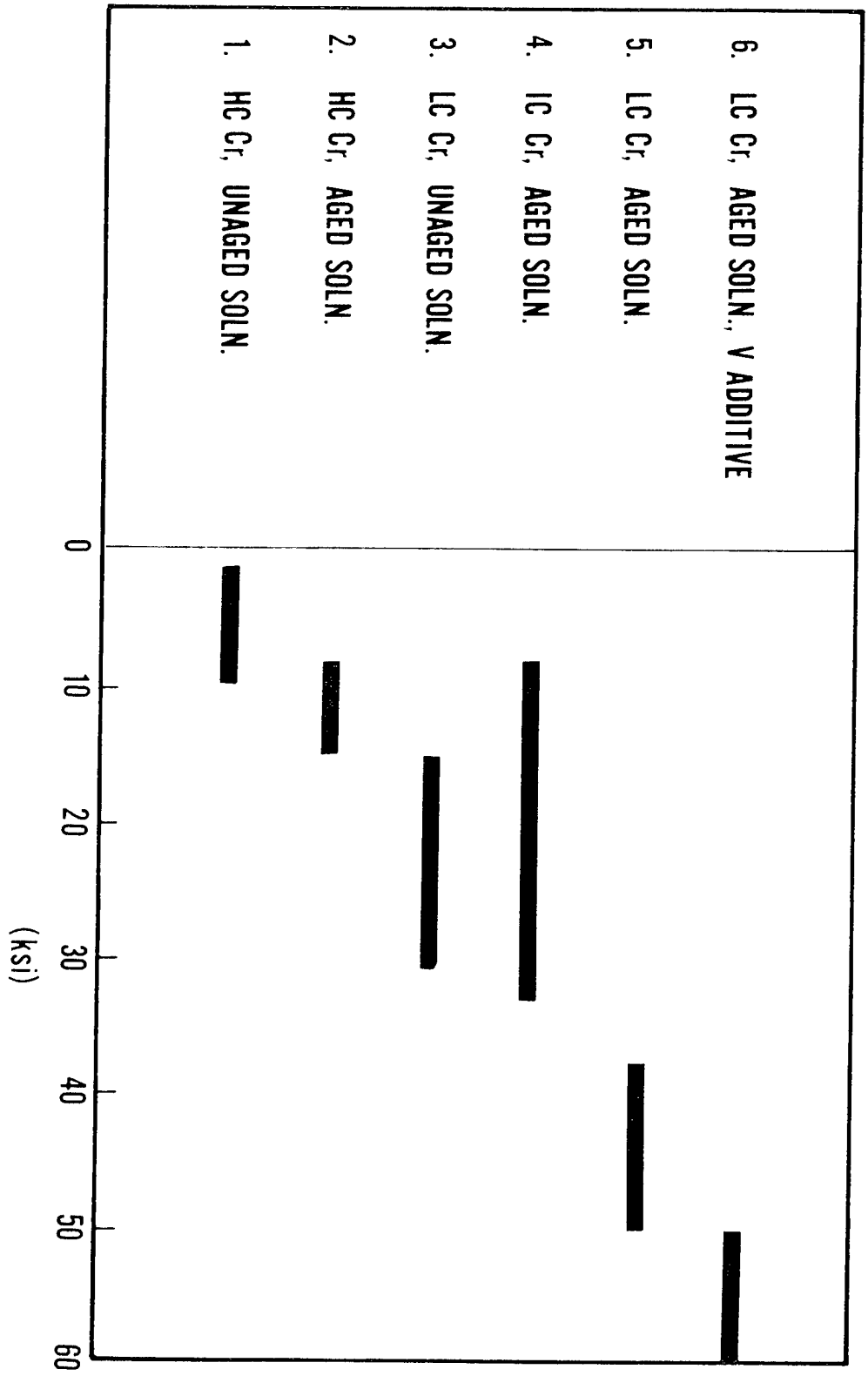

5. Strength of Electrodeposited Chromium.

EROSION RESISTANT COATINGS FOR GUN BORE PROTECTION

J A Sheward

RARDE, Fort Halstead
Sevenoaks, Kent, UK

ABSTRACT

The mechanisms responsible for the erosion of high pressure tank gun barrels are outlined together with the means being developed to prolong barrel life. The use of erosion resistant coatings is shown to be most effective and techniques for the deposition of suitable coatings are reviewed. The advantages and limitations of the various coatings available are described.

INTRODUCTION

There are two types of degenerative change which occur on firing high pressure, large calibre, tank gun barrels, namely the growth of cracks through the barrel wall (fatigue) and the progressive removal of steel from the bore (wear or erosion). The application of modern metallurgical techniques especially electro-slag refining, has meant that the fatigue life of barrels has been considerably extended. However, current ballistics requirements, which demand high temperature propellants result in severe in-bore conditions and unacceptably high erosion rates (up to 25μm per round).

The mechanisms of erosion are complex, and to some extent depend on firing conditions, but three principal factors have been identified ([1]). The intense thermal/pressure pulse on firing produces craze cracking due to thermal fatigue in the bore surface layer and a well defined heat affected zone is produced. By allowing the hot propellant gases to penetrate the bore surface, these microcracks facilitate the erosion of bore material by a variety of processes. In addition it has been shown that the reactive propellant gases produce brittle layers on the bore surface containing free carbon, carbides and nitrides, which are easily removed. Thirdly, the engraving forces of the driving band (usually nylon) produce mechanical wear effects, which would not be expected to be significant except possibly in removing brittle or cracked phases.

It may be concluded that if the bore could be protected, at least to some extent, from the thermal pulse produced on firing, then undesirable physical/chemical changes resulting in the formation of cracks and brittle phases would be reduced and the barrel life would be greatly extended. It has been shown that two general methods are available which are capable of doing this. The heat release which occurs is primarily due to the recombination of energetic species from the hot propellant gases at the bore surface. By using certain propellant additives especially fine powders such as talc, it is possible to reduce the outward diffusion of these energetic species, so that the heat intensity at the bore is reduced to some extent. The second method involves the application of a resistant coating to the bore, which is able to withstand the thermal pulse without suffering undesirable physical or chemical changes. This means that heat accepted by the

coating during firing is subsequently conducted away at a relatively slow rate, so that the gun steel substrate is not adversely affected. Since this method seems to offer the possibility of complete protection to the gun bore, considerable effort is being made to develop a suitable coating technique.

There are several important property requirements which need to be considered in the selection of a suitable coating material, these include high melting point, thermal capacity and yield strength, low thermal conductivity, a coefficient of thermal expansion and elastic modulus compatible with gun steel and chemical/physical inertness at high temperatures. These requirements have suggested that the most promising coating materials are certain refractory metals (W, Cr, Mo, Ta, Nb and Ti), their alloys and compounds (especially titanium nitride).

COATING TECHNOLOGY

Because of the peculiar rifled tube configuration of a gun barrel, any suitable deposition processes must possess good throwing power to ensure near uniform coating of land and groove of the rifling. In addition, exposure to high temperatures must be minimised to avoid degrading the mechanical properties of the gun steel. However, this limitation can be overcome by using a coated liner. Adequate coating/substrate adhesion is essential and usually relies on effective substrate cleaning, also the coating thickness must be sufficient to prevent the subsequent formation of a heat affected zone in the underlying gun steel. Present work indicates that the coating thickness for most materials must lie in the range 50 to 200μm to ensure adequate barrel life.

Coating porosity is undesirable and the density of the coating should be similar to that of the bulk material. The microstructure of the coating is very important. The columnar growth morphology associated with many deposition techniques is known to be particularly unsuitable since crack growth between the columnar grains is likely. This leads to undermining of the coating when the cracks reach the substrate. The formation of a fine grain coating structure is therefore an important consideration in the selection of a suitable coating process.

Four types of coating process and/or surface treatment are being considered (Table 1).

LIQUID PHASE ELECTRODEPOSITION

Conventional hard chromium plate will almost certainly be used in the UK to protect the bores of the next generation of tank guns. The limitations of HC chromium as an erosion resistant coating have been investigated and the failure modes observed (Fig 1) seem to be due to the high crack density and residual stresses present in this particular coating ([2]).

An experimental coating rig using a vertical barrel section is being set up to determine the effects of current density, electrolyte temperature and flow, entrained hydrogen etc on coating structure under carefully controlled conditions. This work will include the deposition of substantially crack-free chromium (LC) and the interrupted deposition technique will also be investigated.

There are several fused salt electrolyte systems which may be used to deposit a far larger range of metals than is available from aqueous electrolytes. Initially the molten fluoride (FLiNaK eutectic) system was used to deposit tantalum at temperatures around 700°C but the results were disappointing. This electrolyte is difficult to use since even minute traces of moisture have an adverse effect and it has now been ruled out because of operating temperature requirements. Two relatively low temperature systems ($\ll$600°C) are now being investigated which show promise for the deposition of refractory metals (Cr, Ta etc). The first of these being developed at Imperial College, uses a eutectic alkali metal chloride electrolyte (LiCl, KCl) to deposit chromium from the Cr^{++} ion at 470°C. Smooth fine grain adherent coatings about 30μm thick have been produced on small flat plates.

The second system operates at an even lower temperature ($\lesssim$200°C) with a molten eutectic alkali metal thiocynate system which has been developed by the Wolfson Centre for Electrochemical Science at Southampton University. Preliminary work is aimed at identifying the various ionic species that may be exploited in any electrodeposition process for metals of interest and in using additives (eg cyanates and urea) to improve electrolyte stability.

VAPOUR DEPOSITION

Vapour deposition processes may be subdivided into physical vapour deposition PVD and chemical vapour deposition CVD, which were developed from the original vacuum evaporation and hot wire pyrolysis techniques by applying modern vacuum technology and utilising low pressure plasma discharges as a convenient means of energy exchange.

PHYSICAL VAPOUR DEPOSITION

The sputtering process using a co-axial target electrode seems to be particularly suitable for coating the inside of tubes. The process relies on bombarding the target with energetic gas ions (usually argon from a glow discharge) so that small fragments are ejected and deposited on nearby substrates. The process may be conveniently combined with sputter cleaning of the substrate in the glow discharge prior to coating, although in the tubular geometry of the gun, impurities tend to be transferred to the target and then back to the barrel during coating. Electropolishing seems to be a good preliminary surface cleaning treatment to use; it also radiuses slightly the corners of the lands which is beneficial in avoiding folds and other defects in the coating.

An important development which differentiates it from the original technique is the application of a small negative bias (about 150v) to the substrate which attracts some ions from the plasma during the deposition process ([3]). These and probably other excited species from the plasma interact at the substrate during deposition and tend to produce a more coherent, finer grained coating structure than conventional sputtering. However because the electric field intensity is significantly different across the rifling (lands, grooves and land sides), with a corresponding variation in the intensity of the ion bombardment, there is some variation in coating structure.

Work on the sputter coating of 30mm RARDE barrel sections/liners for firing trials is complicated by the small bore diameter which creates design problems. In order to obtain adequate throwing power it is necessary to use comparatively high gas pressures (~0.3mbar) which lead to a rapid heat build up. Tungsten and tantalum coatings have been produced, but adhesion was poor due to the formation of a thin brittle iron oxide layer on the substrate during sputter cleaning. Work is in hand to investigate the use of argon hydrogen mixtures to minimise oxide formation and to improve substrate cooling.

The columnar growth structure of homogeneous vapour deposited coatings is known to be related to self shadowing effects during deposition, associated with the uniform size of the deposited particles. It has been shown that alloy coatings containing roughly equal proportions of tantalum and tungsten have significantly improved coating structures as compared to single component coatings. The target used consisted of a bundle of 1mm thick tungsten and tantalum rods.

A 120mm Chieftain tank barrel is 6.60m long and weighs over 1000Kg and therefore because of its size must serve as its own vacuum chamber. A pilot scale plant is being constructed so that the barrels can be processed in the vertical position with end flanges supporting a central electrode. A study of the glow discharge characteristics within a 120mm barrel is being made and it has been proved necessary to utilise power sources fitted with arc suppression. A study of sputtering deposition using RF techniques inside an unrifled 120mm cylinder with a removable test section is underway at Salford University. Experiments have been carried out using a variety of shaped central target electrodes (screw thread, multirod) but the deposition rates obtained were low ($<$1µm per hour).

DC sputtering work on smooth bore and on rifled 120mm barrel sections has also been carried out at AERE using a central tungsten target electrode with a small negative bias applied to the barrel. Attempts were made to increase the deposition rate towards 1µm per hour by using various target geometries. An open cage of rods placed on the circumference of a circle 80mm in diameter has been particularly successful. This design uses the hollow cathode effect to stabilise and intensify the plasma discharge over a wide range of operating pressures and ion currents.

Ion plating and reactive ion plating processes were developed by combining evaporation (from an electron beam hearth for refractory metals) with ion bombardment of the substrate during deposition. As before the ions (usually argon) are derived from a low pressure glow discharge, but by introducing a reactive gas compounds may be deposited (eg nitrides by introducing nitrogen). Since only a limited degree of scattering of the evaporant occurs, the process does not have enough throwing power to coat the inside of a gun tube without moving the electron beam hearth along the barrel axis. This does not seem to be feasible at present.

CHEMICAL VAPOUR DEPOSITION

This technique uses a volatile metallic compound, which is pyrolysed or reduced (usually by hydrogen), to produce a coating on a heated substrate. The flow system used is particularly suitable for gun tubes and there seems to be no limitation imposed by the throwing power of the process.

The deposition of tungsten from tungsten hexafluoride WF_6 on gun steel substrates has been studied at the Fulmer Research Institute at temperatures around 500°C. The coatings obtained were very crystalline and attempts to refine the grain structure by co-depositing tungsten carbides were not successful. Recently, non-crystalline coatings of tantalum, molybdenum and niobium have been obtained by reduction of the appropriate chloride at temperatures above 600°C. The chloride is prepared immediately before use by passing chlorine over the metal at a temperature of about 500°C. The conditions required to deposit these metals are similar, so that alloy deposition should be feasible.

A particular disadvantage of thermally activated CVD processes is the requirement for substrate heating. An interesting development is to repeat what has been done with PVD processes and use a plasma derived from a glow discharge to supply energy to decompose or reduce the metallic volatile. Such a procedure confers many of the advantages of PVD processes including sputter cleaning, yet retains the high throwing power capability of CVD. Thin coherent coatings of molybdenum and tungsten have been produced by this technique on small flat plates, using the metal hexacarbonyls which were evaporated from a hot water heated crucible into a hydrogen/helium plasma. Carbon contamination of the coatings can be reduced by the addition of small quantities of water vapour to the gas stream.

A study of the glow discharge assisted decomposition of titanium tetrachloride vapour at Southampton University has shown that the metal deposition rate is a function of the plasma electron temperature and therefore deposition may be explained solely by regarding the plasma as an energy exchange medium.

THERMAL SPRAY TECHNIQUES

Plasma spraying is generally more satisfactory than oxy-fuel gas spraying in producing dense carbon free coatings, but even so some porosity is likely. A short section of 120mm barrel has been plasma sprayed with tungsten using an external gun with a coating flux incidence angle of 45°. Fitments are available to plasma spray at near normal incidence inside a 120mm barrel and recently low pressure spraying in an inert atmosphere has been shown to produce coatings of superior quality, but as yet this process is not available in the UK. The flame detonation process has produced promising coatings on small flat plates but is not suitable for the coating of internal surfaces. At present, it seems unlikely that thermal spray techniques as such are capable of producing coatings of sufficient quality and consistency for use inside gun barrels.

SURFACE MODIFICATION TECHNIQUES

These may be divided into two main types, namely those which are concerned with treating gun steel substrates and those which modify the structure of predeposited coatings.

GUN STEEL SURFACE MODIFICATION

Since the steel itself is already in an optimum physical state controlled to a large extent by its composition and pretreatment, any modification technique must seek to alter the chemical composition of the surface layers only, so as to produce enhanced erosion resistance. A number of diffusion techniques are available in which nitrogen, carbon, boron etc penetrate the steel surface and react with it giving very hard diffusion bonded surface deposits with enhanced hardness and frictional wear resistance. Processes such as plasma nitriding (boriding, carburizing etc) do not significantly alter the dimensions of treated components and substrate heating is not a problem, but unfortunately most of these coatings are too thin ($\leq$10μm). In order to utilise the properties of stable refractory nitrides eg titanium nitride TiN, which has been shown to possess useful erosion resistant properties, predeposited ion plated titanium coatings were diffused into steel substrates at 700°C prior to nitriding. However the diffusion of titanium inwards was restricted by the formation of the intermetallic phase Fe_2Ti and it has not been possible to produce satisfactory diffused coatings of titanium nitride.

It is possible to obtain much greater substrate penetration by ion implantation techniques, although unlike the plasma process ion implantation is very much a line of sight process. Small ion sources have recently been developed by AERE capable of treating the insides of tubes down to about 75mm diameter. Nitrogen implantation of low carbon steel results in enhanced hardness and frictional wear properties and there is evidence that implanted nitrogen is not present initially as a separate nitride phase but in the atomic state. The atomic nitrogen migrates along substrate dislocations so that mechanical properties improve on ageing. Of greater interest is the possibility of implanting metallic ions such as yttrium and chromium together with nitrogen possibly underneath coatings.

COATING MODIFICATION

There are certain readily applicable coating processes (in particular plasma spraying and electrodeposition) which produce refractory metal coatings with defective features such as microcracks or porosity. There is evidence that the structure of these coatings could be radically improved by exposure to fast high intensity thermal treatments which transform the coating structure but leave the substrate largely unaffected. Promising techniques include scanning the coated surface with laser or electron beams or by exposure to a sufficiently energetic plasma.

Laser glazing studies of electrodeposited chromium coatings at Imperial College have been carried out in an argon atmosphere inside a glove box to prevent embrittlement of the chromium by nitrogen. By varying the laser energy, spot size and traverse rate it is possible to obtain partial melting of the coating and a limited degree of diffusion of chromium into the substrate occurs. The annealed chromium layer produced is softer, contains far fewer cracks than originally, also the coating is bonded to the substrate by diffusion. However a well defined heat affected zone is produced underneath the diffused zone, which is harder than the original gun steel and may well be more susceptible to thermally induced fatigue failure leading to the formation of microcracks.

The glazing of stub 30mm chrome plated barrels for subsequent firing is now being attempted (Fig 2). It is probably not necessary to glaze the entire rifled profile of a barrel and only those regions of the coating that have been shown to be most likely to fail (viz land corners) will be glazed initially.

Since the erosion mechanisms observed in both coated and uncoated gun barrels often seems to be associated with the formation and growth of cracks of some kind, the presence of an amorphous layer on the bore surface could be an effective crack barrier. Cambridge University have developed amorphous metallic glasses based on gun steel alloys containing carbon, phosphorus and/or boron additions, which may be obtained in ribbon form by splat cooling ($\sim 10^6$ deg/s). Small coated steel samples with an amorphous surface have been prepared by exposing clad or plasma sprayed coatings to electron beam treatment in vacuo. The cladding process is clearly impracticable inside tubes and plasma sprayed coatings contain trapped gases which are released on exposure to the electron beam with disruptive results.

Attempts have been made to sputter suitable alloy coatings and these have been shown to be partly amorphous in the as deposited state. Work is continuing to obtain thicker coatings. Unfortunately the amorphous alloys so far investigated contain elements such as phosphorus, which react with hot propellant gases. Other less reactive alloy systems are being investigated and the possibility of using ion implantation to produce these in situ on the bore surface is being considered.

ASSESSMENT TECHNIQUES

A number of small scale assessment techniques have been developed in order to determine the comparative erosion resistance of test coatings. The standard chosen for comparison has been an electrodeposited chromium coating of comparable thickness. The techniques used include traversing a plasma torch across a 4cm square flat coated gun steel sample, eroding a coated nozzle sample with a jet of propellant gas and firing out a coated 30mm stub RARDEN barrel under erosive conditions ([2]). The thin layer activation technique has been used to determine erosion rates after just a few firings.

Recently the development of a 30mm liner system has started. This will be used to determine the in-bore performance of coatings produced by high temperature processes ($>500°C$) including fused salt electrodeposition and CVD.

ACKNOWLEDGEMENT

The author is indebted to his colleagues for much of the material used in the preparation of this report.

© Crown Copyright Reserved

TABLE 1. POTENTIAL COATING PROCESSES AND SURFACE TREATMENTS

Type	Process	Typical Coating Structure	Remarks
Liquid Phase Electro-deposition	Hard Chrome Plating	Microcracked	In use
	Soft Chrome Plating	Fewer cracks	Under investigation
	Fused Salt Deposition	Diffused at high temperatures	Temperature limitation
Physical Vapour Deposition PVD	Sputter Ion Plating	Variable	Promising
	Ion Plating	Variable	)Point
	Reactive Ion Plating	Variable	)source)limitation
Chemical Vapour Deposition CVD	Thermally Induced	Columnar	Temperature Limitation
	Plasma Activated	?	Promising
Thermal Spray Techniques	Plasma Spraying	Porous	Unlikely
	Detonation Gun	Dense	Very directional
Surface Modification Techniques	Plasma Nitriding	Diffused	Not suitable
	Ion Implantation	Diffused	?
	Laser Glazing	Variable	Promising
	Amorphous Coatings	-	Resistant coating development needed

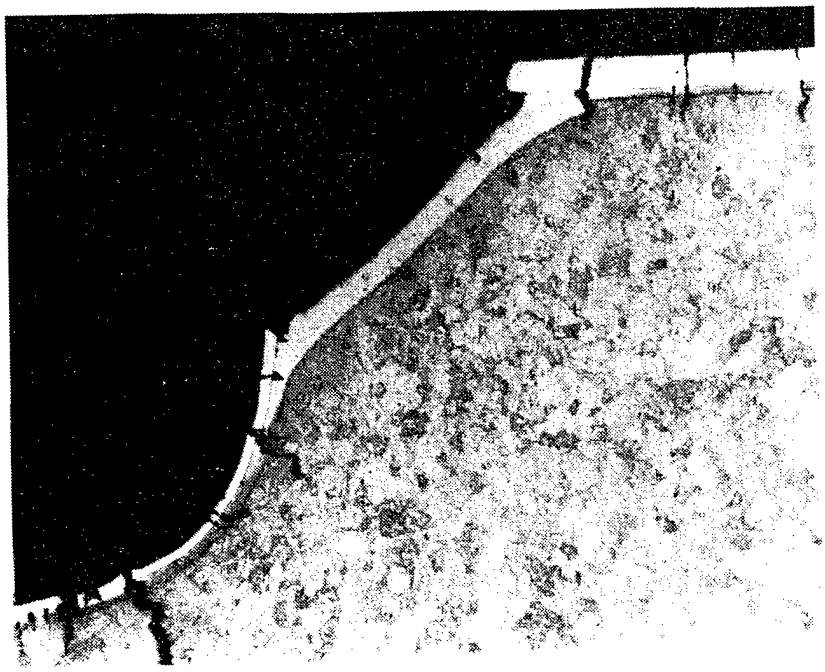

Fig 1. Typical spalling of a hard electroplated chromium coating at a land corner in a 120mm barrel. Coating detachment is followed by erosion of the land and heat affected zone formation is conspicuous.

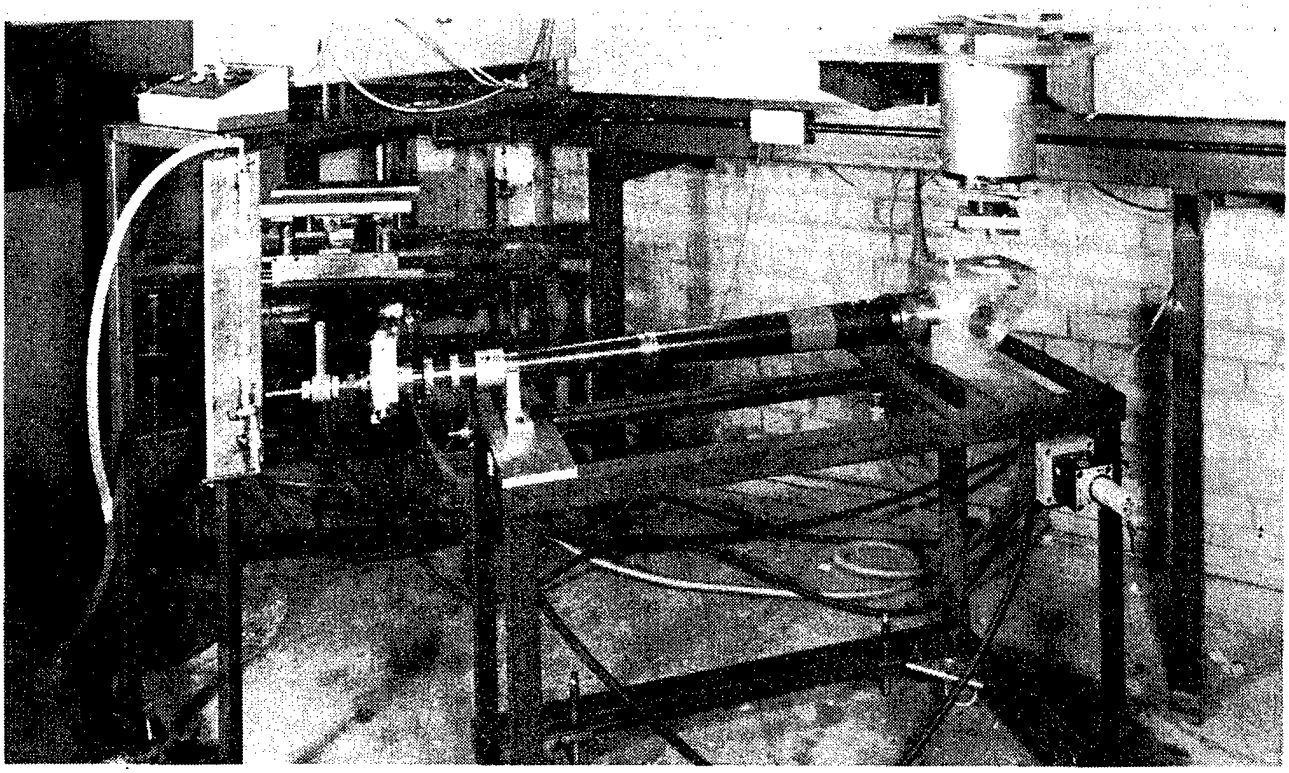

Fig 2. Equipment for the laser glazing of stub 30mm barrels.

REFERENCES

1. Glue D R, Sheward J A, Young W J and Gibson I P

   "Erosion Resistant Coatings for Gun Bore Surfaces",
   Inst of Metallurgists Conference, Environmental Degradation of High Temperature Materials Douglas ICM1980, also RARDE Technical Report 1/81, unlimited.

2. TTCP Sub Group P, Technical panel PTP-1 Operating Assignment: Gun Wear and Erosion. Proceedings of meeting held at RARDE, UK 14-18 June 1982.

3. Gibson I P

   "Erosion Resistant Coating of Tubes by Physical Vapour Deposition",
   Thin Solid Films 83, 27-35 (1981). Presented at the International Conference on Metallurgical Coatings, San Francisco, April 1981, also RARDE Technical Report 3/82, unlimited.

REFRACTORY METAL COATINGS FOR CONTROL OF GUN TUBE EROSION

M. Levy and S. K. Pan

Army Materials and Mechanics Research Center
Watertown, Massachusetts 02172

ABSTRACT

The feasibility of densifying plasma sprayed refractory metal coatings on 4340 steel by means of a 15kW CO_2 laser was investigated. The coating metals included tantalum, Ta-10W, molybdenum and columbium alloys WC103 and WC3015 Although density was significantly improved, full densification with minimal dilution of substrate was not achieved. It may be possible to overcome the problem by improving the protective atmosphere used during processing and by laser processing the refractory metals in powder form directly on the surface rather than as a plasma sprayed layer. Laser processing of Stellite 12 powders was successful. Recent results of efforts to electrodeposit niobium, tungsten and molybdenum from molten salts were presented.

INTRODUCTION

The Army has a continuing need for improved methods of minimizing erosion and extending the life of long range cannon because of problems associated with the upgrading of field guns, reducing the variety of different items in supply and lowering overall costs[1]. Although the NMAB review recognized that the problem of gun tube erosion has to some measure been alleviated, the board stated that there was no implicit assurance that advanced gun systems could be designed with acceptable wear life, based on current state-of-art. Efforts to promote a better understanding of the mechanism of gun erosion was recommended.

Erosion of gun tubes is a complex problem which spans the sciences of metallurgy, chemistry, physics and mechanics. Research efforts must be designed to recognize the multidisciplinary nature of the problem. However, the NMAB concluded that an improved understanding of the complex erosion phenomenon will not be achieved through purely analytical treatments. Rather, any predictive models developed would necessarily be mainly empirical.

Further a multi-faceted study of the erosion problem was suggested which included the following factors: 1. Test/scale-up, 2. Erosion-reducing additives, 3. Propellant composition, 4. Rotating band materials, 5. Insulation/Lubrication, 6. Wear-resistant inserts, 7. Cooling, and 8. Protective surface coatings.

Characteristics required of candidate coating materials include: high melting point (>1534°C), chemical inertness to propellant by-products, high thermal ductility and fracture toughness, fabricability and economic availability. Additional requirements include good adhesion and thermal, mechanical and metallurgical compatibility with gun steels.

Many conventional techniques are available for producing coatings on steel substrates including electroplating, diffusion (e.g., carbiding, chromizing, nitriding and metalliding), hot dip, vapor deposition (e.g., sputtering and glow discharge) and thermal spray processes (e.g., arc plasma, oxyacetylene and detonation).

A cursory review[2] of the available techniques indicated that the following processes can meet the requirements for coating a gun tube: 1. Electroplating, 2. Thermal spray, 3. Sputtering, 4. Chemical vapor deposition. Electroplating is being economically used on a large scale. Unfortunately, many promising materials such as Mo, W, Cb and Ta can not be electrodeposited in aqueous solutions. But electrodeposition of refractory metals from fused salt baths is feasilbe. Plasma arc spraying methods can be used to apply most materials in a gun tube provided the diameter is large enough to accomodate the torch unit. Sputtering can produce execellent coating-substrate systems. But this method is not economically feasible for large gun tubes because of limited capabilities for producing thick coatings. Chemical vapor deposited coatings generally require unacceptable heating of the steel substrate to achieve a good bond. Therefore, electrodeposition and plasma arc spray techniques appear to be the more promising of the conventional coating processing techniques for applying candidate coatings to gun tubes.

The objective of this study is to develop protective surface coatings capable of increasing the service life of gun barrels by investigating and optimizing coating processing techniques and new coating systems with erosion resistant potentials. Initial studies were conducted with high temperature materials (melting point greater than gun steel) applied by (I) the plasma arc process and (II) fused salts electrodeposition. The feasibility of minimizing or mitigating porosity inherent in the layers of plasma sprayed refractory metals on gun steel using a large industrial laser was investigated.

I. LASER DENSIFIED PLASMA SPRAY COATINGS

MATERIALS AND PROCEDURES

The metals and alloys selected for this study were tantalum, Ta-10W, molybdenum and the columbium base alloys WC 103 and WC 3015. These alloys were selected in order to give a range of melting points from a high of 2995°C for tantalum to approximately 2468°C for WC 103 and WC 3015. Pure columbium metal was not included in this study, because laser processing of plasma sprayed columbium had been investigated in an earlier limited program[3]. In that investigation, it was shown to be possible to obtain densification of plasma sprayed columbium on SAE4340 substrates, but complete melting of the

Cb-layer could not be achieved without damage to the substrate. Laser processing electroplated chromium on 4340 samples, for the purpose of consolidation, surface melting and substrate hardening had also been performed earlier[4]. It was found that chrome plated steel could be laser hardened, but blistering and softening of the chromium took place. Chromium was therefore not considered in this work. However, it was decided to include a lower melting commercial hardfacing alloy with good high temperature hardness and erosion resistance. Stellite 12 was selected for this purpose.

Originally, it was planned to include tungsten in the program, but the very high melting point of tungsten (3410°C), well above the melting point of steel (1534°C), would have made it impossible to obtain laser cladding by melting or densification of plasma sprayed tungsten without collapse of the 4340 steel substrate.

The compositions of the six materials studied are listed in Table I. The specimens for laser processing were prepared by plasma spraying these materials on hardened 4340 steel substrates measuring 4" X 4" X 1/2". The specimen preparation was performed by AMMRC using a Metco type 3MB plasma flame spray gun. The plasma spray parameters are summarized in Table II.

All laser processing was performed* on an Avco HPL 15 kW, CO_2 laser with continuous wave output. A focused laser beam with a nominal diameter of 0.05" (0.127 cm) in the focal plane was used for processing the samples. This spot was scanned back and forth in a direction normal to the processing direction by means of an oscillating copper mirror. The frequency of oscillation was 42 Hz and the amplitude could be varied from 0.5" (1.27 cm) to 0.25" (0.635 cm). In this manner, a rectangular laser spot with length 0.05" (0.127 cm) in the processing direction and a width equal to the amplitude of oscillation could be generated in the focal plane.

The specimens were mounted on a motor driven slide inside a metal enclosure as shown in Fig. 1. This enclosure was evacuated prior to laser processing by means of a rotary vacuum pump, and backfilled with welding grade argon gas. The laser beam entrance port on top of the enclosure was closed during evacuation and opened just prior to start of processing. In order to reduce the influx of air into the enclosure, the argon gas atmosphere was kept streaming to the enclosure at a slight over-pressure. But some contamination by oxygen and nitrogen was unavoidable.

The specimens were laser processed by moving them at a pre-set speed under the stationary laser beam. In this way, a strip of laser processed material across the specimen, equal to the width of the beam, could be obtained.

---

*Laser processing work was performed by Ole Sandven at AVCO Everett Research Laboratory, Everett, MA 02149, Contract No. DAAG 46-80-C-0044

After each run, the specimen was allowed to cool, and the enclosure was then re-evacuated and backfilled with fresh argon gas before the next run. Several runs could be made on each specimen for the purpose of determining the most suitable processing parameters.

The cladding of the 4340 steel samples with Stellite 12 was less difficult and was performed with the arrangement shown in Fig. 2. In this set-up, a 0.5" X 0.5" (127 cm X 127 cm) laser spot was generated on the specimen surface by means of an optical integrator. During the initial processing runs with this equipment, plasma sprayed specimens were used, but excessive oxidation occurred. In later work, the Stellite material was applied to the substrate surface in the form of loose powder by means of an automatic powder feeder. This proved much more satisfactory, and thick continuous laser cladding without visible oxide formation could be obtained. In all processing of Stellite the reaction zone was protected by an off-axis argon jet operating with a flow rate of 12.5 ft 3/hr (103cc/sec).

Metallographic specimens were prepared from the laser processed samples by making cuts normal to the processing direction. The refractory metal specimens were not etched, because the etchtant needed to reveal the structure of these metals, tended to attack the substrate severely.

The Stellite 12 cladded samples were etched in Glyceregia (30cc Glycerol, 25cc HCl, 10cc HNO_3) followed by immersion in Murakami's etchtant (10g $K_3Fe(CN)_6$, 10g KOH in 100cc H_2O).

Metallographic inspection of the specimens were performed by AVCO with a Leitz metallograph and hardness measurements were carried out by means of a Wilson Knoop microhardness tester, using a 500g load. Hardness measurements were made at 0.005" intervals from the surface. The observed Knoop hardness numbers (KHN) were translated to Rockwell C units (R_c) by means of standard tables.

RESULTS

MOLYBDENUM A total of 30 test runs were performed at power densities ranging from 168 kW/in^2 (26.0 kW/cm^2) to 440 kW/in^2 (68.2 kW/cm^2). The range of processing speed was from 4 to 35 in/min (0.17 to 1.48 cm/sec). The corresponding dwell time, that is, the time a given spot on the surface is exposed to the laser beam was 0.17 sec to 1.50 sec. It proved difficult to obtain consistent results, particularly at the higher processing speed. This was apparently caused by variation in laser energy absorption from specimen to specimen and even from one area to another on the same specimen. Porosity was observed in all cases regardless of processing speed and a suitable set of processing parameters could not be established for molybdenum. Figure 3 shows the extensive porosity present at the interface after slow laser processing.

TANTALUM A total of 50 test runs were completed on tantalum. The range of power density was from 168 to 440 kW/in^2 (26.0 to 68.2 kW/cm^2) at a processing speed range from 6 to 40 in/min (0.25 to 1.69 cm/sec). The

corresponding range of dwell time was from 0.15 to 1 sec. Again, variation of absorptivity was apparent, as was the case with all plasma sprayed material tested. Nevertheless, significant densification could be obtained at high power and speed levels as shown in Fig. 4. At lower power and speed, deep inmelting and alloying with the substrate occurred as shown in Fig. 5. At medium power and speed, considerable melting took place but extensive porosity was observed at the interface. The hardness profile obtained under these conditions is shown in Fig. 6. The high hardness of the tantalum surface layer indicates a high level of impurities due to contamination by the ambient atmosphere during processing.

Ta-10W A total of 37 test runs were made on this material with processing parameters ranging from 110 to 440 kW/in^2 (17.0 to 68.2 kW/cm^2) in power density, and with processing speed levels from 9 to 30 in/min (0.38 to 1.27 cm/sec). The range of dwell time was 0.2 to 0.67 sec. In Ta-10W, surface melting could be obtained, but again with formation of large pores at the melt-solid interface (Fig. 7). Processing at lower speed resulted in massive void formation and partial collapse of the substrate surface. The hardness profile obtained indicates a high level of impurities.

WC 103 Fifty test runs were made on WC 103 in order to establish optimum processing parameters. The test parameters ranged from 172 to 440 kW/in^2 (42.1 to 68.2 kW/cm^2) for power density, 10 to 45 in/min (0.42 to 1.91 cm/sec) for processing speed, and 0.13 to 0.6 sec for dwell time. At low processing speed, extensive alloying with the substrate material occurred, as shown in Fig. 8. At higher speed the resulting structure retained same porosity. However, considerable densification did occur as indicated in Fig. 9 showing laser processed material on the right and uprocessed, plasma sprayed material on the left. The hardness of the alloy layer is not as high as for tantalum and Ta-10W, but some contamination is still indicated by the magnitude of the hardness and its variation form spot to spot.

WC 3015 About forty test runs were made on WC 3015 with power densities in the range 156 to 432 kW/in^2 (24 to 67 kW/cm^2) and processing speed varying from 20 to 70 in/min (0.82 to 2.96 cm/sec), with corresponding dwell times in the range 0.09 to 0.3 sec. At low processing speed, extensive alloying with the substrate occurred with concomitant improvement in density. At higher speed, no power setting could be found that resulted in any visible effect on the plasma sprayed material without damaging the substrate. A hardness of R_c 66 was found for the bulk of the WC 3015 alloy.

STELLITE 12 The processing of this material was performed with the system shown in Fig. 2. The optimum processing parameters were determined to be 38.8 kW/in^2 (6 kW/cm^2) at a processing speed of 20 in/min (0.85 cm/sec) with a corresponding dwell time of 1.5 sec. At these parameters, dense, pore free deposits with a thickness of 0.07" (0.178 cm) could be obtained. By overlapping consecutive runs, a continuous clad layer could be obtained as shown in Fig. 10. The hardness of the Stellite layer was, as expected, around R_c 50. The slight drop in hardness at the interface showed that the dilution of the Stellite

layer, by substrate melting, was very slight. Table III summarizes the parameters employed for laser densification of each material and lists the optimum parameters developed for maximum density and minimum dilution of substrate.

SUMMARY AND CONCLUSIONS

The cladding of SAE4340 steel with Stellite 12, yielded the best results. Little dilution (inmelt into the substrate), good bonding and satisfactory hardness of the cladded layer were obtained. By overlapping adjacent individual laser runs by approximately 50%, it was possible to obtain a continuous clad layer over the entire 4" X 4" (10.2 X 10.2 cm) sample surface area.

The results of the laser processing of the refractory metals/alloys show that true laser cladding of steel substrates with these materials is very difficult to achieve (full density with minimal dilution of substrate) due to the reactivity of the materials and to the great difference in melting points between the cladding materials and the steel substrate. Considerable densification of the plasma sprayed refractory metal surface layers could be obtained, but attempts to fully melt the surface layers resulted in damage to the substrate or alloying between substrate material and the cladding material. Some porosity was also evident when melting of the plasma sprayed surface layer occurred. Another problem encountered in the laser processing of the refractory materials, was contamination by oxygen and nitrogen from the processing atmosphere. This is shown by the high hardness of the processed materials.

In order to obtain more satisfactory results, improved processing techniques, in particular, an improved protective atmosphere must be used. It should then be possible to obtain better densification, and for the lower melting columbium alloys WC 103 and WC 3015, true cladding by melting may be possible. Further, if the material is applied to the gun steel surface in the form of loose powder, rather than by plasma spraying, it may also prove possible to obtain true cladding by melting. Absorptivity of the laser beam will be enhanced while heat conduction to the substrate will be less than for a solid layer.

II. FUSED SALT ELECTEODEPOSITION OF REFRACTORY METALS

MATERIALS AND PROCEDURES

The work reported herein summarizes progress we have made in electrodepositing niobium, molydenum, and tungsten, particularly niobium, on copper and steel substrates. The process employed for the electrodeposition of these refractory metals was developed by Mellors and Senderoff[5,6] and involves high temperature electrolysis in a bath of molten fluoride salts (FLINAK). These electrolytes are made up of a ternary eutectic of alkali fluorides, i.e., LiF, NaF and KF. The following operations are involved in the over-all process: electrolyte preparation; plating cell design , pre-electrolysis and plating.

ELECTROLYTE PREPARATION The electrolyte was prepared by melting a mixture of Li, Na, and K fluorides in the following proportion to form the ternary eutectic (m.p. 453^{O}C): LiF 26.2%, NaF 10.5%; KF 47.0%[7,8]. Ten weight percent

will react with tungsten chips to form the lower valence tungsten.

$$W^{6+} + W^{O} \longrightarrow 2W^{+++}$$

Figure 15 shows the set-up for this procedure. After pre-electrolysis to adjust the mean valence to about 4 (4.5 is the upper limit) electrodeposition of tungsten will follow. The same procedure will be applied to molybdenum plating, but here MoF_6 will be used as the gas to react with molybdenum chips to form a mean valence of three.

CHARACTERIZATION OF TANTALUM ELECTRODEPOSITS - A metallurgical examination of several tantalum plated specimens provided by Union Carbide Corp. and General Metals Technologies Corp.[9,10] was carried out. Figure 16 shows the microstructure of (a) the as-deposited plate and (b) after heat treating at 1500°C. There is no evidence of recrystallization after the heat treatment. The columnar structure observed remains unchanged. Figure 17 contains X-ray diffraction scans taken at two different locations in the tantalum plate. The tracing in (a) shows the presence of both α and β phases, but is predominantly β phase. The α phase only is present in scan (b). Figure 18 shows the Knoop hardness indentations on the α and β tantalum grains and the steel substrate. The hardness values listed in Table VI show that the β phase is about double the hardness of the α phase.

SUMMARY AND CONCLUSIONS

Niobium electrodeposited from a molten salts bath exhibited good adhesion to substrate, uniform thickness, high density, and some preferred orientation. Examination of tantalum deposited in a similar fashion showed that the plate is thermally stable with a controllable grain structure. Our efforts will continue with further evaluation of niobium, electrodeposition of molybdenum and tungsten with emphasis on molybdenum because it has the highest potential for gun tube applications. Also, for improved properties, refractory metal alloys will be investigated employing pulse current electrodeposition[11] and electrometalliding[12] techniques. We recognize that the relatively high temperature of the molten salts bath may degrade the mechanical properties of the gun tube steel. The utilization of liners and/or the development of lower temperature baths comprised of fused chlorides, cyanides and carbonates is both feasible and desirable.

REFERENCES

1. Erosion in Large Gun Barrels, National Materials Advisory Board, Publication NMAB-321-1975
2. Gun Tube Erosion and Control, Proceedings of the Interservice Technical Meeting, Watervliet Arsenal, February 25 & 26, 1970, p3,4-10
3. AVCO Everett Research Laboratory Contract DAAG 46-79-M-1044 (AMMRC)
4. AVCO Everett Research Laboratory Contract DAAA 77-C-0243 (Watervliet Arsenal)
5. G. W. Mellors and S. Senderoff, Canadian Patent 688,546 (1964)
6. S. Sanderoff, Metallurgical Review, 11, 97-111 (1966)

of ammonium bifluoride was added to the melt in a graphite crucible in order to remove residual moisture and to convert impurity elements in the salts to fluorides. Then the melt was cast into small ingots ready for the pre-electrolysis step.

PLATING CELL AND PRE-ELECTROLYSIS OF NIOBIUM BATH Figure 11 is a schematic drawing of the plating cell. Ingots of the purified salts and K_2NbF_7 (16.2 wt%) were placed in the nickel crucible inside the plating cell where an argon atmosphere was maintained at all times. A gate valve seals off the electrolyte from the atmosphere when the cell is opened. The cell is heated up by means of a pot furnace which surrounds it. The rate of heating is about 200°C/hr to 800°C. This temperature was maintained during the entire pre-electrolysis period. Commerically pure niobium sheet (99%) was used as anode along with a copper cathode for the low current (10 mA/cm^2) electrolysis for 10 hours. During this pre-electrolysis any residual impurities in the melt were deposited on the surface of the copper cathode as shown in Fig. 12. Concomitantly, niobium was reduced to a mean valence of approximately 4. Above mean valence 4.2 the current efficiency is reduced significantly.

PLATING OF NIOBIUM Electrodeposition of niobium was carried out according to the following parameters:

Anode:	Niobium sheet, 3" X 2" (7.6 X 5.1 cm)
Cathode:	Copper sheet, 3" X 1" (7.6 X 2.5 cm)
	Steel sheet, 3" X 1" (7.6 X 2.5 cm)
Current density:	15 to 50 mA/cm^2 (96.8 to 332.6 mA/in^2)
Plating time:	0.5 to 18 hr
Bath temperature:	750 to 810°C

Typical platings on copper and steel substrates are illustrated in Fig. 13. Coatings of uniform thickness with good adhesion are obtained. A columnar structure with some epitaxial growth is observed in the deposit on copper, i.e., grain boundaries extend into the deposit. A slight preferred orientation of <223> was revealed by X-ray diffraction. Table IV shows that the hardness of the niobium plate is 160(KNH) compared to a hardness of 120(KHN) for the mild steel substrate.

The deposition rate of niobium at the cathode current density of about 13 mA/cm^2 was 0.65 mil/hr (Fig. 14). The cathode current efficiency (CCE) varied with plating time. Based on the reduction of niobium from a valence of four.

$$Nb^{+4} + 4\ e \longrightarrow Nb^{0}$$

the CCE was calculated as shown in Table V. The current efficiency was essentially 100% for the niobium plating.

ELECTRODEPOSITION OF TUNGSTEN AND MOLYBDENUM Efforts to electrodeposit these metals from molten salt baths will commence soon. Generally, the procedures will be similar to those described for niobium. Again the basic ingots of ternary eutectic of alkali fluorides will be used. But after melting, and prior to pre-electrolysis, WF_6 gas will be bubbled into the melt, where WF_6

7. G. W. Mellors and S. Senderoff, J. Electrochem, Soc., 112, 266-271 (1965) also this jounal 113, 66-71 (1966)
8. G. W. Mellors, personal communication
9. S. K. Pan, (Unpublished previous work)
10. I. Ahmad and E. Chen, personal communication
11. R. Weil, personal communication
12. N. C. Cook, U.S. Patent 3,024,175 (1962)

Table I Composition of Material

MATERIAL	WEIGHT %															
Mo	Mo															
	99+															
Ta	W	Cb	Fe	Ni	Mo	Ti	Zr	C	O	TA						
	0.93	0.042	0.005	0.001	0.017	0.001	0.025	0.0038	0.088	Bal						
Ta-10W	W	Cb	Fe	Ni	Mo	Ti	Zr	Si	Co	N	Ta					
	10.6	0.098	0.0035	0.002	0.002	0.002	0.002	0.0067	0.079	0.004	Bal					
WC-3015	Ti	Zr	Hf	C	W	Ta	Fe	Mo	Al	Si	B	O	H	N	Cb	
	4.5	1	26.7	0.3	10.9	1.7	0.0265	0.02	<0.002	0.0106	$<10^{-4}$	0.162	0.013	0.183	Bal	
WC-103	Ti	Zr	Hf	C	W	Ta	Fe	Mo	Al	Si	B	O	H	N	Cb	
	1	0.7	10	0.062	10.9	1.7	0.0265	0.02	<0.002	0.0106	$<10^{-4}$	0.162	0.013	0.183	Bal	
Stellite #12	W	Cr	C	Co												
	9	29	1.8	Bal												

Table II Plasma Spraying Parameters

MATERIAL	POWDER MESH SIZE	THICKNESS DEPOSIT	SPRAY PARAMETERS			
			AMPS	VOLT	SPRAY DIST.	SPRAY RATE
Mo	-200/+30	0.045"	500	60-70	3" - 5"	9.5 lb/hr
Ta	-120/+200	0.045"	500	60-70	4" - 7"	8 lb/hr
Ta - 10W	-120/+200	0.045"	500	60-70	4" - 7"	8 lb/hr
WC-3015	-200/+325	0.045"	500	60-70	3" - 5"	9.5 lb/hr
WC-103	-200/+325	0.045"	500	60-70	3" - 5"	9.5 lb/hr

Substrate: SAE4340 steel hardened to R_c 53-55, Atmosphere: A + 10% H_2

Table IV Microhardness (KHN) of Nb-Platings

Specimen	B 12	A21	F4
Nb Plating	194	142	144
Substrate*	91	70	118

* B12 &A21 copper, F4 mild steel

Table III. Summary of Processing Parameter Study

MATERIAL	POWER DENSITY (KW/IN^2)	PROCESSING SPEED (IN/MIN)	DWELL TIME (SEC)	OPTIMUM PARAMETERS
Mo	168 - 440	4 - 35	0.17 - 1.5	------
Ta	168 - 440	6 - 40	0.15 - 1	194 kW/in^2 at 16.8 in/min
Ta-10W	110 - 440	9 - 30	0.2 - 0.67	198 kW/in^2 at 16.8 in/min
WC 103	272 - 440	10 - 45	0.13 - 0.6	187 kW/in^2 at 34 in/min
WC 3015	156 - 440	20 - 70	0.09 - 0.3	------
STELLITE #12	32 - 38.8	5 - 25	1.2 - 6.0	38.8 kW/in^2 at 20 in/min

Table V. Niobium Plating on Copper

Specimen No.	C.D. (mA/cm^2)	Time (min)	Thickness (mil)	C.C. Eff. (%)
A-12	13.6	60	0.43	78
A-13	14.1	120	1.08	94
A-14	13.5	180	1.83	111
A-17	12.5	240	2.54	125
A-18	11.0	300	2.42	108

Table VI. Microhardness (KHN) of Ta-plating

Specimen		TA	TB	TC	TD	Average
Tantalum Plating	α	250	340	169	388	286
	β	700	697	650	640	672
Substrate (steel)		403	388	307	286	346

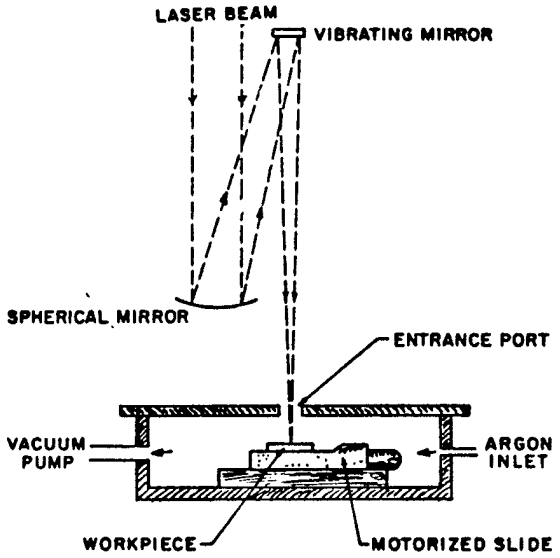

Fig. 1 Experimental set up for laser treatment.

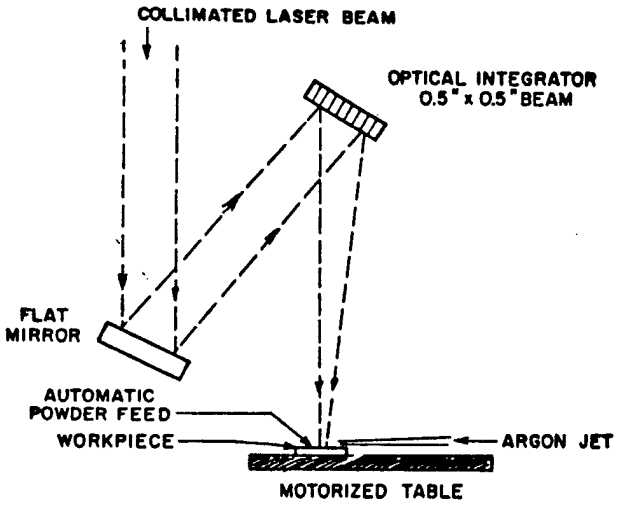

Fig. 2 Laser cladding of Stellite 12 on steel.

(18X)

Fig. 3 Laser treated Mo-coating (184 kW/in^2, 12.3"/min).

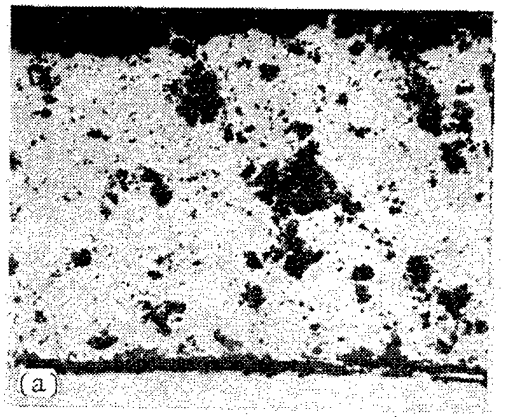

(75X)

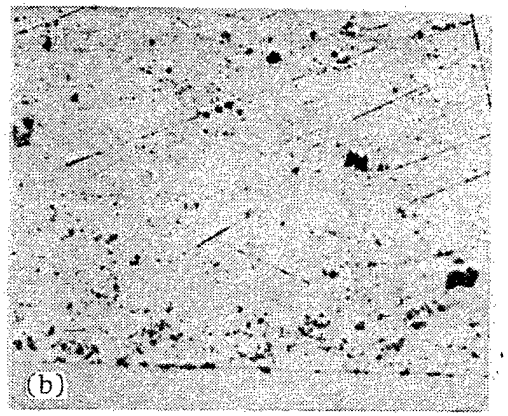

(75X)

Fig. 4 Tantalum coating (a) as-sprayed, (b) laser treated, laser parameters 424 kW/in^2, 31.5"/min.

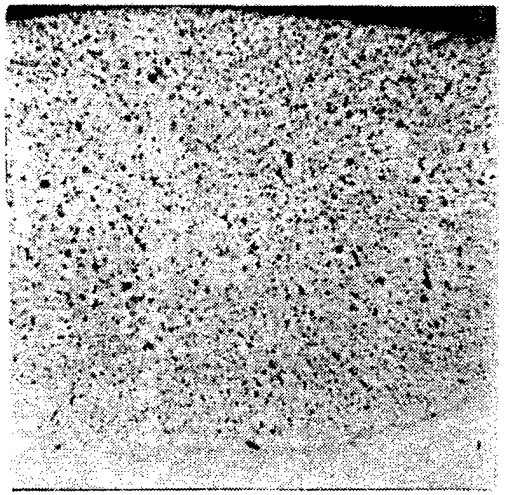

(18X)

Fig. 5 Laser treated Ta-coating (186 kW/in^2, 6"/min).

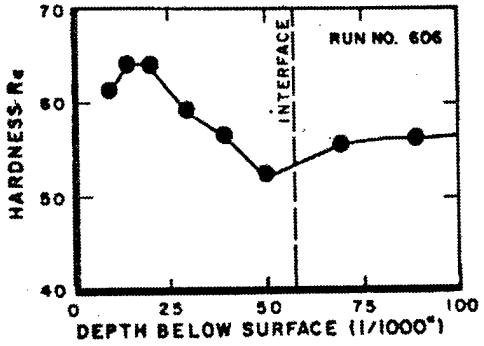

Fig. 6 Hardness of laser treated Ta-coating on 4340 steel.

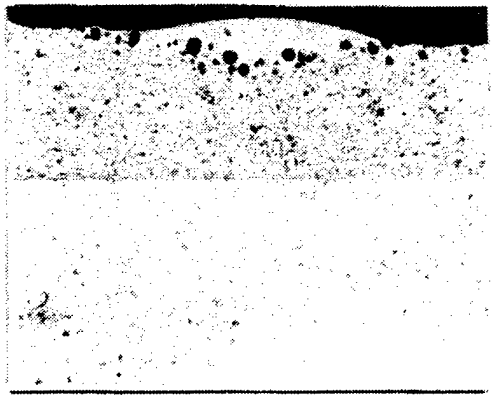

(18X)

Fig. 7 Laser treated Ta-10W coating (160 kw/in^2, 15.25"/min).

(18X)

Fig. 8 Laser treated WC103 coating (400 kW/in^2, 10.3"/min).

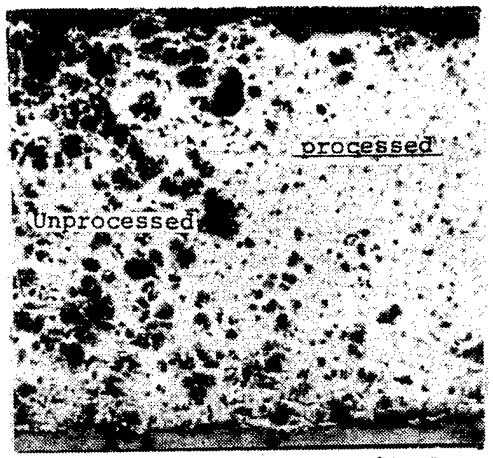

(45X)

Fig. 9 WC103 coating partially laser treated (187 kW/in^2 34"/min)

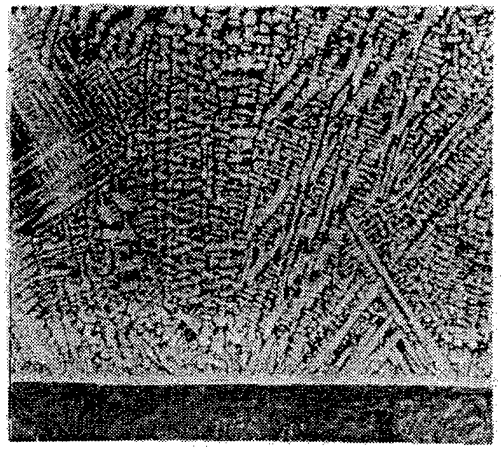

(120X)

Fig. 10 Laser cladded Stellite 12 (38.8 kW/in^2, 20"/min).

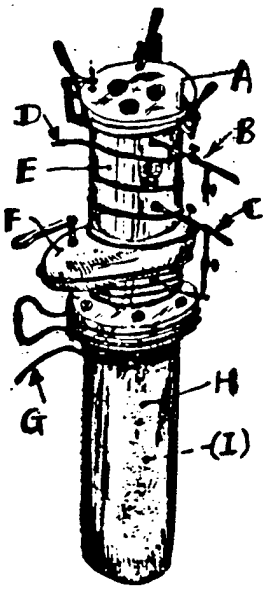

A - Cell top lip
B - Argon outlet
C - Argon inlet
D - Cooling water inlet
E - Cooling chamber
F - Gate valve
G - Cooling water outlet
H - Hot chamber
I - Ni-Crucible (inside)

Fig. 11 Schematic diagram of molten-salts electrodeposition cell.

Fig. 12 Pre-electrolysis cathodes showing powdery deposits.

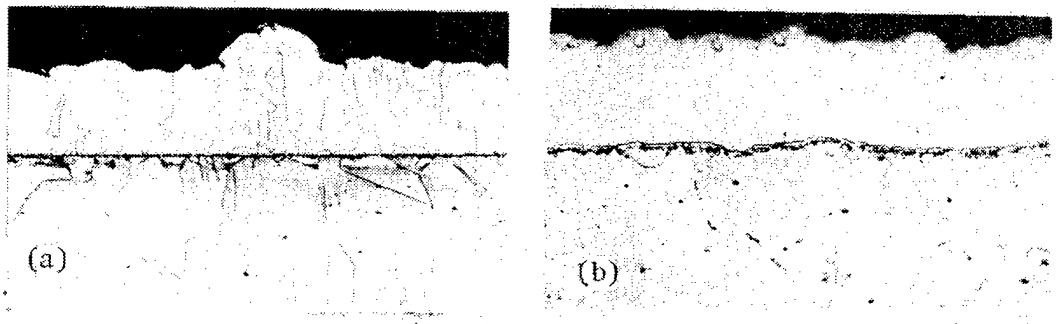

(225X) (225X)

Fig. 13 Niobium platings on (a) copper and (b) steel (deposit unetched).

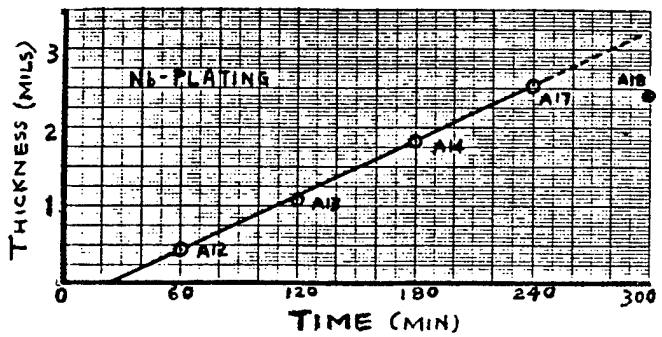

Fig. 14 Electrodeposition of niobium as a function of time.

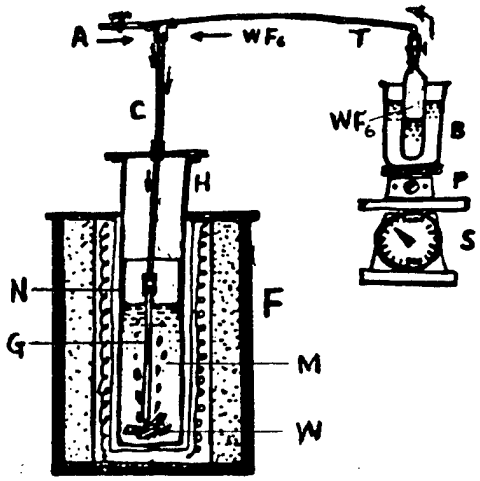

S --- Weighing scale
P --- Hot plate
B --- Water bath
WF_6 - WF_6 gas
A --- Argon gas
C --- Copper tubing
H --- Hastalloy can
N --- Ni-Crucible
G --- Graphite tubing
M --- Molten Fluorides
W --- Tungsten Chips
T --- Tefelon tubing
F --- Pot furnace

Fig. 15 Apparatus and gas flow for the preparation of tungsten electrodeposition bath.

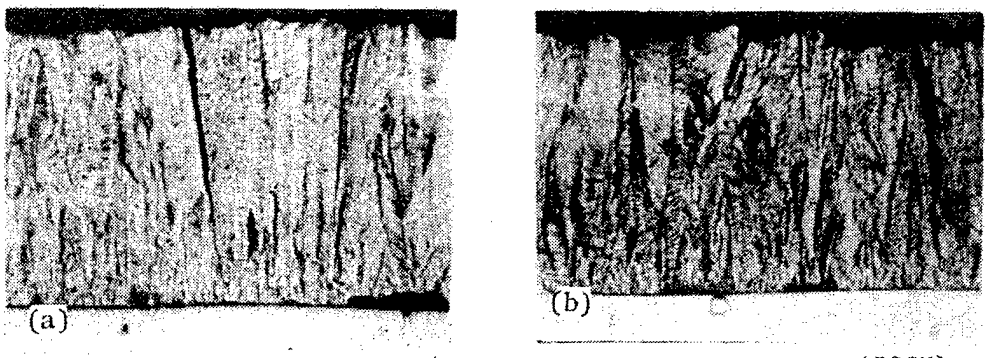

(320X) (320X)

Fig. 16 Electrodeposited tantalum (a) as-deposited (b) heat treated at 1500°C.

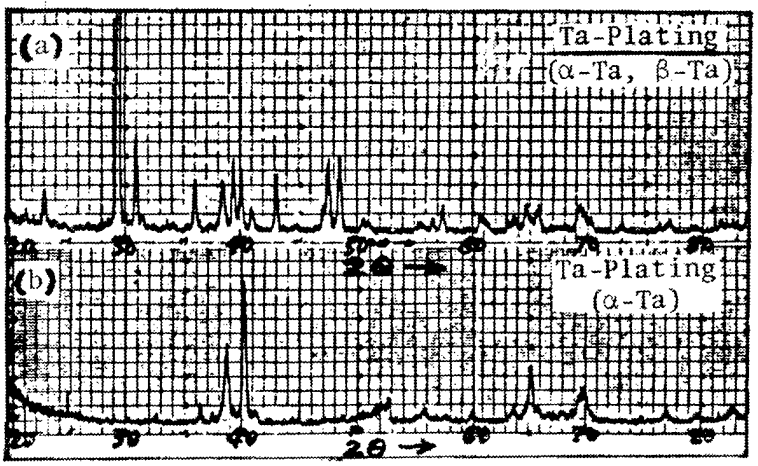

Fig. 17 X-ray diffraction patterns of tantalum plating (a) presence of α-Ta and β-Ta (b) α-Ta.

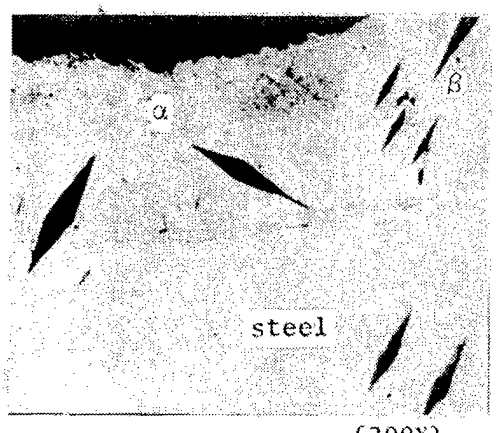

(200X)

Fig. 18 Tantalum plating on steel showing hardness indentations.

MATERIALS FOR DE-COPPERING EROSION-RESISTANT GUN TUBES

Dr. G.C. Vezzoli and Dr. M. Otooni
U.S. Army Armament Research and Development Center
Dover, NJ

ABSTRACT

Recent developments in the plating of gun tubes for the purpose of resisting wear and erosion, combined with progress in high energy propellants, has led to a renewed concern on the subject of copper deposition from the rotating band onto the interior tube. In previous experience, lead and lead-carbonate have been successfully utilized to remove copper residue. The processes that are operative in the removal of copper are determined to be embrittlement and dissolution. Efforts during the past few years have been focused on developing decoppering agents of lower toxicity and lesser density that that of lead and lead-carbonate. Toward achieving this goal, we have studied bismuth subcarbonate, lead carbonate hydroxide, lead sulfate, tin, indium and bismuth antimonide. Under laboratory elevated pressure-temperature conditions the ternary compounds $Bi_2O_2CO_3$, $Pb_3(CO_3)_2(OH)_2$, and $PbSO_4$ undergo decomposition to form free metal, metal oxide, and liberated oxygen, and are experimentally suitable decoppering agents. Our results on liquid tin indicates the presence of two liquid states interpretable in terms of two different atomic species having unique coordination number and chemical potentials. Microscopy reveals that (1) the recovered sample from each liquid field is structurally unique and (2) that the diffusion depth of each liquid through compressed polycrystalline copper pellets is different (the lower temperature liquid showing greater diffusion). The T vs P statistical boundary differentiating the two liquids is initially negatively sloped and appears to intersect the melting curve of tin near the triple point in the vicinity of 30 kbar. This boundary then becomes discontinuous and changes sign to a positive slope at higher pressure. These observations suggest that tin is a suitable decoppering agent for small caliber tubes where propellant energetics are relatively low. Lead carbonate hydroxide and bismuth subcarbonate, on the other hand, are expected to be suitable decoppering agents for large caliber tubes.

Introduction

The phenomenon which is referred to under the term "coppering" is due to the deposition of copper metal from the rotating band of a spin-stabilized projectile onto the interior of a gun tube. The increased erosion resistance due to the chromium plating of the 8-inch tube and the increased energy of modern propellents have the combined effect of causing the build-up of coppering to the eventual condition that a round can no longer be chambered. Prior to the advent of chromium plating the coppering problem was compensated or offset by the effect of subsequent rounds causing normal gun tube wear and hence removing the copper. The build-up of the copper appears to be due to the combination of abrasion and surface melting, and may involve interfacial solid solution with the refractory coating metal or with the base metal.

In the past the removal of built-up copper and/or the prevention of coppering has been accomplished through the action of lead (Pb) metal or lead carbonate- which is added to the bag charge. Normally 12 to 15 rounds, each containing one (1) pound of lead or lead carbonate are required to de-copper the deposition from about 100 eight-inch rounds (XM650) using M107 propellent (thus removing about 8 mils of copper film).

The process of decoppering is believed to be due to the dual effects of dissolution and embrittlement of the copper by the decoppering agent. The low melting point of the decoppering agent (such as Pb) allows the agent to operate in the liquid state and take the copper into solution according to the Pb-Cu binary phase diagram. The Cu-Pb phase diagram at 1 atm shows an exsolution dome of two liquid melts between 954 and 990°C[1]. The solid solubility of Cu in Pb is less than 0.007 wt % Pb. The eutectic for the dissolution of Cu by liquid Pb occurs at 0.11 wt % Cu at 328°C. Liquid Pb also embrittles

the deposited Cu and allows it to be more easily chiped or blown off by the action of the round.

Although Pb is proven to be a chemically suitable decoppering agent it has the disadvantage of high toxicity and high density, coupled with high required weight of Pb to dissolve a given weight of Cu in the neighborhood of 1000°C. The toxicity causes unacceptably high concentrations of lead vapor in the immediate surroundings of a gun crew in an enclosed or partly enclosed area (as attested by OSHA). The high density of Pb and low solubility of Cu in Pb detracts from the energetic potential of the propellent charge because of the weight of inert material. Furthermore indications exist that lead and lead-tin solder decoppering agents have the effect of increasing crack propagation rates in certain tubes. For these reasons a laboratory study was conducted to develop a substitute decoppering agent of lower toxicity and lesser density than Pb.

Thus it is the purpose of this paper to describe the interaction of a variety of materials with copper at high pressure and temperature. The materials that were chosen as candidate decoppering agents were bismuth, bismuth subcarbonate, tin, indium, and bismuth antimonide. To better establish the cause of the decoppering process studies were also conducted utilizing lead, lead carbonate, lead carbonate hydroxide, two forms of lead oxide, and lead sulfate. Data were taken on all of the above materials to establish their P-T phase diagrams (including decomposition), their interaction with free copper, and their interaction with copper that had been deposited on chromium which in turn was deposited on gun tube steel.

The ternary compunds were studied because of the expectations that P-T

induced decomposition would generate free metal for dissolution and embrittlement of Cu, oxygen for bonding with Cu to form Cu_2O that could blow-off with propellent gasses as well as for possible protection of the gun tube against erosion, and a non metal such as carbon to possibly place a film of low wettability on the interior gun bore to oppose subsequent coppering.

Experimental Procedures

The apparatus for these experiments consisted of a Bridgman anvil pressure system operating typically from 1 to 30 kbar at 20 to 450°C, and a high temperature furnace operating at 1 atm in flowing argon or in air at 20 to 1200°C. In situ electrical measurements were conducted by use of mica gaskets and direct electrical contact to tungsten carbide anvils or via use of platinum contacts on the top and bottom of the sample. A complete description of the high pressure Bridgman anvil system is given in Ref 2a.

Samples consisted of pressed powders of the decoppering agent in the form of pellets of diameter 0.10 inch and thickness 0.015 inch. Interface experiments utilized either copper foil or pressed copper powder (1 to 10μ packed in Argon). See Ref 2b.

Examination and characterization of samples that were recovered from high pressure and high temperatue conditions were performed by x-ray diffraction (Gandolphi & Debye Scherrer) and by scanning and transmission electron microscopy with energy dispersive x-ray analysis techniques.

Experimental Results

A. Lead (See Ref 3)

The melting curve of lead (Pb) was determined by the method of in-situ

electrical resistance (R). At the melting point (m.p.) the resistance of Pb was observed to decrease 2%. The melting curve is positive and linear to the limits of the experiments at 28 bar. At peak gun tube pressures corresponding to 8 inch ordnance and zone 9 charge, Pb melts at temperatues no higher than 345°C and no lower than the 1 atm m.p of 327°C. An electrical anomaly (change in sign of dR/dt from - to +) occurs in the solid state in the 300° temperature region at pressures up to 40 kbar but is not identified with a known polymorphic phase transformation. Liquid Pb diffuses through Cu foil at gun tube pressures and embrittles the Cu. Thus a combined dissolution-embrittlement phenomenon causes the decoppering effect of Pb. In the high pressure study no evidence was found for a second liquid Pb species at temperatures up to 470°C. The cubic closest packing structure of the solid state is believed to be preserved in the short range environment in the liquid field. Upon cooling the melt, the resolidification P-T data points were essentially co-linear with the melting data points (no significant supercooling effects.) High-temperature measurements at 1 atm confirmed the binary Cu-Pb phase diagram given in Ref 1.

B. Bismuth (Ref 4)

The melting curve of Bismuth (Bi) was established and shows negative slopes up to 27 kbar followed by positive slopes to the limits of the experiment at 35 kbar. In gun tube environment Bi melts at between 250 and 270°C. The melting of Bi could not be detected at 1 atm or at high pressure by sensitive electrical techniques unless the Bi was in contact with copper foil. Under such a configuration melting was detected as a very faint but reproducible anomaly in the negative dR/dT data. As temperature is further increased above the m.p., at pressures up to the 30 kbar region a change in sign of dR/dT

from - to + is observed in the liquid state when Bi is in contact with Cu or Pt. At still somewhat higher tempratures the sign of dR/dT returns to minus. At interior gun pressures the temperature for this liquid state anomaly is about 300^{o}C. The anomaly identifies P-T conditions for a liquid-liquid reaction whereby the high temperature liquid appears to be more reactive relative to Cu and Pt (either forming a compound, a solution, or simply embrittling due to grain boundary effects). Liquid Bi diffuses through 0.122mm Cu foil at high pressure and causes severe embrittling as well as some dissolution. In experiments without the use of Cu or Pt the solidified recovered Bi product showed vastly different morphology and texture depending upon whether it was derived from above or below the liquid-liquid boundary. This liquid-liquid zone correlates with a Soviet study (Ref 5) indicating a Bi liquid state zone of anomalous sound velocity. The zone is reported up to 7.7 kbar at between 270 and 290^{o}C. Extrapolation to 1 atm of the P-T liquid-liquid region in the present study correlates very well with the maximum conductance turning point reported in two earlier studies (Ref 6 and 7).

Data taken at 1 atm and high temperature confirms points on the phase diagram of Cu-Bi given in Ref 1 and show that the mutual solid solubility of Bi and Cu is very small (less than 0.5 atomic percent). There is no indication of separate Bi and Cu liquids, and at 1000^{o}C liquid Bismuth can dissolve a much greater weight percent of Cu than can Pb. Bismuth also shows lesser toxicity and lesser density than Pb as well as a lower m.p. at gun tube pressures and a decreasing m.p. as pressure increases. Bi is far more embrittling to Cu than is Pb. For all of these reasons it is believed that under laboratory conditions Bi is a superior decoppering agent than Pb. Bismuth does not interact strongly with steel and wets copper in a superior manner than does Pb.

C. Lead Carbonate Hydroxide (Ref 8).

The P-T induced decomposition of lead carbonate hydroxide or hydrocerrusite $(PbCO_3)_2 \cdot Pb(OH)_2$ follows the sequence: (1) $(PbCO_3)_2 \cdot Pb(OH)_2 \rightarrow [(PbCO_3)_2 \cdot Pb(OH)_2]_{(1-x)} + uPbO + yCO_2 + zH_2O$; (2) $PbO \rightarrow Pb + O_2$; (3) $(PbCO_3)_2 \cdot Pb(OH)_2 + PbO \rightarrow Pb_{10}(CO_3)_6(OH)_6O$ [lead carbonate hydroxide oxide or Plumbonacrite] ; (4) Pb(solid)→Pb liquid. At about 3-4 kbar the respective temperatures for these effects are 100, 300, 340 and 350°C. In the low pressure range the effect of increasing pressure is to drastically decrease the temperature of the initial decomposition. The pressure dependence for the decomposition of both forms of PbO (Litharge & Massicot) as a starting material is only very slight, however, if the pressure cell is not sealed (as it is not sealed in a gun tube), oxygen can escape during the initial decomposition of the $Pb(OH)_2$ groups (before Pb and O_2 can bond to form PbO) and free lead can be generated at temperatures much less than 300°C. The lead is detected by a large decrease in resistance and identified by x-ray diffration. When a Pb path bridges the electrodes a very large increase in conductance occurs. The pressure dependence of the reconstitution reaction (in the above sequence reaction #3) is also only slight. The reconstitution reaction is associated with increased resistance and identified by x-ray diffraction. At higher temperatures the Plumbonacrite (grey black in color) will decompose probably to $PbCO_3$, PbO, Pb, O_2, CO_2 and H_2O as well as compounds thereof. Therefore use of lead carbonate hydroxide (white lead or hydrocerrusite) may provide an iterative decoppering process due to decomposition to free lead followed by reconstitution followed again by decomposition. Lead carbonate hydroxide is believed to be a superior decoppering agent as compared to Pb or $PbCO_3$ because of the above reasons as well as the expected reaction forming Cu_2O and the driving of O_2 or atomic oxygen into the tube

or liner wall to decrease erosion. It is also possible that any residual carbon will reduce the tendency toward further coppering.

D. Lead Carbonate (Ref 9)

The decomposition of lead carbonate ($PbCO_3$) also known as cerussite involves six stages prior to the melting of free lead. At temperatures up to 400°C the molar fraction of free lead is much less as derived from the $PbCO_3$ starting material contrasted to $(PbCO_3)_2 \cdot Pb(OH)_2$ starting material. The stages of decomposition involve the development of PbO and then the bonding of PbO as a group in addition to the bonding of water molecules derived from included moisture. In the 300°C neighborhood a region of disordered electrical behavior is observed at high pressure and may be associated with the formation of lead carbonate oxide $PbOCO_3$ which is identified by x-rays and is a grey black material in the recovered product. At temperatures even above the melting of free Pb, products of decomposition exist such as $(PbCO_3 \cdot PbO) \cdot 3H_2O$, $PbCO_3$ PbO, and $PbCO_3 \cdot 2PbO$ as well as $PbOCO_3$. Experiments with $PbCO_3$ in contact with Cu at high P-T and at 1 atm at temperatures up to 1000°C show alteration of the above effects due to the interaction with Cu itself.

E. Lead Sulfate (Ref 9)

Lead sulfate $PbSO_4$ or natural Anglesite undergoes decomposition to a transparent material and a black phase. Both phases give rise to the x-ray pattern of natural Anglesite. The electrical data show a large increase in conductivity (followed at higher temperature by a minimum resistance turning point) in the 200 to 300°C neighborhood, suggesting the formation of free Pb. However free Pb is not identified by x-ray diffraction, hence either Pb exists in

less than 5%, or perhaps all of the reactions in $PbSO_4$ are associated with electronic transitions or defects rather than structural rearrangements. The use of $PbSO_4$ as a decoppering agent may be successful to remove copper, however, the fear exists that the presence of moisture may cause the formation of sulfuric acid which could lead to serious gun tube erosion.

F. Bismuth Subcarbonate (Ref 9)

Bismuth subcarbonate ($Bi_2O_2CO_3$) undergoes P-T induced decomposition to Bi_2O_3 plus free bismuth. The electrical profile at a given pressure indicates a minimum resistance condition at about 250°C (probably indicating decomposition to $Bi_2O_3 + CO_2$) followed by a sharp increase in conductance around 270°C (the latter being probably associated with free Bi and precipitated by some irregular behavior). At low pressures the decomposition is to the β phase of Bi_2O_3 whereas from 30 to 40 kbar the yellow α phase is recovered. In the 50 kbar region the recovered product contains Bi plus Bi_2O_5. The melting of Bi is detected (in the experiments that utilized $Bi_2O_2CO_3$ starting material) in the form of maximum or minimum resistance turning points depending upon the solid phase (I,II,III,VII, or VI) from which the liquid was derived. Bismuth subcarbonate then fills the criteria of generating free metal with superior laboratory decoppering properties than Pb. It also allows for free oxygen to bond with Cu or to diffuse into the gun tube surface, as well as giving rise to the possibility at high temperatures of some free carbon developed during decomposition (for possibility of decreased wettability toward future coppering due to very thin carbon film).

G. Tin (Ref 10)

The P-T phase diagram of tin (Sn) was established and reveals a positively sloped melting curve as well as a liquid field boundary. The m.p. of Sn increases from 231°C at 1 atm to about 240°C at 4 kbar. Over this pressure range the liquid - liquid boundary decreases from about 400°C to about 360°C. This boundary continues to be negatively sloped as pressure increases and intersects the melting curve near the triple point at 31 kbar 300°C. At higher pressures the liquid-liquid boundary takes on a positive slope but is displaced upward in temperature (apparently discontinuous at the triple point).

The melting curve to 31 kbar is identified by an increase in electrical resistance, however above 31 kbar melting occurs without detectible elecrical change. The liquid-liquid boundary is established by a change in sign of dR/dT from + to - abserved essentially isobarically. The recovered product from each of these liquid fields shows a contrasting characteristic grain structure upon solidification. The lower temperature of the two liquids appears to be more reactive to copper. This may explain why Sn is a good decoppering agent for small caliber tubes but actually causes tinning of large caliber tubes. The high temperature liquid form of Sn may be based on either a structure similar to the closed packed structure of Pb or similar to the tetrahedral structure of α-Sn (grey Sn - diamond structure). The white Sn (β) - grey Sn (α) phase transformation was studied in the solid state. Results showed that as pressure increases, the temperature for the $\beta \rightarrow \alpha$ transformation decreases and the kinetics become increasingly sluggish such as to cause a large degree of required superco ling. The electrical profile for the $\beta \rightarrow \alpha$ transformation at high pressure and under vacuum shows a plateau behavior in resistance. Since this type of behavior is not observed at high temperature during the liquid-liquid transition, it is believed that this transition is more apt

to be toward a Pb-like liquid rather than a diamond-like liquid. It should be pointed out however, that a two liquid model for Sn is predicted by Soviet researche. and includes a soft sphere phase and a tetrahedral structure. Thus a diamond type liquid is still tenable. The liquid-liquid boundary was confirmed at 1 atm by optical scattering as well as electrical resistance measurements. Experiments at 1 atm show confirmation of the Cu-Sn solid solution phases described in Ref 1. The eutectic is at 227°C at 99.3 atomic per cent Sn. The solid solubility of Cu in Sn at the eutectic is 0.01 atomic percent or 0.006 wt. percent. The rich phase equilibria of the Cu-Sn binary suggests decoppering capability provided tinning does not occur.

H. Indium

In the first experiment on indium in contact with Cu we were unable to electrically detect the melting of indium or any indication of a liquid-liquid transition. Indium solidified in a highly striated fashion. Some electrical indication of reaction with Cu in the liquid state of indium was observed. The Cu-In binary phase diagram shows solid solution phases $\alpha, \beta, \gamma, \delta, \eta$ and suggesting reactivity at high pressure and initiating interest in indium as a possible decoppering agent.

I. Bismuth antimonide

In very recent work on BiSb in contact with Cu electrical resistance measurements at high pressure clearly showed indication of either interaction or reaction with Cu. Examination of the recovered product on the BiSb surface showed grey and black materials in the central regions and blue and purple material on the perimeter. Examination of the Cu side showed clear cut regions

of shiny grey and dull grey material. Some BiSb extruded from a crack in the mica gasket presumably developed when presure was rapidly decreased at high temperature. This material appeared dull grey and quite brittle. The temperature at which the first electrical indication of P-T induced reaction was under 200°C. BiSb appears to be a promising candidate as a decoppering agent.

J. Decoppering Agent Interface Experiments with Copper Deposited on Chromium

A thin film of Cu was deposited on a thin film of Cr which was in turn deposited on an iron substrate. Decoppering agents were placed within steel washers on top of the Cu film. The assembly was heated to 1000°C in a Lindberg furnace in air (as well as a separate experiment being performed in Argon). Upon cooling and examining the recovered samples it was clearly evident that the Cu under the $Bi_2O_2CO_3$ sample was more completely removed as constrasted to the $PbCO_3$ and $(PbCO_3)_2 \cdot Pb(OH)_2$ samples. At 1 atm, electrical resistance effects in $Bi_2O_2CO_3$ were observed in the 500 to 750°C temperature range. In air severe oxidation of the iron substrate was produced at these temperatures.

Conclusions

The major conclusions from this study to date are as follows:

(1) Bi and $Bi_2O_2CO_3$ seem to be superior decoppering agents than Pb or $PbCO_3$ and are of reduced toxicity and reduced density.

(2) $(PbCO_3)_2 \cdot Pb(OH)_2$ appears to be a superior decoppering agent relative to Pb and $PbCO_3$ because of the P-T properties of the $Pb(OH)_2$ group.

(3) Tin seems to be a suitable decoppering agent for small caliber tubes.

(4) BiSb is a promising candidate for decoppering and should be studied.

SESSION V

LINERS, ROTATING BANDS, AND DESIGN

CHAIRMAN: James O'Brasky

further.

Recommendations

It is recommended that during the course of the next two years field tests are run on bismuth and bismuth subcarbonate as candidates for decoppering agents.

Acknowledgement:

The authors wish to acknowledge the support of Dr. Thomas Davidson of ARRADCOM under the AHGO Research in Armaments Program, and Dr. Wayne Robertson of Rockwell International for fruitful discussions.

References:

1. M. Hansen Constitution of Binary Alloys (McGraw-Hill, New York, 1958).

2. a. M. Meyers, F. Dachille & R. Roy, Rev. Sci Instrum. 34, 401 (1963)

   b. Vezzoli, F. Dachille, & R. Roy J. Am. Ceram. Soc. 54, 221 (1971)

3. The detailed data on Pb are given in: G.C. Vezzoli, High Temperatures High Pressures 10 707-709 (1978).

4. The detailed data on Bi are given in: G.C. Vezzoli, High Temperatures High Pressures 12, 195-203 (1980).

5. V. Ablordeppey, Phys. Rev. A 3, 1680 (1971).

6. Y. I. Dutchak, Phys. Met. Metallogr. (USSR) 11, 133 (1961).

7. G.C. Vezzoli Phys. Status Solidi A 48K, 75-77 (1978).

8. Data on lead carbonate hydroxide and the red & yellow forms of lead oxide are given in detail in: G.C. Vezzoli and S. Krasner, High Temperatures- High Presures (in press 1st paper)

9. Data on lead carbonate, lead sulfate, and bismuth subcarbonate are given in: G.C. Vezzoli and S. Krasner High-Temperatures High Pressures (in press, 2nd paper)

10. For data on tin see the comprehensive paper: G.C. Vezzoli and M. Otooni Phys. Rev (in press).

CERAMIC MATERIALS FOR LIGHTWEIGHT GUNS

P. Wong
Army Materials and Mechanics Research Center
Watertown, Massachusetts 02172

ABSTRACT

The potential for the implementation of ceramic liners in small and intermediate gun barrels is presented. Three promising candidate ceramic materials are described and the method for their selection is outlined. A procedure for producing rifled ceramic liners is also included. The feasibility of using ceramic liners in gun barrels and the prospect for its future success is discussed.

INTRODUCTION

The continuing problem of severe erosion/corrosion and wear of small and large calibre gun tubes have plagued the efforts for upgrading field weapons for many years. Understanding the mechanics and the behavior of wear and erosion in gun barrels requires analyses into three major areas which include thermal, chemical, and mechanical processes. Scientists and engineers have been striving for years to understand gun tube erosion and the demand for more advanced high performance weapons continually generate new or intensify old problems.

A measure of success in counteracting wear and erosion has been achieved in the .50 caliber chromium plated and nitrided gun barrels by using stellite liners.[1] Stellite is a cobalt based alloy containing small quantities of Cr and Mo. In recent years, materials in a critical category such as Co and Cr have experienced extreme price and availability turbulence. Such a position of uncertainty of supply is unacceptable for national security and, therefore, has stimulated interest in seeking non-critical materials that are readily available for use as gun tube liners. Many of the ceramic materials considered as candidates for implementation, contain no critical or strategic elements. The recent development of advanced ceramic materials and fabrication techniques have opened and increased the prospects of using ceramic materials as liners in gun tubes. In particular, the ceramic turbine engine program has demonstrated that new ceramic materials have high temperature wear and erosion resistance, high strength and chemical inertness. These are exactly the characteristics in a material that is desired for the development of newer high performance gun systems. The development of more advanced weapon systems have projected requirements of longer range, higher velocities, and rapid rates of fire, all of which, collectively create greater erosion and wear problems. Therefore, the development of any new gun systems depends heavily on the availability of high wear and erosion resistant materials. Ceramic liners for gun barrels are potentially an excellent candidate to provide the life and accuracy requirements for the next generation of weapon systems.

Approved for public release; distribution unlimited.

OBJECTIVE

Our program objective is to determine and establish the feasibility of using ceramic materials as wear and erosion resistant liners in small and intermediate calibre gun barrels. The purpose is to introduce to the ordnance community the potential that ceramic materials can offer in the way of providing improved materials for advanced weapon systems. Ceramic materials offer unique combinations of properties and has had such diverse applications in the Army as providing ballistic protection for air crew personnel, survivability of equipment in the field, missile guidance, efficiency in fuel engine technology, and also reducing the requirements for strategic materials.

Ceramics have traditionally been recognized as being brittle materials, however, it does not necessarily follow that the material is weak. On the contrary, in some cases, ceramics can be stronger than metals. Brittleness is a characteristic of a material which can best be described as a condition where excessive stresses cannot be relieved by local yielding as in the case of metals. Under this condition, the material fails in a brittle manner. Having this knowledge about the characteristic of ceramics, designers can take this into consideration and maximize on the other beneficial properties of the material. New design tools such as computer-based finite element stress analysis are enabling designers to more precisely define the actual local stresses which the ceramic component will experience in service. As a result, ceramic materials are finding their places in more and more areas where other materials are unable to keep up with requirements for higher operating temperatures. An example of this is in the high temperature gas turbine engine where engineers envisioned ceramics offering the promise of a low cost, efficient, and uncooled turbine engine.[2] After considerable research effort in this area it has been determined that ceramic materials can be properly designed for conditions that require high temperature wear and erosion resistance, high strength and chemical inertness. These attributes are also required in many other areas, one of which is in the gun barrel erosion problem. Ceramic engineering has come a long way in terms of understanding its properties better and also in the technology required to fabricate improved ceramics. A survey done by Battelle Columbus Laboratories for AMMRC, reports that the state-of-the-art in ceramic technology presently has three promising candidate ceramic materials which can be considered for gun barrel liners.[3] These include alpha silicon carbide, a fiber reinforced glass matrix composite and an improved zirconia which were analyzed taking into consideration; cost, fabricability, availability as well as their physical properties. AMMRC is presently studying these materials for their program in ceramic liners for gun barrels in the .50 calibre weapons.

APPROACH

In an attempt to determine the feasibility of using ceramic materials as liners in .50 caliber gun barrels, we decided to establish a procedure by which to evaluate candidate materials and a selection process by which

to choose likely prospects for testing. We obtained the services of Battelle Columbus Laboratories to conduct an independent survey of ceramics in gun barrels. Their recommendations on candidate ceramic materials agreed with our list and helped to narrow the choices on the basis of performance, availability, and fabricability. We, therefore, focussed our efforts on those materials judged to have a high probability of success.

The initial testing of alpha silicon carbide was conducted at Maremont, Saco, Maine; for an ARRADCOM program supported by the Army Advanced Concepts Team;[4] where a gun barrel lined with this material was test fired up to 1000 rounds and showed no detectable bore wear. To maintain consistency in the program, we will continue to have Maremont prepare the liners and do further testing. Preparing the liners involves shrink fitting in two steps where the liner is fitted into a steel sleeve which in turn is fitted into a steel jacket making up the test module.

The shrink fitting process is a very critical part of the procedure for installing the ceramic liner in a gun barrel. Ceramic materials, because of their nature, must be continually under compressive stresses to maintain their high strength properties. The shrink fitting of the steel sleeve and jacket over the ceramic liner accomplishes this condition by constantly squeezing on the ceramic liner during service. The amount of compressive stresses generated depends upon the differential of the liner O.D. and the I.D. of the sleeve and jacket. In some cases, the configuration of the module caused circumferential cracking to occur about $\frac{1}{2}$" from the muzzle end of the module. This problem was partially resolved by decreasing the differential or misfit between the liner and sleeve/jacket. We feel that this is strictly a design problem and proper designing through stress analysis could allow more flexibility in obtaining the compressive stresses desired in the lined gun barrel.

The Carborundum Company of Niagara Falls, the supplier of the silicon carbide tubes that were originally test fired, being aware of the cracking problem that occurred during shrink fitting, offered their design and fabrication expertise towards the production of silicon carbide lined gun tube modules. This presented an opportunity for a ceramic fabricator to use their technology base to design for a ceramic lined gun barrel module which had originally been designed for metal components. With the proper design, it is expected that silicon carbide lined gun barrel modules will survive testing under conditions more severe than single shot rounds. We have contracted Carborundum to supply us with a number of silicon carbide lined gun barrel modules ready for testing. These will include smooth bore and rifled bore modules.

One of the major obstacles that has slowed progress in the acceptance of utilizing ceramics as gun tube liners has been the ability to rifle ceramic tubes. The conventional means of rifling metal barrels cannot be applied to most ceramic materials easily. This is particularly true for the very hard materials such as silicon carbide. Ceramic materials of this high hardness must use diamond cutting tools. The bore diameter of a .50 calibre does not allow much room for cutting a number of grooves in a spiral configuration using diamond cutting techniques. While investigating other alternatives for machining ceramics, ultrasonic machining

techniques appeared to have the greatest potential. Cutting ceramics by ultrasonic techiques involves transmitting ultrasonic energy to an abrasive medium that does the actual cutting. We contracted Bullen Ultrasonics of Eaton, Ohio to use their technique to rifle two 7" long silicon carbide tubes with $\frac{1}{2}$" I.D.

Although silicon carbide has shown great potential as a candidate material for liners, other ceramic materials have displayed extraordinary physical properties that deserve investigating for gun barrel applications. These materials are also mentioned in more detail in the Battelle report and include glass matrix fiber reinforced material and a transformation toughened zirconia material. We are presently in the process of evaluating these materials in gun barrel test modules. United Technologies Research Corporation supplied us with three graphite fiber reinforced borosilicate composite gun barrel test modules. These modules survived single shot test firing of up to 10 rounds with only a slight indication of wear. This material concept has the potential for demonstrating advantages over metal alloys such as low density, low thermal expansion, higher operating temperatures and contain no critical elements.[5] Further evaluation of this material concept is continuing.

Another material of considerable interest is the transformation toughened zirconia. This material has shown exceptional physical properties and looks particularly attractive as a gun tube liner. One particular characteristic of this material is that its thermal expansion coefficient is closer to the value for gun steel than any other ceramic material. This material will be obtained and put through the evaluation process to determine its value as a gun barrel liner material.

The program as it stands now, will be capable of screening prospective ceramic materials as the technology improves. Using the present candidate materials as a basis of comparison allows us some degree of certainty whether any future material has potential as liners. As test firing is time consuming and expensive, we can make our selection of the best material knowing what properties we should be looking for.

RESULTS AND DISCUSSIONS

The past few years has seen an influx of improved ceramic materials. Although ceramics have been considered experimentally for applications in gun barrels, it isn't until recently when the improvement in properties of ceramic materials have become so pronounced that real potential can be realized. In order to get a better feel for what the ceramic industry can offer at this time, AMMRC contracted Battelle Columbus Laboratories to conduct a survey on the past, present, and future applications and studies on ceramic materials in gun barrels.

A final report was submitted by P. Stephan and A. Rosenfield entitled "Survey of Ceramics in Gun Barrels."[3] The report gives a good literature review on past experimental studies of ceramics as gun barrel liners conducted at the three Armed Services Research Centers. Basic gun barrel design considerations are presented as well as structural designs for ceramic materials in particular including suggested safety factor estimates. Finally, a guide for the selection of the proper ceramic material

Table I PROPERTIES OF CERAMIC MATERIALS

Material	Density g/cm³	Melting Point C	Thermal Expansion Coefficient 10^{-6}/C	Knoop Hardness kg/mm²	Poisson's Ratio 25 C	Tensile Strength MPa 25 C	Tensile Strength MPa 1000 C
Alpha SiC	3.15	~2800 vaporizes	4.02(RT-700)	2800	0.14	459	442
Reaction-Bonded SiC	3.10	~2800 vaporizes	3.44(RT-500)	2740	0.127	383	461
Hot-Pressed Si_3N_4[1]	3.2	>1900 sublimes	3.5(RT-1000)	3500	0.24	700	600
ZrO_2	5.6-5.75	2715	10.6(RT-1400)	1160	-	620(PSZ)	345(PSZ)
Al_2O_3[1]	3.92-3.98	2050	9.0(RT-1400)	2100	0.22	250-300	234
Mullite ($3Al_2O_3 \cdot 2SiO_2$)	3.15-3.23	1870	5.1(RT-1000)	-	-	83	48
MgO[1]	3.6	2800	12(RT-1000)	800	0.20	131	69
Graphite Fiber - Borosilicate Glass Matrix	1.98	~600 (glass softens)	4.7(RT-600)	~500 (glass)	0.19	950	350 (700 C)
SiC Fiber - LAS Glass-Ceramic Matrix	2.5	~1000 (glass softens)	2.2(RT-1000)	~600 (glass)	-	600	850
Gun Steel	8.0	1450	15(0-800)	380	0.3	1172	758
Desired for Ceramic Liner	low	>1500	compatible with sleeve	high	low	high	

Material	Compressive Strength MPa 25 C	Compressive Strength MPa 1000 C	Elastic Modulus GPa 25 C	Elastic Modulus GPa 1000 C	Fracture Toughness MPa-m 1/2 25 C	Fracture Toughness MPa-m 1/2 1000 C	Thermal Conductivity cal/cm-sec-C 25 C	Thermal Conductivity cal/cm-sec-C 1000 C	Thermal Diffusivity cm²/sec 25 C	Thermal Diffusivity cm²/sec 1000 C
Alpha SiC	-	-	409	-	4.6	6.4	0.208	0.08	0.413	0.12
Reaction-Bonded SiC	1034	-	332	-	7.6	7.6	0.25	0.076	0.49	0.085
Hot-Pressed Si_3N_4[1]	552	-	310	-	4.7	4.7-12	-	0.011	-	0.018[2]
ZrO_2	2068(PSZ)	1034(PSZ)	210(PSZ)	-	9.5	5.0	0.004	0.005	0.0069[2]	0.0064[2]
Al_2O_3[1]	2206	552	407	-	5.0	3.6	0.075	0.015	0.90[2]	0.02[2]
Mullite ($3Al_2O_3 \cdot 2SiO_2$)	1000	-	143	69	-	-	0.015	0.010	-	-
MgO[1]	827	276	303	276	-	-	0.11	-	-	-
Graphite Fiber - Borosilicate Glass Matrix	320	-	193	-	21.4	19 (600)	-	-	-	-
SiC Fiber - LAS Glass-Ceramic Matrix	-	-	138	110	17	25	0.0035	-	0.0073[2]	-
Gun Steel	~1100	-	207	-	110	-	0.184	0.10	0.21[2]	0.08[2]
Desired for Ceramic Liner	high		low		high		low		low	

Notes: (1) Some data may be outdated.
(2) Calculated values.
(3) See references 18-20.

Conversion Factors
1 MPa = 145 lb f/in.^{2} (psi)
1 GPa = 1.45 X 10^5 lb f/in.^{2} (psi)
1 meter (m) = 3.28 feet (ft)

for consideration for test as a gun barrel liner is outlined. Table I lists the physical properties of selected ceramic materials including gun steel for comparison and is also found in the report. At the bottom of each table gives the desirable trend of that property for a potential liner material. The data on these tables were collected from a variety of sources and as such they may have been obtained under differing test conditions. As a result, a direct comparison between materials should only be regarded as differences of a general magnitude and not absolute values. As an excercise, a group of researchers at Battelle were asked to rate the materials from 1 to 6 (one being best) based on their own information on the materials. Table II gives a summary of four evaluations where the lowest total scores represents the best materials. The total

Table II GUN BARREL MATERIAL SELECTION

Material	Ranking (Low Score is Best) Overall Properties (Mechanical, Thermal)	Cost	Fabricability	Availability	Totals
Alpha SiC	13	17	12	12	54
Hot Pressed Si_3N_4	12	23	17	16	68
Zirconia	9	13	11	11	44
Si_3N_4/ZrO_2 Ceramic Matrix Composite	13	17	19	24	73
SiC/LAS Glass Matrix Composite	13	10	17	17	47
Stellite (Cr-Mo-V Steel) (Currently Used)	24	4	4	4	36

score takes into consideration cost, fabricability, and availability as well as the overall physical properties. The best ceramic material according to this experiment is zirconia followed by the fiber reinforced glass matrix composite and silicon carbide. Stellite appears as the best material according to the ranking, but it does not measure up to the wear and erosion resistance of ceramic materials. At this time, this method of selecting materials is only a guide and more study must be made to determine its usefulness. This is only one of many techniques that can be used to evaluate the data but one we'll use until we can get all the materials into the system and analyze the results. The Si_3N_4/ZrO_2 composite is not presently available, but was included as a new idea for comparative purposes.

Discontinuous graphite fiber reinforced glass matrix composites has been and is an active part of United Technologies Research Corporation research program. The materials they developed exhibited excellent strength (100 ksi) and fracture toughness ($K_{Ic} > 20$ ksi $\sqrt{in.}$) and could be designed for particular requirements such as oxidation resistance at high temperatures, moderate or low thermal expansion coefficient, and designated anistropic properties.[5] In particular, the graphite reinforced glass matrix composite exhibited excellent friction and wear properties. The high strength and low modulus characteristics of this composite coupled with its wear properties made this material a good prospect for gun barrel applications. UTRC was subsequently contracted by AMMRC to determine the feasibility of fabricating cyliners of graphite fiber reinforced borosilicate glass composites.

The contract called for three gun barrel test modules lined with this material and test fired. However, there was much more involved in the program in that as a feasibility study, it included the investigation of a variety of fabrication techniques and a design analysis by Maremont Corp., who was a subcontractor, to evaluate the effect of liner thickness and amount of liner/sleeve/jacket interference fit on the resultant liner stresses. They also fabricated the test barrel assembly and test fired

each for 10 rounds single shot. This information is described in detail on the final report submitted to AMMRC for this program.

Although other fabrication techniques such as hot isostatic pressing (HIP) and creep forming of cylinders were investigated, hot pressing was most successful method for producing this particular composite material. Fig. 1 shows the hot pressed ingot of the graphite fiber reinforced borosilicate glass composite and the cylinders that were cored out of it. These cylinders were machined and shrink fitted as liners into gun barrel test modules (Fig. 2) and test fired.

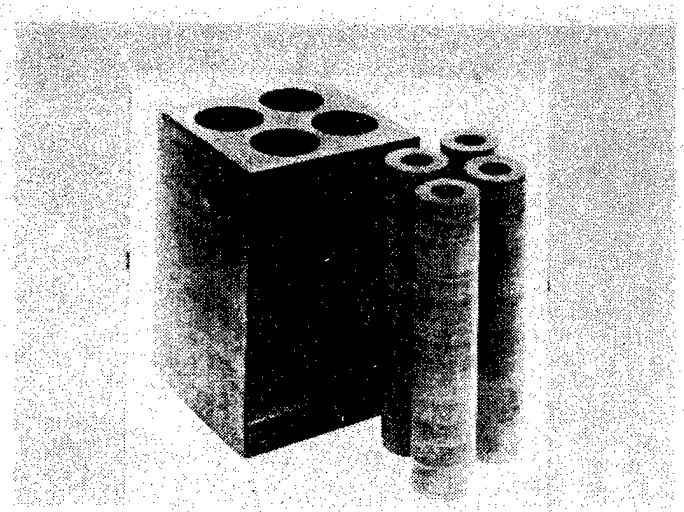

Fig. 1 BOROSILICATE/GRAPHITE FIBER REINFORCED INGOT AND CORE DRILLED CYLINDERS

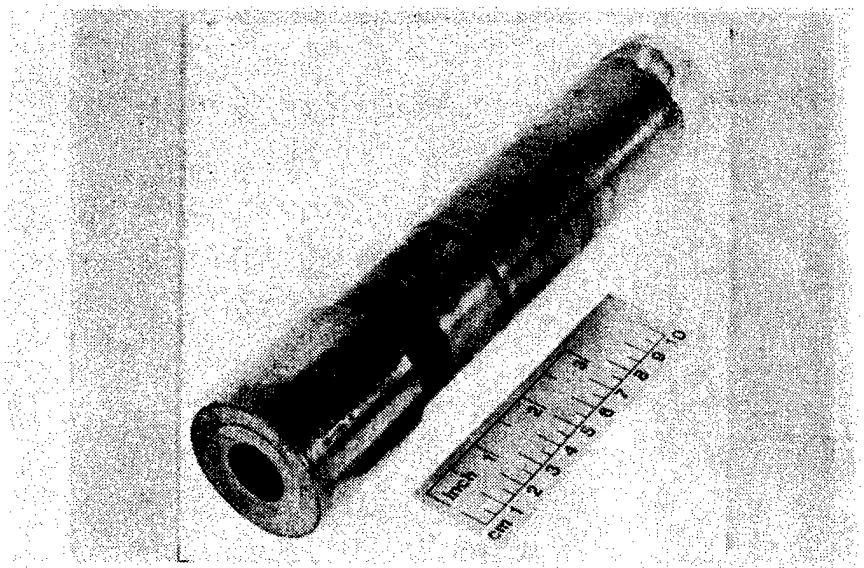

Fig. 2 BARREL ASSEMBLY WITH BOROSILICATE/GRAPHITE FIBER REINFORCED LINER

The results of this program demonstrated that the concept of a fiber reinforced glass matrix composite as a lightweight, low modulus and tough material can survive as a gun barrel liner. Testing at this point has only been under single shot conditions, but the use of higher temperature glass and fibers can conceivably withstand multiple shot conditions. However, further testing must be conducted to evaluate the extent of wear the liner undergoes at extended firing conditions of around 1000 rounds.

Ceramic liners in gun barrels have been test fired single shot using smooth bore tubes. A critical factor in the acceptance of the concept of using ceramic liners is the matter of rifling. Conventional rifling techniques at this time cannot be easily adapted to ceramic materials. This has been a major obstacle in visualizing ceramics in gun tube liner applications. Most of the ceramic materials that can be considered for application in gun barrels are extremely hard and require diamond tooling to machine. The I.D. of a small calibre barrel such as a .50 calibre is limited in space for any kind of cutting tool to be manipulated properly. In the past few years, a machining technique for brittle materials has been developed using ultrasonics.

Ultrasonic machining is a method where a high frequency (20 kHz) energy is imparted to a cutting medium such as a slurry of abrasives (boron carbide) to chip away the brittle material microscopically in areas where the cutting action is required. Bullen Ultrasonics of Eaton, Ohio was contracted to rifle two alpha silicon carbide tubes which were 7" long and $\frac{1}{2}$" in bore diameter. The rifling consisted of eight grooves and lands with a spiral of one revolution in 15". The procedure consisted of tooling that could cut the eight grooves all at one time. The tooling does the ultrasonic cutting and a fixture designed to rotate the tube for the proper rotation. After much trial and error, the procedure was refined and rifling of the inside diameter of ceramic tubes was accomplished. Fig. 3 shows the comparison of the rifling seen in a typical stellite liner with that recently accomplished in a silicon carbide tube. As you can see by the photos, the ultrasonic process does a nice job producing the rifling in the silicon carbide tube.

This procedure is ideal for rifling ceramic liners but several questions remain to be answered. The rifled tube will now have to be shrink fitted into the test module and so it remains to be seen how these grooves will affect the material. There is still, however, the alter- native of rifling the ceramic liner after it has been shrink fitted into the module. This would require considerable modification of the fixture used to rifle the ceramic tube as the added weight and size would have to be accommodated. The design of the rifling has been duplicated from the stellite tube, therefore, redesign of the configuration would have to be considered if the rifled liner suffers adversely during the shrink-fitting and, of course, during the test firing. Although there is now a procedure for producing rifling in a ceramic liner, there are still these questions that have to be resolved and we will be concentrating on these.

Included in our program for selecting candidate materials for evaluation is the new form of zirconium oxide. This material is characterized as transformation toughened or partially stabilized zirconia and is vastly

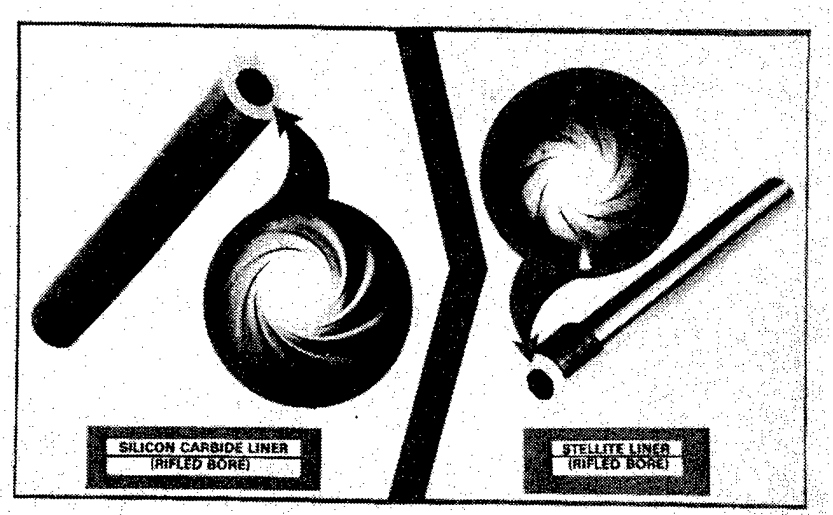

Fig. 3 RIFLED CERAMIC TUBE FOR POTENTIAL REPLACEMENT OF STELLITE LINERS

improved over the zirconia product of the past. The sales promotion describes this as the "strongest and toughest" ceramic oxide available today.[6] Potential applications are where toughness, resistance to chemical attack, and ability to withstand rapid temperature changes are required. Partially stabilized zirconia has the lowest coefficient of friction against steel of any of the ceramic materials (.55 for zirconia versus .77 for hot pressed silicon nitride).[6] In contrast to other ceramic materials where damage due to surface grinding lowers the strength, grinding of this material increases the transverse rupture strength from 490 MPa (71 ksi) to 600 MPa (87 ksi).[6] All of these properties make this material ideally suited for gun barrel liners. One drawback for this material is its high density which makes it heavier than most ceramics, but its mechanical properties look very promising and deserves evaluation as a liner material. We are now in the process of procuring this material and expect to put it into the system for testing and evaluation.

CONCLUSION

The results of this study has suggested a criteria by which ceramic materials may be screened for possible application as gun tube liners. The preliminary tests on some of the materials selected by this process indicate that they can survive the shrink fitting procedure and the single shot firing tests conducted on them. Further evaluation will be continued on these candidate materials selected to determine if this selection procedure has merit. Other factors such as fabricability, availability, and cost; will also have to be considered in the future. However, for this first round, candidate ceramic materials will continue to be selected by this criteria.

All the data indicates that ceramics can offer all the physical requirements necessary for surviving the severe conditions generated by

the next generation of advanced high performance weaponry. The increased wear and erosion resistance and high temperature operation that ceramic materials can provide is the major factor in its acceptance as gun barrel liners. The added feature of producing rifled ceramic liners enhances its future for gun barrel applications. Once the concept of ceramic liners is accepted, extensive designing for its application can be implemented. Proper designing of gun tubes using ceramic liners has the potential of producing a weapon that will last longer, maintain performance and be lighter in weight. Although ceramic liners at this time may cost more than stellite liners, for instance, the potential for longer life expectancy would make it cost effective.

Future study on ceramic liners will concentrate on the three candidate materials selected and any others that satisfy the physical requirement. At this time, test firing of these liners are conducted on a .50 calibre test gun under single shot conditions. The ultimate test for those materials that survive this stage of testing will be under rapid fire conditions. Multiple-fire testing will determine the feasibility of ceramic liners surviving under more realistic conditions.

REFERENCES

1. National Materials Advisory Board (NAS-NAE), "Erosion in Large Gun Barrels." Technical Report #AD-A017-104, National Technical Information Service, Springfield, VA (1975).

2. Katz, R.N., "Ceramics for Vehicular Engines: State-of-the-Art," Report AMMRC #MS-80-2, Army Materials and Mechanics Research Center, Watertown, MA (June 1980).

3. Stephan, P.M. and Rosenfield, A.R., "Survey of Ceramics in Gun Barrels," Technical Report #TR-SP-82-1, Army Materials and Mechanics Research Center, Watertown, MA (1982).

4. Bunning, E.J., Claxton, D.R. and Giles, R.A., "Ceramic Liners for Gun Tubes - A Feasibility Study," Presented at the Ceramic-Metal Systems Division Fifth Annual Conference, Merrit Island, FL (January 1981).

5. Prewo, K.M. and Brennan, J.J. "The Fabrication and Testing of Glass Matrix Composite Cylinders for Gun Barrel Liner Applications," Technical Report AMMRC #TR-82-7, Army Materials and Mechanics Research Center, Watertown, MA (February 1982).

6. Brochure, "Nilsen Sintered Products," Nilsen (USA) Inc., Glendale Heights, IL (1982).

FEASIBILITY OF GLASS MATRIX COMPOSITE CYLINDERS FOR GUN BARREL LINER APPLICATIONS

R. A. Giles and E. Bunning
Saco Defense Systems Division
Maremont Corporation
Saco, Maine

ABSTRACT

The feasibility of using glass matrix composite materials for gun barrel liners was investigated. Liner blanks were fabricated by United Technology Research Center from borosilicate glass reinforced with discontinuous graphite fibers. Fiber orientation of the liner was in the radial plane. Three liners were machined to configurations selected by analytical studies, assembled into modified .50 caliber barrels, and test fired for ten rounds each. The firing tests indicated that a low modulus, fracture tough, ceramic composite such as graphite reinforced glass is capable of withstanding the pressure stresses resulting from firing without failure and exhibits potential as a gun barrel liner material.

BACKGROUND

The erosion and wear of gun barrels has long been recognized as a serious problem and considerable effort has been directed towards finding a solution. The stellite lined chrome plated barrel design developed during World War II was very effective in increasing barrel life by significantly reducing erosion and wear in small caliber rapid fire weapons. Today's new large caliber, high performance gun systems present even more severe erosion problems. This, and the potential shortage of critical materials make it desireable to develop new barrel liners from non-critical materials having improved wear and erosion resistance. One such class of materials is ceramics. The Saco Defense Systems Division of Maremont Corporation (SDSD), under contract to U.S. Army ARRADCOM has demonstrated the feasibility of applying ceramics in this application by successfully firing 1000 rounds, single shot, in a modified M2 .50 caliber machine gun barrel equipped with a silicon carbide liner (Figure 1).

The work described in this paper was performed by United Technology Research Center under contract (DAAG46-81-C-0026) to AMMRC. Saco Defense Systems Division of Maremont Corporation served as subcontractor to UTRC for design consultation, test barrel fabrication, and verification testing.

Approved for public release; distribution unlimited.

Although silicon carbide exhibits the high temperature wear and erosion resistance required of a successful liner material, its inherent properties impose limits on the design and fabrication processes. The combination of relatively low tensile strength and a modulus of elasticity exceeding that of steel - causing the liner to carry a large share of the pressure load - requires that the liner be installed with considerable compressive prestress (shrinkfit) in order to prevent the tensile strength limit from being exceeded during firing. Low impact resistance and high notch sensitivity make the material sensitive to structural or surface imperfections and require careful control of the manufacturing process.

Recognizing the limitations imposed by the mechanical properties of monolithic ceramic materials, the U.S. Army Materials and Mechanics Research Center (AMMRC) awarded a contract to United Technologies Research Center (UTRC) to investigate the feasibility of fabricating a glass matrix composite material as a liner for gun barrels. Because of prior experience in this area, SDSD was selected as subcontractor for engineering consultation, test barrel fabrication and verification firing.

MATERIAL SELECTION

The family of composite materials known as COMPGLAS^{TM} was considered for evaluation. These materials consist of glass and glass-ceramic matrices reinforced with a variety of fibers, including graphite, SiC and AL_2O_3 and possess good fracture toughness and low notch sensitivity when compared with monolithic ceramics. Although their strength is relatively low, their modulus of elasticity is much less than that of steel. For this reason, liner pressure loads are largely reacted by the surrounding barrel, and liner stresses for any given pressure load are reduced. Tensile strength, therefore, becomes less of a critical factor than for monolithic ceramics.

The specific material selected by UTRC for initial liner fabrication was a boro-silicate glass matrix (Corning 7740) with graphite fiber reinforcement. Although this particular material has insufficient long term high temperature capability and a low coefficient of thermal expansion which will result in loss of shrinkfit at elevated temperature, it was judged suitable for inital concept verification and readily lent itself to the proposed fabrication method. After successful verification, efforts could then be directed toward optimizing the fiber/matrix combination to obtain a more favorable coefficient of thermal expansion and improved high temperature capability.

METHOD OF FABRICATION

Three possible fabrication concepts for the composite liner were investigated by UTRC. These are depicted in Figure 2. Since fiber orientation in the composite material is planar, the method of manufacture determines the fiber orientation and, therefore, the directions of maximum strength in the liner. For this reason, the manufacturing method must be based on structural as well as manufacturing considerations.

Concept 3, with fiber orientation in the radial and tangential directions, was chosen for the fabrication of test liners because it resulted in maximum material strength in the plane of the two principal liner stresses. As it happened, this concept was also the easiest to manufacture.

A billet of COMPGLASS^{TM} was first fabricated by uniaxially hot pressing glass powder impregnated plies of chopped graphite fiber paper in square dies. The structure of the billet is shown on Figure 3. Fiber orientation is in the plane defined by Axis 1 and 2.

Liner blanks were then core drilled from the billet. The axis of the liner lies along Axis 3. This process is depicted in Figure 4.

MATERIAL PROPERTIES

Selected properties of the proposed liner material are summarized in Table I. Strength and elastic properties are shown both in the plane of the fibers (Prinicipal Axis 1 and 2) and perpendicular to the fibers (Principal Axis 3). It is apparent that the selection of fiber orientation in the liner is an important design parameter because of the highly directional strength properties. Material properties for sintered alpha silicon carbide and Cr-Mo-V barrel steel are also shown for comparison.

DESIGN OF TEST BARRELS

A computer program, previously developed by SDSD, was used to evaluate design parameters in the following areas:

- The structurally important material properties and their influence on liner design parameters.

- The effect of variable liner wall thicknesses and modulus of elasticity on the maximum liner stresses resulting from bore pressure.

- The liner geometry and interference fits required for three test barrels to be used in room temperature verification tests.

The general design guidelines for the barrel liner can be summarized as follows:

- Because the modulus of elasticity of the liner material is considerably lower than that of the barrel itself (8 Msi vs 30 Msi) the bore pressure loads are largely reacted by the barrel and liner stresses remain at relatively low levels. Thus, lower material strength properties become acceptable if accompanied by a sufficiently low modulus of elasticity. (Figure 5)

- The tangential (tensile) liner stresses due to bore pressure decrease substantially as the liner wall thickness is reduced. The radial (compressive) stresses, however, are not significantly affected by decreasing liner wall thickness. It is, therefore, concluded that the lowest practical liner wall thickness should be selected. (Figure 6)

- Radial compressive stresses at the bore surface are numerically equal to the bore pressure (approximately 55,000 psi max.). The liner material must be capable of handling this stress level.

- The pressure stresses are dynamic in nature, and therefore, direct comparison with the static strength properties of the liner material is misleading. Until information on the dynamic strength and fatigue properties of ceramic liner materials becomes available, the computed data can only serve as a guideline.

- Pressure stresses in the liner wall are not uniform but subject to substantial gradients. It is suggested, therefore, that the modulus of rupture (flexural strength), or some modification thereof, is perhaps a more valid criterion for the evaluation of liner tensile capability than the direct tensile strength.

- The low coefficient of thermal expansion of this material results in rapid loss of shrinkfit at elevated (stabilized) barrel temperatures. In order to maintain at least wall to wall contact between liner and barrel at realistic maximum barrel temperatures (assumed at 1200°F), shrinkfits would have to be employed which would result in compressive stresses exceeding the yield strength of the material. Without such shrinkfits, a gap would form between liner and barrel which would, presumably, result in immediate tensile liner failure of the liner under bore pressure conditions. (Figure 7)

The barrel assembly designed for test firing of the glass matrix composite liner is similar to that employed previously as a test bed for the SiC liner. A breech and muzzle section are slip fit together and held in position with a retaining nut. The breech section consists of the liner, a steel sleeve, jacket and retainer. Shrinkfits are employed between the liner and sleeve and sleeve and jacket to maintain the liner in compression. In view of the low interference fit required in this installation, a separate sleeve is theoretically not necessary but was retained because it facilitates liner installation.

The three configurations selected for fabrication are summarized in Table II. The liner wall thicknesses and interference fits shown were selected such that the calculated resultant tangential stress was in reasonable conformance with the known static strength properties of the liner material. A liner wall thickness of .150" was thought to be the minimum practical thickness to insure liner integrity during handling and installation. Configuration 1 has a stress exceeding the material ultimate (static) limit. Configuration 2 has a stress approximately at this limit, while the stress in Configuration 3 is below this limit.

Figure 8 is a graphical presentation of the radial and tangential stresses throughout the barrel wall as calculated by the computer for verification test Assembly #1. The other configurations have similar stress profiles.

BARREL ASSEMBLY AND FIRING TEST

Three test barrel assemblies were manufactured by SDSD to obtain the diameters and interference fits previously selected.

The actual diameters and interference fits obtained on the various components are summarized in Table III. The results achieved were very close to the desired target values.

After assembly, each liner was inspected for ID size, surface finish, and evidence of cracks using fluorescent penetrant inspection techniques. All assemblies were observed to have circumferential indications of cracks in the bore approximately 1/4 to 3/4" from the muzzle end of the liner. It is suspected that crack formation is connected with nonuniform heating or cooling of the jacket when shrink fitting the liner/sleeve subassembly. The heating method to be used for future assemblies will be modified to obtain more uniform heating and cooling.

Each barrel assembly was fired for a total of 10 rounds single shot. The liner bore surface was monitored periodically with a bore scope to check for evidence of new cracks or the growth of pre-existing ones. No changes were observed.

Figure 9 shows Assembly #3 after the firing tests. Liner bore diameters were measured at 1" intervals before and after firing and the results are shown in Figure 10. The average growth in bore diameter was .0002 inch with individual values ranging from -.0002 to +.0007 inches.

The liner ID surface finish was measured before and after firing and the results are summarized in Table IV. A noticeable increase in surface roughness was observed.

SUMMARY

Test results indicate that a low modulus composite ceramic material deserves consideration as a candidate for barrel liners. Initial verification tests on this first generation material have shown that it is capable of withstanding the pressure and thermal stresses induced by firing at least under ambient temperature conditions. The material also exhibits a high degree of insensitivity towards surface defects. Even with cracks present in the original assembly, no tendency towards crack growth or catastrophic failure was observed.

Wear and erosion data still need to be determined through extended firing tests. These tests are now being conducted by SDSD under contract to AMMRC. The low coefficient of thermal expansion of the material tested is a definite shortcoming. The thermal coefficient of expansion of a practical liner material must be matched to that of the barrel material to allow operation at elevated temperatures without the loss of the initial interference fit.

CONCLUSION

It is our hope that this presentation will provide the material designer with some insight into the parameters of barrel liner design and provide guidance in the development of improved materials.

REFERENCES

1. K.M. Prewo and J. J. Brennan, "The Fabrication and Testing of Glass Matrix Composite Cylinders for Gun Barrel Liner Applications", AMMRC TR 82-7, Feb. 1982.

2. Robert A. Giles, Ernst Bunning, Dave Claxton, "Feasibility of Ceramic Lined Gun Tubes", ARRADCOM Contractor Report ARLCD-CR-30058, Feb. 1981.

3. E. J. Bunning, D. R. Claxton, R. A. Giles, "Ceramic Liners for Gun Tubes - A Feasibility Study", Proceedings of the 5th Annual Conference on Composites and Advanced Ceramic Materials, July-August, 1981.

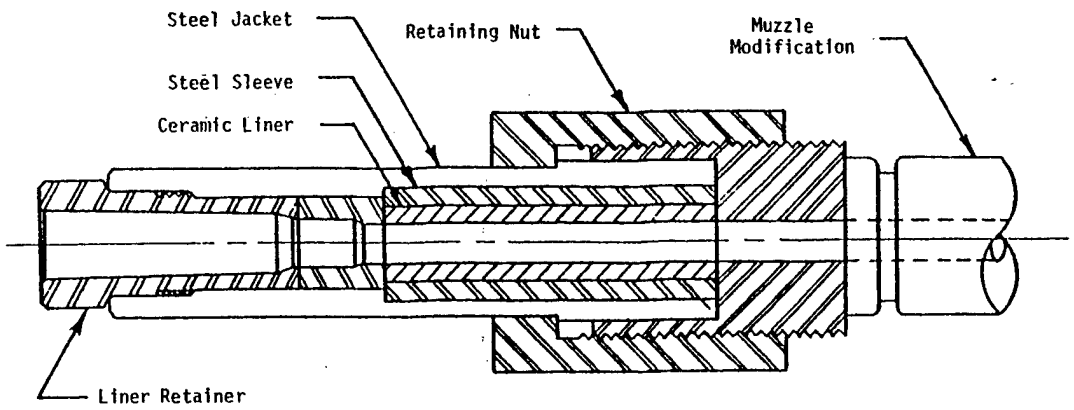

Fig. 1. Test barrel.

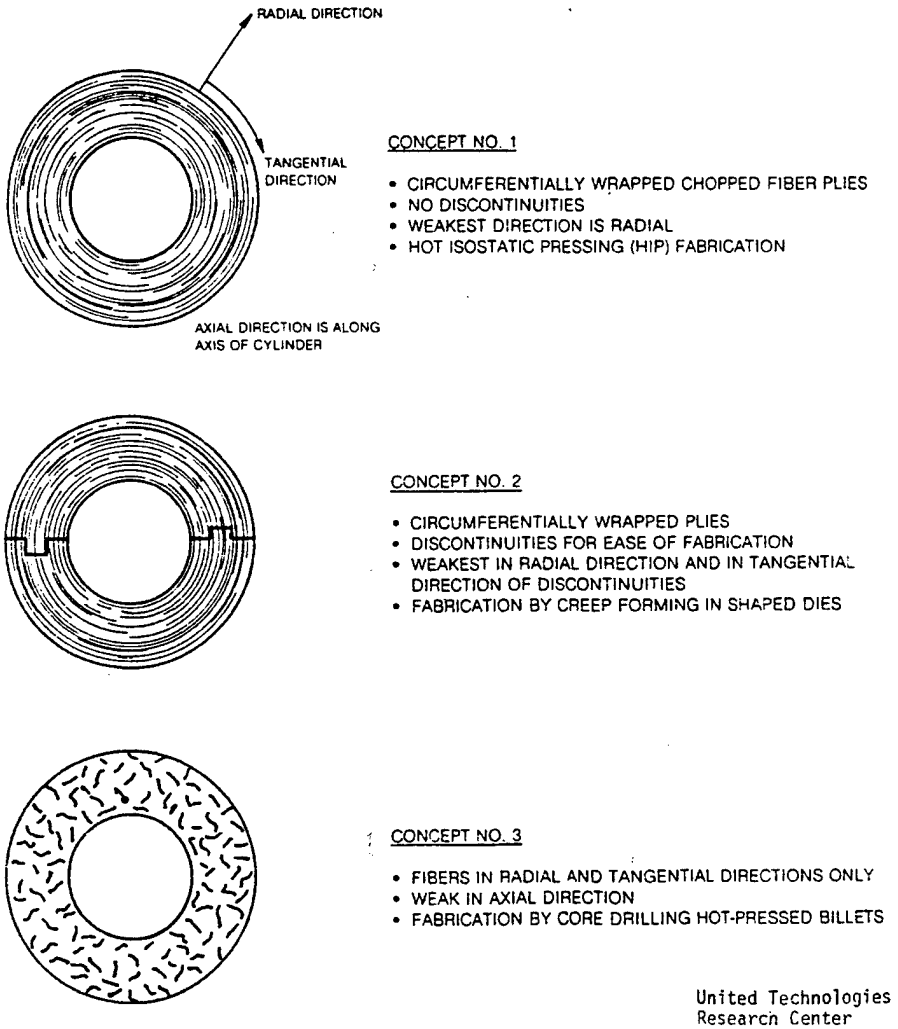

Fig. 2. Liner concepts.

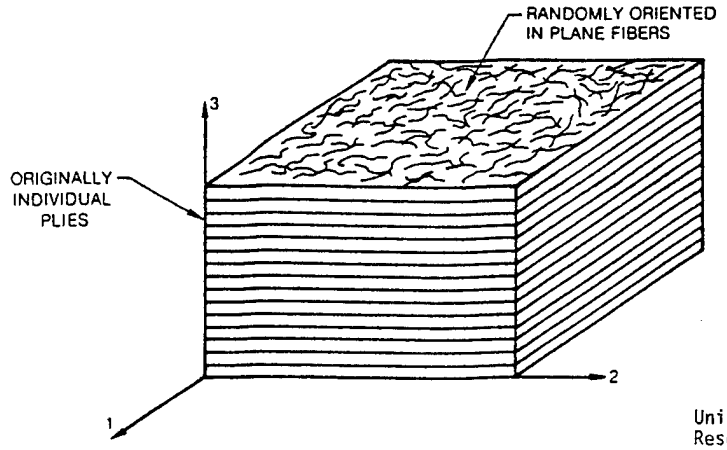

Fig. 3. COMPGLASS™ billet.

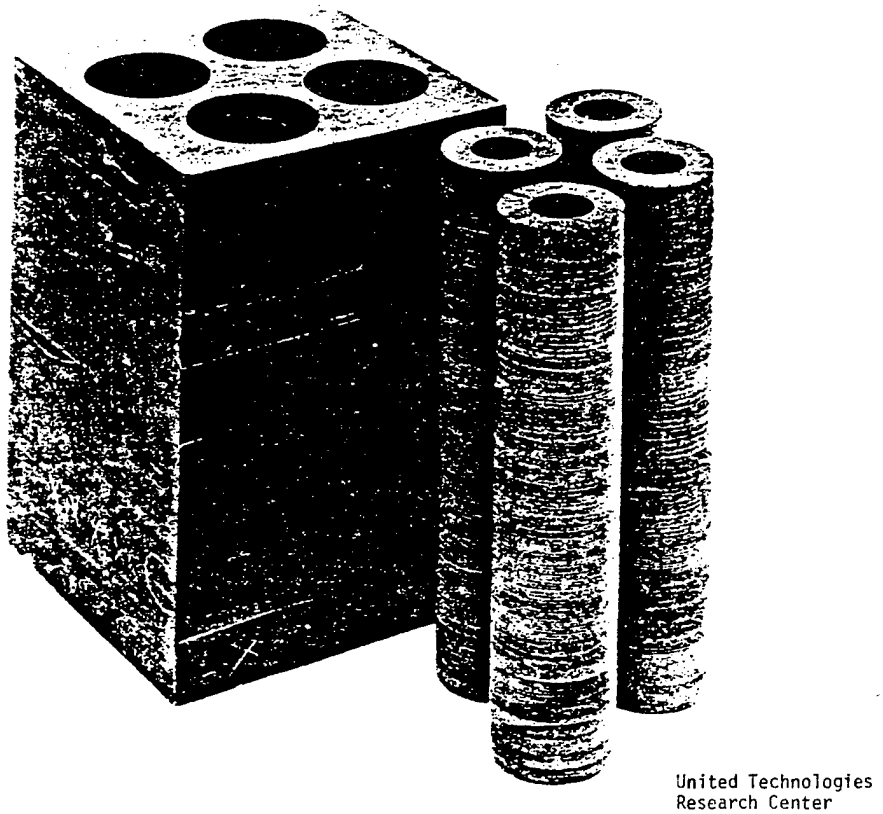

Fig. 4. Core drilled liner blanks

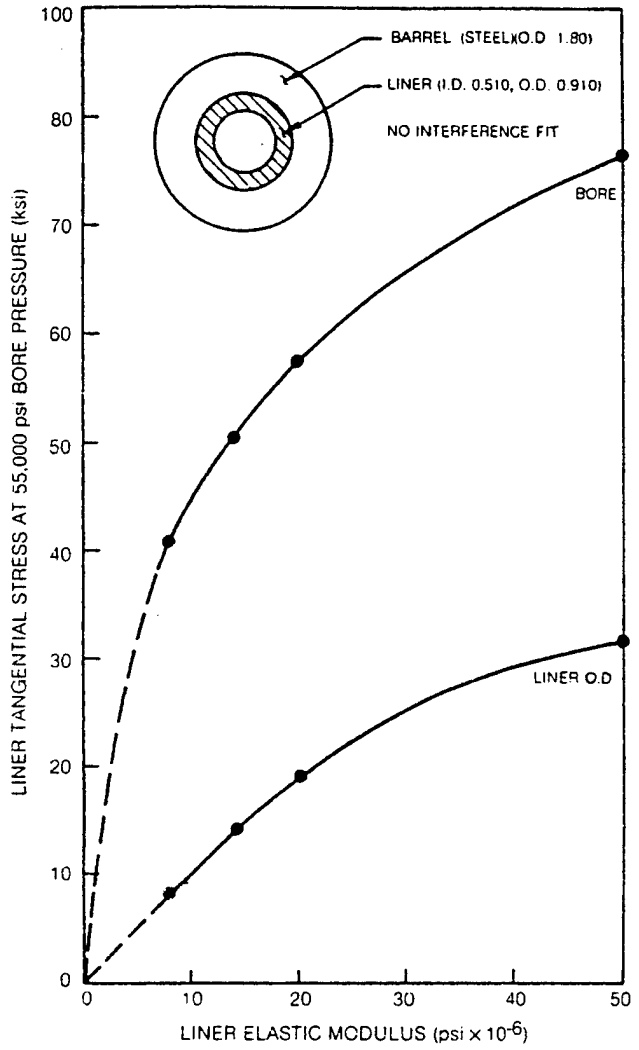

Fig. 5. Liner stress vs. elastic modulus.

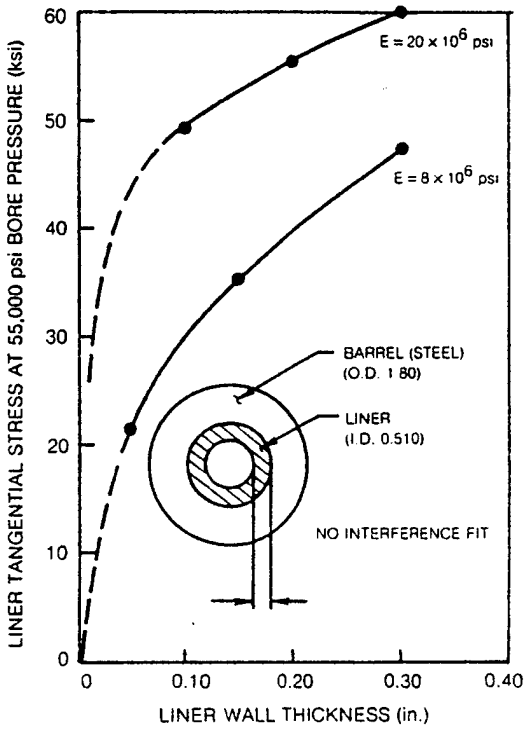

Fig. 6. Liner stress vs. wall thickness.

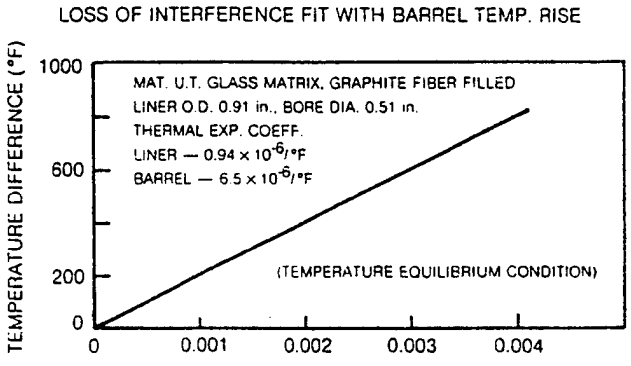

Fig. 7. Loss of interference fit.

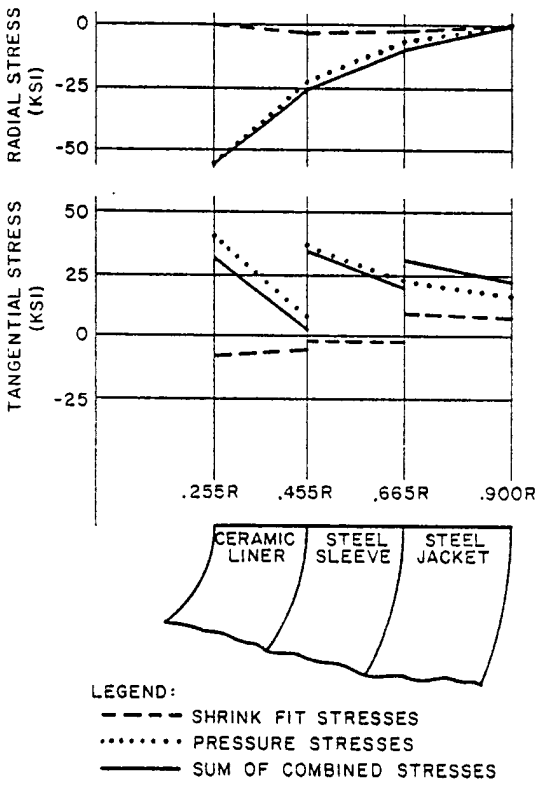

Fig. 8. Stress diagram.

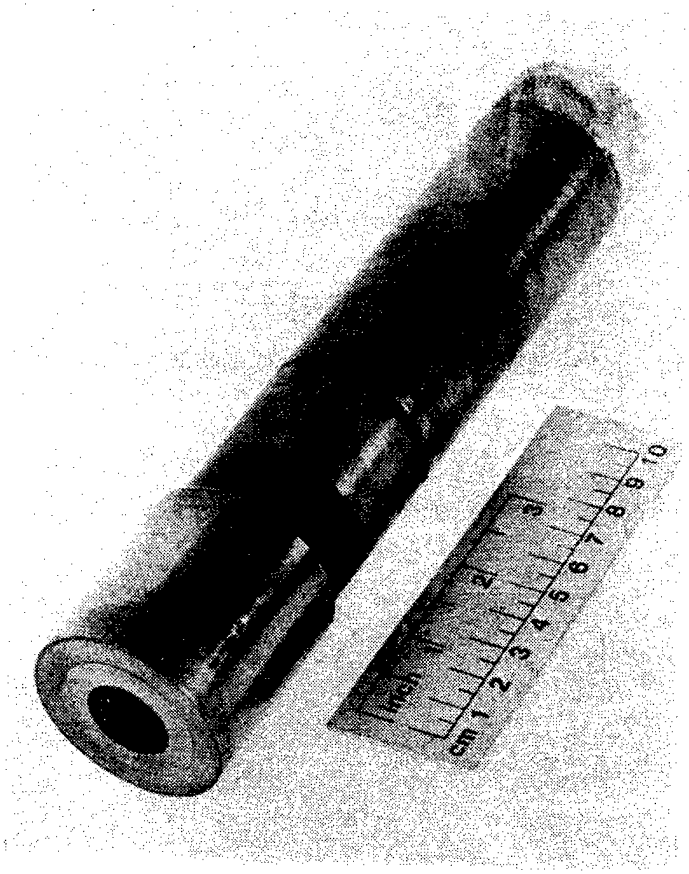

United Technologies Research Center

Fig. 9. Test assembly.

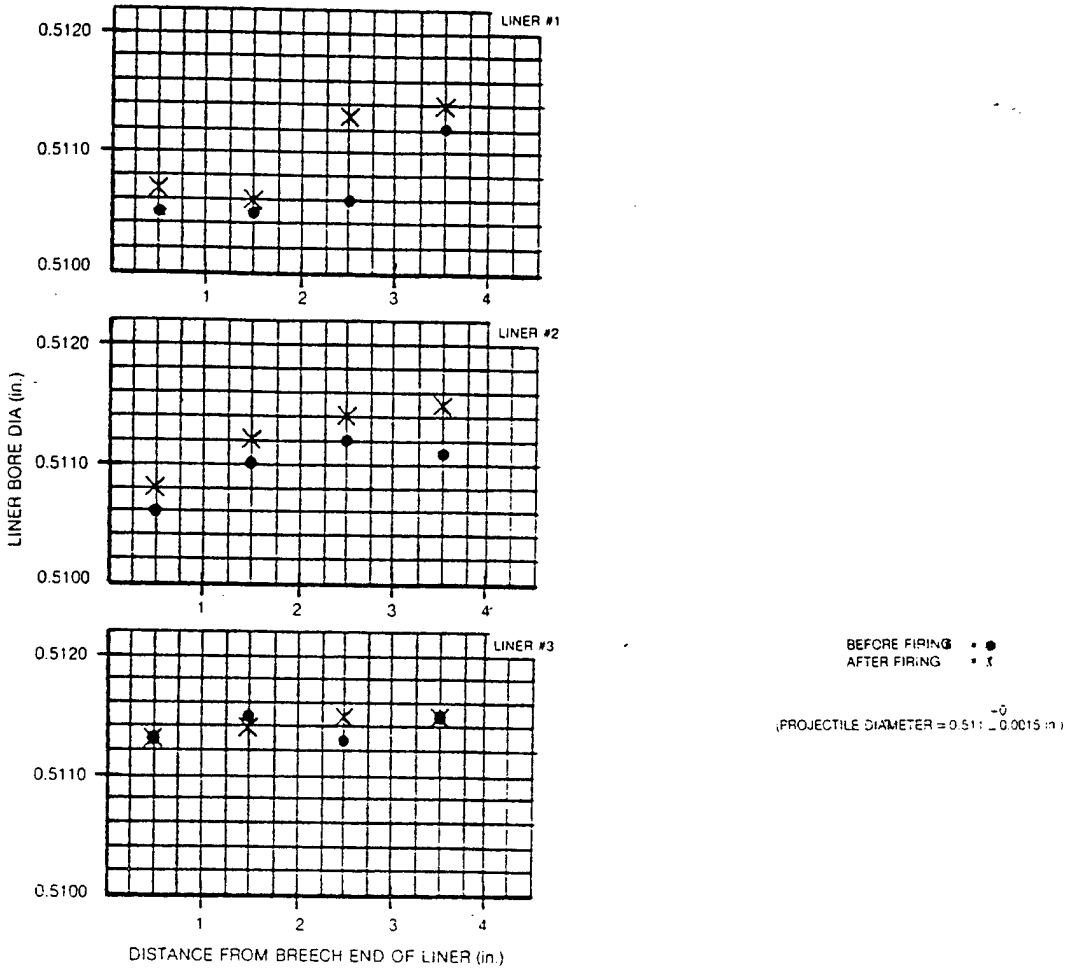

Fig. 10. Bore diameters.

TABLE I

COMPARATIVE PROPERTIES OF LINER AND BARREL MATERIALS
AT AMBIENT TEMPERATURE CONDITIONS EXCEPT AS NOTED

	Graphite/Class Composite		Sintered Alpha Silicon Carbide (at 1472°F)	Cr, Mo, V Gun Steel
	Principal Axis 1-2	Principal Axis 3		
Thermal Conductivity BTU-in./Hr-°F-ft^2 (C)	Unk.	Unk.	343	324
Modulus of Rupture (psi) (R)	45,300	-	64,100	
Young's Modulus (psi) (E)	8×10^6	5.2×10^6	59.4×10^6	30×10^6
Coefficient of Thermal Expansion (1/°F) (A)	$.94 \times 10^{-6}$		2.67×10^{-6}	6.3×10^{-6}
Poisson's Ratio	.19	-	0.142	0.30
Ult. Tensile Strength (psi)	19,400	1,000	48,000	200,000
Compressive Strength (psi)	46,400	113,000	500,000	200,000

TABLE II

SELECTION OF LINER GEOMETRY AND INTERFERENCE FITS
FOR VERIFICATION TEST HARDWARE

Configuration	Comp. Run	Liner Wall (in.)	Diametral Interference		Tangential Stress At Liner Bore		
			Liner/ Sleeve (in.)	Sleeve/ Jacket (in.)	Resultant Stress Max. (ksi)	Pressure Stress (ksi)	Shrink Stress (ksi)
1	1	.200	.0005	.0005	32.2	40.3	-8.1
2	2	.200	.0015	.0005	20.7	40.3	-20.7
3	9	.150	.0015	.0017	9.1	35.4	-26.3

TABLE III

Summary of Dimensional Inspection Results

Liner/Sleeve Dimensions (in.)	Assembly No. 1	2	3
Liner OD	.9100	.9102	.8102
Sleeve ID	.9095	.9086	.8087
Interference (Actual)	.0005	.0016	.0015
Interference (Target)	.0005	.0015	.0015
Sleeve/Jacket Dimensions (in.)			
Sleeve OD	1.3102	1.3126	1.3107
Jacket ID	1.3095	1.3119	1.3090
Interference (Actual	.0005	.0007	.0017
Interference (Target)	.0005	.0005	.0017

TABLE IV

Effect of Firing on Liner ID Surface Finish (RMS)

ID Finish	Assembly No. 1	2	3
Before Firing	12	11	12
After Firing	45	20	25

ADVANCED HIGH PERFORMANCE GUNS WITH REFRACTORY LINERS FOR EROSION RESISTANCE

P. D. Aalto, G. P. O'Hara, and G. D'Andrea
U.S. Army Armament Research and Development Command
Large Caliber Weapon Systems Laboratory
Benet Weapons Laboratory
Watervliet, NY 12189

ABSTRACT

An overview of liners and their application to advanced high performance guns is presented. Technology efforts with 20 mm and large caliber 105 mm gun barrels/tubes are reviewed. The facility used for shrinking a liner into the tube is explained. Structural analysis performed during the design, manufacturing, and testing phases is described. Results of tests conducted with the shrink facility and results of the test firing of the tube and liner are given.

INTRODUCTION

Many future large caliber cannon/gun tubes will be designed for higher muzzle velocity and higher rates of fire. As a result, the tubes will have to endure higher chamber pressures, higher propellant flame temperatures, and unless the current trend in tube design is altered, the tube bore will wear excessively even though it is plated with conventional hard chromium.

Tube liners utilizing advanced technology are a viable option for reducing the wear of the tube bore. Liners will be required because the cost of using advanced technology coatings to protect the complete bore of the tube will make the cost of a future tube exceptionally and possibly prohibitively high. Also the cost of gun tube forgings, the raw material, has risen dramatically over the past several years. Inserting advanced technology erosion resistant liners into gun tubes may provide the option that is needed for the future. The liners will have a longer wear life, will be far more resistant to the erosive effects due to high propellant pressure and flame temperatures and, when worn, will be replaceable by removing the worn liner and inserting a new liner.

Liners have been used in the past. During the 1940's and 1950's, the 8" Gun M1 and the 280 mm 'Atomic Cannon' both were fabricated with a liner.[1,2] Loose liners have been used in the Army 75 mm and 90 mm gun tubes.[3] For many years, the Navy has also made use of both loose and shrink fitted liners. A recent Navy test of a prototype 5"/54 gun barrel with loose insert further demonstrated the feasibility of using liners.[4] Many small arm rifle barrels are constructed today using stellite liners. The work described in this paper will show that it is now possible to insert advanced technology erosion resistant liners into large caliber gun tubes.

20 MM LINER TECHNOLOGY

Three recent reports detail the extensive work performed with 20 mm liners.[5-7] A total of 18 gun barrels (20 mm M24A1) were used. Fourteen (14) of these had

Distribution limited to US Government Agencies only because of test and evaluation; September 1982. Other requests for this document must be referred to Commander, ARRADCOM, ATTN: Benet Weapons Laboratory, DRDAR-LCB-RT, Watervliet, NY 12189.

liners. In all, 45,982 rounds of 20 mm M99A1 cartridges were fired during the entire test program.

Table I is a summary of the liners and barrels that were tested. Tantalum plated 20 mm liners performed better than all other plated liners tested including hard (HC) and ductile (LC) chromium.

TABLE I. SUMMARY OF 20 MM LINERS - PLATINGS AND MATERIALS TEST FIRED

	Barrel No.	No. Rds.
Ta/Steel #1	301349	1097
Ta/Stellite	301356	1010
Cr/Steel #1	300156	5204
Ta/Steel #2	301353	4923
Steel Liner #1	300204	2315
Steel Liner #2	300231	1001
LC Cr/Steel #1	300134	5046
LC Cr/Steel #2	300273	5010
Ta/Steel #3	300288	5034
Cr/Steel #2	301221	4983
Ta/10W	301165	513
Nb/Pyrotool V	332165	1527
Ta/Pyrotool V	300289	996
CG-27	332207	1966

105 MM LINER TECHNOLOGY

Since tantalum plate performed well in the 20 mm lined barrels, tantalum was selected for study in a large caliber 105 mm M68 gun tube with liner. The M68 gun was chosen because it is currently in production and adequate quantities were available for use as prototypes.

This preliminary work did not attempt to optimize either the liner design or the tantalum plating process.

A facility for shrinking liners into large caliber gun tubes was designed, fabricated, and successfully used. The unshrinking of liners prior to firing has been equally successful.

FIXTURE DESCRIPTION

A shrink fixture (facility) was designed, manufactured, and used to shrink a liner into a 105 mm M68 gun tube. The fixture serves two basic functions: support for the tube and other components, and alignment for liner and tube. The fixture stands approximately 18 feet high in a vertical position.

Figure 1 shows the induction coil at the lower half of the fixture and the liner release mechanism above the breech end of the tube.

Figure 2 shows the upper half of the rifling index bar (RIB) with the adjustment rods used to align the RIB with the bore center line of the tube. The RIB, placed into the barrel and inserted into the tube rifling, allows the liner, when dropped, to properly align itself with the rifled tube.

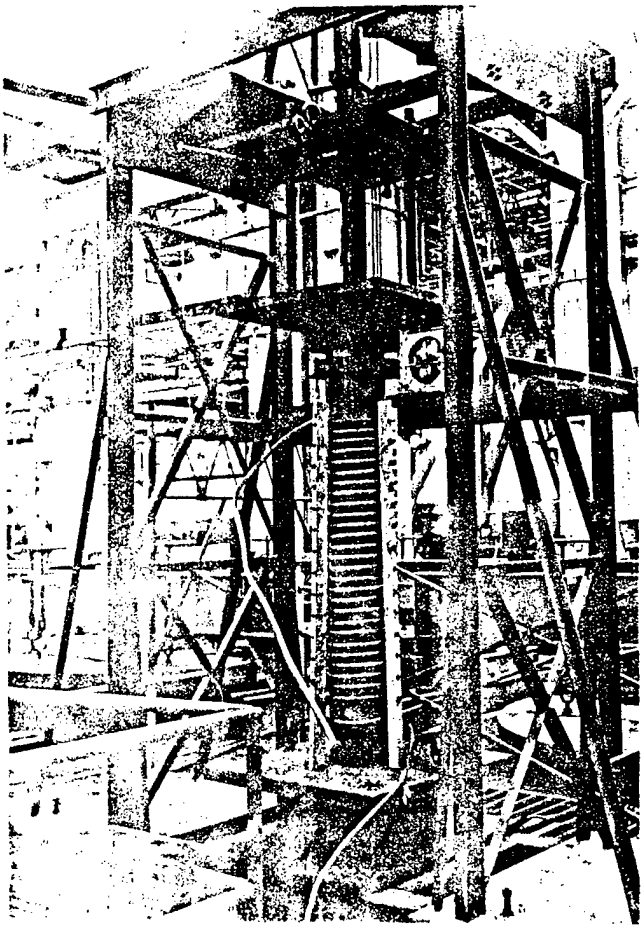

Fig 1. Shrink Fixture (lower half).

Fig. 2. Shrink Fixture (upper half).

STRUCTURAL ANALYSIS

The structural analysis of the stresses and deformations of the various components were done for one of three reasons. First was a check analysis of the lined tube design. The second was analysis in support of the manufacturing operations. The third was the analysis of unusual experimental results. Because

this was a technology program and had to be done using available hardware and material, most of the analysis was done to "check out" a design for structural integrity and not to optimize or improve a current design.

This paper will only give a quick outline of the work done. Nearly all of this work was done from old, well established theory or with the NASTRAN finite element code.

A. Lined Tube Design - An example of the first type of analysis was the analysis of the tube and liner combinations. Figure 3 shows the four basic problems that had to be checked:

1. Liner material requirements.
2. The tube-liner interface.
3. The interior corner at the muzzle end of the liner.
4. The "feather edge" at the chamber end of the liner.

The basic tube for this study was the M68 105 mm tank cannon, which is 100 percent autofrettaged with a long history of excellent service. Because of material and design constraints, a thin liner was selected. The material in this liner was not necessary to contain pressure; therefore, the material requirements are related only to the stress concentration in the fillets of the rifling projections. A finite element analysis was done of the stresses in the fillets using three different loading conditions. Typical results for this analysis are shown in Figure 4 as contour plots of the maximum principal stress. Figure 4 is the plot for stresses due to a pressure of 75,000 psi including the stresses due to a shrink fit thin liner. A problem associated with Figure 4 is that the contours away from the fillet are influenced by the discontinuous stress at the tube-liner interface.

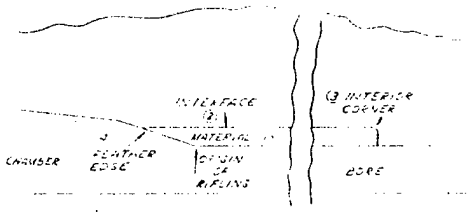

Fig. 3. Schematic Cross-Section of Tube. Four Basic Areas Analyzed.

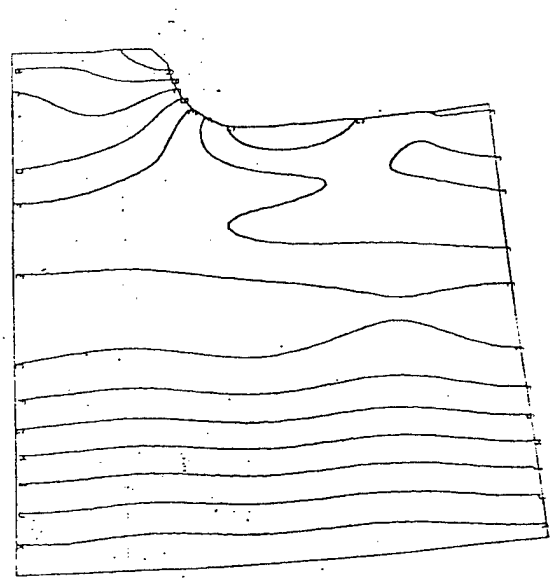

Fig. 4. Plot of Stresses. Pressure P = 75 Ksi.

The tube-liner interface conditions were analyzed from the closed form shrink equations. These equations were previously coded into a program which was improved for the general Multiple-Concentric Tube Design Analysis (MCTDA). Here there are two stresses of interest. The first is the radial stress at the interface which must be sufficient to resist the torque applied during firing and the second is the minimal residual circumferential stress at the bore which should be sufficient to control the maximum stress during firing. The maximum permissible shrink was set by the temperature the tube could be heated to without loss of autofrettage stresses. Figures 5 and 6 show the circumferential bore stress and radial interface stress as a function of shrink interference for 0.0 and 75,000 psi internal pressure. The small residual bore stress due to shrink does reduce the maximum bore stress to a reasonable value; however, the liner must still retain good properties to prevent overstress of the rifling fillets. The minimum radial interface stress of about 4,000 psi at zero internal pressure will easily lock the liner in place to resist the 70,000 inch pound projectile torque. In fact, when this maximum torque is applied, a large portion of the liner is pressurized.

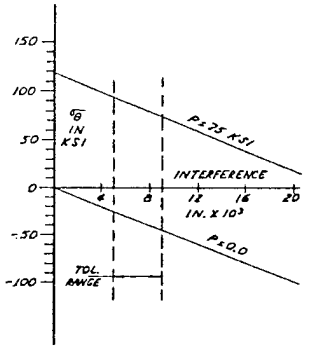

Fig. 5. Circumferential Stress Vs. Interference.

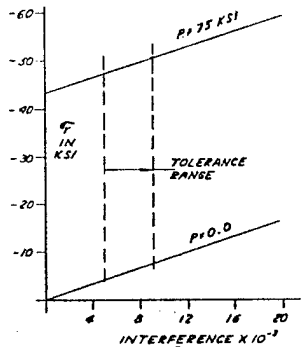

Fig. 6. Radial Stress Vs. Interference.

The interior corner (Item 3) at the muzzle end of the pocket was considered to be a problem because of possible high tensile stresses from two sources. First was the stress due to pressure in the radial gap at the end of the liner. Second was the stress due to uneven expansion of the tube. Gas pressure penetrating into the tube-liner interface from the muzzle end was also a possibility in this area.

A finite element stress analysis was made of this problem. Figures 7 and 8 show deformed grid plots from this study. In these figures, the deformations are exaggerated to become visible and, in fact, the gap between the tube and the liner represent the shrink interference. Figure 7 is the deformed grid with a uniform pressure in the tube. Figure 8 shows the deformations when a step pressure loading is used where the pressure is applied only to the liner.

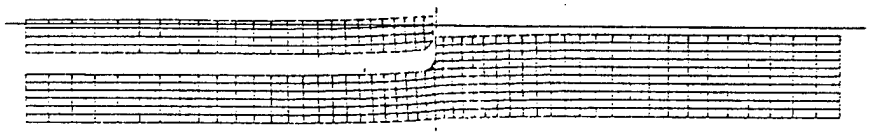

Fig. 7. Finite Element Stress Plot. Deformed Grid with Uniform Pressure.

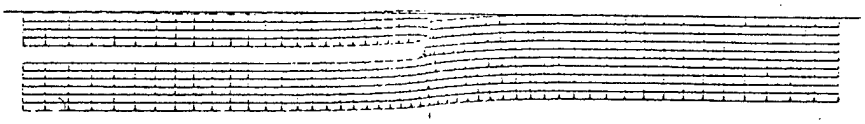

Fig. 8. Finite Element Stress Plot. Deformation with Step Pressure Loading.

The results of this work were largely negative, in that no problems were discovered. The residual stresses due to autofrettage would protect the interior corner from tensile stresses with any reasonable fillet radius. There were, however, other interesting results. It was shown that the radial gap at the end of the liner would tend to close as the pressure front passed the end of the liner and then open as the pressure became more uniform.

It was further shown that the radius on the exterior of the liner at the muzzle end would help to form a seal to prevent gas pressure from penetrating into the liner-tube interface.

The matter of the elastic stability of the "feather edge" of the liner at the chamber end was finally solved using Reference 8, in which the author provided equations for the shrink buckling of a thin ring in a circular opening. These equations are for the upper and lower bound of interferences on the zero slip and zero friction conditions on the interface. Figure 9 shows these results on a plot of interference vs. ring thickness where the results divide the plot into three regions where the behavior is stable, unstable, or when behavior is dependent on friction. On this plot the range of interferences is shown and appear to indicate that a very thin ring is elastically stable and the thin edge should present no problem.

B. Manufacturing - Analysis in support of manufacture could take on several forms; however, two examples will be shown. The first is a problem that resulted from the necessity of making steel liners from M68 gun tubes. These liners were to be used as a base for various electroplated coatings and therefore, had to be slightly larger than the final bore size. It was known, however, that the tube bore would expand as the residual autofrettage stresses were relieved by machining from the outside. Figure 10 shows this expansion plotted against the finished radius. This plot shows a family of lines for different initial outer radii. Because the M68 tube is tapered, there may be an optimum location to cut the liner from the tube.

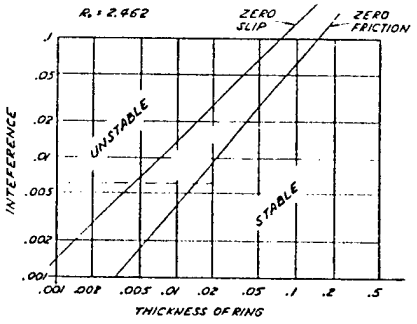

Fig. 9. Plot of Interference Vs. Ring Thickness.

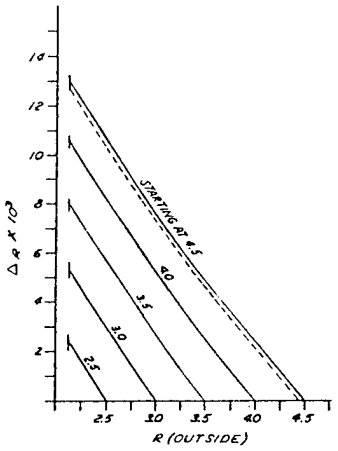

Fig. 10. Plot of Expansion Vs. Finished Radius.

The alternative problem was also done where the exterior of a tube will contract as the interior is cut away. Figure 11 is the results of this study where the data for all initial outside radii basically fall on the same line.

These solutions were done using the von Mises yield autofrettage equations and the radial stress replacement method. The results agree well with experiments, except for an error probably created by the small deviation of the actual residual stress pattern in the M68 from the calculated stresses. This deviation reduces the residual stress at the bore, due to either the swage autofrettage process or compressive reyield at the bore.

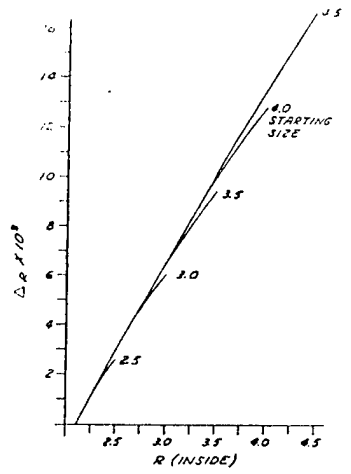

Fig. 11. Plot Showing Results of OD Contraction as Bore is Machined.

C. Testing - During the early testing of the 20 mm tantalum coated steel liners, the rifling "disappeared" while the tantalum coating seemed to remain intact. This result lead to the explanation that the steel liner changed hardness during the tantalum plating process. To study this problem, an elastic-plastic analysis was performed using the M68 rifling model (Figure 12). This study demonstrated that the rifling projection is actually a region of material moderately stressed in compression. This region sits on a band of high tensile stressed material that runs along the rifling grooves, and then under each projection. When the liner material consists of very low properties, there is plastic flow in the tensile band with each loading cycle. The net result is a slow movement of material from under the projection into the groove area.

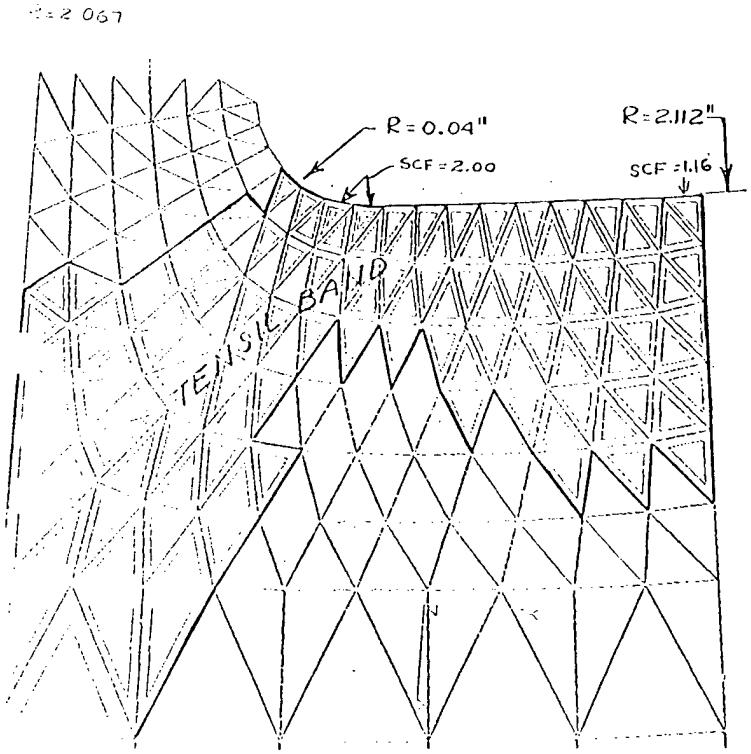

Fig. 12. Finite Element Plot of Land and Groove of 105 mm M68 Gun Tube.

This conclusion was supported by the experimental evidence obtained during the wear test of the 20 mm. For this test, the "land" diameter of the tube became longer and the groove diameter became smaller. Also, in the photomicrographs of the tube after firing, the outline of steel projections can be seen below the tantalum coating. One interesting part of this is that the coating has sufficient ductility to flow with this problem and retain its integrity without loss of thickness or cracking.

TESTING

Shrink Fixture - Before a liner could be shrink fitted into a tube, a number of tests had to be performed to develop assurance and confidence in the fixture. The tests verified that the fixture fulfilled the functions for which it was designed.

"Cold tests" were initially conducted. Steel liners with outside diameter smaller than the bore of the tube, by a few mils, were placed onto the RIB and held by the release mechanism. The release mechanism would be actuated and the liner would drop into the tube. These tests allowed checking of items such as alignment, effects due to liner drop, component function, etc.

Heat tests, using an induction coil, were conducted to determine the bore temperature when the tube was heated. The temperature at the outside diameter was monitored with a surface probe pyrometer. Bore temperatures were monitored by thermocouples placed against the bore wall.

Figure 13 is a curve of the temperature versus time that was generated for the shrink cycle. The oscillations about 700°F were made to insure adequate thermal "soak" of the tube prior to drop of the liner. The RIB was cooled by running water through it just prior to liner drop. Every 10 minutes the power to the induction coil was turned off to permit taking and recording temperatures at the tube outside diameter.

Figure 14 is a curve of temperature versus time for the unshrink cycle.

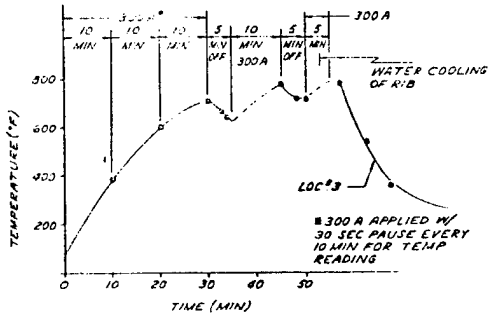

Fig. 13. Temperature Vs. Time Cycle for Shrink.

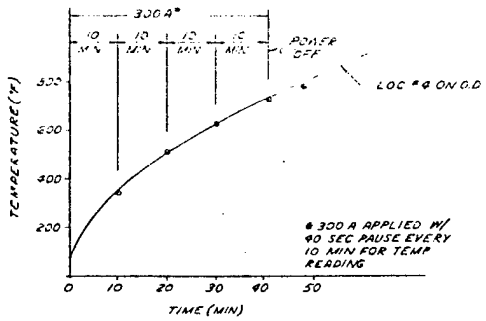

Fig. 14. Temperature Vs. Time Cycle for Unshrink.

Some factors of significance that were noted during the heat tests were:

A. The bore or inside diameter of the tube dilates ideally according to the linear equation

$$BE = .0000065 \frac{\text{in}}{\text{in}} \frac{1}{^\circ\text{F}} \times D(\text{in}) \times T(^\circ\text{F})$$

where:

$.0000065 \frac{\text{in}}{\text{in}} \frac{1}{^\circ\text{F}}$ ≡ Thermal Coefficient of Linear Expansion of Steel

D ≡ Diameter of Bore in Inches

T ≡ Temperature of Bore in Degrees Fahrenheit

BE ≡ Bore Enlargement in Inches

Considering a plot of bore enlargement versus temperature, larger bore diameters produce larger bore enlargements for a given temperature. For example, if the 105 mm, the 120 mm, the 155 mm, and the 8 inch (203 mm), all standard large caliber bore diameters, are compared, the largest bore enlargement at a given temperature will be obtained with the 8 inch tube. The conditions for shrink fitting liners into gun tubes are better for larger caliber tubes.

B. Using the induction coil to heat a large thick-wall tube, a temperature gradient is built up from outside to inside diameter. There can be up to a 150°F difference that will exist when the outside diameter (OD) temperature is 500°F to 600°F. A separate study was conducted to develop the parameters of this phenomenon more fully.[9]

C. The temperature measured on the OD surface of the tube beneath the induction coil varies from low readings at each end of the coil to a high reading at the coil center.

FIRING TESTS

The 105 mm M68 gun tube with tantalum plated liner was test fired, during the period November 1981 through June 1982, with a total of 110 rounds of 105 mm M490 without additive. Both liner and plating have performed well. Other details of the test will be covered in a future publication.[10]

In December 1976, a 105 mm M68 gun tube with full length 5 mil thick hard chrome (HC) plate was test fired. The same ammunition, 105 mm M490 without additive, was used. Figure 15 shows the origin of rifling after 100 rounds. Figure 16 shows the origin of rifling after 150 rounds.

The tantalum plated liner used in the recent test had approximately 3 to 4 mil tantalum on the lands and 2 mil in the grooves. The results obtained with a tantalum plated liner compare favorably with the results obtained with 5 mil HC plate (see Figure 17).

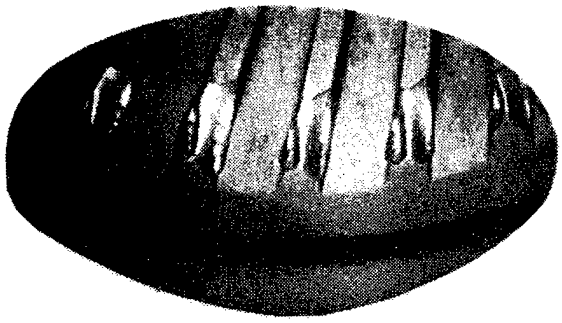

Fig. 15. Origin of Rifling 5 Mil HC Plated Tube After 100 Rounds M490 W/O Additive.

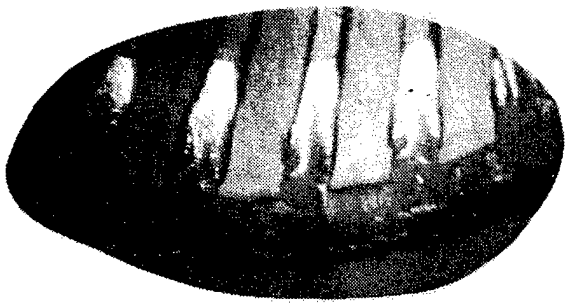

Fig. 16. Origin of Rifling 5 Mil HC Plated Tube After 150 Rounds M490 W/O Additive.

If Figure 17 is used for comparison, the following remarks must be considered:

a. The thickness of the HC plate, while close, was not equal to the thickness of the tantalum plate.

b. No attempt was made to optimize the parameters of the tantalum plate.

c. This was the first test ever conducted in large caliber.

d. Land height of the tantalum plated liner was still present at the origin of rifling after 110 rounds, whereas land height of the HC plate was virtually gone.

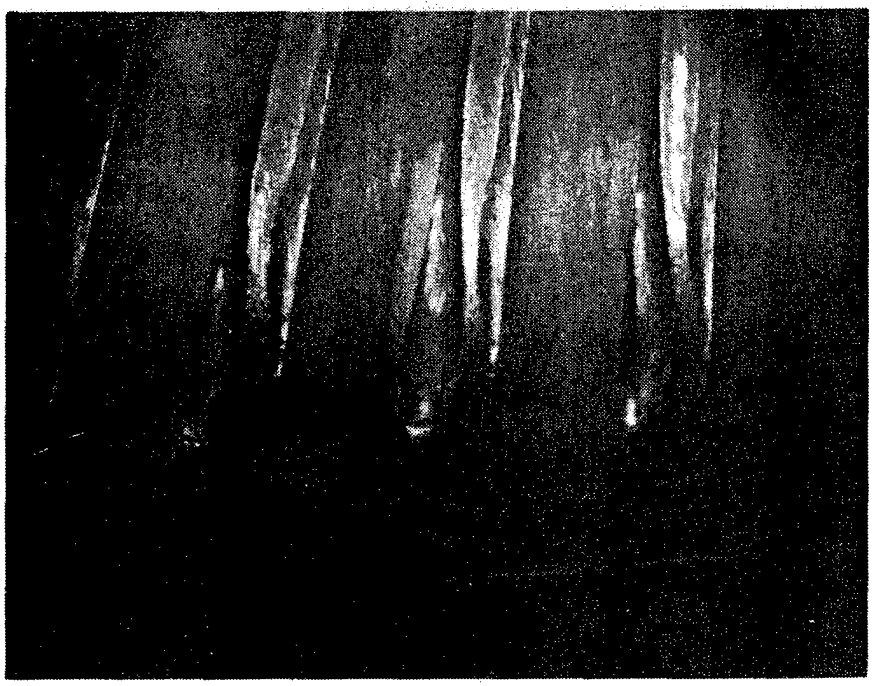

Fig. 17. Origin of Rifling Tantalum Plated Liner After 110 Rounds M490 W/O Additive.

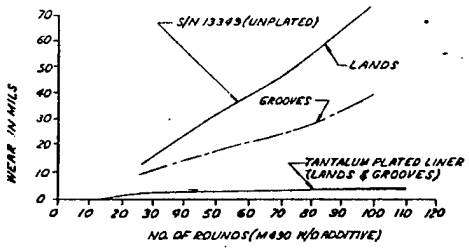

Fig. 18. Comparison of Unplated Tube Vs. Tube With Tantalum Plated Liner.

Figure 18 shows the results obtained with the tantalum plated liner compared with an unplated 105 mm M68 gun tube. The unplated tube reached the condemnation limit of 75 mil after 100 rounds. The stargage data for the tantalum plated liner shows no appreciable wear after 110 rounds.

CONCLUSIONS

Tantalum plated liners in the 105 mm M68 gun tube compare very favorably with HC plated tubes.

It is now possible to insert advanced technology erosion resistant liners into large caliber gun tubes.

REFERENCES

1. "Material for Induction Heat Report, Books I and II," Property of Res. and Dev. Planning Room, Watervliet Arsenal, September 1946 - May 1947

2. "Dev. and Prod. of Artillery Cannon," Watervliet Arsenal Report, 1946 - 1955.

3. "Replaceable Steel Liners for Medium Caliber Guns," OSRD Report, Circa 1953.

4. "Design, Development, and Testing of Prototype 5"/54 Ex 18 MOD 6 (Loose Insert) Gun Barrel," NOSL-R-335, October 1979

5. Cullinan, R. L., et al, ARLCB-TR-80027, USA ARRADCOM, Benet Weapons Laboratory, Watervliet, NY, December 1980.

6. Cullinan, R. L., et al, ARLCB-TR-81001, USA ARRADCOM, Benet Weapons Laboratory, Watervliet, NY, March 1981.

7. Cullinan, R. L., et al, ARLCB-TR-81046, USA ARRADCOM, Benet Weapons Laboratory, Watervliet, NY, December 1981.

8. Chicurel, R., "Shrink Buckling of Thin Circular Rings," Journal of Applied Mechanics, September 1968, pp. 608-610.

9. Disposition Form, Subject: Heating Cycle for Dropped Liner Testing," 7 May 1981, USA ARRADCOM, Benet Weapons Laboratory, DRDAR-LCB-RA (John Vasilakis), Watervliet, NY.

10. Aalto, P. and D'Andrea, G., USA ARRADCOM Technical Report, Benet Weapons Laboratory, Watervliet, NY, to be published.

ENGRAVING OF ROTATING BANDS - A MODIFICATION OF METAL FLOW PATTERN

Dr. Boaz Avitzur
U.S. Army Armament Research and Development Command
Large Caliber Weapon Systems Laboratory
Benet Weapons Laboratory
Watervliet, NY 12189

ABSTRACT

An evaluation of the commencement-of-rifling (C.O.R.) geometry suggests that the mode of deformation of the rotating band by the rifling is inefficient. Observation of rotating bands of fired and retrieved projectiles confirms the above evaluation. Engravers, simulating the conventional design of C.O.R. as well as the proposed modification, were fabricated. Slugs of rotating band material were engraved with the simulated engravers. Metallographic data on the laboratory engraved slugs were compared with those of retrieved projectiles; results from the two simulating designs were also compared. Similarities were found between retrieved bands and simulated conventional design, while the simulated modification resulted in change in metal-flow pattern close to the intended one. Reduced engraving forces is observed as predicted and is explained by reduced deformation forces when the modified design of C.O.R. is being simulated. It is suggested that reduced deformation forces will reduce wear at the commencement-of-rifling.

INTRODUCTION

Engraving is a process by which a rotating band, on a spin-stabilized projectile, assumes a complimentary form with the firing tube's rifling. As the name implies, its primary purpose is to impart a rotational motion to the projectile. In addition, by filling the grooves in the tube's rifling, the rotating band slows down leakage of propellant gases past the projectile. Ideally it would stop such leakage completely.

Design dimensions of the grooves in the tube and of the O.D. (outer diameter) of the rotating band call for interference; the O.D. of the rotating band is made larger than the rifling's grooves' diameter. For an 8 inch gun tube the grooves' diameter is $8.140^{+.006}_{-.000}$ while the O.D. of the rotating band on a corresponding projectile is $8.195^{+.000}_{-.005}$, or an interference of .044 inch to .055 inch in diameter (which is .54 percent to .67 percent of the diameter, and it is to be compared with grooves' depth of .070 inch on each side). If such an interference prevails during firing, the excess material (.044 inch to .055 inch) will be shaven at the rifling grooves and in between it will be pushed backward by the rifling lands. To accommodate for the backward metal-flow, the rotating bands are provided with periodic circumferential channels called canntilleures. This investigator is convinced that the longitudinal push along the circumferential surfaces and the shear along the radial (side) surfaces of the riflings lands (see Figure 1) at the

commencement-of-rifling (C.O.R.), are too severe. The energy required to engrave the band in this fashion is high and the wear on the tube's rifling is severe. Hence, I suggest a modification of the flow pattern in the rotating bands material during engraving through a change in the designs of the commencement-of-rifling (C.O.R.). This change is intended to maintain the configuration of the rifling beyond its commencement. The concept involved can accommodate any change in the rifling configuration and/or surface treatment and thus be complimentary to such a change rather than a substitute for it.

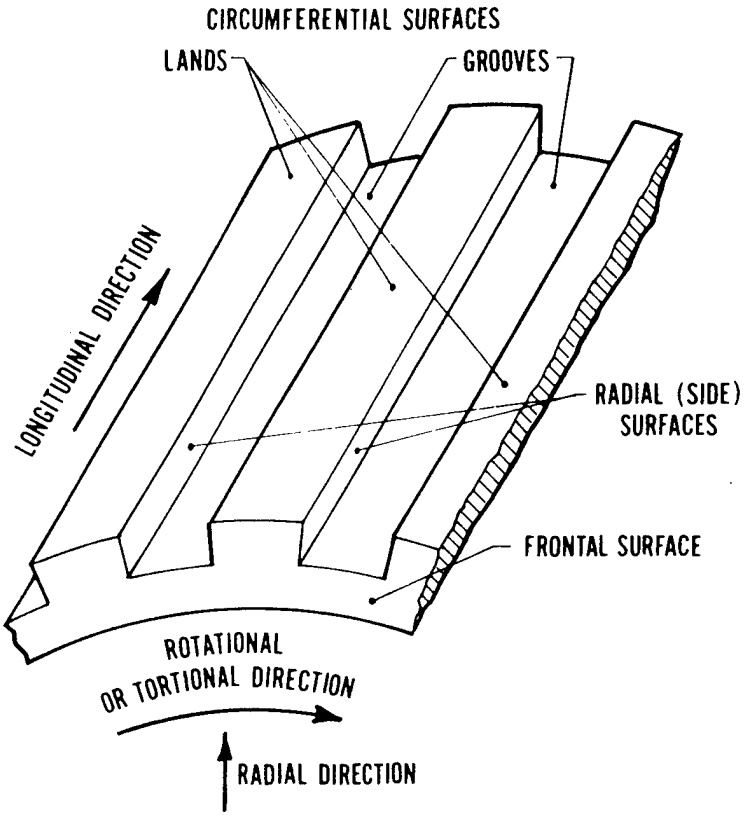

A SEGMENT OF AN ENGRAVED ROTATING BAND

Fig. 1.

OBSERVATIONS

Visual and microscopic evaluation of the rotating bands of fired and retrieved projectiles revealed the following:

a. As seen in Figure 2, material removed by the rifling's land has been pushed backward by the lands. In some locations, the rotating band material between the rifling's land failed to fill the rifling's grooves. This is evidenced by the retention of machining marks on the rotating band. During firing the tube below the projectile is subjected to the propellant's pressure and thus to radial expansion. Under the same pressure, the projectile's tail end may contract radially. These

forces may be augmented by the radial component of the engraving forces. However, as mentioned above for the 8 inch tube and projectile, the interference between the as-machined gun tube and the as-machined rotating band is between .54 percent to .67 percent of their nominal diameter. It is beyond the scope of this investigation to accurately determine the factors that contribute to the band's failure to completely fill the rifling's grooves. Nevertheless, this observation will be referred to in the discussion of the simulated engraving. (Namely simulating both designs - the prevailing one as well as the suggested modification.)

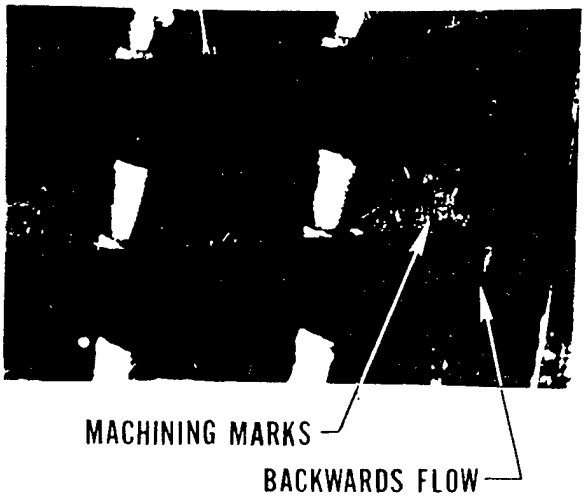

Fig. 2.

b. The microstructure of a transverse cut through the rotating band's groove (Figure 3b) reveals that in a retrieved rotating band of a 105 mm projectile up to about .008 inch below the surface, has been heavily deformed and recrystallized, and that a layer of up to .055 inch to .075 inch (total) was deformed to a noticeable degree.

c. The above micrograph (Figure 3a) also reveals a total groove depth of about .028 inch in the rotating band, while the rifling's land's height is (designed to be) .030 inch to .032 inch. This reemphasizes point "a" above, suggesting an incomplete filling of the riflings grooves by rotating band material. Moreover, according to Figure 3a, the width of the engraved groove is .1664 inch to .2158 inch, whereas the designed width of the rifling land is only .1500 inch. Since this retrieved projectile was fired from a howitzer with degressive twist (of its rifling), the widening of the groove on the rotating band can be partially attributed to the change in twist angle and partially to torsional wear. The slope of one side of the band's groove can be attributed to progressive torsional wear at the early stages of engraving (at the commencement-of-rifling). Usually, however, torsional wear develops gradually throughout the length of the tube. Whatever the mechanism is, the widening of the grooves allows for gas leakage to the front of the projectile.

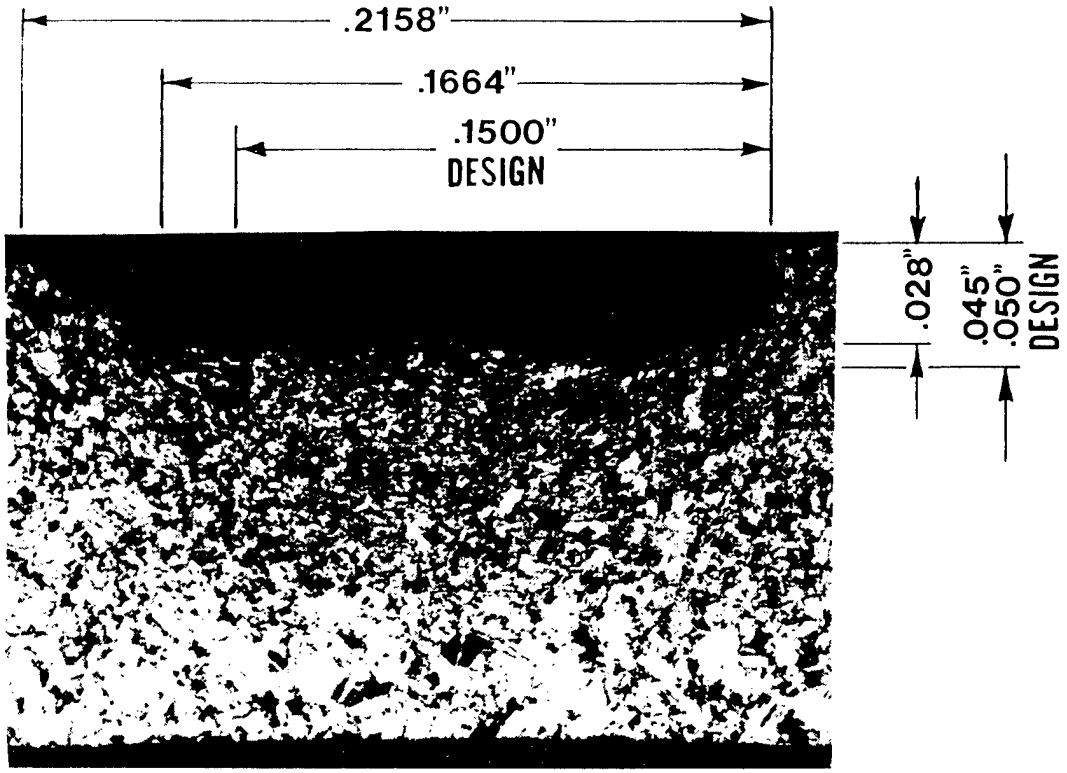

Fig. 3a. Engraved Rotating Band on a 105 MM Projectile - Transverse Section.

Cross section of a rotating band from a retrieved 8 inch projectile (Figure 4) shows engraving depth of .057 inch to .066 inch (or about 81 percent to 94 percent of the design height of the rifling's land). However, the width of the engraved groove is .2193 inch, whereas the designed width of the engraving land is only .1571 inch (or about 40 percent larger than it was designed to be). If these numbers are representative ones (the verification of which is beyond the scope of this investigation), then one conclusion is that despite the almost complete filling of the rifling grooves, gas leakage is still a possibility.

In summary, the above numbers suggest that the wear in the rotating band of the 105 mm projectile fired through a howitzer, was between 4.5 percent and 18 percent of its circumference, while on the retrieved 8 inch projectile it was about 15.8 percent. It is anticipated that these values will vary also with the firing zone (for the same projectile size and weight).

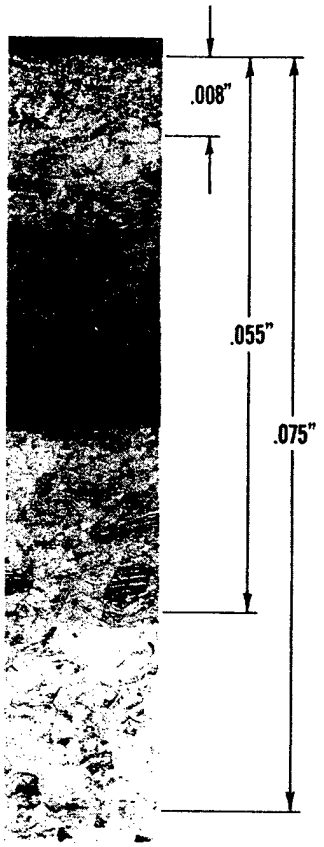

Fig. 3b. Transverse Cut Through an Engraved Groove of a Rotating Band of a 105 MM Projectile - Reduced 50 Percent from 100X Magnification.

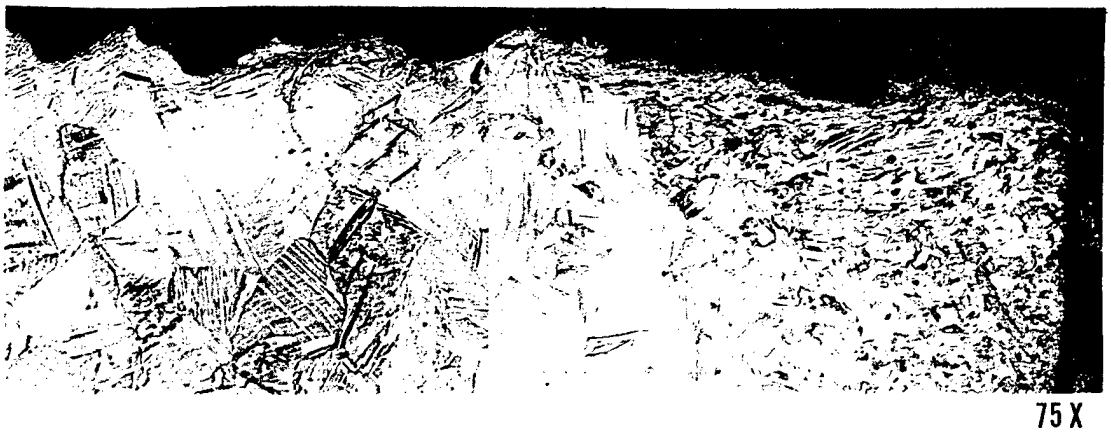

Fig. 3c. Transverse Cut Through the Land of an Engraved Rotating Band of a 105 MM Projectile - Reduced to 75 Percent of 100X Magnification.

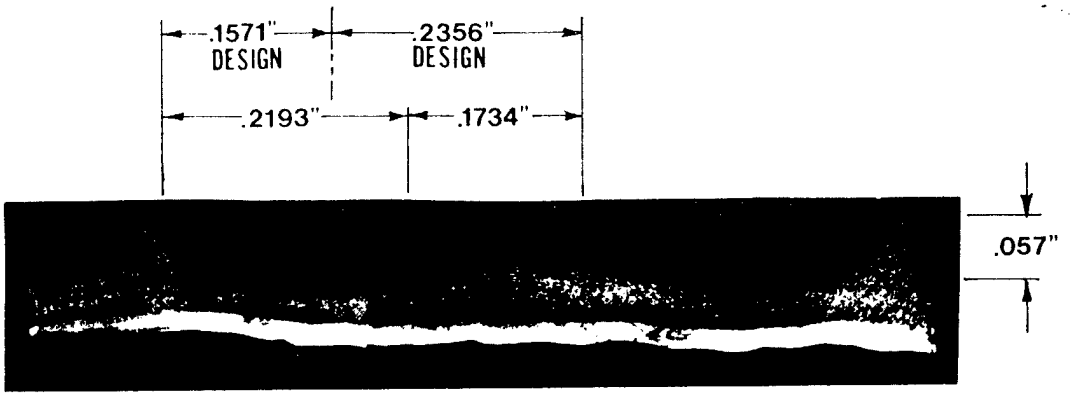

Fig. 4. A Transverse Cut Through a Rotating Band of an 8" Projectile - Reduced to 75 Percent of a 75X Magnification.

BACKGROUND

Most available studies where gross plastic deformation is involved address themselves to continuous processes such as wire drawing or rolling.[1,2] In these processes one can divide the material into three zones:

a. Rigid incoming material.
b. Deformation zone.
c. Rigid outcoming product.

Except at the start and end of the process, the size and shape of the deformation zone is independent of time and so is the stress and/or strain rate distribution throughout the deformation zone. The two leading methods of approximating these stress and strain rate fields are:

a. Limit analysis, which is discussed intensively by Avitzur.[1]
b. The slip line field method, which is discussed by Thomsen et al.[2]

The problem at hand, however, deals with a deformation where the shape of all three zones, the incoming material, the deformation zone, and the final product, vary as the process progresses.

The above mentioned literature,[1,2] as well as others, treats such processes also. (For example, simple forging of a disc or deep drawing of sheet metal into a cup). However, as the process deviates from one of rotational symmetry, it becomes more tedious to analyze the stress and/or strain rates at each instant of the process while in progress. Such studies can be aided experimentally by splitting the samples and imbedding grid lines which will be evaluated as the process progresses.[2] Such a process is tedious and costly. It was not used in this study. An intensive search for such studies by past investigators can be summarized as follows: "The engraving process was not analyzed," so far, "due to lack of adequate data for loading input and the reliability of results in an elastic-plastic modeling problem."[3]

In view of the above background, this investigator bypassed any analytical evaluation of either the prevailing design of commencement-of-rifling, or of his suggested modification of the latter. I was guided by the principal that reducing redundant work (of engraving) should reduce the required energies and engraving forces. Professor Backhoffen's definition of redundant work, as

$$D = \frac{L}{h}$$

where h equals depth of deformation zone and L equals width of deformation zone, was one of my criteria in modifying the design of the commencement-of-rifling.

LABORATORY SIMULATION

The simulator consists of a steel block, an engraving plate, and a moving cage that contains a slug to simulate the rotating band (Figure 5). The first tested engraving plate simulates the rifling and its commencement in an 8 inch tube. In order to simplify the process and to reduce complications by factors of secondary importance, lateral movement of the slug was eliminated. Therefore, a straight rifling was used instead of the rotational twist in actual gun tubes.

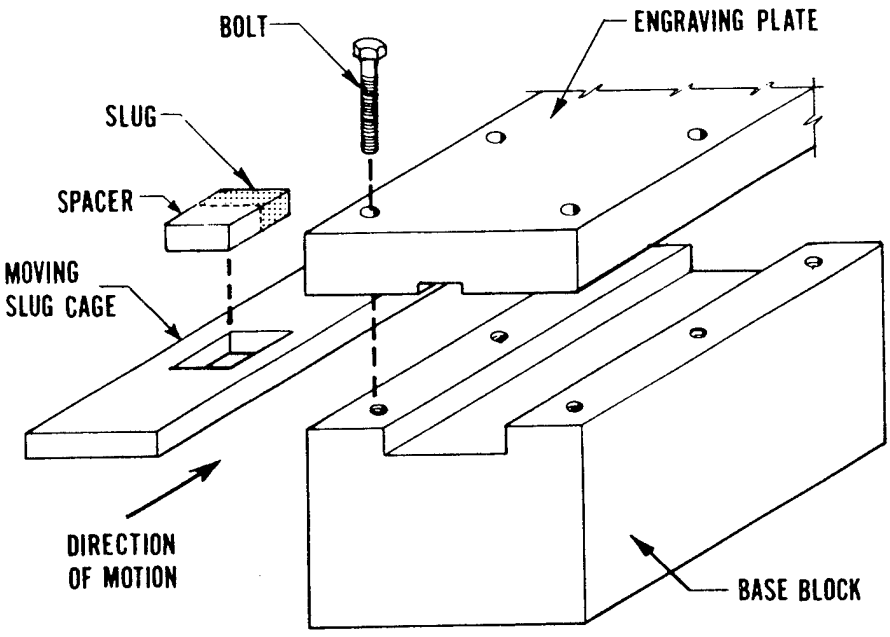

ENGRAVING SIMULATION APPARATUS

Fig. 5.

While the total width of a rotating band on an 8 inch projectile is two inches (with four canntilleures), most of the simulations made so far were with .500 inch long slugs, (Figure 6); .282 inch, x .500 inch, x .800 inch. Visual examination of the engraved slugs reveals the following:

a. The backwards push of engraved material by the simulated rifling land was exaggerated when compared with that of the actual retrieved rotating band.

b. The dull surfaces on the slugs' lands (Figure 7a) suggests, like the retention of machining marks on the retrieved rotating bands, that the simulator's rifling grooves were not completely filled with the engraved slug's material. This is also supported by the grooves depth "B" - height of the groove (Table I and in Figure 6), which reaches the full design depth of .070 inch only at the shiny spots. The total thickness of the engraved slug at its tail end, which is also where the grooves attain the full height of the engraver's land, is larger than its original (unengraved) thickness (by .015 inch to .018 inch). This agrees with the observation that (in an 8 inch tube) despite prefiring interference of .044 inch to .055 inch, there is an incomplete filling of the rifling grooves. The mechanisms leading to this similarity are not necessarily the same, i.e., there is no radial pressure due to propellant gases in the simulator, although elastic strain might be imposed on the simulator's engraving plate's bolts due to the normal component of the engraving force which is similar to the radial component in the actual gun tube during firing.

c. Micrographs reveal the following similarities between a rotating band engraved during firing and a laboratory slug engraved in the above simulator.

1. A cross section through the band/slug material's land (filling the grooves space of the gun/simulator rifling) is by and large undeformed (compare Figure 3c with Figures 8a and 9a). A narrow strip at the (band/ slugs) land's edge underwent deformation (compare Figure 3c with Figure 9b). The latter should be attributed to the shearing of the groove in the simulated slug and/or due to torsional wear in the rotating band of a fired projectile.

2. In the engraved groove the following was observed: a layer of .008 inch below the surface of the fired band (of 105 mm projectile) was heavily deformed and recrystallized (Figure 3b). In the simulated slug a layer of up to .015 inch was heavily deformed (without recrystallization) (Figure 10a). Below the heavily deformed layer one can detect deformation up to .055 inch to .075 inch below the surface of the fired rotating band and about .046 inch to .068 inch in the simulated slug.

On the other hand, comparing the engraved slugs simulating the present design of commencement-of-rifling with those of the modified design, led to the following observations:

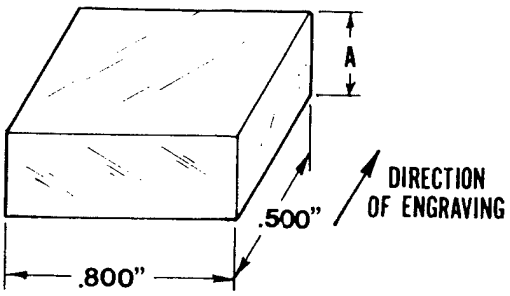

A = .282" FOR SIMULATING CONVENTIONAL C.o.R.
A = .252" FOR SIMULATING MODIFIED VERSION OF C.o.R.

6a. SIMULATING SLUG BLANK

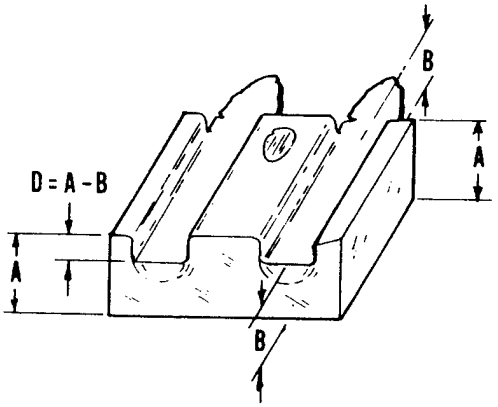

6b. ENGRAVED SLUG SIMULATING CONVENTIONAL C.o.R.

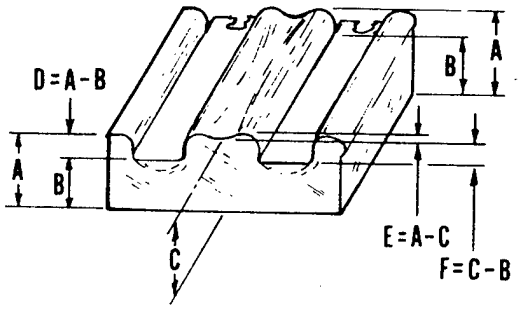

6c. ENGRAVED SLUG SIMULATING MODIFIED C.o.R.

Fig. 6.

TABLE IA. DIMENSIONS OF SIMULATED ENGRAVING

Sample Number	Original Thickness 1. Bare 2. (With Shims)	"A" Total Height		"B" Height at the Groove		"C" Height at Channel in Lane	
		Front	Back	Front	Back	Front	Back
	.282	.282	.309	.2335	.2405		
	.282	.3017	.3049	.2353	.2358	.2953	.3022
1	.282	.287	.298	.227	.228		
2	.282	.286	.300	.229	.231		
3	.282	.2785	.2960	.2250	.2260		
4	.282	.2810	.2970	.2255	.2270		
8	.252	.280		.218		.255	
9	.252	.282		.218		.256	
10	.252	.283		.2175		.2545	
12	.252	.2815		.2165		.2585	
13	.252	.2795		.2120		.2585	
	(.257)						
14	.252	.278		.2092		.2585	
	(.260)						
15	.252	.275		.2090		.2560	
	(.260)						
19	.252	.266		.224		.2610	
20	.252	.266		.2177		.2605	
	(.257)						
21	.253	.266		.2134			
	.266					.2608	
22	.2535	.2666		.2080		.2610	
	(.2735)						
23	.2800	.2773		.2250		.2763	
24	.2800	.2883		.2266		.2781	
26	.282	.3052	.3018	.2367	.2362	.2979	.2958

TABLE 1B. DIMENSIONS OF SIMULATED ENGRAVING

Sample Number	Original Thickness 1. Bare 2. (With Shims)	"D" = A-B Front	"D" = A-B Back	"E" = A-C Front	"E" = A-C Back	"F" = C-B Front	"F" = C-B Back	Material	Simulators Design	Remarks
	.282	.0485	.0685					Copper	Conventional	2.000" long
	.282	.0668	.0687	.0064	.0027	.0600	.0664	Copper	2nd Modification	2.000" long
1	.282	.0600	.0700					Copper	Conventional	
2	.282	.0570	.0690					Copper	Conventional	
3	.282	.0535	.0700					Copper	Conventional	
4	.282	.0555	.0700					Copper	Conventional	
8	.252	.062		.025		.037		Copper	1st Modification	Incomplete
9	.252	.064		.026		.038		Copper	1st Modification	
10	.252	.0655		.0285		.037		Copper	1st Modification	
12	.252	.065		.0230		.042		Copper	1st Modification	
13	.252	.0675		.0210		.0465		Copper	1st Modification	
14	(.257) .252	.0688		.0195		.0492		Copper	1st Modification	
15	(.260) .252	.066		.0190		.047		Copper	1st Modification	Incomplete
19	(.260) .252	.042		.0050		.037		Gilding	2nd Modification	
20	.252	.0483		.0055		.0428		Gilding	2nd Modification	
21	(.257) .253	.0526		.0052		.0474		Gilding	2nd Modification	
22	.266 .2535	.0586		.0056		.0530		Gilding	2nd Modification	
23	(.2735) .2800	.0523		.0010		.0513		Gilding	2nd Modification	
24	.2800	.0617		.0102		.0515		Copper	2nd Modification	
26	.282	.0684	.0655	.0073	.0060	.0611	.0595	Copper	2nd Modification	2nd Slug in tandum of two

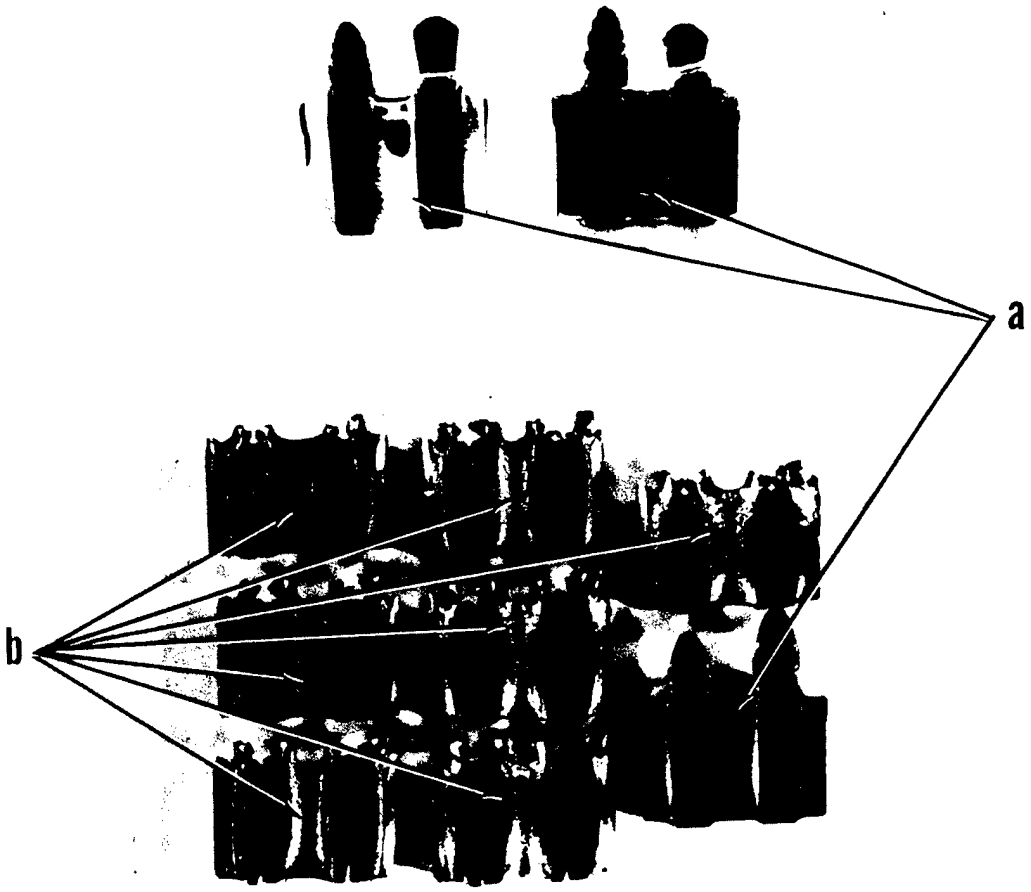

a – Simulation of the prevailing design of C.o.R.

b – Simulation of the 1st modified design of C.o.R.

ENGRAVED SIMULATING SLUGS

Fig. 7.

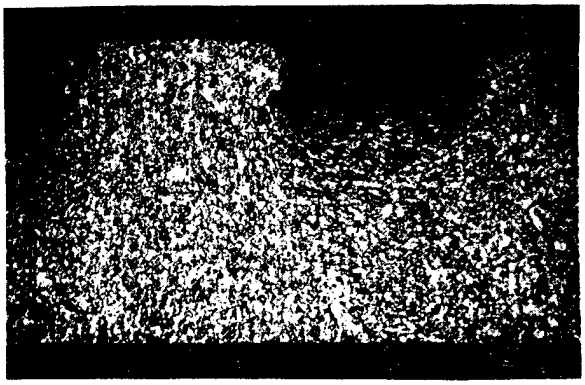

8a. SIMULATING CONVENTIONAL C.o.R.

8b. SIMULATING MODIFIED C.o.R.

TRANSVERSE SECTIONS THROUGH ENGRAVED SLUGS

Fig. 8.
Reduced to 75 Percent of a 7X Magnification.

a. In both cases swelling of the slug took place, although to a significantly lesser extent in the modified design. This is attributed to elastic tension in the bolts that hold the engraving plate onto the base block (of the simulator). In both cases, this tensile strain (in the bolts) is believed to result from the vertical component of the engraving force acting on the engraving plate (and transmitted to the bolts). And indeed, the engraving forces with the simulated modified design are significantly lower than those applied with the simulated conventional engraving (Figure 11).

b. In simulating the conventional design (of commencement-of-rifling) the groove's material was pushed backward by the engraver's lands and the land section (of the slug) remained almost intact. (See Figures 9a and b). This is evidenced by the narrow strips of deformed material at the groove's edges, while the rest of the (slugs') land remains unaffected by the deformation. In the slugs that were engraved through the modified design, however, a larger volume of material was deformed. (A larger 'h' in Backhoffen's equation for redundant work, hence less of the latter.) More significantly, the engraved land shows a buildup of material from the grooves being moved, which is the intent of the modified design. That indeed, this is the mode of deformation during engraving through the modified design, is evidenced from the following:

1. Very little material was pushed backwards (see Figure 7b), compared with slugs simulating conventional engraving (see Figure 7a).

2. The total height of the slug at its land is significantly larger than its undeformed thickness (see Figure 6 and Table I). At the same time, the slug's thickness at the grooves is comparable with the one to be anticipated from the engraver's lands' penetration of only .042 inch (out of a final anticipated lands' height of .070 inch). A correction for a slug swelling of .003 inch to .0188 inch should be considered.

3. The flow pattern, as evidenced through grains distortion in Figures 10, 12, and 13, confirms the above points 1 and 2; a thicker layer than the one observed

in slugs simulating conventional engraving has been deformed under the groove. Moreover, it is clear from Figures 10b and 13b that this material flows towards the slug lands. The microstructures in Figures 13a and 13b clearly demonstrate this difference in deformation (metal-flow) patterns. Figures 9c and 9d confirm that indeed the grains in the slug's land are deformed and together with Figure 13b show that they are indeed part of a continual flow from the material under the slug's grooves. Figures 9a and 9b, on the other hand, suggest that no such flow took place in the engraving that simulates the conventional commencement-of-rifling. Figure 9d also suggests, however, that there is less deformation at the center of the slug's land than at the lands edge. This will explain the failure to completely fill the grooves (Figure 8b).

9a. LAND SECT. - SIMULATING CONV. C.o.R.

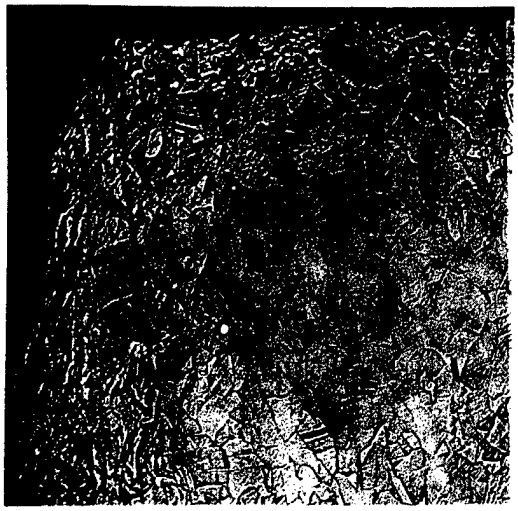

9b. LAND SECT. - SIMULATING CONV. C.o.R.

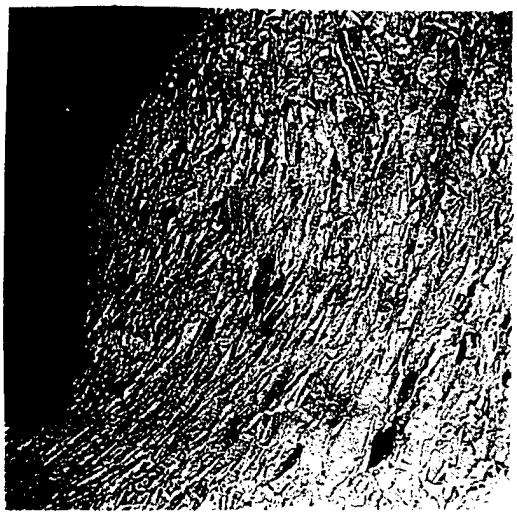

9c. GROOVE & LAND - SIMULATING MODIFIED C.o.R.

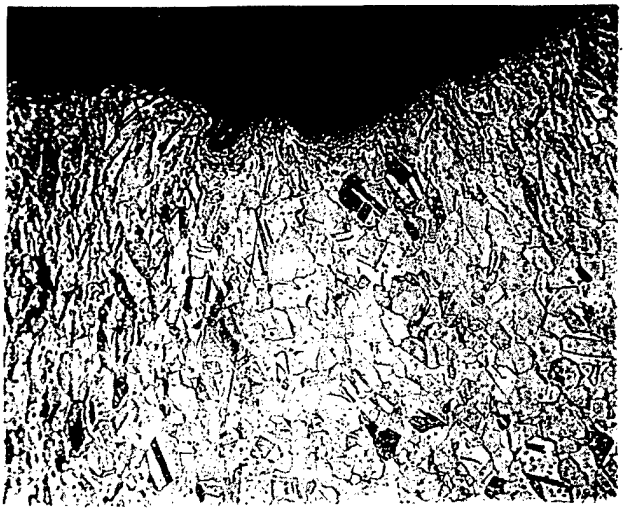

9d. LAND SECTION - SIMULATING MODIFIED C.o.R.

TRANSVERSE SECTIONS THROUGH ENGRAVED SLUGS

37.5 X

Fig. 9.

Reduced from 50X Magnification.

The failure to completely fill the engravers grooves with the modified design led to a second modification in the design of the commencement-of-rifling. The improvement in deformation flow pattern with the latest modification and the effects of other possible factors, are presently being studied.

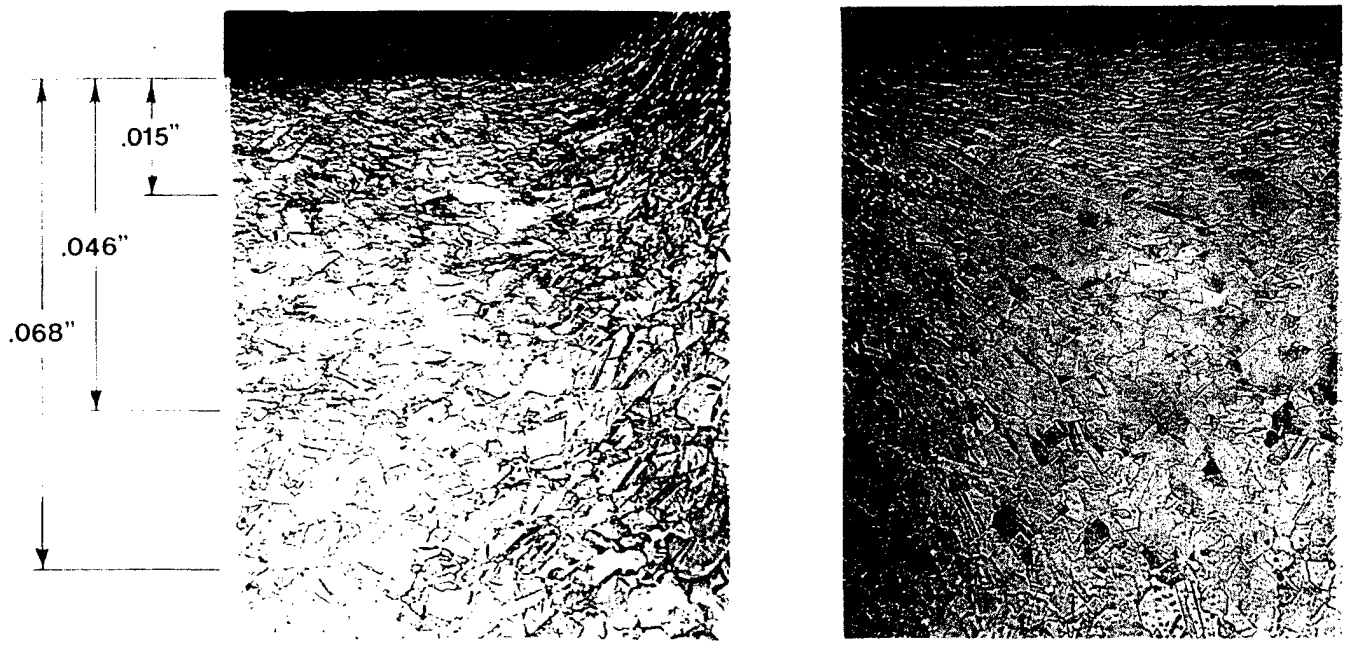

10a. SIMULATING CONVENTIONAL C.o.R.

10b. SIMULATING MODIFIED C.o.R.

TRANSVERSE SECTIONS THROUGH ENGRAVED SLUG GROOVES
37.5 X

Fig. 10.

Figure 11 represents characteristic plots of engraving force vs. slugs displacement (through the engraving plate). These graphs suggest a significant reduction in engraving force with the modified design, compared with the conventional design. A slight improvement over that of the first modification is also suggested for the second modification. However, other factors, not yet identified, might contribute to these differences. On the other hand, one should bear in mind that for reasons of expediency and economics, the engraving plates made in accordance with both of the modified designs are rough in the direction of the anticipated metal-flow, while the engraving plate that simulates the conventional design has a high degree of smoothness, particularly in the flow direction. Thus, in a smoother engraver, further lowering of engraving forces is to be anticipated for engraving with the modified design. In addition, in order to compensate for the unknown swelling of the engraving space due to transverse elastic strain in the bolts that hold the engraving plate, the undeformed slugs have been thickened. This led to a high pre-engraving friction or even shaving, which distorts the pre-engraving share of energy consumption. Once the amount of prefiring interference is determined (in actual gun tube), these forces will be replaced by those required for a slight extrusion through the forcing cone (or be eliminated all together).

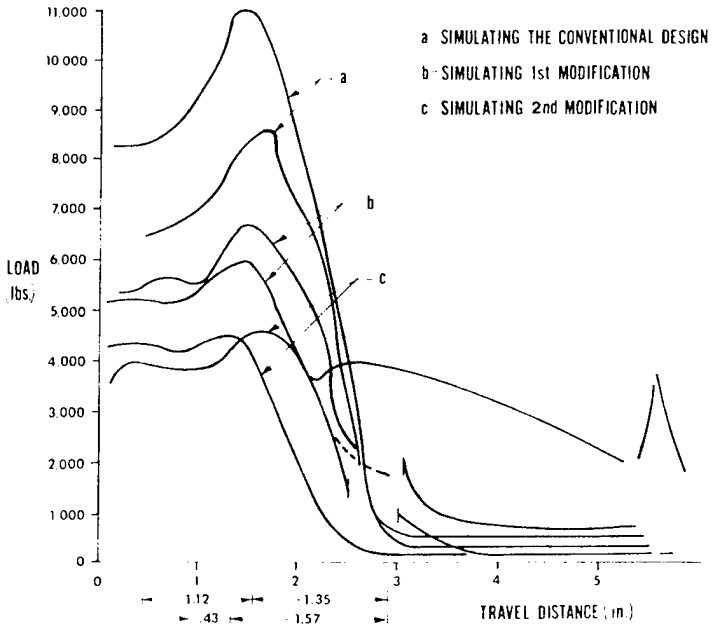

ENGRAVING FORCE AS TRAVEL DISTANCE
(of the slug, through the engraving plate)

Fig. 11.

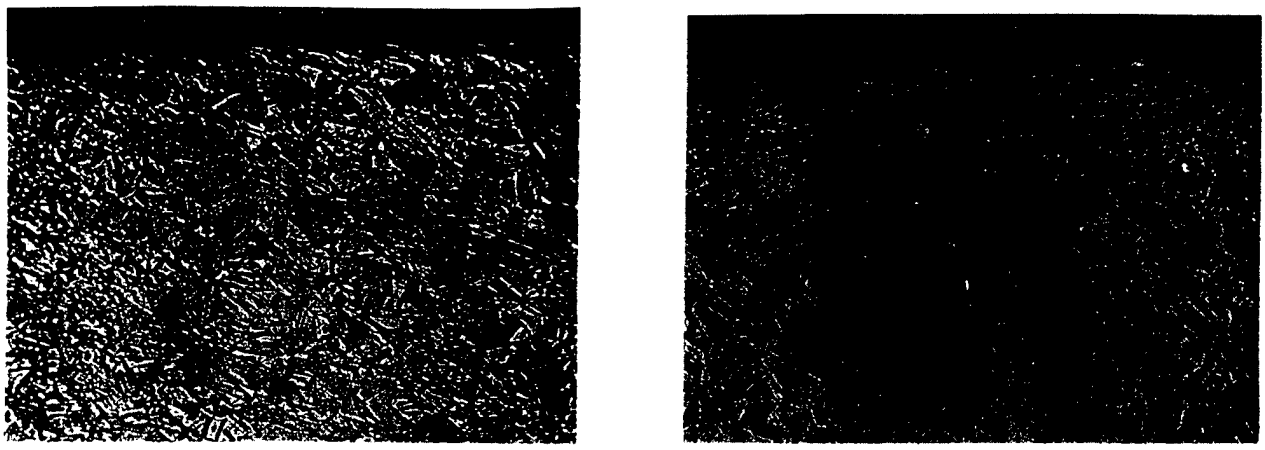

12a. SIMULATING CONVENTIONAL C.o.R.

12b. SIMULATING MODIFIED C.o.R.

LONGITUDINAL SECTIONS THROUGH ENGRAVED SLUG GROOVES

Fig. 12.

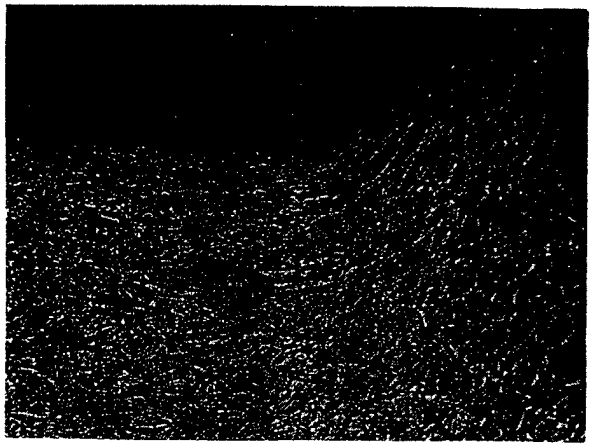

13a. SIMULATING CONVENTIONAL C.o.R.

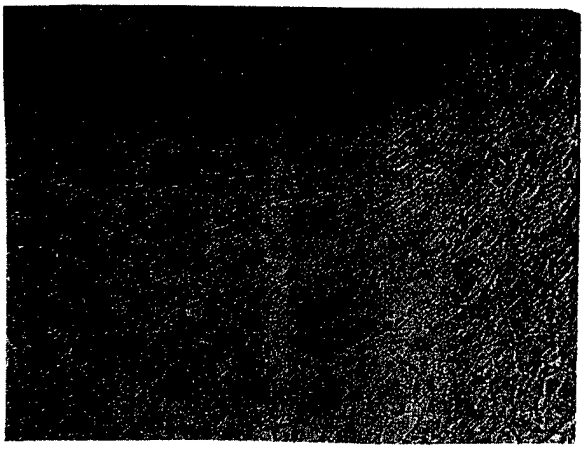

13b. SIMULATING MODIFIED C.o.R.

TRANSVERSE SECTIONS THROUGH TO ENGRAVED SLUG GROOVES
37.5 X

Fig. 13.

CONCLUSIONS

This study was based on the assumptions that:

1. Conventional commencement-of-rifling forces the displaced metal backwards during engraving.

2. Associated with such a mode of deformation, there is a lot of redundant work involved and as a result, higher forces are required during engraving. This means that a larger amount of energy is being consumed by the process. This excess energy can be better used for propelling the projectile.

3. The mode of deformation associated with larger redundant work and larger engraving forces will also result in higher wear.

This study was aimed at testing these assumptions, and set to modify the design of commencement-of-rifling in a way that will replace the above mode of deformation by one where metal-flow will be transverse to the slug/rotating bands motion. Moreover, with the transverse metal-flow, larger volumes of material will participate in the deformation, being displaced shorter distances and with less redundant work and an overall lower engraving force and less energy consumption.

Assumptions 1 and 2 have been verified and two successive modifications of the design of the commencement-of-rifling were tested. These modified designs resulted in a transverse metal-flow at a reduced engraving force as they were set-up to do. Factors affecting the total engraving force other than the mode of deformation were not fully identified yet, and their effect was not separated from the total force requirement. Also, the transverse metal-flow obtained so far failed to fully fill up the engravers grooves as desired. Further studies are planned to identify and separate these other factors and to improve the transverse flow of the material.

ACKNOWLEDGEMENTS

I would like to express my appreciation for the help I received from Mrs. Theresa Brassard and Mr. Christopher Rickard in the preparation of macrographs and micrographs, to Mr. Richard Warenchak and Mr. Leo Szymanski's help in simulating the engravings, to Dr. Fritz Sautter for his moral support and encouragement in undertaking this assignment and to Dr. Paul Cote for coediting the manuscript.

REFERENCES

1. Avitzur, B., Metal Forming: Processes and Analysis, McGraw-Hill, 1968.

2. Thomsen, E. G., Yang, C. T., and Kobayashi, S., Mechanics of Plastic Deformation in Metal Processing, The MacMillan Co., NY, 1965.

3. Rottenberg, M. M. and Bowers, J. M., "Rotating Band for High Velocity Thin Walled 30 mm Projectiles," Air Force Armament Laboratory Technical Report, AFATL-TR-79-73, August 1979.

THE SLIDING BEHAVIORS OF COPPER ALLOYS

R. S. Montgomery
U.S. Army Armament Research and Development Command
Large Caliber Weapon Systems Laboratory
Benet Weapons Laboratory
Watervliet, NY 12189

ABSTRACT

Several copper alloys were rubbed against steel, chromium electroplate, and tantalum at sliding speeds of 1.7 meters per second without lubricants. The friction, wear, metal transfer, and scuffing tendencies were observed with a view to correlating these with the properties of the alloys.

Except for aluminum bronze and the welded overlay rotating band materials, harder alloys showed less wear. Metal transfer, scuffing (rough deposits), and friction were not found to correlate with any property. Attempt was then made to attribute behavior to special microstructure, crystal orientation, mutual solubility, and position in the periodic table but no trend was found.

Heavy transfer was not usually associated with high wear and rough deposits were not usually associated with either.

INTRODUCTION

Metal surfaces sometimes scuff and adhere to each other during sliding. It is believed that much of the severe wear sometimes shown by projectile rotating bands is caused by scuffing of their surfaces during engraving and initial travel before a lubricating molten film has been formed. The purpose of this research was to develop a basis for prediction of scuffing of copper alloys and hopefully of other metals.

Mutual solubility has been considered the most important factor in the metal transfer or seizure of metals. Goodzeit[1] stated that scuffing of two metals was principally determined by their alloying characteristics (mutual solubility). He pointed out that, surprisingly, some miscible pairs have fair resistance to seizure and some immiscible pairs have poor resistance to seizure. Ernst and Merchant[2] suggested that mutual solubility should be a factor in friction and wear - the best metal pairs being those that are immiscible. Roach et al[3] stated that while mutual solubility of pin and disk metals is necessary to avoid seizure, another factor measured by the metal's position in the periodic table is also required.

Approved for public release; distribution unlimited.

Wear often correlates with hardness although it has been overemphasized as a wear preventive property. Yet, Erickson[4] found no consistent influence of hardness or indeed of any bulk property on wear behavior. It has also been stated that friction is inversely proportional to hardness.[5-9] However, Moore and Tegart[10] found that while the coefficient of friction of a hard material sliding on the softer beryllium copper was markedly dependent on the hardness of the beryllium copper, it was very erratic and there was no such relationship when the slider was softer than the plate.

The behaviors of copper alloys in dry sliding on steel, while pertinent to the study of the sliding of projectile rotating bands on cannon bores, were expected to be irregular. Rabinowicz and Tabor[11] reported that copper sliding on mild steel resulted in over three times the metal transfer as did steel sliding on copper. On the other hand, Goodzeit[1] reported that copper on steel usually runs fair (i.e. the pair fails at high load in the test machine) but when the geometry was reversed and the hard metal slid on the softer one, the pair performed poorly. In addition, Roach et al[3] reported that copper sliding on a steel disk marginally lubricated with kerosene exhibited erratic behavior. Anderson[6] reported that there was no correlation between the median coefficient of adhesion and hardness for copper and attributed this to work hardening. Semenov[12] states that the influence of chemical composition on seizure is known to be considerable in the case of copper alloys. Merchant[13] reported that there was no scoring between the copper-iron pair in his tests. He also pointed out that copper and iron are quite mutually insoluble at room temperature, but that their solubility becomes very considerable at temperatures such as those occurring at contact points of sliding surfaces. However, molten copper has been reported not to wet iron.[14]

There is not much information about copper sliding on either chromium or tantalum, but Goodzeit[1] reported that a chromium slider performed fairly well when run against a copper disk, but a tantalum slider had poor resistance to seizure. Copper is immiscible with chromium and with tantalum.

EXPERIMENTAL METHOD

The present study was carried out using a "pin-on-disk" friction and wear machine. The coefficient of friction was determined from instantaneous measurements of load and friction forces. Wear was determined by measurements of changes in length of the test pin, and amount and character of metal transferred from the pin to the rotating disk were estimated by visual observation.

The design of the test machine was fairly typical. Differences between it and usual pin-on-disk machines are related to the extremely soft and rapid-wearing pin materials. The pin which is continually loaded is held out of contact with the disk supported by means of a rotating cam and sear arrangement. When the sear is triggered, the pin is let down a very short distance into contact with the rotating disk and then quickly picked up again by the rotating cam. The sear then reengages thereby preventing the pin from again contacting the disk.

The disk was 305 mm (12 inches) in diameter. It was made from AISI 4340 steel which approximates the composition of conventional gun steel. Plates of tantalum and chromium electroplated steel fixed to the rotating steel disk were used to obtain data for pins sliding on these materials. The disk was designed to be of relatively large mass so that its rotational speed would not change during an experiment. The properties of the disk surface materials are given in Table I.

TABLE I. PROPERTIES OF THE DISK METALS

	4340 Steel	Chromium Electroplate	Tantalum
m.p. (°C)	1530°	1890°	3000°
Conductivity ($cal/cm^2/cm/sec/°C$)	0.108	0.16*	0.130
Elast. Mod. (kN/m^2)	$200x10^6$	$110x10^6$	$186x10^6$
Hardness (KHN)	235	1000	140
Ultimate Stress (kN/m^2)	744,000	103,000	758,000
Yield Stress (kN/m^2)	472,000	103,000	690,000
Elongation (%)	22	0	3

*From fused salt deposition.

The pin was plane-ended and 4.75 mm (0.187 inch) in diameter. In the work reported at this time, pins were made of OFHC copper; sintered copper; two copper alloys containing iron (0.31 and 1.20 wt. %); two dispersion hardened coppers (Glidcop AL-20 and AL-60 with 0.4 and 1.1 wt. % aluminum oxide respectively); gilding metal (90-10 copper zinc alloy); an aluminum bronze; and welded overlay band materials from recovered M483 (gilding metal), M549 (copper), and M650 (copper) projectiles. Unfortunately, the material from the band of the recovered M483 projectile was not typical and was not within specifications. In the case of the welded overlay band materials, pins were machined from the bands with their axes perpendicular to those of the projectiles. In this way sliding of the pins was the same as for actual bands sliding on a cannon bore. The copper alloys containing iron were made from powders of the individual metals and were heat treated to eliminate the sintered microstructure. The compositions and properties of all the pin metals are given in Tables II and III.

The experiments described in this report were made at a sliding speed of 1.7 m/s (67 inches/sec). This corresponds to projectile velocities close to the origin-of-rifling in a cannon. Bearing pressures ranged between 55,000 kN/m^2 (8,000 psi) and 83,000 kN/m^2 (12,000 psi).

TABLE II. COMPOSITIONS AND PROPERTIES OF THE COPPER ALLOYS

	OFHC Cu	Sintered Cu	0.31% Fe Cu	1.20% Fe Cu	AL-20 Cu	AL-60 Cu	Gilding Metal
Cu (wt. %)	100.	99.82	99.44	97.92	99.6	98.9	90.0
Fe (wt. %)	0	0.012	0.313	1.197	-	-	0
Zn (wt. %)	0	0	0	0	-	-	10.0
Al_2O_3 (wt. %)	0	0	0	0	0.4	1.1	0
O_2 (wt. %)	0	0.09	-	-	-	-	-
Hardness (KHN)	88	73	70	77	174	175	85
m.p. (°C)	1083°				1082°	1082°	1021-1043°
Conductivity ($cal/cm^2/cm/sec/°C$	0.958				0.843	0.768	0.450
Mod. of Elast. (kN/m^2)	$110x10^6$	$110x10^6$	$110x10^6$		$113x10^6$	$137x10^6$	$137x10^6$
Ultimate Stress* (kN/m^2)	220-240,000				470,000	520,000	258,000
Yield Stress* (kN/m^2)	69-76,000				370,000	450,000	69,000
Elongation (%)*	45-55				19	10	45

*With no cold work.

TABLE III. COMPOSITIONS OF ROTATING BAND AND ALUMINUM BRONZE ALLOYS

	Band Mat'l from M483	Band Mat'l from M549	Band Mat'l from M650	Aluminum Bronze
Cu (wt. %)	85.25	96.74	96.77	87.22
Fe (wt. %)	1.58	1.25	2.07	2.31
Zn (wt. %)	7.46	0	0.02	0
Al (wt. %)	5.21	0	0	9.72
Sn (wt. %)	0.34	0.99	0.68	0
Hardness (KHN)	132	144	137	146

The data reported at this time are for pins sliding on smooth, fresh surfaces. They were produced by removing all traces of transferred metal by abrading with 100 grit emery cloth at speed, then polishing with 400 grit emery also at speed. The pin was matched to the disk before the first sliding experiment (i.e. there was complete contact on the bottom surface of the pin).

Measurement of wear by pin length changes was neither extremely sensitive nor precise. Sometimes there was metal transfer but the measured wear was zero (i.e. the pin length appeared unchanged).

Several experiments were routinely conducted with each metal pair. Friction data were taken from the first portion of the experiment after almost full load was reached. Typical contact times were about 100 msec. Friction data were never taken during the very short time of sliding at the end of an experiment when the pin was sliding on a previously contacted part of the disk. Wear was taken as the length of pin lost during an experiment and measured to the nearest 0.025 mm (0.001 inch).

DISCUSSION

The copper alloys used as pin materials in this research are of interest in explaining the sliding behavior of projectile rotating bands. They also are a group of metals with very similar melting points, chemical properties, and modulus of elasticity. On the other hand, their hardnesses and microstructures are very different and their ductilities quite different.

The three disk materials investigated, tantalum, AISI 4340 steel, and chromium electroplate, are of interest or potential interest as bore surfaces in cannons. Most cannon bores are of gun steel which is closely approximated by AISI 4340; in some cannons the steel bore is protected by a coating of chromium electroplate; and liners of tantalum or of tantalum alloys are being considered because of their resistance to "erosion". In addition, these three metals are very different in their chemical, physical, and mechanical properties.

METAL TRANSFER

Data from the sliding experiments are given in Tables IV and V and wear as a function of metal transfer is shown in Figure 1. There was sometimes extreme variation in the wear and transfer data. This extreme variation doubtlessly resulted from the very small sliding area and very short time of sliding.

TABLE IV. AVERAGE RESULTS FROM SLIDING EXPERIMENTS

	Cu OFHC	Cu Sintered	Cu 0.31% Fe	Cu 1.20% Fe	Cu AL-20	Cu AL-60	Gilding Metal	
$\bar{f}$	0.31 ± .03	0.39 ± .02	0.30 ± .02	0.40 ± .01	0.33 ± .01	0.33 ± .01	0.45 ± .02	
wear (mm)	0	0.02	0.06	0.04	0	0	0.01	
transfer	none to light	very slight to heavy	none to light	very slight to light	none to light	moderate to very heavy	light	Steel
rough	no	occasionally	no	no	no	occasionally	no	
$\bar{f}$	0.52 ± .05	0.36 ± .03	0.38 ± .03	0.35 ± .02	0.38 ± .02	0.39 ± .02	0.27 ± .02	
wear (mm)	0.005	0	0.03	0.005	0	0	0	
transfer	none	none	very slight to moderate	none	none to very slight	none	none	Cr Plate
rough	no	no	occasionally	no	no	no	no	
$\bar{f}$	0.33 ± .02	0.35 ± .03	0.33 ± .01	0.38 ± .03	0.31 ± .02	0.36 ± .01	0.37 ± .01	
wear (mm)	0.01	0.008	0.025	0.025	0.008	0.005	0.02	Ta
transfer	very slight to light	none to very slight	very slight to heavy	none to very slight	very slight	very slight	light to moderate	
rough	no	no	no	no	no	no	occasionally	

$\bar{f}$ = average coefficient of friction.

TABLE V. AVERAGE RESULTS FROM SLIDING EXPERIMENTS

	M483 Projectile Band Mat'l	M549 Projectile Band Mat'l	M650 Projectile Band Mat'l	Aluminum Bronze	
$\bar{f}$	0.35 ± 0.01	0.29 ± 0.03	0.40 ± 0.02	0.38 ± 0.02	Steel
wear (mm)	0.02	0.25	0.02	0.01	
transfer	v. slight to light	v. slight to moderate	moderate	v. slight to light	
rough	no	occasionally	yes	no	
$\bar{f}$	0.25 ± 0.04	0.32 ± 0.02	0.38 ± 0.03	0.32 ± 0.02	Cr Plate
wear (mm)	0.0025	0	0.0025	0.005	
transfer	none to light	none	none to light	none	
rough	no	no	no	no	
$\bar{f}$	0.40 ± 0.02	0.29 ± 0.02	0.28 ± 0.02	0.29 ± 0.03	Ta
wear (mm)	0.085	0.15	0.02	0.045	
transfer	v. slight to v. heavy	light to heavy	light to v. heavy	moderate to v. heavy	
rough	occasionally	occasionally	yes	occasionally	

$\bar{f}$ = average coefficient of friction.

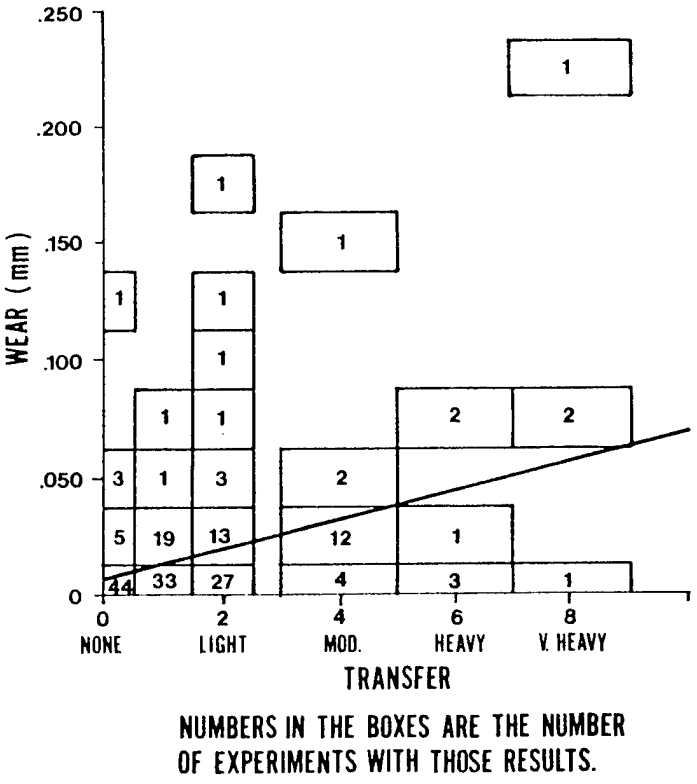

Fig. 1. Wear as a Function of Metal Transfer.

While there was a tendency for more transfer to occur at higher wear rates, heavy and very heavy transfer occurred even at zero wear.* The transferred metal was rough in a minority of the cases. If experiments with none, very slight, and light transfer were not considered, there would be no correlation between wear and metal transfer. Even rough transferred metal was not usually associated with high wear or heavy transfer.

Mutual solubility with a particular disk metal, melting point, elasticity, and chemical properties of all the copper alloys are about the same, but metal transfer was sometimes very different. Therefore, these properties could not be the controlling factor. In addition, small amounts of iron in the copper did not lead to transfer or scuffing even in sliding on steel. Even microstructure is not the important factor controlling metal transfer. The microstructures of AL-60 and AL-20 coppers are identical as are those of copper containing 0.31 percent Fe and copper containing 1.20 percent Fe, while the sliding behaviors of the former on steel and the latter on chromium electroplate were very different.

WEAR

An important observation from this study is that both metal transfer and wear of aluminum bronze and the welded overlay band materials were essentially different from the other copper alloys investigated. These alloys often scuff and sometimes transfer to the mating surfaces more and show unexpectedly high wear. Although the difference in the case of material from the band of the M483 projectile could be attributed to chemical composition, it certainly can not in the cases of the alloys from the bands of M549 and M650 projectiles. These alloys are 96.74 percent and 96.77 percent copper, respectively. It also apparently cannot be attributed to microstructure. The microstructures of the alloys behaving differently show a wide variation. Gilding metal and OFHC copper both have annealed structures of relatively small grains; copper containing 0.31 and 1.20 percent Fe have heat treated structures of large grains; AL-20 and AL-60 coppers are dispersion hardened alloys with grains so small that they cannot be resolved even at 1000X; and sintered copper has a sintered structure with a large amount of foreign material (probably oxide) at the grain boundaries. The welded overlay microstructures, too, are not all the same. The material from the bands of the M549 projectile shows the columnar grains expected in a welded structure and the materials from the bands of the M483 and the M650 projectiles have been recrystallized by heat treatment to small equiaxed grains.

X-ray diffraction studies were made on the band materials from the M483, M549, and M650 projectiles. As expected from its microstructure, the band material from the M549 projectile showed large grains and preferred crystalline orientation. However, both the other band materials showed only little crystalline orientation. Therefore, the welded overlay band materials did not all possess crystalline orientation; so this is not an explanation for their different sliding behaviors.

*Zero wear in this report implies wear less than 0.025 mm, the limit of the experimental measurement.

Excluding the data on aluminum bronze and the welded overlay band materials, there was a correlation of wear with hardness. The effect of hardness, however, was different for the different mating surfaces. The data is plotted in Figure 2. There was always wear for all alloys sliding on tantalum with less wear for the harder alloys. The wears of copper alloys sliding on steel and on chromium were similar. No wear was measured if the alloys were harder than about 86 KHN. If the copper alloys were softer than this, their wear sliding on steel was about double that obtained sliding on chromium. The wear data for aluminum bronze and the welded overlay band materials, all of which had hardnesses of about 140 KHN, did not fit this correlation. With the exception of hardness, no other property of the copper alloys could be correlated with wear.

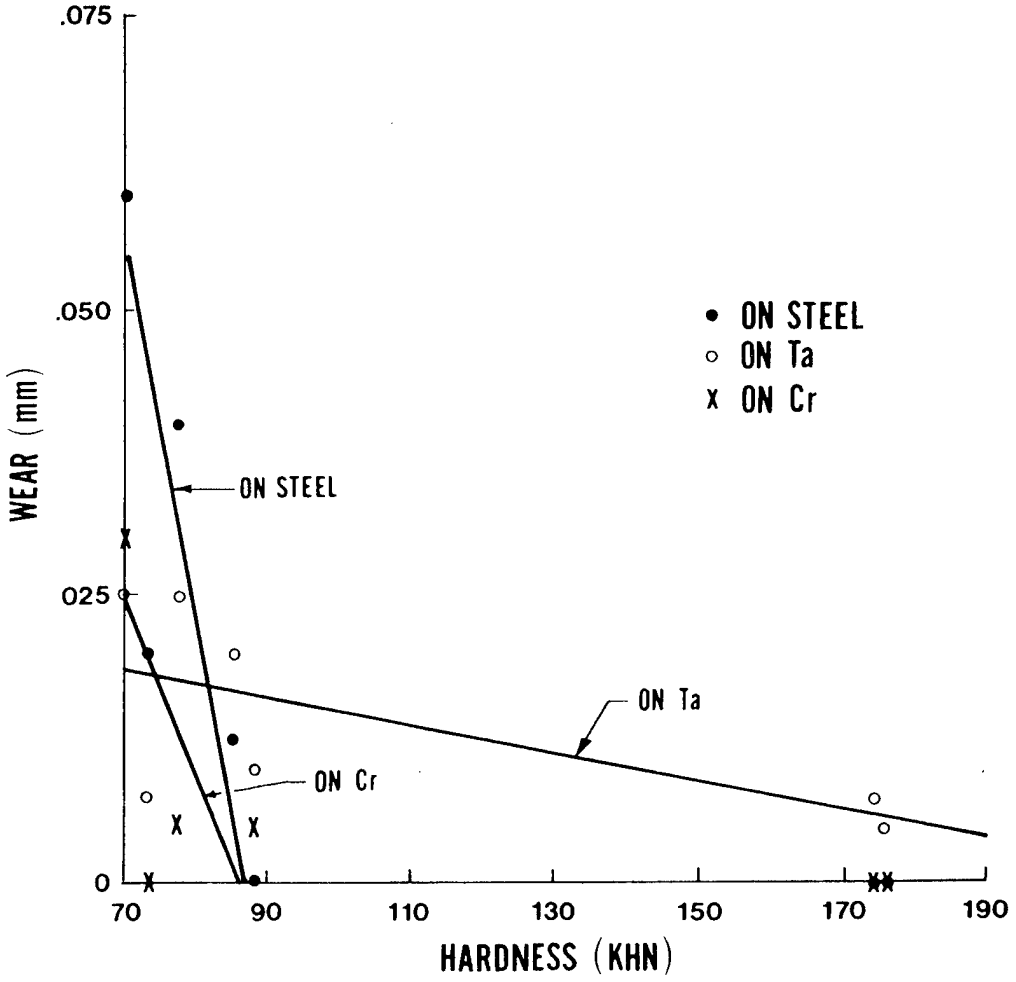

Fig. 2. Effect of Hardness on Wear for Similar Copper Alloys.

FRICTION

The coefficients of friction measured in these experiments could not be correlated with any bulk property. However, since the hardness of the slider was always considerably less than that of the plate (except in the cases of some of the alloys sliding on tantalum), a correlation hardness would not be expected on the basis of the work of Moore and Tegart[10] or Montgomery.[15]

The correlation of friction with adhesion between the surfaces could not be tested because adhesion was not measured. However, such a correlation seems unlikely because of the large difference in friction of copper containing 0.31 and 1.20 percent Fe sliding on steel and OFHC and sintered copper sliding on both steel and chromium. The adhesions of these alloys would be expected to be quite similar.

Although the effect of load on the coefficients of friction was not investigated in more than a few cases, some examples are plotted in Figure 3. The coefficients of friction were high at low loads and decreased asymptotically as the load increased. At loads greater than about 890 N (200 lbf) there was usually little further change with load. This was the general behavior found by McFarlane and Tabor.[16] The exact friction-load curve was different for all metal pairs investigated.

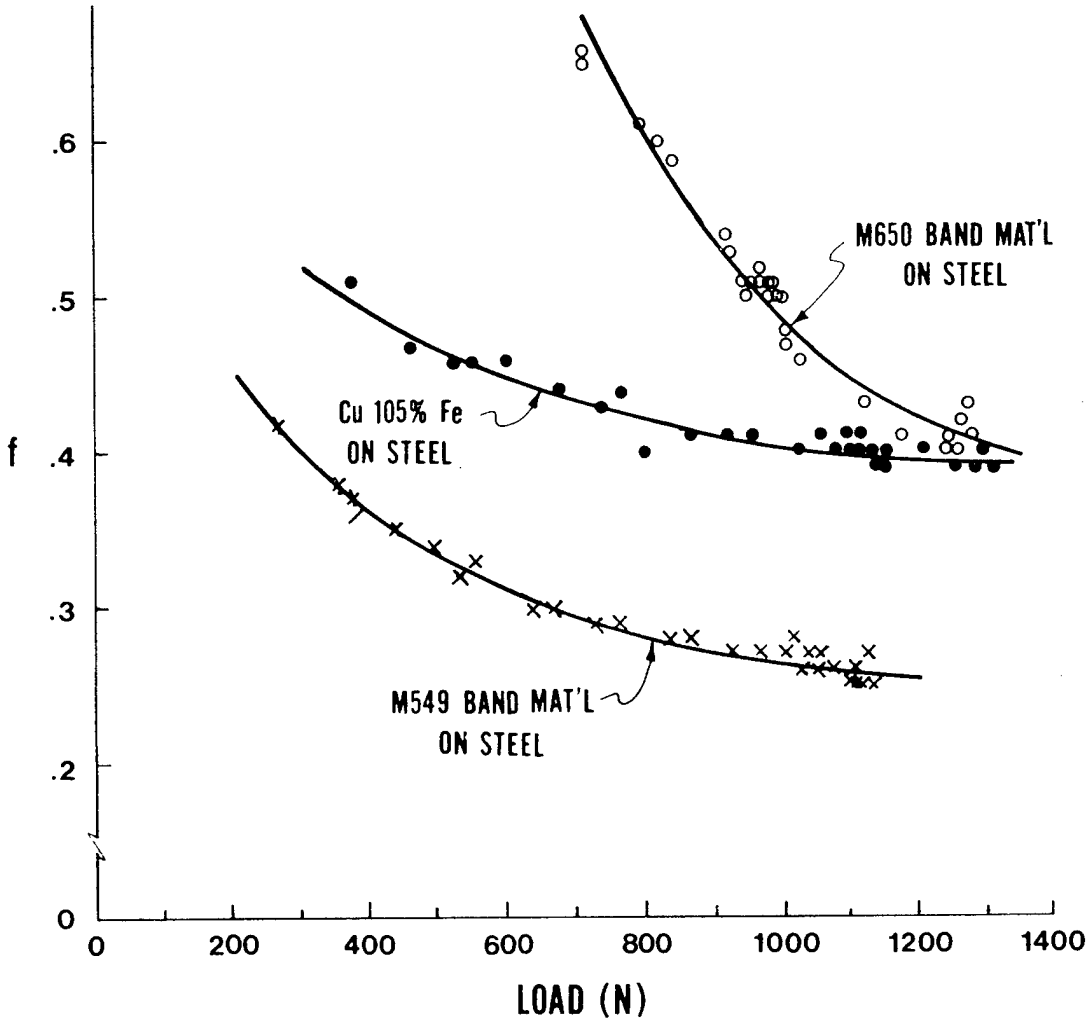

Fig. 3. Effect of Load on Coefficients of Friction.

CONCLUSIONS

1. It was not possible to correlate metal transfer, scuffing (rough deposits), wear, or friction with the properties of the metal pair except for the one exception discussed below. However, the sliding behaviors of the copper alloys were expected to be irregular perhaps because of their propensity to work harden.

2. Excluding the data on aluminum bronze and the welded band materials, there was a correlation of wear with hardness with less wear with higher hardness. The effect of hardness was different for the different mating surfaces.

3. Mutual solubility with the disk metals and position in the periodic table did not control metal transfer and scuffing with the copper alloys investigated.

4. While there was a tendency for more transfer to occur at higher wear rates, heavy and very heavy transfer did occur even at very low rates. Heavy and very heavy transfer were not usually associated with high wear, and rough deposits were not usually associated with high wear or heavy transfer.

5. Metal transfer was not the first step in the production of loose wear particles with the copper alloys because there was wear sometimes without metal transfer.

6. Wear of aluminum bronze and the welded overlay band materials investigated was essentially different from the other copper alloys investigated. These alloys often scuffed and sometimes transferred to the mating surface more and showed unexpectedly high wear when sliding on steel and tantalum. The reason for this for the welded overlay band materials was not the result of a particular microstructure or crystalline orientation.

7. Small amounts of iron in the copper alloys did not result in scuffing and high metal transfer even when sliding on steel.

ACKNOWLEDGEMENTS

Most of the experimental work was done by L. J. Szymanski and some of the initial work was done by K. J. Lansing. The metallography was done by Theresa Brassard and C. Rickard. The x-ray study was done by G. Capsimalis.

REFERENCES

1. Goodzeit, C. L., Proc. Symp. on Friction and Wear, p. 67, Elsevier Pub. Co. (1957).

2. Ernst, H. and Merchant, M. E., Special Summer Conf. on Friction and Surface Finish, M.I.T., Cambridge, MA 76 (1940).

3. Roach, A. E., Goodzeit, C. L., and Hunnicutt, R. P., Trans. ASME 78, 1659 (1959).

4. Erickson, R. C., ASLE Paper 81-5A-3, presented at 1981 ASLE/ASME Lubrication Conference (1981).

5. Drozdov, Yu. N. and Archegov, V. G., Wear 69, 299 (1981).

6. Anderson, O. L., Wear 3, 253 (1960).

7. Sikorski, M. E., J. Basic Engr. 85, 279 (1963).

8. Rabinowicz, E., J. Applied Physics 32, 1440 (1961).

9. Bowden, F. P. and Tabor, D., The Friction and Lubrication of Solids, Oxford University Press (1950).

10. Moore, A. J. W. and Tegart, W. J. McG., Proc. Royal Soc. (London) A212, 452 (1952).

11. Rabinowicz, E. and Tabor, D., Proc. Royal Soc. (London) A208, 455 (1951).

12. Semenov, A., Wear 4, 1 (1961).

13. Merchant, M. E., Trans. ASME 78, 1669 (1956).

14. Olsen, L. O., Smith, C. S. and Critenden, E. C., Jr., J. Applied Physics 16, 425 (1945).

15. Montgomery, R. S., Wear 15, 373 (1970).

16. McFarlane, J. S. and Tabor, D., Proc. Royal Soc. (London) A202, 244 (1950).

INTERFACE CONSIDERATIONS IN MEDIUM AND MAJOR CALIBER GUNS

J. S. O'BRASKY

NAVAL SURFACE WEAPONS CENTER

DAHLGREN, VIRGINIA

ABSTRACT

A review of the interface considerations in the design of medium and major caliber gun systems is presented. The interface considerations under consideration include:

1. The design of the chamber-projectile interface to enable ramming.

2. The rotating band-forcing cone interface to ensure sticking and a reproducible seating position.

3. The rotating band-rifling interface and its effects on condemnation criteria.

4. The seating chracteristics of extensively worn guns.

The propelling charge ignition and combustion phenomena have significanat interface implications which have been treated elsewhere at great length. Therefore, these phenomena are not treated in this paper. Also, down bore travel/projectile interfaces, although important for projectile flight and fuze performance, are not treated herein.

INTRODUCTION

Gun tube-projectile interface design is one of those arcane disciplines which is rarely the subject of mathematical analysis. The usual procedure associated with rotating band, chamber, and rifling design has been to draw on the accumulated experience for the preliminary design and to work out difficulties in the evaluation of prototypes. During the first four decades of this century, this approach was reasonably efficient. In that period, new guns and projectiles were continuously in development and the design establishments were staffed by long term employees. As a result, interface design became highly evolutionary. At least one establishment published a fairly detailed account of this evolution to preserve the knowledge so painfully won, Reference 1. In recent years, the number of new gun and projectile developments has become much smaller. As a result, each new project seems to start with a new and inexperienced design team which constitutes a diminishing fraction of the development effort. Although these teams have the benefit of modern, highly sophisticated models, the evolutionary chain has usually been broken. One of the more unfortunate circumstances of engineering science is that few engineers bother to master the history of their own specialties; particularly if the literature is not in the easily available forms, e.g., textbooks and journal papers. This paper is presented in the hope that some of the researchers attending this conference may come to appreciate certain of the more obscure interface issues and understand how their work might impact upon them.

THE CHAMBER-PROJECTILE INTERFACE

The chamber of a gun serves two primary functions. The chamber contains the propellilng charge during the loading and firing sequence and provides one of the breech end obturating surfaces. The second function of the chamber is to serve as a cam surface which allows the projectile to be delivered to the seated position in a smooth and centered manner. This secondary function is of prime interest in this paper.

Three basic ramming schemes are in common use:

1. Constant contact ramming,
2. Catapult ramming, and
3. Flick ramming.

In constant contact ramming, a chain rammer or human hand delivers each single component to its desired location. Classic examples of this technique are the hand rammed tank gun ammunition and the separate loading power rammed procedures of major caliber naval guns and self-propelled artillery pieces.

Catapult ramming is the classic method used in separated cased naval guns. In this procedure, a projectile and separate cartridge case are rammed as a unit. The rammer spade is in contact with the cartridge case base until the breech-face is reached. The projectile continues under its own momentum to the seated positions.

Flick ramming is one of the more popular schemes for use in stroke limited situations such as automated self-propelled guns. In this case, the projectile is accelerated to full ram velocity in a very short stroke and then flies across an air gap into the chamber. Although this procedure can be useful in loading propelling charges, it is rarely used for this purpose.

Each of these techniques imposes different constraints on the gun chamber design. These differences will be examined below.

The best illustration of the sophistication which can be built into the chamber-cam profile is contained in the 16"/50 MK 7 Mod 0 gun design. This weapon has a choke at the breech end. The choke was used to reduce force level on the breech block by presenting the smallest reasonable breech opening. The projectile is rammed across the spanning tray through the choke. As the projectile center of gravity extends beyond the choke, the projectile tips into the chamber, Figure 1. The rammer head is still at the choke level. Note that the tip angle must be small enough so that the windshield is not damaged and the projectile base does not bind on the choke. The projectile base then slides down the choke face until the projectile rests on the high lip of the rotating band and the forward bourrelette. Note that the point of contact of the rammer head is slightly above the projectile centerline. As the projectile slides forward the rammer head crawls down the choke face and re-establishes itself in contact with the projectile base, Figure 2. The ogive now picks up the centering slope. The projectile nose is cammed up. Note that the height and location of the rotating band high lip limits the maximum nose excursion. As the projectile center of gravity passes the forward edge of the centering slope, the projectile tips aligning itself with the bore. At this point the rammer head point of contact has again changed. It is important that the centering slope be sufficiently shallow and the rammer head be sufficiently high so that the rammer cannot jam the projectile. At this point, the projectile is delivered centered to the forcing cone, i.e., the seated position. It should be noted that the projectile is the follower operating on the cam profile provided by the chamber. The dynamics of ramming are functions of the geometry, projectile mass properties, point of application of the ramming force, and velocity of ram. It is entirely possible in a poorly designed system for the "follower" to leave the "cam" and ballot against the upper chamber wall. This action can cause jamming or a loss in ram velocity. The projectile is delivered to the forcing cone at a velocity of seven to twelve feet per second. Seven feet per second is usually considered the sticking threshold .

In catapult ramming of semi-fixed ammunition, the projectile and cased propelling charge are rammed as a unit. The camming action is similar to that observed in constant contact ramming. In this case, the projectile point of contact with the cartridge case closure plug does change somewhat. The cartridge case is stopped by its flange's impact on the chamber. The projectile continues to run under its own momentum until the rotating band encounters a seating slope. The free run distance varies from one inch to twenty inches depending on weapon caliber and erosion state. In this ramming mode, sufficient energy must be supplied to ensure the projectile seats in the most worn gun condition when the weapon is at maximum loading elevation. In the 5"/54 MK 42 gun mount, this elevation angle is 85°. Typical catapult ram velocities vary over a range of seven to forty-five feet/second depending on system rate of fire requirement.

Flick ramming is the most difficult scheme to make reliable. In this concept, a projectile is given enough energy in the rammer to transit an air space outside the breech, slide through the chamber and arrive at the seated position with enough velocity remaining to stick in the forcing cone. For some systems, this process must be achieved at any load angle between 0° and 70°. The obvious first prerequisite for a successful flick rammmer is to reliably release any projectile the gun system may use from the rammer at a consistent velocity and in an attitude maintained within strict yaw limits. The chamber profile should be quite gentle and the rotating band should have a high lip to assist in centering a projectile which may be balloting badly. If the system is an any load angle design, the ram velocity is usually established by the high angle energy requirement. This situation can result in "follower" separation in a chamber with rapid slope changes. In the flick rammer scheme, the projectile is in free flight except when it contacts the chamber wall.

The specific point of this discussion of elementary chamber-projectile kinematics in an erosion symposium is that certain chamber and rotating band characteristics which may not be desirable from an erosion or ignition phenomena point of view may be dictated by the kinematics of this interface. Typical parameters of interest are the rotating band high lip diameter and location, multi-taper chambers, and chamber surface finishes and protective coatings.

THE ROTATING BAND-FORCING CONE INTERFACE

A second interface of significant interest is the interface between the rotating band and the forcing cone. This interface controls the seating position, sticking, and seating consistency.

Over the years, the general trend in forcing cone design has been toward a single shallow cone with one to three degree slope. Figure 3 illustrates this trend. The single deviation from this trend was the Piobertized forcing cone which was based on the theory that "what is not there, cannot erode". In fact, experience indicates that the complicated forcing cone always eroded into a conical form anyway. The single major erosion phenomena encountered in the forcing cone region is the gas wash pocket, Figure 4. Current naval practice calls for gun tube condemnation if these pockets exceed 10% of the wall thickness, Reference 2. The causes of gas wash pockets are somewhat obscure. It has been observed that such pockets occur most often where a local area of surface roughness or a surface enclusion has previously been known to exist. In addition, propellant gas stagnation under the rotating band during the early stages of engraving may also be implicated.

The rotating band-forcing cone interface determines the shape of the velocity-loss curve. In Figure 5, the 5"/54 MK 19 gun barrel-MK 64 projectile rotating band interface is illustrated. Note that in a new gun the front edge of the band controls the projectile seating distance. Only when the bore-enlargement exceeds 0.100 inch does the projectile seating distance begin to change. Very rapidly, the seating control shifts to the rotating band high lip. Figure 6 is the velocity loss curve for this weapon. In Figure 7 the 5"/54 MK 19 gun barrel-MK 73 projectile interface is illustrated. The 5"/54 MK 73 projectile uses a plastic rotating band with a very high lip which seats on a part of the forcing cone which does not erode. Figure 8 contains the

5"/54 MK 73 projectile velocity loss curve. Note that muzzle velocity level is maintained even under high erosion conditions and that the velocity loss curve is decreasing linearly.

THE ROTATING BAND-RIFLING INTERFACE

The rotating band-rifling interface establishes the maximum erosion condition which can be tolerated if accuracy is the criteria. Figure 9 parameterizes the experience using both Army and Navy data. Note that rotating bands without high lips invariably lead to gun condemnation levels of $\frac{\Delta Do}{\Delta Do} = .02$. A high lip without a body of band interference leads to to condemnation at $\frac{\Delta Do}{\Delta Do} = .03$. A high lip and a body of band interference results in $.04 < \frac{\Delta Do}{\Delta Do} < .055$. The impact of this situation can be seen in Figure 10. Note that the difference beweeen a $\frac{\Delta Do}{\Delta Do} = .02$ and a 0.04 condemnation level is a 3:1 increase in gun barrel accuracy erosion life.

where: ΔD_o = change in bore diameter
ΔD_o = initial bore diameter

It should be noted that fuze reliability and allowable maximum range reduction are also erosion life condemnation criteria. These matters were covered in Reference 3.

SEATING CONDITIONS IN EXTREMELY WORN GUNS

Occasionally a gun system may have such a poor erosion performance that it becomes necessary to allow extreme erosion conditions. This situation usually arises in rapid fire, high performance guns using medium or high flame temperature propellants. In this case, the projectile seats on an eroded bore surface. As the surface erodes, the projectile seats further and further down bore. This process results in significant velocity variability because the rotating band tolerances now effect seating, Figure 11.

CONCLUSIONS

The proper design of the gun-projectile interfaces can have a significant impact on the service life of the weapon and on its ability to accept erosion conditions. These design features are rarely analyzed.

REFERENCES

1. Carl F. Jeansen' Notes on Gun Chamber, Projectile Bands and Accuracy Life of U. S. Naval Guns, (Navy Department, Bureau of Ordance, Washington, D. C.), February 1937

2. SW300-BB-GTP-010 Servicability of Naval Gun Barrels, (Naval Sea Systems Command, Washington, D. C.) Nov 1981

3. James S. O'Brasky and M. C. Shamblen, "End of Life Criteria", Proceedings of the Tri-Service Gun Tube Wear and Erosion Symposium, 29-31 March 1977

16-IN./50 GUN BARREL/PROJECTILE INTERFACE

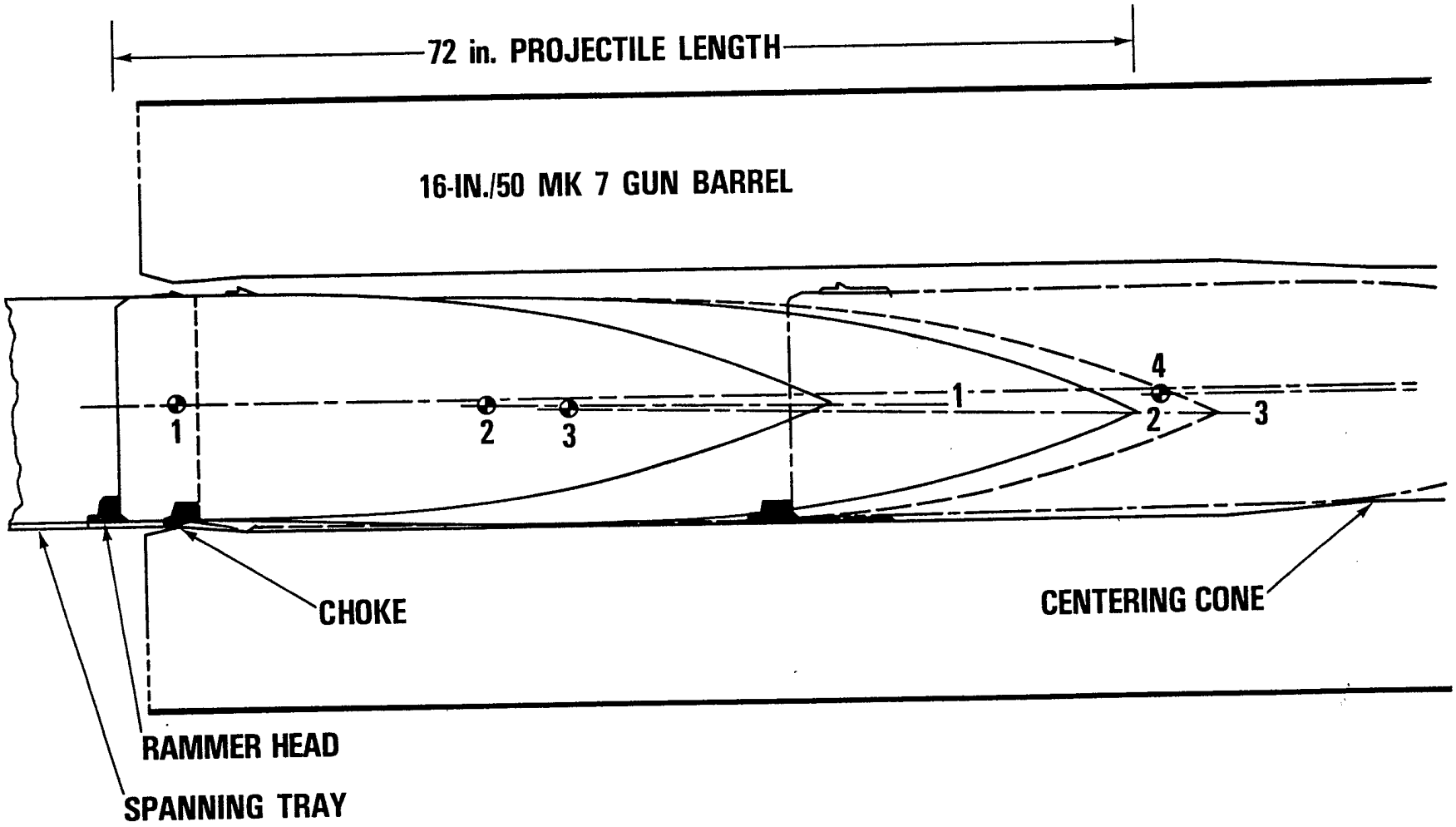

V-450

Figure 1

16-IN./50 GUN BARREL/PROJECTILE INTERFACE—SEATING

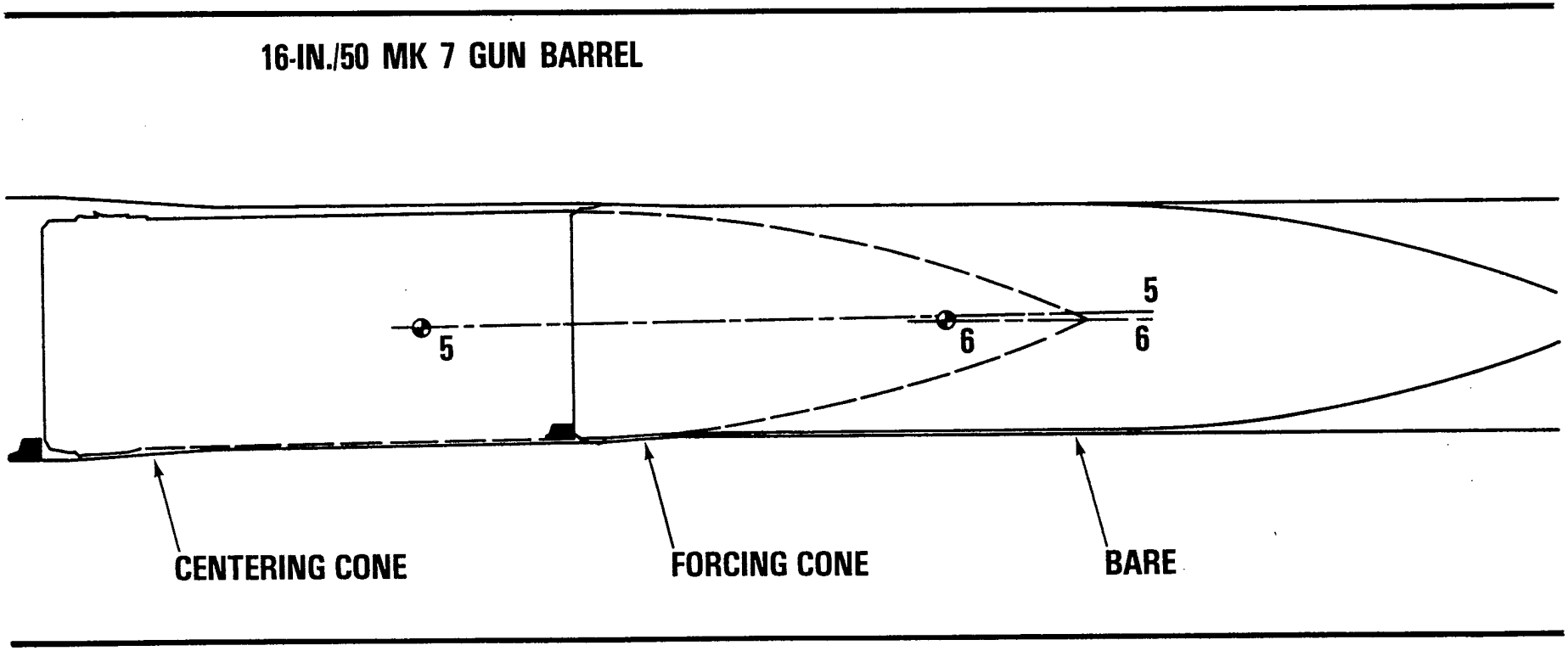

V-451

Figure 2

8-IN./45 GUN MK IV–2

DR. 36655–2 FEB. 1911

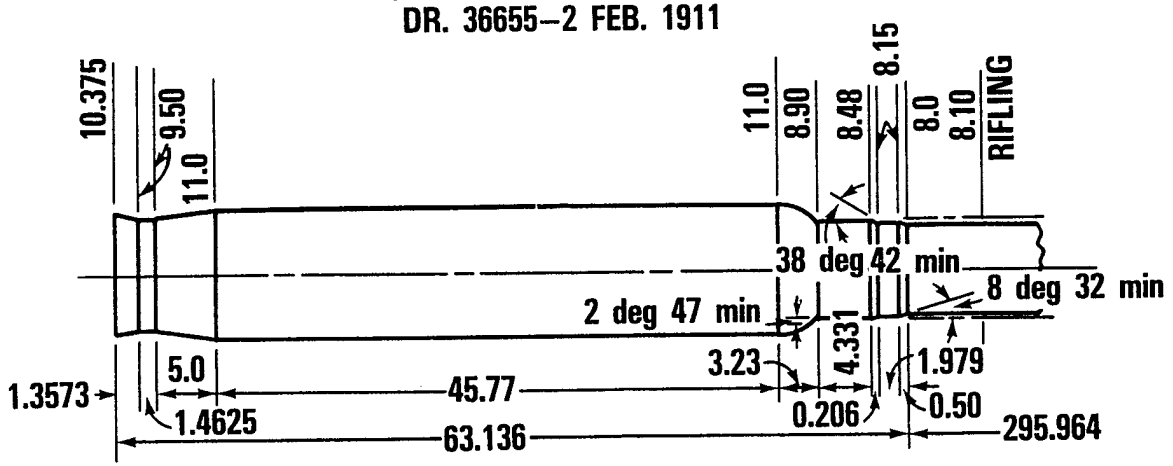

8-IN./45 GUN MK IV–3

DR. 38162–6 NOV. 1915 (REV. B)

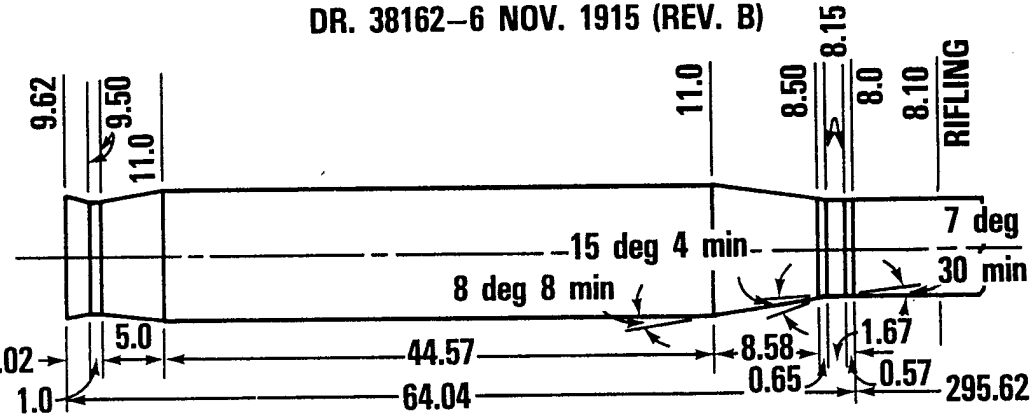

8-IN./55 GUN MK XII

DR. 150905–17 APR 30

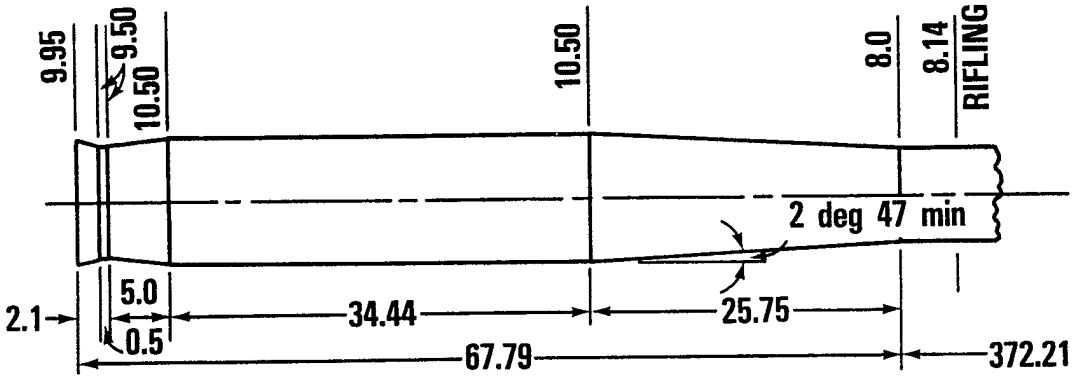

SEVERE CASE OF FLAME WASHING, HEAT CRACKS, AND HEAT CHECKS

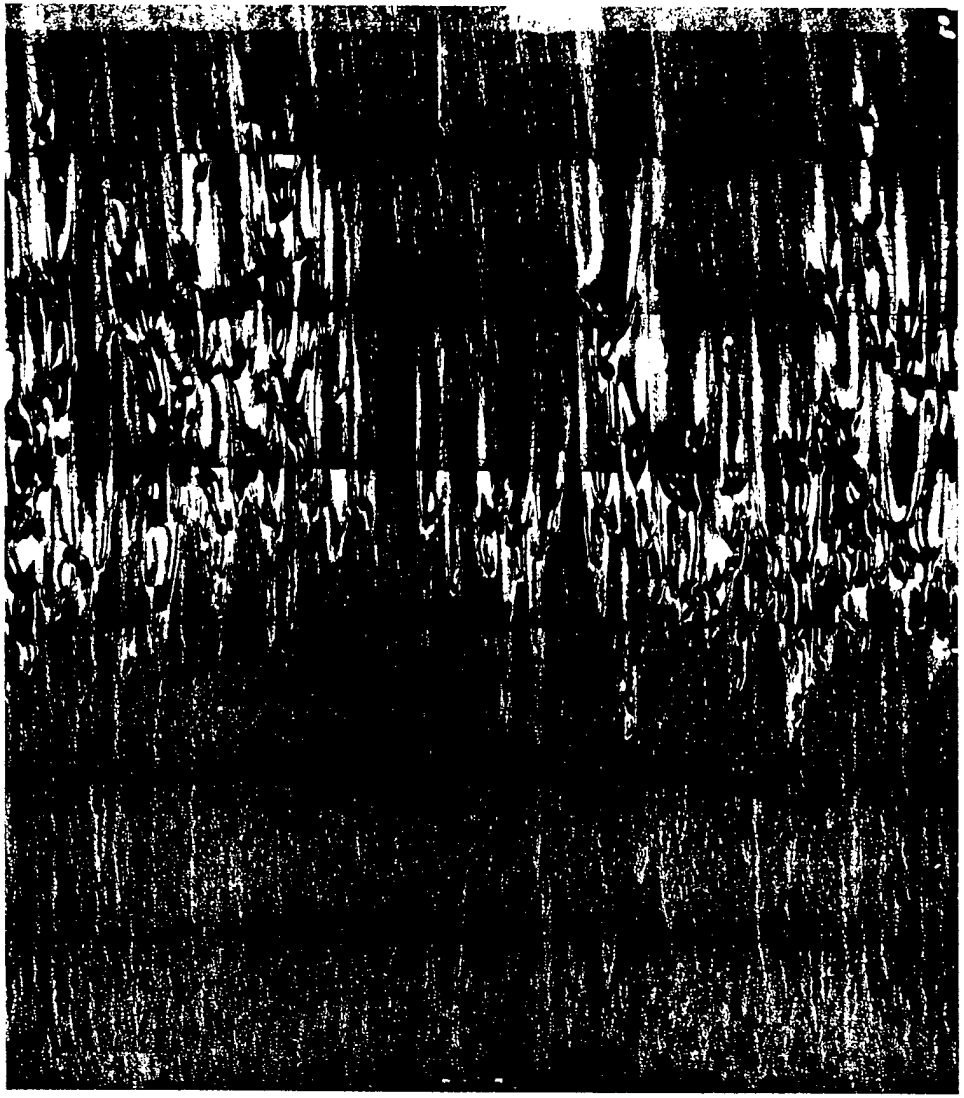

V-453

Figure 4

5-IN./54 MK 41 PROJECTILE SEATED IN NEW GUN

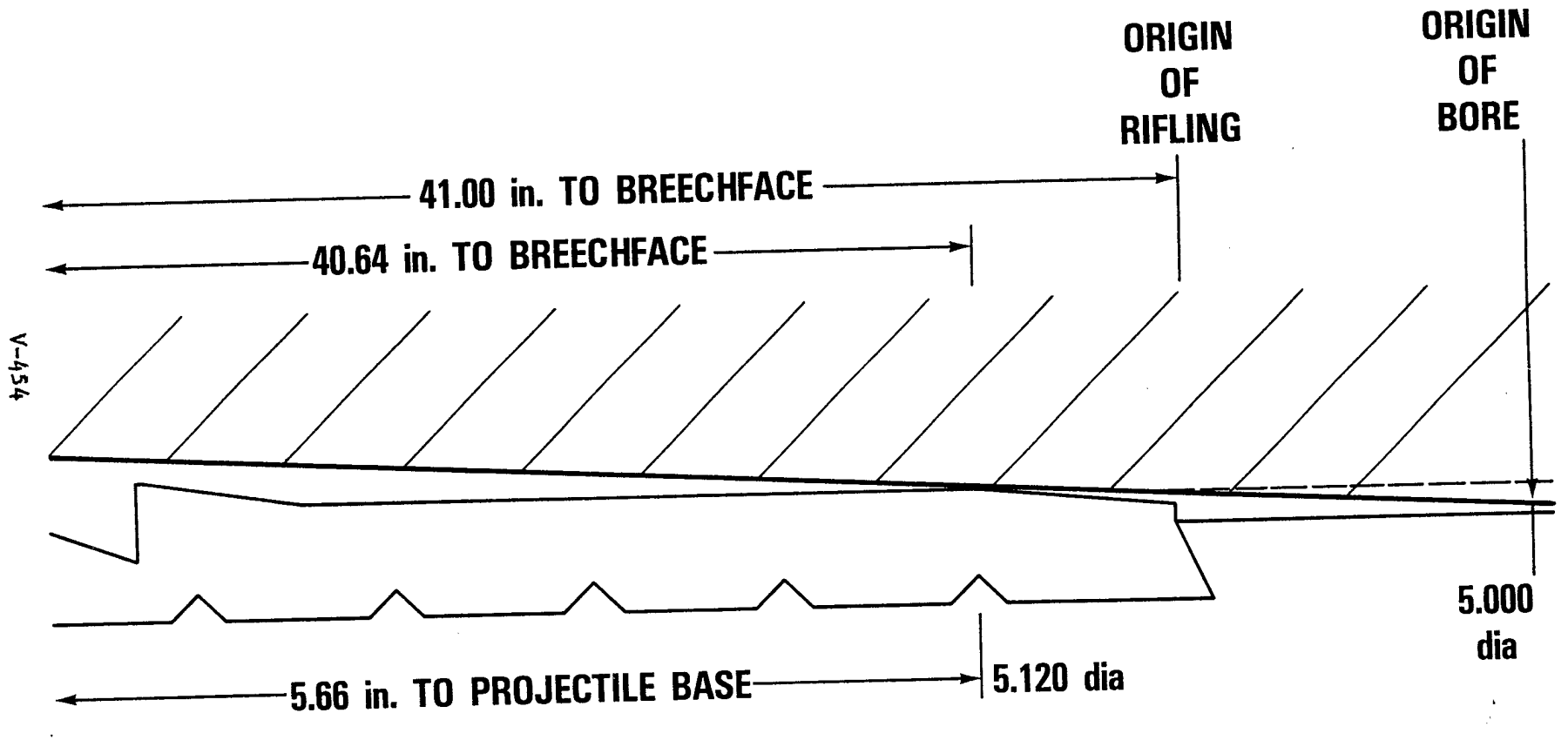

Figure 5

5-IN./54 VELOCITY LOSS CURVE MK 19 GUN BARREL MK 64 PROJECTILE

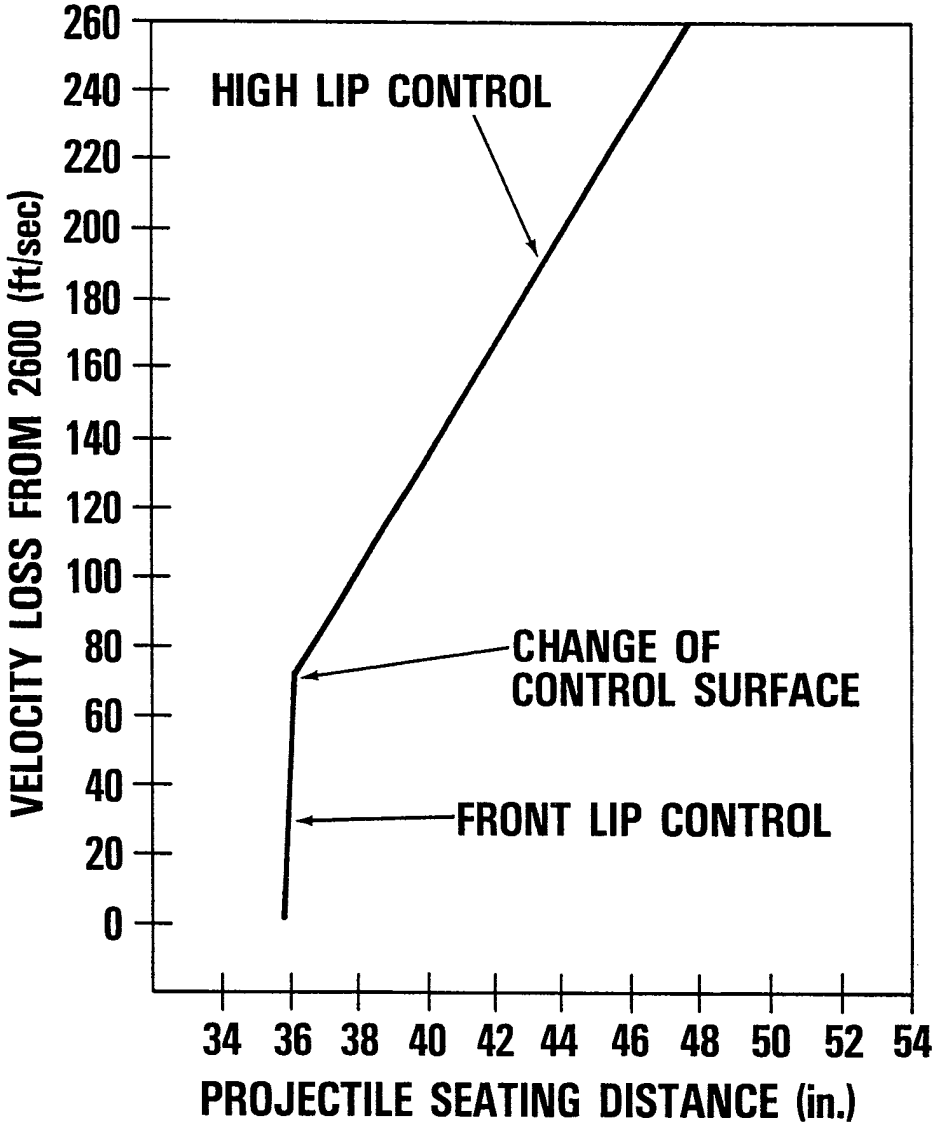

Figure 6

5-IN./54 MK 19 GUN BARREL/MK 73 PROJECTILE INTERFACE

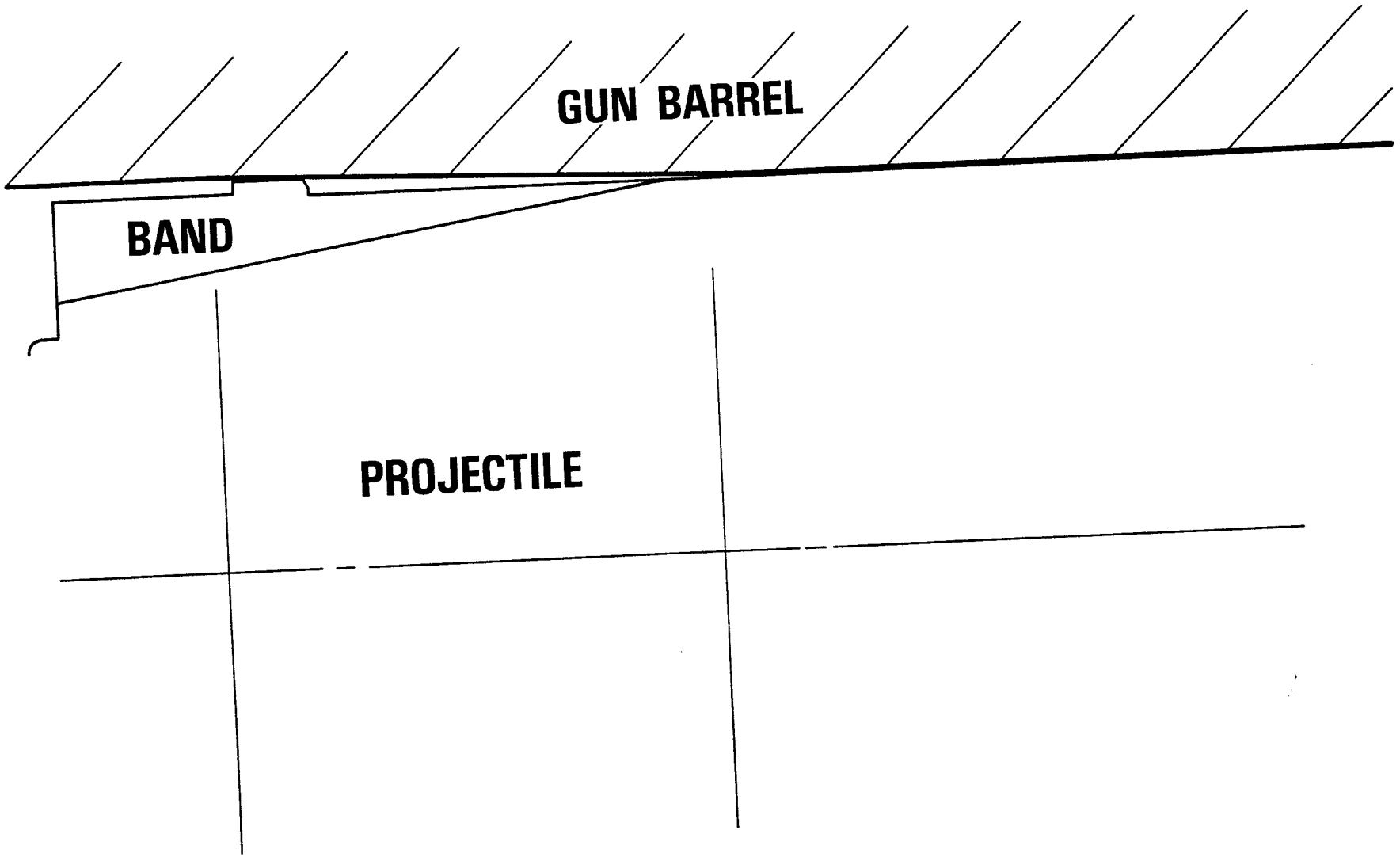

V-456

Figure 7

VELOCITY LOSS CURVE 5-IN./54 MK 19 GUN BARREL MK 84 PROJECTILE, SUPER CHARGE

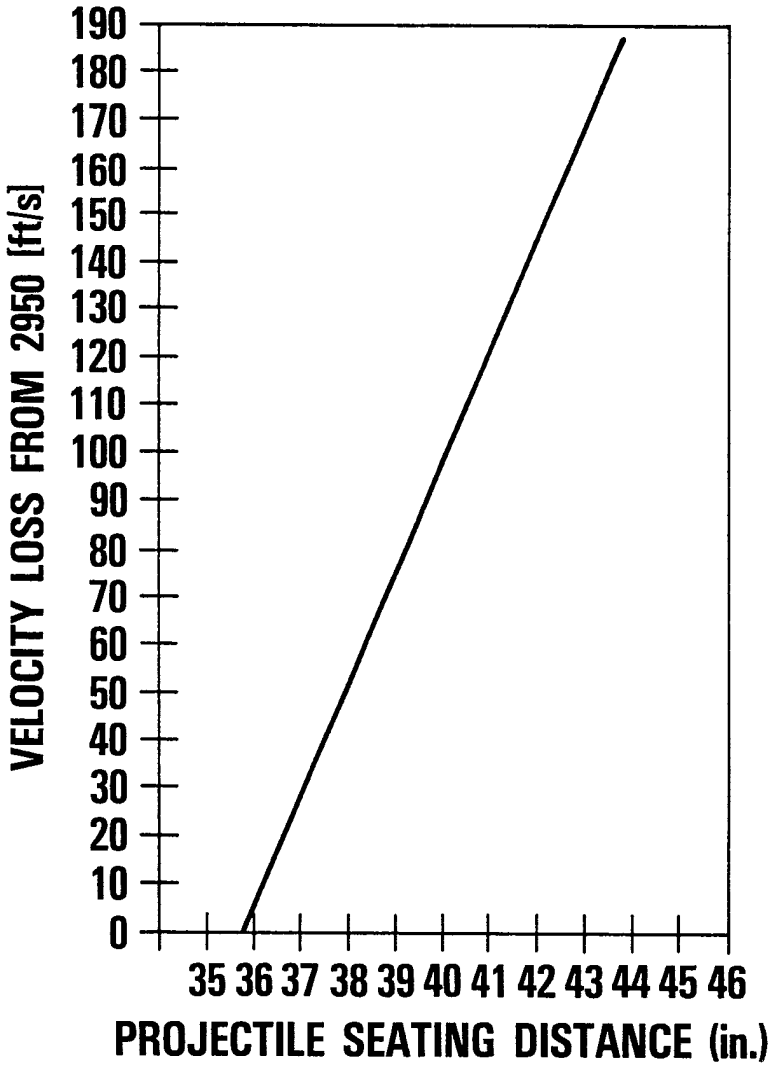

Figure 8

HIGH LIP	BAND BODY	CONDEMNATION LIMIT $\frac{(\Delta D_o)MAX}{D_o}$
NONE	0.1 in. > GROOVE DEPTH	≤ 0.02
0.04 D_o	EQUAL GROOVE DEPTH WITH OPTURATOR	$= 0.03$
0.04 D_o	0.020 in. > GROOVE DEPTH OR 0.004 D_o > GROOVE DEPTH	$0.04 \leq \frac{(\Delta D_o)MAX}{D_o} \leq 0.06$

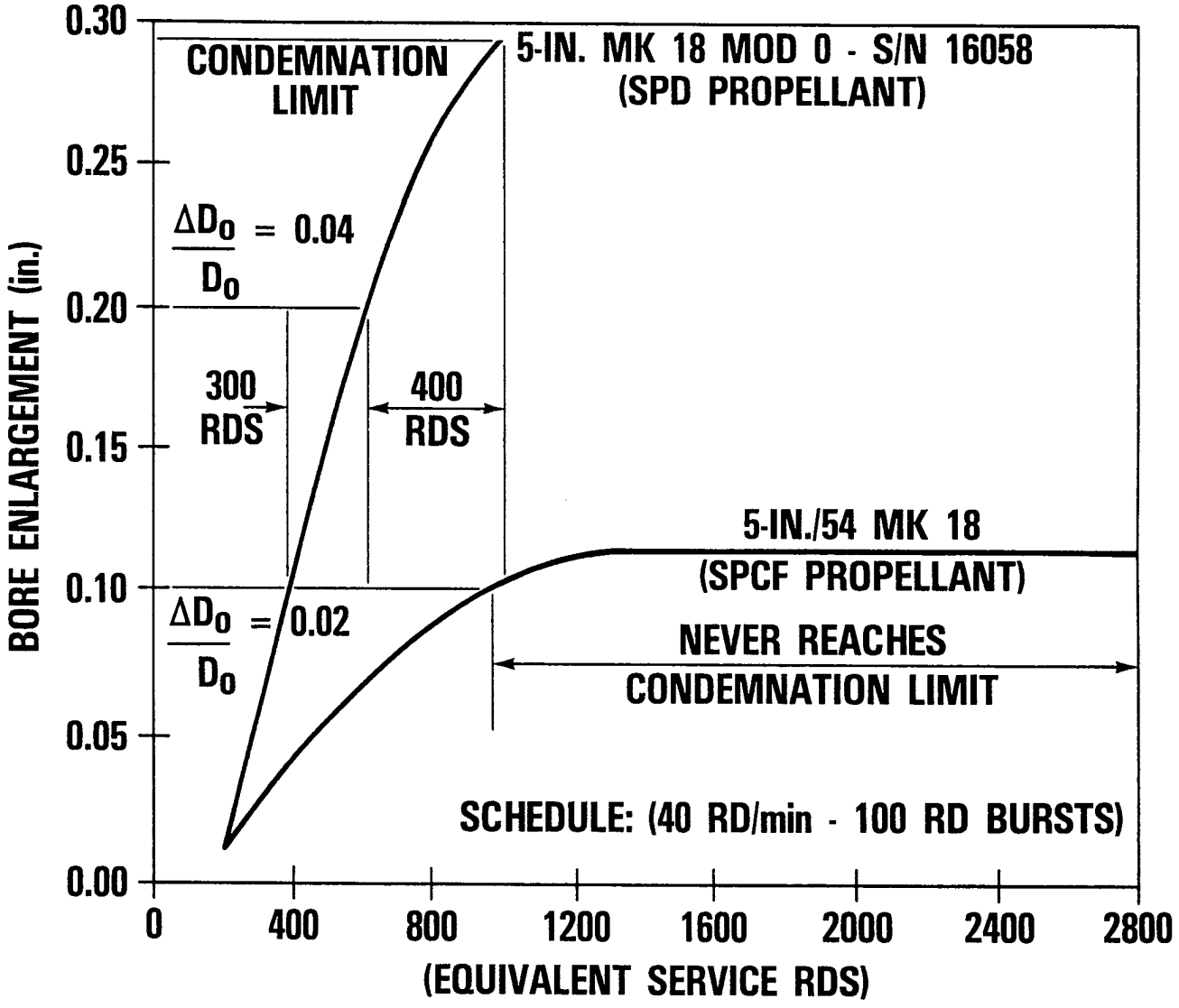
0.30
0.25
0.20
0.15
0.10
0.05
0.00
BORE ENLARGEMENT (in.)
CONDEMNATION LIMIT
5-IN. MK 18 MOD 0 - S/N 16058
(SPD PROPELLANT)
ΔD0/D0 = 0.04
300 RDS
400 RDS
5-IN./54 MK 18
(SPCF PROPELLANT)
ΔD0/D0 = 0.02
NEVER REACHES
CONDEMNATION LIMIT
SCHEDULE: (40 RD/min - 100 RD BURSTS)
0
400
800
1200
1600
2000
2400
2800
(EQUIVALENT SERVICE RDS)

Figure 10

5-IN./54 MK 41 PROJECTILE SEATED ON EROSION CONE IN VERY WORN GUN

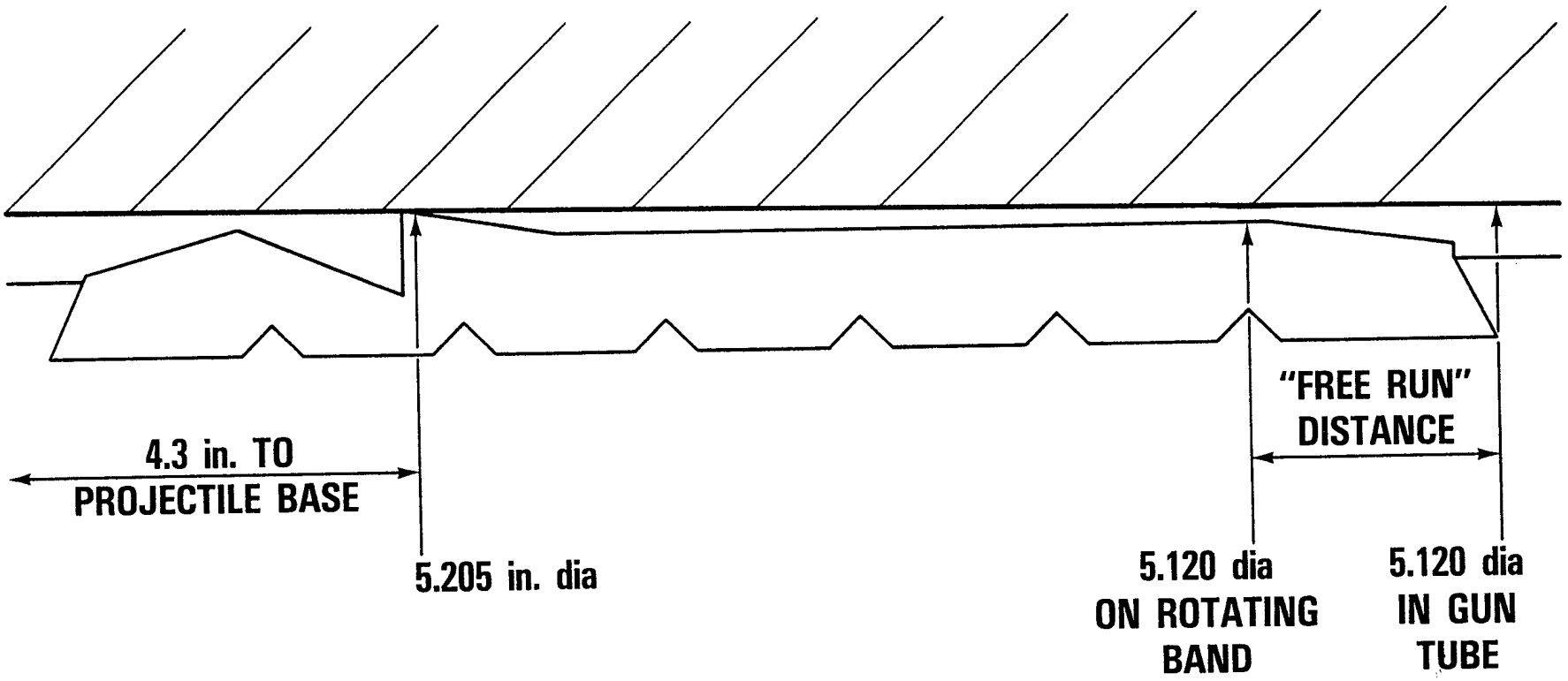

Figure 11

SESSION VI

PROPELLANTS AND ADDITIVES

CHAIRMAN: Dr. Jean-Paul Picard

MITIGATION OF HEATING AND EROSION IN HIGH-ENERGY ANTI-ARMOR AUTOMATIC CANNONS

Franklin A. Vassallo
CALSPAN CORPORATION
Buffalo, New York 14225

ABSTRACT

Heating conditions in current high-performance anti-armor cannons have been found sufficient to produce single-shot bore surface melting when uninhibited ammunition is fired. Heating/erosion testing of uninhibited ammunition in unique instrumented test fixtures at Calspan suggested intolerably short tube life without use of effective erosion inhibitors.

This paper describes the results of a developmental program in which Calspan designed and fabricated thermal/erosion research fixtures, conducted single-shot heating and erosion evaluations of candidate inhibitors, and assembled prototype inhibitor packages for use in burst fire weapon's evaluation.

The effectiveness of silicone ablatives and TiO_2/wax inhibitors on bore heating and erosion is presented. Results of test evaluations of a number of inhibitor compositions and deployments are presented. Outstanding performance is shown for a unique ablator design based upon ablator injection. For it, erosion life is shown to increase at least thirtyfold over that of uninhibited ammunition. Large reductions in bore heating are also demonstrated with use of ablator injection.

INTRODUCTION

The desire for increased terminal effectiveness of kinetic energy penetrators has led to the development of high charge-to-mass ratio ammunition with resulting increased single-shot tube erosion and heating. Basic causes of such increased heating and erosion are due to the need for the utilization of increased pressures, propellant gas temperatures, and propellant gas velocities which are required to achieve the needed superior firepower. Furthermore, the cannon systems which are intended to employ this ammunition in the anti-armor role derive much of their lethality from relatively high-rate operation. This mode of operation naturally impacts unfavorably on cannon thermal performance and tube erosion life.

Calspan has for a number of years been actively engaged in assessment and alleviation of tube heating and erosion for anti-armor automatic cannon systems. Early efforts[1,2] resulted in extension of tube erosion life for the ARES 75mm HIMAG cannon by as much as thirtyfold, using ablative additives within the ammunition. In those efforts, it was found that, although materials and plating

solutions to tube erosion were found to extend tube life in research fixtures, problems associated with implementation of such solutions as well as their limited extension of operational range suggested the development of ablative ammunition additive packages to be the solution having the greatest potential long-range benefit.

The use of a silicone ablative composition added to the basic 75mm telescoped round in the ARES HSTV-L was found to virtually eliminate tube erosion in single-shot firings.[3] Additionally, there was evidence that the ablative composition lowered the bore heating such that the onset and/or growth of bore surface cracking was alleviated. Subsequent erosion phenomenology investigations at Calspan[4] revealed that bore heating and erosion severity is related to the rate at which projectile kinetic energy is generated in the interior ballistics cycle. High rates of projectile kinetic energy generation as present in current anti-armor cannons lead to tube diametrical erosion rates measured in thousandths of an inch per shot. Again, ablative erosion inhibitors were found to show promise toward significant reduction of these severe rates of erosion.

This paper deals with additional findings regarding mitigation of heating/erosion using the ablative approach for telesoped medium caliber anti-armor ammunition.

HEATING/EROSION TEST APPARATUS AND PROCEDURES

GENERAL

As a means of measuring and evaluating heating/erosion in actual firing tests, Calspan designed, fabricated, and installed a unique test fixture at its Ashford Experimental Site. This single-shot test fixture was designed to represent the essential features of a medium-caliber anti-armor cannon but had provisions for measurement of local heating and erosion along the gun tube. Measurement of heating and erosion for shots, to be discussed later, permitted Calspan to evaluate a number of candidate erosion inhibitors quickly through limited single-shot firings of each. Generally speaking, erosion inhibitors were tested in groups of typically 3 to 4 shots of each type, at which time test data was reduced and the performance of the inhibitor analyzed. Many variations in erosion inhibitor deployment, type, and composition could therefore be assessed in the test program.

HEATING/EROSION TEST FIXTURE

Figure 1 illustrates schematically the erosion test fixture design. It consists of several components that are joined together to permit assessment of both heating and erosion at various axial stations along the gun tube. A primary member of the fixture is the support frame which effectively houses the chamber and two short barrel sections. The support frame supports the ammunition endcaps between the breech plate and the first short barrel section during firing.

The ammunition fired in this fixture is of the telescoped variety which consists of metallic endcaps and a plastic case. The telescoped projectile is

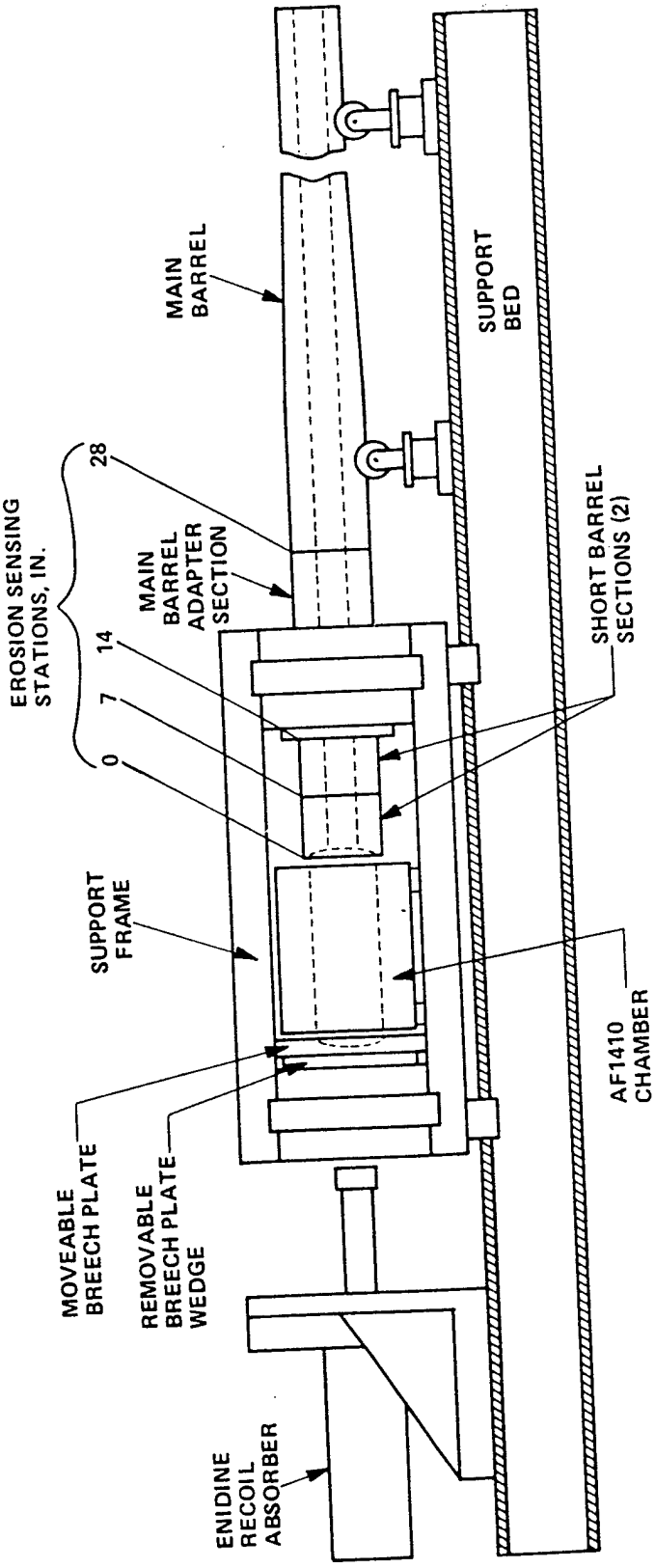

Figure 1 SCHEMATIC OF 90 MM HEATING/EROSION FIXTURE

guided in its initial passage into the gun tube through the use of metallic guide sleeve internal to the round. The view of the primary components involving the erosion inhibitor is given later in this paper. In loading, the telescoped ammunition is placed into the chamber while the chamber is at a lateral position to the side. A removable breech plate is retracted slightly during the operation. A sideward movement of the chamber and forward movement of the breech plate engages both endcaps with corresponding cutouts in the breech and barrel faces. The wedge breech plate holds the movable plate forward, assuring adequate resistance against ammunition rupture. The main feature of the technique is that, once the ammunition is placed between the first short-barrel section and the movable breech plate, it is supported on-line with the bore of the tube and is locked in place between these positions.

The support frame and main barrel together provide a mass which, during firing, recoils rearward sliding along the support bed. Recoil energy is absorbed using an hydraulic shock absorber.

INSTRUMENTATION AND DATA REDUCTION

The erosion and heating data were acquired at various axial stations, as indicated in Figure 1. Erosion measurements were obtained using test rings installed at sections of the barrel as was done in prior 75mm testing.[2,3] The positions of the test rings were at the entrance of the tube and at 7, 14, and 28 inches from the tube entrance. Post-test removal of the test rings was accomplished by breaking threaded joints and withdrawing specific test rings. Gas obturation was through the use of "O" rings at each section. The qualitative surface effects characterization of each ring was through the use of Indium replicas of the surface and optical examination. The actual material loss associated with firing was established by weighing each test ring and computing the average diametrical loss on the basis of density-volume considerations. This method was deemed most appropriate since, for the conditions of test, the weight losses associated with these firings were easily observed by use of analytical balance measurements.

The heat input determinations for all instrumented locations were made through the use of in-wall thermocouples of a type previously used at Calspan. These were fabricated and installed as is illustrated in Figure 2. Thermoelectric output of the thermocouple is converted to total heat input through application of data reduction methods of reference 1.

In addition to the basic erosion and heating measurement, Calspan also determined the pressures in the chamber and tube during each shot utilizing conventional piezoelectric transducers. A gross maximum pressure in the cartridge case was also recorded using M11 type copper ball crusher gages for each shot. Velocity measurements for each round were determined through the use of downrange break wire screens and an oscilloscope timing indicator. Basic utilization of the velocity measurement was to assess differences in ammunition performance as a result of changes in erosion inhibitor.

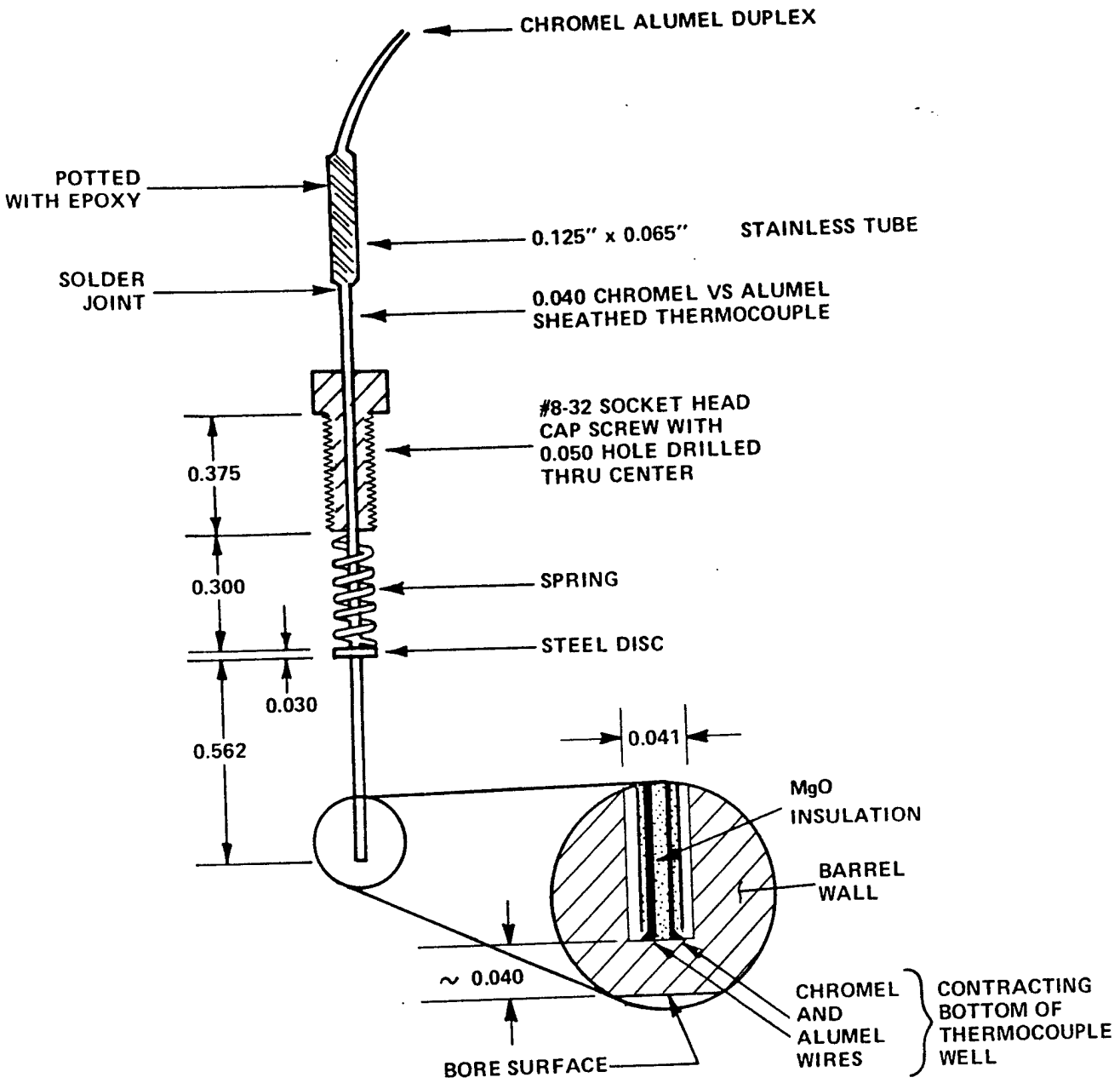

Figure 2 IN-WALL THERMOCOUPLE DESIGN AND INSTALLATION

TEST RESULTS AND DISCUSSION

Evaluations of erosion and heating were made for telescoped proof-slug armor piercing ammunition (PSAP) at ammunition temperatures ranging from -45 to +145°F. The composition of the ablator formulation was varied as was its basic deployment. Evaluations of TiO_2 additive and two general ablator deployments were made.

EROSION EVALUATIONS

Non-Ablative Ammunition

Firing tests for the purpose of establishing both heating and erosion were conducted initially utilizing non-ablative proof-slug ammunition. These firings were to obtain baseline values upon which erosion inhibitor tests of ablative configurations could be compared. In the firings, both interior ballistics data and heating and erosion data were gathered. Generally, the erosion at the various axial stations was found to increase greatly as the charge level was increased. In examining the characteristics of the surface of the test rings in these non-ablative firings, it was found that all the test rings exhibited surface melting erosion with gross material loss. Bore diametrical enlargements, measured in thousandths of an inch per shot, were indicated. Hence, the tube service life, when firing non-ablative ammunition, would be expected to be very short -- measured in tens rather than hundreds of shots per barrel. Hence, effective mitigation of erosion was shown to be essential in order to achieve an effective rapid fire cannon system.

TiO_2/Wax Liner Configuration

A brief examination of the viability and efficacy of the common TiO_2/wax liner was performed early in the test program. For these evaluations, typical 105mm TiO_2/wax liners were placed inside the plastic cartridge case at the wall and were intended to operate in similar fashion to that used in 105mm cased ammunition. A number of shots were conducted to establish the heating erosion profile for this type of erosion inhibitor. Results of the erosion tests are presented in Figure 3. Here, it is observed that, compared to the non-ablative ammunition, the liner provides some measurable reduction in erosion near the tube entrance but shows rapid loss of effectiveness at downbore locations in the tube. As indicated in Figure 3, the percentage benefit utilizing the liner appears to be essentially negligible at approximately four calibers into the tube. Furthermore, although the percentage reductions in erosion at the tube entrance are significant, they are far removed from what is actually needed to produce the desired major increases in tube erosion life. It was found that firings utilizing the TiO_2/wax additive exhibited bore surface melting also measured in thousandths of an inch per shot. Furthermore, the surfaces beneath any residual TiO_2 deposits after firing showed evidence of bore surface melting. It is felt that under the conditions of firing present in these high energy charges, the integrity of the TiO_2/wax surface deposits is insufficient to withstand the severe hyperthermal

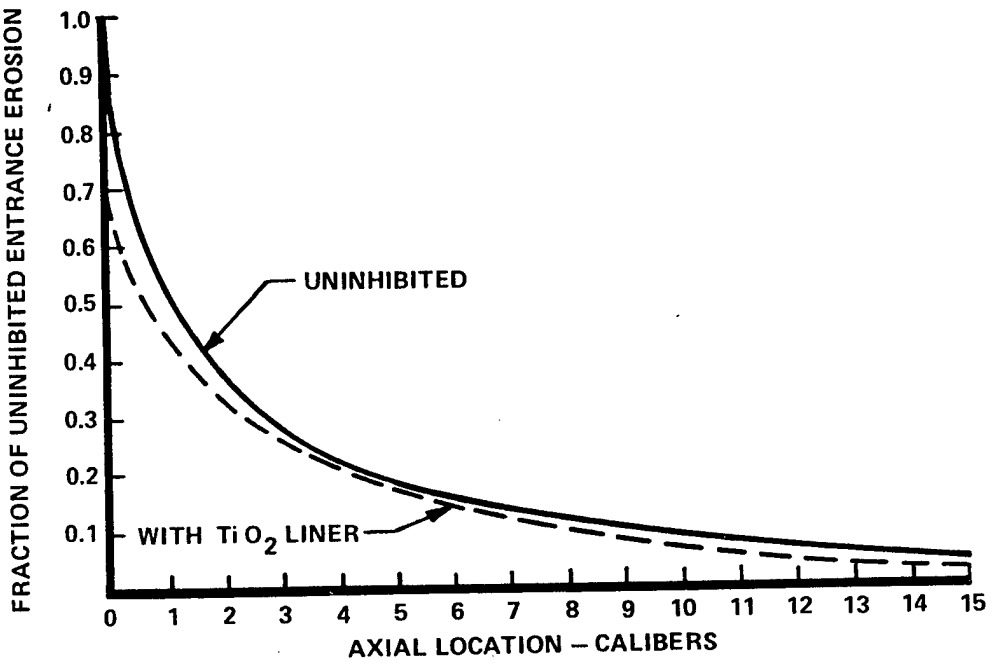

Figure 3 EFFECT OF TiO_2 LINER ON EROSION FOR A TYPICAL TELESCOPED CARTRIDGE

environment of the gun firing. Deposits observed at the completion of each individual shot are those which can withstand later aspects of the ballistic cycle without loss, but surface damage has already taken place. Because of its rather poor performance at the entrance of the tube, it appears that simple utilization of TiO_2 wax liners would not be adequate to provide needed erosion protection in these telescoped ammunition types.

Conventional Ablator Package Configurations

First investigations of ablator modifications to the PSAP ammunition were based upon techniques and packaging configurations utilized earlier in the 75mm ammunition HSTV-L. This conventional system is illustrated in Figure 4. It consists essentially of an outer plastic sleeve extension or side wall in which the ablator is inserted and a plastic cover to separate the ablative composition from the main propellant charge. The ablative material itself was formulated of various mixes of dimethyl silicone fluid, Mica, Cab-O-Sil and Triton X100 wetting agent. The proportions of each ingredient varied depending upon the composition being evaluated. In general, the dimethyl silicone fluid proportion constituted the main ingredient of the ablator mix being from 60 to 90 percent of the mix itself.

The study of the test data, generated through firings of many variations in ablator formulation and deployment, revealed that the ablative compositions, in general, provided very large reductions in the maximum bore erosion and did operate to extend dramatically the tube erosion life. It was found that all provided significant benefit relative to erosion over that of the non-ablative charges. Individual formulations and deployments indicated each to perform successfully at various stations of the tube. On the other hand, each was observed to show inadequate protection at some axial station or the other, such that the actual increase in erosion life of the tube was limited to no more than five times that of the non-ablative charge for general ablator weights below 5 percent of the charge weight. Following the initial tests whereby insufficient ablator protection was obtained, ablative firings at a weight level approaching 8 percent of the charge were conducted using a Mica enriched ablator. Figure 5 shows the relative effectiveness of this best conventional configuration on erosion. Here, we observe that very great reductions are produced in erosion near the entrance of the tube. Some effectiveness of the ablator is lost as one proceeds axially downbore reaching a maximum erosion at a location of approximately five calibers into the tube. Beyond this location, some further increased protection appears to be gained. The typical erosion profile as illustrated in Figure 5 is representative of that known as the secondary wear profile. At this level of inhibitor, the resulting benefit in erosion life over that of the non-ablative ammunition appears to be increased to about 7 to 1.

Later brief investigation of the efficiency of ablator coating deposits on the bore surface revealed that the protection afforded by the Mica ablator and in this configuration appeared to be approaching the limit of performance within the ablator amount feasible for application in this round type. Hence, it was believed that other means for deployment of the ablator must be sought, if complete protection of the tube is to be obtained.

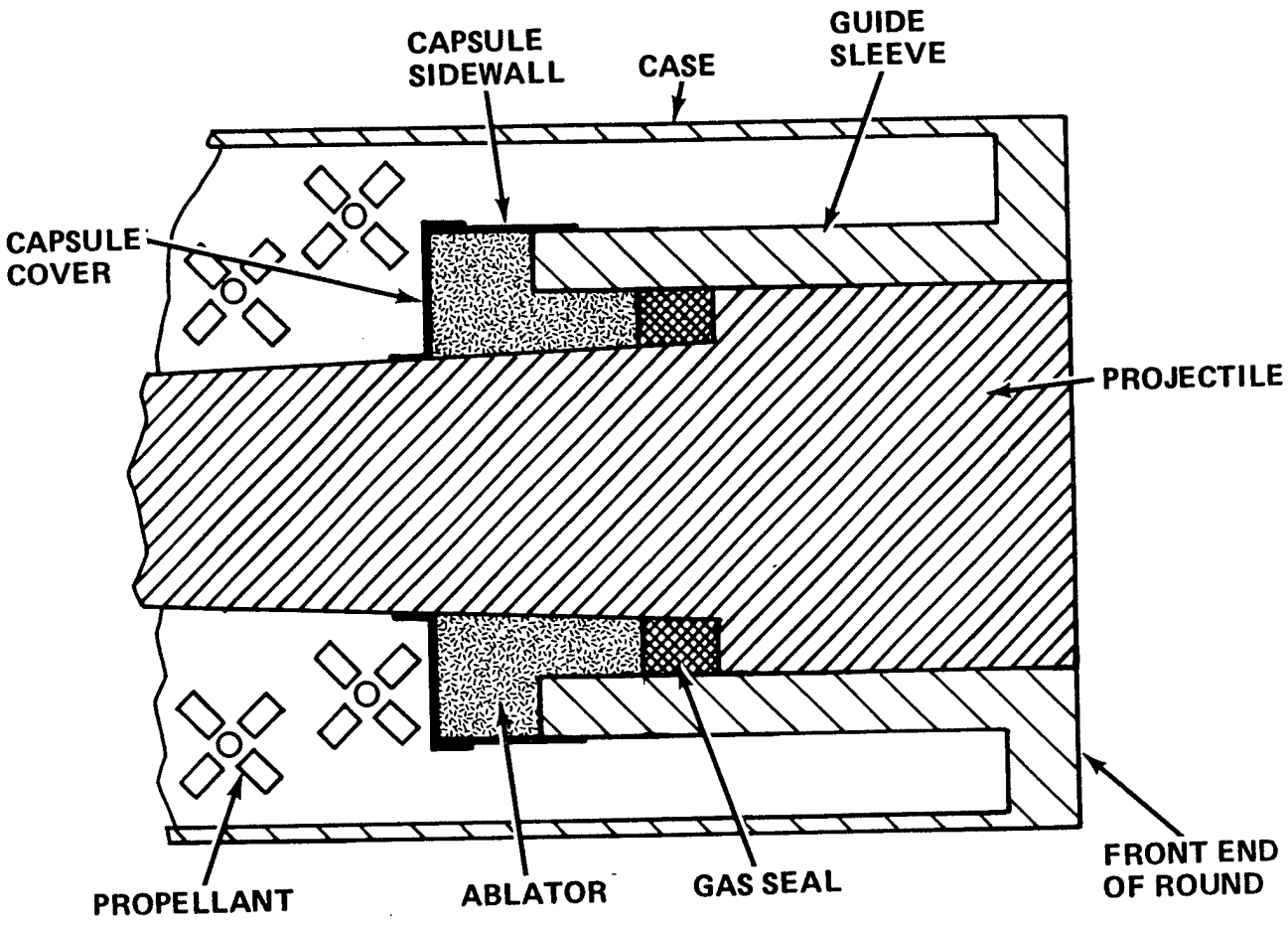

Figure 4 CONVENTIONAL ABLATOR CONFIGURATION

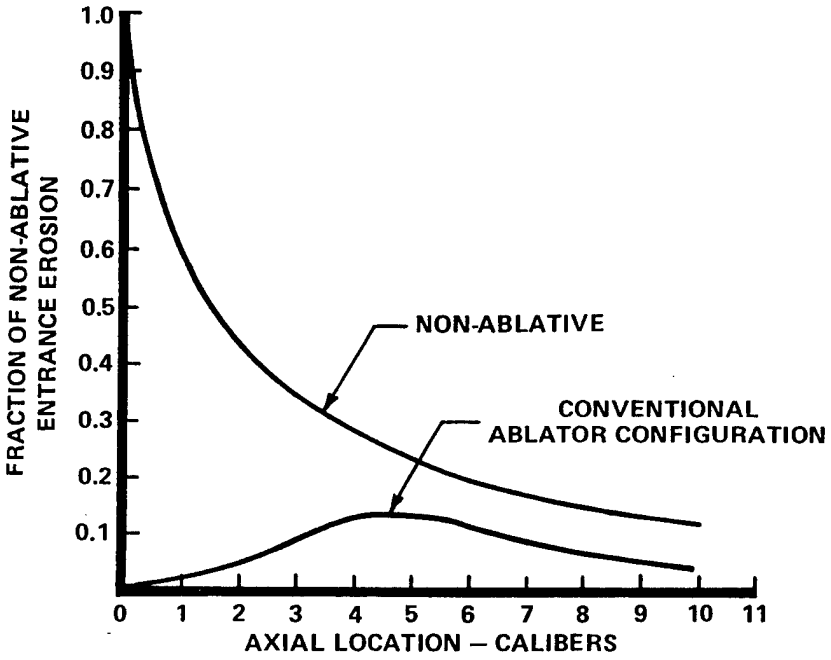

Figure 5 RELATIVE EFFECTIVENESS OF THE CONVENTIONAL ABLATOR CONFIGURATION ON EROSION

Ablator Injection

The basic drawback of the conventional ablator package above is in its inability to provide continuous application of coating to the bore surface. The mechanism by which the ablator is coated along the tube is simply be adhesion between the ablator component and the tube wall as the ablator package is forced along the tube following the projectile. Therefore, any ablator which has finally passed the point of interest on the tube has no further chance to return and continue the coating mechanism in the far upstream sections of the barrel. Therefore, any thickness of raw ablator coating deposit on the tube must of itself provide complete protection throughout the entire firing period. A method which would permit possibly greater efficiency would be to insert the ablator material further into the cartridge case and have it come out more slowly during the ballistic cycle, thereby continually coating the tube. Through inspection of the measured pressure time histories in the round, it was recognized that during the firing of the telescoped cartridge, a substantial pressure difference exists across the steel round control guide sleeve in the front endcap.

It was believed that ablator placed in the annular space between the round control guide sleeve and the outer case could be injected into the propellant gas flow stream through suitable ports drilled through the round control guide sleeve. As an aid to movement of the ablator material, it was thought that a diaphragm placed upon the thickened ablator fluid would act as a piston pusher. Hence, the full pressure drop across the round control guide sleeve could be effective in forcing ablator through the ports. A suitable choice of injector port size and ablator viscosity could allow one to arrive at an optimum injection of ablator fluid which would run along the surface of the bore, thereby protecting it from the hot propellant gases. Figure 6 illustrates schematically the general concept for the ablator injection scheme.

Calspan entered into an evaluation of the scheme in an effort to establish whether the technique could be practically implemented. Investigations were conducted to establish approximate port sizes required to obtain uniform deposition of injected ablator fluid throughout the ballistic cycle. Furthermore, Calspan systematically determined the required amount of ablator to provide total protection of the bore surface.

Tests of the resulting ablator injection configuration at ambient temperature indicated essentially no erosion along the tube. Very minor losses associated primarily with mismatch of test rings with that of the general bore were observed. In general, very tenacious protective bore coating residue was found on post-test examination of the bore and test rings. The photograph of Figure 7 illustrates the effectiveness of the ablator deployment in the vicinity of the injector ports. Here, we see that the areas immediately downstream of the injector ports appear to show essentially no erosion beneath the deposits generated through decomposition of the silicone fluid. On the other hand, the areas between the injector ports which have no protection from injection of fluid show a surface wash and melting due to bore surface heating. In this ablator injection scheme, the basic protection and operating principle for protection appear to be related to flow of the ablator fluid along the bore surfaces during the interior ballistic cycle. So long as ablator flow persists, protection appears to be rather

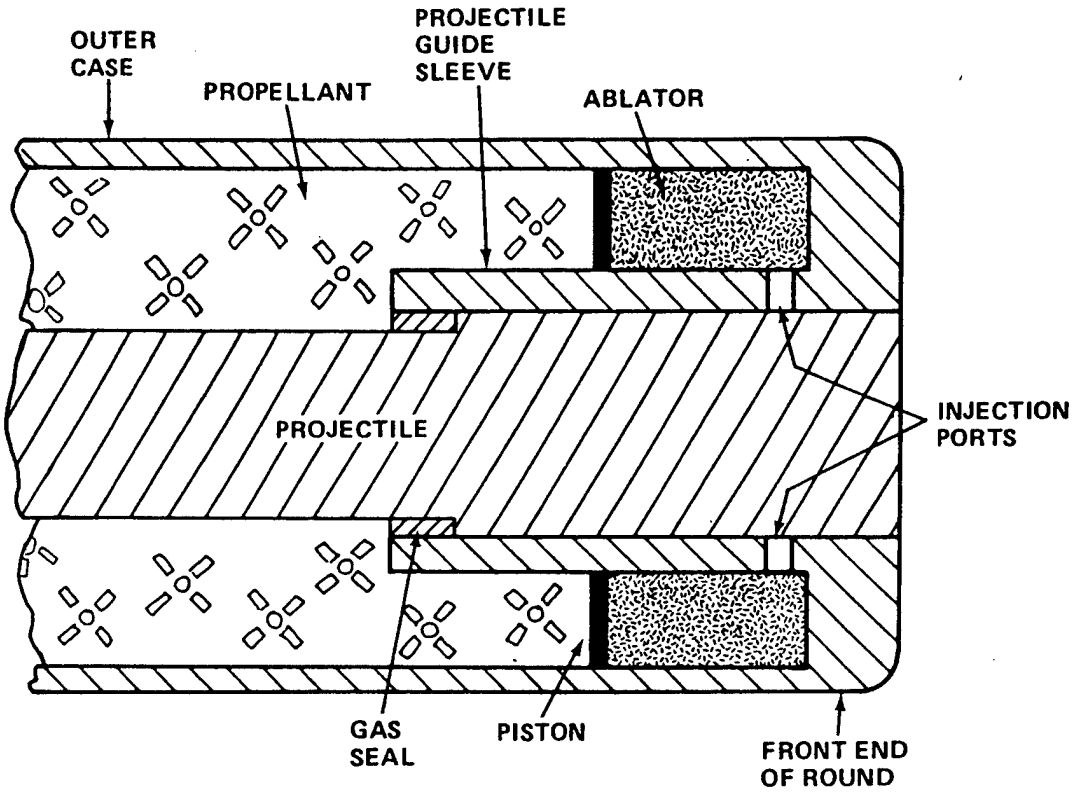

Figure 6 ABLATOR INJECTION CONCEPT

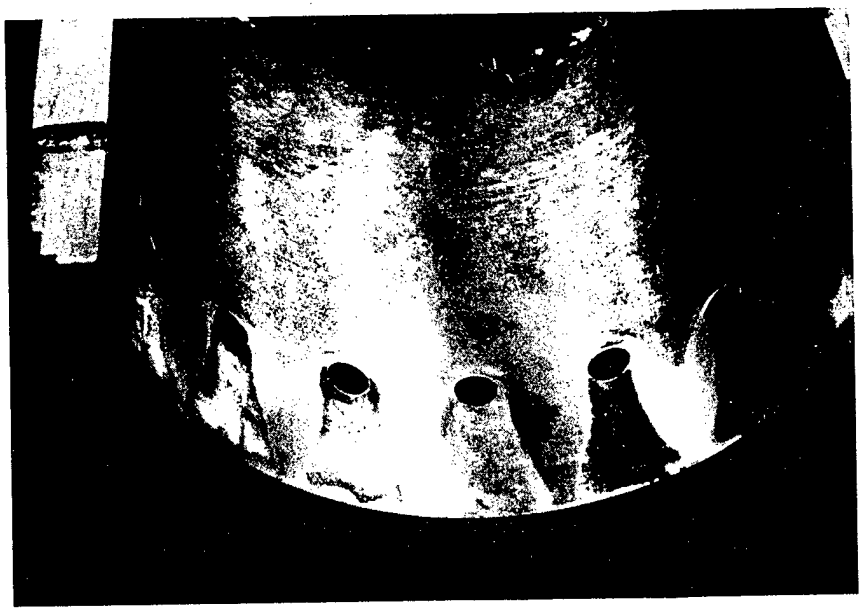

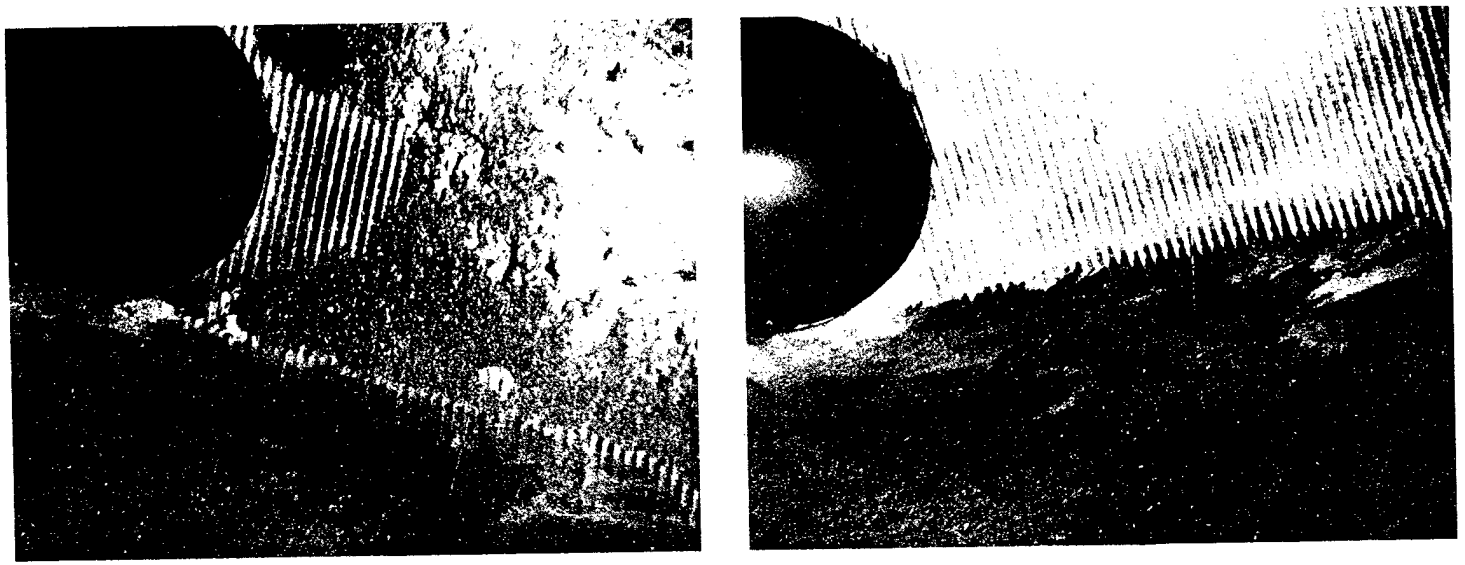

Figure 7 ILLUSTRATION OF ABLATOR EFFECTIVENESS IN THE NEIGHBORHOOD OF THE INJECTOR PORTS

complete. Therefore, it is essential that ablative material be injected through the ports for a duration at least sufficient to preclude erosion throughout the interior ballistic cycle.

It was found that test rings downbore are protected to nearly the same extent as that portrayed near the ports (Figure 7) when the ablator injection is operating successfully. There was evidence in the firings that bore surface coating deposits were measured to be less than 1-1/2 to 2 thousandths thick. This should not interfere with projectile travel or stability in the tube.

Figure 8 illustrates the relative erosion distributions for non-ablative ammunition compared to that modified using ablator injection. At 70°F ambient, erosion life is observed to be increased by as much as thirtyfold over that of uninhibited ammunition. Furthermore, erosion using ablator injection is in evidence at all only beyond 5 calibers into the tube. Erosion values are essentially nil near the tube entrance.

At increased ammunition temperature to 145°F, some loss in ablator effectiveness is observed; but, nonetheless, very significant protection is observed. At subzero temperatures (data not shown), no erosion was observed.

HEATING EVALUATIONS

Heat input determinations for the different charges were made at various axial stations along the tube. It was found that heating values for the very high kinetic energy charges produced heat input values upwards of 145 Btu's per square foot near the entrance of the tube, diminishing somewhat along the tube axis. Figure 9 illustrates the typical heat input distribution along the tube for the three basic charge types investigated. As one may observe, the heat input for the non-ablative charges diminishes roughly 15 percent over the first 8 calibers of the tube and this is the basic reason why there is a significant reduction in the axial erosion for this charge as one proceeds downbore. The heat input distribution for the conventional ablator configuration is shown to show greatest protection near the entrance of the tube and less downbore; this accounts for the loss of downbore protection with respect to erosion for this particular configuration. The heat input distribution for the ablator injection technique indicates substantial reductions in heating along the tube out as far as 8 calibers and beyond. Heating reductions of as much as 40 percent compared to non-ablative are observed near the entrance of the tube and become nearly constant at this percentage throughout the initial sections of the barrel. The rather large reductions in heating observed should be expected to result in major gains in rapid-fire erosion life in that bore temperatures and barrel average temperatures will be diminished significantly over those of non-ablative ammunition in the multi-shot firings for which the anti-armor cannons are designed.

INTERIOR BALLISTICS PERFORMANCE

Assessment of the interior ballistics performance of all ammunition containing ablative components indicated very minimal increase in maximum chamber

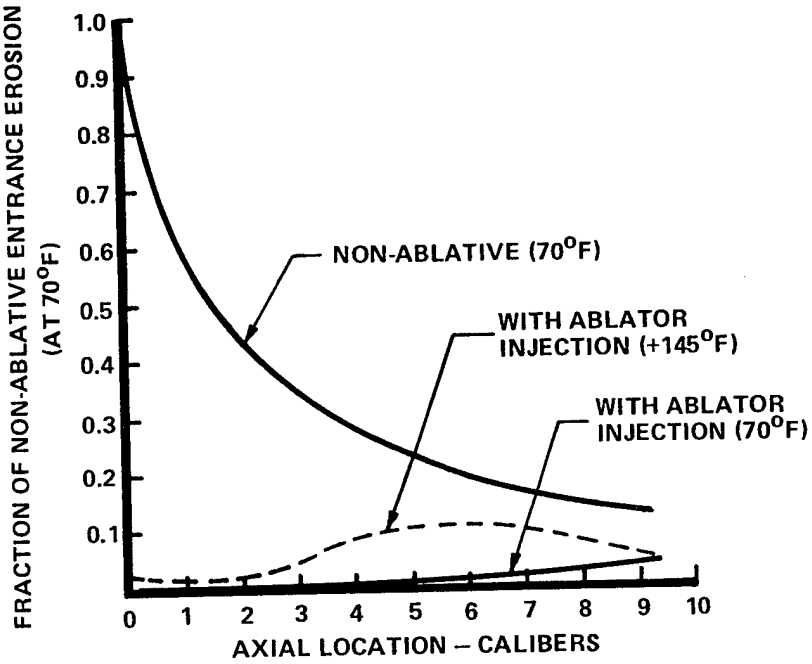

Figure 8 RELATIVE EFFECTIVENESS OF ABLATOR INJECTION ON EROSION

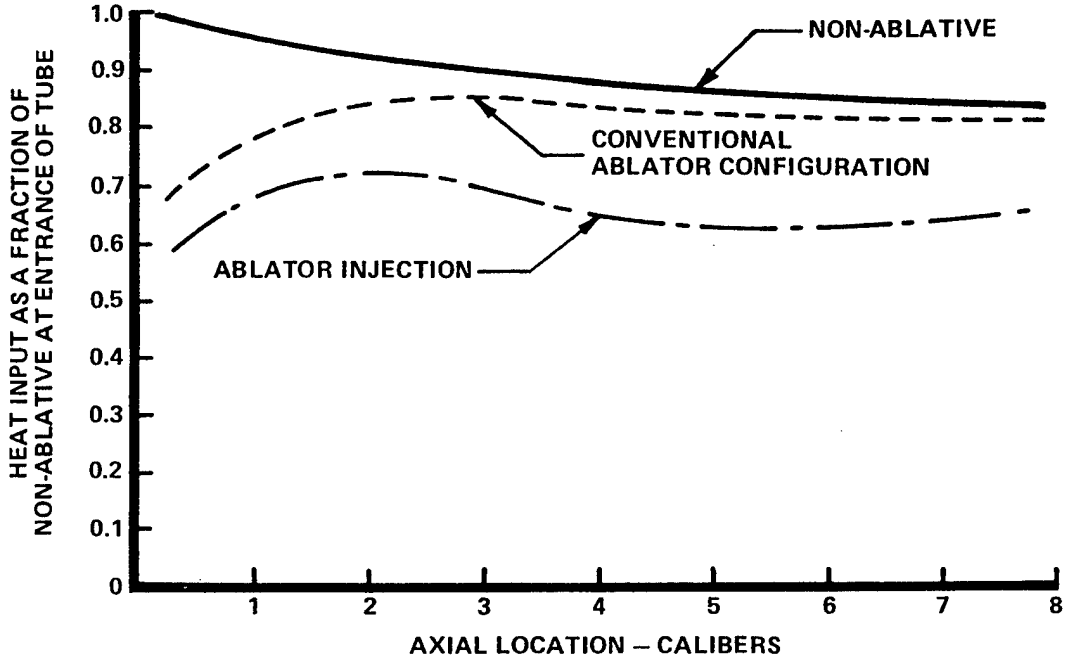

Figure 9 TUBE HEATING COMPARISONS (TELESCOPED AMMUNITION)

pressure compared to that of the non-ablative ammunition. It was also found that the resulting muzzle velocities for the inhibited ammunitions were indistinguishable from those for the non-ablative ammunition. Hence, it is felt that little ballistic performance is sacrificed with the inclusion of the ablative-erosion inhibitor and injection scheme described in the earlier sections.

CONCLUSIONS

Calspan's investigations of heating and erosion for the high-energy anti-armor ammunitions permit a number of conclusions to be drawn.

1. Instrumented single-shot heating and erosion test fixtures can permit efficient assessment of these factors for candidate ammunition types and modifications.

2. Erosion conditions in high-energy anti-armor cannons can exceed the bore surface melting threshold in single-shot firings of uninhibited ammunition.

3. Only very limited protection of the tube appears to be attainable in telescoped cartridge designs through the use of TiO_2/wax liners.

4. Ablative formulations applied as additives in a conventional aft configuration can provide significant protection against heating and erosion. Severalfold increases in tube life are suggested.

5. Efficient application of ablative erosion inhibitors suggests virtual elimination of bore erosion in telescoped cartridge designs for which ablator injection is feasible.

6. The effect of the erosion inhibitors on the interior ballistics performance of the round appears to be minimal. Tests show minor increase in maximum chamber pressure as a result of the reduced chamber volume associated with introduction of the ablator package. Little, if any, measurable loss of muzzle velocity has been observed.

7. Heating reductions through the use of effective ablative erosion inhibitors have been found to be significant. Heating reductions of as much as 40 percent were observed for the ablative injection configuration. Optimization of the ablator formulation could undoubtedly improve this percentage.

REFERENCES

1. Vassallo, F.A., "Heat Transfer and Erosion in the Ares 75mm High-Velocity Cannon," Calspan Technical Report No. VL-5645-D-1, October 1975.

2. Vassallo, F.A., and Brown, W.R., "Heat Transfer and Erosion in the Ares 75mm High-Velocity Cannon," Vol. II, Calspan Technical Report No. VL-5873-D-1, October 1977.

3. "Thermal/Erosion/Fatigue Studies of the Ares 75mm Advanced Development Cannon," Calspan Quarterly Reports 1-10, April 1978-July 1980.

4. Vassallo, F.A., "Thermal and Erosion Phenomenology in Medium Caliber Anti-Armor Cannons," ARRADCOM Report ARLCD-CR-81028, November 1981.

A COMPARISON OF BARREL-HEATING PROCESSES FOR GRANULAR AND STICK PROPELLANT CHARGES

A. W. Horst
US Army Armament Research and Development Command
Ballistic Research Laboratory
Aberdeen Proving Ground, Maryland

ABSTRACT

The natural flow channels offered by propelling charges composed of bundles of stick propellant significantly reduce the resistance to gas flow when compared to that of granular propellant charges, virtually eliminating potentially damaging pressure waves in the gun chamber. However, this same feature which reduces pressure waves may also result in more propellant remaining in the chamber, burning behind the origin of rifling, and perhaps increasing barrel erosion. In this study, a two-phase flow interior ballistic code (NOVA) is employed to compare propellant motion and heat transfer processes for ballistically-equivalent stick and granular propellant charges. A large difference in the motion of the solid phase during ignition and combustion is predicted for the two configurations, leading ultimately to an approximately 300 K higher maximum wall temperature for the stick propellant charge.

INTRODUCTION

Stick propellant is finding increasing application in high-performance artillery charges. Currently employed in a number of European top-zone propelling charges, stick propellant is now being introduced into US artillery as a product improvement to the existing 155-mm, M203 (Zone 8S) Propelling Charge. Further, its use is all but assured in future advanced artillery weapon systems under consideration in the United States.

The current popularity enjoyed by stick propellant can be attributed to a number of very desirable ballistic advantages associated with its use, some of them only potential but others clearly demonstrated. The natural flow channels associated with bundles of sticks reduce the resistance offered to gas flow by several orders of magnitude when compared to that resulting from the tortuous path required of flow through a granular propellant bed[1]. Locally high pressure gradients cannot therefore be supported in a stick propellant charge, and potentially damaging longitudinal pressure waves are all but unseen. In addition, the regular packing of propellant sticks yields higher loading densities than for randomly packed granular propellant, allowing equivalent performance with stick propellant charges using a slightly increased mass of a lower energy, lower flame-temperature propellant formulation. It is widely purported, and not unreasonable to expect, that the lower flame temperature should lead to increased barrel life and perhaps reduced muzzle flash and blast. Alternatively, a larger possible charge mass of the existing formulation may allow performance increases in an otherwise volume-limited gun system. With such worthwhile benefits in the offing, exploitation of the stick propellant concept certainly appears well-motivated.

Approved for public release; distribution unlimited

In this paper, we wish to raise concern in respect to one of these potential benefits - that of increased tube life with stick propellant charges. Under the assumption that heat transfer to the tube wall is the dominant mechanism for gun barrel erosion, the use of cooler propellant made possible by the higher packing density of propellant sticks has been deemed adequate to assure a reduction in barrel wear. However, an interior ballistic analysis scheme devised by Nordheim[2] during World War II purports heat transfer to the tube at the origin of rifling to be strongly affected by the distribution of burning propellant grains in the gun tube. According to this picture, heat transfer would be the greatest when the burning propellant remained in the chamber; the least when the propellant was uniformly distributed throughout the gun. Thus, the very feature of stick propellant which reduces pressure waves should also reduce motion of the solid phase considerably, leading to increased heat transfer to the tube and perhaps increased erosion rates as well.

Indeed, recent calculations[3] based on Nordheim's hypothesis yielded an 18% higher heat input for a stick propellant charge assumed to remain in the chamber when compared to a granular propellant distributed throughout the gun. These calculations were performed using ballistically-equivalent candidate stick (XM208) and granular (XM203E2) propellant charge configurations for the US 155-mm, M198 Towed Howitzer. The same study reports limited experimental measurements of heat transfer for the two charges (without wear-reducing additives) to differ by 13%, the stick propellant charge again yielding the larger value. In fact, based on Nordheim's analysis, the flame temperature for a ballistically-equivalent stick propellant charge must be reduced by 300 K to obtain comparable heat transfer to that of the granular propellant, top-zone, 155-mm howitzer charge. While Nordheim's analysis is admittedly crude and confirmatory experimental data sparse, further study of this problem appeared warranted in view of the major commitment to stick propellant under consideration by the US Army.

THEORY

Calculations reported in this paper were performed using the NOVA code[4], a two-phase, unsteady flow representation of the interior ballistic cycle. The balance equations describe the evolution of macroscopic flow properties accompanying changes in mass, momentum, and energy arising out of interactions associated with combustion, interphase drag, and heat transfer. Functioning of the igniter is included by specifying a predetermined mass injection rate as a function of position and time. Flamespreading then follows from axial convection, with grain surface temperature deduced from a heat transfer correlation and the unsteady heat conduction equation, and ignition based on a surface temperature criterion. Noteworthy features of NOVA pertinent to this study include mechanisms leading to motion of the solid phase (explicit description of igniter functioning, interphase drag forces, the gas pressure gradient, and intergranular stresses) and the processes of heat transfer to and conduction in the tube wall.

While the code remained unchanged except for input data for granular and stick propellant charge calculations, differences do exist in the forms of correlations employed within the code to relate those microprocesses responsible for interphase drag and intergranular stresses for the two propellant geometries to the overall governing equations for macroscopic flow in the gun. Reference is made to the empirical, steady-state correlations of Ergun[5] and Andersson[6] for

resistance to flow through fixed and fluidized beds of granular propellant, while drag is deduced from heat transfer by means of a Reynolds analogy for stick propellant, where it is expected to be dominated by the boundary layer. Similarly, intergranular stress in a granular propellant bed is described as being an irreversible function of bed porosity, while a stick propellant bundle is treated as being elastic and capable of sustaining tension as well as compression. In both cases, individual grains/sticks are assumed incompressible.

Convective heat transfer to the tube is calculated using a simple turbulent pipe flow correlation[7] based on a hydraulic Reynolds number to account for the presence of the solid phase:

$$q = h\ (T_g - T_s)$$

$$h = \frac{k_f}{D_h}\left[0.023\ Re_D^{0.8} Pr^{0.4}\right]$$

where

$$Re_D = \rho_f u\ D_h/\mu_f$$

$$D_h = 2\varepsilon R_T/\left[1 + 2R_T\ \frac{\varepsilon}{D_p}\right]$$

The local temperature at the inside surface of the tube is then determined, as driven by the convective boundary condition, using an approximate cubic profile integral solution to the one-dimensional heat conduction equation. This approximation has been previously shown[8] to produce a 2% error in predicted temperature change for a constant heat flux and 6% for a linearly increasing flux.

Results presented are not to be interpreted as firm, quantitative predictions of wall temperature. Certainly such confidence awaits a considerably more detailed representation of the microprocesses occurring in the chemically-reacting, unsteady (and perhaps multiphase) boundary layer, as well as processes occurring on the bore surface itself. Nevertheless, the NOVA code provides a phenomenologically much more complete picture of the interplay of charge motion and heat transfer than does Nordheim's procedure, and quantitative trends revealed during this study may warrant consideration by the charge design community.

RESULTS

Figure 1 presents bore-surface temperature histories at the origin of rifling calculated for ballistically-equivalent, top-zone, granular (M203) and stick (XM208) propellant charges for the 155-mm, M198 Howitzer. The M203 charge employs a conventional seven-perforation granulation, while the XM208 made use of charge-length, slotted, single-perforation sticks. Both charges employ the same M30A1 propellant formulation, yet significantly higher wall temperatures are predicted for the stick propellant charge. Loci of maximum wall temperatures as a function of axial position for the two charges are displayed in Figure 2, again

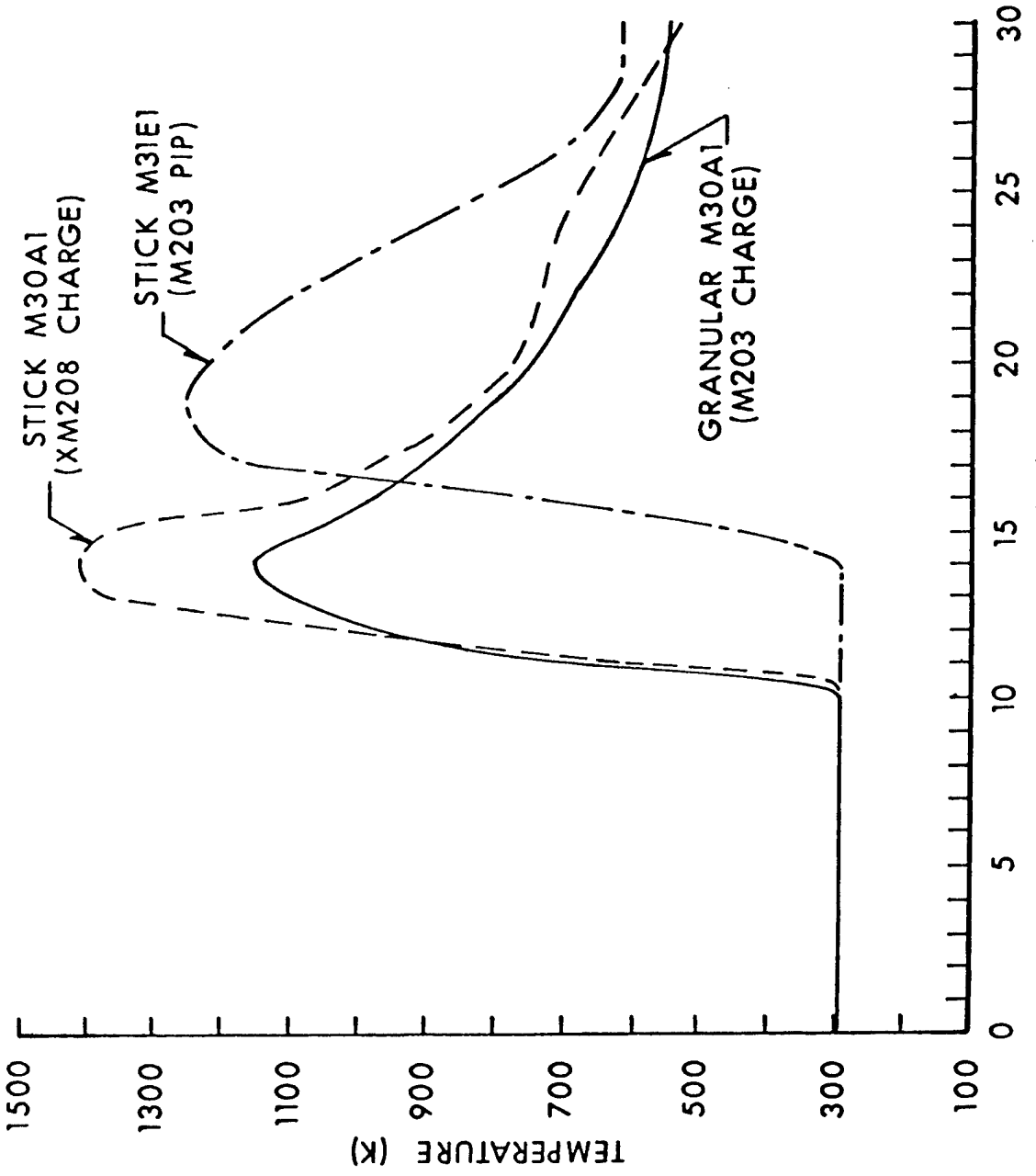

Figure 1. Predicted Bore-Surface Temperature Histories

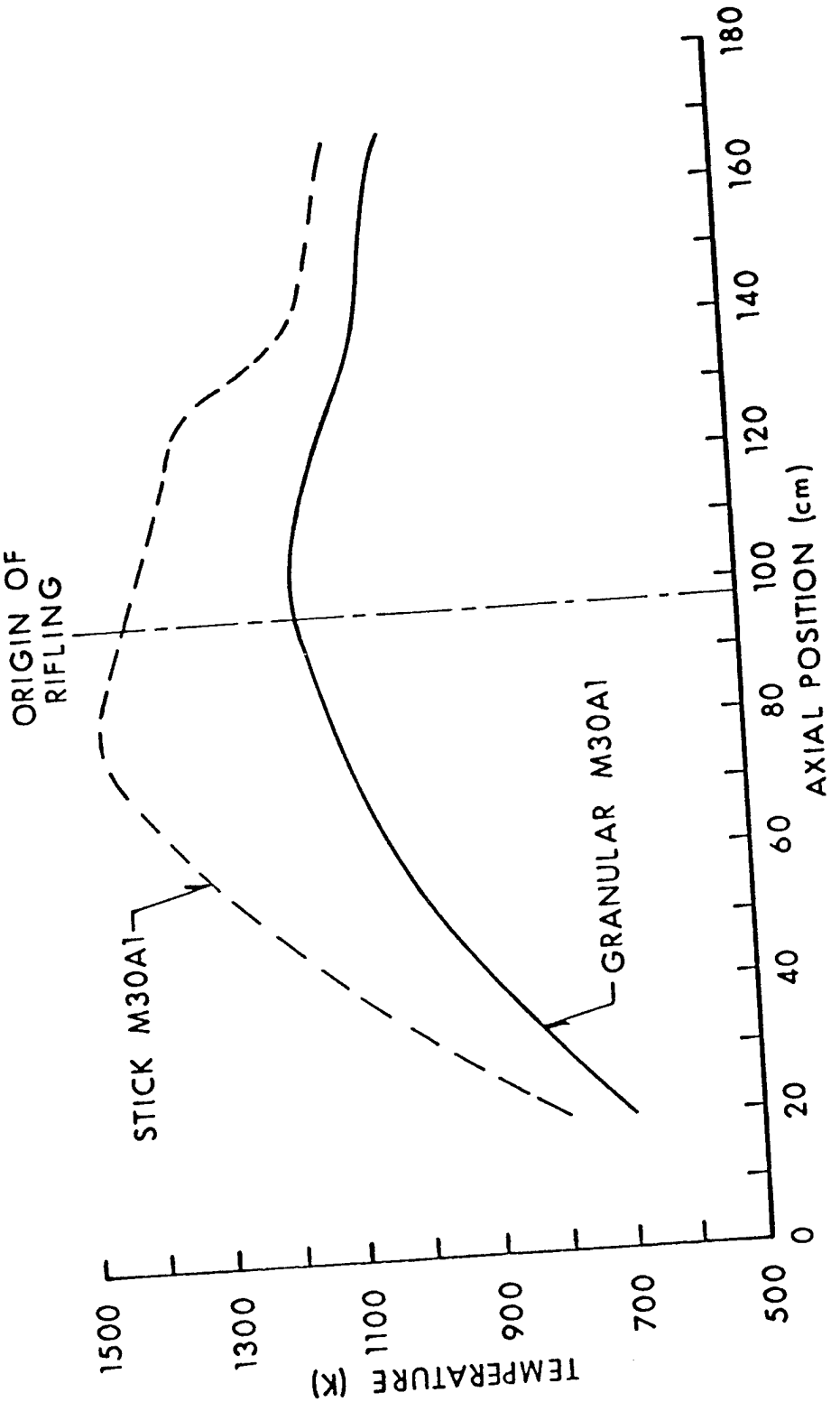

Figure 2. Maximum Predicted Wall Temperatures

indicating a more severe heating environment associated with the stick propellant.

If Nordheim's hypothesis is correct, the mechanism for this difference should involve a difference in the motion and distribution of the burning propellant, an integral part of the two-phase flow dynamics described by NOVA. Figure 3 depicts the distribution of solid propellant at various times during the interior ballistic cycle for the two propellant configurations. The granular propellant, indeed, becomes more widely dispersed in the gun tube during much of the combustion phase, resulting in a significant portion of the total charge burning ahead of the origin of rifling and hence not contributing to its erosion. Virtually all of the stick propellant, however, is predicted to remain in the chamber during the combustion cycle. While these distributions do not mimic precisely the limiting-case assumptions of Nordheim, the data of Figure 3 clearly identify the difference in granular and stick propellant motion as an important factor in barrel heating and perhaps erosion.

A logical extension to Nordheim's hypothesis might include the role of gas velocities in the heat transfer process. Figure 4 depicts gas velocities for the two charges at the moments of their respective maxima at the origin of rifling. While it must be cautioned that these figures represent core-flow velocities, we note again that the lowered resistance to flow offered by the stick propellant charge leads to a condition which exacerbates heat transfer to the tube.

To confirm this effect, an additional calculation was performed employing the granular propellant configuration, this time with the interphase-drag friction factor reduced to a value corresponding to stick propellant[1]. As expected, propellant motion was substantially less than that predicted for the unmodified granular propellant (also shown in Figure 3); further, the predicted maximum bore-surface temperature rose to nearly 1500 K.

Finally, we recognize the compensating effect associated with the use of a cooler propellant (i.e. lower flame temperature) made possible by the higher loadable charge weights of bundles of sticks. Specifically, the M203 Product Improvement Program (PIP) calls for replacement of M30A1 granular propellant with M31E1 stick propellant. However, based on computed results for this propellant formulation, also shown in Figure 1, the accompanying decrease in flame temperature of approximately 400 K falls somewhat short of totally compensating for the increase in bore-surface temperature at the origin of rifling associated with the stick geometry. Desired gains in cannon wear life will have to result from other features of the new propelling charge.

CONCLUDING REMARKS

A phenomenologically reasonable hypothesis has been presented that suggests that stick propellant geometries may be inherently more erosive based on hydrodynamic considerations alone. Calculations employing the NOVA code substantiate earlier predictions to this effect based on the simple analysis of Nordheim. While quantitative predictions of bore-surface temperature provided by the current analysis must be viewed with some uncertainty, we have no justification for rejecting the basic message that stick propellant erosivity may not equate with granular propellant erosivity. Planned commitments to stick propellant

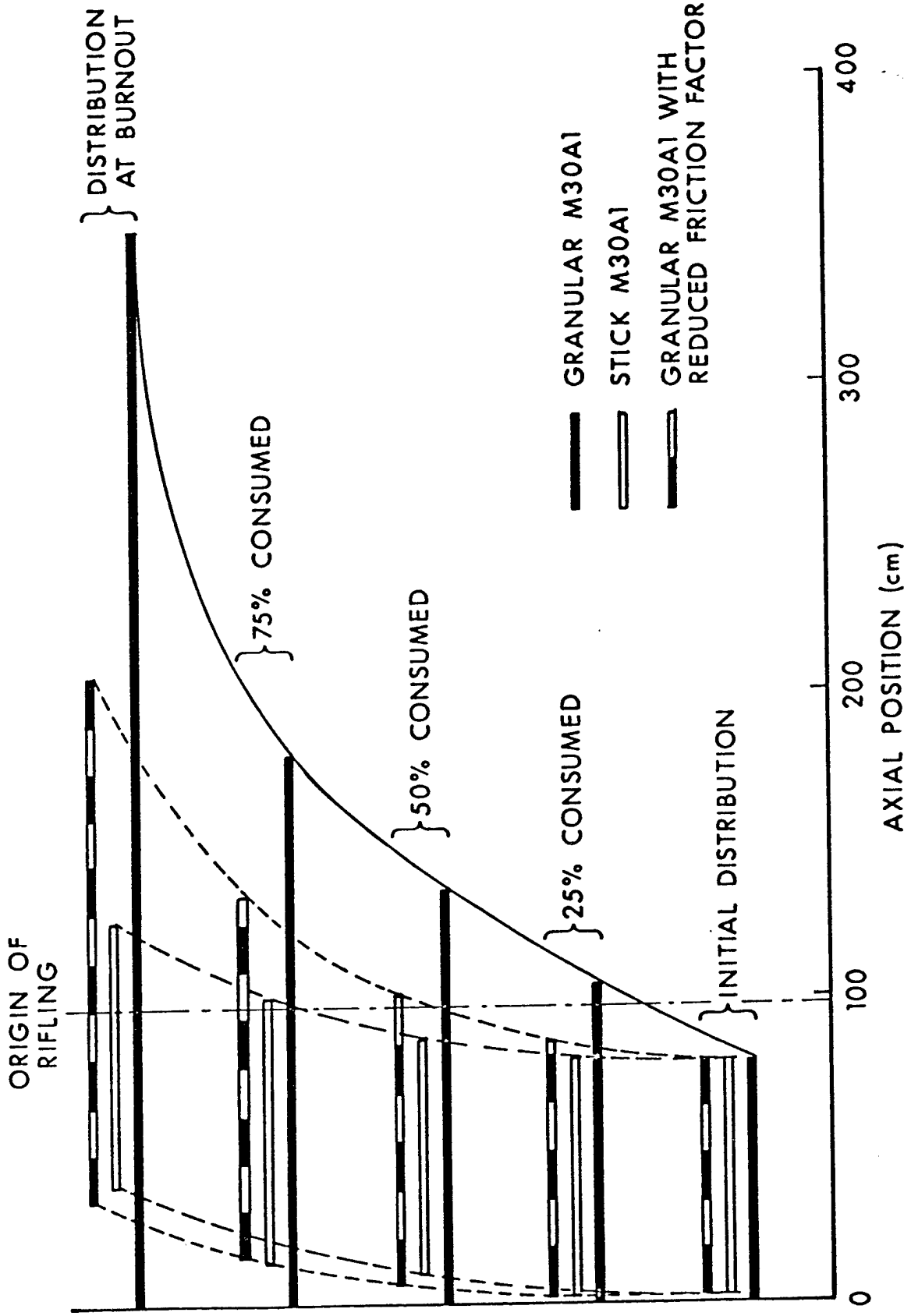

Figure 3. Calculated Distributions of Propellant

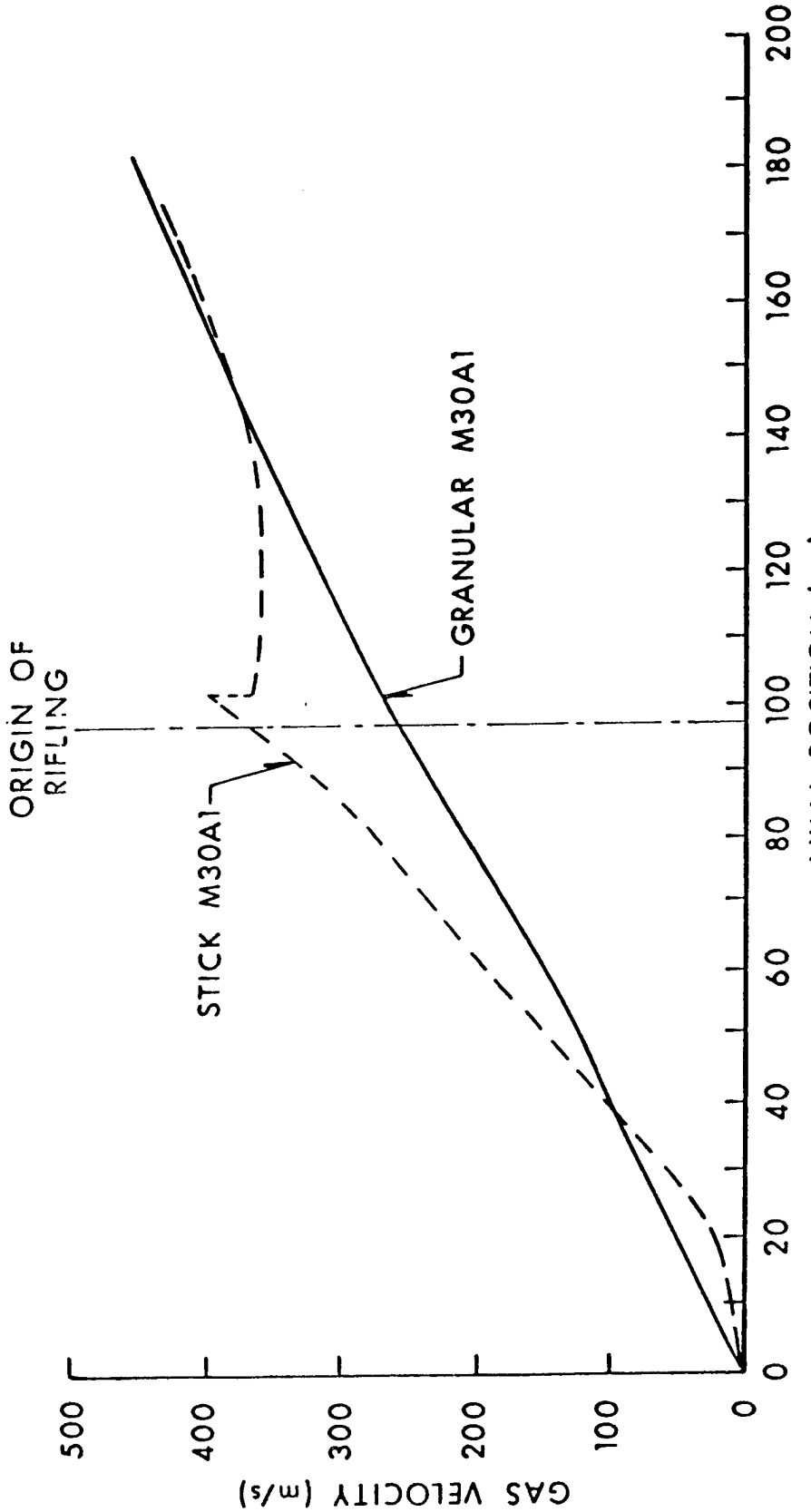

Figure 4. Predicted Gas-Velocity Profiles

charges warrant immediate experimental investigation of this problem. The coincidental use of a rigid, combustible cartridge case (with or without additives) may well help to provide the substantial improvement in wear life over conventional bagged, granular propellant charges as suggested by British experience. Further, the use of several tiers of shorter sticks being considered to facilitate propellant manufacture and blending may also be shown to promote distribution of the burning propellant throughout the gun tube. If this can be accomplished without the return of undesirable pressure waves, the problem of excessive heat transfer, if real, may be eliminated.

REFERENCES

1. F.W. Robbins, et al., "Experimental Determination of Stick Charge Flow Resistance," 17th JANNAF Combustion Meeting, CPIA Publication 329, Vol. II, pp. 97-118, November 1980.

2. L.W. Nordheim, H. Soodak, and G. Nordheim, "Thermal Effects of Propellant Gases in Erosion Vents and Guns," NDRC Armor and Ordnance Report No. A-262, National Defense Research Committee, Washington, DC, March 1944.

3. J.R. Ward and I.C. Stobie, "On the Erosivity of Stick and Granular Propellant," USA ARRADCOM, Ballistic Research Laboratory, Aberdeen Proving Ground, MD (report in preparation).

4. P.S. Gough, "THE NOVA CODE: A User's Manual, Volume 1. Description and Use," IHCR 80-8, Naval Ordnance Station, Indian Head, MD, December 1980.

5. S. Ergun, "Fluid Flow Through Packed Columns," Chem. Eng. Progr., Vol. 48, pp. 89-95, 1952.

6. K.E.B. Andersson, "Pressure Drop in Ideal Fluidization," Chem. Eng. Sci., Vol. 15, pp. 276-297, 1961.

7. J.P. Holman, "Heat Transfer," McGraw-Hill, 1968.

8. C.W. Nelson, "On Calculating Ignition of a Propellant Bed," ARBRL-MR-02864, USA ARRADCOM, Ballistic Research Laboratory, Aberdeen Proving Ground, MD, September 1978.

NOMENCLATURE

D_p particle diameter

D_h hydraulic diameter

h convective heat transfer coefficient

k_f thermal conductivity of gas at film temperature

Pr Prandtl number

q heat transfer rate

R_T tube radius

Re_D Reynolds number

T_g gas temperature in core flow

T_s bore-surface temperature

u gas velocity in core flow

ε macroscopic bed (or bundle) porosity

μ_f gas viscosity at film temperature

ρ_f gas density at film temperature

EROSIVITY OF STICK PROPELLANT

J.R. Ward and I.C. Stobie
USA Ballistic Research Laboratory
Aberdeen Proving Ground, MD

ABSTRACT

During the second World War, Nordheim and co-workers at Duke University derived an interior ballistic scheme to compute heat transfer to gun barrels. Nordheim claimed that the distribution of unburned propellant affected heat transfer at the commencement of rifling (CR) region. Heat transfer was greatest if the unburned propellant stayed in the chamber, while the heat transfer was least if the unburned propellant were evenly distributed. Stick propellant should remain in the chamber in contrast to granular propellant, so stick propellant should be more erosive.

This article summarizes experimental data on 155-mm zone 8S propelling charges which affirm Nordheim's hypothesis. Heat inputs were measured in separate laboratories with the XM208 (stick M30A1 propellant) and the XM203E2 charges (granular M30A1 propellant) as well as a zone 8S charge for the FH70 which has stick cordite N propellant. The heat input measurements made without additives show the XM208 charge has a higher heat input than the XM203E2 charge with the difference diminishing as one goes down the barrel in accord with Nordheim's prediction.

The experimental measurements also claimed that the cartridge 3 charge in the FH70 which is ballistically matched to the zone 8S charge gave higher heat input. The cartridge 3 charge tested used stick cordite N and a polyurethane foam liner. Wear test data for the FH70 was culled and by using intervals where only cartridge 3 charges were fired and the same axial downbore distance relative to the CR, it was shown that the cartridge 3 charge was more erosive than the M203 and M30A1 propellant and a TiO_2-wax liner, despite the 500K lower flame temperature of cordite N.

An important corallary in this comparison was the demonstration that wear in the 155-mm cannons (M199 and M185) was unaffected by the different forcing cone design.

INTRODUCTION

An extensive investigation of gun barrel wear in hypervelocity guns was sponsored by the National Defense Research Committee during World War II[1]. A key problem was how to compute heat transfer to gun barrels. Nordheim and co-workers at Duke University[2] devised an interior ballistics scheme to compute heat flux from combustion gases using Reynolds' analogy between energy and momentum transfer for the convective heat transfer coefficient.

Nordheim observed that the assumption as to the distribution of unburned powder significantly changed heat transfer. The heat transfer at the commencement of rifling was least when the propellant was evenly distributed behind the projectile; the heat transfer was greatest when the unburned propellant remained in the chamber, since all the combustion gases had to pass the commencement of rifling. The difference in heat transfer diminished down the barrel to the point where all the propellant was consumed. Nordheim provided results for both assumptions; he felt

Approved for public release;
distribution unlimited.

the short, granular propellants conformed to the assumption of evenly distributed grains.

Nordheim's work implied that propellant charges made with stick propellants would be more erosive than propelling charges with equivalent interior ballistics made with granular propellants, since the unburned stick propellant would remain in the chamber.

During the course of investigations to discern the unusual wear produced by the 155-mm XM201E2 charge, heat transfer and erosion sensor measurements were done with a series of 155-mm propelling charges in which the wear-reducing additives were removed.[3,4] Among the charges tested was a stick propellant version, XM208, of the XM203E2 charge with granular propellant. Since heat transfer data had been collected in separate laboratories, and the use of the heat transfer technique and erosion sensors was in its infancy, the larger wear and heat input for the XM208 charge stirred little interest. In this report, the heat input and wear data are collected, placed on a common basis, and compared to see if the stick propellant is more erosive. In addition, the prediction from the heat input measurements that the cartridge 3 charge for the FH70 is more erosive than the M203 charge is tested by comparing wear data from the FH70 with wear from the M199 cannon with the M203 charge.

HEAT TRANSFER DATA

Table I lists characteristics of the XM203E2 charge and two stick propellant analogs, the XM208 and the FH70 cartridge 3.

Calspan Corporation measured total heat input at three axial locations on the M185 barrel with thermocouples imbedded in the barrel wall. The thermocouples were placed so they were directly over a groove. One thermocouple was placed forward of the commencement of rifling where remaining tube life is estimated from the bore enlargement.[5] Another thermocouple was mounted one-third the distance between the commencement of rifling and the muzzle, while the third thermocouple was mounted at the muzzle. Bore surface temperatures at the commencement of rifling were computed from the total heat input and interior ballistic trajectories.[6] At BRL, the total heat input was measured at the commencement of rifling with four thermocouples imbedded at different distances from the bore surface.[7] In order to obtain equivalent units of energy per unit area, the BRL measurements are divided by the bore perimeter (613.7mm).

Table II summarizes which zone 8S charges were tested. The goal of the tests was to reduce the wear of the XM201E2 charge, so no systematic testing of zone 8S charges was planned.

Table III summarizes the results obtained by Calspan with the zone 8S charges. The BRL results are summarized in Table IV.

One should note first that the Calspan and BRL data for the XM203E2 charge cannot be compared directly since the BRL heat input represents heat input with a "clean-out" round after each shot. The Calspan heat input is the average of five

TABLE I. CHARACTERISTICS OF 155-MM ZONE 8S CHARGES EVALUATED

Charge	Additive	Propellant	Type	Flame Temp, K	Charge Mass, kg	Peak Chamber[a] Pressure, MPa	Muzzle Vel,[a] m/s
XM203E2	TiO_2-wax	M30A1	7-perf	3,000	11.8	318	830.0
XM208	TiO_2-wax	M30A1	Stick	3,000	11.3	308	817.2
Cartridge 3	Polyurethane Foam	Cordite N	Stick	2,470	12.3	316	813.5

a - Inert-loaded M549 RA Projectiles

TABLE II. ZONE 8S CHARGES EVALUATED FOR HEAT TRANSFER

Propelling Charge	Additive	Calspan	BRL
XM203E2	TiO_2-wax	X	X
XM203E2	None	-	X
XM208	TiO_2-wax	X	-
XM208	None	X	-
Cartridge 3	Polyurethane Foam	X	-
Cartridge 3	None	-	-

TABLE III. CALSPAN HEAT INPUT AND WEAR DATA FOR ZONE 8S CHARGES[a]

Charge	No. Shots	Heat Input, J/mm^2 1.006m	2.108m	6.007m
XM203E2	5	1.119	0.863	0.673
Cartridge 3	5	b	.892	.554
XM208	3	b	.971	.610
XM208 (no additive)	2	1.518	1.106	.666

a - Axial distances measured from rear face of tube (RFT).
b - Data unavailable.

TABLE IV. HEAT INPUTS FOR XM203E2 CHARGE MEASURED AT BRL

Charge	Heat Input, 1.006 RFT, J/mm^2
XM203E2 (no additive)	1.292
XM203E2	1.144

consecutive XM203E2 shots. In order to see how well heat inputs agree between the two sets of measurements, charges without wear-reducing additives are compared in Table V. One sees the Calspan measurements are 3% greater. Using 1.034 as a correction factor, the BRL heat inputs corrected to be consistent with Calspan are 1.336 J/mm^2 and 1.183 J/mm^2 for the XM203E2 charge minus its additive and XM203E2 charge, single-shot respectively.

TABLE V. HEAT INPUTS MEASURED BY BOTH CALSPAN AND BRL

Charge	Heat Input, J/mm^2 Calspan	BRL	Ratio, Calspan, BRL
M119	1.138	1.103	1.032
XM119E4 (minus liner)	1.290	1.245	1.036

Figure 1 summarizes the heat inputs from Table III and the modified BRL heat inputs. Interpretation of some of the data is confounded by the wear-reducing additives and missing values in the commencement of rifling region. Nonetheless, one sees that the XM208 charge produces greater heat input than the XM203E2 even when the wear-reducing additive is taken from both charges. The difference between the stick and granular propellant decreases downtube as expected from Nordheim's

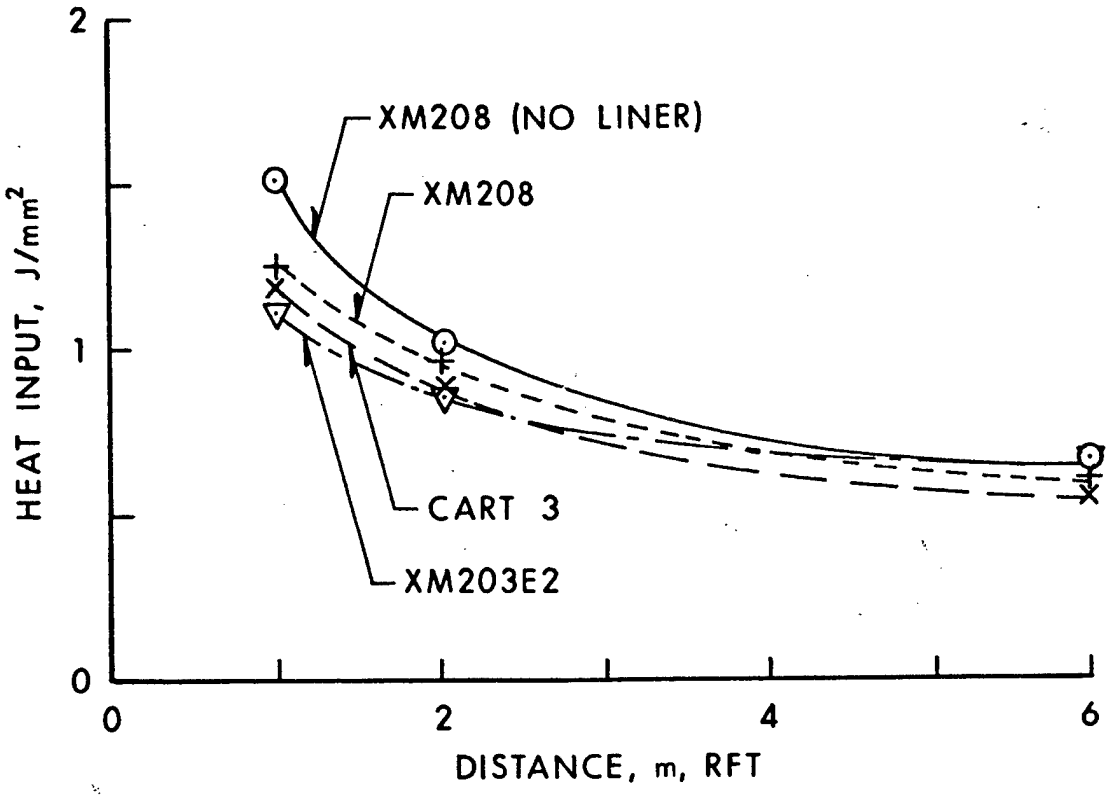

Figure 1. Heat Input vs Axial Distance for Zone 8S Charges

hypothesis that the distribution of unburned propellant accounts for the greater heat input near the commencement of rifling. At the muzzle the cartridge 3 charge with cordite N has the smallest heat input. The trend from the muzzle to 2.108m RFT, suggests the stick cordite N propellant is more erosive than the granular M30A1 propellant at the commencement of rifling.

WEAR FROM CARTRIDGE 3 CHARGE

In order to corroborate wear predictions from the heat input data, wear data[8] from the cartridge 3 charge in the FH70 will be compared to that for the XM203E2 charge.

One area leading to confusion when discussing gun wear is the way tube life is determined on either side of the Atlantic. The monitors are located in the lands in both cases, however, their axial positions in the gun tube vary. The US positions sensors one-quarter inch (6.4 mm) from the commencement of rifling. The Europeans monitor gun wear at one inch (25.4 mm) from the CR. This report attempts to compare wear from the cartridge 3 and XM203E2 charges at a common distance from the CR. Comparisons are made for intervals where no lower zone charges were fired.

Central to this comparison is the assumption that the different chamber designs in the 155-mm cannons do not affect wear. It has been assumed that a steeper forcing cone fosters wear. This assumption has never been tested, since any change in the slope of the forcing cone alters the interior ballistic cycle such that

differences in wear could be attributed to changes in chamber pressure or muzzle velocity. To isolate the role of the forcing cone, one needs to compare guns with equal chamber volumes, so that the interior ballistic cycle (pressure-time, velocity-time curves) are identical.

Over the course of development of a new 155-mm towed howitzer, the Army tested two version with different forcing cone slopes, but with equivalent interior ballistics. A review of the test data showed that one experimental version of a zone 8 charge had been fired in sufficient numbers in each cannon[9], so that one can see whether the forcing cone affects wear.

Table VI lists pertinent gun dimensions taken from engineering drawings supplied by Watervliet Arsenal. The CR is the point where the lands first reach full height beyond which the cannons are identical. The forcing cone is the region between the chamber and the CR, one can see that the forcing cone is twice as steep in the M185. Since axial distances downbore are measured relative to the RFT, wear should be compared relative to the CR to compensate for differences in the chamber and forcing cone. In this article, wear will be reported at 0.25 inches (6.4 mm) from the CR.

TABLE VI. GUN DIMENSION FOR M185 AND M199 HOWITZERS

Cannon	Chamber Length, mm	Forcing Cone Region, mm	Diametral Taper, mm	Commencement of Rifling, mm*
M185	923.5	76	0.203	990.5
M199	995.5	59	0.101	1054.1

*Distance measured from the rear face of the tube (RFT).

Table VII lists the wear data for the M199 cannon (shallow forcing cone) in which 208 low-velocity rounds were fired prior to the test with the XM201E5 charges. The wear vs rounds fired was fit with a linear, least-squares program which computed best-fit values of the slope and intercept as well as the wear with these best fit values. The slope for the M199 cannon was 1.4 μ/round; the wear computed with the best-fit values for the slope and intercept are also listed in Table VII. The agreement between the measured and computed wear shows that the wear vs rounds fired was linear over this interval.

Table VIII lists similar wear data for the M185 cannon (steep forcing cone) in which 1,050 XM201E5 charges were fired after proofing. The slope computed with the linear, least-squares program was 1.5 μ/round suggesting that the forcing cone slope did not affect wear. This assertion is strengthened by considering tube to tube variation in wear. Table IX lists wear for three 105-mm M68 cannons firing M456A1 HEAT rounds[10] which suggests that a difference in wear of 0.1 μ/round is not significant.

TABLE VII. WEAR OF M199 CANNON SN74 FIRING M107 PROJECTILES WITH THE XM201E5 CHARGE

Tube Round No.	Test Round No.	Wear, mils (mm)*	Wear, Cal'd, Mils (mm)
208	---	3 (0.08)	3 (0.08)
308	100	8 (.20)	8 (.20)
408	200	13 (.33)	13 (.33)
508	300	19 (.48)	19 (.48)
608	400	23 (.58)	24 (.61)
708	500	28 (.71)	29 (.74)
808	600	36 (.91)	35 (.89)

*Vertical land wear measured at 1,060 mm RFT with a stargauge. Zero wear corresponds to 155.00 mm (6.100 inches).

TABLE VIII. WEAR OF M185 CANNON SN22684 FIRING M107 PROJECTILES AT ZONE 8 WITH THE XM201E5 CHARGE

Tube Round No.	Test Round No.	Wear, mils (mm)*	Wear, Cal'd, mils (mm)
1	----	4 (0.10)	4 (0.10)
41	40	6 (.15)	6 (.15)
151	150	11 (.28)	13 (.33)
261	260	17 (.43)	19 (.48)
371	370	28 (.71)	25 (.64)
481	480	34 (.86)	32 (.81)
601	600	39 (.99)	39 (.99)
751	750	49 (1.24)	48 (1.22)
901	900	54 (1.37)	56 (1.42)
1051	1050	65 (1.65)	65 (1.65)

*Vertical land diameter measured at 1,006 mm RFT, measured with a pullover gauge. Zero corresponds to 155.00 mm (6.100 inches).

TABLE IX. 105-MM M68 GUN WEAR FIRING HIGH-EXPLOSIVE ANTI-TANK ROUNDS

SN	Rounds Fired	Wear, mm	Wear/Round, μ
3864	1,120	1.77	1.6
4360	1,952	2.92	1.5
6600	1,931	2.92	1.5

Since the XM201E5 charge has a TiO_2-wax liner, these results with the M185 and M199 cannons suggest that the forcing cone slope did not affect the action of the wear-reducing additive. These results may be of interest as a test case for those modeling boundary layer flow in guns with the aim of understanding how additives such as TiO_2-wax reduce wear[11,12].

In order to estimate wear from the cartridge 3 charge with the FH70, inspection sheets from reference 8 were collected for intervals when only zone 8S (cartridge 3) charges were fired. Wear data for the XM203E2 charge will be taken from the M199 wear test at Yuma Proving Ground.[13]

To compensate for differences in chamber design, wear between the two cannons, FH70 and M199, will be compared at points equidistant from the CR. The CR for each cannon measured from RFT is listed below.

	FH70	M199
CR, mm, RFT	994.8	1054.1
CR, in, RFT	39.16	41.50

Table X compares entries on each inspection sheet relative to the respective CR to see which entries, if any, are common to both cannons.

TABLE X. INSPECTION SHEET ENTRIES ADJUSTED TO CR

FH70		M199	
Distance RFT, mm	Distance, CR, mm	Distance, RFT, mm	Distance, CR, mm
996	1.2	1056.6	2.5
1006	11.2	1060.4	6.4
1016	21.2	1066.8	12.7
1020.2	25.4	1092.2	38.1

One sees that no entries are identical, but two positions (996-1056.6 and 1006-1066.8) are within two millimeters of each other.

In addition to matching distances from the CR, one needs to compare wear from the same starting diameter, since wear/round is not linear past a certain barrel diameter as illustrated in Figure 2 for the M199 cannon firing XM203E2 charges. For this reason, wear data from the M199 cannon starting with tube round number 521 will be the starting point for comparing wear between the two cannons.

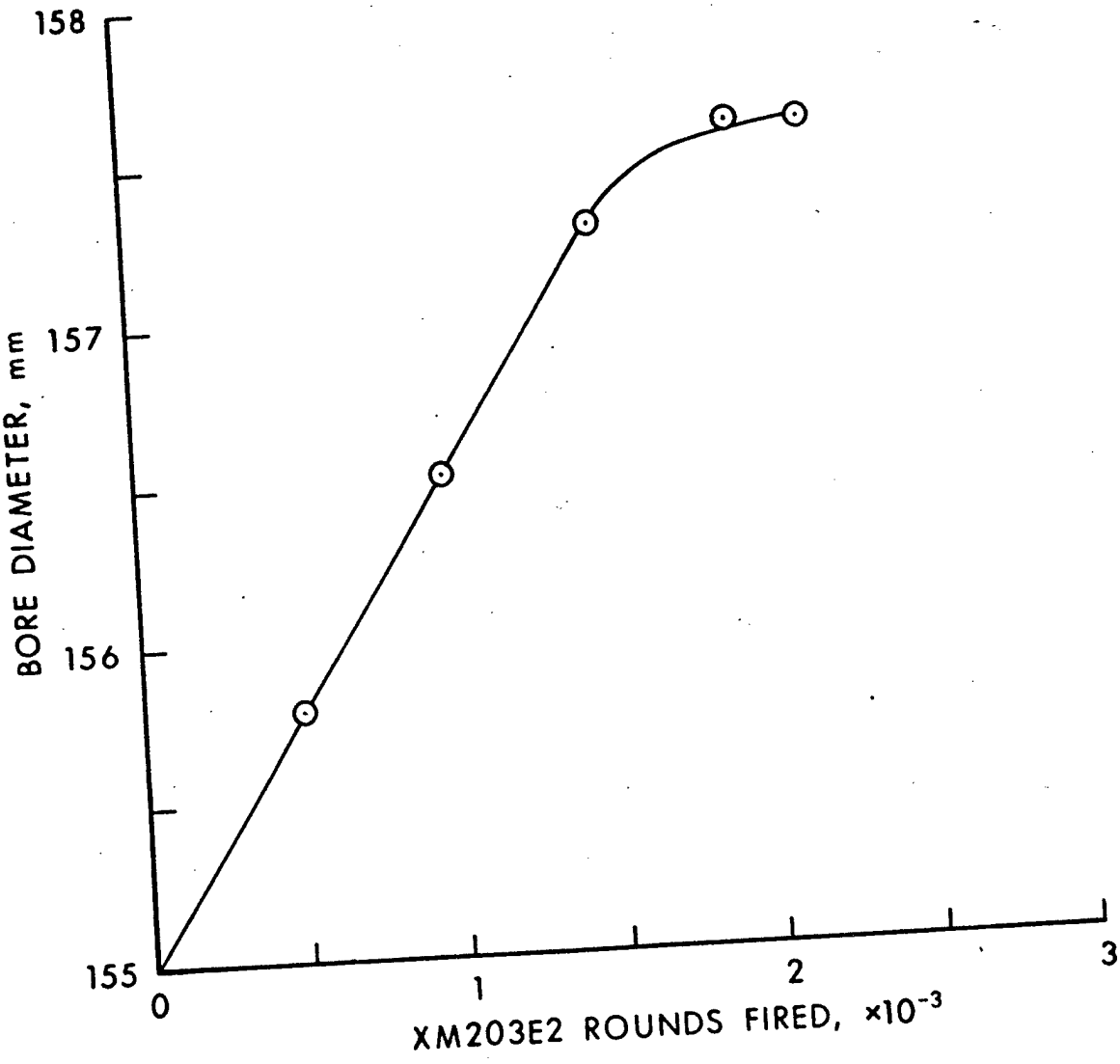

Figure 2. Bore Diameter at 1057 mm RFT vs XM203E2 Rounds Fired

Tables XI and XII collect pertinent wear data from the FH70 and the M199 cannons from which relative erosivity of the cartridge 3 and XM203E2 charges will be determined. Figures 3 and 4 are plots of wear vs zone 8S rounds fired. In both instances, the FH70 wear seems somewhat greater than the M199 wear firing the XM203E2 charges which seems to corroborate the prediction from the heat input measurements.

So far no distinction has been made between the XM203E2 and the M203 charge regarding wear. The M203 is identical to the XM203E2, save for a higher melting point wax in the TiO_2-wax additive to preclude unburned residue being left in the chamber.[14] Calspan heat input measurements were equivalent for the two charges

TABLE XI. VERTICAL LAND DIAMETERS FOR FH70 (996 MM RFT) AND M199 (1057 MM RFT)

FH70[a]				M199[b]			
Tube Rd No.	Cart. 3 Rd	Diameter, mm	Wear, mm	Tube Rd No.	XM203E2 Rd[c]	Diameter, mm	Wear, mm
951	-----	156.07	-----	521	-----	155.79	-----
1458	507	156.98	0.91	1000	469	156.52	0.73
1992	1041	157.56	1.49	1527	976	157.29	1.50
2457	1506	158.16	2.09	2001	1430	157.59	1.80
3047	2096	158.63	2.56	2235	1654	157.59	1.80

a - Wear measured 11.2 mm from CR.
b - Measurement 12.7 mm from CR.
c - Excluding Zone 7 M4A2 rounds fired for precision.

TABLE XII. VERTICAL LAND DIAMETERS FOR FH70 (1006 MM RFT) and M199 (1067 MM RFT)

FH70[a]				M199[b]			
Tube Rd No.	Cart. 3 Rd	Diameter, mm	Wear, mm	Tube Rd No.	XM203E2 Rd[c]	Diameter, mm	Wear, mm
951	-----	155.95	-----	521	-----	155.64	-----
1458	507	156.92	0.97	1000	469	156.40	0.76
1992	1041	157.42	1.47	1527	976	157.11	1.47
2457	1506	158.14	2.19	2001	1430	157.51	1.87
3047	2096	158.38	2.43	2235	1654	157.54	1.90

a - Wear measured 1.2 mm from CR.
b - Wear measured 2.5 mm from CR.
c - Excluding Zone 7 M4A2 charges fired for precision.

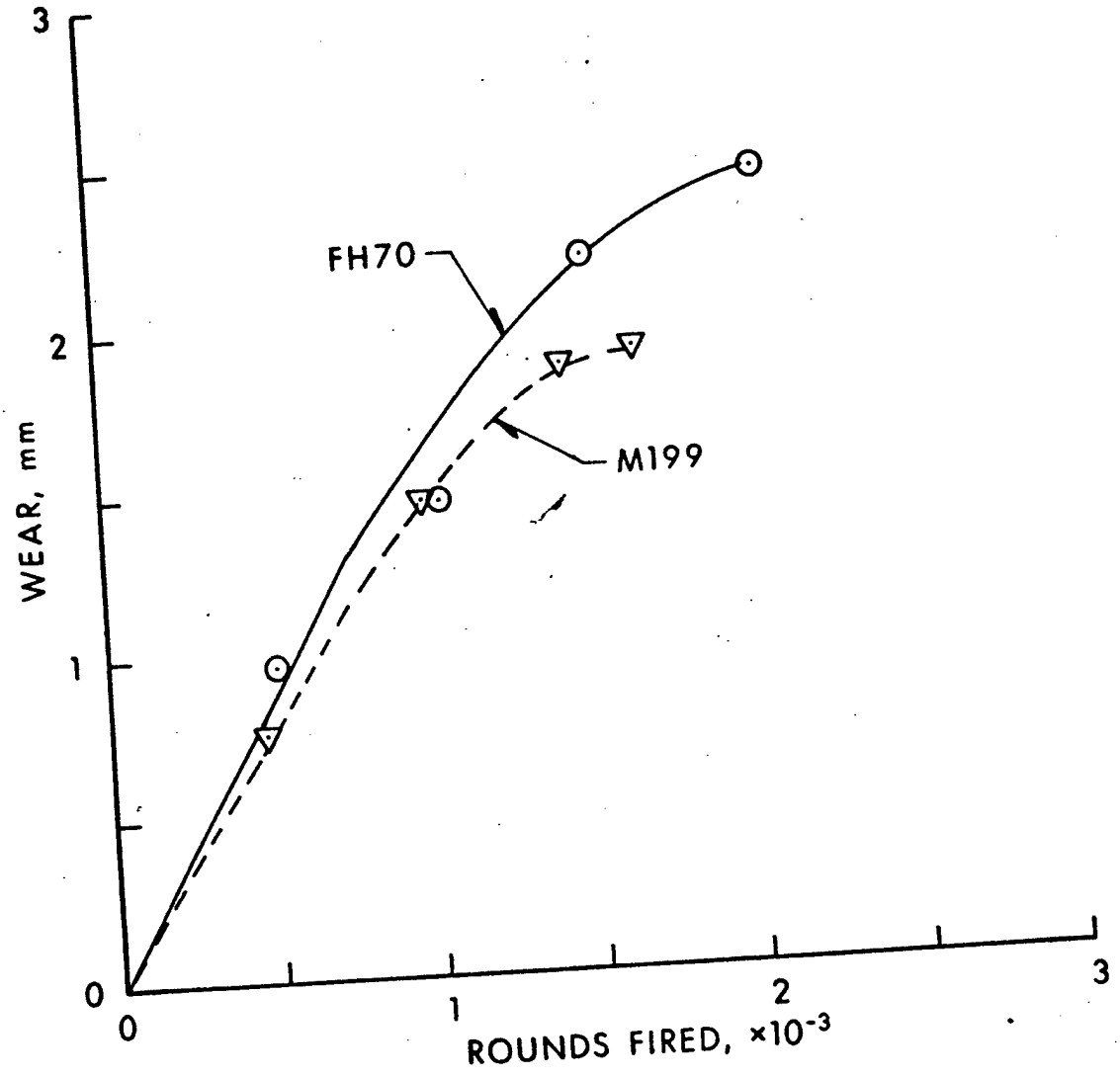

Figure 3. Wear vs Zone 8S Rounds for FH70 (996 mm RFT) and M199 (1057 mm RFT) Cannons

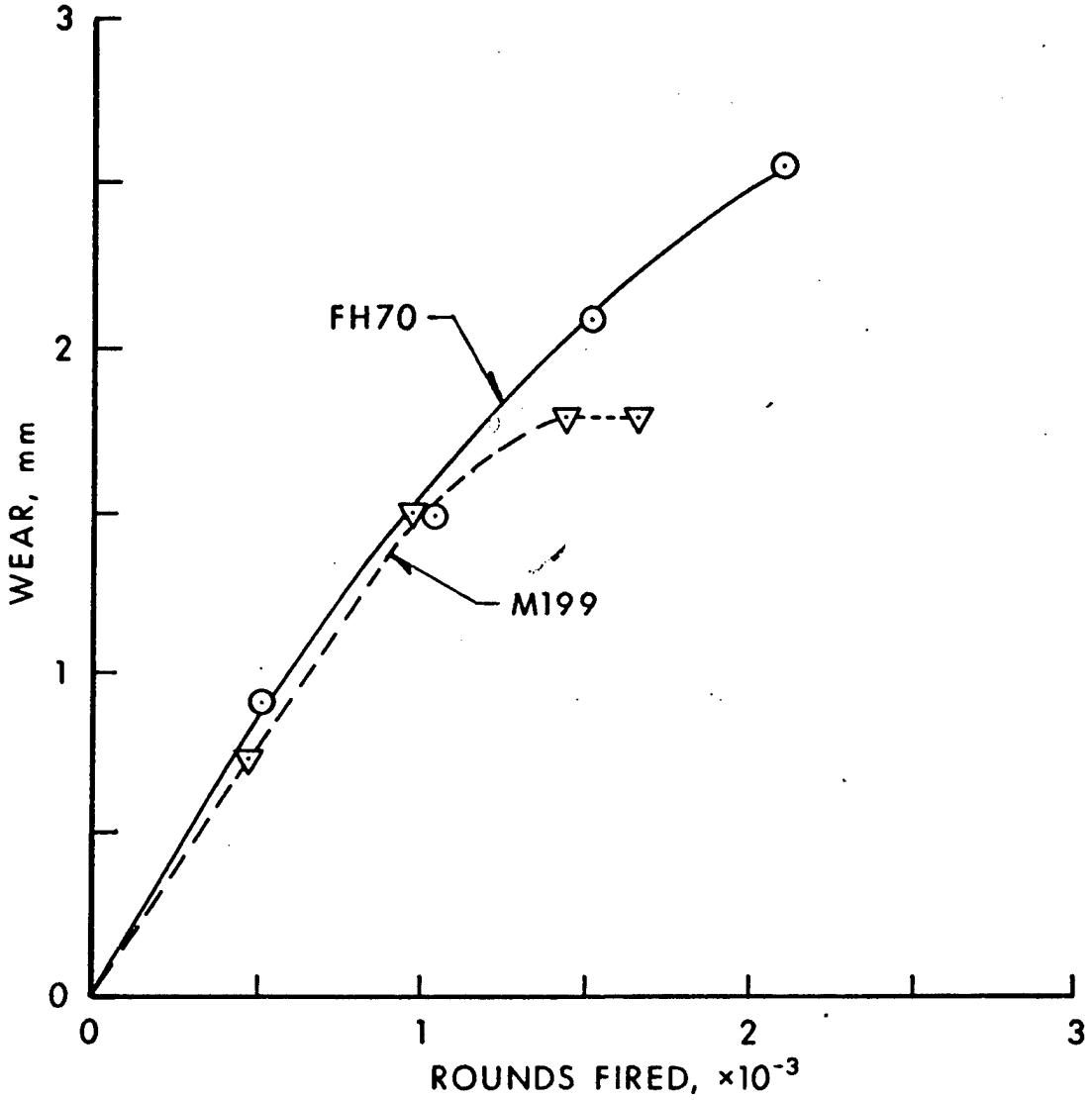

Figure 4. Wear vs Zone 8S Rounds for FH70 (1006 mm RFT) and M199 (1067 mm RFT) Cannons

implying the new wax did not change the wear appreciably.[15] Recently, a wear test was fired with the M203 charges for which data at 6.4mm CR are available.[16] Table XIII collects wear from this test along with data for the XM203E2 charge. Figure 5 is a plot of wear vs zone 8S rounds fired which suggests the M203 and XM203E2 wear the M199 cannon equally.

The above analysis of wear data corroborates the heat transfer data by Calspan, as well as reinforces the assumption by Nordheim that stick propellant is inherently more erosive than granular propellant based on the hydrodynamics of the flow. This contention was given further support recently when Horst[17] used the NOVA code to compare the interior ballistics of the M203 and XM208 charges. The results showed that most of the unburned stick propellant remains in the chamber in contrast to the granular propellant which is evenly distributed behind the projectile. Peak bore surface temperature in the CR region for the XM208 charge was 300K higher than the M203 charge. A calculation was also performed with stick M31E1 propellant, in place of stick M30A1 which showed that the peak temperature of the stick charge was still higher than the granular charge, despite the reduction of 400K in flame temperature by use of the M31E1 propellant in place of M30A1 propellant.

CONCLUSIONS

1. Examination of heat transfer data collected by Calspan and BRL shows the heat input from the XM208 charge without additive is 13% greater than the XM203E2 charge without additive in the commencement of rifling region in accord with Nordheim's assumption that erosion is greater for stick propellant.

2. The 155 mm zone 8S cartridge 3 charge with cordite N stick propellant and a polyurethane foam liner appears to be at least as erosive as the M203 charge based on analysis of wear data from the FH70 and heat input measurements by Calspan Corp.

3. The wear in the 155 mm M185 and M199 howitzers is the same for the XM201E5 charge. Hence, the different forcing cone design in the two cannons does not affect wear.

TABLE XIII. COMPARISON OF WEAR BETWEEN M203 AND XM203E2 CHARGES

Tube Rd No.	Diameter, mm	Wear, mm	M203 Rd	Tube Rd No.	Diameter, mm	Wear, mm	XM203E2 Rd
1	155.02	----	1	1	155.00	0	1
257	155.22	0.20	245	521	155.69	0.69	1501
502	155.71	.69	478	1000	156.45	1.45	970
752	156.18	1.17	716	1527	157.16	2.16	1477
1002	156.46	1.45	954	2001	157.51	2.51	1931
1252	156.84	1.83	1192	2001	157.51	2.51	1931
1520	157.17	2.16	1448	2235	157.57	2.57	2155
1871	157.45	2.44	1787				

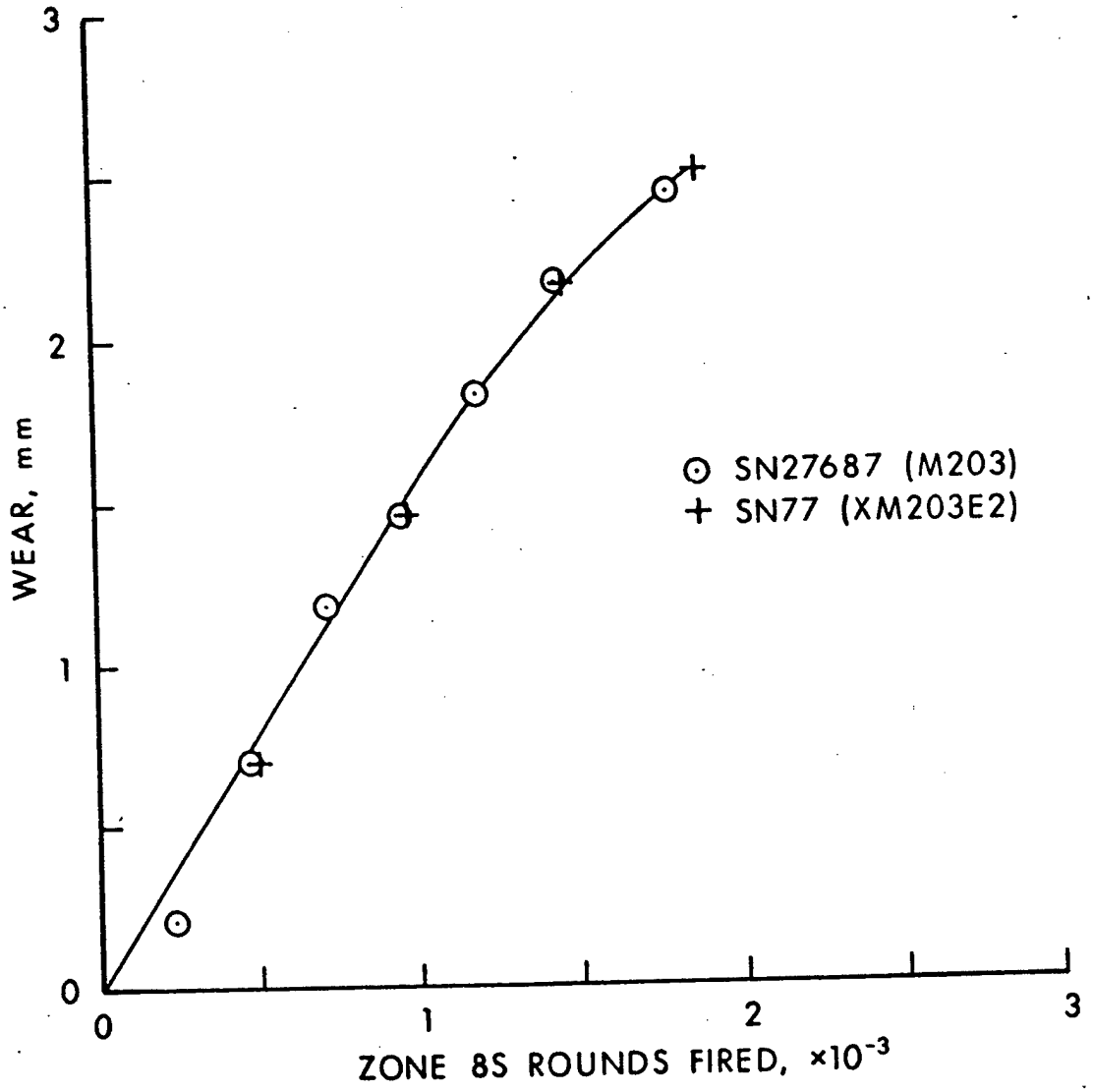

Figure 5. Comparison of Wear for XM203E2 and M203 Charges

REFERENCES

1. "Hypervelocity Guns and the Control of Gun Erosion", Summary Technical Report of Division 1, National Defense Research Committee, Washington, DC, 1946.

2. L.W. Nordheim, H. Soodak, and G. Nordheim, "Thermal Effects of Propellant Gases in Erosion Vents and Guns", NDRC Armor and Ordnance Report No. A-262, March 1944.

3. F.A. Vassallo, "An Evaluation of Heat Transfer and Erosion in the 155-mm M185 Cannon", Calspan Technical Report No. VL-5337-D-1, July 1976.

4. J.R. Ward and T.L. Brosseau, "Effect of Wear-Reducing Additives on Heat Transfer Into the 155-mm M185 Cannon", BRL Memorandum Report No. 2730, February 1977 (AD A037374).

5. "Evaluation of Cannon Tubes", Dept. of the Army Technical Manual TM-9-1000-202-14, November 1976.

6. F.A. Vassallo, "Mathematical Models and Computer Routines Used in Evaluation of Caseless Ammunition Heat Transfer", Calspan Report No. GM-2948-Z-1, June 1971.

7. T.L. Brosseau, "An Experimental Method for Accurately Determining the Temperature Distribution and Heat Transferred in Gun Barrels", BRL Report No. 1740, September 1974 (AD B000171L).

8. "Technical Evaluation of FH 155mm Mod 70 (FH70), Wear Life Determination (Test Series Nr 385, Part II)", July 1973 and Addendum, November 1975 (German).

9. T.G. Hughes, "DT II Test of Propelling Charge, XM201E5", APG Firing Record P-82646, APG, MD, July 1977.

10. R.P. Grepps, "Final Report on Product Improvement Test of Ammunition Additive Effect on M41 and M68 Gun Tube Life", DPS Report No. 1520, APG, MD, December 1964.

11. S.W. Kang and J.L. Levitan, "Surface Heating Due to a Turbulent Boundary Layer Flow", Numerical Methods in Thermal Problems, Vol. II, p. 1235, R. Lewis, K. Morgan, and B. Schreffer, Eds., Pineridge Press, Swansea, UK, 1981.

12. A.C. Buckingham and W.J. Siekhaus, "Simulating Interactions Between Turbulence and Particles in Erosive Flow and Transport", Numerical Methods in Laminar and Turbulent Flow, p. 929, C. Taylor and B. Schreffer, Eds., Pineridge Press, Swansea, UK, 1981.

13. J.D. Kruger, "DT II of Howitzer, 155mm, Towed, XM198 (Tube Wear Phase with the XM203 Propelling Charges)", YPG Firing Report No. 13703, March 1977.

14. D.S. Downs and L.E. Harris, "Relationship of Residue Formation to Wax Used in H203 Propelling Charge Liner", ARRADCOM Tech Report ARLCD-TR-79042, December 1979.

15. D.S. Downs, J.A. Lannon, and L.E. Harris, "Prediction of Wear Characteristics of Artillery Propelling Charges", ARRADCOM Technical Report ARLCD-TR-80016, March 1981.

16. J. Whitcraft, "Product Validation Test - Government (PVT-G) of Howitzer, Medium, Towed, 155mm M198", MTD Report No. 5403, July 1980.

17. A.W. Horst, "A Comparison of Barrel-Heating Processes for Granular Stick Propellant Charges", BRL Memorandum Report No. 3193, August 1982.

A CRITICAL EXAMINATION OF THE CONCEPT OF WORN GUN CHARGE ASSESSMENT

B. Z. Jablovskis and J. S. O'Brasky
Naval Surface Weapons Center
Dahlgren, Virginia

ABSTRACT

When it became necessary to change the propellant granulation in the assembly of a service round of shipboard ammunition, problems arose in the assessment of a lot of propellant for the new assembly. Causes for the problems were ascertained and a modified procedure was devised as a "quick fix" for the assessment of this assembly. When other assemblies for other calibers exhibited similar assessment problems, the theories and practice of propellant evaluation were closely examined. A new procedure was developed and approved. Subsequent tests have shown tremendous success with the new procedure.

BACKGROUND

From 1948 to 1976, the U.S. Navy followed a worn gun assessment procedure. This procedure is specified in MIL-P-22314. The worn gun charge assessment technique was developed during World War II when it was realized that a single gun charge assessment technique was producing variable results and that new guns might not always be available.

The basic scheme involved establishing the muzzle velocity vs charge weight relationship for a given test and master propellant at two stages of erosion life, nominally first and third quarter. A minimum of two gun barrels was thus required for 8" caliber or greater and four guns were used for less than 8" guns, two guns for each erosion stage whenever possible. At each stage of gun life, an average matching charge was estimated to produce the same velocity performance as the master round in the same worn gun on the same day. The worn gun matching charge weights and velocity loss points were then used as data points in a charge weight, velocity loss space. A curve of specified form was forced through this data and extrapolated to zero velocity loss, i.e., new gun performance, to produce the assigned charge weight for a given lot.

Over the years, the worn gun charge assessment procedure was used for propellants of significantly different relative quickness, flame temperatures, and compositions. In theory, as long as one was dealing with small differences in these parameters, accurate results should have been attained. When a test propellant of significantly different ballistic characteristics was assessed against the master propellant, accuracy severly deteriorated.

In 1971-1972, as a result of a malfunction investigation[1], it was determined necessary to change the propellant composition and grain geometry in the reduced charge for the 8"/55 Caliber Guns, MARK 16 (case), to eliminate shock waves to the projectile which were causing close aboard prematures. Firing tests were conducted in an instrumented 8"/55 caliber case gun using six different compositions

Approved for public release; distribution unlimited

and grain geometry combinations of propellant in the inventory at that time and the normal primer and case. The instrumented barrel has piezoelectric gauge ports at the cartridge case mouth position, ahead of the projectile rotating band to measure forces acting on the projectile during its travel in the barrel, and six inches aft of the muzzle to obtain muzzle signature pressure. In addition, there were two piezoelectric gauges in the base of each cartridge case. In addition, to obtain data on 8"/55 projectile response during the early-time gun environment, four instrumented 8"/55 projectiles were fired as part of the test program.

Instrumentation consisted of piezoelectric pressure gauges and accelerometers mounted in the projectile base, which were monitored via the "hardwire" technique.[2] Velocity was measured by induction coils. All propelling charges were pre-conditioned to +90 $\pm$ 3°F which is Navy baseline temperature.

An extensive review was undertaken of all pressure-time profiles, the analyses of the shock spectra results, and all other generated data. Consideration of all parameters resulted in the selection of the 6"/47 caliber pyro granulation/composition as the "best available" propellant to eliminate the pressure wave anomaly in the reduced charge assemblies for the 8"/55 caliber case guns.

DISCUSSION

ORIGINAL PROCEDURE. Following the selection of the 6"/47 propellant for the 8"/55 replacement reduced charge, a charge assessment was conducted in accordance with MIL-P-22314 as summarized below:

a. Two guns were selected having a known difference in mean muzzle velocity of about 50 f/s (when firing the master propellant for the reduced charge) and which had exhibited no unusual velocity performance.

b. The propellants used in ballistic testing for determination of charge weight were preconditioned at 90°F for at least seven days immediately prior to firing and were maintained at a temperature as close as possible to 90°F during charge assembly, transporation, etc., prior to firing. Projectiles were inert loaded to the specified weight and all assembled rounds used in the charge assessment contained no more than one lot number of any single component such as case or primer.

c. The number of firing days (occasions) equalled the number of guns used (in this case two guns = two firing days).

d. For the particular reduced charge in question, there are no established velocity and pressure vs charge weight slopes. The firing scheme used required that on each occasion's firing, three rounds of the test powder be fired with charges estimated to produce approximatley 75% of the intended muzzle velocity, three appropriate master charges, four test propellant rounds with charges estimated to match the master velocity mean within 20 f/s, and one test charge estimated to yield a velocity exceeding that of the master by 100 f/s.

Since a pressure differential was expected between the master propellant and the test propellant, the master and test groups were fired in sequence rather than in matched pairs with one of the test rounds serving as a conditioning and probing round. Muzzle velocity and maximum breech pressure were taken with induction coils and copper crusher gauges, respectively.

Since a velocity-quickness (i.e., a propellant effect which determines rate of velocity loss with gun erosion) difference exists, a least squares line was fitted to the velocity vs matching charge "of the occasion" for both guns to obtain a "quickness corrected" assigned charge. This fitted curve was then extrapolated to the "average new gun condition", i.e., zero velocity loss.

The results of this powder proof together with the results of a validation firing in a new gun are shown in Figure 1 as the original procedure. The quickness corrected charge clearly did not give the performance anticipated in a new gun. Verification firing of the assigned charge weight in a new gun indicated that the desired velocity of 2220 f/s was not obtained; instead a velocity of 2145 f/s was realized. Needless to say, the performance illustrated in Figure 1 was completely unacceptable.

What happened that could have caused such an inaccurate determination of an assigned charge? What changes must be made to the firing scheme and/or analyses procedures in order to determine an accurate charge which would produce the nominal new gun velocity for this assembly in a new gun?

First things first. A valid charge had to be determined so it could be loaded and issued to the Fleet.

MODIFIED PROCEDURE. Following the validation firing, a total of 35 rounds fired from four different guns in three different states of wear with six different charge weights was available for analysis. It was known that the new reduced charge produces a pressure-time-travel relationship which is grossly different from that produced by the previous 8"/55 reduced propelling charge. It was also known from the powder proof conducted in accordance with MIL-P-22314 that the new reduced charge would exhibit quite different velocity loss characteristics. Since all previous propelling charges including the master propellant are no longer service acceptable because of the ballistic forcing functions generated therein, it was decided that no attempt would be made to match their velocity loss characteristics in that such a match can be achieved at only one point in the wear life of the weapon.

Based upon these factors, the objective assigned to the interim charge assessment method was that for all individual guns, the new or unworn gun muzzle velocity should be 2220 $\pm$ 10 f/s with 8" projectiles weighing 260 pounds at the assessed charge weight.

An additional firing program was conducted in another new gun to avoid extrapolation to "new gun condition." The program consisted of firing four data rounds at the previously estimated charge and four data rounds at a charge estimated to produce approximately 2230 f/s. See Figure 1 (Liner S/N 1132.) A linear least squares relationship was calculated for the velocity vs charge weight data from new guns, Liners S/Ns 1059 and 1132. Using this relationship (the modified procedure on Figure 1), it was determined that the nominal new gun velocity of 2220 f/s would require a charge weight of 52.03 lbs of 6"/47 caliber propellant Lot SPDN-8291. The propellant lot was assembled into the reduced charge assembly and issued to the Fleet. There have been no problems reported to date.

COMPARATIVE ERROR ANALYSES. The failure of the original procedure of MIL-P-22314 to produce an accurate determination of the charge weight of SPDN-8291

8"/55 CALIBER GUN, MARK 16 REDUCED CHARGE

VELOCITY VS CHARGE WEIGHT

MODIFIED PROCEDURE - - - - - - -

ORIGINAL PROCEDURE ———————

POWDER: SPDN-8291 (6"/47)
ASSIGNED CHARGE: 52.03 LB.

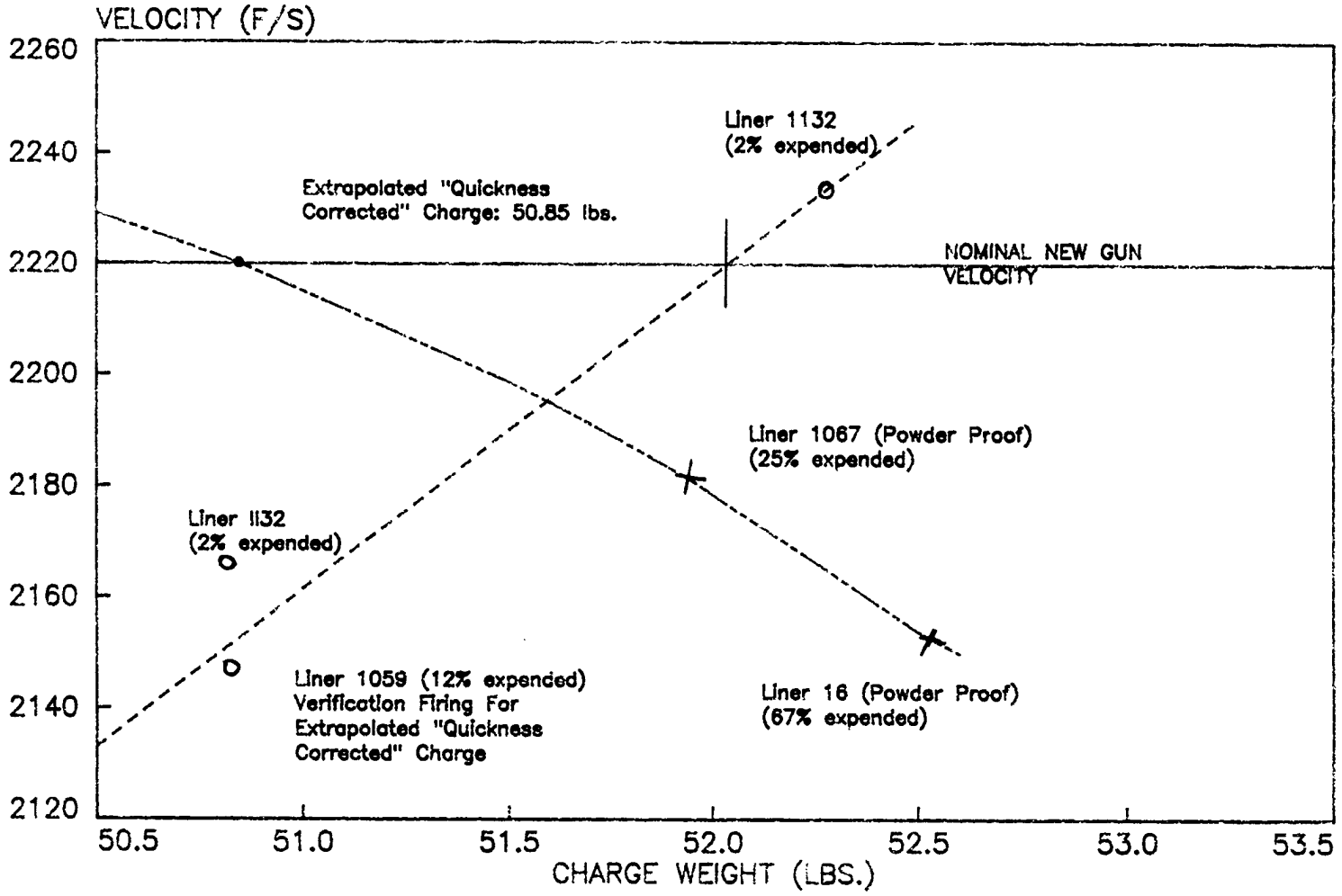

FIGURE 1

required for the replacement 8"/55 reduced charge demands explanation. Similarly, the modified procedure finally used to assess that charge must be shown to be more significantly accurate to justify its application. An analyses was therefore undertaken to examine the sources and magnitude of error in each procedure. Standard statistical techniques were employed to establish confidence means and slopes where required. These techniques are documented in references (3) and (4).

The "matched powder" method of propellant proof which is the basis of the procedures of most proof methods carries within it the implicit assumption that the master propellant at its assessed charge weight provides nominal new gun performance in an unworn gun. If the master propellant has changed in performance it is assumed that all service propellants have also changed in the same manner. The fallacy in this argument is that the master propellant must be check fired periodically in unworn guns to determine its performance and this is not always done. The effect of an undetected change in master propellant performance can have a decisive effect upon the assessed charge weight for the test propellant. If the actual velocity performance of the master propellant is less than expected, then, on the matching charge vs velocity plane, the actual velocity loss for the test guns will be over estimated which will result in an abnormally low "quickness corrected" charge weight when extrapolated to zero loss. If the actual velocity performance of the master exceeds the nominal velocity in a new gun, the reverse will result.

Another source of possible error in assessment is the interpretation of "Fit a straight line to the velocity versus charge weight results." The subsequent reference in MIL-P-22134 to a least squares operation at another step in the analysis would lead one to believe that in the analysis of the individual firing data, least squares regression is not required. In actuality, the procedure used for many years has required that the arithmetic average of the muzzle velocities be taken at each charge weight (two rounds at 75% service velocity and five rounds at near-service velocity only) and that a straight line be drawn through these two points and then extended until it intercepts the "velocity of the occasion" established by the firing of the master propellant. The charge weight of the test powder corresponding to that intercept is designated the matching charge.

To perform an error analyses on this technique, it is necessary to establish the confidence with which each mean is established, remembering that the low velocity mean is based on a sample size of two rounds per firing while the near-service mean is based upon at least four rounds (usually five). Thus, for each firing, 95% confidence limits can be assigned to the matching charge. These confidenced matching charges can then be used to extend the error analyses to the velocity loss versus matching charge plane to determine the error range for the "quickness corrected" charge in the new gun condition. By this process, at 95% level of confidence, it was determined that the "quickness corrected charge" required to match the Master could have been anything between 50.25 lbs and 52.60 lbs whereas the assessed was 50.85 lbs.

In the particular case of the attempted powder proof on the replacement 8"/55 reduced charge, the master propellant, SPDN-9836, was firing 35 f/s below its nominal velocity performance in a new gun (Liner S/N 1132). Depot loaded charges fired during the malfunction investigation were also performing below standard. The result was the assessment of an artificially low quickness corrected charge weight. A perfectly executed powder proof under the provisions of MIL-P-22314 would give a

"quickness corrected" charge range of 2.35 lbs at a 95% level of confidence in this particular case.

The error in charge assessment of the modified procedure was also established. It was noted that the method used to determine the replacement 8"/55 reduced charge assignment has several outstanding characteristics:

a. Two new guns were used, therefore eliminating the need to extrapolate to the new gun condition.
b. Two charge weights were used giving muzzle velocities which bracketed the desired performance, thus eliminating another extrapolation.
c. At each charge weight, a sufficient sample size was obtained to allow confidence in the means established.
d. A linear least squares regression was then used to establish the muzzle velocity vs charge relationship for the new gun condition.
e. The velocity to be matched was the nominal new gun velocity an absolute quantity, rather than the day-to-day performance of the master propellant which was of a different granulation than the test propellant.

The correlation coefficient calculated for the least squares line was R = .9657. The percentage of the variance removed by the regression line is 93.26% by analysis. This result indicates that the assumption of a linear relationship between charge weight and muzzle velocity is not unreasonable in this case.

Analyses[1] at the 95% level of confidence indicates that the charge weight assessed by the modified procedure is 52.03 $^{+.15}_{-.11}$ lbs.

Another way to look at this result is that 95% of all sample mean muzzle velocities obtained with 52.03 lb of SPDN 8291 when fired in a new 8" MARK 16 MOD 1 liner with 260 lb. 8" MARK 25 projectiles will fall within 7.5 f/s of the nominal new gun velocity, 2220 f/s.

ADDITIONAL TESTS. The Navy occasionally conducts firing tests as a part of the propellant surveillance program to determine actual gun performance in addition to the laboratory tests normally performed.

5"/38 Caliber Guns. In January 1972, a surveillance firing test was conducted on 19 lots of Navy Cool (NACO) propellant. This composition of propellant had been hastily introduced into the Fleet in this caliber in 1969 for its reduction in gun wear characteristics; NACO has a flame temperature of approximately 2250°K where previous compositions for this caliber are 2550°K. The propellant lots had been assessed in accordance with the procedures and aceptance criteria of MIL-P-22314 (original procedure as discussed in 8"/55 section) and matched against a master propellant of another composition (PYRO), the only one available. The firing test for the surveillance test was conducted on three different days in one new gun (proof series only) and no master was fired for comparison or gun ballistic level per event. A total of ten rounds from each of the 19 propellant lots were locally assembled and fired. Figure 2 is a plot of the Nominal New Gun Velocity (NNGV) minus the Test Propellant Mean Velocity ($\overline{TPV}$) vs the propellant lot in order of manufacture. Note that the range of differences in the velocity means is 88 f/s (53 f/s and -35 f/s) for the 19 lots! It is felt that some of this significantly large range may have been reduced by matching against the Master used in the assess-

5"/38 NACO PROPELLANT SURVEILLANCE

Nominal New Gun Velocity Minus Test Propellant Mean Velocity vs. Propellant Lot

____Represents mean of 10 rounds
-----Break in time of manufacture

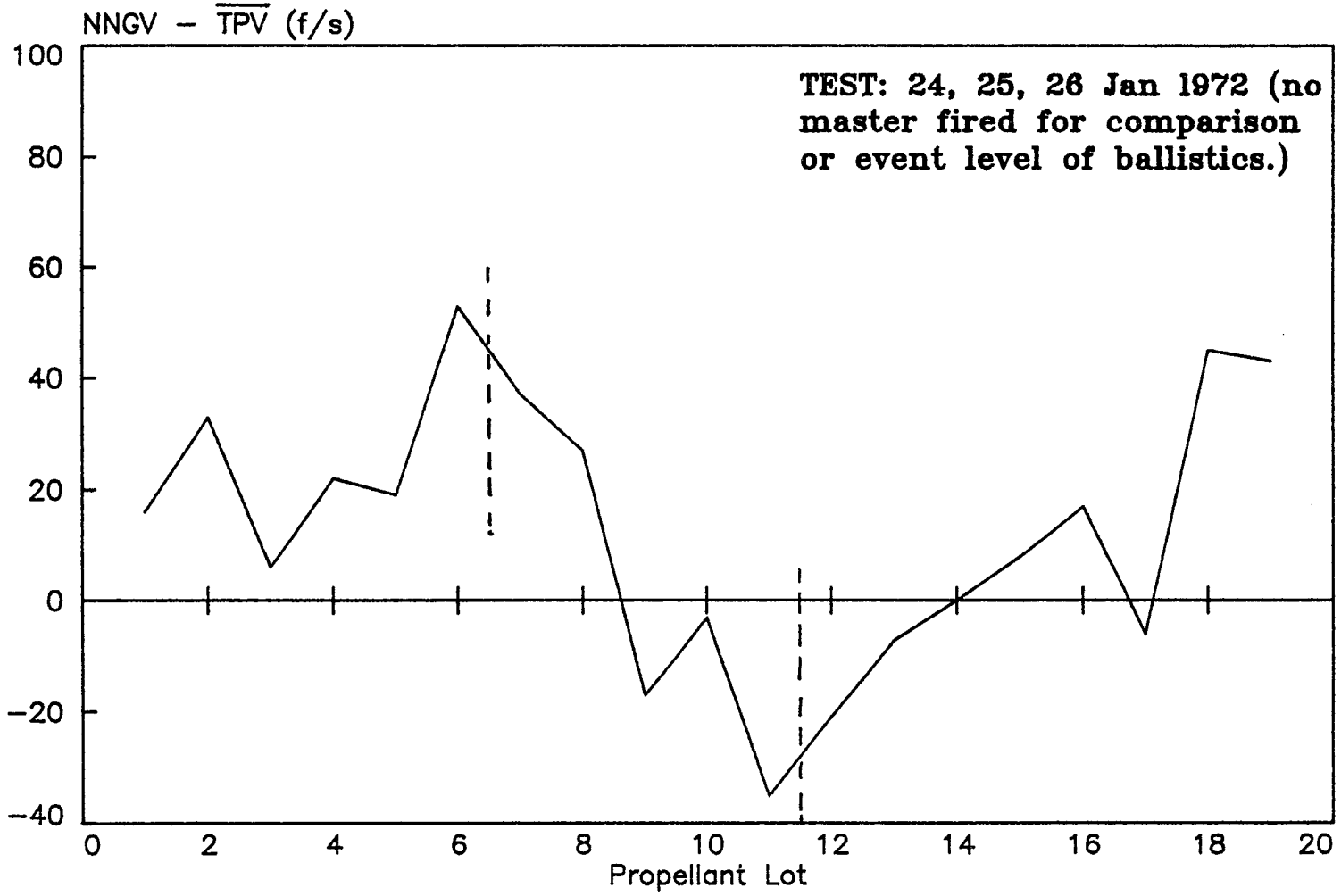

VL-512

Figure 2

ments. This propellant composition is no longer used in this caliber because of an adverse primer-propellant relationship (shock waves) which was discovered in 1974. No surveillance firing test has been conducted in this caliber since 1972.

5"/54 Caliber Guns. In June 1973, a surveillance firng test was conducted on 15 lots of NACO propellant. This composition of propellant had been hastily introduced into the Fleet in this caliber in 1967 for the same reasons mentioned for the 5"/38 NACO propellant. Nine of the 15 lots were assessed against a Master propellant of different composition (PYRO) and six lots were assessed against a NACO Master propellant. All 15 lots were assessed in accordance with the procedures and acceptance criteria of MIL-P-22314, "original procedure." Propellant from the first nine lots was received in depot loaded propelling charges (separated loading ammunition) and propellant from the latter six lots was received from bulk storage and locally loaded prior to firing. The test was designed to compare the performance of each propellant lot against the Master propellant it was assessed against. The Master was locally loaded. Ten rounds of each propellant lot were fired during the three day test and again the gun had only proof of barrel rounds fired prior to the test. The data are graphically presented in Figure 3. A significant lot-lot variation range of 66 f/s around the Masters was noted for all lots. The change in the Master propellant composition to the same as the test propellant significantly decreased the range between lots (21 f/s), but it was still greater than desired.

RESULTS

ACTION. As a result of the information presented in Figures 1, 2, and 3, funds were made available in Fiscal Year (FY) 1975 to revise MIL-P-22314 as recommended by reference (5). Applicable specifications, assorted test procedures and related documents were perused and discussed with knowledgeable personnel at a variety of DOD activities. Firing schemes (e.g., number and order of rounds, guns, temperatures, days, mounts, etc.), acceptance criteria, and analyses procedures were examined. Monte Carlo simulations were conducted to examine the reliability and confidence of a proposed charge estimator. A firing program was conducted to check-out the proposed procedure, the proposed analyses of data were performed, and the final assessed charge was test fired for verification. The velocity means produced by the "test propellant" assessed charge and the Master Propellant on that occasion differed by one f/s!

The proposed revision to MIL-P-22314 was submitted to the sponsor[6] and approved.[7] The new procedure has been used by the U.S. Navy since April 1976. As of 1 September 1982, a total of 40 lots of propellant spanning three calibers of guns has been assessed by the new procedure with very good results. Figure 4 is a graphical presentation of some of test results showing the decrease in lot-lot variation and difference of Master Propellant and test propellant mean velocities as Master and test propellant compositions changed and especially as the test procedure changed.

CURRENT PROCEDURE. The current procedure for evaluation of all U.S. Navy shipboard gun ammunition propellant lots is presented as Figure 5.

Master Propellant. Test lots of propellants are matched against a Master of the same composition and granulation. If there is no Master, then the Master rounds are obviously omitted from the firing scheme and the Nominal New Gun Velocity (NNGV)

5"/54 NACO PROPELLANT SURVEILLANCE

Master Propellant Mean Velocity Less Test Propellant Mean Velocity vs Propellant Lot

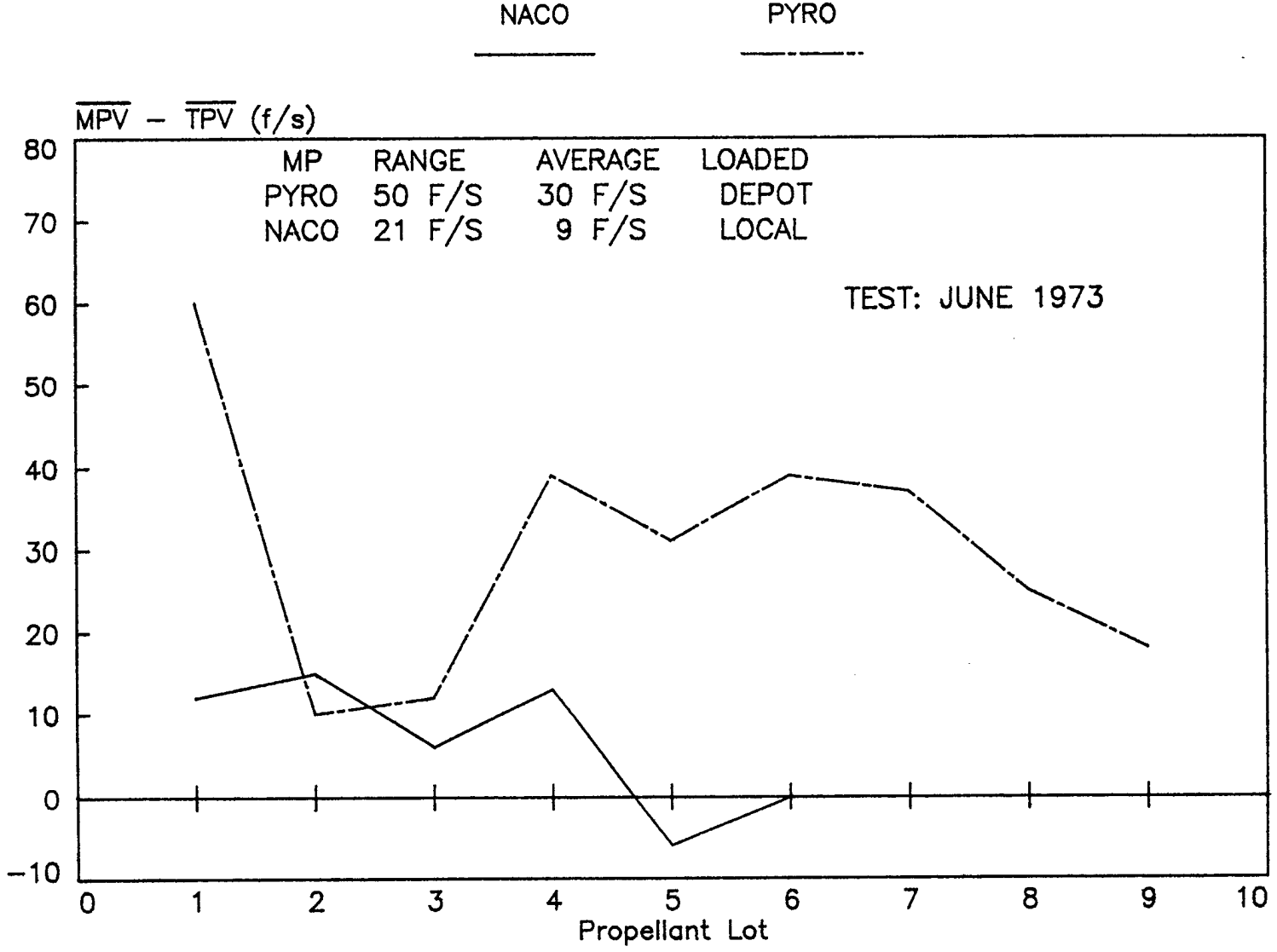

Figure 3

5"/54 CALIBER NACO PROPELLANT

Master Propellant Mean Velocity Minus Test Propellant Mean Velocity vs. Ammunition Lot

Old Pyro ..... Old NACO ——— — ——— New NACO ———

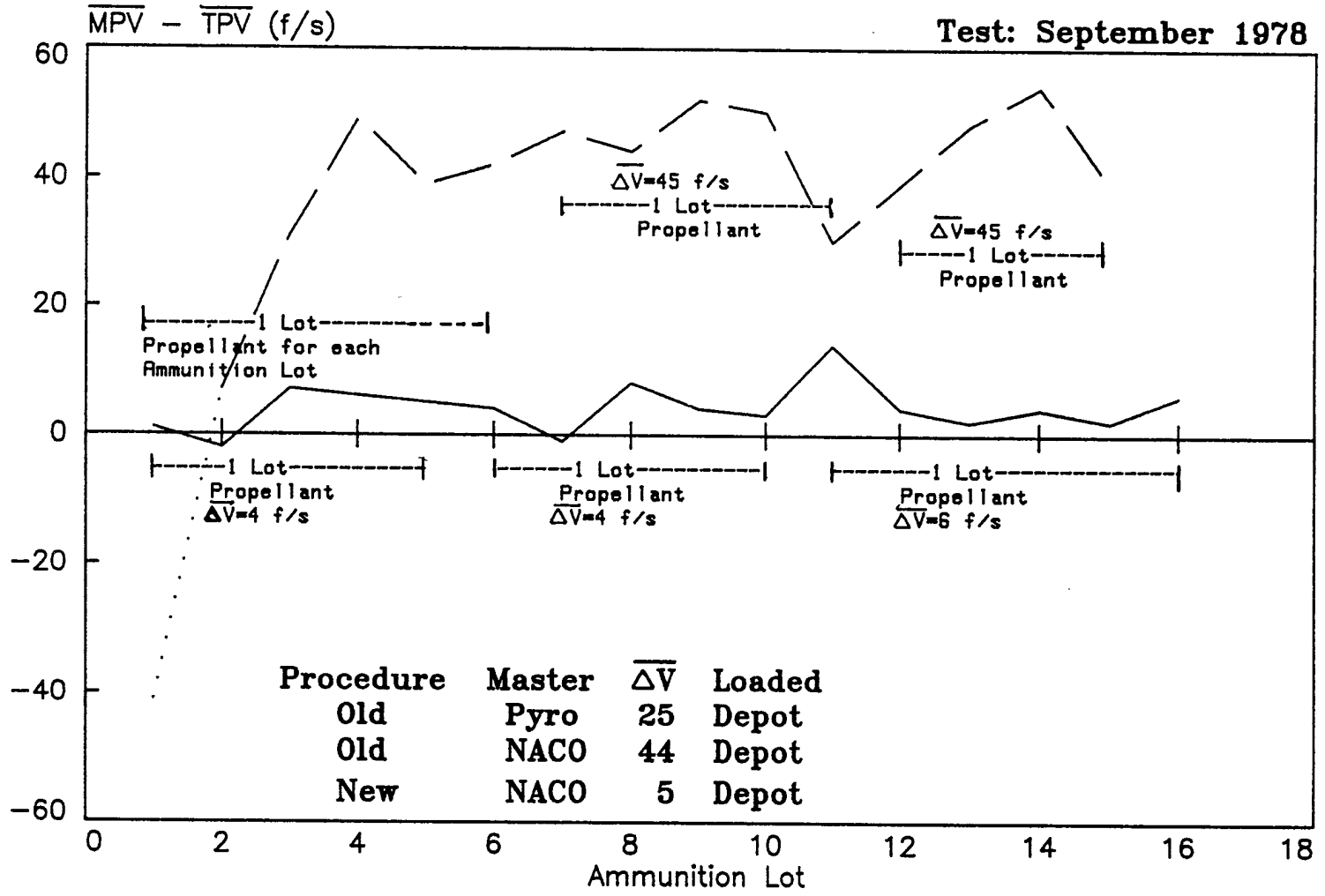

Figure 4

for the assembly is used instead in the analyses.

Guns. If there is a Master, the guns used shall not have a velocity loss greater than two and one-half % of the NNGV for the assembly. If there is no Master, the guns shall not have a velocity loss greater than one and one-half % of the NNGV for the assembly. No more than one gun shall be fired each day.

Mount. If the system has both an automatic and single fire mount, the tests shall be conducted in the automatic mount. Firing shall be in the single fire mode but the ammunition shall be automatically loaded into the gun barrel utilizing the mount hoist and ram mechanisms.

Instrumentation. Instrumentation must measure muzzle velocity (NSWC/DL uses a G.E. transceiver doppler radar, KU-band, mounted on the gun barrel) and maximum chamber pressure (NSWC/DL uses U.S. Navy copper crusher gauges). Ejection time is measured as backup information. The quantity of flash is measured by photocell, also as backup information.

Charges. An estimated charge for the test propellant lot, C_1, is determined either from a probing round firing test or from the combination of test experience and chemical/closed bomb/geometrical information provided for each lot by the propellant manufacturer (Powder Description Sheet Data). This charge is estimated to produce Master velocity or NNGV. Determine two extreme charges for the test propellant. Charge C_2 is a charge estimated to produce a velocity approximately 50 f/s less than charge C_1. Charge C_3 is a charge estimated to produce a velocity approximately 50 f/s greater than charge C_1. Charges C_2 and C_3 should result in a velocity range of approximately 100 f/s for the test instead of the approximate 600 f/s for full service charge lots by the former procedure. Charges C_2 and C_3 also should bracket the Master velocity or NNGV thereby eliminating the need to extrapolate in each gun.

Firing Tests. The firing scheme for each gun is presented on the right of Figure 5. Charge groups C_2 and C_3 should be randomized for each gun. If there is a Master, the Master should be randomized with the C_1 charge. The first round of the day is considered to be a warming round and as such is not used in the analyses of data. The first four groups (three if there is no Master) of the firing scheme shall be fired. The linear least squares velocity vs charge weight relationship for the test propellant (TP) shall be calculated. The data from all of the TP rounds shall be used, thereby eliminating round off to means. If there is a Master, calculate its mean velocity ($\overline{MPV}$). Substitute the $\overline{MPV}$, or the NNGV if there is no Master, in the Velocity vs Charge Weight linear fit and determine the estimated charge weight (TPMC) for the TP required to match the $\overline{MPV}$ or NNGV. Assemble and fire four rounds (first round is a warming round and not used in data analyses) with the TPMC. Calculate the mean velocity for the MC rounds ($\overline{TPMCV}$) and determine its difference (Δ) from the $\overline{MPV}$ or NNGV. Repeat the above process for each of the remaining three guns.

Assessed Charge. To determine the assessed charge (AC) for the TP, solve the statistically weighted formula presented in Figure 5. MC_i is the test propellant matching charge for each gun and Δ_i is the difference in the velocity produced by the test propellant matching charge and the Master or from the NNGV. If the Δ for any gun is determined to be zero, replace the zero with a one.

PROPELLANT EVALUATION
VELOCITY VS CHARGE
EACH OF 4 BARRELS

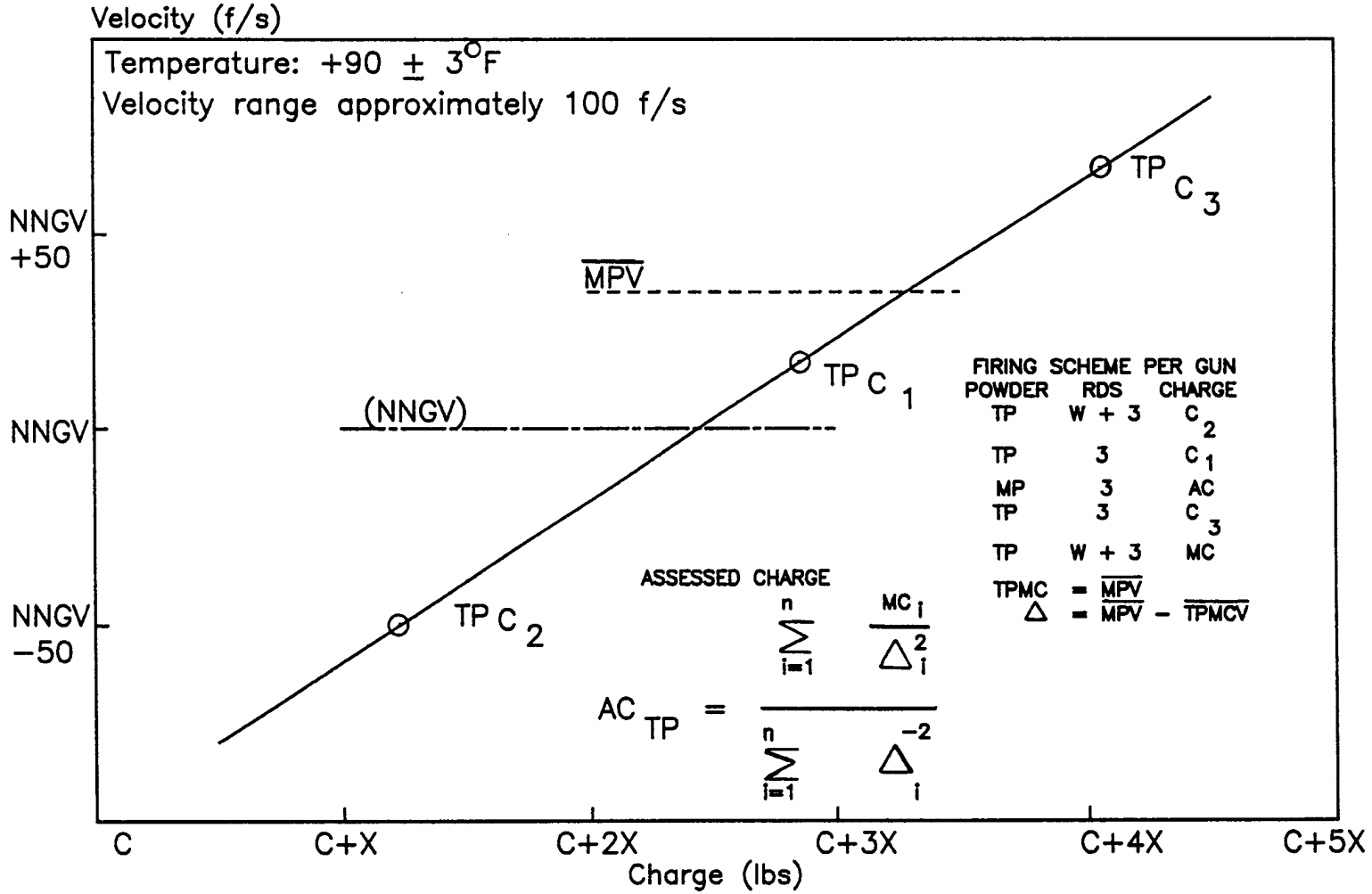

Figure 5

Validity. The validity of the assessed charge shall be determined by a firing program in any of the guns used in the assessment. The program shall consist of five or 10 rounds each of the Master and each lot evaluated (depends on caliber). The rounds, including the Master, shall be randomized to eliminate any gun erosion or hot gun effect.

Pressure Determination. The mean pressure produced by the matching charge in each of the i^{th} guns shall be calculated. To this value is algebraically added the pressure erosion loss of the Master for that gun. The overall estimate of the maximum chamber pressure is then obtained by averaging these four pressures. If there is no Master, average the four pressures across the guns.

Ballistic Uniformity. The velocity and maximum chamber pressure standard deviations shall be determined from the matching charge data per gun. For each standard deviation:

a. Calculate the sum of the squares of the deviations from the mean per gun.
b. Sum across the guns.
c. Divide by the quantity of the sum of the total number of rounds minus the number of guns.
d. Take square root to nearest unit of acceptance criteria.

Acceptance/Rejection. The acceptance or rejection of each lot is determined by comparing the acceptance criteria with the values determined above.

REFERENCES

1. NWL Techincal Report TR-2753 of April 1973 by M. C. Shamblen and J. S. O'Brasky, Investigation of 8"/55 Close Aboard Malfunctions, Naval Weapons Laboratory, Dahlgren, Virginia.

2. NWL Technical Report TR-2624 of December 1971 by D. W. Culbertson, M. C. Shamblen, and J. S. O'Brasky, Investigation of 5" Gun In-Bore Ammunition Malfunctions, Naval Weapons Laboratory, Dahlgren, Virginia.

3. "Applied Statistics for Engineers" by W. Volk (McGraw-Hill Book Company, Inc., New York, 1958).

4. "Statistical Methods" by G. W. Snedecor (Iowa State College Press, Ames, Iowa, 1956).

5. NWL, Dahlgren ltr TPB:BZJ:pjc 8010/1-21 of 27 Dec 1972.

6. NSWC, Dahlgren ltr DT-41:BZJ:ges 8010/1-21 of 29 Aug 1975.

7. NAVSEA ltr 9921/RLH Ser 118 of 15 Jan 1976.

WEAR TESTING OF M30A1 AND M31E1 PROPELLANT IN STICK CONFIGURATION PACKAGED IN BAGS AND COMBUSTIBLE CASES

Dr. J.A. Lannon
Dr. A.J. Bracuti
C.J. Gardner
LCWSL, ARRADCOM
Dover, New Jersey

and

D. Adams
G. Sturbutzel
Calspan Corporation
Buffalo, New York

ABSTRACT

A limited series of firing tests were conducted to compare the wear and erosion, and heating effects of the standard, high zone 155mm M203 propelling charge with a variety of stick charges in bags or combustible cases. The test charges were made from M30A1, M31E1 and Nitramine propellants, and were configured to achieve a ballistic match with the M203 charge.

Data was taken to provide comparisons between the standard and test charges, M30A1 and M31E1 stick and between bag and combustible case with both M30A1 and M31E1 propellants.

Preliminary examination of the summary data table of heating effects indicate such comparisons as:

1. The standard M203 propelling charge wear performance is as good as all test charges at the origin of rifling.
2. M31E1 stick in a combustible case without a TiO_2/wax liner is better than bag.
3. Performance of the M31E1 and M30A1 stick indicates that the M31E1 stick produces less heating and less erosion than M30A1 stick.

Comparison of wear profiles for U.S. 155mm M198 Howitzer and a similar NATO system firing similar propelling charges and projectiles shows that the British zone 8 stick propelling charge in combustible case with 10% talc causes less downbore wear than the U.S. M203 granular propelling charge.

INTRODUCTION

One of the major problems of the 155mm M198 weapon system continues to be the wear life of the gun tube, which is roughly one sixth of the fatigue life. Artillery systems have a requirement to fire at the extremes of both long and short ranges using a constant firing chamber volume. This prevents the use of cooler propellants with their associated larger chamber volumes to reach the longer ranges since the peak pressure and pressure rise time in this larger volume may not be sufficient to insure that the projectile will exit the tube when smaller charges are fired to reach the shorter ranges. Granular propellant has a limit in the

packing density to which it can be loaded without incurring serious ignition problems. Thus, in order to reach the longer ranges required at an acceptable charge loading density, an intermediate chamber volume was chosen which necessitated the use of a propellant with a correspondingly higher flame temperature. A sufficient quantity of cooler burning granular propellant such as M31 would not fit into the chamber to reach the longer ranges.

It has been determined for granular nitrate ester propellants that the higher the flame temperature of the propellant, the greater the erosion. Stick propellant can be loaded at higher loading densities than granular propellant. Thus, it is possible to use the cooler stick propellants in the intermediate chamber volumes. However, stick propellant burns differently from granular propellant, and its wear characteristics have not been fully assessed.

This test program was designed to provide wear data to help quantify the thermal and erosion effects of stick propelling charges and to permit direct comparisons with the present standard M203 granular propelling charge. Wear reducing additives were not specifically addressed, but one series of M30A1 stick propellant in propelling charge bag was tested with the same TiO_2/wax wear reducing liner as is contained in the granular charge.

EXPERIMENTAL

PROPELLING CHARGES

Propelling charges containing M30A1, M31E1, and Nitramine stick propellants in bags and combustible cases were configured to achieve a ballistic match with the standard M203E2 propelling charge. Seven-round series of propellants and charge container combinations were fired in which thermal and erosion data were measured. These data were compared with anologous data obatined from M203 and M203 without the TiO_2/wax wear reducing liner. The Nitramine stick series was discontinued after the first round due to excessive chamber pressure. Table 1 describes each series fired. M549A1 projectiles were fired with all test charges. M107 projectiles fired with M4A2 propelling charges were used as cleaners before each test series. Figures 1 and 2 illustrate two typical test charges.

GUN TUBE

A 155mm M199 gun tube, serial number 29943, was instrumented with thermal and erosion sensors at the locations shown in Figure 3. This test program, including cleaner founds, comprised rounds 104 through 171 of all rounds fired through tube serial number 29943.

HEAT SENSORS

Three thermocouple wells were drilled in the tube at the origin of rifling to receive thermocouples (heat sensors). Each well was flat-bottom drilled to a measured distance of about 1mm from the bore surface at the center of a groove in order that the entire heating cycle be completed prior to achievement of maximum temperature at this depth. A fourth thermocouple was located at 1.65 meters (65 inches) from the rear face of the tube (RFT) also 1mm from the bore surface at the center of a groove. A typical heat sensor installation is shown in Figure 4.

Wires of stainless steel sheathed, 40 gauge chromel-alumel are forced into contact with the flat-bottomed hole by the action of a compression spring. When contact is maintained, a thermocouple junction is formed at the contact points of the wires with the bottom of the well. If contact is lost for any reason, electrical continuity is also lost and no output will result. Thus, when an output is generated, it directly represents the change in temperature at the contact point. Subsequent analysis yields the total local amount of heat input per unit area to the gun barrel. As is shown in Figure 4, a small amount of silicone grease is placed in the thermocouple well prior to insertion of the thermocouple to fill void spaces and to decrease the small thermal resistance introduced by the presence of the hole. The thermocouple assembly is held in place by use of a 10 - 32 machine screw, which also imposes the required force to the thermocouple loading spring.

EROSION SENSORS

Three erosion sensors were installed in lands in tube serial number 29943; two at the origin of rifling region and one at 1.65m (65 inches) RFT. At the origin of rifling, the sensors were placed at 1.06m (41.85 inches) and 1.09m (42.85 inches) RFT.

These sensors were fabricated such that they could be replaced after each series of shots in order to keep the data for each series separate. Thus, erosion sensor holders were designed for adjusting surface match between sensor, holder and tube face, as well as to firmly fix the sensors axial position after adjustment. After fabrication, each holder was inserted into its respective location in the tube and honed to produce an excellent fit to the bore curvature. Gas seals were provided by use of conventional O-rings. The erosion sensor can be seen in Figure 5.

The erosion sensors were machined in the shape of cylinders having a single O-ring groove at the approximate mid-point (Figure 5). The sensor was made from 4340 steel heat treated to a hardness $R_c 34$ and sheathed in Tantulum - 10% tungsten alloy. The inner face of the sensor was contoured to match the bore curvature. This face, after polishing, was fitted with a series of three different Knoop impressions of various depths and one square indentation which were made with a microhardness tester.

A diamond indenter of the Knoop type was employed for all erosion sensors. This indenter produces a sharp impression with a constant length to depth ratio of 30:1, independent of depth, as illustrated in Figure 6. Variation in impression depth could be obtained by changing the load on the indenter tool. The impressions served as a gauge by which erosion or wear could be measured after firing. The approximate depths of the Knoop impressions on each sensor range from 1.2 to 10.7 microns. After forming the surface impressions, the surface of each sensor was characterized prior to being used in the gun testing by photomicrographs (SEM) at 275X magnification. The smallest impression was further photographed at 900X.

Post test examination of the erosion sensor can indicate the amount of erosion in several ways. When severe erosion occurs, one or several impressions may be completely removed, thus indicating surface loss. When normal erosion occurs, the impression lengths will shorten in direct proportion to depth change.

PROCEDURE

TEST FIRINGS

The tests were conducted jointly at ARRADCOM in Dover, N.J. by ARRADCOM and Calspan Corporation personnel. The types of charges tested are listed below and in Table 1:

1. The standard M203.
2. The standard M203 without TiO_2/wax additive liner but with lead foil.
3. M31E1 stick propellant in propelling charge bag without TiO_2/wax additive liner but with lead foil.
4. M30A1 stick propellant in propelling charge bag with TiO_2/wax additive liner.
5. M30A1 stick propellant without TiO_2/wax additive liner or charge container, but with lead foil.
6. M31E1 stick propellant in combustible case without TiO_2/wax additive liner.
7. M30A1 stick propellant in combustible case without TiO_2/wax additive liner but with lead foil.
8.* Nitramine stick propellant in combustible case without TiO_2/wax additive liner but with lead foil.

* 1 Round only.

The tests were fired in seven round series with M549A1 projectiles. Temperature - time profiles were recorded directly from the thermocouples during and after firing at a point approximately 1mm from the bore surface for each heat sensor location. See Figures 3 and 4. Erosion was measured for each series by the change in Knoop impression dimensions and divided by the number of rounds per series to yield averaged values per round. See Figures 3, 5, and 6.

DATA REDUCTION

The data reduction consisted of 1, conversion of thermocouple data from a point 1mm below the bore surface, to bore heat input per unit area at the surface, and 2, assessment of the bore surface erosion by examination of the erosion sensors. Conversion of in-wall temperature to heat input was based upon the theory (Reference 2) that bore heat input per unit area is given by the expression

$$Q = \sqrt{\pi k c \rho_m}\ \theta\ (T\ (\theta) - T_o)$$

where Q is the local heat input per unit area at the heat sensor location

T_o is the initial in-wall temperature

θ is the time after firing

K is the thermal conductivity

$c\rho_m$ is the heat capacity per unit volume

Q is evaluated at successive time intervals of 0.1, 0.2, 0.3 seconds, etc., result-

ing in a plot of Q vs θ. The curve produced approached the calculated heat input asympotically.

The amount of erosion experienced by each erosion sensor was determined by comparison of the pretest and posttest scanning electron microscope (SEM) photographs. This comparison was made after careful ultrasonic cleaning (as confirmed by use of the SEM in the x-ray mode) and included visual study of the surface condition and measurement of impression length change.

RESULTS

The reduced heat data for the tests conducted are summarized in Table 2. This table shows the averaged heat input and standard deviation for each test series for each heat sensor location. See Figure 3.

Table 3 provides a list of chamber pressure and muzzle velocity data averaged for each test series together with each standard deviation.

Table 4 lists the relative ranking of each test series for both heat and erosion data. Data from the thermal sensors at the 41.85 in RFT station has been averaged to show a single ranking value for each type of sensor at each axial location. Table 4 also briefly describes the coating observed on the erosion sensors and the presence of coppering of these same sensors.

Evaluation of the test charges was performed by 1, comparisons of the heat inputs for each type of charge, 2, comparisons of the relative rankings of the erosion data, and 3, comparisons of the relative rankings as provided by the heat and erosion methods. All comparisons were made relative to the standard M203 charge. Series 8, the Nitramine stick propellant in a combustible case without TiO_2/wax additive liner but with lead foil was discontinued after the first round due to excessive chamber pressure. Results for this series will not be discussed further, but the single round data will be included in the tables.

DISCUSSION

Relative rankings of all test series based on thermal and erosion data for each axial sensor location as shown in Figure 3 is given in Table 4. Figure 7 compares the averaged heat input for each series, for each of the four thermal sensors, plus or minus one standard deviation.

Examination of the erosion sensor surfaces shows that the only series for which Knoop impressions remained visible after testing were series 1 and 4, at 41.85 inches RFT, and series 1 at 42.85 inches RFT. Therefore, the examination was extended to include machining marks on the tantalum - 10% tungsten sleeve around the sensor, the amount of recession of the steel beyond the sleeve, and the amount of erosion visible on the sleeve. An assessment was also made of the general character of the coating that was observed on the erosion sensors and whether copper was present. This is briefly summarized in Table 4.

A cursory examination of the heating data as described by Figure 7 shows that thermal sensors 4, 5, and 6 consistently yield progressively higher readings for each series.

Since previous test programs fired in this tube with the same instrumentation also produced readings which increased consistantly in the same order as the sensor numbers, and since different thermocouples were used from one test program to the next and were sometimes changed during a test, this effect may be caused by some inconsistancy in the thermocouple wells or that the heat distribution around the firing chamber is not uniform. However, the data would still be adequate to yield relative rankings as Figure 7 shows.

None of the series fired, including the standard M203, produced the same relative ranking for all the sensors. Further, there does not appear to be a correlation between the relative rankings based on the heat data and the erosion data, although some agreement is shown for the 41.85 inches RFT location for series 1, 4, and 5. Note, also, that Table 4 and Figure 7 show that some series produced similar results for individual sensors so that relative rankings were given as ties.

From the relative rankings listed in Table 4 and the heating data with its associated variability given in Figure 7, observations can be made comparing the performances of the several propelling charges tested. In general, none of the charges performed better than the standard M203 propelling charge, although series 6, the M31E1 stick propellant in combustible case without the TiO_2 wear additive liner appeared to perform equally well, indicating that the same charge with a wear reducing additive may be superior to the M203 propelling charge.

Comparing series 3 and 6, M31E1 stick propellant without wear additive liners in charge bag and combustible case indicates that the combustible case may offer a significant improvement in heat input. The addition of talc to the combustible case, which is scheduled to be evaluated shortly, is expected to reduce both erosion and heating.

Comparison of series 3 and 4, M31E1 and M30A1 stick propellant in charge bags shows almost identical performance. However, since series 4 was fired with a wear reducing liner, this suggest that if the M31E1 propellant also was fired with TiO_2/ wax liner, its performance might have been better.

Series 5, M30A1 stick propellant wrapped only in lead foil, appeared to be consistantly poorest in both heating and erosion, indicating that a charge container helps to reduce both effects. Comparing series 5 with series 7 indicates that the combustible case should greatly reduce the gun tube erosion.

Clearly, considerably more tests are necessary to accurately compare stick propellants with granular propellants and combustible cases with charge bags - M31E1 stick propellant with wear additive liner, and M31E1 stick propellant in a combustible case with talc should be evaluated. M30A1 stick propellant in combustible case with talc should also be tested.

It should also be emphasized, that these tests are performed at only two axial tube locations; the origin of rifling and a point approximately 23 inches further down the tube toward the muzzle. The entire wear profile of the tube and the resultant effect on tube condemnation has not been addressed for any of the stick propellants tested as it has for the M203 propelling charges. See Reference 3 and Figure 8.

Figure 8 compares the wear profile of the standard M203 propelling charge in steel 155mm M199 Howitzer tube firing M549 projectiles to a zone 8 British stick propelling charge in a combustible case containing 8% to 10% talc, firing a similar projectile. The NATO test was conducted in a German 155mm Howitzer similar to the M198 U.S. weapon system. Approximately 2000 rounds were fired for both tests. See References 3 and 4.

From Figure 8 it can be seen that although the wear at the origin of rifling for both charges was comparable, the wear for the British charge dropped off much more quickly proceeding toward the muzzle than did that of the M203 charge.

The wear condemnation limit for the 155mm M199 tube firing the M203 propelling charge is normally 1750 rounds. This condemnation limit for the M198 Howitzer system firing M549A1 projectiles is based on a combination of premature fuze functioning and short rounds. These effects are believed to be caused by down bore wear in the U.S. tube. The German tube firing the British charge was tested to a total of 3047 rounds and was still serviceable. For these reasons it will be necessary to more fully characterize the wear effects of stick charge such as the M30A1 and M31E1 propellants.

SUMMARY

1. The standard M203 granular propelling charge appears to perform as well or better at the origin of rifling than all of the test charges. The performance of series six, M31E1 stick propellant in combustible case without wear reducing additive was indistinguishable from the standard charge. Addition of a wear reducing additive in the combustible case for the M31E1 stick charge could significantly improve its performance.

2. The performance of M31E1 stick propellant in combustible case without wear reducing additive was better than M30A1 stick propellant in the same configuration, indicating that the cooler burning M31E1 propellant is potentially superior.

3. Comparison of the heat data for series 3 and 6, M31E1 stick propellant in bag and combustible case indicates that combustible cases offer a reduction in heating.

4. Examination of the heat input data for series 5, M30A1 stick propellant without charge container shows that this charge produced the highest heating of all charges tested. Comparison of this data to series 7, the same charge in a combustible case shows that a charge container significally reduces heating at the origin of rifling.

5. Heat input and erosion data did not always produce the same relative rankings. However, once the Knoop impressions have been removed from the erosion sensor surfaces, the erosion sensors have been used beyond their intended limit and the data becomes somewhat doubtful.

6. Development of high zone stick charges and extension of gun tube wear life are both major areas of concern for Army artillery systems. In view of the fact that much of the performance definition derrived from the test data for this pro-

gram is within the experimental variability of the measurement techniques, it is of vital importance that the accuracy of these results be confirmed by extended testing.

7. Comparisons of a wear profile of the U.S. 155mm M198 Howitzer firing the M203 propelling charge with the M549 projectile, to that of a similar system developed by NATO shows that the wear life of the M199 tube could be greatly improved by using the M31E1 stick propellant in a combustible case with talc. The NATO system fires a British zone eight stick propelling charge containing an N Q propellant with a flame temperature 200° higher than that of the U.S. propellant. The charge is contained in a combustible case containing talc and is fired from a German tube. The wear test of the NATO system was conducted to almost double the wear life of the M199 tube, more than 3000 rounds, and the tube was still serviceable. Further development and more complete evaluation of the M31E1 propellants in combustible case is necessary and it should offer considerable potential for improving the wear.

REFERENCES

1. D.S. Downs, J.A. Lannon and L.E. Harris, "Prediction of Wear Characteristics of Artillery Propelling Charges", ARRADCOM Tech Report ARLCD-TR-80016, March 1981.

2. F.H. Vassallo, "Mathematical Models and Computer Routines Used in Evaluation of Caseless Ammunition Heat Transfer", Calspan Corp., Report No. GM-2948-Z-1, Buffalo, N.Y., June 1971.

3. J.A. Lannon and A.C. Vallado, "155mm M199 Chrome Plated Cannon Tube S.N. 83 Wear Test", ARRADCOM Report, January 1979.

4. Final Report, Field Howitzer Test, FH155-1, Operating-Life Firing (Test Series No. 385, Part II).

Table I

TEST CHARGES

Series	Remarks
1	The standard M203
2	The standard M203 without TiO_2/wax additive liner but with lead foil.
3	M31E1 stick propellant in propelling charge bag without TiO_2/wax additive liner but with lead foil.
4	M30A1 stick propellant in propelling charge bag with TiO_2/wax additive liner.
5	M30A1 stick propellant without TiO_2/wax additive liner or charge container, but with lead foil.
6	M31E1 stick propellant in combustible case without TiO_2/wax additive liner.
7	M30A1 stick propellant in combustible case without TiO_2/wax additive liner but with lead foil.
8*	Nitramine stick propellant in combustible case without TiO_2/wax additive liner but with lead foil.
*	1 Round only.

Table II

AVERAGED HEAT INPUT

Series	Sensor #4 Heat	σ	Sensor #5 Heat	σ	Sensor #6 Heat	σ	Sensor #7 Heat	σ
1	105.4	4.1	106.2	6.7	114.2	4.9	94.2	5.2
2	111.4	5.9	121.7	10.5	133.7	4.7	106.9	7.4
3	114.9	2.4	117.7	3.4	131.3	1.4	105.3	1.6
4	111.9	4.5	126.4	1.9	127.1	3.0	94.8	4.8
5	136.6	5.4	143.9	2.9	157.5	5.1	120.4	7.4
6	102.1	4.7	108.4	4.5	118.5	11.6	100.9	3.4
7	114.6	7.4	124.2	7.0	129.6	4.9	109.1	4.9
8	100.1	---	109.1	---	118.1	---	95.6	---

Table III

AVERAGED CHAMBER PRESSURE (PSI) AND AVERAGED MUZZLE VELOCITY (FPS)

Series	Chamber Pressure	σ	Muzzle Velocity	σ
1	47,429	390.4	2726	4.1
2	46,429	495.7	2723	8.3
3	50,386	857.2	2716	11.9
4	46,400	553.8	2665	6.2
5	44,543	457.7	2674	10.7
6	49,114	552.1	2685	9.1
7	49,143	457.7	2717	7.0
8	55,600	-----	2683	---

Table IV

SUMMARY OF RESULTS

Series No.	Description	Rankings 41.85 in. RFT Heat Input	41.85 in. RFT Erosion	42.85 in. RFT Erosion	65.0 in. RFT Heat Input	65.0 in. RFT Erosion	Character of Coating	Copper on Sensors?
1	Standard M203	1	1	3	1	6	Glassy	Yes
2	M203 w/Lead w/o TiO_2/wax Liner	4	3	1	6	2	Thin, Black;+ Plastic Piece	Slight Amount
3	XM203 w/M31E1 Stick in Bag w/Lead w/o TiO_2/wax Liners	6	2	2	5	2	Thin, Black;+ Plastic on sides of Sensor	Slight Amount
4	XM208 w/M30A1 Stick in Bag	4	4	-	3	-	Thin, Black	No
5	XM208 w/M30A1 Stick w/Lead w/o TiO_2/wax Liner	8	8	6	8	4	Reddish-Brown, Gummy	No
6	XM203 w/M31E1 Stick in Combustible Case w/o Liner	3	6	3	4	6	Dark Brown Pieces;+ Metallic Pieces on Sleeve	Yes
7	XM203 w/M30A1 Stick in Combustible Case w/Lead w/o TiO_2/wax Liner	6	7	6	7	5	Brown Spots; Reddish-Brown, Gummy	Slight Amount
8	Nitramine Stick in Combustible Case w/Lead w/o TiO_2/wax Liner	2	5	5	2	1	Thick, Grey Granular, Loose; + Metallic Pieces on Sleeve	Yes

FIGURE 1: Typical Test Charge - Series 6

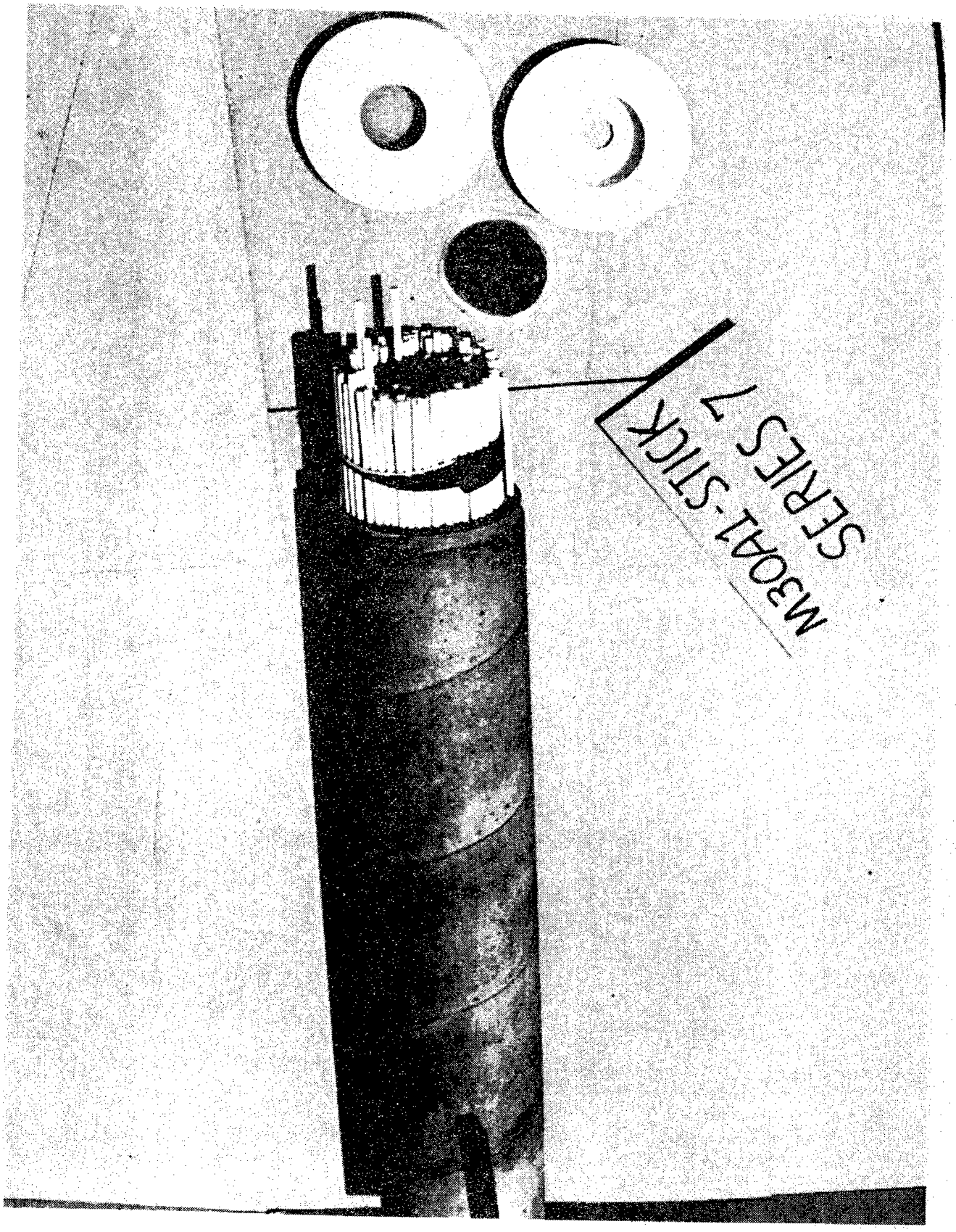

FIGURE 2: Typical Test Charge - Series 7

INSTRUMENTATION LOCATIONS - 155MM GUN TUBE SN29943

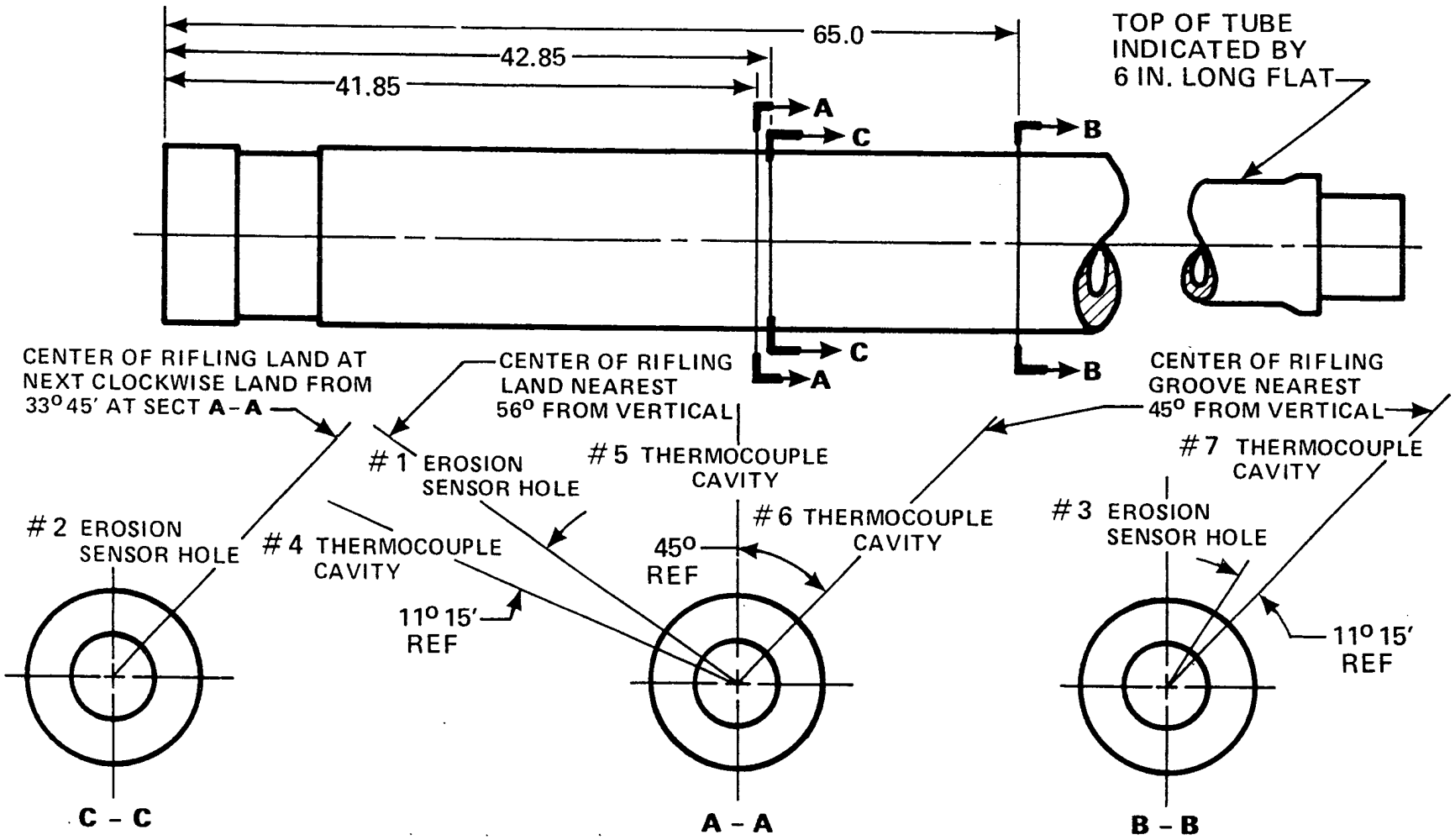

- ALL THERMOCOUPLE CAVITIES TO BE CENTERED ON RIFLING GROOVES
- ALL EROSION SENSOR HOLES TO BE CENTERED ON RIFLING LANDS

FIGURE 3

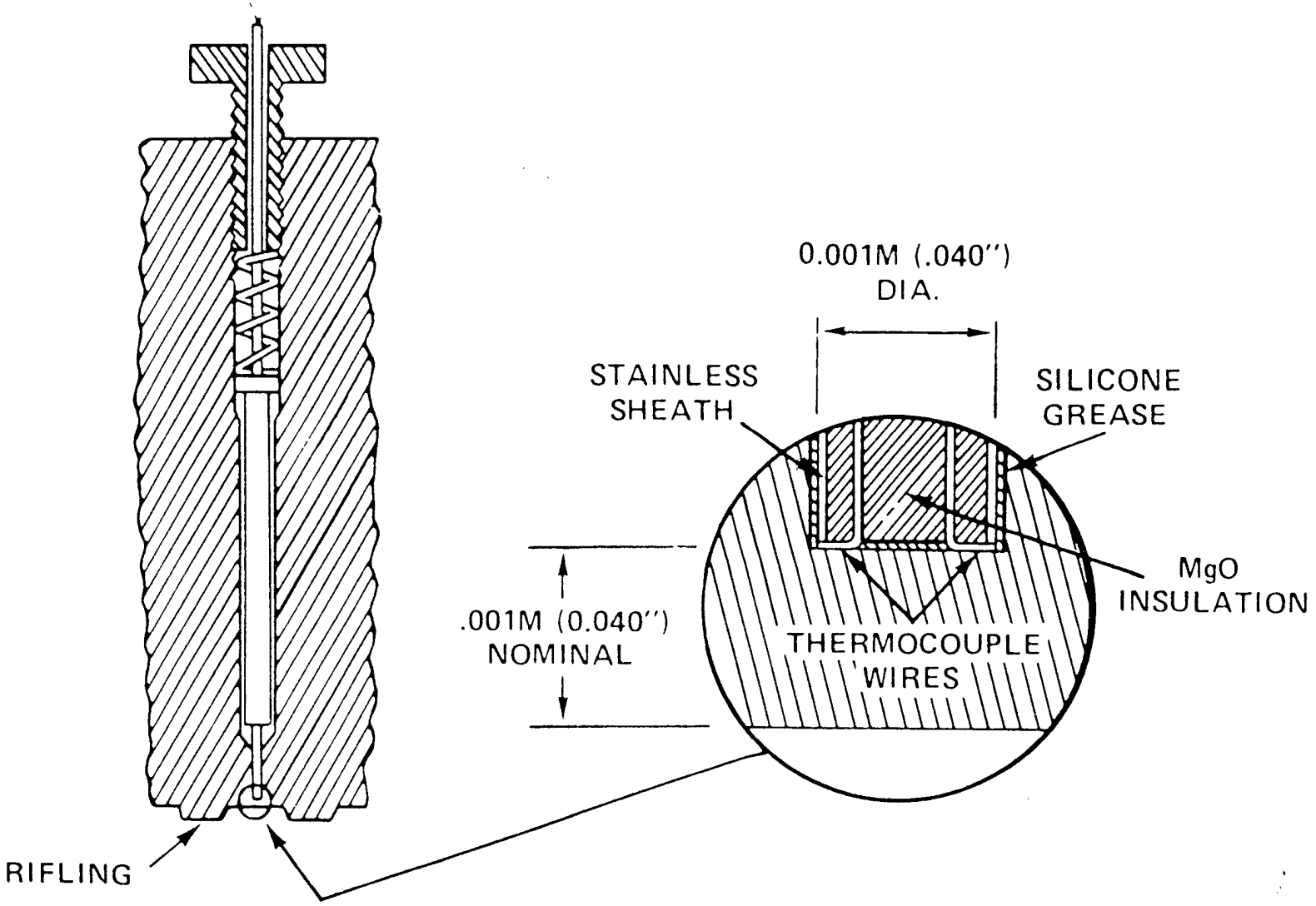

In-wall thermocouple (heat sensor) installation

FIGURE 4

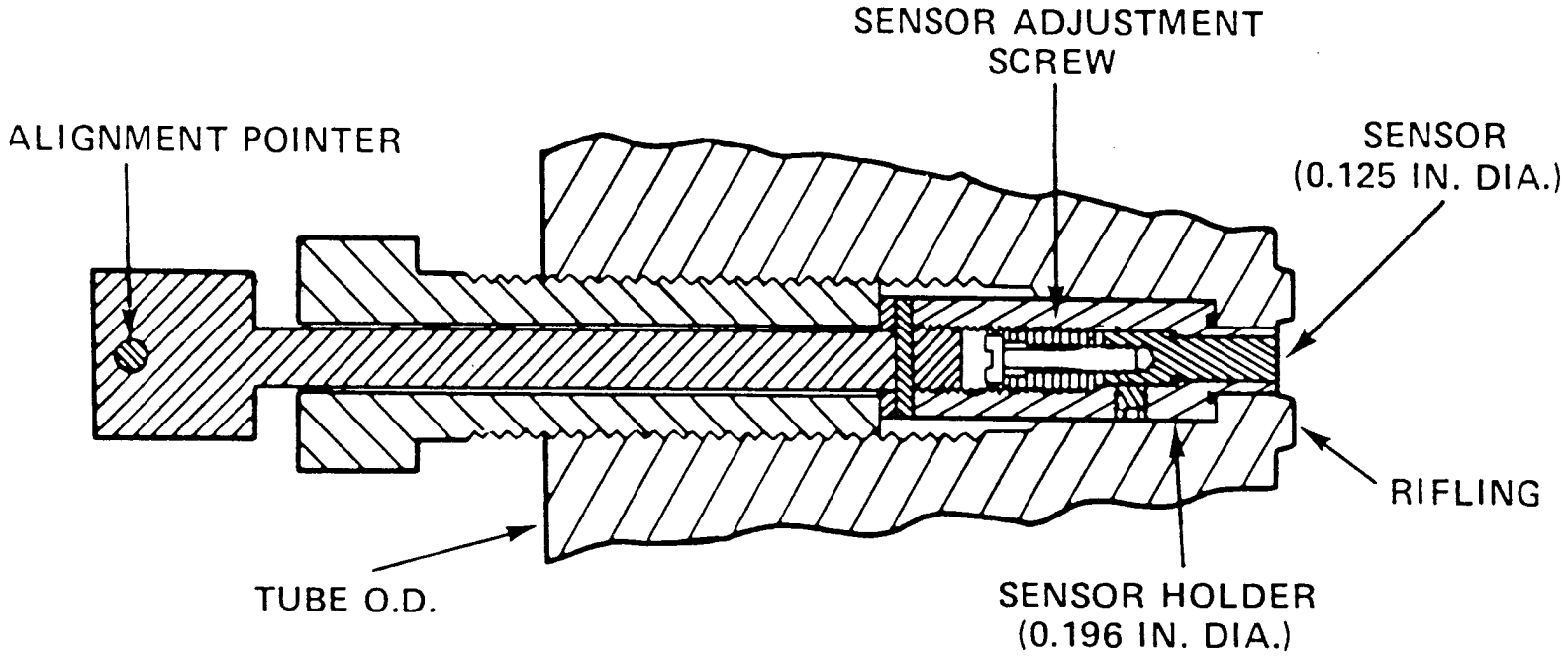

Erosion sensor installation

FIGURE 5

WEAR PROFILES OF U.S. AND NATO 155MM HOWITZER TUBES AT 2000 ROUNDS

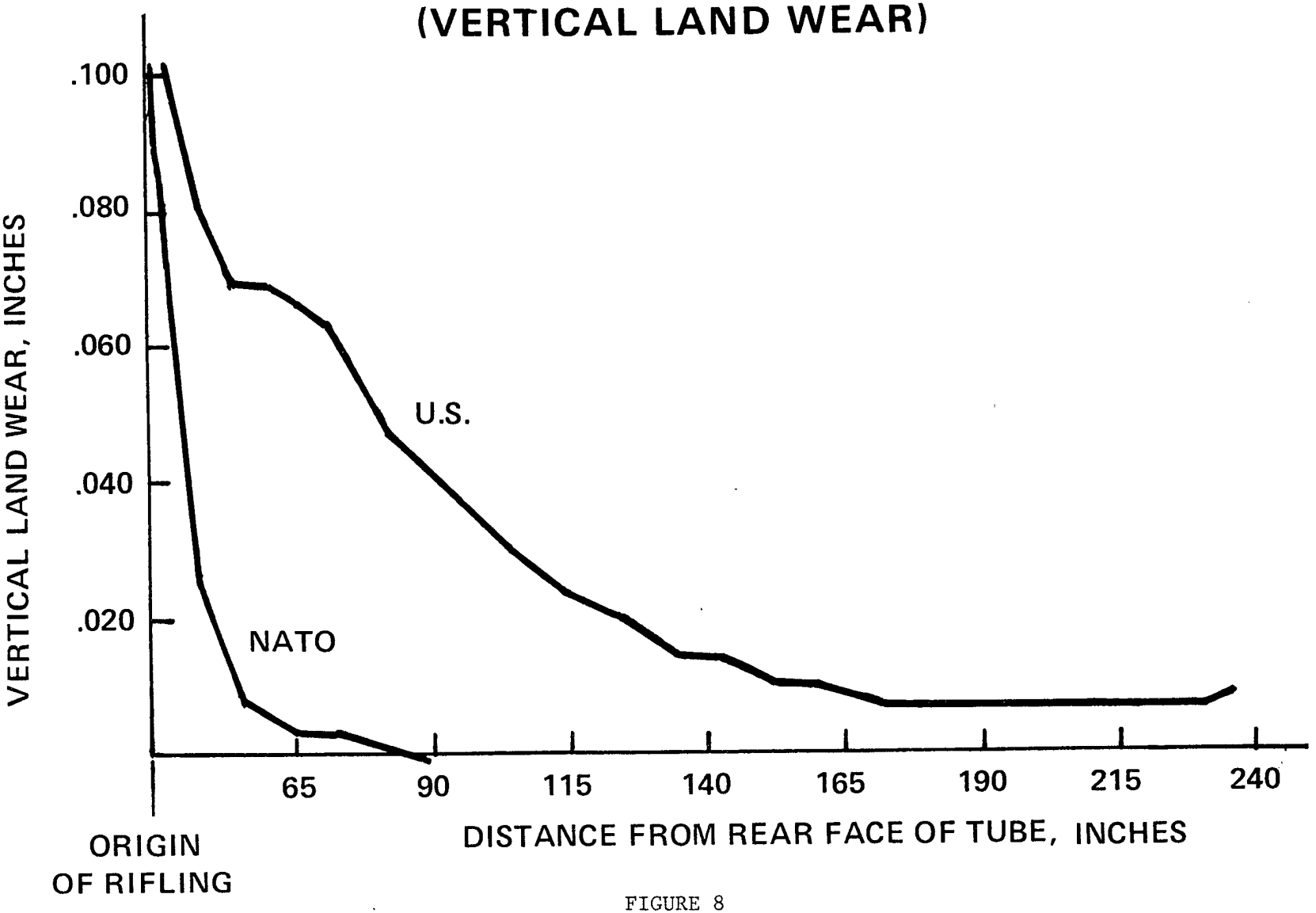

FIGURE 8

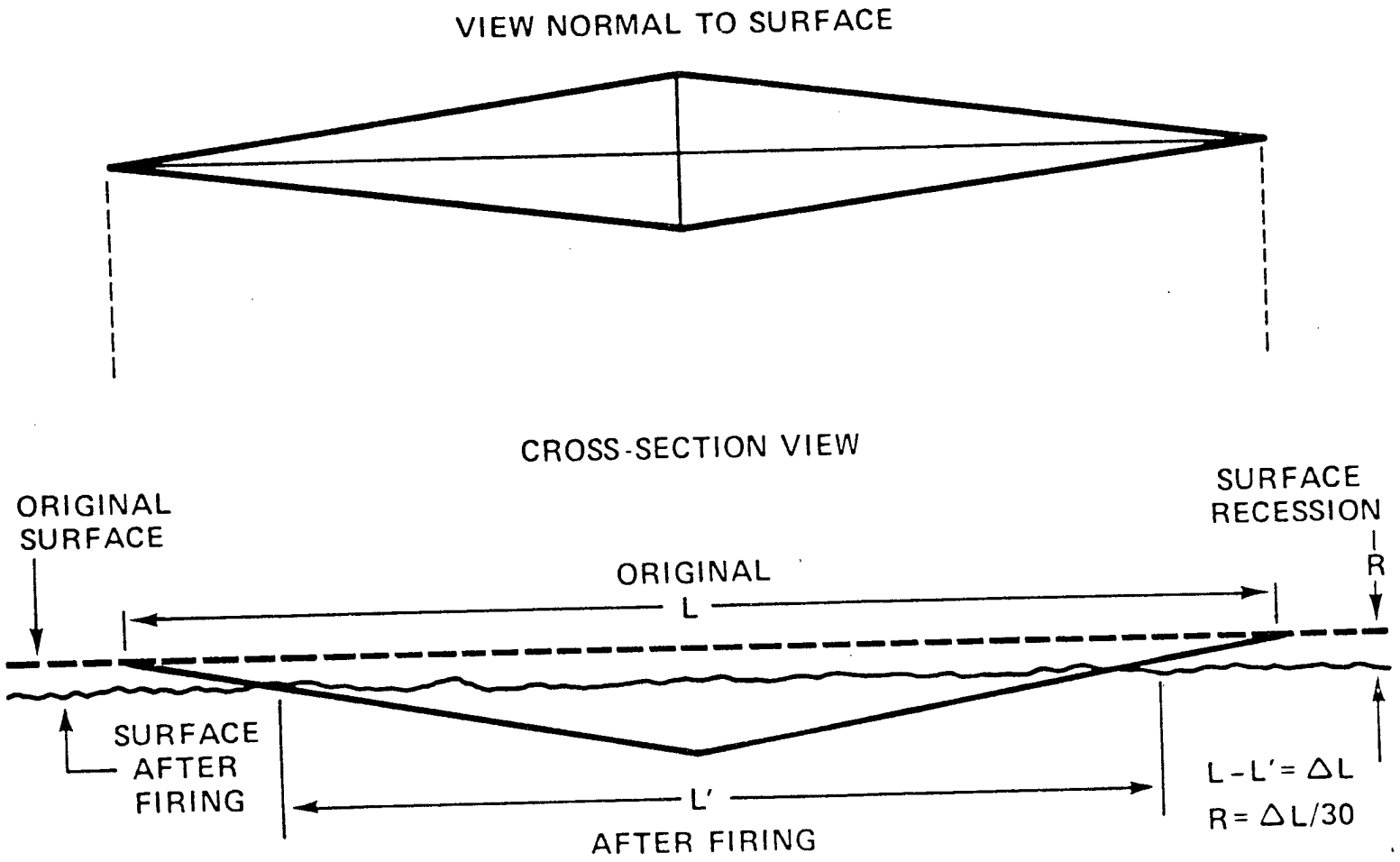

NOTE: In practice, actual length of indentation is from 10 to 400 micrometers.

Knoop microhardness indenter configuration

FIGURE 6

AVERAGED HEAT INPUT DATA FOR EACH TEST SERIES AT EACH SENSOR LOCATION

± 1 STANDARD DEVIATION

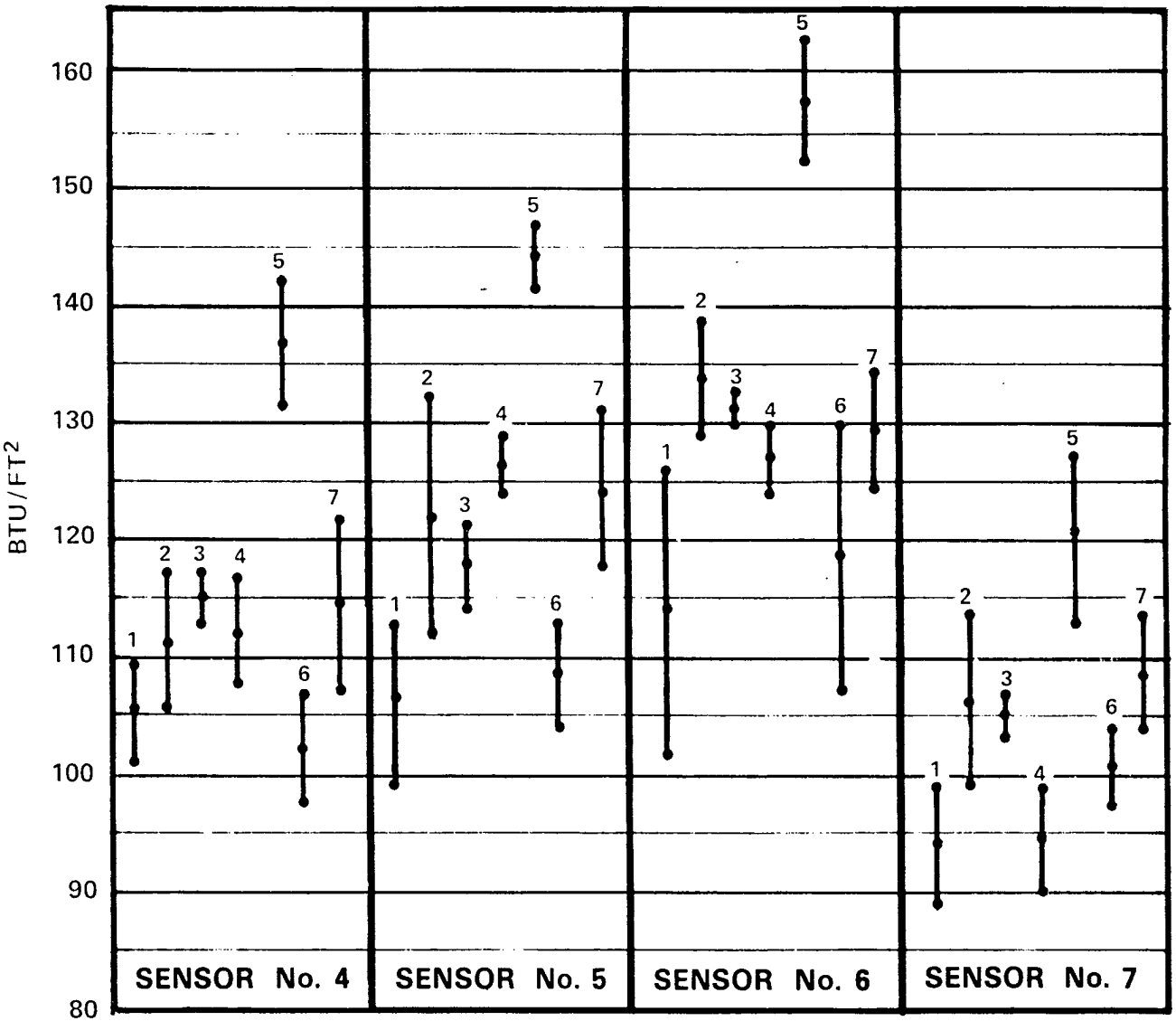

FIGURE 7